UNIVERSITÀ
DEGLI STUDI
DI PADOVA

Sede Amministrativa: Università degli Studi di Padova

Dipartimento di Scienze Chimiche

CORSO DI DOTTORATO DI RICERCA IN: SCIENZE MOLECOLARI
CURRICOLO: SCIENZE CHIMICHE
CICLO XXXII

Peptide-based foldamers for applications in self-recognition, supramolecular propagation, and photo-induced folding.

Tesi redatta con il contributo finanziario della Fondazione Cariparo

Coordinatore: Ch.mo Prof. Leonard Prins
Supervisore: Ch.mo Prof. Alessandro Moretto

Dottorando : Giulia Marafon

INDEX

Abstract

Self-recognition and propagation

Two appropriately functionalized nucleobases, thymine and adenine, have been covalently linked at the N- and C-termini of α-aminoisobutyric acid-rich helical peptide foldamers, at a set of selected chromophores and at fully adenine-capped gold nanoparticles, aiming at driving self-assembly through complementary recognition. These systems were studied in terms of their self-recognition abilities to generate ordered nano-architectures. A crystal-state analysis (by X-ray diffraction) shows that adenine···thymine base pairing, through Watson–Crick intermolecular H-bonding, does take place between either end of each peptide molecule. Evidence for time-dependent foldamer···foldamer associations in solution is provided by circular dichroism measurements. The self-assembly of foldamers, through living supramolecular polymerization, eventually leads to the formation of twisted fibers. It was found that adenine···thymine binding allowed the formation of precisely assembled nano-systems that depend powerfully on their morphologies from the nature of the chromophores utilized. These well-organized supramolecular architectures are able to undergo morphologically self-shaping processes under illumination by visible light, through the activation of the plasmon resonance of gold nanoparticles.

Moreover, three building blocks have been designed to chemically link to a gold surface and vertically self-assemble through thymine–adenine hydrogen bonds. Starting from these building blocks, two different films were engineered on gold surface. These films were characterized by electrochemical and spectroscopic techniques, and were very stable over time and when in contact with solution. Under illumination, they generate current with higher efficiency than similar previously described systems.

Self-recognition and polymerization

A set of four organogelators, from an α-amino acid derivative to a tetrapeptide, covalently linked to an acetylenic moiety, was studied in terms of polymerization efficiencies to afford peptide polyacetylenes (PAs) and polydiacetylenes (PdAs). Peptides were designed to improve the organogelator behavior via formation of intermolecular H-bonding-mediated β-sheet networks as a function of their main chain length. The polymerization experiments were run under appropriate conditions for the various monomers with the aim at elucidating how the monomer self-assembly process might influence polymer formation. Starting

compounds and their corresponding polymers were characterized by a variety of spectroscopic and microscopic techniques.

A symmetrical dipeptide-based diacetylene system (DAs) was found to be able to self-assemble in dichloromethane and to form a compact fiber network which resulted in a stable organogel. As a consequence of the organogel formation, we explored the possibility to run a light-induced topochemical polymerization. Evidence for the generation of peptide-based polydiacetylenes is provided by Raman, UV-Vis, and CD spectroscopies and a set of microscopic techniques. Finally, we succeeded in processing a polymeric composite by use of the electrospinning technique, starting from a mixture of a dipeptide-based diacetylene and polymethyl methacrylate.

Photo-induced supramolecular folding

Peptides are well known to play a fundamental therapeutic role and to represent building blocks for numerous useful biomaterials. Stabilizing their active 3D-structure by appropriate modifications remains, however, a challenge. We have expanded the available literature information on the conformational propensities of a promising backbone change of a terminally blocked δ-amino acid residue, a dipeptide mimic, by replacing its central amide moiety with an (E) Cγ=Cβ alkene unit. By DFT calculations, X-ray diffraction in the crystalline state, and FT-IR and NMR spectroscopies in solution we examined the extended *vs*. folded preferences of analogs of this prototype system. The theoretical and experimental results obtained clearly point to the conclusion that increasing the number of adequately positioned methylations will enhance the preference of the original sequence to fold, thus opening interesting perspectives in the design of conformationally constrained peptidomimetics.

Systems in which an external stimulus elicits a response through some sort of modification at the molecular or supramolecular level bear potential for the development of smart materials and devices. A simple, unsaturated, *E–Z* photoisomerizable β-amino acid, (Z)-3-aminoprop-2-enoic acid, has been introduced into peptide foldamers through a one-pot chemical coupling, based on Pd/Cu-catalyzed olefin oxidative amidation, between two peptide segments carrying, respectively, a -Gly-NH_2 residue at the C-terminus and an acryloyl group at the N-terminus. Reversible conversion between the *Z* and *E* configurations of the 3-aminoprop-2-enoic linkage was achieved photochemically. A crystallographic analysis on two model compounds shed light on the consequences, in terms of 3D structure and self-

association properties, brought about by the different configuration of the unsaturated linkage. As a proof of concept, *E–Z* photoisomerization of a 3-aminoprop-2-enoic acid residue, inserted as the junction between two conformationally distinct peptide domains (one helical while the other β-sheet promoter), allowed supramolecular self-association to be reversibly turned on/off.

Finally, we developed a versatile synthetic approach suitable for the stepwise incorporation of multiple, even consecutive, units of the simplest $C^{\alpha,\beta}$-unsaturated β-amino acid, [(*E*/*Z*)-3-aminoprop-2-enoic acid] in peptide-based foldamers.

Riassunto

Auto-riconoscimento e propagazione

Due basi azotate opportunamente funzionalizzate, timina e adenina, sono state legate covalentemente alle estremità N- e C- terminali di foldameri peptidici, diversi cromofori e nanoparticelle d'oro, in modo da promuovere il processo *self-assembly* di questi sistemi sfruttando il riconoscimento tra basi complementari. Questi sistemi sono stati studiati per osservare la loro capacità di auto-associarsi e di generare nano-architetture ordinate. Tramite diffrazione dei raggi X abbiamo potuto osservare che su entrambe le estremità dei peptidi, a cui sono legate le basi azotate, si formano interazioni intermolecolari non covalenti del tipo Watson-Crick tra le basi complementari, mentre analisi di dicroismo circolare evidenziano l'associazione foldamero···foldamero tempo-dipendente in soluzione. Il *self-assembly* dei foldameri, attraverso una polimerizzazione supramolecolare *living*, da origine a strutture fibrose spiralizzate. E' stato osservato che il *binding* adenina···timina permette la formazione di nano-sistemi precisamente assemblati la cui morfologia dipende fortemente dal cromoforo utilizzato. Le strutture supramolecolari ben organizzate possono subire processi di auto-modellamento sotto irraggiamento con luce visibile, attraverso l'attivazione del plasmone di risonanza delle nanoparticelle.

Inoltre, le basi azotate timina e adenina sono state covalentemente legate a tre *building blocks* che sono stati successivamente legati chimicamente a una superficie d'oro, ed è stato studiato il processo di *self-assembly* attraverso legami a idrogeno tra adenina···timina. In questo modo sono stati ottenuti due diversi film, che sono stati caratterizzati attraverso tecniche spettroscopiche ed elettrochimiche, risultando molto stabili nel tempo anche a contatto con la soluzione. In seguito ad irraggiamento, è stato osservato che essi generano corrente con efficienza maggiore rispetto ai sistemi preesistenti.

Auto-riconoscimento e polimerizzazione

Un set di quattro gelatori organici, da un α-amminoacido a un tetrapeptide, legati covalentemente a un residuo acetilenico, sono stati studiati per verificare la loro efficacia di polimerizzazione con lo scopo di formare poliacetileni e polidiacetileni. I peptidi sono stati progettati per essere in grado di aumentare la capacità di gelazione tramite la formazione di legami a idrogeno intermolecolari che stabilizzano un network di strutture β-sheet, in funzione della lunghezza della catena principale del peptide stesso. Gli esperimenti di polimerizzazione sono stati condotti in condizioni appropriate ai singoli monomeri con lo

scopo di chiarire come il processo di *self-assembly* del monomero influenza la formazione dei polimeri. I composti di partenza e i corrispondenti polimeri sono stati caratterizzati attraverso diverse tecniche spettroscopiche e microscopiche.

E' stato studiato, inoltre, il comportamento di un dipeptide simmetrico basato su un sistema diacetilenico, capace di auto-assemblare in diclorometano generando un network di fibre compatto che risulta in un organogel stabile. Come conseguenza della formazione dell'organogel, abbiamo esplorato la possibilità di eseguire una polimerizzazione topochimica indotta dalla luce. Polidiacetileni a base peptidica sono stati studiati attraverso spettroscopia Raman, UV-Vis e dicroismo circolare, oltre che con tecniche di microscopia.

Folding supramolecolare foto-indotto

E' noto che i peptidi rivestono un ruolo fondamentale in ambito terapeutico e nello sviluppo di nuovi materiali. Per questo motivo, stabilizzare la loro struttura 3D attraverso appropriate modifiche del backbone è sempre più una sfida. Uno dei sistemi studiati durante questo Dottorato è un δ-amminoacido, che mima un dipeptide, in cui l'ammide centrale è stata sostituita da una unità (E) Cγ=Cβ. attraverso calcoli DFT, diffrazione ai raggi X nello stato cristallino e spettroscopia FT-IR e NMR in soluzione sono state studiate le preferenze conformazionali di diversi analoghi di questo sistema. Dai risultati teorici e sperimentali è emerso che un numero crescente di posizioni metilate aumenta la propensione del sistema a formare strutture foldate, aprendo interessanti prospettive nella progettazione di peptidomimetici conformazionalmente rigidi.

I sistemi in cui uno stimolo esterno provoca una risposta attraverso una qualsiasi modificazione a livello molecolare o supramolecolare offrono un potenziale per lo sviluppo di materiali intelligenti e dispositivi. Un semplice, insaturo, β-amminoacido *E-Z* isomerizzabile, l'acido (Z)-3-aminoprop-2-enoico, è stato inserito all'interno del backbone di foldameri peptidici attraverso una reazione di ammidazione ossidativa *one pot* Pd/Cu catalizzata tra due segmenti peptidici opportunamente funzionalizzati rispettivamente con un residuo -Gly-NH_2 al C- terminale e un gruppo acrile al N- terminale. Fotochimicamente è stato possibile ottenere la conversione, reversibile, tra le configurazioni *Z* ed *E* dei foldameri. L'analisi cristallografica dei foldameri ottenuti evidenzia le conseguenze, in termini di struttura tridimensionale e proprietà di *self-assembly*, determinate dalle diverse configurazioni (*Z* ed *E*) del linkage insaturo. Come *proof of concept*, la fotoisomerizzazione dell' acido (Z)-3-aminoprop-2-enoico, inserito come giunzione tra due domini peptidici conformazionalmente

distinti, un'elica 3_{10} e il residuo 16-20 dell'amiloide β, permette di "accendere" e "spegnere" reversibilmente l'associazione supramolecolare.

E' stato infine sviluppato un nuovo approccio sintetico ottimizzato per incorporare più di un residuo dell' acido (Z)-3-aminoprop-2-enoico, anche consecutivamente, in foldameri peptidici.

Introduction

From the second half of the twentieth century, the field of synthetic oligomers able to achieve well-defined conformations has attracted the attention of many scientists, due to the ability of these molecules to mimic the folding of biomolecules. The folding process of proteins, for instance, into secondary and ultimately into tertiary and quaternary structures, represents the key point for their correct function and reactivity. These complex structures are supported mainly by non-covalent interactions like hydrogen bonding, and ionic, Van der Waals and hydrophobic interactions, which give proteins the favorite degree of specificity in form and function.[1] These non-covalent interactions are moreover characterized by reversibility, that means their reactivity can be tuned by local environmental changes. Thus, the correct folded structure of a protein is the result of a delicate combination between non-covalent interactions and local environmental conditions. The Levinthal's paradox describes that even a short polypeptide would require a very long time to reach its correct native conformation.[2] For this reason, cooperativity is a crucial aspect in the folding process, to obtain the precise folded structure in a biologically relevant time. First of all, the driving force of a folding process is the minimization of the interactions between the non-polar side chains and the solvent, in order to stabilize the structure, a mild equilibrium between the loss in conformational entropy and increase in enthalpy.[3] Therefore, the incomparable specificity of biomolecules structures it's kind of what scientists are going for. To do so, they possess an infinite number of building blocks, and imagination is the only limit.

The molecules artificially synthetized with this scope in mind are foldamers, oligomers with the specific characteristic to fold into well-defined structures with the driving force of non-covalent interactions, or, as stated in Gellman's definition, "any polymer with a strong tendency to adopt a specific compact conformation". [4,5] Some of the most attractive features possessed by this class of molecules are their synthetic availability, readiness to modifications and the predictability and stability of their folding configurations.[6] Since the first few synthetic foldamers were described, there has been an exceptional growth in this field.[4–19] Many of these are inspired from the aliphatic chains found in polypeptides (C. Toniolo), others are based on β-amino acids, or on aromatic ring systems not found in biomolecules (S. Hecht and I. Huc). In the design of a foldamer, the initial step must therefore be to identify those elements of the backbone, which will impart well-defined secondary structural preferences to the folded structure.

Depending on the choice of the monomers, it is possible to develop several folded artificial molecular architectures, covering peptidic foldamers, nucleic acid foldamers, abiotic oligomers, metallofoldamers, and folded polymers. The intrinsic properties of the monomers are translated from the *micro* to the *macro* scale level, producing molecules with remarkable properties. Thanks to synthetic foldamers, it was possible to generate artificially biological structural motif such as helices, sheets, columns, and cavities, able to mimic the reactivity and functions of biomolecules.[20-27] Another aspect that has to be considered in the design of a biomimetic folded structure is the intrinsic conformational dynamism, which characterized proteins and biomolecules. Here we are introducing dynamic foldamers[28] (J. Clayden), not only supramolecular conformationally uniform architectures but molecules that mimic also properties and functions of allosteric proteins and receptors. Due to the fact that the folding process is driven by non-covalent interactions, their nature allow scientists to easily modify the folded conformation, by means of an external stimulus, to tune functions. In this way, with dynamic foldamers, it is possible to achieve, with a chemical output, control of reactivity and selectivity,[29-32] acting on foldamers able to adopt more than one switchable conformations, each of which still characterized by a defined folded structure.

References

1. G. A. Jeffrey and W. Saenger, *Hydrogen Bonding in Biological Structures*, Springer-Verlag, Berlin, **1991**.
2. C. Levinthal, in *Mossbauer Spectroscopy in Biological Systems, proceedings of a meeting held at Allerton House, Monticello, Illinois*, University of Illinois Press, Urbana, IL, **1969**.
3. K. A. Dill, *Biochemistry*, **1990**, 29, 7133.
4. S. H. Gellman, *Acc. Chem. Res.*, **1998**, 31, 173.
5. D. J. Hill, M. J. Mio, R. B. Prince, T. S. Hughes and J. S. Moore, *Chem. Rev.*, **2001**, 101, 3893.
6. I. Huc, *Eur. J. Org. Chem.*, **2004**, 17.
7. *Foldamers: Structure, Properties and Applications*, ed. S. Hecht and I. Huc, Wiley-VCH, Weinheim, **2007**.
8. A. D. Bautista, C. J. Craig, E. A. Harker and A. Schepartz, *Curr. Opin. Chem. Biol.*, **2007**, 11, 685.
9. R. P. Cheng, *Curr. Opin. Struct. Biol.*, **2004**, 14, 512.
10. B. Gong, *Acc. Chem. Res.*, **2008**, 41, 1376.
11. C. M. Goodman, S. Choi, S. Shandler and W. F. DeGrado, *Nat. Chem. Biol.*, **2007**, 3, 252.
12. Z.-T. Li, J.-L. Hou and C. Li, *Acc. Chem. Res.*, **2008**, 41, 1343.
13. A. R. Sanford and B. Gong, *Curr. Org. Chem.*, **2003**, 7, 1649.
14. C. E. Schafmeister, Z. Z. Brown and S. Gupta, *Acc. Chem. Res.*, **2008**, 41, 1387.
15. D. Seebach and J. Gardiner, *Acc. Chem. Res.*, **2008**, 41, 1366.
16. M. T. Stone, J. M. Heemstra and J. S. Moore, *Acc. Chem. Res.*, **2006**, 39, 11.
17. K. D. Stigers, M. J. Soth and J. S. Nowick, *Curr. Opin. Chem. Biol.*, **1999**, 3, 714.
18. A. Violette, S. Fournel, K. Lamour, O. Chaloin, B. Frisch, J. P. Briand, H. Monteil and G. Guichard, *Chem. Biol.*, **2006**, 13, 531.
19. N. P. Chongsiriwatana, J. A. Patch, A. M. Czyzewski, M. T. Dohm, A. Ivankin, D. Gidalevitz, R. N. Zuckermann and A. E. Barron, *Proc. Natl. Acad. Sci. U. S. A.*, **2008**, 105, 2794.
20. H. Juwarker, J.-M. Suk and K.-S. Jeong, *Chem. Soc. Rev.*, **2009**, 38, 3316.
21. R. B. Prince, S. A. Barnes and J. S. Moore, *J. Am. Chem. Soc.*, **2000**, 122, 2758.
22. D.-W. Zhang, X. Zhao and Z.-T. Li, *Acc. Chem. Res.*, **2014**, 47, 1961.

23. Q. Gan, Y. Ferrand, C. Bao, B. Kauffmann, A. Grélard, H. Jiang and I. Huc, *Science*, **2011**, 331, 1172.
24. V. Azzarito, K. Long, N. S. Murphy and A. J. Wilson, *Nat. Chem.*, **2013**, 5, 161.
25. M. Reggelin, S. Doerr, M. Klussmann, M. Schultz and M. Holbach, *Proc. Natl. Acad. Sci. U. S. A.*, **2004**, 101, 5461.
26. R. A. Smaldone and J. S. Moore, *J. Am. Chem. Soc.*, **2007**, 129, 5444.
27. M. M. Müller, M. A. Windsor, W. C. Pomerantz, S. H. Gellman and D. Hilvert, *Angew. Chem.*, **2009**, 121, 940.
28. B. A. F. Le Bailly and J. Clayden, *Chem. Commun.*, **2016**, 52, 4852.
29. M. De Poli, W. Zawodny, O. Quinonero, M. Lorch, S. J. Webb, and J. Clayden, *Science*, **2016**, 352, 575.
30. D. Mazzier, M. Crisma, M. De Poli, G. Marafon, C. Peggion, J. Clayden, and A. Moretto, *J. Am. Chem. Soc.*, **2016**, 138, 8007.
31. N. Eccles, B. A. F. Le Bailly, F. della Sala, I. J. Vitòrica-Yrezàbal, J. Clayden, and S. J. Webb, *Chem. Commun.*, **2019**, 55, 9331.
32. M. Vallade, P. S. Reddy, L. Fischer, and I. Huc, *Eur. J. Org. Chem.*, **2018**, 5489.

Project aims

The main purpose of this project is the development of new families of peptides and peptide-mimic foldamers, built on chemically modified peptides and peptide hybrid-organic molecules. Applications therefore will explore (i) self-recognition and propagation, (ii) photo-induced supramolecular folding, (iii) β-turn mimic.

(i) Self-recognition and propagation. One of the most important examples of realization of highly selective molecular process in biology is the mutual recognition of complementary nucleobases by means of multiple hydrogen-bonding patterns. In this work, we want to realize and to study a set of novel N-terminally thymine- and C-terminally adenine-functionalized peptides, with alternating achiral α-aminoisobutyric acid (Aib) and L-Ala residues. Additionally, fully adenine-capped, water soluble, gold nanoparticles (GNPs) and other photo-active and nucleobases functionalized chromophore will also synthesized. These systems will be study in terms of their self-recognition abilities to generate ordered nano-architectures with the aim to investigate novel electronic applications. Moreover, a set of alkyne-functionalized short peptides, with strong tendency to form highly organized β-sheet structures, will be synthetized with the aim to generate electroactive peptide based-polymers, via acetylene or diacetylene polymerization.

(ii) Photo-induced supramolecular folding. With the aim of finding an alternative to the well know azobenzene unit to be inserted directly into a peptide backbone, we want to explore the possibility to synthetize the simplest unsaturated (*E*-*Z* photoisomerizable) β-amino acid, namely (*Z*)-3-aminoprop-2-enoic acid (Δ^ZβAla). For this purpose, we will consider some organic synthetic methodologies. We thought that the reversible conversion between the Δ^ZβAla and Δ^EβAla configurations will exhibit remarkable 3D-structure consequences, especially in terms of molecular self-association.

(iii) β-turn mimic. Intermolecular backbone-backbone hydrogen bonding is observed in quaternary structures and is believed to be an significant stabilizing force in protein-protein interactions. It is possible to remove the amide functionality in a single dipeptide substructure by replacing it with an E-alkene moiety. We will explore new (E)olefin dipeptide systems to investigate the relationship between chemical structure and folding.

Most of the work of these three years has already been published on different scientific journals as papers, for which permission to reuse the text has been requested and granted by the copyright holder. Personally, I have been involved in the conceptual design of the experiments and in drafting the manuscripts, together with my Ph.D. supervisor, Prof. Alessandro Moretto, but especially I was responsible for the synthetic design, the synthesis and the characterization of all the studied compounds.

Needless to say, all the work wouldn't have been possible without the collaboration and the efforts of other people, with whom I worked and which have helped me for the completion and outcome of this Ph.D. thesis. In particular, all the X-Ray diffraction structures reported have been resolved by Dott. Marco Crisma, Prof. Mariano Venanzi, Dott. Emanuela Gatto and their collaborators at the University of Roma "Tor Vergata" and at the Technische Hochschule in Wildau (Germany) have been involved in the electrochemical studies and characterizations, and at last I have to thank for the computational measurements Prof. Carlos Alemán and Prof. David Zanuy Gomara from the Universitat Politècnica de Catalunya.

Abbreviations

A	=	Adenine
Ac	=	acetyl
Ac_2O	=	acetic anhydride
AcOH	=	acetic acid
AFM	=	atomic force microscopy
Aib	=	α-Amino*iso*butyric acid
Ala	=	L-Alanine
Arg	=	L-Arginine
Boc	=	*tert*-butyloxycarbonyl
Boc_2O	=	di-*tert*-butyl dicarbonate
CD	=	circular dichroism
CF	=	carboxyfluorescein
COSY	=	correlation spectroscopy
CQDs	=	carbon quantum dots
CV	=	cyclic voltammetry
Cys	=	L-cysteine
Cys(Me)	=	S-methyl-L-cysteine
DAs	=	diacetylenes
DBU	=	1,8-diazabicyclo[5.4.0]undec-7-ene
DIC	=	N,N'-di*iso*propylcarbodiimide
DIPEA	=	N,N-di*iso*propylethylamine
DLS	=	dynamic light scattering
DMAP	=	4-dimethylaminopyridine
DMF	=	N,N-dimethylformamide
DMPA	=	2,2'-dimethoxy-2-phenylacetophenone
DMSO	=	dimethylsulphoxyde
DPPA	=	diphenylphosphoryl azide
E-SEM	=	environmental scanning electron microscopy
EDC	=	N-ethyl-N'-(3-dimethylamino)propyl-carbodiimide
ESI	=	electrospray ionization
ET	=	electron transfer
Et_2O	=	diethyl ether
EtOAc	=	ethyl acetate
EtOH	=	ethanol
Fmoc	=	(9*H*-fluoren-9-yl)methoxycarbonyl

FT-IR	=	Fourier transform infrared spectroscopy
FTIR-RAS	=	Fourier transform infrared reflection absorption spectroscopy
Gly	=	Glycine
GNPs	=	Gold nanoparticles
HATU	=	1-[bis(dimethylamino)methylene]-1H-1,2,3-triazolo[4,5-b]pyridinium 3-oxid hexafluorophosphate
HBTU	=	N,N,N′,N′-tetramethyl-O-(1H-benzotriazol-1-yl)uronium hexafluorophosphate
HFIP	=	1,1,1,3,3,3-hexafluoro-2-propanol
HMBC	=	^{1}H-^{13}C Heteronuclear Multiple-Bond Correlation
HMQC	=	^{1}H-^{13}C Heteronuclear Multiple Quantum Correlation
HOAt	=	1-hydroxy-7-azabenzotriazol
HPLC	=	high performance liquid chromatography
IR-RAS	=	infrared reflection absorption spectroscopy
ITO	=	indium tin oxide
Leu	=	L-Leucine
Lys	=	L-Lysine
MALDI	=	Matrix-Assisted Laser Desorption/Ionization
MeOH	=	methanol
M_w	=	molecular weight
NMR	=	nuclear magnetic resonance
NOESY	=	nuclear Overhauser effect spectroscopy
OMe	=	Methoxy
O*t*Bu	=	*tert*-butoxy
PAs	=	polyacetylenes
PdAs	=	polydiacetylenes
Phe	=	phenylalanine
PMMA	=	poly(methyl methacrylate)
Prop	=	propargyl
RCM	=	ring-closing metathesis
ROESY	=	rotating frame nuclear overhouser effect spectroscopy
ROP	=	ring opening polymerization
SAMs	=	2D self-assembled monolayers
SEC	=	size-exclusion chromatography
SEM	=	scanning electron microscopy
SPPS	=	solid phase peptide synthesis
T	=	Thymine
TEA	=	triethylamine

TEM	=	transmission electron microscopy
TEOA	=	triethanolamine
Tfa	=	trifluoro acetyl
TFA	=	trifluoroacetic acid
TFE	=	trifluoroethanol
TGA	=	thermogravimetric analysis
THF	=	tetrahydrofuran
TIS	=	triisopropylsilane
TMEDA	=	N,N,N′,N′-Tetramethylethylenediamine
TMS	=	tetramethylsilane
$TMSCHN_2$	=	(Trimethylsilyl)diazomethane
TOCSY	=	total correlation spectroscopy
Trt	=	triphenylmethyl
UV-Vis	=	ultraviolet-visible spectroscopy
Val	=	L-Valine
XPS	=	X-ray photoemission spectroscopy
ZnTPP	=	zinc-tetraphenylporphyrin

1.1 Shaping bioinspired photo-responsive microstructures by the light-driven modulation of selective interactions[a]

The design and creation of bioinspired self-shaping microstructures represent a new way to develop shape-adaptation in synthetic materials. In distinction to shape-memory polymers, the self-shaping abilities in these bioinspired materials are located at the nanoscale, rather than the molecular, level.[1] In this view, self-assembly can be considered as the most powerful autonomous organization of components able to produce structures at any scale level, and this phenomenon takes part in many essential biological, chemical, and physical processes. In these complex systems, the self-organization is synergically driven by specific intermolecular interactions, like π-π stacking interactions, hydrogen bonds, electrostatic interactions and hydrophobic forces.[2–4] Nowadays, following the bio-inspiration concept, many new types of functional materials have been readily achieved through the selective molecular recognition between defined components.[5–9] One of the most important examples of the realization of highly selective molecular process in Nature is the mutual recognition of complementary nucleobases by means of the selectivity, directionality, reversibility, and cooperativeness of hydrogen bonds.[10–14] While the Watson–Crick base pairing is dominant within nucleic acids constrained by the geometry of the double helix, it is important to note that the nucleobases linked to synthetic systems may change their binding behaviour.[15] Thus, reverse Watson–Crick, Hoogsteen, 'wobble' base pairs and other nucleobase binding modes play important roles in any artificial-nucleobase self-assembly process mainly controlled by its hydrogen bonding network.[16] Furthermore, in the hybrid-nucleobase systems the chemical nature of the linked molecules play, additionally, an important role in the self-assembly process. Finally, hydrogen-bonding interactions alone cannot yield significant driving forces for molecular recognition in bulk water due to the strong competitive binding of water molecules.[17] In this perspective, a prior design of the directional mode of complementary hydrogen bonding may overcome the competition of the aqueous environment and the self-recognition antagonism between the same type of nucleobases.[18] We have studied the selective adenine-thymine binding (A-T) occurring between complementary self-organized complex systems, such as gold nanoparticles, with suitable functionalized chromophores, such as tetraphenylporphyrin, azobenzene and carbon quantum dots (CQDs),[19] that resulted in well-organized supramolecular architectures. Importantly, we reported three examples of governable

[a] Reprinted (adapted) with permission from (RSC Adv., 2016, 6, 73650). Copyright (2019) Royal Society of Chemistry."

morphological transition processes, induced by the light activation of the plasmon resonance of the gold nanoparticles.

Synthesis of thymine- and adenine-functionalized chromophores

The chemical structures of functionalized molecules are presented in Fig. 1.

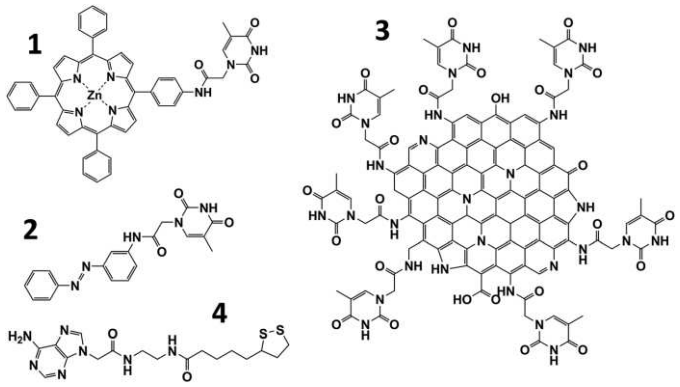

Fig. 1 Representation of the chemical structures of the compounds synthesized and studied.

Briefly, thymine was first converted into its corresponding acetic acid derivative, namely thymine-1-acetic acid,[20] while adenine was converted into its acetic ethyl ester derivative, namely ethyl adenine-9-acetate.[21] Then, thymine-1-acetic acid was coupled either (i) with 5-(4-aminophenyl)-10,15,20-triphenyl porphyrin and subsequently converted into its metallated Zn-form, yielding **1**, (ii) with 4-aminoazobenzene, yielding **2** and (iii) amino-doped CQDs,[19,22–24] yielding **3**. Ethyl adenine-9-acetate was converted into its monoacetyl ethylen-diamino amide derivative and subsequently coupled with racemic lipoic acid, yielding **4**. Compounds **1**–**3** were chemically and spectroscopically characterized as illustrated in Fig. 2. Fig. 2A shows a comparison of the UV-Vis absorption spectra of **1** (red line) and its non-metallated form (black line) in tetrahydrofuran (THF) solution. The two spectra exhibit the characteristic UV-vis profiles of metallated porphyrin and porphyrin, respectively.[25] Fig. 2B displays the UV-vis profiles of **2** recorded after three cycles of irradiation (at 350 or 420 nm) that reveal the reversible isomerization process occurring between the trans and cis forms.[26] This phenomenon was additionally investigated by ^{1}H-NMR. In this case, the chemical shifts of the protons belonging to the thymine part of the molecule are affected by the photoinduced isomerization process. The comparison of the FT-IR absorption spectra recorded for pristine CQDs and **3** was the first evidence to confirm the occurrence of the chemical modification of pristine CQDs after coupling with thymine-1-acetic acid. Successively, Fig. 2C and D

illustrates a comparison of TEM analyses and fluorescence spectra of pristine CQDs[23] and **3**, respectively. In particular, TEM analyses (Fig. 2C and D, inserts) revealed the formation of strongly aggregated structures occurring for **3** (probably resulting from thymine self-recognition). Importantly, as shown from a comparison of the fluorescence experiments (recorded in MeOH solution, Fig. 2D, right), the multi-colored emission properties (taking place for pristine CQDs) are preserved in **3**.

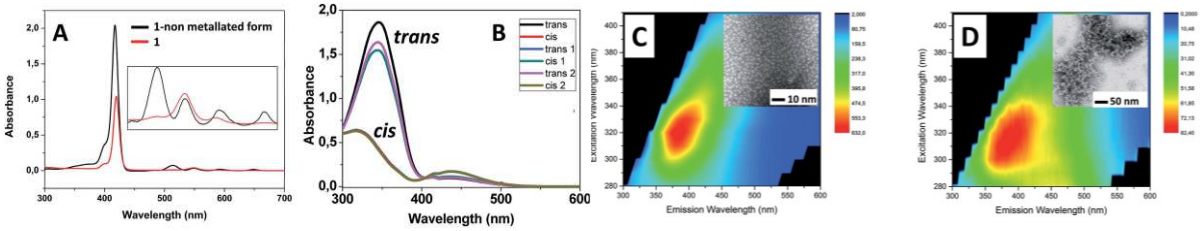

Fig. 2 (A) UV-Vis absorption spectra recorded for **1** (red line) and its non-metallated analog (black line) in a THF solution. (B) UV-Vis absorption spectra of a THF solution of **2** recorded after three complete irradiation cycles with light at 350 and 420 nm. (C) Fluorescence 2D spectrum recorded for pristine CQDs. Inset: TEM image of pristine CQDs. (D) Fluorescence 2D spectrum recorded for **3**. Inset: TEM image of **3**.

Self-aggregation studies

A part of this work was devoted to the study of the self-aggregation properties of compounds **1**–**3** that may arise from thymine–thymine self-recognition.[16,27] To this aim, compound **1** was dissolved in THF. Upon addition of water to the THF solution, flake-like structures were recovered after few hours, as shown in Fig. 3A and B. Compound **2** was examined in its trans and *cis* conformers. Interestingly, it was found that slow evaporation from a THF/MeOH (methanol) solution provided different microstructure morphologies for the trans and the *cis* isomers (Fig. 3C and D, trans isomer, and Fig. 3E and F, cis isomer). Finally, slow evaporation from a water solution of **3** provided formation of ordered microstructures as shown in Fig. 3G and H. It is worth noting that the same experiments repeated for 5-(4-aminophenyl)-10,15,20-triphenyl porphyrin, trans 4-aminoazobenzene and cis 4-aminoazobenzene and pristine CQDs did not produce any type of microstructures. With this set of self-recognition experiments we demonstrated the strong aptitude of functionalized thymine to bind itself in a mixed THF/water solution.

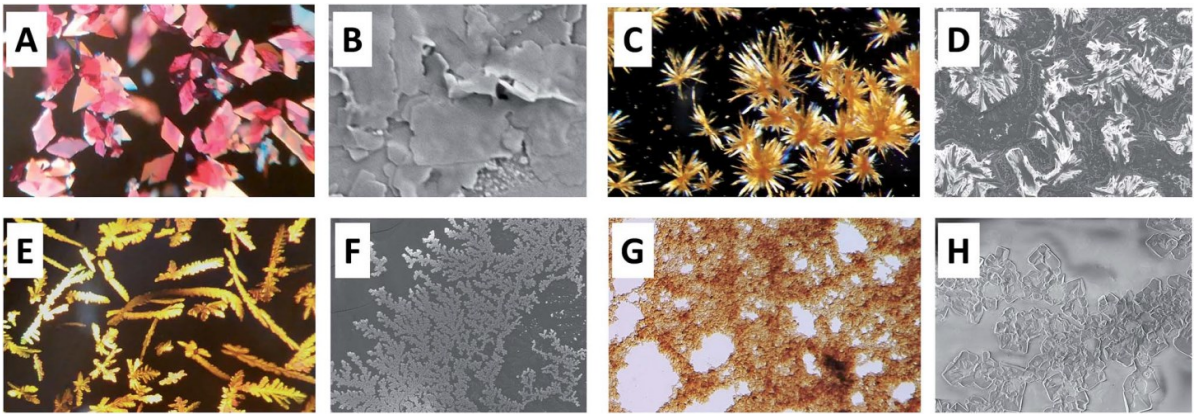

Fig. 3 (A) Optical microscope and (B) SEM images showing organized microstructures obtained from 1. (C, E) Optical microscope and (D, F) SEM images revealing different structures adopted by **2** in its trans and its cis forms, respectively. (G) Optical microscope and (H) SEM images showing organized microstructures obtained from 3.

Synthesis of adenine-capped gold nanoparticles

Then, nanometric-sized GNPs (**5**) covered by **4** (Fig. 4A) were synthesized. **4** was combined with tetrachloroauric acid in THF, and after an appropriate time of complexation the mixture was rapidly reduced by adding $NaBH_4$.[28] After 48 h aging, GNPs were recovered by filtration and fully characterized using transmission electronic microscopy (TEM), UV-Vis absorption spectroscopy, thermogravimetric analyses (TGA), and dynamic light scattering (DLS). From the TEM images (sample dissolved in water), it was possible to highlight the strong self-aggregation tendency of this nanosystem, due to the self-recognition mediated by intermolecular hydrogen bonds occurring among the adenine moieties (Fig. 4B). By using a DMSO/water mixture, it was possible to reduce the self-aggregation propensity and to detect a distribution of single GNPs (Fig. 4C). In Fig. 4D, the graph displays a narrow size distribution centered at a diameter of 1.5 nm observed for GNPs. The UV-Vis absorption spectrum of a diluted solution of nanoparticles in water resembles closely that of GNPs with a size lower than 2 nm, as confirmed by the presence of a slightly pronounced plasmonic resonance located at 520 nm (Fig. 4E). TGA analyses revealed a chemical composition of 42% of the organic part and 58% of the inorganic part (Fig. 4F).

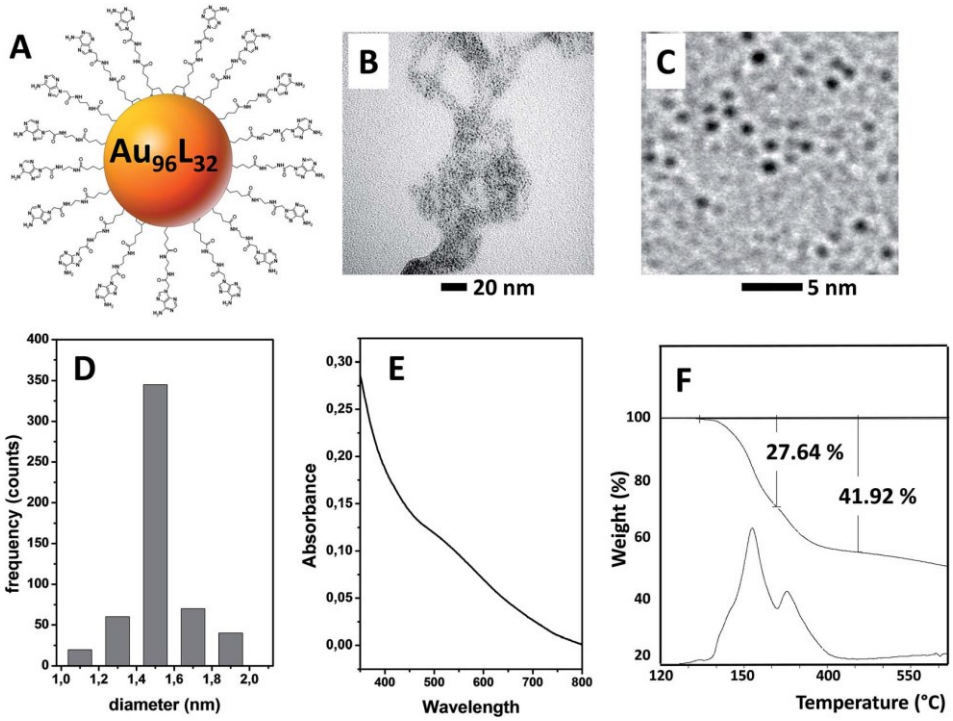

Fig. 4 (A) Schematic representation of adenine-capped GNPs. (B) TEM image of self-aggregated adenine-capped GNPs. (C) TEM image of dispersed adenine-capped GNPs. (D) Size distribution graph obtained considering a large number of dispersed adenine-capped GNPs. (E) UV-Vis absorption spectrum of adenine-capped GNPs dissolved in a DMSO/water mixture. (F) TGA analyses run on a solid sample of adenine-capped GNPs.

Thus, the number of Au atoms in the corresponding GNPs can be calculated from the dimensions of the metallic core observed by TEM images taking into account the density of bulk gold metal (55 atoms per nm^3, if a spherical model is applied). The number of adenines conjugated to the inorganic cluster was calculated from the TGA weight loss (corresponding to the weight fraction of the organic coating monolayer on the inorganic cluster) divided by the molecular weight of the related adenine conjugated to the inorganic core.[29] From all this information, we may estimate that the average chemical formula for these GNPs would be $Au_{96}L_{32}$. This formula is in good agreement with that of similarly sized GNPs resolved by X-ray crystallographic analyses that revealed a closely related number of gold atoms for a very similar core size diameter, but concomitantly displayed a larger number of organic ligands.[30] In this connection, it is worth emphasizing that we used the disulfide-containing lipoic acid, which affords a double number of sulfur atoms for the molecular unit (if compared to that of the GNPs resolved by X-ray crystallographic analyses). Thus, a lower number of ligands is required to passivate the gold core. From DLS measurements of a diluted water solution of adenine-capped GNPs, an average diameter of 6.5 nm per GNP was found (Fig. 5A). This

value is in agreement with a hypothetical structure where the organic ligands (**4**) are placed in a fully-extended conformation.

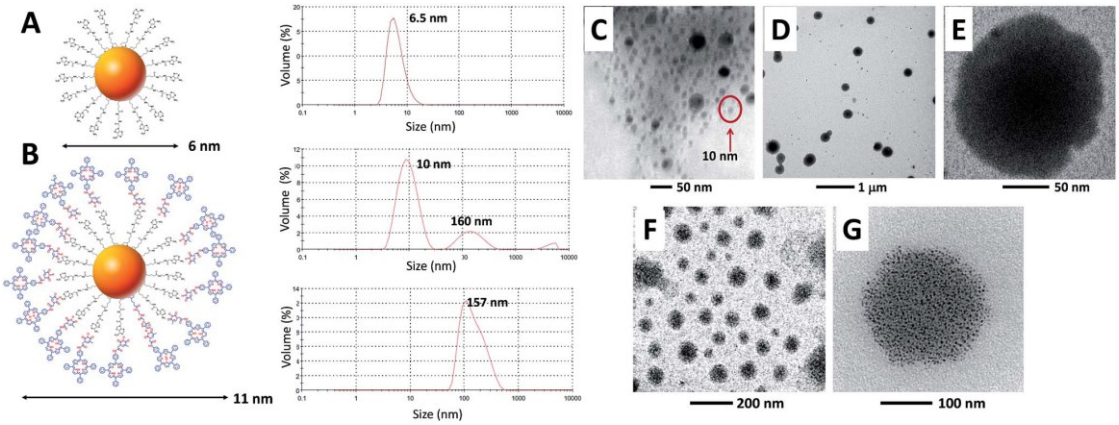

Fig. 5 (A and B) Representation and DLS analysis of **4**-capped GNPs and **4**-capped GNPs mixed with **1**, respectively. (C) TEM image showing monomeric, self-recognized **1**/adenine-capped GNPs. (D) TEM images showing a large view of **1**/adenine-capped GNPs self-assembled nanosystems. (E) TEM image showing a detailed view of a single aggregate. (F) TEM images showing a large view of **1** (in its non metallated form)/adenine-capped GNPs self-assembled nanosystems. (G) TEM images showing a detailed view of **1** (in its non metallated form)/adenine-capped GNPs nanosystems.

Molecular recognition between adenine-capped GNPs and thymine-functionalized chromophores

By mixing a solution composed of **5** and **1**, a step toward a molecular recognition process mediated by thymine/adenine interactions was carried out. The basic idea is to detect molecular recognition through the formation of a double sized nanoparticle (with an estimated diameter of 11 nm, considering an extended conformation taking place for both **1** and **4**), which may result from the selective interaction of the adenine layer of the GNPs and **1** (Fig. 5B). To run this experiment, **5** was first dissolved in water and subsequently an equivalent of 1 (referred to as the adenine ligand) was added from a highly diluted THF solution. After a mixing time of 24 h at 30 °C, a large number of single monomeric **1**/**5** nanosystems of 10 nm diameter were detected by DLS experiments (Fig. 5B) and TEM analyses (Fig. 5C). It is worth noting that the presence of the Zn^{2+} ion inside the porphyrin ring allowed detection of the 10 nm assembled nanoparticle core, which was present in this case, by TEM. By both techniques a small amount of large round aggregates were also detected. With the aim to understand the origin of such large spherical microstructure aggregates we repeated the

above-described experiment keeping constant the number of GNPs and **1** equivalents but varying the concentration. In particular, after a slow addition of a THF solution of **1** to a water solution (20-times concentrated with respect to the previously reported experiment) of adenine-capped GNPs, the solution turned slightly opaque, and only large **1**/**5** nanosystems of 160 nm diameter were almost quantitatively detected by TEM analyses (Fig. 5D and E) and DLS experiments (Fig. 5B). Since, by TEM analyses it was hard to distinguish the presence of adeninecapped GNPs, we repeated the self-assembly experiment by using **1** in its non-metallated form. Also this case the TEM analyses confirmed the exclusive formation of large spherical aggregates (Fig. 5F) and moreover, from a detailed view of a single spherical aggregate (Fig. 5G) it was possible to distinguish single **5** nanosystems that are not aggregated to each other, but rather seemed precisely spatially located within the aggregate. Because TEM analyses were run under ultra-high vacuum conditions, atomic force microscopy (AFM) (Fig. 6A) and environmental scanning electron microscopy (E-SEM) (Fig. 6B) analyses were carried out on the large **1**/adenine-capped GNPs nanosystems, to provide more detailed morphological information under wet-like conditions. By both techniques, formation of spherical-shaped aggregates, with similar dimensions of those observed by TEM, was detected. To understand the origin of these spherical superstructures, which could be related to the onset of a set of cooperative non-covalent bonds mediated by hydrogen bonding, π–π stacking and hydrophilic/hydrophobic interactions, we carried out UV-Vis absorption measurements. The UV-Vis absorption spectrum of **1**, recorded in THF, exhibits an intense Soret band at 419 nm, together with two weaker Q-bands at 547, and 587 nm (Fig. 6C, red line). In contrast, in the UV-Vis absorption spectrum of the spherically-shaped aggregates obtained, the Soret band is red shifted to 429 nm, while the frequency of the two Q-bands falls at longer wavelengths, at 561 and 600 nm (Fig. 6C, black line, insert). The red-shift of the absorption bands of **1** indicates the formation of J-aggregates (Fig. 6D).[31]

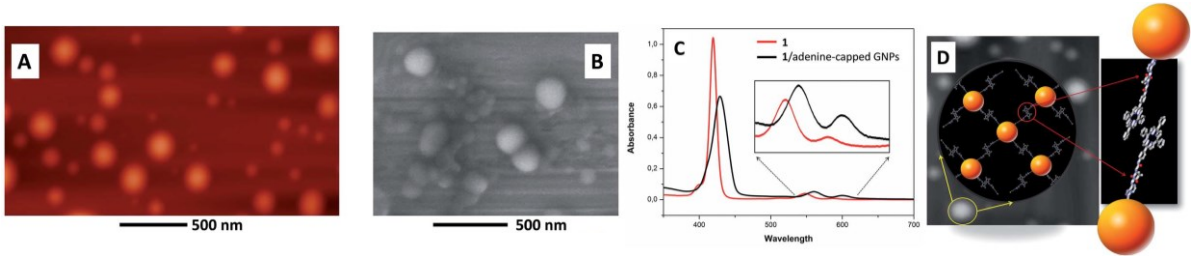

Fig. 6 (A and B) AFM and E-SEM images, respectively, showing a large view of **1**/adenine-capped GNPs self-assembled nanosystems. (C) UV-Vis absorption spectra in THF of **1** (red line) and **1**/adenine-capped GNPs (black line) self-assembled nanosystems. (D) Schematic representation of the hypothetic bulk network interactions occurring for these assembled nanosystems.

We decided to use light at 500 nm to promote an eventually occurring molecular reorganization. The principle is that at this wavelength the gold core of GNPs absorbs light, thus the resulting vibrational energy (heat) may flow from the gold core[32] across the adenine capping layer following excitation of the nanoparticle plasmon resonance, and finally could affected the adenine/thymine binding mode with consequences extending to the spatial distribution of the overall self-assembled systems (Fig. 7). Thus, we irradiated a solution of large spherical aggregates by using a LED at 500 nm. Under illumination, the opaque solution turned into a suspension after a few minutes and this suspension was analysed directly by TEM. Fig. 7A (stained TEM) displayed the morphological transition that occurred from large spherical to straight fiber structures, while Fig. 7B (non-stained TEM) showed the details of the nanoparticle disposition within the fiber structures. As a control experiment, we used LED at different wavelengths (405, 465 and 585 nm), and under these condition no microstructures transition were found.

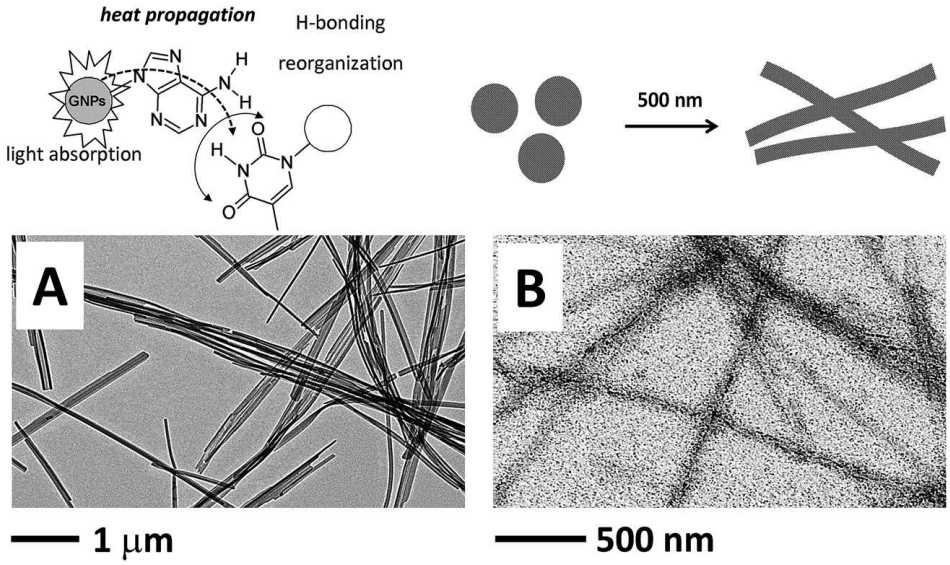

Fig. 7 (Upper part) Schematic representation of the light induced activation of the microstructure transition occurring in the **1**/**5** self-assembled system. (A) TEM images (stained) showing the formation of fibers. (B) TEM images (non-stained) showing the GNPs within the fiber network.

We repeated the same type of experiment by mixing together **5** and **2** under the above experimental conditions. Interestingly, in the case of **2** in its trans form, a rapid formation of a suspension of straight fiber networks was observed after mixing the two components, as detected by SEM (Fig. 8A and B). Additionally, the same sample was further characterized by TEM (Fig. 8C and D, under stained and non-stained conditions, respectively) which revealed the spatial arrangement of the GNPs inside the novel microstructure formed. Moreover, after a prolonged irradiation at 365 nm (*trans* to *cis* azobenzene isomerization), the previous

suspension was converted into a milk-like suspension, that resulted froma dense network of bent fibers, as detected by SEM (Fig. 8E and F). The same sample was further characterized by TEM (Fig. 8G and H, under stained and non-stained conditions, respectively) and the results confirmed the bent morphology adopted by this supramolecular system under light exposure, and highlighted the presence of adenine-capped GNPs inside the fiber networks. The possibility to convert the straight fiber network into a bent fiber network by a photo-induced process suggested that the azobenzene moieties are not densely packed within the fiber network, so that they are able to isomerize, under irradiation, between their *trans* and *cis* forms. Moreover, the isomerization process seems not to affect recognition with the nanoparticles, but rather it appears to act only on the directional propagation of the resulting fibers.

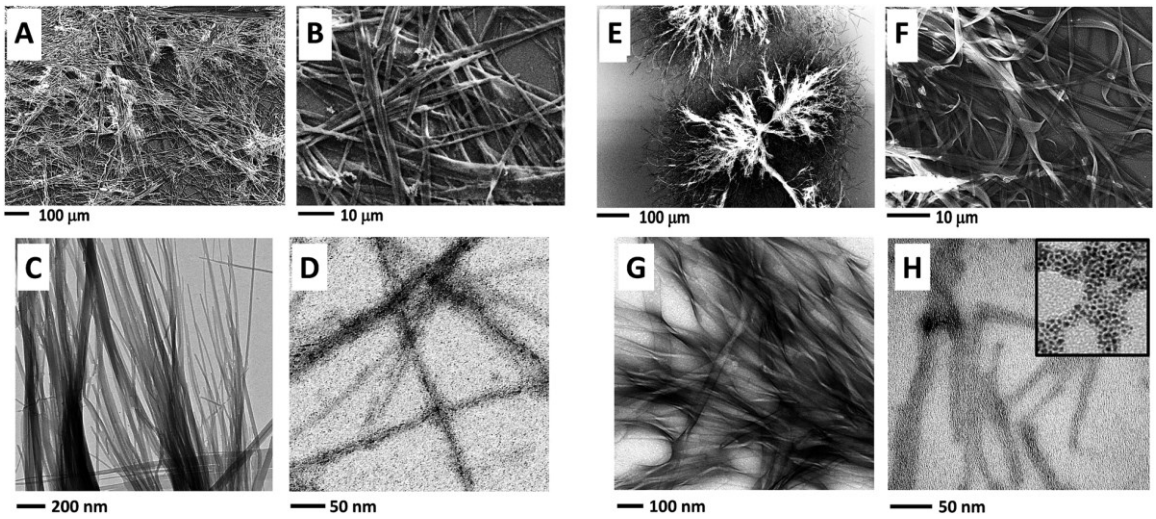

Fig. 8 (A and B) SEM images showing the formation of microstructures composed of a straight fiber network, occurring by the mixing of **2** (in its trans form) with adenine-capped GNPs. (C and D) Corresponding TEM images, stained and un-stained, respectively, showing the fibrous nature of the network, and highlighting the adenine-capped GNPs inside the fibers. (E and F) SEM images showing the formation of novel microstructures composed of dense network of bent fibers, after irradiation at 350 nm of the "trans" microstructures (**2** is in its cis form). (G and H) Corresponding TEM images, stained and un-stained, respectively, showing the fiber type nature of the network, and highlighting details of the GNPs within the fiber network.

Moreover, after irradiation by LED at 500 nm of the bent fiber network, bunch-like microstructures were readily obtained (Fig. 9A stained, and Fig. 9B non-stained, conditions). Finally, this approach was extended to **3** with the aim of obtaining branched structures due to the multivalent nature of both components, thymine-functionalized CQDs and adenine capped GNPs. Surprisingly enough, the resulting mixture appeared as a transparent solution even under different *w/w* ratios of **3**/adenine-capped GNPs (both mixed from mother water

solutions). We found that the photoemission activities of the resulting mixtures were still present, but with a significant intensity decrease (Fig. 10A). These mixture were further examined by TEM and the results from these analyses showed the formation of large aggregates (Fig. 10B, under stained condition). The TEM measurements under non-stained condition (Fig. 10C) show the disposition of the adenine-capped GNPs inside the aggregate. Thus, formation of solid aggregates was forced by slow diffusion of THF vapors to these water solutions. In all cases, we observed formation of "swelled-type" precipitates that were collected, allowed to dry under ambient conditions, and morphologically analyzed by SEM. In particular, Fig. 10D reports the morphological characterization of the material collected from a 4:1 *w/w* ratio of the **3**/adenine-capped GNPs mixture, which proved the occurrence of a uniform sponge-like morphology for this sample. We exploited the electron-donating capabilities of photoexcited CQDs, which eventually enable reduction of silver salts to the corresponding AgNPs on the surface of the CQDs themselves.[24] A water solution of silver nitrate was directly mixed with a 4:1 *w/w* ratio of the 3/adenine-capped GNPs mixture. After the slow diffusion of THF vapors to this mixture, the "swelled-type" precipitate was collected and allowed to dry on a thin glass support. This material was directly photoexcited with UV light (365 nm) over a period of 1 h. Formation of AgNPs within the resulting material was confirmed by UV-Vis absorption spectroscopy, via the detection of a strong Ag plasmonic resonance and by TEM analyses (Fig. 10E and F). Additionally, after irradiation by LED at 500 nm of the swelled-type precipitate, flat-like microstructures were obtained as shown by TEM analyses.

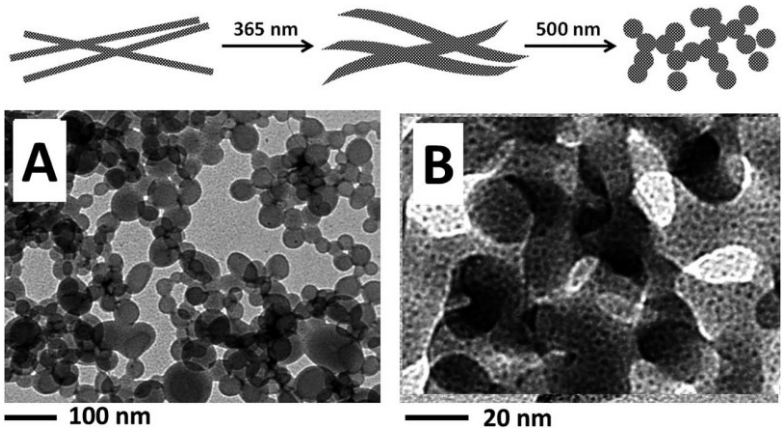

Fig. 9 (A and B) TEM images showing the detail of bunch-like microstructure (stained) and detail of the GNPs within the bunch-like network, respectively.

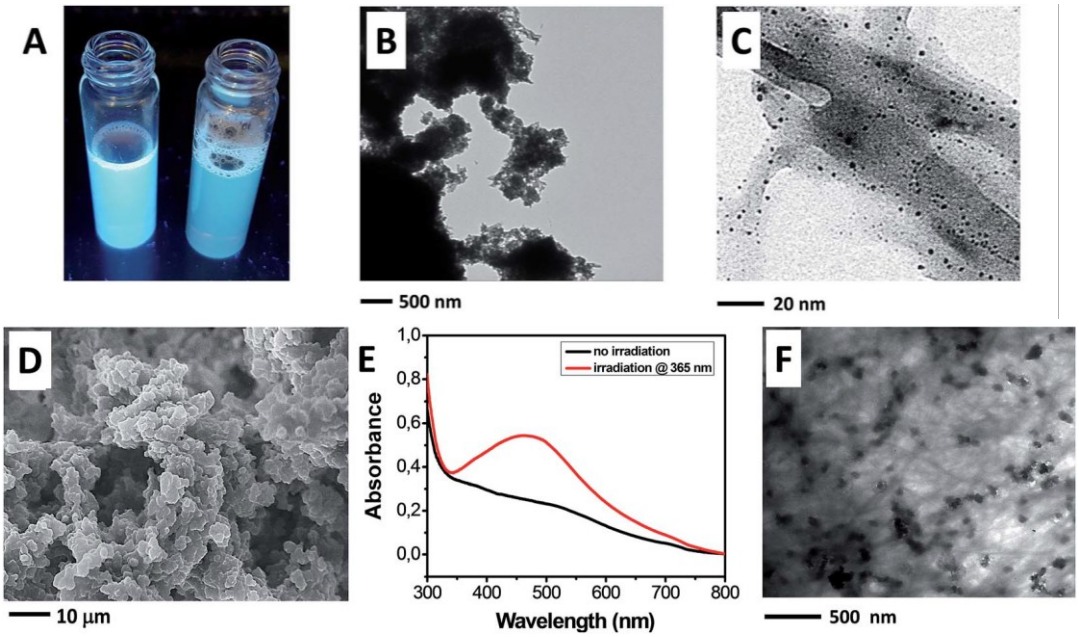

Fig. 10 (A) Pictures showing a solution of **3** in water (left) and a **3**/adenine-capped GNPs water mixture (right) under exposure of light at 365 nm. (B) TEM image (stained) recorded from the **3**/adenine-capped GNPs water mixture showing the formation of aggregates. (C) TEM image (nonstained) recorded from the **3**/adenine-capped GNPs water mixture showing the presence of adenine-capped GNPs within the aggregate. (D) SEM image of the solid material collected from a **4**:**1** w/w ratio of the **3**/adenine-capped GNPs mixture. (E) UV-vis absorption spectra recorded before and after irradiation at 365 nm. (F) TEM image showing formation of large Ag clusters.

Molecular recognition on polymer support

Once we proved the occurrence of selective recognition between functionalized adenine and thymine, we expanded our studies on this phenomenon at the surface level. To this purpose, we used a thiol functionalized polymer that is readily accessible by a two-component thiol-ene chemistry polymerization, between a 2,4,6-triallyloxy-1,3,5-triazine and 2,2'-(ethylendioxy)diethanthiol. The resulting gummy, highly cross-linked polymer (Fig. 11A and B) presents a large number of free thiols on its surface, and it is spectroscopically transparent to light above 390 nm (Fig. 11D, blue line). We took advantage of these free thiol groups to anchor **4**-capped GNPs to the polymeric matrix via a thiol-to-thiol exchange reaction (Fig. 11A). The resulting slightly colored polymer, after washing extensively with water and MeOH, displayed an UV-Vis absorption spectrum with a slightly higher absorption with respect to that of the non-functionalized polymer (Fig. 11C, black line). To this functionalized polymer selective recognition experiments was carried out by using **1** (non-metallated form) and **2** (a schematic representation of the overall process is reported in Fig. 11A). In particular,

THF solutions of **1** (non-metallated form) and **2** were placed over the **4**-GNPs functionalized polymer for 30 min. After this time, the solutions were removed and both polymeric matrices were washed several times with THF to remove the unbound **1** (non-metallated form) and **2**. As a result, the polymeric matrix changes in color (for **1** in its non-metallated form, see Fig. 11D). For both samples, solid-state UV-Vis absorption spectra were recorded, which demonstrated the binding of **1** (in its non-metallated form, Fig. 11D, red line) and **2**. This last compound was reversibly isomerized directly on the surface by using light at 365 or 420 nm (Fig. 11E). As a control experiment, the direct absorption of **1** (non-metallated form) or **2** on the surface of the non-functionalized polymer did not take place in the absence of **4**-GNPs.

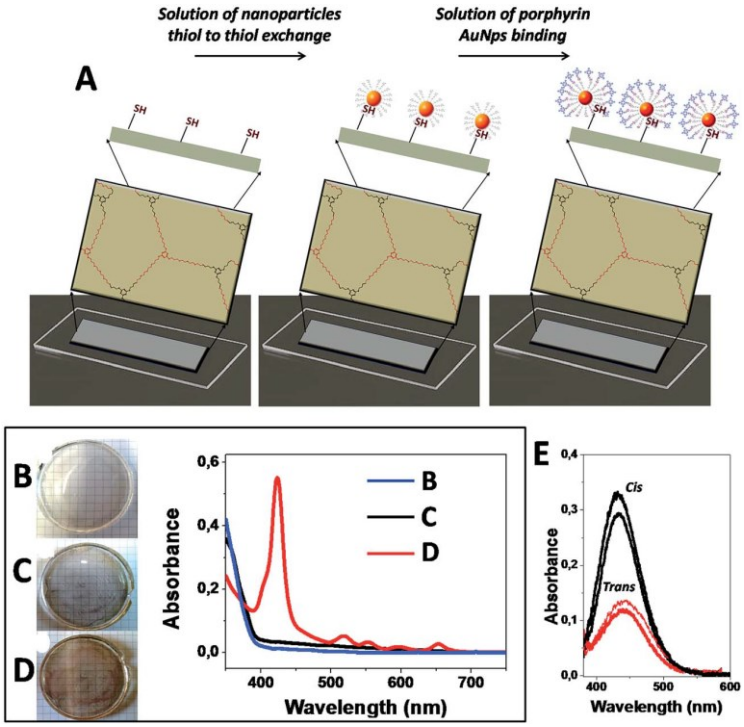

Fig. 11 (A) Schematic representations of the surface binding experiments occurring over the thiol-functionalized polymer (left), by using **4**-GNPs (center), and **1** in its non-metallated form (right). (B and D) Pictures showing, respectively, the thiol-functionalized polymer, the **1**-GNPs/functionalized polymer, and the **1**-GNPs/functionalized polymer and the corresponding solid-state UV-Vis absorption spectra recorded for: the thiol-functionalized polymer (blue line); the **4**-GNPs/functionalized polymer (black line); and the **1** (in its non-metallated form)/**4**-GNPs/functionalized polymer (red line). (E) Solid-state UV-Vis absorption spectra recorded during three reversible cycle of isomerization (cis/trans) occurring directly on the **2**/**4**-GNPs/functionalized polymer surface, using light at 365 or 420 nm.

Conclusions

We have shown selective adenine-thymine binding occurring between complementary self-organized complex systems. These interactions result in precise supramolecular architectures that are morphologically dependent on the nature of the chromophore used. In particular, adenine capped gold nanoparticles combined with tetraphenylporphyrin afforded supramolecular spherical aggregates, which combined with azobenzene generated straight fiber networks and were further able to reorganize into bent fiber networks under *trans*-to-*cis* isomerization. The multifunctional nature of thymine-CQDs combined with adenine-capped GNPs generated a hybrid porous material which retained the characteristic electron-donating capabilities of the photoexcited pristine CQDs. Importantly, we successfully explored the self-shaping properties of the resulting microstructures by inducing a "shake-up" of supramolecular binding mode, promoted by the activation of the plasmon resonance of the adenine capped gold nanoparticles. In our view, the mixing process between adenine-GNPs and thymine-chromophores yields kinetically controlled microstructures, where all of the possible binding modes are cooperatively involved. Then, following the vis-illumination (vibrational energy converted in heat propagation), the microstructures undergo H-bonding modes (including chromophores-chromophore interactions) that afford an ordered, self-shaped, morphological transition, morphologically dependent on the nature of the chromophores. We are currently investigating the nature of this interesting binding mode selection. Moreover, we successfully explored the selective binding at the surface level, proving spectroscopically its occurrence on a polymeric surface, where the adenine-capped GNPs were initially attached via a thiol-to-thiol exchange reaction and subsequently used as molecular sites for binding of thymine-functionalized tetraphenylporphyrin and azobenzene.

Experimental section

Instruments and Methods

Nuclear Magnetic Resonance. ^{1}H and ^{13}C NMR spectra were recorded at room temperature on a Bruker AC-200 (200 MHz) instrument using the partially deuterated solvent as the internal reference. Chemical shifts (δ) are expressed in ppm. The multiplicity of a signal is indicated as: br - broad, s - singlet, d - doublet, t -triplet, m - multiplet, etc.

Mass Spectrometry. ESI-MS experiments were performed using an ESI-ToF MarinerTM BiospectrometryTM Workstation of Applied Biosystems by flow injection analysis using MeOH as the mobile phase. High-resolution mass spectra were obtained by electrospray ionization on a Perseptive Biosystem Mariner ESI-ToF spectrometer (Foster City, CA). An 1 x 10^{-9} M solution of neurotensin, angiotensin I, and bradykinin in an 1:1 CH_3CN/H_2O mixture, containing 1% formic acid, was used for calibration.

Transmission electron microscopy (TEM). Samples were analyzed on a Jeol 300PX instrument. Samples were prepared immediately before used. A small drop of solutions was floated on a glow discharged carbon coated grid and excess was removed by #50 hardened Whatman filter paper. For the samples with negative staining, the grid was then floated on 2% uranyl acetate solution for 10 seconds, and the excess was removed by #50 hardened Whatman filter paper.

Scanning electron microscopy (SEM). A Carl Zeiss Merlin field emission scanning electron microscope operating at 5kV accelerating voltage was used. A small drop of the milk-like aqueous suspension was placed on a microscope glass cover slip and allowed to dry overnight.

FT-IR absorption. FT-IR absorption spectra were recorded with a Perkin-Elmer 1720X spectrophotometer.

UV-Vis Absorption Spectroscopy. The UV-Vis absorption spectra were recorded using a Varian Cary 5000 UV-Vis-NIR spectrophotometer. A 1-cm path length quartz cell was used.

Fluorescence Emission Spectroscopy. The fluorescence spectra were measured upon excitation at different wavelengths using a Varian Cary Eclipse Fluorimeter. A 1 cm path length quartz cell was used. The samples prepared for UV Vis were used to collect the fluorescence data.

Atomic Force Microscopy. AFM experiments were performed on Ntegra Aura (NT-MDT) instrument operating in tapping mode at 200−400 kHz drive frequency and using a single crystal silicon tip coated with TiN (NSG01/TiN, 0.01-0.025 Ω-cm, antimony dope).

Synthesis and Characterization

Materials

1-hydroxy-7-aza-1,2,3-benzotriazole (HOAt) was purchased from GL Biochem (Shanghai) Ltd. N-(3-Dimethylaminopropyl)-N′-ethylcarbodiimide hydrochloride (EDC·HCl) and dimethylsulfoxided6 were obtained from Iris Biotech (Germany). N,N-Diisopropylethylamine (DIPEA) was purchased from Fluka (Switzerland). Triethylamine (TEA), 1,5-Diazabicyclo[5.4.0]undec-5-ene (DBU), bromoacetic acid, ethyl bromoacetate, 4-(phenylazo)aniline, 5-(4-aminophenyl)-10,15,20-triphenyl porphyrin, tetrachloroauric acid and lipoic acid were obtained from Sigma-Aldrich. The deuterated solvent $CDCl_3$ was purchased from Euriso-Top (France). All other chemicals and solvents were Sigma-Aldrich, Fluka or Acros products and used as provided without further purifications.

Synthesis of thymine-1-acetic acid

Thymine (4 g, 31.7 mmol) was dissolved in a solution of KOH (6.82 g, 121 mmol) in 20 ml of water. The solution was warmed at 40°C and a solution of bromoacetic acid (6.25 g, 45 mmol) dissolved in 10 ml of water was added in 30 minutes. The reaction was stirred for another 30 minutes at this temperature. The solution was cooled at room temperature and the pH was adjusted to 5.5 with conc. HCl. The reaction was cooled for 2 h in the refrigerator. After filtration of the precipitate formed, the solution was adjusted to pH 2 with conc. HCl and it was put in the freezer for 2 h. The product was filtrated, washed with water and dried (4.7 g, 85% yield). White solid. Melting point: 252-255°C

^{1}H NMR: (200 MHz, DMSO-d_6): δ 1.75 (s, 3H, CH_3), 4.36 (s, 2H, CH_2), 7.49 (s, 1H, CH), 11.33 (s, 1H, NH), 13.09 (s, 1H, OH).

MS (ESI-TOF): [M] calc. = 184.1494 m/z; $[M+H]^+$ found = 185.0567 m/z; [2M] calc. = 368.2988 m/z; $[2M+H]^+$ found = 369.1056 m/z.

IR (KBr): 3178, 3073, 3026, 2962, 1739, 1706, 1664, 1633 cm^{-1}.

Synthesis of ethyl adenine-9-acetate

Adenine (4 g, 30 mmol) was suspended in dry DMF (60 ml) and NaH (0.82, 34 mmol, washed with petroleum ether) was added. The reaction was stirred for 2 h at room temperature. After this time, ethyl bromoacetate (6.64 ml, 60 mmol) was added dropwise in 3 h and the solution was stirred for another 3 h. the solvent was removed by evaporation in vacuo. The remaining oil was shaken with water and the resulting white precipitate was isolated by filtration, washed with water and dried (3.7 g, 56% yield). Melting point: 227-229°C

^{1}H NMR: (200 MHz, $CDCl_3$): δ 1.21 (t, 3H, CH_3), 4.15 (q, 2H, CH_2), 5.06 (s, 2H, CH_2), 7.25 (s, 2H, NH_2), 8.11 (d, 2H, CH).

MS (ESI-TOF): [M] calc. = 221.2159 m/z; $[M+H]^+$ found = 222.2057 m/z.

IR (KBr): 3103, 2924, 1741, 1671, 1604, 1582 cm^{-1}.

Synthesis of thymine-4-phenilazoanilide (2)

Thymine-1-acetic acid (0.5 g, 2.7 mmol) was dissolved in dry DMF and activated with HOAt (0.36 g, 2.7 mmol) and EDC·HCl (0.52 g, 2.7 mmol). The solution was cooled with an ice/water bath and stirred for 30 minutes. Separately, 4-(phenylazo)aniline (1.33 g, 6.7 mmol) was dissolved in dry DMF and it was added to the active ester. Triethylamine (376 µl) was added until basic pH. The reaction was stirred for 1 h. Subsequently, the solvent was concentrated by evaporation in vacuo and the product was isolated by mean of chromatographic column (eluent CH_2Cl_2:CH_3OH 9:1).

^{1}H NMR (cis): (200 MHz, DMSO-d_6): δ 1.76 (s, 3H, CH_3), 4.46 (s, 2H, CH_2), 6.80-6.86 (m, 4H, CH azo), 7.78-7.97 (m, 5H, CH azo), 10.38 (s, 1H, CH), 11.32 (s, 1H, NH); (trans) (200 MHz, DMSO-d_6): δ 1.78 (s, 3H, CH_3), 4.55 (s, 2H, CH_2), 7.43-7.65 (m, 4H, CH azo), 7.73-7.97 (m, 5H, CH azo), 10.62 (s, 1H, CH), 11.32 (s, 1H, NH).

MS (ESI-TOF): [M] calc. = 363.3699 m/z; $[M+H]^+$ found = 364.1413 m/z.

IR (KBr): 3291, 1692, 1668, 1598, 1551 cm^{-1}.

Synthesis of thymine-(aminophenyl) porphyrin

Thymine-1-acetic acid (0.1 g, 0.54 mmol) was dissolved in dry DMF and activated with HOAt (0.073 g, 0.54 mmol) and EDC·HCl (0.104 g, 0.54 mmol) and the solution was stirred for 30 minutes. 5-(4-aminophenyl)-10,15,20-triphenyl porphyrin (0.07 g, 0.11 mmol) was added at the solution and the pH was adjusted to basicity with TEA (100 µl). The reaction was

stirred for another 3 h, then water was added to the solution. The resulting precipitate was isolated by mean of a spin-dryer and dried (0.08 g, 90% yield).

^{1}H NMR: (200 MHz, DMSO-d_6): δ 1.22 (s, 2H, NH pyrrole), 1.84 (s, 3H, CH_3), 4.69 (s, 2H, CH_2), 7.64 – 8.83 (m, 27H, porphyrinic ring), 10.74 (s, 1H, NH), 11.41 (s, 1H, NH).

MS (ESI-TOF): [M] calc. = 795.8844 m/z; $[M+H]^+$ found = 796.3231 m/z.

IR (KBr): 3314, 1702, 1675 cm^{-1}.

Synthesis of metallated thymine-(aminophenyl) porphyrin (1)

Thymine-(aminophenyl) porphyrin (0.035 g, 0.044 mmol) was dissolved in $CHCl_3$ (10 ml). Subsequently, a saturated solution of zinc acetate in CH_3OH (4 ml) was added to the solution of thymine-(aminophenyl) porphyrin and the mixture was refluxed for 1 h. The excess of acetate was removed by treatment with water (3v), then the solution was dried over Na_2SO_4, filtered and evaporated under reduced pressure (0.034 g, 90% yield).

MS (ESI-TOF): [M] calc. = 858.3913 m/z; $[M+H]^+$ found = 859.2334 m/z.

Synthesis of adenine-9-ethylenamide amine

Adenine-9-acetate (0.3 g, 1.35 mmol) was dissolved in ethylenediamine (10 ml, 149 mmol) and DBU was added as catalyst. The reaction was stirred for 2 h at 50°C, then it was allowed to cool the solution at room temperature. The product was precipitated by adding ethyl ether, filtered, washed with ethyl ether and dried (0.278 g, 87% yield).

^{1}H NMR: (200 MHz, DMSO-d_6): δ 2.61 (m, 3H), 3.07 (m, 3H), 4.82 (s, 2H, CH_2), 7.18 (s, 2H, NH_2), 8.08 (d, 2H, CH), 8.24 (s, 1H, NH).

IR (KBr): 3356, 3265, 3098, 1669, 1602 cm^{-1}.

Synthesis of 4

Lipoic acid (0.206 g, 1 mmol) was activated in dry DMF (10 ml) by adding HOAt (0.136 g, 1 mmol) and EDC·HCl (0.192 g, 1 mmol). The mixture was stirred for 30 minutes, then adenine-9-ethylenamide amine (0.235 g, 1 mmol) was added to the solution. DIPEA (200 µl) was added until basic pH and the reaction was stirred overnight. The solvent was concentrated under reduced pressure. The residue was shaken with CH3CN resulting in precipitation. The solid recovered after filtration was dried obtaining 0.28 g of product as a solid (66% yield).

^{1}H NMR: (200 MHz, DMSO-d_6): δ 1.25-1.75 (m, 5H, CH_2 lipoic ac.), 1.75-1.98 (m, 1H, CH_2 lipoic ac.), 2.01 (m, 2H, CH_2 lipoic ac.), 2.42 (m, 1H, CH_2 lipoic ac.), 3.13 (m, 5H, CH_2 lipoic

ac.), 3.60 (m, 1H, CH_2 lipoic ac.), 4.80 (s, 2H, CH_2), 7.19 (s, 2H, NH_2), 7.82 (s, 1H, NH), 8.09 (d, 2H, CH), 8.31 (s, 1H, NH).
IR (KBr): 3297, 3122, 2933, 1665, 1643, 1605, 1560 cm^{-1}.

Synthesis of adenine-capped gold nanoparticles

4 (0.105 g, 0.35 mmol) was dissolved in THF (5 ml) and cooled with an ice/water bath. Separately, tetrachloroauric acid (0.069 g, 0.177 mmol) was dissolved in THF (5 ml), cooled and added dropwise to the solution of 4. The reaction was stirred overnight to allow the complexation. $NaBH_4$ (0.07 g, 17 mmol) dissolved in water (2 ml) and cooled was added quickly and the solution. After 48 h of aging, the gold nanoparticles were recovered by filtration, washed with CH_3OH and dried.
IR (KBr): 3355, 3095, 2929, 1646 cm^{-1}.

Synthesis of Carbon Quantum Dots (CQDs)

Chlorohydrated Arginine (10.2 g, 48.4 mmol) and ethylendiamine (3.56 ml, 53.3 mmol) are introduced in a 100 or 250 ml beaker containing 26.6 ml of ultrapure water. The solution was stirred at r.t. until complete dissolution of reactants and then it was irradiated in a domestic microwave oven for 4 minutes at 1000 W. During this lapse of time, white-gray aqueous vapor came out from the vents of the oven. A porous black-reddish solid was obtained and it was washed in a gooch filter with 4x20 ml aliquots of acetonitrile and 4x20 ml of diethyl ether. The solid was dried for several minutes in air and dissolved in the minimum volume of ultrapure water to obtain a dark and turbid solution, which is filtered through a cellulose syringe filter (0.45 μm cut-off). The purified solution was freezed using a bath of acetone and solid carbon dioxide (T ≈ -78 °C) and then dried under vacuum through a lyophilization process, which brought to a brownish final compound.

Synthesis of thymine doped CQDs (3)

Thymine-1-acetic acid (0.590 g, 3.2 mmol) was dissolved in dry DMF (2.5 ml) and activated with HOAt (0.48 g, 3.8 mmol) and EDC·HCl (0.288 g, 1.62 mmol) and the solution was stirred for 15 minutes with an ice/water bath. Separately, CQDs (0.28 g) were dissolved in dry DMF (1 ml) and the solution was stirred for 15 minutes. This solution was added to the active ester and pH was adjust to basicity with TEA (0.984 ml). After 10 minutes the ice/water bath

was removed and the reaction was stirred overnight. The product was precipitated with CH_3CN and washed with CH_2Cl_2.

Synthesis of functionalized polymer based on 2,4,6-triallyloxy-1,3,5-triazine and 2,2'-(ethylendioxy)diethanthiol

2,4,6-triallyloxy-1,3,5-triazine (1.82 g, 7.3 mmol) and 2,2'-(ethylendioxy)diethanthiol (2 g, 11 mmol) were stirred in presence of 2,2'-dimethoxy-2-phenylacetophenone (DMPA, 0.40 g, 1.5 mmol) as photoiniziator for the polymerization. The solution was irradiated at 365 nm in to the appropriate mold and the cross-linker polymer was obtained as a rubber-like material.

Self-assembly procedures

(i) Thymine self-recognition experiments were performed as follow: a lyophilized samples of **1** and **2** (in its trans form) were dissolved in a THF solutions to the final concentration of 2 mM. To these solutions water was slowly added to the final concentration of 1 mM for **1** and 0.5 mM for **2**. The solutions were allowed to stay at room temperature to the open air thus to let part of THF mixture evaporate. During this time, formation of crystals was observed. Crystals from **2** (in its cis form) were obtained after a prior isomerization of **2** run directly in the THF solution. Organized microstructures from 3 were obtained starting from a lyophilized sample that was dissolved in pure water to the final concentration of 3 mM. The solvent was allowed to slowly evaporate over a flat area vessel.

(ii) Adenine-thymine recognition experiments were performed as follow: a 0.6 mM stock solution of adenine-capped GNPs was prepared starting from 100 mg of lyophilized sample dissolved in 5 ml in water. (a) **1**/adenine-capped GNPs monomeric nanosystems: to a 200 μl of adenine-capped GNPs stock solution (corresponding to 4 μmol of ligands), 1 was slowly added from a its solution prepared dissolving 3.2 mg (4 μmol) in 2 ml of THF. After an appropriate mixing time the solution was examined by DLS and TEM. (b) 1/adenine-capped GNPs large aggregates: Similar conditions were adopted for the formation of large aggregates, with the experimental difference that **1** was added from a 10 to 20 times concentrated THF solution. Similar experimental conditions were adopted for the formation of **2**/adenine-capped GNPs microstructures.

(iii) **3**/adenine-capped GNPs nanosystems: to a 400 μl of adenine-capped GNPs stock solution (corresponding to 8 μmol of adenine ligands), **3** was slowly added from a its solution

prepared dissolving 9.5 mg (corresponding to 32 μmol of thymine ligands) in 2 ml of water at pH 8. The resulting mixture was allowed to equilibrate for 1 hr. Successively, a slow addition of THF to the mixture allowed the formation of a nanostructurated material.

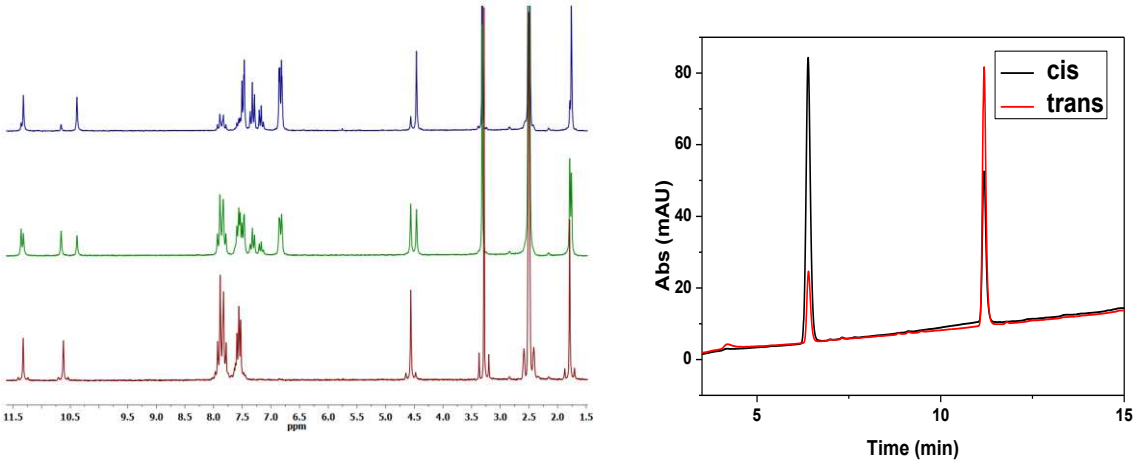

Fig. 12 Left: ^{1}H-NMR spectra of **2** after different times of irradiation at 350 nm (*cis* form in blue, *trans* form in red, and *cis*/*trans* mixture in green). Right: HPLC chromatogram of **2** showing interconversion between *trans* form (red line) and *cis* form (black line).

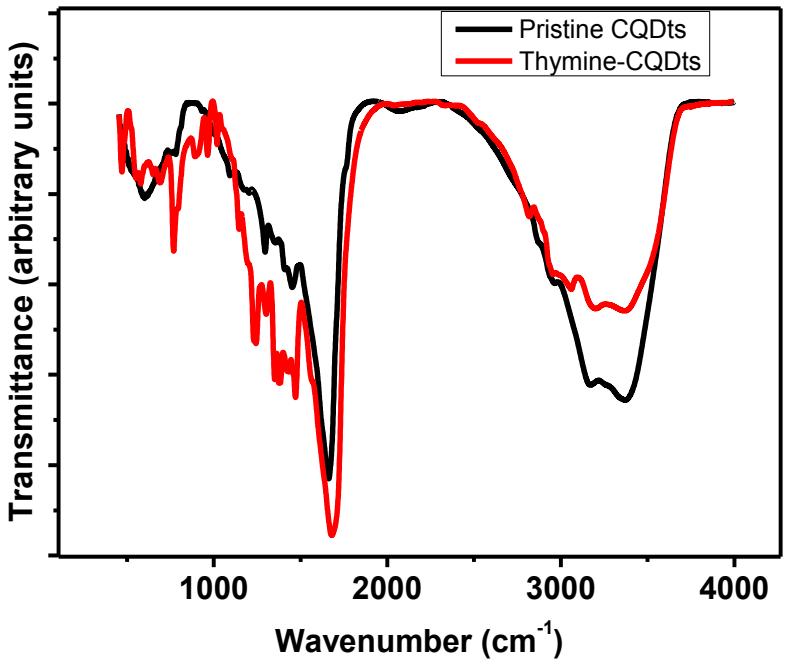

Fig. 13 Solid-state FT-IR absorption spectra recorded for **3** (red line) and its pristine CQDs precursor (black line).

References

1. A. R. Studart and R. M. Erb, *Soft Matter*, **2014**, 10, 1284.
2. J. M. Lehn, *Proc. Natl. Acad. Sci. U. S. A.*, **2002**, 99, 4763.
3. G. M. Whitesides and B. Grzybowski, *Science*, **2002**, 295, 2418.
4. J. F. Stoddart and H.-R. Tseng, *Proc. Natl. Acad. Sci. U. S. A.*, **2002**, 99, 4797.
5. E. Persch, O. Dumele and F. Diederich, *Angew. Chem., Int. Ed.*, **2015**, 54, 3290.
6. K. Ariga, H. Ito, J. P. Hill and H. Tsukube, *Chem. Soc. Rev.*, **2012**, 41, 5800.
7. G. Yu, K. Jie and F. Huang, *Chem. Rev.*, **2015**, 115, 7240.
8. A. K. Boal, F. Ilhan, J. E. DeRouchey, T. Thurn-Albrecht, T. P. Russell and V. M. Rotello, *Nature*, **2000**, 404, 746.
9. E. Busseron, Y. Ruff, E. Moulin and N. Giuseppone, *Nanoscale*, **2013**, 5, 7098.
10. J. L. Sessler, C. M. Lawrence and J. Jayawickramarajah, *Chem. Soc. Rev.*, **2007**, 36, 314.
11. S. Sivakova and S. J. Rowan, *Chem. Soc. Rev.*, **2005**, 34, 9.
12. J. L. Sessler and J. Jayawickramarajah, *Chem. Commun.*, **2005**, 1939.
13. L. Liu, D. Xia, L. H. Klausen and M. Dong, *Int. J. Mol. Sci.*, **2014**, 15, 1901.
14. A. Ciesielski, M. El Garah, S. Masiero and P. Samorì, *Small*, **2016**, 12, 83.
15. W. Saenger, *Principles of Nucleic Acid Structures*, Springer, New York, **1984**.
16. A. G. Slater, Y. Hu, L. Yang, S. P. Argent, W. Lewis, M. O. Blunt and N. R. Champness, *Chem. Sci.*, **2015**, 6, 1562.
17. A. R. Fersht, *Trends Biochem. Sci.*, **1987**, 12, 301.
18. S. Choi, S. Park, S.-A. Yang, Y. Jeong and J. Yu, *Sci. Rep.*, **2015**, 5, 17805.
19. L. Wang, S. J. Zhu, H. Y. Wang, S. N. Qu, Y. L. Zhang, J. H. Zhang, Q. D. Chen, H. L. Xu, W. Han, B. Yang and H. B. Sun, *ACS Nano*, **2014**, 8, 2541.
20. A. R. Katritzky and T. Narindoshvili, *Org. Biomol. Chem.*, **2008**, 6, 3171.
21. K. L. Dueholm, M. Egholm, C. Behrens, L. Christensen, H. F. Hansen, T. Vulpius, K. H. Petersen, R. H. Berg, P. E. Nielsen and O. Buchardt, *J. Org. Chem.*, **1994**, 59, 5767.
22. K. Suzuki, L. Malfatti, D. Carboni, D. Loche, M. Casula, A. Moretto, M. Maggini, M. Takahashi and P. Innocenzi, *J. Phys. Chem. C*, **2015**, 119, 2837.
23. D. Mosconi, D. Mazzier, S. Silvestrini, A. Privitera, C. Marega, L. Franco and A. Moretto, *ACS Nano*, **2015**, 9, 4156.

24. D. Mazzier, M. Favaro, S. Agnoli, G. Granozzi, S. Silvetrini, M. Maggini and A. Moretto, *Chem. Commun.*, **2014**, 50, 6592.
25. M. Gouterman, *J. Mol. Spectrosc.*, **1961**, 6, 138.
26. G. Sudesh Kumar and D. C. Neckers, *Chem. Rev.*, **1989**, 89, 1915.
27. W. Mamdouh, M. Dong, S. Xu, E. Rauls and F. Besenbacher, *J. Am. Chem. Soc.*, **2006**, 128, 13305.
28. Z. Wu, J. Suhana and R. Jin, *J. Mater. Chem.*, **2009**, 19, 622.
29. E. Longo, A. Orlandin, F. Mancin, P. Scrimin and A. Moretto, *ACS Nano*, **2013**, 7, 9933.
30. P. D. Jadzinsky, G. Callero, C. J. Ackerson, D. A. Bushnell and R. D. Kornberg, *Science*, **2007**, 318, 430.
31. S. Ogi, K. Sugiyasu, S. Manna, S. Samitsu and M. Takeuchi, *Nat. Chem.*, **2014**, 6, 188.
32. M. Schade, A. Moretto, P. Donaldson, C. Toniolo and P. Hamm, *Nano Lett.*, **2010**, 10, 3057.

1.2 Tuning morphological architectures generated through living supramolecular assembly of a helical foldamer end-capped with two complementary nucleobases.[b]

Nucleobase pairing is one of the most powerful tools used by Nature for the programmable arrangement of complex functional molecular architectures. Not surprisingly, the electronic, H-bonding, stacking, and cation binding properties of DNA, or its smaller constituents, such as nucleosides or nucleotides[1] have been exploited in supramolecular chemistry and molecular recognition fields to enable the formation of planned nanostructures by directed base pairing.[2] Therefore, these features have become extremely attractive for many different scientific fields,[3] and in particular for materials chemistry. Here, by combining nucleobase recognition with organic building blocks, it is possible to create novel systems, potentially endowed with interesting properties, i.e. for the development of nanoelectronic devices. In this area, the properties of such self-assembled products strongly depend on the molecular components and the type of interactions responsible for recognition.[4] Foldamers are synthetic, sequence-specific oligomers similar to natural oligopeptides, proteins, and oligonucleotides that fold into well-defined three-dimensional structures.[5] Clearly, *inter alia* they offer to chemists a broad set of building blocks for the construction of templates for the production of complex arrays of functional groups in virtually unlimited geometrical patterns.[6] Therefore, foldamers provide attractive opportunities for the design of innovative molecules in many different chemical areas. Successful examples of the potential offered in supramolecular and materials chemistry by the combination of nucleobases and foldameric units in the same molecule have been reported.[7] In most of those studies, nucleobases were placed at multiple sidechain positions, whereas in few instances a single nucleobase was appended at the N-terminus of an oligopeptide chain.[7c,e] To the best of our knowledge, examples of foldamers decorated with a base at each end have not been reported yet. We describe here the results of our study on short, synthetic (but biomimetic) peptide foldamers based on helicogenic Aib (a-aminoisobutyric acid)[8] or Aib/Ala residues, covalently linked to a thymine (T) and to an adenine (A) at their N- and C-termini, respectively. These foldamers acted as monomers able to spontaneously self-organize (in isolation or in the presence of other nucleobase systems) in precisely controlled 3D-architectures via a non-covalent, supramolecular, living polymerization process.

[b] Reprinted (adapted) with permission from (Soft Matter, 2017, 13, 4231). Copyright (2019) Royal Society of Chemistry".

Results and discussion

The syntheses of the two nucleobase-functionalized foldamers presented in this work required a prior design of the appropriate linkers. Thus, T was converted into its corresponding carboxymethylene derivative, thymine-1-acetic acid. On the other hand, A was first modified to its ethylcarboxylate methylene derivative, ethyl adenine-9-acetate, which was subsequently amidated (with ethylenediamine) into its monoacetyl-ethylendiamino amide. The chemical structure of the first foldamer (compound **1**), prepared by solution methods is shown in Fig. 1.

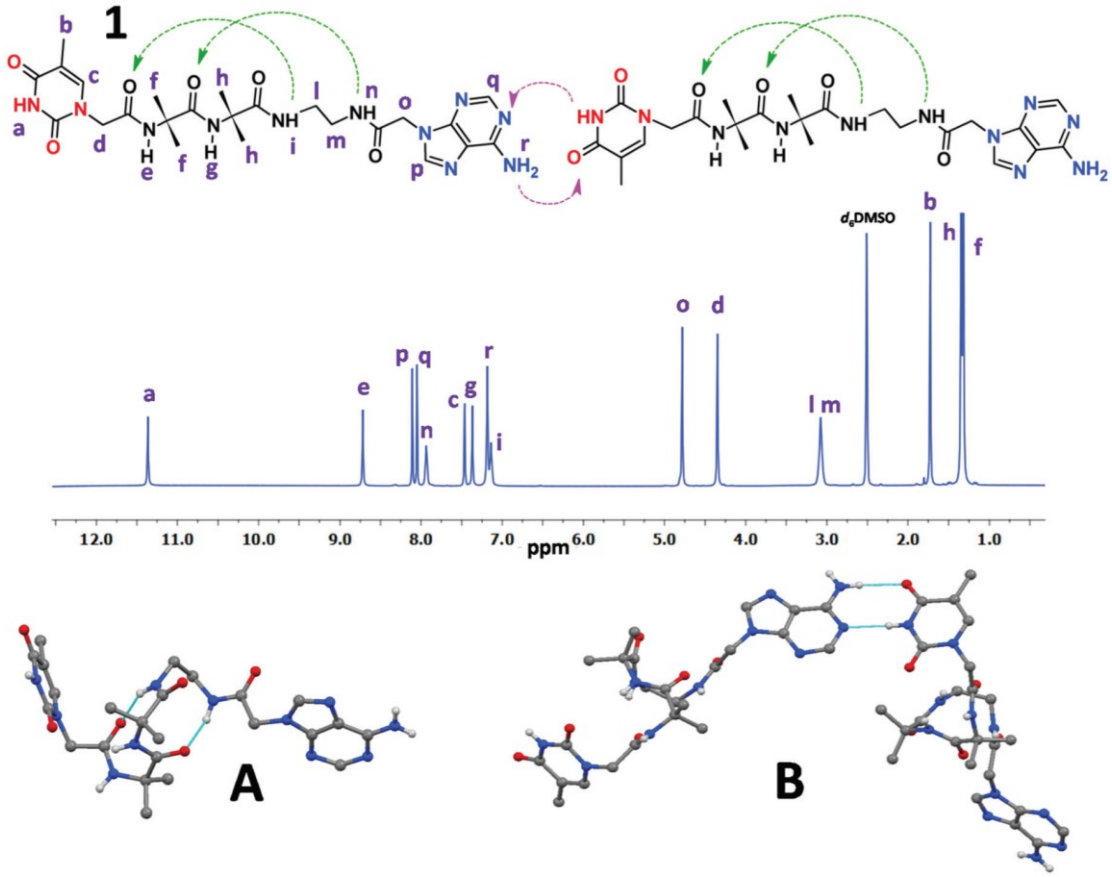

Fig. 1 Upper part: Chemical structure of the achiral foldamer **1** (with a schematic representation of its expected inter- and intramolecular H-bonding interactions) and its ^{1}H-NMR spectrum (DMSO) with proton assignments. Middle part: (A) X-Ray diffraction structure of the molecule of foldamer **1** highlighting the two consecutive intramolecular backbone H-bonds. (B) Intermolecular A···T base pairing through H-bonds in the X-ray diffraction structure of foldamer **1**.

Compound **1** was planned as a suitable system to obtain single crystals for X-ray diffraction analysis, which would have allowed us to properly understand details of the self-organization of the T···A moieties in the crystal state. The choice of a homo-peptide sequence based on Aib is related to the propensity of this C^{α}-tetrasubstituted α-amino acid to support β-

turn/incipient helical conformations and provide ordered crystal packing motifs even in case of very short homo-oligomers.[8] In particular, this foldamer is expected to generate a pair of intramolecular H-bonds which constrain the two Aib residues, the ethylenediamine unit, and part of the A linker as well, in two consecutive turns (one β-turn and one β-like turn).[9] On the other hand, we also envisaged formation of intermolecular H-bonds occurring between the two complementary nucleobases (Fig. 1). Interestingly, despite the hydrophobic nature of Aib, compound **1** was found to be highly soluble in water. Single crystals of **1** were grown by slow evaporation from a methanol-water solution. The X-ray diffraction structure of **1** (Fig. 1A) highlights the two consecutive turns (each with ten atoms encompassed in the H-bonded pseudo-cycle) which are formed between the first and second amide C=O groups of the chain and, respectively, the two consecutive amide N–H groups of the ethylendiamine linker (for the backbone torsion angles).

The packing mode of terminally protected helical peptides is usually characterized by head-to-tail intermolecular H-bonds between backbone N–H and C=O groups that are not involved in the intramolecular H-bonding scheme.[10] Conversely, in the crystals of **1**, the C-terminal A of one molecule is H-bonded to the N-terminal T of a (x + 1, -y + 1/2, z-1/2) symmetry related molecule (Fig. 1B). Such a double H-bond motif corresponds to the standard Watson–Crick A···T base pairing. The propagation of this motif gives rise to a H-bond mediated, supramolecular foldamer (Fig. 2A), in which molecules characterized by opposite screw senses of their helical backbones alternate. Lateral connection between zig-zagging rows is provided by a H-bond between the N–H group of Aib(2) and a (x-1, y, z) translational equivalent of the C=O group of the adenine-9-acetyl moiety. Most of the additional intermolecular H-bonds involve the co-crystallized water molecules. Another relevant feature of the packing mode is the occurrence of π-stacking between pairs of H-bonded A···T dimers (Fig. 2B). Specifically, two distinct, alternating pairing modes are observed. In one of them (upper part of Fig. 2B), the T ring belonging to the asymmetric unit (x, y, z) nicely stacks to the neighboring A ring (symmetry: -x, y + 1/2, -z + 1/2) and concomitantly, the (x-1, -y + 1/2, z + 1/2) A ring stacks to the (-x-1, -y + 1, -z + 1) T ring. The second pairing mode (lower part of Fig. 2B), is off-register, in the sense that the (x, y, z) T ring overlaps to the H-bonds of the neighboring A···T dimer, so that the shortest separation is between the edges of the (x, y, z) T ring and its (-x, -y + 1, -z + 1) counterpart, rather than between T and A.

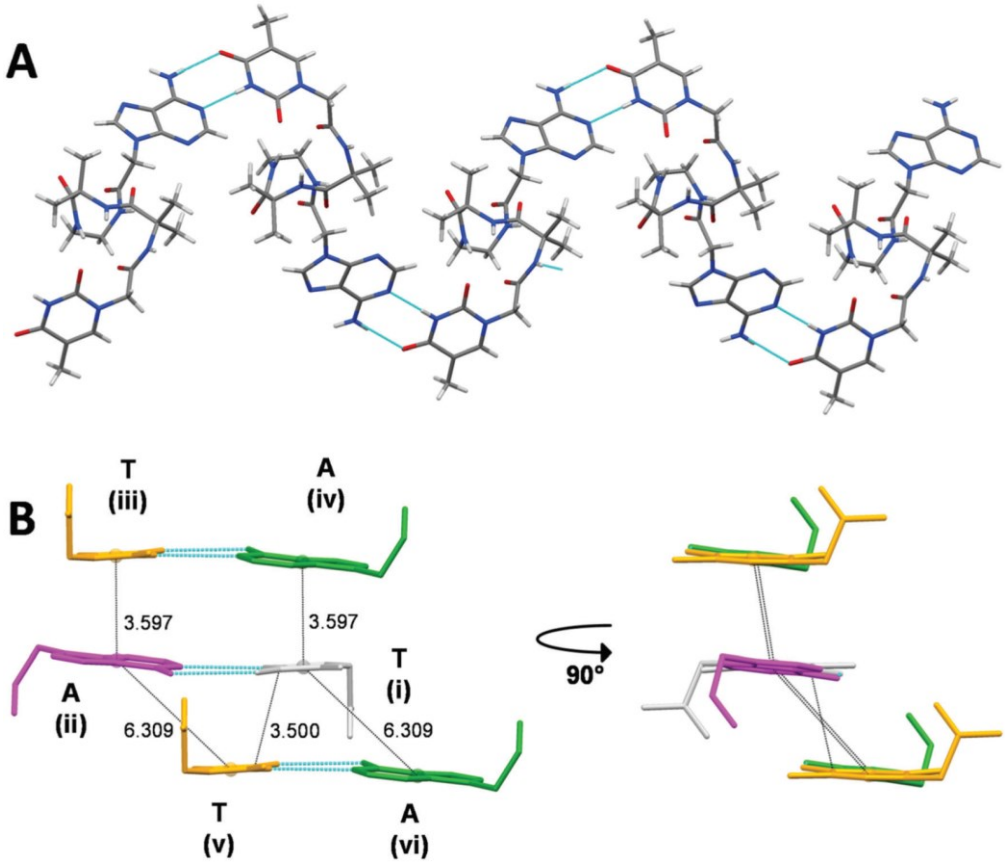

Fig. 2 (A) The supramolecular polymer generated through propagation of the A···T base pairing (five molecules of foldamer **1** are shown). (B) Nucleobase stacking in the packing mode of foldamer **1**. Three H-bonded A···T dimers are shown. Symmetry transformations used to generate equivalent atoms are the following: (i) x, y, z; (ii) x-1, -y +1/2, z+1/2; (iii) -x-1, -y + 1, -z + 1; (iv) -x, y + 1/2, -z + 1/2; (v) -x, -y + 1, -z + 1; (vi) -x + 1, y + 1/2, -z + 1/2. The distances between centroids of neighboring A and T bases are indicated. In the lower part, the distance between the C4 atoms of T moieties of symmetry (i) and (v) is also shown.

The chemical structure of foldamer **2**, synthesized by the solid-phase methodology, is illustrated in Fig. 3. It is based on an -(L-Ala-Aib)$_4$- octapeptide sequence,[11] expected to give rise to a 3_{10}-/α-helical structure (for a possible intramolecular H-bonding scheme, see Fig. 3) of right-handed screw sense dictated by the L-configuration of the Ala residues. In the ^{1}H-NMR spectrum of **2** in DMSO (d_6) (Fig. 3), the splitting of the signals of the two methylene CH protons belonging to the T linker and of the four CH protons of the A (ethylenediamine) linker (highlighted in red and orange, respectively) indicates that these protons are diastereotopic. This observation suggests that the chiral information residing in the right-handed helical peptide backbone of foldamer **2** is propagated up to the T-cap at the N-terminus and to the last ‘‘reverse’’ amide at the C-terminus.

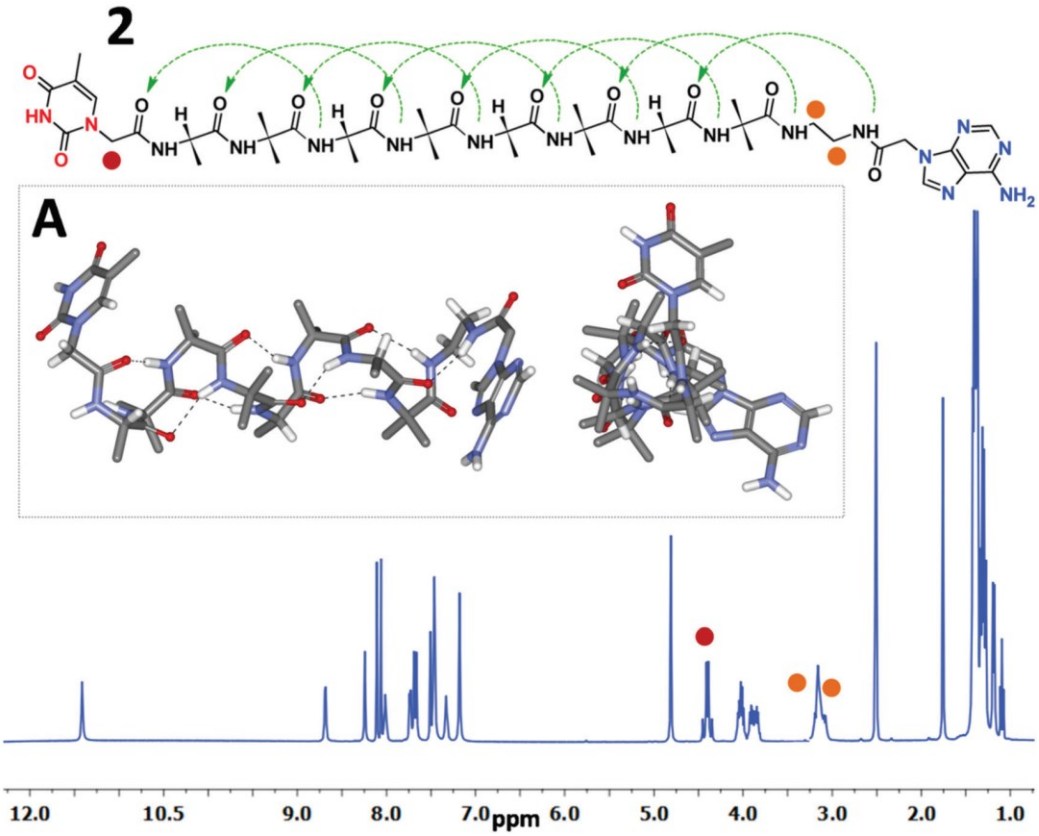

Fig. 3 Chemical structure of the chiral foldamer **2** (with a schematic representation of its expected intramolecular H-bonding interactions) and its ^{1}H-NMR spectrum (DMSO). The signals of the methylene groups connecting the bases to the peptide backbone are highlighted. (A): 3D-representation of foldamer **2** (side and axial views).

The conformation adopted by **2** in water was investigated using CD spectroscopy, including a comparison with its carboxylic acid precursor T-(L-Ala-Aib)$_4$-OH. This latter compound exhibits a spectrum indicative of a right-handed, mixed 3_{10}-/α-helix,[8b,12] characterized by two negative maxima at 224 and 205 nm of medium intensity with an ellipticity ratio (R) of 0.68,[13] and an additional, weak positive maximum located at 265 nm related to the T chromophore[14] close to the N-terminal, chiral L-Ala residue (Fig. 4A). If compared to its carboxylic acid precursor, foldamer **2** displays a CD spectrum similar in shape, but characterized by significantly more intense negative maxima. This finding might be related to an extension of the helix through formation of two additional intramolecularly H-bonded turns encompassing the C-terminal ethylenediamine linker, similar to those observed in the crystal structure of foldamer **1**. In this way, the (otherwise achiral) ethylenediamine linker would be forced to twist by retaining the right-handed screw sense of the preceding peptide helix. The slightly increased intensity and variation in shape of the positive maximum near 265 nm, observed on going from T-(L-Ala-Aib)$_4$-OH to foldamer **2**, suggests that the C-

terminal A chromophore of the latter might also somehow experiencing a chiral environment. Interestingly, by recording the CD spectra of **2** in a 8 : 2, v/v, tetrahydrofuran (THF)/water solution, we found a strong, general, and time-dependent enhancement of the CD intensity, as shown in Fig. 4B. The CD spectra were recorded at the concentration of 1 mM, immediately and at different times (30 min, 2 h, and 8 h) after sample dissolution. In particular, a comparison between the first and the last measurement (black and green lines, respectively) well illustrates the impressive eightfold boost of the CD signal intensity. We ascribe this amplification effect to the formation of supramolecularly assembled, well organized species in the organic/water solvent mixture. We explored the thermal stability of such supramolecular aggregates by monitoring the CD signal at 224 nm as a function of the temperature in the 25-65°C range (Fig. 4G). A marginal variation of the signal intensity is observed up to 50°, followed by a dramatic decrease between 50°C and 60°C. The CD spectrum collected at 60°C (*Experimental Section*, Fig. 14) is virtually superimposable to that of the monomeric species at 25°C shown in Fig. 4B (black line). This latter finding supports the view that the temperature increase does not affect the helical folding of foldamer **2** (the thermal stability of Aib-rich, helical peptides is well documented in the literature),[15] but rather it induces the disassembly of the supramolecular aggregates.

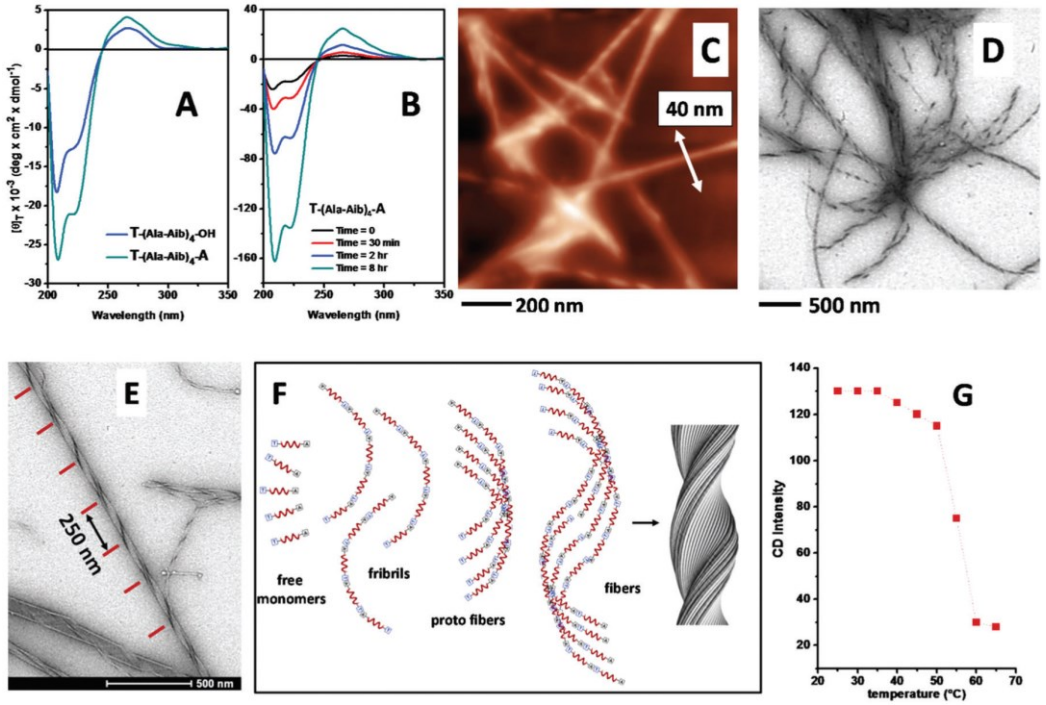

Fig. 4 (A) CD spectra of foldamer **2** (green line) and its precursor T-(L-Ala-Aib)$_4$-OH (blue) (concentration: 1 mM in water for both compounds). (B) CD spectra of foldamer **2** in a 8:2 (v/v)

THF/water mixture, recorded at different times after dissolution (concentration: 1 mM). (C and D) AFM and TEM (stained with uranyl acetate) images, respectively, of the precipitate collected starting from a 25 mM solution of **2** in 8 : 2, v/v, THF/watermixture. (E) Detail of TEM (stained with uranyl acetate) images highlighting the fiber pitch. (F) Proposed mechanism of self-assembly of foldamer **2** leading to the formation of twisted fibers. (G) Temperature dependence of the CD signal at 224 nm for foldamer **2** after incubation for 8 h in a 8 : 2 (v/v) THF/water mixture (concentration: 1 mM).

To prove self-assembly, we repeated the experiment starting from a 25 mM solution of **2** in the same solvent mixture used for the CD analysis. After dissolution of **2** (by the aid of sonication at 30°C), the mixture was let to stand for 24 h at room temperature in a closed vessel. The precipitate which formed was then collected and analyzed by AFM and TEM techniques (Fig. 4C and D, respectively). By using either technique, it is possible to observe formation of long, twisted fibers characterized by a quite regular pitch of 250 nm (this latter feature is clearer in the TEM images recorded under stained conditions, Fig. 4E). From these data, we are inclined to suggest that such a fiber morphology might arise from the process schematically reported in Fig. 4F. Specifically, molecules of **2** may recognize each other through complementary base-pairing, intermolecular interactions similar to those obtained for **1**. However, at variance with **1** in which a zig-zagging supramolecular polymer is generated by the alternation of molecules with opposite screw sense, in foldamer **2** there are eight amino acid residues folded in a right-handed helical conformation which dictates the distance between the terminal nucleobases and their relative orientation (Fig. 3A). Thus, the base-paring mediated assembly of foldamer **2** may give rise to bent fibrils, proto-fibers, and eventually fibers characterized by a longer spiral-likemotif. This hypothesis is supported by the results obtained from the CD analysis discussed above. With increasing concentration, fibrils start to interact, generating fibers, possibly stabilized by nucleobase p-stacking interactions and characterized by a spiral mode of propagation. Interestingly, from the TEM analysis (Fig. 4D and E) the screw sense of the twisted fibers appears to be exclusively right-handed. Also, TEM images taken at different incubation times (*Experimental Section*, Fig. 15) suggest that the twisting of the fibers takes place slowly after their formation. In our next step, with the aim at controlling the directionality of the supramolecular propagation of foldamer **2**, we made use of pristine T as ‘‘terminator’’. In principle, by using an appropriate ratio of **2** and the terminator, it might be possible to selectively bind (or block) the C-terminus of foldamer **2** (which is capped by an A) and to concomitantly allow propagation of the supramolecular growth of **2** from the opposite end. The results of some experiments carried out to test this hypothesis are shown in Fig. 5A-C. Foldamer **2** was combined with pristine T

in different terminator/foldamer molar ratios of 0.05%, 0.5%, and 5%. In Fig. 5A we report the TEM and AFM images which refer to the 0.05% molar ratio condition (all of the results discussed below made use of a prolonged time of sonication of a 7:3 THF/water, *v/v*, mixture with a fixed **2** concentration of 20 mM prior to be analyzed), which clearly indicated formation of long fibers characterized by a different packing of the twisted motif (Fig. 5A and inset). The most densely packed fibers (inset of Fig. 5, left) displayed an average diameter of 20 nm and a fixed pitch of 150 nm, while the ribbon-like fibers showed an average diameter of 40 nm and an ordered pitch of 200 nm. A first observation of an onset of supramolecular propagation under the 0.5% experimental conditions, is reported in Fig. 5B. A mixture of flat/twisted, short fibers (100-400 nm long and 15–25 nm wide) were indeed produced. Interestingly, a detailed view of the microstructures reveals a precise molecular organization within the fibers. The fiber borders are particularly dense. This result is compatible with a semi-cylinder-like morphology occurring for these structures (Fig. 5B, inset). At 5% molar ratio, only very short (20–80 nm), poorly ordered microstructures were obtained (Fig. 5C).

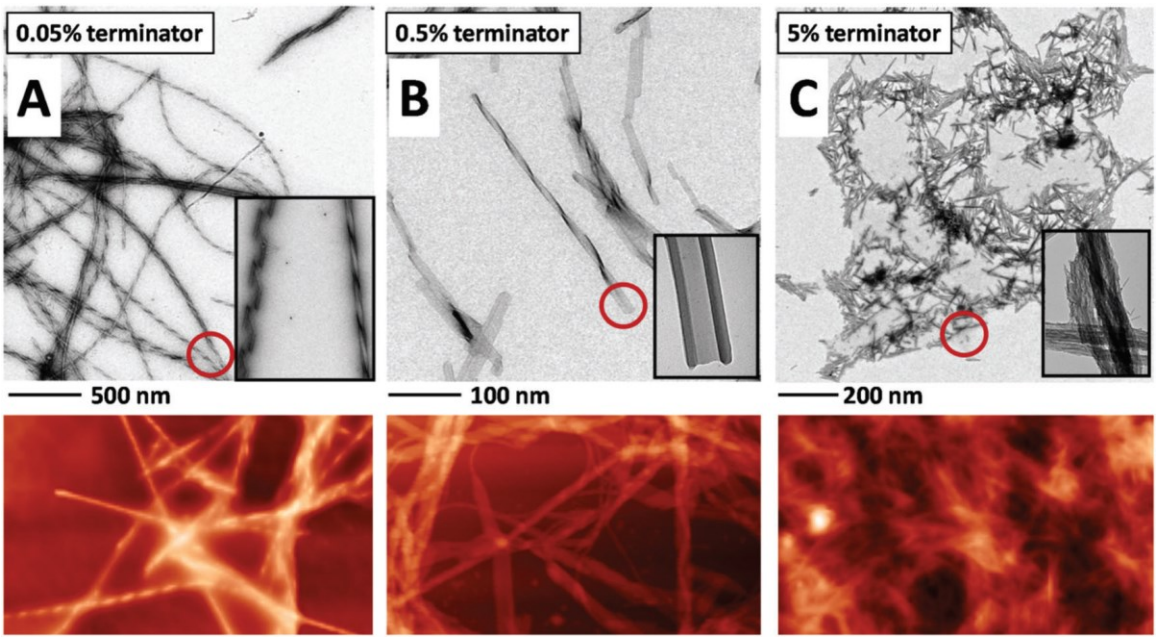

Fig. 5 (A-C) TEM (above) and the corresponding AFM (below) images of three different sample preparations, referred respectively to 0.05%, 0.5%, and 5% molar ratio of pristine T to **2**. TEM insets show the related microstructure organizations.

On the basis of this set of experiments we concluded that a well defined amount of terminator allows one to control the supramolecular propagation of foldamer **2**. To obtain more information about the mode of interaction of T with foldamer **2**, we prepared a T derivative carrying a chromophoric probe, i.e. 5-(4-aminophenyl)-10,15,20-triphenylporphyrin

(compound **3,** Fig. 6B).16 Binding of **3** to foldamer **2** was investigated by CD spectroscopy in the absorption range (375–500 nm) of the Soret band of the porphyrin chromophore.[17] Specifically, we performed a titration experiment in 2:1, *v/v*, THF/water (to minimize self-aggregation of **2** and to allow solubilization of **3**), by keeping constant the concentration of **2** while adding increasing amounts of **3** (Fig. 6A).

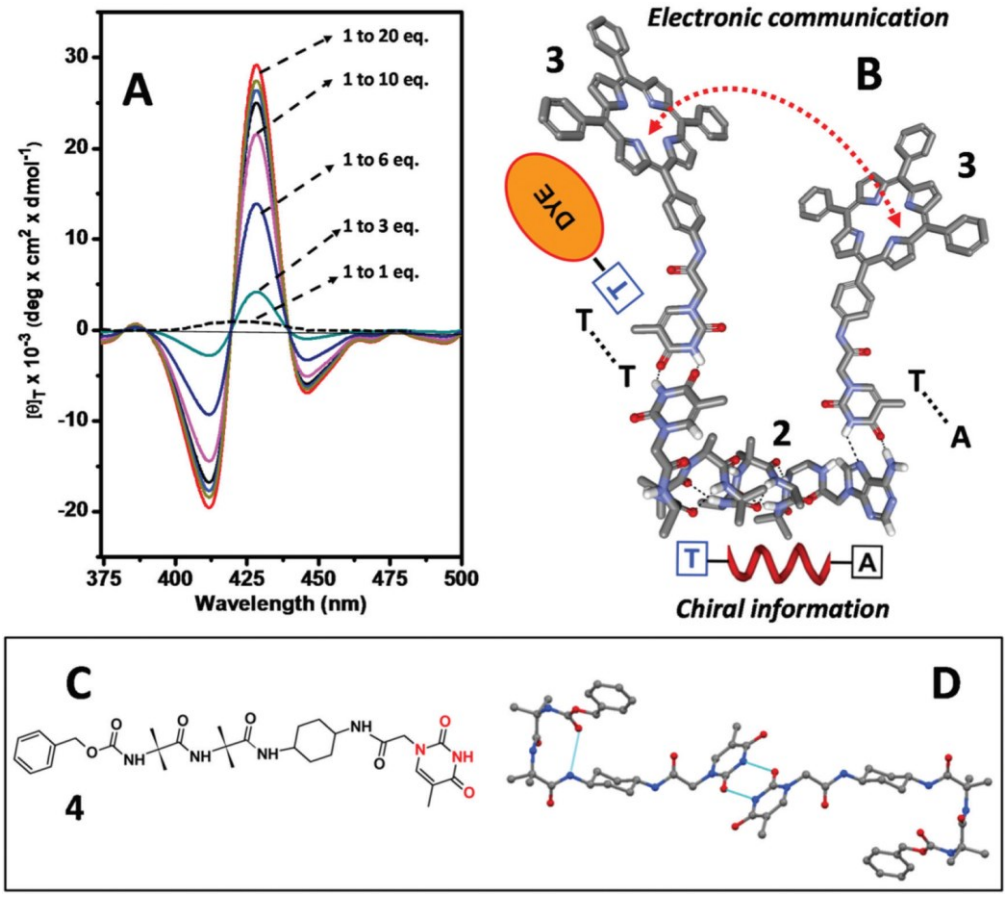

Fig. 6 (A) CD spectra, recorded upon addition in different molar ratios of the porphyrin-derivatized T **3** to a 0.01 mM, 2 : 1, v/v, THF/water solution of foldamer **2**. (B) Schematic representation of the proposed **3**-to-**2** binding mode and the related electronic coupling between two porphyrin chromophores. (C) Chemical structure of **4** and (D) its X-ray diffraction structure showing the formation of an intramolecular β-turn conformation and an intermolecular T···T base pairing.

As expected, prior to addition of **3**, foldamer **2** does not give any CD signal in the selected wavelength range. After addition of one equivalent of **3**, the CD spectrum displays only a weak positive band centered at 424 nm. This result should be related to a **3**-to-**2** association, which allows chirality transfer from the chiral peptide foldamer to the achiral porphyrin chromophore. Quite interestingly, all of the subsequent additions of **3** (from 3 to 20 equivalents) give rise to exciton split CD profiles of increasing overall ellipticities which exhibit two clear isosbestic points. These CD curves are necessarily related to an electronic

communication between the porphyrin chromophores confined in a chiral environment.[17] These findings support the view that at 1:1 molar ratio of **3** to **2**, only a mono-associated species is formed (in all probability, the T site of **3** is base-paired to the A site of **2**), but higher amounts of **3** are able to progressively populate a bis-associated species, in which **3** binds also to the N-terminus of **2** through T···T base-pairing (Fig. 6B). The possible occurrence of this latter feature is supported by the results obtained for peptide foldamer **4** (Fig. 6C), that consists in an Aib homo-dimer connected to a T moiety via an 1,4-diaminocyclohexyl linker. In particular, the X-ray diffraction structure of **4** (Fig. 6D) shows, in addition to the well-known, intramolecularly H-bonded β-turn encompassing the -Aib-Aib- sequence,[8] an intermolecular T···T base pairing. These considerations prompted us to investigate the supramolecular co-assembly of foldamer **2** with the porphyrin derivatized T **3** at varying molar ratios. In all of these experiments, we employed an 8:2, v/v, THF/water mixture (i.e., the solvent which led foldamer **2** alone to fiber formation) and the concentration of **3** was kept constant at 0.05 mM, while the **2**-to-**3** molar ratio was increased from 10:1 to 500:1. All solutions were sonicated for **2** h at 30°C and subsequently allowed to stand in close vials for 3 days at room temperature. Finally, they were examined by TEM (Fig. 7A-C).

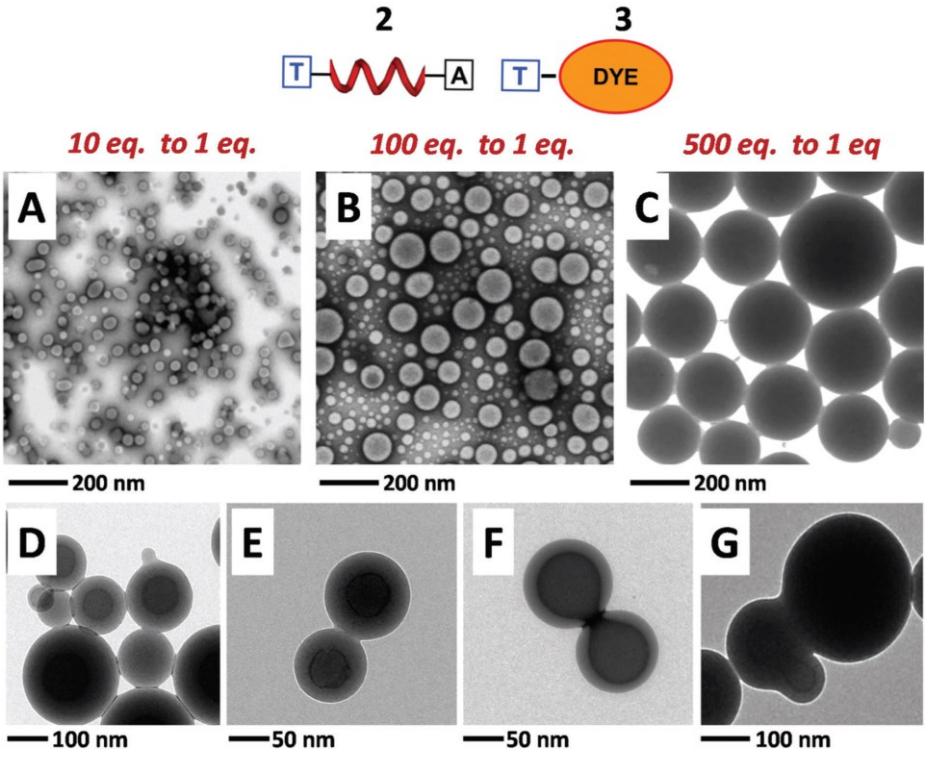

Fig. 7 (A–C) TEM images recorded for three different experiments of co-assembly of foldamer **2** and the porphyrin-derivatized T **3** in an 8 : 2, v/v, THF/water mixture, at the **2**-to-**3** molar ratios of 10: 1, 100 : 1, and 500: 1, respectively. (D–G) Cryo TEM images of samples from the 500: 1 **2**-to-**3** molar ratio preparation.

The results of these analyses clearly indicate: (i) the occurrence of an assembly process that produces spherical superstructures, and (ii) the dependence of their size and distribution on the **2**-to-**3** molar ratio. Specifically, at 10:1 molar ratio, 40 nm dispersed spherical structures were obtained. Conversely, at 100:1 and 500:1 molar ratios, 100 nm poly-dispersed and 200 nm narrowly dispersed spherical structures were produced, respectively. We believe that the presence of the large, flat and hydrophobic porphyrin chromophore, connected through T···A base pairing to one end of a fraction of the molecules of foldamer **2**, may induce formation of more stable spherical aggregates rather than linear chains in the supramolecular assembly process. To better understand the spherical aggregate morphology, the samples obtained from the 500:1 molar ratio of **2**-to-**3** (i.e., the largest spherical aggregates observed) were further analyzed by cryo-TEM (Fig. 7D–G). The results suggest formation of hollow vesicles (Fig. 7D and E) that are in contact to each other through part of their external surface. Interestingly, it was found that the surfaces of the vesicles may undergo a fusion process (Fig. 7F) that dynamically create larger vesicles (Fig. 7G). We also explored the possibility that modifications of the environmental conditions might induce a transition from supramolecular vesicles to the fiber morphology we previously observed for the self-assembly of foldamer **2** alone. Indeed, we found that repeated additions of 0.2, 2, and 10% volumes of 2,2,2-trifluoroethanol (TFE) to the 200 nm vesicles prepared from the 500:1 **2**-to-**3** molar ratio allowed a straightforward transition from vesicles to fiber microstructures (Fig. 8A–C). As clearly shown in Fig. 8A, upon the first addition of 0.2% TFE, the vesicles start to lose part of the peptide foldamer content from their surface. This phenomenon results in the formation of holes in the vesicles and the generation of a fibrillar network (Fig. 8A, red and blue squares, respectively). Upon the second addition of 2% TFE, the new TEM analysis (Fig. 8B) indicates a progressive disappearance of the vesicular (Fig. 8B, blue square) and the fibrillar morphologies which begin to be replaced by formation of proto-fibers and fibers (Fig. 8B, red square). After the last addition of 10% TFE, an ordered fiber network appears (Fig. 8C, and its blue square), although with smaller size (Fig. 8B, red square) with respect to those obtained by foldamer **2** alone in THF/water solution. The effect of TFE on the vesicles formed by co-assembly of foldamer **2** and the porphyrin-derivatized thymine **3** might be related, at least in part, to the H-bonding capability (as the donor) of this fluoroalcohol, stronger than that of aliphatic alcohols.

Indeed, addition of ethanol (up to 10% *v/v*) to the vesicles did not affect their morphology. However, the competition of TFE with the A–T base pairing is not effective enough to

hamper formation of fibers (Fig. 8C). Tentatively, TFE may also be involved in the solvation of the porphyrin-derivatized thymine **3** in a way that favors destabilization of the vesicles.

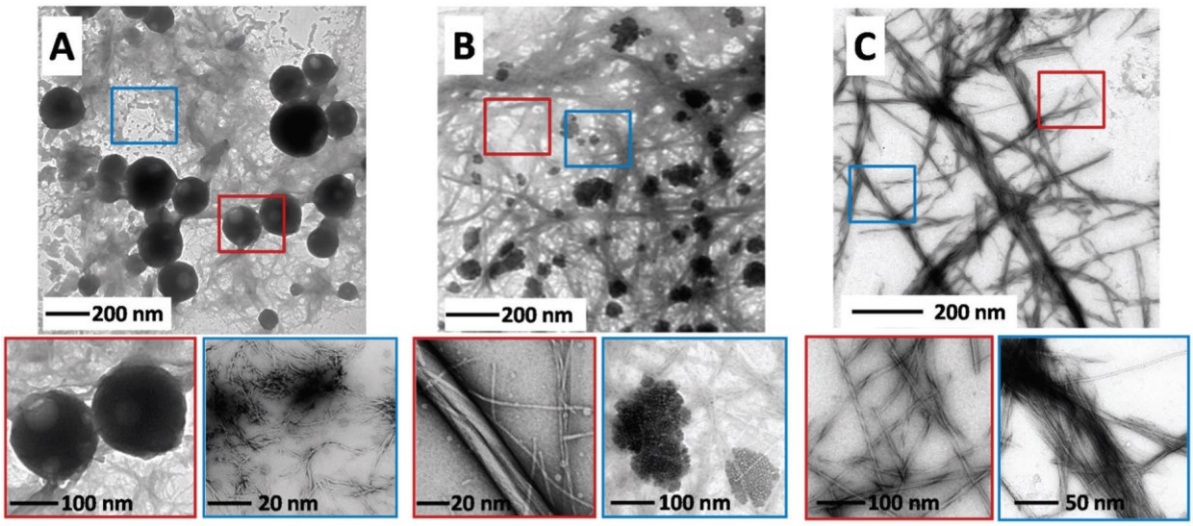

Fig. 8 (A–C) TEM images recorded after addition of 0.2, 2, and 10% volumes of TFE, respectively, to the vesicles formed by co-assembly of foldamer **2** and the porphyrin-derivatized T **3** in an 8 : 2, v/v, THF/water mixture, at the **2**-to-**3** molar ratio of 500 : 1.

Finally, we made use of A-capped gold nanoparticles (5, Fig. 9A)[16] to control the supramolecular growth of **2**. Gold nanoparticles **5** and peptide foldamer **2** were combined at different molar ratios in pure water solution. The most interesting information obtained from these experiments was found in the case of a large (500 eq.) excess of **2** with respect to **5**. Under these conditions, after a slow evaporation of the solution to dryness, homogenous spherical aggregates (up to 200–300 mm in diameter) were detected by optical microscopy (Fig. 9B). A SEM analysis revealed that these microstructures are made of thick fibers that seem to grow from a central core (Fig. 9C and D). At the periphery of the aggregates, these fibers tend to fray into thinner filaments following a sort of dendrimeric process (Fig. 9E). Overall, these results suggest that the A-capped gold nanoparticles **5** exert an efficient templating effect, driving the supramolecular assembly of foldamer **2** towards a star polymer-like form.

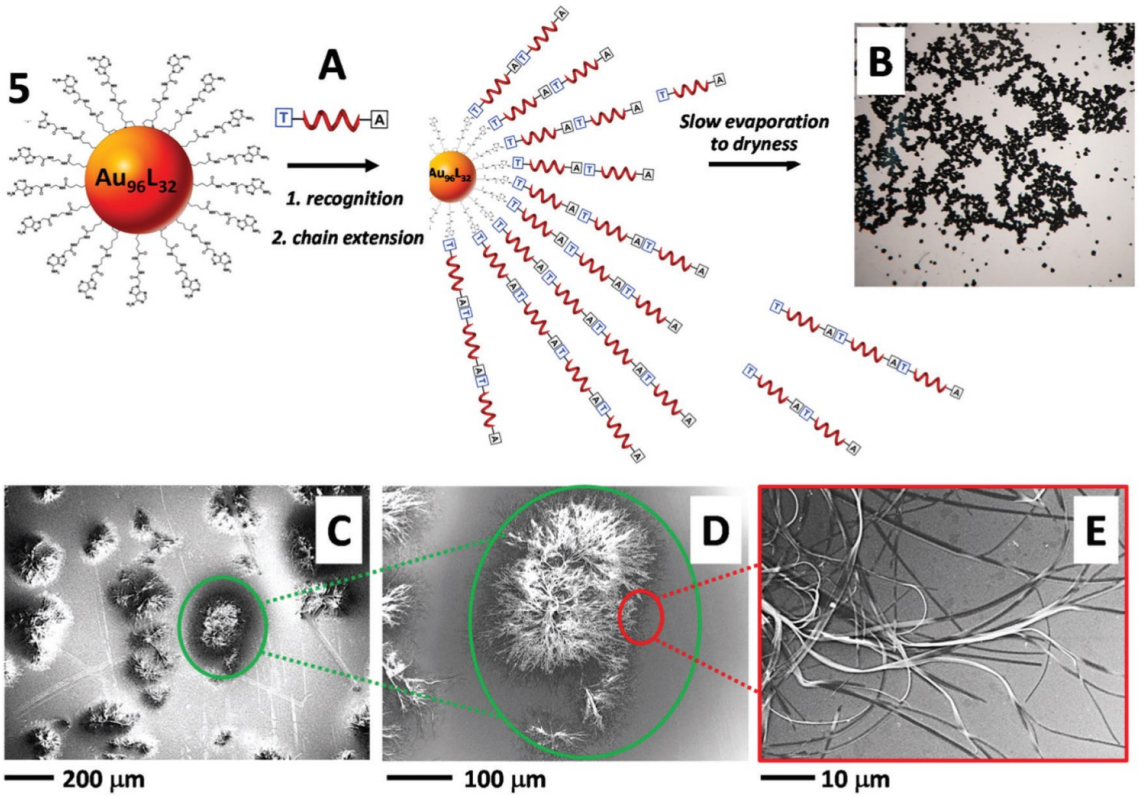

Fig. 9 (A) Schematic representation of the recognition and chain extension processes occurring between A-capped gold nanoparticles (**5**) and peptide foldamer **2**. (B) Optical microscope image recorded after slow evaporation from a water solution of the **5**/**2** mixture, showing formation of 200–300 mm spherical aggregates. (C and D) SEM images illustrating details of the microstructures (E) SEM details of the external part of the aggregates which highlight the dendrimeric nature of the fibers.

Conclusions

Introduction of a dyad of complementary, appropriately functionalized nucleobases covalently linked to the N- and C-termini of a peptide helical foldamer allows its precise self-recognition, that ends up into a well-defined supramolecular structure control at the nanoscale level. The interacting dyad of nucleobases is orthogonally compatible with the intramolecularly H-bonded 3D-structure of the peptide foldamer in the sense that the nucleobases do not interact with any of the amide groups of the peptide backbone. Depending on the experimental conditions, the resulting microstructures may be easily controlled in size and shape and converted into different architectures. In the future, this system may represent a valuable structural platform for the design of functional foldamers in which biomimetic functions are appropriately developed.[18]

Experimental section

Instruments and Methods

Nuclear Magnetic Resonance. ^{1}H and ^{13}C NMR spectra were recorded at room temperature on a Bruker AC-200 (200 MHz) and a Bruker Avance III 400 spectrometer (400.13 MHz ^{1}H frequency and 100.62 MHz ^{13}C frequency) instrument using TMS (tetramethylsilane) as the internal reference. The multiplicity of a signal is indicated as s, singlet; d, doublet; t, triplet; m, multiplet; and br, broad. Chemical shifts (δ) are expressed in ppm.

FT-IR absorption. FT-IR absorption spectra were recorded with a Perkin-Elmer 1720X spectrophotometer.

Mass Spectrometry. ESI-MS experiments were performed using an ESI-ToF MarinerTM BiospectrometryTM Workstation of Applied Biosystems by flow injection analysis using MeOH as the mobile phase. High-resolution mass spectra were obtained by electrospray ionization on a Perseptive Biosystem Mariner ESI-ToF spectrometer (Foster City, CA). An 1 x 10-9 M solution of neurotensin, angiotensin I, and bradykinin in an 1:1 CH_3CN/H_2O mixture, containing 1% formic acid, was used for calibration.

Electronic Circular Dichroism. ECD measurements were carried out at room temperature using a Jasco J-715 spectropolarimeter. A fused quartz cell of 1-mm path length (Hellma) was used.

Transmission Electron Microscopy. Samples were analyzed on a Jeol 300 PX TEM instrument. A glow discharged carbon coated grid was floated on a small drop of the nanosphere suspension and excess was removed by #50 hardened hatman filter paper.

Scanning Electron Microscopy. A Carl Zeiss Merlin field emission scanning electron microscope operating at 5kV accelerating voltage was used. A small drop of the milk-like aqueous suspension was placed on a microscope glass cover slip and allowed to dry overnight.

Atomic Force Microscopy. AFM experiments were performed on Ntegra Aura (NT-MDT) instrument operating in tapping mode at 200−400 kHz drive frequency and using a single crystal silicon tip coated with TiN (NSG01/TiN, 0.01-0.025 Ω-cm, antimony dope).

Synthesis and Characterization

Materials

1-Hydroxy-7-aza-1,2,3-benzotriazole (HOAt) was purchased from GL Biochem (Shanghai) Ltd. N-(3-dimethylaminopropyl)-N′- ethylcarbodiimide hydrochloride (EDC·HCl) was obtained from Iris Biotech (Germany). Trifluoroacetic acid, N,N'-diisopropylcarbodiimide (DIC), 4-(dimethylamino)-pyridine (DMAP), di-tert-butyl dicarbonate (Boc_2O), 1,8-diazabicyclo[5.4.0]undec-7-ene (DBU), triethylamine (TEA), bromoacetic acid and ethyl bromoacetate were obtained from Sigma-Aldrich. The deuterated solvent dimethylsulfoxide (DMSO-d_6) and $CDCl_3$ were purchased from Euriso-Top (France). All other chemicals and solvents are Sigma-Aldrich, Fluka or Acros products and used as provided without further purifications.

Synthesis of thymine-1-acetic acid[1]

Thymine-1-acetic acid was synthetized as previously reported at page 16.

Synthesis of ethyl adenine-9-acetate[1]

For the synthetic details about the preparation of ethyl adenine-9-acetate please refer to page 17.

Synthesis of adenine-9-monoacetyl-ethylendiamino amide[1]

Adenine-9-monoacetyl-ethylendiamino amide following the procedure described at page 18.

Synthesis of thymine-(aminophenyl) porphyrin (3)

The synthetic procedure for thymine-(aminophenyl) porphyrin was previously reported at page 17.

Synthesis of Z-$(Aib)_2$-OCH_3[2]

Z-Aib-OH (3.67 g, 17.5 mmol) was dissolved in dry DCM and activated with HOBt (2.36 g, 17.5 mmol) and EDC·HCl (3.36 g, 17.5 mmol) and the solution was stirred for 20 minutes. In the meanwhile, H-Aib-OCH_3 (5.13 g, 43.8 mmol) was dissolved in dry DCM, the pH was adjusted to basicity with TEA and it was added at the solution of the active ester. The reaction was stirred overnight. After evaporation of the solvent, the residue was dissolved in ethyl acetate and washed with $KHSO_4$ 5% and $NaHCO_3$ 5%, dried, filtered and concentrated. The

product was precipitate from ethyl acetate and petroleum ether.

^{1}H NMR: (400 MHz, $CDCl_3$): δ 1.53 (s, 12H, CH_3 Aib), 3.73 (s, 3H, CH3), 5.12 (s, 2H, CH2), 5.30 (s, 1H, NH), 6.91 (s, 1H, NH), 7.36 (s, 5H, CH).

^{13}C NMR: (101 MHz, $CDCl_3$): δ 26.03, 26.24, 53.71, 56.32, 57.85, 67.23, 128.05, 128.95, 129.40, 137.84, 156.87, 175.54, 175.89.

MS (ESI-TOF): [M] calc. = 336.3828 m/z; $[M+H]^+$ found = 337.2547 m/z.

IR (KBr): 3381, 3364, 3318, 3279, 2986, 1727, 1657, 1522 cm^{-1}.

Synthesis of Z-$(Aib)_2$-OH[3]

Z-$(Aib)_2$-OCH_3 (0.30 g, 0.89 mmol) was dissolved in dry THF, then LiOH liquefied in water (0.06 g, 2.67 mmol) was added and the solution was stirred for 2 hours at 40°C. After evaporation of the organic solvent, pH was adjust to 4 with solid $KHSO_4$. The product was extracted with ethyl acetate, then the organic phase was washed with brine, dried over anhydrous Na_2SO_4, filtered and concentrated. The product was precipitate from ethyl acetate and petroleum ether.

^{1}H NMR: (200 MHz, $CDCl_3$): δ 1.52 (s, 12H, CH_3 Aib), 5.13 (s, 2H, CH2), 5.24 (s, 1H, NH), 6.91 (s, 1H, NH), 7.37 (s, 5H, CH).

^{13}C NMR: (101 MHz, $CDCl_3$): δ 25.45, 26.12, 56.53, 57.92, 67.31, 128.11, 129.02, 129.71, 137.96, 157.01, 175.68, 175.91.

MS (ESI-TOF): [M] calc. = 322.3563 m/z; $[M+H]^+$ found = 323.4652 m/z.

IR (KBr): 3430, 3299, 2989, 1722, 1704, 1653, 1534, 1510 cm^{-1}.

Synthesis of Z-$(Aib)_2$-diaminocyclohexane

Z-$(Aib)_2$-OH (0.5 g, 1.55 mmol) was dissolved in dry CH_3CN and activated with HOAt (0.21 g, 1.55 mmol) and EDC·HCl (0.29 g, 1.55 mmol) and the solution was stirred for 20 minutes. trans-1,4-diaminocyclohexane was dissolved in dry CH_3CN and added at the solution. TEA was used to basify to pH 8. The reaction was stirred overnight. After evaporation of the solvent, the residue was dissolved in ethyl acetate and washed with $KHSO_4$ 5% and $NaHCO_3$ 5%, dried, filtered and concentrated. The product was precipitate from ethyl acetate and petroleum ether and directly used for the next synthetic step, after mass characterization.

MS (ESI-TOF): [M] calc. = 418.5297 m/z; $[M+H]^+$ found = 419.6421 m/z.

Synthesis of peptide foldamer 4

Thymine-1-acetic acid (0.06 g, 0.32 mmol) was dissolved in dry DCM and activated with HOBt (0.044 g, 0.32 mmol) and EDC·HCl (0.062 g, 0.32 mmol) and the solution was stirred for 30 minutes. Z-(Aib)2-diaminocyclohexane (0.14 g, 0.32 mmol) was added at the solution of the active ester and DIPEA was used to basify to pH 8. The reaction was stirred overnight. After evaporation of the solvent, the residue was dissolved in ethyl acetate and washed with $KHSO_4$ 5% and $NaHCO_3$ 5%, dried, filtered and concentrated. The product was precipitate from ethyl acetate and petroleum ether.

^{1}H NMR: (400 MHz, DMSO-d_6): δ 1.28 (s, 12H, CH_3 Aib), 1.74 (s, 5H, CH_2), 2.07 (s, 1H), 4.22 (s, 2H, CH_2), 5.08 (s, 2H, CH_2), 7.06 (d, 1H, NH, J=6Hz), 7.34 (s, 5H, CH), 7.52 (s, 1H, NH),7.61 (s, 1H, NH), 8.03 (d, 1H, NH, J=5Hz), 11.25 (s, 1H, NH).

^{13}C NMR: (101 MHz, $CDCl_3$): δ 12.23, 26.14, 30.97, 49.57, 50.15, 51.23, 56.55, 57.16, 66.82, 107.23, 128.42, 128.51, 128.67, 137.25, 141.89, 152.31, 156.37, 164.91, 170.43, 175.39, 175.73.

MS (ESI-TOF): [M] calc. = 584.6639 m/z; $[M+H]^+$ found = 585.2979 m/z; [2M] calc. = 1168.3278 m/z; $[2M+H]^+$ found = 1169.5801.

Synthesis of adenine-capped gold nanoparticles (5) [1]

Adenine-capped gold nanoparticles were synthetized as described at page 19.

Synthesis of Boc-$(Aib)_2$-OBzl

Boc-Aib-OH (0.50 g, 2.5 mmol) was dissolved in dry DCM and activated with HOAt (0.34 g, 2.5 mmol) and EDC·HCl (0.47 g, 2.5 mmol) and the solution was stirred for 30 minutes. H-Aib-OBzl (0.57 g, 3 mmol) was added at the solution of the active ester and DIPEA was used to basify to pH 8. The reaction was stirred overnight. After evaporation of the solvent, the residue was dissolved in ethyl acetate and washed with $KHSO_4$ 5% and $NaHCO_3$ 5%, dried, filtered and concentrated. The product was precipitate from ethyl acetate and petroleum ether.

^{1}H NMR: (400 MHz, $CDCl_3$): δ 1.44 (s, 15H, CH_3), 1.57 (s, 6H, CH_3), 4.87 (s, 1H, NH), 5.17 (s, 2H, CH_2), 7.14 (s, 1H, NH), 7.31-7.35 (5H, benzyl ring).

^{13}C NMR: (101 MHz, $CDCl_3$): δ 26.15, 26.38, 28.73, 56.17, 56.27, 67.35, 80.91, 128.39, 128.49, 128.65, 137.21, 155.61, 175.31, 175.44.

MS (ESI-TOF): [M] calc. = 378.4626 m/z; $[M+H]^+$ found = 379.2315 m/z.

Synthesis of thymine-$(Aib)_2$-OBzl

Boc-$(Aib)_2$-OBzl (0.90 g, 2.4 mmol) was treated with a solution 1:1 dichloromethane/trifluoroacetic acid to remove the tert-butyloxycarbonyl protecting group. After evaporation of the solvent, the product was mixed with the active ester of thymine-1-acetic acid (0.50 g, 2.7 mmol) prepared with HOAt (0.37 g, 2.7 mmol) and EDC·HCl (0.52 g, 2.7 mmol), and TEA was added to basify the solution. The reaction was stirred overnight. After evaporation of the solvent, the residue was dissolved in ethyl acetate and washed with $KHSO_4$ 5% and $NaHCO_3$ 5%, dried, filtered and concentrated.

^{1}H NMR: (400 MHz, DMSO-d_6): δ 1.30 (s, 6H, CH_3), 1.34 (s, 6H, CH_3),1.75 (s, 3H, CH_3), 4.27 (s, 2H, CH_2), 5.02 (s, 2H, CH_2), 7.32-7.35 (5H, benzyl ring), 7.39 (s, 1H, NH), 7.44 (s, 1H, CH), 8.27 (s, 1H, NH), 11.34 (s, 1H, NH).

^{13}C NMR: (101 MHz, $CDCl_3$): δ 12.25, 26.17, 26.23, 50.13, 56.45, 56.93, 67.37, 107.29, 128.36, 128.51, 128.63, 137.19, 141.79, 152.27, 164.89, 170.35, 175.03, 175.37.

MS (ESI-TOF): [M] calc. = 444.4809 m/z; $[M+H]^+$ found = 445.2761 m/z.

Synthesis of thymine-$(Aib)_2$-OH

Thymine-$(Aib)_2$-OBzl (0.85 g, 1.9 mmol) was dissolved in 10 ml of ethanol. Subsequently, Pd/C 10% and 5 ml of cyclohexene were added under nitrogen. The solution was stirred at 80°C until the reaction finished (seen by thin layer chromatography), then filtered on celite and washed with ethanol, acetonitrile and diethyl ether. The resultant solution was dried under vacuum providing the desired compound.

^{1}H NMR: (400 MHz, DMSO-d_6): δ 1.30 (s, 6H, CH_3), 1.34 (s, 6H, CH_3),1.74 (s, 3H, CH_3), 4.28 (s, 2H, CH_2), 7.32 (s, 1H, NH), 7.44 (s, 1H, CH), 8.35 (s, 1H, NH), 11.35 (s, 1H, NH), 12.06 (br, 1H, OH).

^{13}C NMR: (101 MHz, $CDCl_3$): δ 12.21, 24.41, 26.03, 50.11, 56.93, 57.12, 107.14, 141.93, 152.25, 164.97, 170.41, 175.32, 179.23.

MS (ESI-TOF): [M] calc. = 354.3583 m/z; $[M+H]^+$ found = 355.6247 m/z.

Synthesis of 1

Thymine-$(Aib)_2$-OH (0.3 g, 0.85 mmol) was dissolved in acetic anhydride (20 ml, 211 mmol) and the solution was stirred for 1 hour at 130°C. The solvent was removed under vacuum and the oxazolone is added at adenine-9-monoacetyl-ethylendiamino amide (0.21 g, 0.9 mmol) dissolved in anhydrous DMF. The reaction was stirred overnight. After evaporation of the

solvent, the crude product was purified by flash chromatography.
For ^{1}H NMR details and ^{1}H and ^{13}C resonances assignment see the NMR analysis.
MS (ESI-TOF): [M] calc. = 571.2615 m/z; $[M+H]^{+}$ found = 572.2906 m/z.

Synthesis of 2

Peptide foldamer **2** was synthesized using standard solid phase 9-fluorenylmethoxycarbonyl (Fmoc) chemistry on a 2-chlorotrityl chloride resin. For each step, Fmoc deprotection was performed by mixing the resin in a piperidine/N,N-dimethylformamide (DMF) (2:8, v/v) solution for 10 minutes (2x), then washing with DMF, MeOH and CH_2Cl_2. For all of the amino acid couplings we used the following protocol: 5.0 eq. (relative to the resin loading) of Fmoc-protected amino acid were activated externally with 4.9 eq. of O-Benzotriazole-N,N,N',N'-tetramethyluronium hexafluorophosphate (HBTU) and 15 eq. of diisopropylethylamine (DIPEA) in DMF (2.5 ml/mmol of amino acid). This mixture was then added to a peptide chamber containing the resin and mixed for 3 hours. The resin was then drained and rinsed with MeOH, and CH_2Cl_2, then allowed to dry. All coupling and deprotection steps were monitored by performing a Kaiser test on a few resin beads, which were removed from the peptide chamber after drying. As a last coupling, thymine-1-acetic acid (5.0 eq.) was used instead of amino acid residue. The resin was prepared for cleavage by washing with CH_2Cl_2 and MeOH then drying under high vacuum. Cleavage from the resin was accomplished by stirring the resin with 10 ml of TFA, water and TIS (95:2.5:2.5) for 3 hours. The resin was removed by filtration and washed with 3 ml of the cleavage mixture. The filtrate volume was reduced by evaporation under reduced pressure and the peptide was precipitated by the addition of 200 ml cold diethyl ether. The precipitate was filtered and rinsed with cold diethyl ether to obtain the crude peptide. The product was then activated with DIC (0.126 g, 1 mmol) in DMF for 15 minutes, then adenine-9-monoacetyl-ethylendiamino amide (0.47 g, 2 mmol) was added to the mixture. The reaction was stirred at 40°C overnight, then the solvent was evaporated under vacuum. The crude product was washed with water, which was evaporated. The product was purified by flash chromatography.
For ^{1}H NMR details and ^{1}H and ^{13}C resonances assignment see the NMR analysis.
MS (ESI-TOF): [M] calc. = 1026.3091 m/z; $[M+H]^{+}$ found = 1027.5155 m/z.

NMR analysis

NMR experiments were performed at 298 K on a Bruker Avance III 400 spectrometer (400.13 MHz 1H frequency and 100.62 MHz ^{13}C frequency) equipped with a 5 mm multinuclear inverse z-field gradient probe-head. For data processing the Topspin 3.5 software was used.
Foldamer **1** (3 mg) was dissolved in 1 ml of DMSO-d_6 for NMR characterization. The ^{1}H and ^{13}C chemical shifts were reported in ppm and referenced to the ^{1}H residual solvent signal and ^{13}C solvent signal: resonances assignment was obtained using 2D heteronuclear correlation spectroscopy (^{1}H-^{13}C HMQC and HMBC experiments).
^{1}H one-dimensional spectrum was recorded with 8 transients, 14 ppm spectral width, and 32k data points. Exponential multiplication with line broadening of 0.2 Hz was applied prior to Fourier Transform.
The ^{1}H-^{13}C Heteronuclear Multiple Quantum Correlation (HMQC) and the ^{1}H-^{13}C Heteronuclear Multiple-Bond Correlation (HMBC) spectra were acquired with 16 and 200 scans respectively, accumulated for 128 and 180 experiments, and processed with a magnitude calculation; the spectral width was 14 ppm in F2, 180 or 210 ppm in F1. 3.4 ms and 66.7 ms evolution delay were used, respectively for ^{1}H-^{13}C one-bond and ^{1}H-^{13}C long-range coupling constants selection. Zero-filling in both F1 and F2 dimensions, multiplication with a Gaussian function (in F2) and a squared sine function (in F1) were performed prior to 2D Fourier Transform.
Foldamer **2** (7 mg) was dissolved in 1 ml of H_2O/D_2O solution (10:1) for NMR characterization. The ^{1}H and ^{13}C chemical shifts were reported in ppm and referenced to DSS: the resonances assignments were obtained using 2D homonuclear (TOCSY and ROESY) experiments and 2D heteronuclear correlation spectroscopy (^{1}H-^{13}C HMQC and HMBC experiments). ^{1}H one-dimensional spectrum was acquired with the 1D gradient NOESY-presat sequence using an inversion recovery delay of 15 ms, accumulating 32 transients of 32k data points and 10 ppm spectral width. Exponential multiplication with line broadening of 0.2 Hz was applied prior to Fourier Transform.
The TOtal Correlation SpectroscopY (TOCSY) spectrum was acquired with WATERGATE sequence for water signal suppression, with a spectral width of 10 ppm. A total of 512 experiments with 16 scans each one were acquired in TPPI mode. The mixing time was 70 ms and the relaxation delay 1.2 s. The Rotating frame nuclear Overhouser Effect SpectroscopY (ROESY) spectrum was acquired with WATERGATE sequence for water signal suppression,

with a spectral width of 10 ppm. A total of 512 experiments with 64 scans each one were acquired in TPPI mode. The mixing time was 150 ms and the relaxation delay 1.4 s. The TOCSY and ROESY data were processed with a Gaussian function (in F2) and a squared sine function (in F1) multiplication prior to 2D Fourier Transform, and zero-filling in both F1 and F2 dimensions.

The ^{1}H-^{13}C Heteronuclear Multiple Quantum Correlation (HMQC) and the ^{1}H-^{13}C Heteronuclear Multiple-Bond Correlation (HMBC) spectra were acquired with 128 and 400 scans respectively, accumulated for 128 and 180 experiments, and processed with a magnitude calculation; the spectral width was 10 ppm in F2, 180 and 200 ppm in F1. 3.4 ms and 66.7 ms evolution delay were used, respectively for ^{1}H-^{13}C one-bond and ^{1}H-^{13}C long-range coupling constants selection. Zero-filling in both F1 and F2 dimensions, multiplication with a Gaussian function (in F2) and a squared sine function (in F1) were performed prior to 2D Fourier Transform.

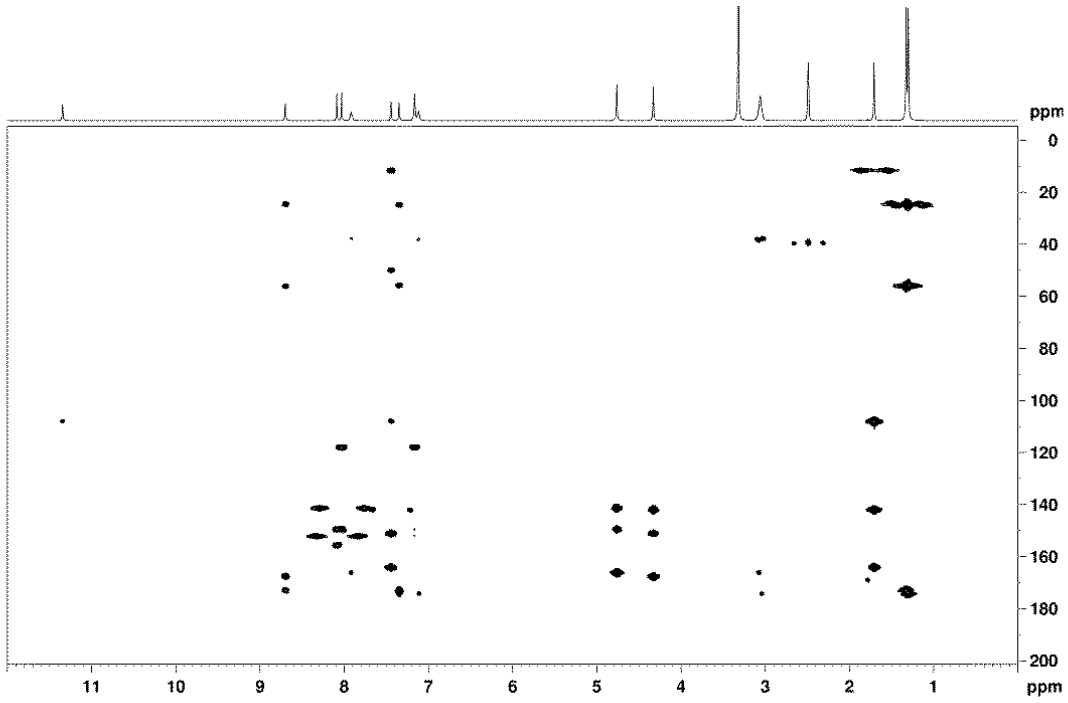

Fig. 10 ^{1}H-^{13}C HMBC spectrum of Foldamer 1 in DMSO-d_6.

Thymine	**2**	**3**	**4**	**5**	**6**	**CH_3**
^{1}H		11.35			7.44	1.71
^{13}C	151.2		164.2	108.0	142.0	11.6
carboxymethylene	**7**	**8**				
^{1}H	4.33					
^{13}C	49.8	167.75				
Aib 1	**9**	**10**	**11**			**CH_3**
^{1}H	8.70					1.33
^{13}C		56.3	173.0			24.7*
Aib 2	**12**	**13**	**14**			**CH_3**
^{1}H	7.35					1.30
^{13}C		55.8	174.4			24.7*
ethylendiamine	**15**	**16**	**17**	**18**		
^{1}H	7.12	3.06*	3.06*	7.92		
^{13}C		38.3	38.0			
carboxymethylene	**19**	**20**				
^{1}H		4.76				
^{13}C	166.25	44.7				
Adenine	**22**	**24**	**26**	**27**	**29**	**NH_2**
^{1}H		8.09			8.03	7.16
^{13}C	149.6	152.1	155.7	118.1	141.5	

Table 1 ^{1}H and ^{13}C resonances assignment of Foldamer **1** in DMSO-d_6.

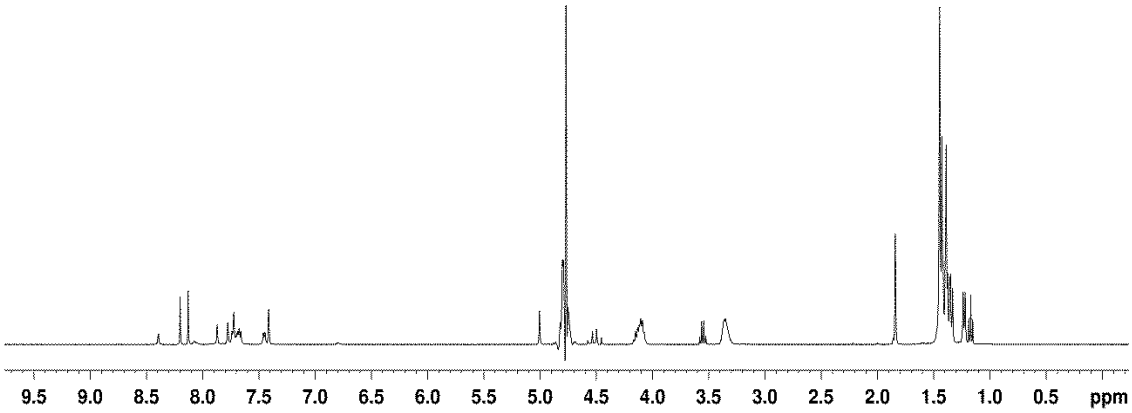

Fig. 11 ^{1}H one-dimensional spectrum of Foldamer **2** in H_2O/D_2O 10:1 solution.

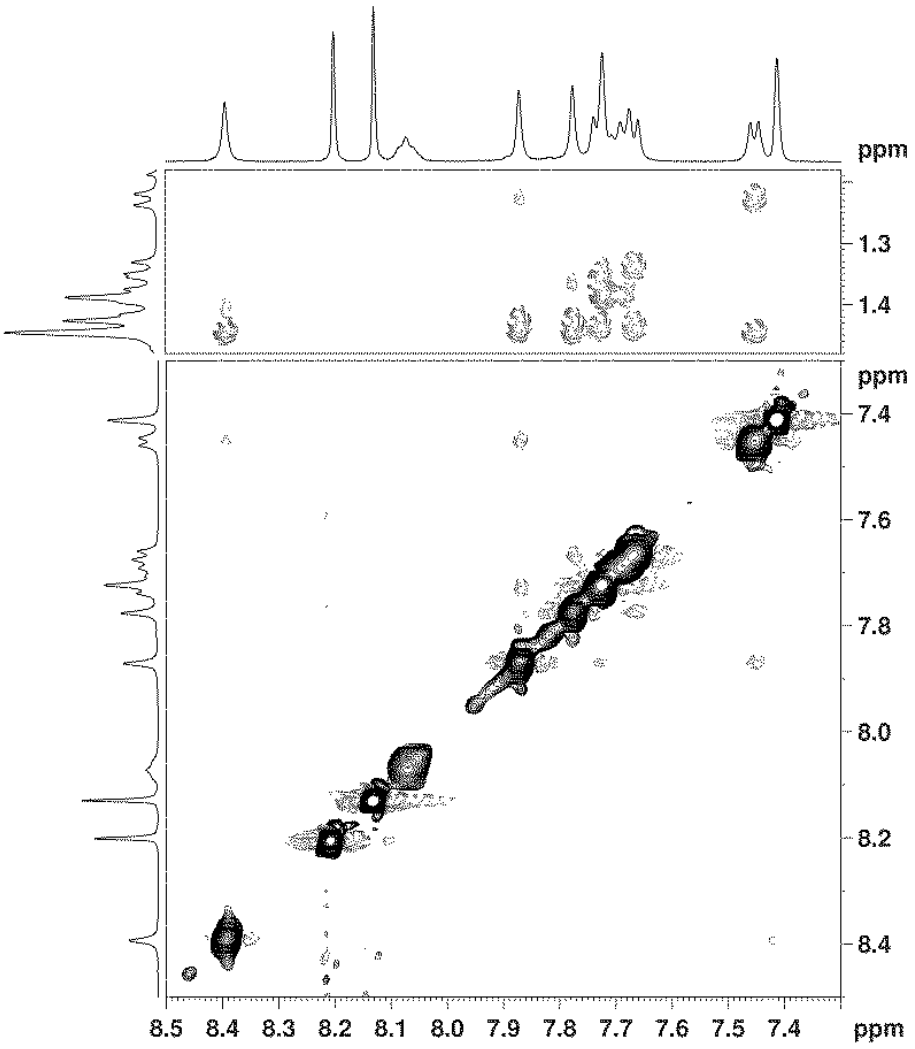

Fig. 12 Two sections of the ROESY spectrum of Foldamer **2** in H_2O/D_2O 10:1 solution. NH-NH and NH-CH_3 ROESY connectivities allows the sequential assignment of Aib and Ala residues.

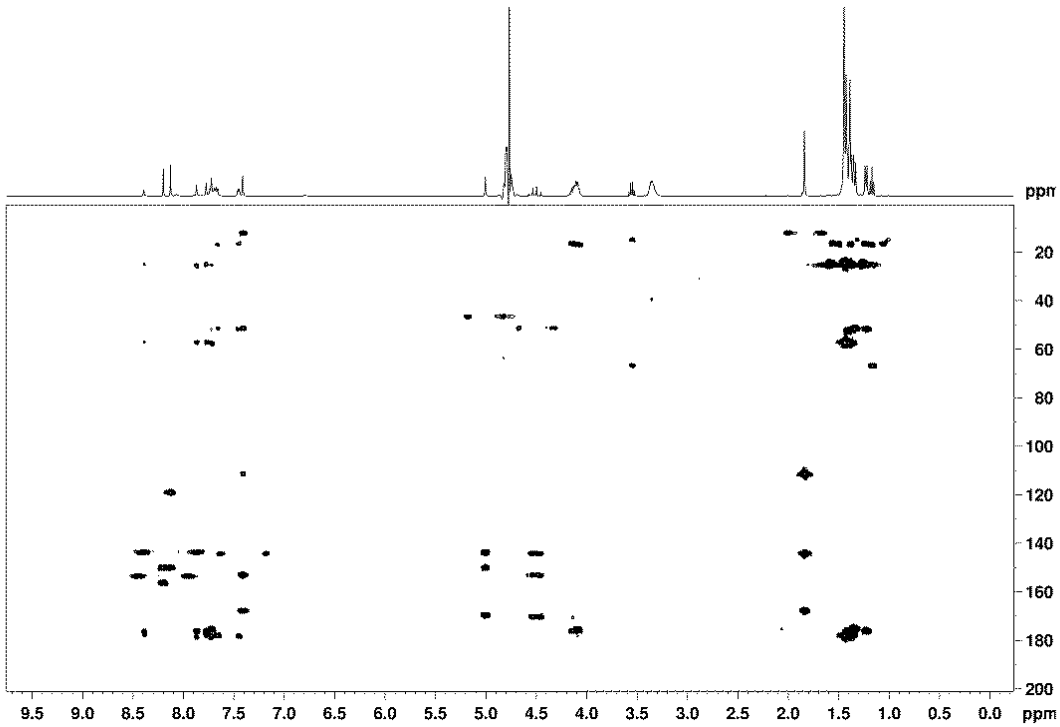

Fig. 13 $^{1}H–^{13}C$ HMBC spectrum of Foldamer **2** in H_2O/D_2O 10:1 solution.

Thymine	**2**	**3**	**4**	**5**	**6**	**CH_3**
^{1}H		nd			7.41	1.84
^{13}C	153.1		167.8	111.4	144.3	12.1
carboxymethylene	**7**	**8**				
^{1}H	4.56-4.47					
^{13}C	51.4	170.4				
Ala 1	**9**	**10**	**11**			**CH_3**
^{1}H	8.75	4.14				1.41
^{13}C		52.3	176.5			16.2*
Aib 2	**12**	**13**	**14**			**CH_3**
^{1}H	8.39					1.45
^{13}C		57.2	178.3			25.0
Ala 3	**15**	**16**	**17**			**CH_3**
^{1}H	7.45	4.10				1.23

^{13}C		51.8	176.1			16.6
Aib 4	**18**	**19**	**20**			**CH_3**
^{1}H	7.87					1.43
^{13}C		57.3	178.5			25.5
Ala 5	**21**	**22**	**23**			**CH_3**
^{1}H	7.73	4.08				1.36
^{13}C		51.9	176.4			16.7*
Aib 6	**24**	**25**	**26**			**CH_3**
^{1}H	7.78					1.45
^{13}C		57.2	177.9			25.1
Ala 7	**27**	**28**	**29**			**CH_3**
^{1}H	7.67	4.11				1.34
^{13}C		51.5	175.5			16.7*
Aib 8	**30**	**31**	**32**			**CH_3**
^{1}H	7.72					1.39
^{13}C		57.6	178.2			25.3
ethylendiamine	**33**	**34**	**35**	**36**		
^{1}H	7.69	3.35*	3.35*	8.07		
^{13}C		39.8*	39.8*			
carboxymethylene	**37**	**38**				
^{1}H		5.00				
^{13}C	169.6	46.5				
Adenine	**40**	**42**	**44**	**45**	**47**	**NH_2**
^{1}H		8.2			8.13	6.79
^{13}C	150.1	153.5	156.4	119.2	143.6	

Table 2 ^{1}H and ^{13}C resonances assignment of Foldamer **2** in H_2O/D_2O 10:1 solution.

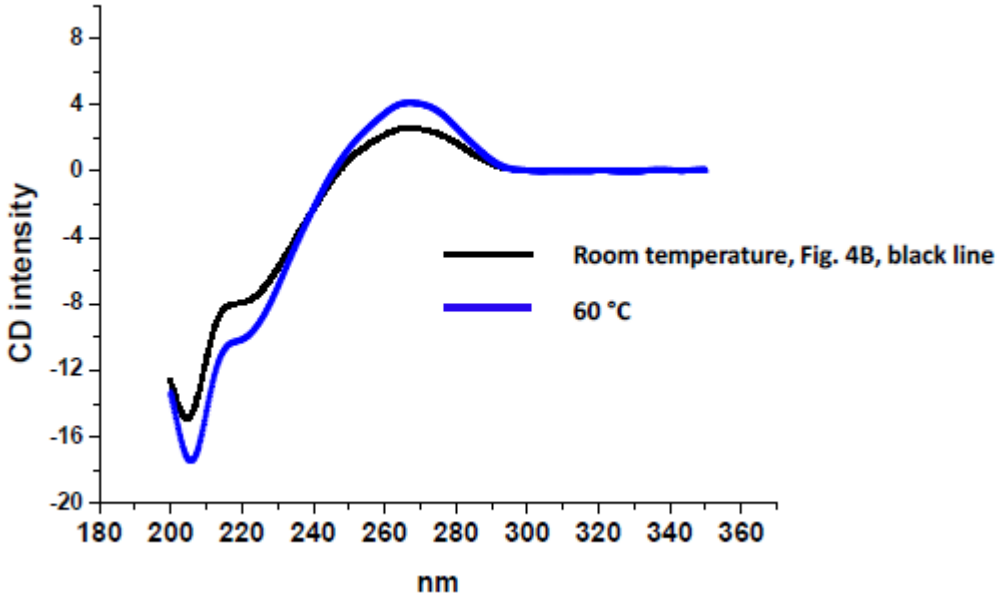

Fig. 14 The CD spectrum collected at 60°C (blue line) is virtually superimposable to that of the monomeric species at 25°C (black line).

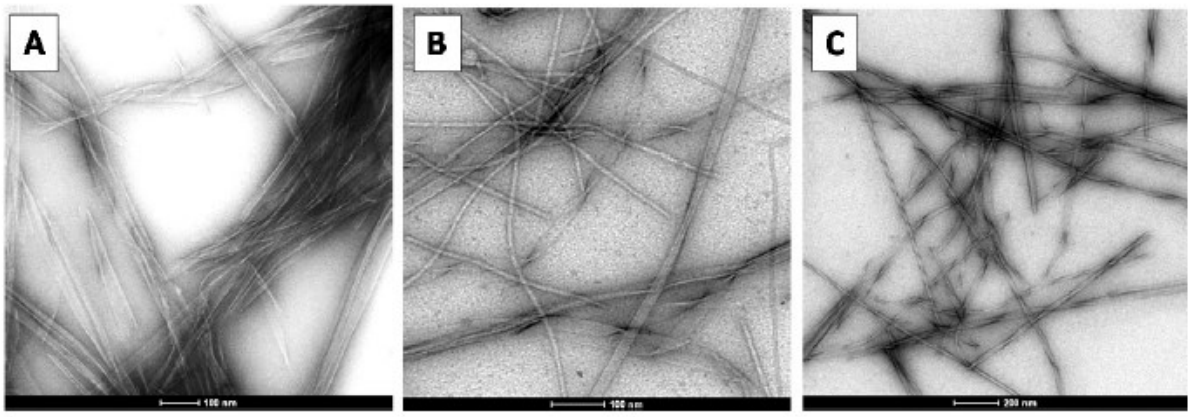

Fig. 15 TEM images recorded at three different times (A 6 hr, B 12 hr, and C 18 hr) during the self-assembly of 2 under the conditions reported in main text, Fig 4.

X-Ray diffraction

Crystals of foldamers **1** and **4** were grown by slow evaporation from methanol-water and ethanol solutions, respectively. X-Ray diffraction data were collected with a Gemini E four-circle kappa diffractometer (Agilent Technologies) equipped with a 92 mm EOS CCD detector, using graphite monochromated Cu Kα radiation (λ = 1.54178 Å). Data collection and reduction were performed with the CrysAlisPro software (Agilent Technologies). A semi-empirical absorption correction based on the multi-scan technique using spherical harmonics, implemented in the SCALE3 ABSPACK scaling algorithm, was applied. Both structures were solved by ab initio procedures of the SIR 2014 program,[19] and refined by full-matrix least-squares on F2, using all data, by application of the SHELXL-2014 program.[20] Non-hydrogen atoms were refined anisotropically, except for two, partially occupied, cocrystallized water molecules in the structure of **1**. The asymmetric unit of **4** includes a co-crystallized ethanol molecule, the methyl group of which is disordered and was refined on two positions, with population parameters of 0.65 and 0.35, respectively. H-Atoms were calculated at idealized positions and refined using a riding model. Relevant crystal data and structure refinement parameters, selected torsion angles, and intra-and intermolecular H-bond parameters are listed in Tables S1-S3 for 1, and in Tables S4-S6 for 4. CCDC 1535890 and 1535891 contain the supplementary crystallographic data for this paper. These data can be obtained from The Cambridge Crystallographic Data Centre via www.ccdc.cam.ac.uk/structures.

Table S1. Crystal data and structure refinement for foldamer **1** heptahydrate.

Identification code	mc268f	
Empirical formula	$C_{24}H_{33}N_{11}O_6$, 7(H_2O)	
Formula weight	697.72	
Temperature	293(2) K	
Wavelength	1.54178 Å	
Crystal system	Monoclinic	
Space group	P 2_1/c	
Unit cell dimensions	a = 9.11756(10) Å	α= 90°.
	b = 21.6446(2) Å	β= 98.1280(10)°.
	c = 17.9917(2) Å	γ = 90°.
Volume	3514.92(6) $Å^3$	
Z	4	
Density (calculated)	1.318 Mg/m^3	
Absorption coefficient	0.915 mm^{-1}	
F(000)	1488	
Crystal size	0.400 x 0.300 x 0.050 mm^3	
Theta range for data collection	3.213 to 70.887°.	
Index ranges	-11<=h<=11, -26<=k<=26, -21<=l<=21	
Reflections collected	45118	
Independent reflections	6749 [R(int) = 0.0278]	
Completeness to theta = 67.679°	100.0 %	
Absorption correction	Semi-empirical from equivalents	
Max. and min. transmission	1.00000 and 0.59078	
Refinement method	Full-matrix least-squares on F^2	
Data / restraints / parameters	6749 / 1 / 432	
Goodness-of-fit on F^2	1.035	
Final R indices [I>2sigma(I)]	R_1 = 0.0565, wR_2 = 0.1647	
R indices (all data)	R_1 = 0.0649, wR_2 = 0.1744	
Extinction coefficient	n/a	
Largest diff. peak and hole	0.549 and -0.427 e.$Å^{-3}$	
CCDC deposition number	1535890	

Table S2. Selected torsion angles [°] for foldamer **1**.

N1T-C01-C0-N1	145.67(19)
C01-C0-N1-C1A	172.11(18)
C0-N1-C1A-C1	58.0(2)
N1-C1A-C1-N2	27.0(2)
C1A-C1-N2-C2A	178.90(18)
C1-N2-C2A-C2	52.3(3)
N2-C2A-C2-N3	37.5(3)
C2A-C2-N3-C31	-175.73(19)
C2-N3-C31-C32	108.9(2)
N3-C31-C32-N4	-57.3(2)
C31-C32-N4-C33	-84.9(3)
C32-N4-C33-C34	164.4(2)
N4-C33-C34-N9A	170.0(2)

Table S3. Hydrogen bonds for foldamer **1** heptahydrate [Å and °].

D-H...A	d(D-H)	d(H...A)	d(D...A)	<(DHA)
N3-H3...O0	0.86	2.28	3.050(2)	148.4
N4-H4...O1	0.86	2.19	2.857(2)	134.0
N3T-H3T...N1A#1	0.86	2.02	2.884(2)	178.0
N6A-H6A1...O4T#2	0.84	2.12	2.949(2)	168.8
N2-H2...O3#3	0.86	2.57	3.014(3)	112.9
N1-H1...O1W	0.86	2.13	2.980(2)	172.2
N6A-H6A2...O4W	0.90	2.56	3.389(4)	155.1
O4W-H4WA...N7A	0.95	1.88	2.791(3)	159.2
O2W-H2WA...O2	0.75	2.10	2.829(3)	165.6
O3W-H3WA...O2	0.94	1.89	2.824(3)	173.7
O2W-H2WB...N3A#4	0.93	2.07	2.980(3)	164.9
O1W-H1WA...O2W#5	0.87	1.94	2.808(3)	171.3
O1W-H1WB...O4W#6	0.85	2.00	2.821(4)	164.1
O3W-H3WB...O5W	0.95	1.89	2.778(5)	155.3
O4W-H4WB...O5W#7	0.82	1.98	2.807(6)	179.8
O5W-H5WA...O7W	0.84	1.88	2.711(12)	170.4
O6W-H6WB...O3W	0.84	2.01	2.850(8)	178.1
O6W-H6WA...O1W#8	0.84	1.95	2.789(7)	177.8

Symmetry transformations used to generate equivalent atoms:

#1 x-1,-y+1/2,z+1/2 #2 x+1,-y+1/2,z-1/2 #3 x-1,y,z

#4 x,-y+1/2,z+1/2 #5 x-1,-y+1/2,z-1/2 #6 -x,y+1/2,-z+1/2

#7 x+1,y,z #8 x+1,-y+1/2,z+1/2

Table S4. Crystal data and structure refinement for foldamer **4** ethanol solvate.

Identification code	mc258d	
Empirical formula	$C_{29}H_{40}N_6O_7$, C_2H_6O	
Formula weight	630.74	
Temperature	293(2) K	
Wavelength	1.54178 Å	
Crystal system	Monoclinic	
Space group	P 2_1/n	
Unit cell dimensions	a = 10.7942(5) Å	α= 90°.
	b = 18.8139(6) Å	β= 98.486(4)°.
	c = 16.8871(8) Å	γ = 90°.
Volume	3391.9(3) Å^3	
Z	4	
Density (calculated)	1.235 Mg/m^3	
Absorption coefficient	0.741 mm^{-1}	
F(000)	1352	
Crystal size	0.500 x 0.400 x 0.250 mm^3	
Theta range for data collection	3.538 to 72.983°.	
Index ranges	-13<=h<=13, -23<=k<=23, -20<=l<=19	
Reflections collected	27911	
Independent reflections	6691 [R(int) = 0.0331]	
Completeness to theta = 67.679°	100.0 %	
Absorption correction	Semi-empirical from equivalents	
Max. and min. transmission	1.00000 and 0.48756	
Refinement method	Full-matrix least-squares on F^2	
Data / restraints / parameters	6691 / 0 / 408	
Goodness-of-fit on F^2	1.037	
Final R indices [I>2sigma(I)]	R_1 = 0.0614, wR_2 = 0.1748	
R indices (all data)	R_1 = 0.0788, wR_2 = 0.1939	
Extinction coefficient	n/a	
Largest diff. peak and hole	0.612 and -0.255 e.Å^{-3}	
CCDC deposition number	1535891	

Table S5. Selected torsion angles [°] for foldamer **4**.

C01-C07-OU-C0	-75.1(3)
C07-OU-C0-N1	170.0(2)
OU-C0-N1-C1A	-177.4(2)
C0-N1-C1A-C1	-58.6(3)
N1-C1A-C1-N2	136.3(2)
C1A-C1-N2-C2A	176.1(2)
C1-N2-C2A-C2	57.0(3)
N2-C2A-C2-N3	30.1(3)
C2A-C2-N3-C31	175.8(2)
C2-N3-C31-C32	-143.8(2)
C2-N3-C31-C36	94.5(3)
N3-C31-C32-C33	-179.0(2)
C36-C31-C32-C33	-56.4(3)
C31-C32-C33-C34	55.4(3)
C32-C33-C34-N4	-177.7(2)
C32-C33-C34-C35	-54.1(3)
N4-C34-C35-C36	177.4(2)
C33-C34-C35-C36	54.6(3)
N3-C31-C36-C35	177.5(2)
C32-C31-C36-C35	56.7(3)
C34-C35-C36-C31	-56.2(3)
C35-C34-N4-C37	117.6(3)
C33-C34-N4-C37	-118.7(3)
C34-N4-C37-C38	178.7(2)
N4-C37-C38-N1T	-147.6(2)

Table S6. Hydrogen bonds for foldamer **4** ethanol solvate [Å and °].

D-H...A	d(D-H)	d(H...A)	d(D...A)	<(DHA)
N3-H3...O0	0.86	2.41	3.098(3)	137.9
N1-H1...O4#1	0.86	2.42	3.234(3)	157.1
C1B2-H1B5...O2T#2	0.96	2.47	3.251(3)	138.8
N2-H2...O2T#2	0.86	2.37	3.190(3)	158.6
N3T-H3T...O4T#3	0.86	2.02	2.860(3)	165.6
O1E-H1OE...O1	0.82	1.97	2.778(3)	167.3
N4-H4...O1E#4	0.86	2.05	2.911(3)	173.8

Symmetry transformations used to generate equivalent atoms:

#1 -x+1,-y,-z+1 #2 -x+2,-y,-z+1 #3 -x+2,-y-1,-z+1

#4 -x+3/2,y-1/2,-z+3/2

References

1. J. Sponer, J. Leszczynski and P. Hobza, *Biopolymers* (Nucleic Acid Sci.), **2002**, 61, 3.
2. (a) M. R. Jones, N. C. Seeman and C. A. Mirkin, *Science*, **2015**, 347, 840; (b) P. Yin, H. M. T. Choi, C. R. Calvert and N. A. Pierce, *Nature*, **2008**, 451, 318; (c) J. T. Davis, *Angew. Chem., Int. Ed.*, **2004**, 43, 668; (d) S. Sivakova and S. J. Rowan, *Chem. Soc. Rev.*, **2005**, 34, 9; (e) A. G. Slater, Y. Hu, L. Yang, S. P. Argent,W. Lewis, M. O. Blunt and N. R. Champness, *Chem. Sci.*, **2015**, 6, 1562.
3. J. L. Sessler, C. M. Lawrence and J. Jayawickramarajah, *Chem. Soc. Rev.*, **2007**, 36, 314.
4. (a) B. J. Cafferty, I. Gallego, M. C. Chen, K. I. Farley, R. Eritja and N. V. Hud, *J. Am. Chem. Soc.*, **2013**, 135, 2447; (b) G. P. Spada, S. Lena, S. Masiero, S. Pieraccini, M. Surin and P. Samorì, *Adv. Mater.*, **2008**, 20, 2433; (c) C. C. Lee, C. Grenier, E. W. Meijer and A. P. H. J. Schenning, *Chem. Soc. Rev.*, **2009**, 38, 671; (d) V. L. Malinovskii, D. Wenger and R. Häner, *Chem. Soc. Rev.*, **2010**, 39, 410.
5. (a) S. H. Gellman, *Acc. Chem. Res*., **1998**, 31, 173; (b) D. J. Hill, M. J. Mio, R. B. Prince, T. S. Hughes and J. S. Moore, *Chem. Rev.*, **2001**, 101, 3893; (c) I. Huc, *Eur. J. Org. Chem.*, **2004**, 17; (d) S. Hecht and I. Huc, *Foldamers: Structure, Properties and Applications*, Wiley-VCH, Weinheim, **2007**; (e) I. Saraogi and A. D. Hamilton, *Chem. Soc. Rev.*, **2009**, 38, 1726; (f) H. Juwarker, J.-M. Suk and K.-S. Jeong, *Chem. Soc. Rev.*, **2009**, 38, 3316; (g) B. A. F. Le Bailly and J. Clayden, *Chem. Commun.*, **2016**, 52, 4852.
6. C. M. Goodman, S. Choi, S. Shandler and W. F. DeGrado, *Nat. Chem. Biol.*, **2007**, 3, 252.
7. See for example: (a) P. Chakraborty and U. Diederichsen, *Chem. - Eur. J.*, **2005**, 11, 3207; (b) Y. Ura, J. M. Beierle, L. J. Leman, L. E. Orgel and M. R. Ghadiri, *Science*, **2009**, 325, 73; (c) X. Li, Y. Kuang, H.-C. Lin, Y. Gao, J. Shu and B. Xu, *Angew. Chem., Int. Ed.*, **2011**, 50, 9365; (d) C. J. Serpell, M. Barlog, K. Basu, J. F. Fakhoury, H. S. Bazzi and H. F. Sleiman, *Mater. Horiz.*, **2014**, 1, 348; (e) D. Yuan, X. Du, J. Shi, N. Zhou and B. Xu, *Angew. Chem., Int. Ed.*, **2015**, 54, 5705; (f) O. Berger, L. Adler-Abramovich, M. Levy-Sakin, A. Grunwald, Y. Liebes-Peer, M. Bachar, L. Buzhansky, E. Mossou, V. T. Forsyth, T. Schwartz, Y. Ebenstein, F. Frolow, L. J. W. Shimon, F. Patolsky and E. Gazit, *Nat. Nanotechnol.*, **2015**, 10, 353.

8. (a) C. Toniolo, M. Crisma, F. Formaggio and C. Peggion, *Biopolymers (Pept. Sci.)*, **2001**, 60, 396; (b) I. L. Karle and P. Balaram, Biochemistry, **1990**, 29, 6747; (c) W. Mayr, R. Oekonomopulos and G. Jung, *Biopolymers*, **1979**, 18, 425; (d) E. Benedetti, A. Bavoso, B. Di Blasio, V. Pavone, C. Pedone, M. Crisma, G. M. Bonora and C. Toniolo, *J. Am. Chem. Soc.*, **1982**, 104, 2437.
9. (a) C. M. Venkatachalam, *Biopolymers*, **1968**, 6, 1425; (b) C. Toniolo, *CRC Crit. Rev. Biochem.*, **1980**, 9, 1; (c) G. D. Rose, L. M. Gierasch and J. A. Smith, *Adv. Protein Chem.*, **1985**, 37, 1.
10. I. L. Karle, *Acta Crystallogr., Sect. B: Struct. Sci.*, **1992**, 48, 341.
11. (a) V. Pavone, E. Benedetti, B. Di Blasio, C. Pedone, A. Santini, A.Bavoso, C. Toniolo, M. Crisma and L. Sartore, *J. Biomol. Struct. Dyn.*, **1990**, 7, 1321; (b) E. Benedetti, B. Di Blasio, V. Pavone, C. Pedone, A. Santini, A. Bavoso, C. Toniolo, M. Crisma and L. Sartore, *J. Chem. Soc., Perkin Trans. 2*, **1990**, 1829; (c) F. Formaggio, M. Crisma, C. Toniolo and J. Kamphuis, *Biopolymers*, **1996**, 38, 301; (d) E. Longo, A. Moretto, F. Formaggio and C. Toniolo, *Chirality*, **2011**, 23, 756; (e) E. Longo, M. Crisma, F. Formaggio, C. Toniolo and A. Moretto, *Polym. J.*, **2013**, 45, 516; (f) D. F. Kennedy, M. Crisma, C. Toniolo and D. Chapman, *Biochemistry*, **1991**, 30, 6541; (g) E. K. S. Vijayakumar and P. Balaram, *Biopolymers*, **1983**, 22, 2133; (h) K. Otoda, Y. Kitagawa, S. Kimura and Y. Imanishi, *Biopolymers*, **1993**, 33, 1337; (i) K. Kitagawa, T. Morita and S. Kimura, *Angew. Chem., Int. Ed.*, **2005**, 44, 6330.
12. (a) C. Toniolo and E. Benedetti, *Trends Biochem. Sci.*, **1991**, 16, 350; (b) S. C. Yasui, T. A. Keiderling, F. Formaggio, G. M. Bonora and C. Toniolo, *Biopolymers*, **1986**, 25, 79; (c) S. C. Yasui, T. A. Keiderling, F. Formaggio, G. M. Bonora and C. Toniolo, *J. Am. Chem. Soc.*, **1986**, 108, 4988.
13. (a) C. Toniolo, A. Polese, F. Formaggio, M. Crisma and J. Kamphuis, *J. Am. Chem. Soc.*, **1996**, 118, 2744; (b) M. C. Manning and R. W. Woody, *Biopolymers*, **1991**, 31, 569.
14. (a) J. Kypr, I. Keynovska, K. Bednarova and M. Vorlickova, in *Comprehensive Chiroptical Spectroscopy*, ed. N. Berova, P. L. Polavarapu, K. Nakanishi and R. W.Woody, Wiley, Hoboken, NJ, **2012**, vol. 2, pp. 575–586; (b) D. Voet, W. B. Gratzer, R. A. Cox and P. Doty, *Biopolymers*, **1963**, 1, 193; (c) J. N. Schimelman, D. M. Dryden, L. Poudel, K. E. Krawiec, Y. Ma, R. Podgornik, V. A. Parsegian, L. K. Denoyer, W.-Y. Ching, N. F. Steinmetz and R. H. French, *Phys. Chem. Chem. Phys.*,

2015, 17, 4589.

15. J. D. Augspurger, V. A. Bindra, H. A. Scheraga and A. Kuki, *Biochemistry*, **1995**, 17, 2566.
16. G. Marafon, D. Mosconi, D. Mazzier, B. Biondi, M. De Zotti and A. Moretto, *RSC Adv.*, **2016**, 6, 73650.
17. S. Matile, N. Berova, K. Nakanishi, J. Fleischhaner and R. W. Woody, *J. Am. Chem. Soc.*, **1996**, 118, 5198.
18. M. J. Webber, E. A. Appel, E. W. Meijer and R. Langer, *Nat. Mater.*, **2016**, 15, 13.
19. M.C. Burla, R. Caliandro, B. Carrozzini, G.L. Cascarano, C. Cuocci, C. Giacovazzo, M. Mallamo, A. Mazzone, G. Polidori, *J. Appl. Crystallogr.,* **2015**, 48, 306.
20. G.M. Sheldrick, *Acta Crystallogr. C,* **2015**, 71, 3.

1.3 Building supramolecular DNA-inspired nanowires on gold surfaces: from 2D to 3D[c]

The three-dimensional (3D) organization of molecules on surfaces remains an ongoing challenge in the field of materials science.[1] In particular, the molecular order and perfect positioning of different redox centres may be of fundamental importance in building artificial photosynthetic systems to control the direction of electronic flow.[2–4] Nature uses lipoproteins as a template to organize chlorophyll dyes in an optimal arrangement to avoid strong intermolecular interactions and to confer directionality to the electron transfer (ET) process. All the macromolecules found in nature are constructed by the self-assembly of different building blocks that capitalise on the formation of noncovalent and reversible interactions, including electrostatic, hydrophobic, van der Waals and metal–ligand interactions, hydrogen bonds, and aromatic π-stacking. Collectively, if sufficient in number, these weak interactions can yield highly stable assemblies.[5] A number of studies have investigated ET processes in supramolecular assemblies in solution, similar to those in nature, in which the interacting chromophores are held together by non-covalent interactions.[6] However, only electrochemical and spectro-electrochemical properties of 2D self-assembled monolayers (SAMs) covalently linked to a gold surface have been reported[7–16] and very few attempts have been made to build 3D supramolecular structures. McGimpsey et al.[17] reported the formation of multilayer thin films on gold via non-covalent interactions between a sulfurcontaining 2,6-dicarboxypyridine ligand, a metal ion, and other 2,6-dicarboxypyridine ligands, which were used as a means to incorporate one or more layers of pyrene chromophores into the film. This group demonstrated that these films were able to generate a photocurrent with quite high efficiency.[17,18] Also, Kimura et al. reported on the possibility of building multi-layered peptide films using hydrogen bonds.[19] To our knowledge, no other studies have reported an approach to obtain 3D supramolecular systems on a surface, especially systems containing peptides. We decided to use the thymine-adenine DNA base pair interaction to generate 3D supramolecular films composed of different 2D layers . To this end, we engineered two types of photocurrent-generating films on a gold surface, as shown in Figure 1. Films **1** and **2** consist of multi-layered systems in which the light-absorbing group (a zinc-tetraphenylporphyrin chromophore, ZnTPP) is noncovalently linked to a gold surface through thymine–adenine hydrogen bonds. These films were assembled by consecutive deposition of

[c] Reprinted (adapted) with permission from (Angew. Chem. 2019, 131, 7386). Copyright (2019) John Wiley and Sons."

each layer. In film **1**, two components are used: adenine linked to a lipoic acid (Lipo–A) to covalently bind the gold surface and ZnTPP linked to a thymine molecule (T–ZnTPP). Film **2** has an additional non-covalently linked layer: an undecapeptide analogue of the trichogin GA IV peptide[20] (defined hereafter as T–Tr(Lys)–A), in which the four glycine residues were replaced by four lysine residues to favour a helical conformation[21] (*Experimental Section*, Figure 6) and reduce conformational flexibility, and the two extremities were functionalized with thymine and adenine for binding of Lipo–A and T–ZnTPP, respectively.

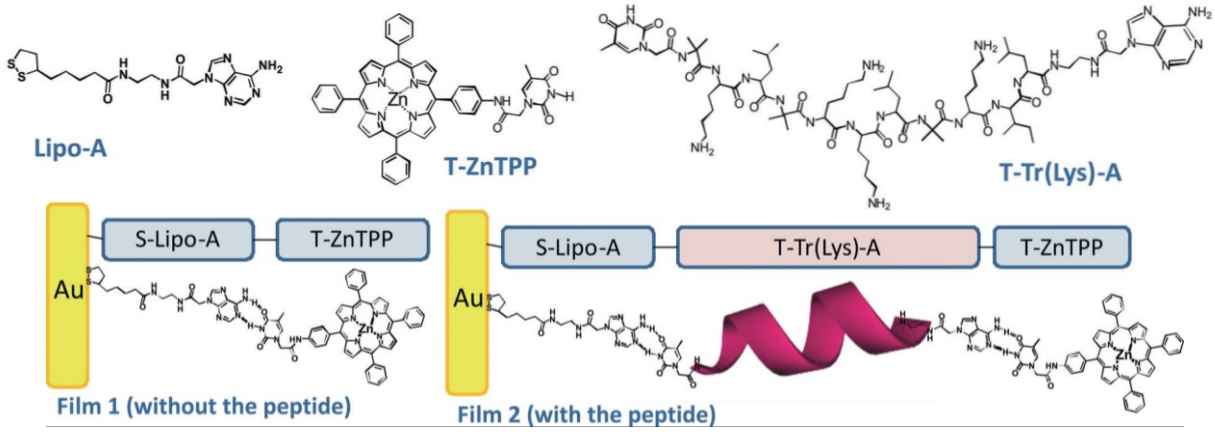

Fig. 1 Chemical structures of the building blocks used for the construction of films 1 and 2.

We have already synthetized similar systems in solution, which can form long filaments through complementary nucleobase interaction by properly tuning the experimental conditions.[22] Similarly, we avoided peptide self-assembly by using a diluted peptide solution (10 μm, e.g., 10 times below the threshold to get the self-assembly), thus obtaining a monolayer. Conductivity, infrared reflection absorption spectroscopy (IR-RAS), ultraviolet/visible (UV/Vis) and fluorescence spectroscopy measurements were carried out for films **1** and **2** after the formation of each layer. Cyclic voltammetry (CV) experiments performed in a 0.1m acetate buffer solution at pH 4.4 determined the Lipo–A density on the surface.[23] By measuring the amount of charge required for complete oxidation of adenine, a molecular density of (7.3 ± 0.8) $x10^{-10}$ mol cm^{-2} was obtained by taking into account the electrode effective surface area, which is 1.1 times larger than the geometric surface area (*Experimental Section*, Figures 8 and 9).[5] From this value, the mean area occupied by a single molecule on the surface is (23 ± 1) $Å^2$. This value can be used to determine the adenine orientation on the gold surface, considering the size of the adenine (treated as a parallelepiped) of 50 $Å^2$ in a horizontal arrangement and 22 $Å^2$ in a vertical arrangement.

From such evaluations, it was concluded that the Lipo–A molecules are densely packed with a perpendicular orientation to the gold surface. The Fourier transform infrared reflection absorption spectroscopy (FTIR-RAS) measurements assessed the presence of the peptide layer and determined its conformation and molecular orientation on the surface. The obtained FTIR-RAS spectrum is shown in Figure 2. Amide I and amide II bands appeared at 1673 cm^{-1} and 1543 cm^{-1}, respectively, confirming the presence of a peptide layer on the surface; in particular, these results indicate an ahelix positioned vertically on the substrate surface.[13b] Calculations based on the amide I/amide II absorbance ratios led to a tilt angle of the helical axis normal to the surface of 588. This value is generally obtained for quite well self-assembled peptide monolayers, indicating that the T–Tr(Lys)–A peptide forms a homogeneous film on the Lipo–A layer, despite the low peptide concentration used in the incubation solution to avoid multi-layer formation.[24–26] Interestingly, in film **1**, these signals are much less intense due to the lower content of amide bonds, confirming the presence of the intermediate layer of film **2**.

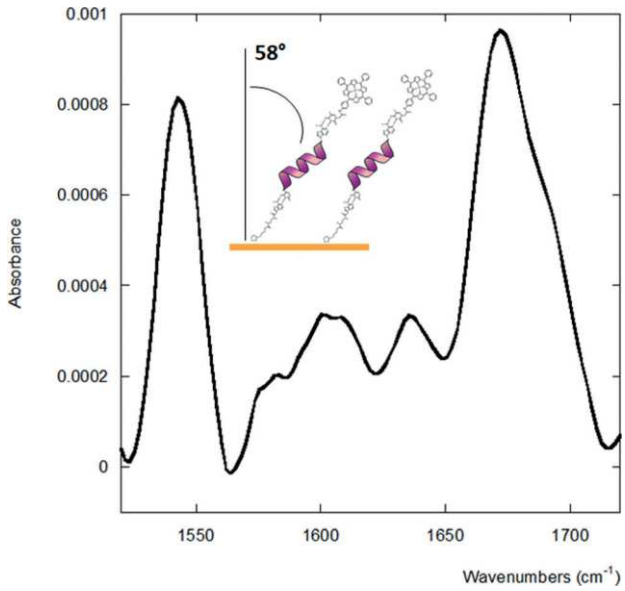

Fig. 2 IR-RAS spectrum of film **2**.

The difference between the spectrum obtained by the IR-RAS measurements of film **2** and that of film **1** is reported in Figure 10 in the *Experimental Section*. The presence of the third layer was evaluated by two different methods. First, the film was deposited on a gold (5 nm)-coated glass slide to perform absorption and fluorescence spectroscopy measurements. The absorption spectra not only confirmed the presence of the T–ZnTPP molecule but also could

be used to determine the amount of porphyrin molecules from the measured absorbance value.[27] This value was (7.0 ± 0.5) x 10^{-11} mol cm^{-2} for film **1** and (3.5 ± 0.8) x 10^{-11} mol cm^{-2} for film **2** (with the peptide). The fluorescence emission spectra confirmed that the absorption bands were those of the porphyrin ring (*Experimental Section*, Figure 11). The different surface densities of T–ZnTPP in films **1** and **2** were also measured by detaching the film from the gold surface by CV and analyzing the visible absorption spectrum of the electrolytic solution after film removal. From the absorption spectrum, the known solution volume and electrode immersion area and by taking into account the electrode surface roughness, the Γ values were determined. The results are reported in Figure 11 in the *Experimental Section* and in Table 1. Herein, to demonstrate the capability of our SAM to give rise to oxygen photoreduction, photocurrent generation measurements were performed in the ZnTPP absorption range. Upon illumination in the visible region and in the presence of a stable and non-corrosive electron donor (triethanolamine, TEOA), high cathodic currents were generated.[28]

System	Absorbance	Γ [mol cm-2] from absorbance on surface	Γ [mol cm^{-2}] from absorbance in solution	Photocurrent intensity [$nAcm^{-2}$]	Photocurrent Quantum Yield (430 nm)
Film 1	0.035	$7.0\pm0.5\times10^{-11}$	$8.5\pm1.5\times10^{-11}$	109	0.3% (0 V) 0.4% (-0.3 V)
Film 2	0.018	$3.5\pm0.8\times10^{-11}$	$4.1\pm1.3\times10^{-11}$	175	1.0% (0 V) 2.3% (-0.3 V)

Table 1 Results obtained using UV/Vis absorption spectroscopy in transmission mode (directly on the gold surface and after film removal in solution) and photoelectrochemical measurements.

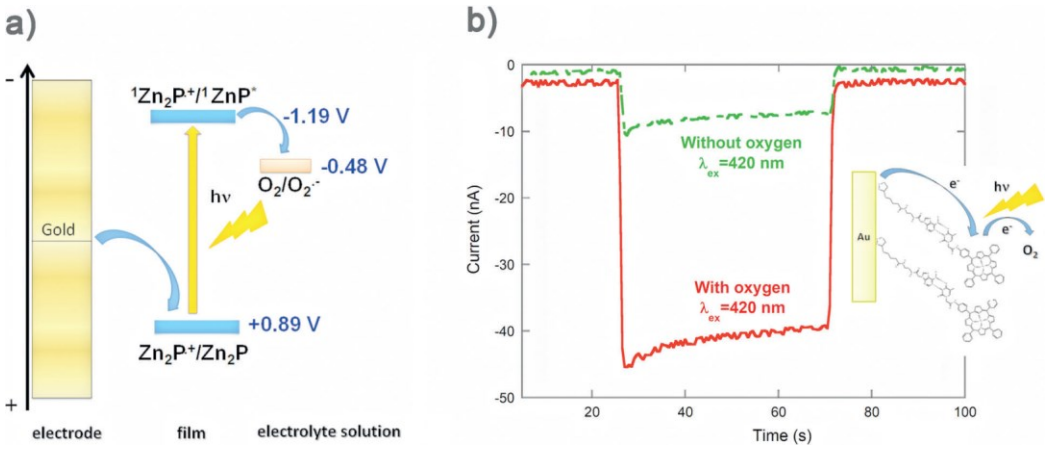

Fig. 3 (A) Photocurrent generation diagram indicating the path of the electron flow; (B) photocurrent

signal obtained by exciting film **1** at 420 nm before and after oxygen removal (inset: scheme of the electron flow).

The electron acceptor in the present system was hypothesized to be O_2 in solution (Figure 3a). To confirm this hypothesis, the same photocurrent generation experiments were performed by exciting the samples at 420 nm after fluxing argon into the solution for 20 minutes. The oxygen removal produced a large decrease in the photocurrent signal, confirming our assumption (Figure 3b).[29] Photocurrent responses of films **1** and **2** are shown in Figure 4.

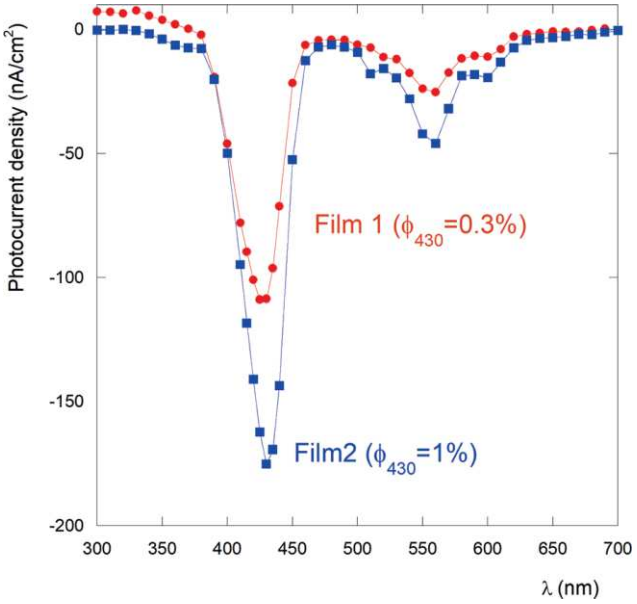

Fig. 4 Photocurrent action spectra of film **1**/Au/TEOA/Pt and film **2**/Au/TEOA/Pt cells.

The photocurrent action spectrum is very similar to the surface absorption spectrum of ZnTPP, confirming that ZnTPP is the photoexcited species responsible for the signal. Interestingly, a significant enhancement in the magnitude of the photocurrent upon inserting the peptide between Lipo-A and the deposited T-ZnTPP SAM was observed, with film **2** having a higher photocurrent value (175 nA cm^{-2} at 430 nm) than film **1** (109 nA cm^{-2} at 430 nm), despite the lower ZnTPP content confirmed by surface absorption spectroscopy both on the surface (Table 1) and after film removal in solution (Table 1). These values are higher than those reported for ZnTPP systems on both indium tin oxide (ITO)[30] and gold[16b,31] surfaces and represent a quantum efficiency at 430 nm of 1.0%for film **2** and 0.3%for film **1**.[32] When a negative potential was applied, the efficiency increased, reaching 2.3% for film **2** and 0.4% for film **1** at an applied potential of -0.3 V. These values are higher than those obtained with other porphyrin–peptide systems covalently linked to a gold surface.[15a,b] The reason for the higher photocurrent value obtained with the peptide-containing film might be

multi-fold. First, it is well known that the porphyrin-excited singlet state is quenched by the gold electrode via energy transfer. This process depends on distance and should be more efficient with film **1**, in which the ZnTPP is closer to the gold surface, giving rise to a lower photocurrent value. In contrast, the ET rate from the gold electrode to the resulting porphyrin cation radical decreases with an increase in chain length, favouring a higher photocurrent value in film **1**. Second, the presence of porphyrin aggregation enhances the rate of the nonradiative pathway in the excited state. The presence of J-aggregates in films **1** and **2** is suggested by the surface absorption spectrum (10 nm shift) and by the maximum photocurrent absorption (which is approximately 430 nm in both films). However, the mean molecular area occupied by the T-ZnTPP layer in the two films is different, being 240 $Å^2$ for film **1** and 476 $Å^2$ for film **2**. This difference suggests that the porphyrin molecular orientation on the gold surface in the two films is different (the size of the molecule is 480 $Å^2$ in a planar arrangement and 200 $Å^2$ in a vertical arrangement).[16b,31] It appears that, along with avoiding ZnTPP quenching, the peptide in film **2** also organizes the dyes in a different arrangement. It has already been demonstrated that porphyrin aggregation and molecular orientation influence photocurrent efficiency.[31,33] Third, the helical peptide spacer also has an active role in the electron transfer process. It is well known that photosynthetic proteins have mostly helical conformations and that this kind of secondary structure has very good electron transfer mediation properties, with tunneling parameters β reaching 0.02 $Å^{-1}$.[11c,34] Moreover, the peptide length of Tr(Lys) (estimated to be about 17 Å)[35] suggests the onset of a tunnelling mechanism for film **2**,[11b] favouring direct ET from the Au electrode to ZnTPP. Tr(Lys) is thus likely to have a promoting effect on the ET rate. It has been demonstrated that the intramolecular hydrogen bonds actively promote ET, and that helical peptides behave like molecular photodiodes, due to the dipole moment[14a] and spin-dependent effects along the helical axis.[36] However, even when the dipole moment and spin effect do not favor ET, this kind of molecular spacers can better mediate the ET process than other molecules (such as alkanethiols). Repeated photoexcitation of films **1** and **2** resulted in a 25–55% loss in photocurrent intensity after approximately 8 hours of measurements of alternating light/dark cycles and at different applied voltages. Interestingly, the day after the measurements, the photocurrent intensities of both films had recovered, suggesting that the films were stable (*Experimental Section*, Figure 13). The films were found to be very stable, giving rise to the same photocurrent intensity (using a fresh electrolyte solution) for more than two months (stored at ambient temperature). Therefore, the current decrease observed after several hours

of measurements was attributed to oxygen consumption. Notably, however, all these results clearly indicate that the bio-inspired noncovalent strategy developed in the present work is a potentially effective and simple means by which to engineer complex modular supramolecular SAMs to control film length for device fabrication purposes, including the conversion of incident light to electronic current and oxygen photoreduction for photodynamic therapy.

Experimental Section

Instruments and Methods

Electrochemistry. Cyclic voltammograms (CVs) were obtained by using a PG 310 potentiostat (Heka Elektronik). CV experiments were carried out at room temperature, adopting a standard three-electrode configuration with a SAM-coated gold electrode as the working electrode, a platinum wire as the auxiliary electrode, and Ag/AgCl as the reference electrode. Experiments to determine the surface area of Au gold foil electrodes were carried out with a 0.5 mM $K_3Fe(CN)_6$ solution in 1 M KCl at a sweep rate of 50 $mV \cdot s^{-1}$. Photocurrent measurements were carried out at room temperature using the three-electrode set-up described above, by using Na_2SO_4 (0.1 M) as supporting electrolyte and TEOA (50 mM) as the electron donor in solution. In this experiment, the SAM-modified electrode was irradiated with a Xe lamp (150 W) equipped with a monochromator and the generated photocurrent was detected by the voltammetric analyzer described above. The incident photon-to-current efficiency (IPCE) has been determined by using the following equation:[6]

$$IPCE(\%) = \frac{100 \cdot i(A/cm^2) \cdot 1240}{I(W/cm^2) \cdot \lambda(nm)}$$

where i is the measured photocurrent, I is the incident light power density, and λ is the incident wavelength (340 nm). The intensity of the incident light was evaluated with a Vector H410 Power Meter (Scientech, USA) and the yields of photocurrent generation were obtained by the following equation:[7]

$$\phi = \frac{\frac{i}{e}}{\frac{W \cdot \lambda}{h \cdot c}(1 - 10^{-A})}$$

where $I=W \cdot \lambda / h \cdot c$, is the number of photons per unit area and unit time, i is the photocurrent density, e is the elementary charge, λ the wavelength of light irradiation, A the absorbance of the adsorbed dyes at λ, W the light power irradiated at λ, c the velocity of light, and h the Planck constant.

CV experiments performed to determine the ZnTPP redox properties, were carried out at room temperature, adopting a standard three-electrode configuration with a SAM-coated gold electrode as the working electrode, a platinum wire as the auxiliary electrode, and an Ag wire

in contact with 0.01 M $AgNO_3$ solution in acetonitrile is used as a reference electrode. Ferrocene was used as an internal reference. Measurements were carried out by bubbling argon in the TBAP 0.1 M in CH_2Cl_2 electrolyte solution for at least 20 min prior the measurement.

Steady-state Fluorescence. Steady-state fluorescence experiments were carried out on a Fluoromax-4 spectrofluorimeter (Jobin-Yvon) operating in the single-photon counting mode. For the fluorescence measurements, the peptide SAMs were immobilized on a transparent glass coated with a 5-nm thick Au layer. The glass was mounted on a solid sample holder and the signal detected at 45°.

Circular Dichroism. CD spectra were recorded using a J600 spectropolarimeter from Jasco (Tokyo, Japan). The temperature was controlled at 25 ± 0.1 °C with a thermostatted cuvette holder. The reported CD signals were normalized with respect to peptide molar concentrations.

Fourier transform infrared reflection-absorption spectroscopy (FTIR-RAS). FTIR-RAS experiments were performed by using a Thermo-Scientific (mod. Is50) instrument (Thermo Scientific Inc., Madison, WI, USA), with a VeemaxTM III Variable Angle reflectance Accessory (Pike Technologies, Madison, WI, USA) and a mercury-cadmium-telluride (MCT) detector. Moreover, a polarized incident beam at an incidence angle of 80° with respect to the sample surface was used. A total of 516 scans, with a resolution of 2 cm^{-1}, were collected for each sample.

Synthesis and Characterization

Material

Spectrograde solvents (Carlo Erba) were exclusively used. Water was distilled and passed through a Milli-Q purification system. Other chemicals, triethanolamine (TEOA) (Fluka), potassium chloride (Carlo Erba), sodium sulphate (Carlo Erba), potassium ferricyanide (Aldrich) and potassium hydroxide (Aldrich) were all of reagent grade quality and used without further purification. Gold foil electrodes of 0.05 mm thickness were bought from Sigma-Aldrich and used for electrochemical measurements. Transparent glass coated with a 5-nm thick Au layer were Nanocs products and used for fluorescence measurements.

Preparation of self-assembled peptide thin films. Gold electrodes were etched for 15 min in a freshly prepared piranha solution (2:1 sulphuric acid/H_2O_2, *v/v*), rinsed with bidistilled water

and ethanol before immersion in the peptide solution for the SAM deposition. SAM-coated electrodes were prepared by dipping two cleaned gold electrodes into a 1 mM methanol solution of Lipo-A in a N_2 atmosphere. After 24 h, the electrodes were repeatedly (five times) rinsed with methanol to remove physically adsorbed molecules from the SAM, and immersed into: a 10 μM peptide solution in methanol for film **2** and a 0.1 mM T-ZnTPP solution for film **1**. After 24 h, the electrode containing film **1** (Au/Lipo-A···T-ZnTPP) was dried for 3 min under a gentle argon flow and was ready to be used, while the second electrode was let into the T-Tr(Lys)-A solution for 48 h. After this time, it was dipped into a 0.1 mM solution of T-ZnTPP in a N_2 atmosphere, in order to obtain the three layer system. Subsequent to 24 h, the electrode containing film **2** (Au/Lipo-A···T-Tr(Lys)-A···T-ZnTPP) was dried for 3 min under a gentle argon flow and was ready to be used.

Synthesis. We have developed a novel trichogin GA IV analog, The T-Tr(Lys)-A peptide, the primary structure of which is given in Figure 5, where the four Gly residues at position 2, 5, 6, and 9 were replaced by Lys residues, and two complementary nucleobases were linked at the N- and C-termini. In this synthetic effort we took advantage of an optimized SPPS protocol that allowed us to efficiently incorporate sterically hindered residues such as Aib. The peptide has been synthesized on a ethylendiamine-chlorotrytil resin. The N-terminus has been blocked with Thymine-acetic acid, synthesized as previously described.[5] The peptide, cleaved under mild conditions (hexafluoroisopropanol 30% in CH_2Cl_2) to preserve the side-chain protective groups, has been functionalized at its C-terminus by Adenine-acetic acid, prepared following the procedure described in a previous work.[5] Yield: 45%. Purity: 97%. Characterizations were performed by HPLC, ESI-MS analysis and NMR.

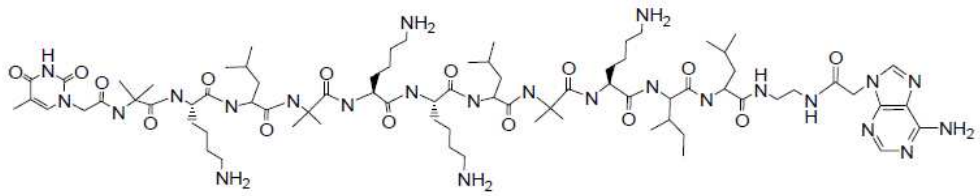

Fig. 5 Chemical structure of T-Tr(Lys)-A. Primary sequence: Thymine-CH_2-CO-Aib-Lys-Leu-Aib-Lys-Lys-Leu-Aib-Lys-Ile-Leu-NH-$(CH_2)_2$-NH-CO-CH_2-Adenine.

Circular Dichroism. The CD spectrum of T-Tr(Lys)-A in methanol, reported in Figure 6, exhibits a strong negative band at 204 nm and a weaker negative band at 222 nm, typical of right-handed helical conformations.[1] The native trichogin GA IV in methanol has an R value

($\theta_{222}/\theta_{204}$) of 0.4,[2] while the analog used in this work has R = 0.6, suggesting that Lys residues favor the helical conformation.[3]

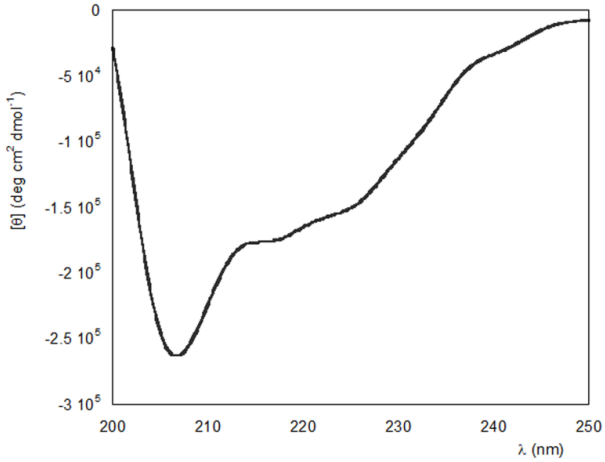

Fig. 6. CD spectrum of T-Tr(Lys)-A in methanol, c=1·10^{-4} M, l=0.1 cm.

We studied the self-assembly of T-Tr(Lys)-A as a function of peptide concentration by circular dichroism (Figure 7). Our CD analysis (Figure 7) registered aggregation (i.e., R>1) at concentrations above 0.2 mM. TEM analysis performed on the same solutions analyzed by CD confirmed that at R>1 molecular fibers are formed. Our analysis demonstrated that the peptide self-assembly occurs only above 0.1 mM. To obtain the monolayer for film **1**, a diluted solution (10 μM, 10 times less concentrated than the threshold for aggregation) was thus employed.

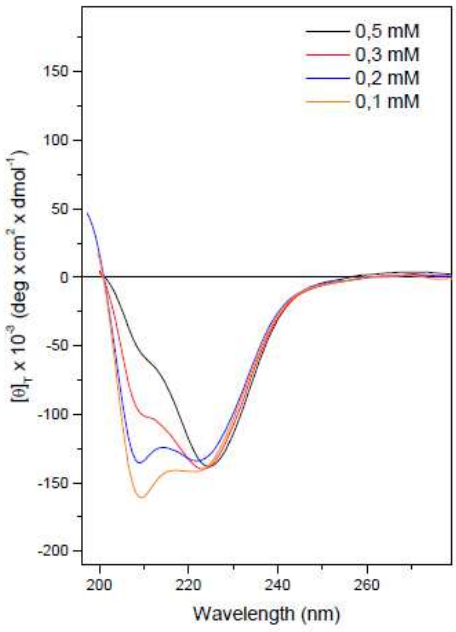

Fig. 7 Circular Dichroism spectra of T-Tr(Lys)-A as a function of increasing peptide concentration in 10:1 v/v acetonitrile/basic water (NaOH 0.1 M) solution.

Cyclic Voltammetry of lipo-adenine. The lipo-adenine (Lipo-A) density on the surface has been evaluated by CV experiments performed in a 0.1 M acetate buffer solution, pH 4.4. A typical CV curve obtained from this experiment is shown in Figure 8. When the gold electrode modified with the lipo-adenine monolayer is immersed in an acid solution and the potential is swept to sufficiently positive values, the first scan shows an oxidation peak with a maximum above 1.17 V, which corresponds to the oxidation of the adenine molecules on the electrode surface.

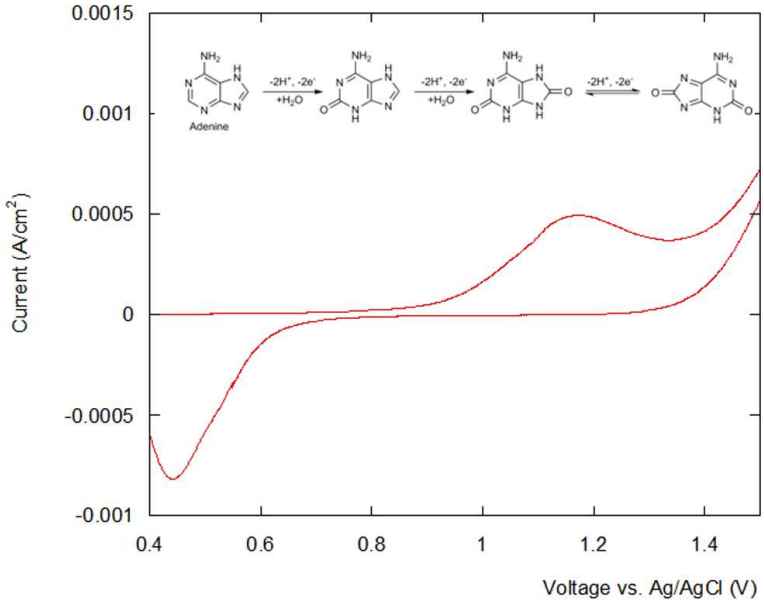

Fig. 8 Cyclic voltammetry experiments in a 0.1 M acetate buffer solution, pH 4.4. Inset: scheme of the electrochemical reactions involved. Scan rate: 100 mV/s.

As each molecule contains one adenine and that six electrons are involved in the oxidation process, the surface coverage of the electrode (ϕ) can be calculated from the peak area (i.e. the charge associated with the reduction process), by the following formula: $\phi=Q/nFA$, where Q is the peak charge, n is the number of electrons involved and A is the effective surface area. By measuring the charge amount required for complete oxidation of the adenine, a molecular density of $(7.3 \pm 0.8)\cdot 10^{-10}$ mol/cm^2 is obtained, by taking into account the electrode effective surface area. The surface area of Au gold foil electrodes was determined from the CV of a $K_4[Fe(CN)_6]$ standard solution, following the Randles-Sevcik equation:

$$i_p = 0.4463\, nFAC(nF\nu D/RT)^{1/2}$$

where i_p is the current maximum, n is the number of electrons transferred in the redox event, A is the electrode area in cm^2, F is the Faraday constant, D is the ferricyanide diffusion coefficient ($7.2 \cdot 10^{-6}$ cm^2/s),[4] C is the electrolyte concentration and v is the scan rate. We found that the electrode active surface is 1.1 times the geometric surface area of the electrode.

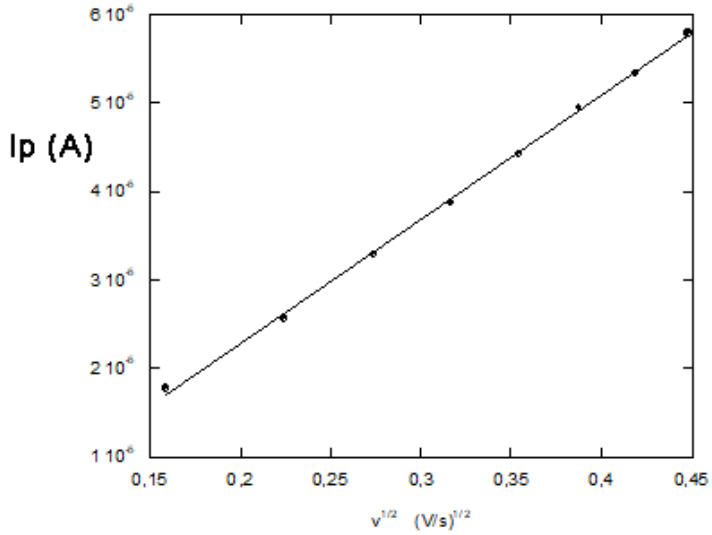

Fig. 9 Plot of the anodic peak current value, as a function of the root square of the scan rate of a $K_4[Fe(CN)_6]$ 50 mM standard solution.

RAS Measurements.

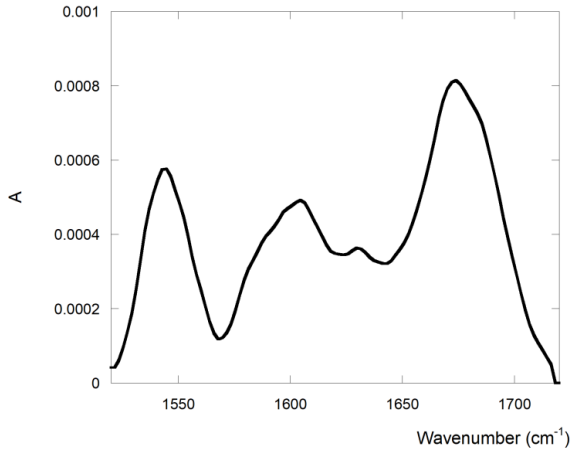

Fig. 10 IR-RAS spectral difference obtained from the spectrum of film **2** minus that of film **1**.

Absorbance and Fluorescence spectra. Figure 11 shows the absorption spectra of film **1** and film **2** on Au/glass substrates in transmission mode and of T-ZnTPP in methanol solution. The Soret band on the gold surface is broadened and red-shifted by 10 nm relative to the corresponding spectra in methanol. The porphyrin Q-bands were also observed. In general, a red shift is observed in J-aggregates of porphyrins (that is side-by-side porphyrin π-

aggregation). However, the red shift observed on gold surface is quite small compared to the one reported in solution,[5-7] indicating the moderate interaction among the porphyrins.

Steady state fluorescence spectra of film **1** and **2** on Au/glass substrates and of T-ZnTPP in methanol solution are shown in Figure 11. Both films exhibit the typical emission band of the ZnTPP fluorophore, with two maxima at 612 and 654 nm, which confirm the T-ZnTPP inclusion into the films. The fluorescence spectra on Au/glass surface are broader compared to one obtained in solution, and slightly red-shifted, suggesting aggregation among the porphyrins in both films.

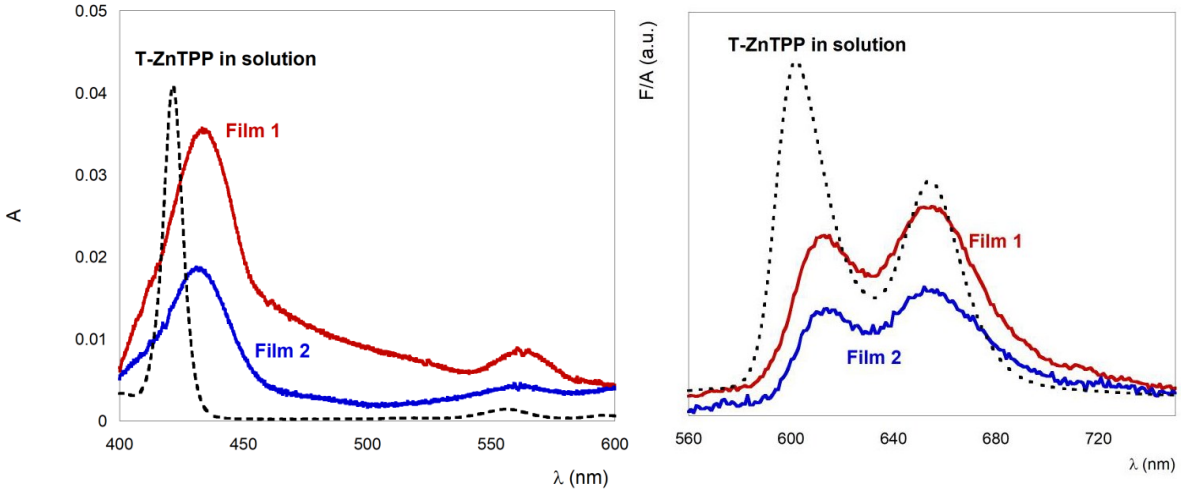

Fig. 11 Left: UV-visible spectra of film **1** and **2** on Au/glass surfaces in transmission mode and of T-ZnTPP in methanol solution. Right: corrected fluorescence spectra of film **1** and **2** on Au/glass substrate and of T-ZnTPP in methanol solution. λ_{ex}=422 nm in solution and 433 nm on surface. The spectra are normalized for comparison.

Cyclic Voltammetry of ZnTPP. Cyclic voltammetry of film **1** and **2** on gold surface was performed in CH_2Cl_2 containing TBAP 0.1 M with a sweep rate of 500 mV/s. Interestingly, irreversible oxidation peaks were observed at 0.89 V and 1.20 V for film **1**, while film **2** gave rise to two reversible oxidation peaks at 0.93 V and 1.23 V (Figure 12).

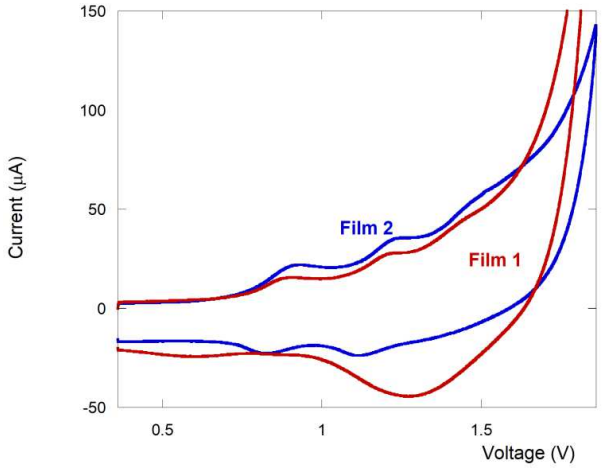

Fig. 12 Cyclic voltammetry experiments of film **1** and **2** on a gold foil surface performed in a CH_2Cl_2 solution containing TBAP 0.1 M. Scan rate: 500 mV/s.

These oxidation peaks are identified as $ZnTPP/ZnTPP^+$ and $ZnTPP^+/ZnTPP^{2+}$, respectively. Film **1** and **2** have been found to be not stable during CV measurements, showing no signal during the second scan. Taking dvantage of these properties, we have estimated the surface coverage, Γ, from the absorption spectrum of the ZnTPP in the electrolyte solution, measured after several CV scans (in order to be sure to have detached the whole film). The complete film removal from the surface was then verified by CV measurements in $K_3[Fe(CN)_6]$ solution. By knowing the solution volume and the electrode immersed area, taking into account the electrode surface roughness, we obtained the Γ values reported in Table 1.

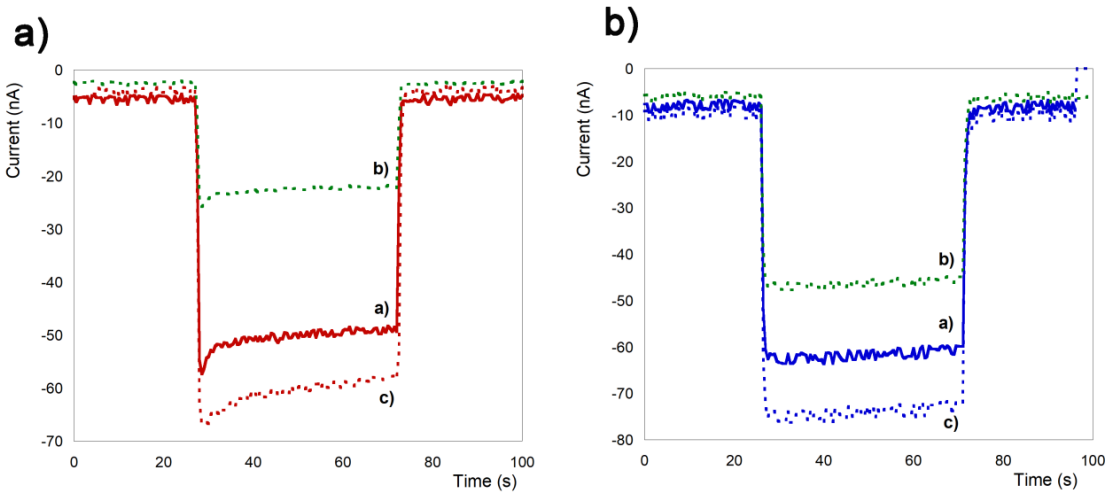

Fig. 13 Photocurrent signal obtained by exciting film **1** (a, left) and film **2** (b, right) at 420 nm: during the firstn wavelength scan (a), after several hours of measurements (b) and the two days after using fresh electrolyte solution (c).

References

1. J. Martin, M. Martin-Gonzalez, J. F. Fernandez, and O. Caballero-Calero, *Nat. Commun.,* **2014**, 5, 5130.
2. (a) M. Morisue, S. Yamatsu, N. Haruta, and Y. Kobuke, *Chem. Eur. J.,* **2005**, 11, 5563; (b) D. M. Guldi, *Chem. Soc. Rev.,* **2002**, 31, 22; (c)W. Kim, E. Edri, and H. Frei, *Acc. Chem. Res.*, **2016**, 49, 1634.
3. M. E. El-Khouly, E. El-Mohsnawy, and S. Fukuzumi, J. *Photochem. Photobiol. C*, **2017**, 31, 36.
4. (a) V. Balzani, A. Credi, and M. Venturi, *ChemSusChem*, **2008**, 1, 26; (b) J. Barber, *Chem. Soc. Rev.*, **2009**, 38, 185.
5. (a) J. M. Lehn, *Proc. Natl. Acad. Sci. USA*, **2002**, 99, 4763; (b) G. M. Whitesides, J. P. Mathias, and C. T. Seto, *Science*, **1991**, 254, 1312; (c) J. M. Lehn, *Science*, **2002**, 295, 2400; (d) G. M. Whitesides, and B. Grzybowski, *Science*, **2002**, 295, 2418.
6. (a) M. R. Wasielewski, *Acc. Chem. Res.*, **2009**, 42, 1910; (b) M. D. Ward, *Chem. Soc. Rev.*, **1997**, 26, 365.
7. (a) R. G. Nuzzo, and D. L. Allara, *J. Am. Chem. Soc.*, **1983**, 105, 4481; (b) L. H. Dubois, and R. G. Nuzzo, *Annu. Rev. Phys. Chem.*, **1992**, 43, 437; (c) M. D. Porter, T. B. Bright, D. L. Allara, and C. E. D. Chidsey, *J. Am. Chem. Soc.*, **1987**, 109, 3559; (d) E. P. Enriquez, C. H. Gray, V. F. Guarisco, R. V. Linton, D. K. Mar, and E. T. Samulski, *J. Vac. Sci. Technol.*, **1992**, 10, 2775.
8. Y. T. Long, E. A. Irhayem, and H. B. Kraatz, *Chem. Eur. J.*, **2005**, 11, 5186.
9. E. Gatto, A. Porchetta, M. Scarselli, M. De Crescenzi, F. Formaggio, C. Toniolo, and M. Venanzi, *Langmuir*, **2012**, 28, 2817.
10. (a) M. Venanzi, G. Pace, A. Palleschi, L. Stella, P. Castrucci, M. Scarselli, M. De Crescenzi, F. Formaggio, C. Toniolo, and G. Marletta, *Surf. Sci.*, **2006**, 600, 409; (b) E. Gatto, L. Stella, C. Baldini, M. Venanzi, C. Toniolo, and F. Formaggio, *Superlattices Microstruct.*, **2009**, 46, 34.
11. (a) N. Amdursky, *ChemPlusChem*, **2015**, 80, 1075; (b) A. Shah, B. Adhikari, S. Martic, A. Munir, S. Shahzad, K. Ahmad, and H. B. Kraatz, *Chem. Soc. Rev.*, **2015**, 44, 1015; (c) H. S. Mandal, and H. B. Kraatz, *J. Phys. Chem. Lett.*, **2012**, 3, 709.
12. "The Electrochemistry of Peptide Self-Assembled Monolayers": E. Gatto, M. Caruso, and M. Venanzi in *Handbook of Nanoelectrochemistry* (Eds.: M. Aliofkhazraei, A.

Makhlouf), Springer, Cham, **2016**.

13. (a) S. Sek, A. Tolak, A. Misicka, B. Palys, and R. Bilewicz, *J. Phys. Chem. B*, **2005**, 109, 18433; (b) J. Watanabe, T. Morita, and S. Kimura, *J. Phys. Chem. B*, **2005**, 109, 14416; (c) S. Sek, A. Sepiol, A. Tolak, A. Misicka, and R. Bilewicz, *J. Phys. Chem. B*, **2004**, 108, 8102; (d) Y. Arikuma, K. Takeda, T. Morita, M. Ohmae, and S. Kimura, *J. Phys. Chem. B*, **2009**, 113, 6256; (e) H. S. Mandal, and H. B. Kraatz, *Chem. Phys.*, **2006**, 326, 246; (f) Y. Arikuma, H. Nakayama, and T. Morita, *Angew. Chem. Int. Ed.*, **2010**, 49, 1800; *Angew. Chem.*, **2010**, 122, 1844; (g) Y. Arikuma, H. Nakayama, T. Morita, and S. Kimura, *Langmuir*, **2011**, 27, 1530.
14. (a) S. Yasutomi, T. Morita, Y. Imanishi, and S. Kimura, *Science*, **2004**, 304, 1944; (b) T. Morita, S. Kimura, S. Kobayashi, and Y. Imanishi, *J. Am. Chem. Soc.*, **2000**, 122, 2850; (c) K. Yanagisawa, T. Morita, and S. Kimura, *J. Am. Chem. Soc.*, **2004**, 126, 12780; (d) S. Yasutomi, T. Morita, and S. Kimura, *J. Am. Chem. Soc.*, **2005**, 127, 14564.
15. (a) H. Uji, Y. Yatsunami, and S. Kimura, *J. Phys. Chem. C*, **2015**, 119, 8054; (b) H. Uji, K. Tanaka, and S. Kimura, *J. Phys. Chem. C*, **2016**, 120, 3684; (c) M. Venanzi, E. Gatto, M. Caruso, A. Porchetta, F. Formaggio, and C. Toniolo, *J. Phys. Chem. A*, **2014**, 118, 6674.
16. (a) H. Imahori,Y. Nishimura,H. Norieda, H. Karita, I.Yamazaki, Y. Sakata, and S. Fukuzumi, *Chem. Commun.*, **2000**, 661; (b) H. Imahori, H. Norieda, Y. Nishimura, I. Yamazaki, K. Higuchi, N. Kato, T. Motohiro, H. Yamada, K. Tamaki, M. Arimura, and Y. J. Sakata, *J. Phys. Chem. B*, **2000**, 104, 1253; (c) H. Imahori, H. Norieda, H. Yamada, Y. Nishimura, Y. J. Sakata, and S. Fukuzumi, *J. Am. Chem. Soc.*, **2001**, 123, 100.
17. E. Soto, J. C. MacDonald, C. G. F. Cooper, and W. G. McGimpsey, *J. Am. Chem. Soc.*, **2003**, 125, 2838.
18. P. F. Driscoll, Jr., E. F. Douglass, M. Phewluangdee, E. R. Soto, C. G. F. Cooper, J. C. MacDonald, C. R. Lambert, and W. G. McGimpsey, *Langmuir*, **2008**, 24, 5140.
19. Y. Miura, G. C. Xu, S. Kimura, S. Kimura, S. Kobayashi, M. Iwamoto, Y. Imanishi, and J. Umemura, *Thin Solid Films*, **2001**, 393, 59.
20. C. Peggion, F. Formaggio, M. Crisma, R. F. Epand, R. M. Epand, and C. Toniolo, *J. Pept. Sci.*, **2003**, 9, 679.
21. M. De Zotti, B. Biondi, C. Peggion, F. Formaggio, Y. Park, K. S. Hahm, and C.

Toniolo, *Org. Biomol. Chem.*, **2012**, 10, 1285.

22. (a) G. Marafon, D. Mosconi, D. Mazzier, B. Biondi, M. De Zotti, and A. Moretto, *RSC Adv.*, **2016**, 6, 73650; (b) G. Marafon, I. Menegazzo, M. De Zotti, M. Crisma, C. Toniolo, and A. Moretto, *Soft Matter*, **2017**, 13, 4231.
23. A. M. Oliveira-Brett, V. Diculescu, and J. A. P. Piedade, *Bioelectrochemistry*, **2002**, 55, 61.
24. M. Kai, K. Takeda, T. Morita, and S. Kimura, *J. Pept. Sci.*, **2008**, 14, 192.
25. S. Okamoto, T. Morita, and S. Kimura, *Langmuir*, **2009**, 25, 3297.
26. K. Takeda, T. Morita, and S. Kimura, *J. Phys. Chem. B*, **2008**, 112, 12840.
27. F. Sabuzi, V. Armuzza, V. Conte, B. Floris, M. Venanzi, P. Galloni, and E. Gatto, *J. Mater. Chem. C*, **2016**, 4, 622.
28. In general TEOA solutions give rise to anodic photocurrent. However, it has been demonstrated in the literature that different porphyrin SAMs favor ET to O_2 in solution, due to the similar electrochemical potential of TPP and TEOA.
29. A. Vecchi, E. Gatto, B. Floris, V. Conte, M. Venanzi, V. N. Nemykin, and P. Galloni, *Chem. Commun.*, **2012**, 48, 5145.
30. (a) H. Yamada, H. Imahori, Y. Nishimura, I. Yamazaki, and S. Fukuzumi, *Adv. Mater.*, **2002**, 14, 892; (b) H. Imahori, M. Kimura, K. Hosomizu, T. Sato, T. K. Ahn, S. K. Kim, D. Kim, Y. Nishimura, I. Yamazaki, Y. Araki, O. Ito, and S. Fukuzumi, *Chem. Eur. J.*, **2004**, 10, 5111.
31. H. Imahori, T. Hasobe, H. Yamada, Y. Nishimura, I. Yamazaki, and S. Fukuzumi, *Langmuir*, **2001**, 17, 4925.
32. The quantum efficiency has been calculated using the absorption values obtained by UV/Vis measurements on surface. Using the surface coverage obtained by CV measurements, higher quantum efficiencies are obtained, with the film **2** value still higher than that of film **1**.
33. B. J. Walker, A. Dorn, V. Bulovic, and M. G. Bawendi, *Nano Lett.*, **2011**, 11, 2655.
34. M. Kai, K. Takeda, T. Morita, and S. Kimura, *J. Pept. Sci.*, **2008**, 14, 192.
35. C. Toniolo, C. Peggion, M. Crisma, F. Formaggio, X. Shui, and D. S. Eggleston, *Nat. Struct. Biol.*, **1994**, 1, 908.
36. (a) A. C. Aragonès, E. Medina, M. Ferrer-Huerta, N. Gimeno,M. Teixidò, J. L. Palma, N. Tao, J. M. Ugalde, E. Giralt, I. Dìez-Pèrez, and V. Mujica, *Small*, **2017**, 13, 1602519; (b) M. Kettner, B. Göhler, H. Zacharias, D. Mishra, V. Kiran, R. Naaman, C.

Fontanesi, D. H.Waldeck, S. Sek, J. Pawlowski, and J. Juhaniewicz, *J. Phys. Chem. C*, **2015**, 119, 14542; (c) F. Tassinari, D. R. Jayarathna, N. Kantor-Uriel, K. L. Davis, V. Varade, C. Achim, and R. Naaman, *Adv. Mater.*, **2018**, 30, 1706423.

2.1 From self-assembled peptide-ynes to peptide polyacetylenes and polydiacetylenes

Amino acids, sugars, lipids, and nucleic acids are naturally occurring bioactive and biocompatible compounds. These properties make them excellent building blocks for the development of novel materials. In recent years, due to these characteristics, peptide-based compounds became a topic of intensive research[1] mainly because peptides exhibit great potential as bio-based alternatives to other types of currently used synthetic materials. When rationally designed, peptide-based materials were shown to offer unprecedented advantages as those to provide modular and generalizable platforms with tunable mechanical, chemical, and biological properties.[2] Whether peptides are made up exclusively of amino acids or are hybridized with other functional moieties (i.e., polymerizable sites), they are known to adopt well specific conformations and interesting self-assembly morphologies, thus providing useful platforms for the development of nanoscale materials.[3–5] Over the last decade, this class of hybrid compounds was extensively investigated by combining their routinely easy peptide synthesis and the possibility to conveniently design a specific secondary structure which may possess a precise function.[6–16] We focused our attention on the chemical polymerizations of triple-bond functionalized peptides that can produce colored (optical absorption above 380 nm) polymers with repeated peptide units joined together by conjugated double or alternating double–triple bonds.[17–25] As a result, such peptide-based polyacetylenes (PAs) or polydiacetylenes (PdAs) are expected to be electronically active and may be good candidates for the preparation of novel materials. Therefore, we rationally varied the polymerizability of the peptide–acetylene monomers by changing the number and types of a-amino acids within the monomers with the aim at exploring the monomer templation effect on the polymerization efficiency and the properties of the resulting materials.

Results and discussion

The first part of this work was devoted to the preparation of peptideyne monomers with a strong propensity to adopt β-sheet conformations. On the basis of the extensive literature existing on oligo- and polypeptides,[26–28] we decided to evaluate the combination of four strongly b-sheet promoter a-amino acids, namely Val, Leu, Phe, and Cys(Me) (S-methyl cysteine).[29–33] In the self-assembly process, both non-covalent side-chain interactions and C=O···H-N intermolecular H-bonds are known to play fundamental roles in molecular

recognition and formation of regular microstructures. Importantly, as we worked in organic media, intermolecular C=O···H-N H-bonds force the molecules to pack each other, while hydrophobic side chains may result to be, at least partially, solvated. Thus, in the sequences we selected for our study the dominant force driving self-assembly is related to the number of amide units present in the monomeric peptides. Amino acid side-chain interactions may help in the formation of microstructures at a later stage. Therefore, we designed and synthesized the following four peptide-ynes: Boc-L-Val-NH-prop (**1**), Boc-L-Phe-L-Val-NH-prop (**2**), Boc-L-Cys(Me)-L-Phe-L-Val-NH-prop (**3**), Boc-L-Leu-L-[Cys(Me)]-LPhe-L-Val-NH-prop (**4**) (prop, propargyl) by following a step-by-step solution protocol. All of them are characterized by a propargyl amine moiety covalently linked to their C-termini (Figure 1). It is worth noting here that the effect of the Boc-NH-urethane group on peptide self-association is not easy to be established. This is related to the ambiguous (partly hydrophobic, the *tert*-butyl moiety, and partly hydrophilic, the -OCONH- function) nature of this type of Na-protection.[34] All of the monomers were treated under appropriate experimental conditions to produce the corresponding PAs or PdAs (Figure 1) as discussed in the next sections.

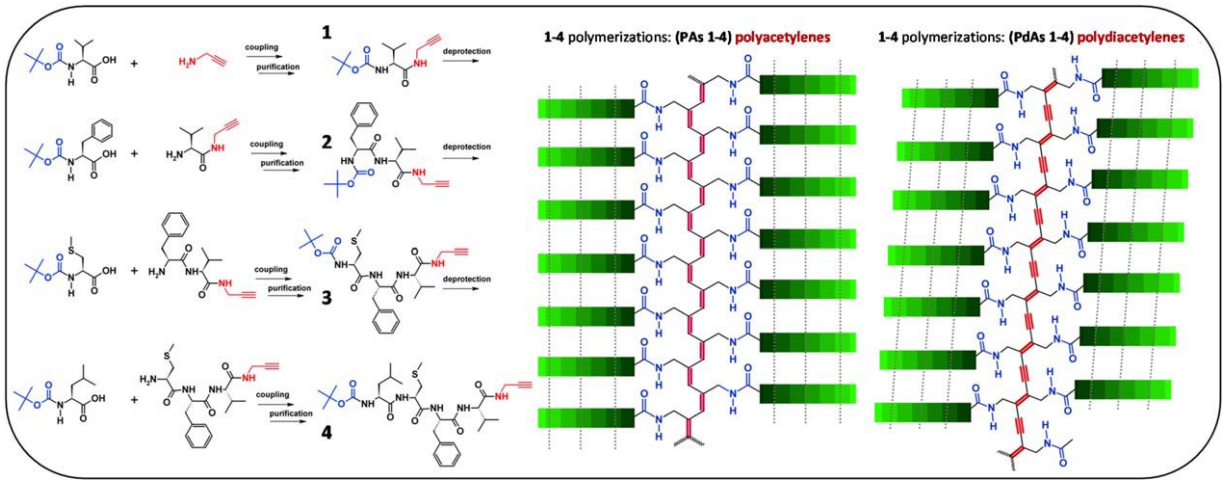

Fig. 1 Left: Syntheses and chemical structures of monomers **1**–**4**. Right: Schematic representations of the polyacetylenes (PAs) and polydiacetylenes (PdAs) polymers. Highlighted in red are the novel, unsaturated and conjugated, polymeric backbones.

Characterization of peptide-yne monomers

In Figure 2A the ^{1}H NMR spectra of peptide-yne monomers **1**-**4** are reported. As a function of the peptide main-chain length, the related NMR spectra showed different signals, which belong to the different α-amino acid constituents. It is worth noting that the NMR spectra

were recorded in CH_3CN-d_3. The use of this solvent of low polarity emphasized the already strong, intrinsic tendency to self-aggregation of these compounds, especially evident for **3** and **4** (as suggested by the presence of broad signals).[35] We also measured the solid-state FT-IR absorption spectra for all of the samples. As it can be seen from Figure 2B, in the amide N-H stretching range (amide A, 3400-3200 cm^{-1}) and in the amide C=O stretching range (amides I-II, 1700-1500 cm^{-1}) all of the peptide bonds of **1**-**4** are involved in intermolecular H-bonds typical of β-sheet-like 3D-structures.[36–38] In particular, all of the amide A and I-II bands of 1 to 4 move progressively to higher energies (amide A: 3303 to 3268 cm21; amide I: 1660 to 1625 cm^{-1}; amide II: 1540 to 1522 cm^{-1}). This overall feature is particularly pronounced for **2**-**4**. This observation suggested that a high supramolecular organization took place in the solid phase for the longest compounds. To prove that this organization may occur in solution as well, we performed CD experiments in different solvents. More specifically, we made use of MeOH (a competitor for H-bond formation) to avoid aggregation and detect the conformation of the isolated, solvated molecule, and THF to promote the onset of intermolecular H-bonds and observe the overall supramolecular organization. The results are illustrated in Figure 2C. In the CD experiments carried out in MeOH (at 1.5 mM concentration for all of the four compounds) we obtained different profiles for **1**-**4**. These distinct features are due to the different amino acid sequences (intrinsic chirality of each residue) and peptide lengths (formation of chiral secondary structures) characteristic of peptides **1**-**4** accompanied by the presence in **2**-**4** of the Phe benzyl chromophores, the electronic transitions of which in the far-UV region are known to overlap those of the peptide group.[33,39]

In THF, however, all of the four compounds exhibited similar CD curves with an intense negative maximum at 230 nm which we attributed to a β-sheet-like conformation (Figure 2D).[40,41] This information suggested that **1**-**4** may self-aggregate in this less polar solvent following a similar molecular recognition pathways. Moreover, not surprisingly, it also indicates that the peptide tendency for β-sheet formation is enhanced in THF relative to MeOH. On the basis of the observations obtained from the CD spectroscopy, we decided to investigate the morphological organization of **1**-**4** in THF. To explore this phenomenon, we prepared a set of THF solutions at different concentrations with the aim at finding the corresponding critical concentration for each compound needed to obtain organogels. In the organogel state, the overall non-covalent interactions (especially those of the H-bonding type) may cooperatively induce formation of ordered nanostructures able to entrap the solvent. After several attempts, we found stable organogels for each compound at the following

critical concentrations (in THF solution): **1**, 15 mM; **2**, 10 mM; **3**, 7 mM; **4**, 5 mM. These values for the critical concentration gave direct information on the intrinsic tendency of each compound to self-aggregate and, in particular, highlighted that **4** displayed the optimal conformational geometry to cooperatively induce gelation of the mixture at the lowest concentration with respect to those of the other compounds.

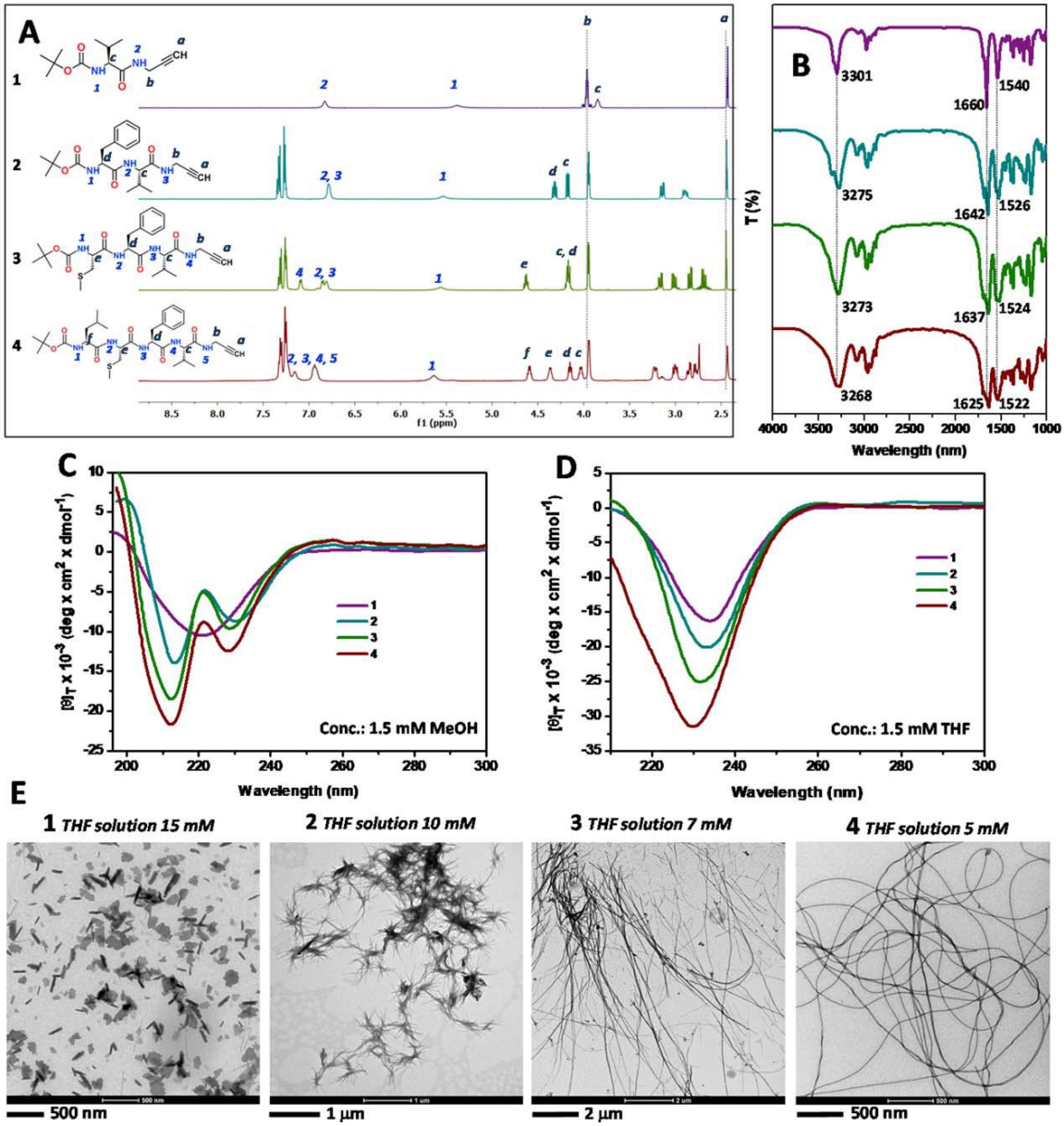

Fig. 2 (A-D) ^{1}H NMR (recorded in CH_3CN), solid-state FT-IR absorption and CD (recorded in MeOH and THF) spectra, respectively, of compounds **1** (purple), **2** (blue), **3** (green), and **4** (red). (E) TEM images of compounds **1**–**4**.

To prove the formation of organized self-assembled structures, we run transmission electron microscopy (TEM) experiments. The results, reported in Figure 2E for the four compounds, were recorded for their specific critical concentration values. The analyses indicated the

occurrence of different self-assembled morphologies. The TEM image of compound **1** revealed formation of a flake-like structure, while compounds **2**-**4** are characterized by fiber-like structures. In particular, long, but not well defined, fibers were obtained for **3**, while **4** afforded accurately defined, regular and long fibers. The overall results obtained from the chemical, physical, and microscopic characterizations performed for the **1**-**4** monomers may be summarized as follows: (i) according to their increased main-chain length, similar strands of H-bonded networks, typical of β-sheet-like structures, are formed in organic solvents for all of the monomers. Interestingly, comparable typologies of intermolecular interactions are found for all of the monomers at both low and high monomer concentrations; (ii) despite the occurrence of similar β-sheet-like H-bonding interactions, the longest peptides (**3** and **4**) afforded more ordered microstructures under their critical self-assembly conditions. This finding may suggest the onset of a templating effect that is progressively induced by the presence of more units (from **1** to **4**) of β-sheet supporting amino acids in the peptide backbone. As a consequence, we now have in our hands a system where the alkyne units are strictly self-assembled with a supramolecular geometry imposed by the corresponding conjugated peptide. Under these conditions, we may consider that polymerization of the triple bonds is controlled by a template effect generated by the molecular preorganization of the **1**-**4** monomers.

Peptide polyacetylenes

We applied the well established acetylene polymerization via rhodium catalysis[42–50] to monomers **1**-**4** following the schematic representation illustrated in Figure 3A. As it is known from this type of polymerization, depending on the catalyst involved, four unsaturated chains of different conformers may be obtained: *cis-transoid*, *trans-cisoid*, *trans-transoid*, and *cis-cisoid* forms (Figure 3B).[44]

The Rh(I) catalyst was suggested as being able to induce a stereospecific polymerization for acetylenes to afford selectively cis-transoid polyacetylene isomers.[51] Thus, what we expected from the β-sheet peptide-yne polymerizations induced by the Rh catalyst was formation of *cis-transoid* polyacetylenes with peptides precisely aligned laterally, with respect to the unsaturated backbone, along their parallel β-sheet axis (Figure 3C, example for polymer **PA 1**).

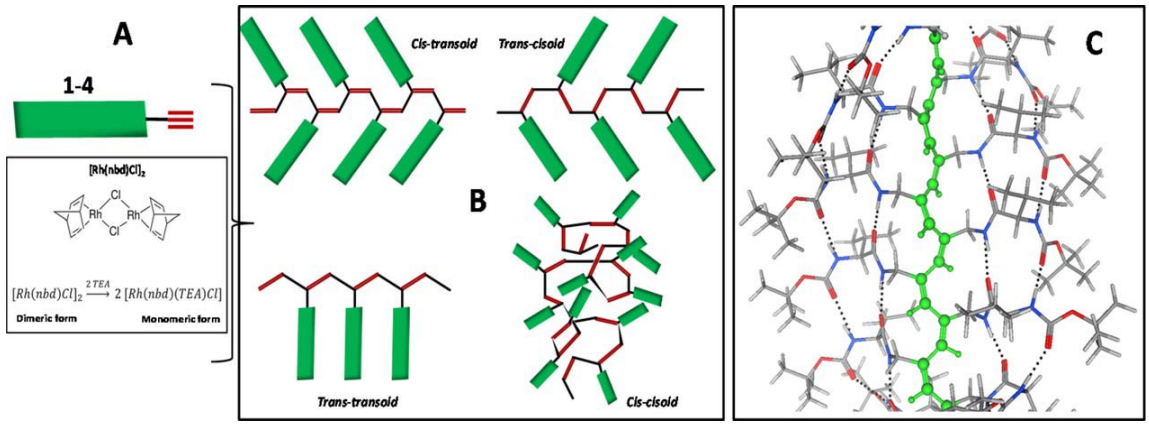

Fig. 3 (A) Chemical structure of the catalyst and its activation by means of the co-catalyst. (B) Schematic representation of the possible conformations adopted by the polyacetylene backbone. (C) Energy minimized structures for the cis-transoid **PA 1**, highlighting the unsaturated backbone and all peptide molecules aligned in the parallel b-sheet conformation.

With this geometry in mind, we also believed that longer peptides should generate more stable structures extra-stabilized by formation of multiple H-bonded interactions between all of the amide groups present in the peptides. Clearly, one of the chemical polymerization pre-requisites is to run the reaction at high monomer concentration. Under these conditions, we already demonstrated that monomers **1**-**4** are susceptible to formation of organized packed structures (organogels). To explore the role of a molecular pre-organization induced by the supramolecular self-assembly of the monomers, we carried out all polymerizations for peptide-ynes (**1**-**4**) at the concentration 0.1 M in THF at 55°C. Under these conditions, all monomers are above their minimum critical concentration, but at temperature 50°C their organogel organization are in the molten state, resulting in a viscous solution or in a solid mixture. After the addition of the catalyst and cocatalyst to the molten organogel solutions, polymerizations proceeded rapidly for monomers **1**-**3** (very dense mixtures were obtained after few minutes of reactions). Conversely, monomer **4** did not undergo this polymerization process. The polymers were collected after precipitation upon MeOH addition and centrifugation. After drying the polymers, we took optical microscope images of the solid materials.

As can be seen from Figure 4, **PA 1**–**3** displayed a yellow/orange color[21] and are present in the form of flakes. We proceeded with the morphological characterization of the polymers by using TEM. The three polymers were dissolved at low concentration in a mixture of DMF/THF, deposited on a TEM grid, and let stand to dryness.

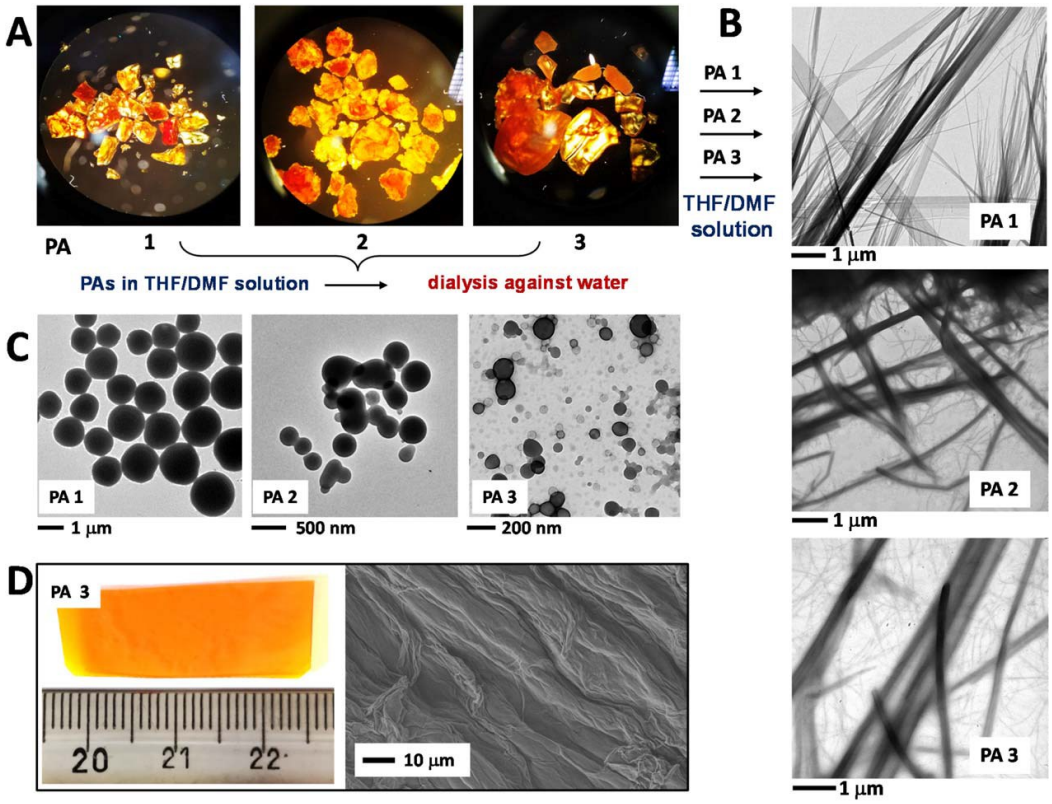

Fig. 4 (A) Optical microscope images of **PA 1**–**3**. (B) TEM images of **PA 1**–**3** in diluted DMF/THF mixtures. (C) TEM images of aqueous solutions of self-assembled **PA 1**–**3**. (D) Macroscopic material from processed **PA 3** and its SEM characterization.

The results are displayed in Figure 4B, which shows formation of linear assemblies of fibers for all samples. In particular, for **PA 1** small fibers were detected prior to their aggregation into larger assemblies, while **PAs 2** and **3** displayed a tendency to aggregate in wide, linear assemblies. We may assume that the solid flakes of polymers obtained after centrifugation would be formed by highly packed and organized polymeric chains kept together in fibrillar-like aggregates. Interestingly, when the organic mixtures were dialyzed against water, the polymeric materials re-assembled in nanoparticle-like structures with the diameter decreasing from **PAs 1** to **3** (Figure 4C). We succeeded in processing the polymers by moulding them into appropriate shapes. As an example, by dissolving **PA 3** at high concentration in DMF (dense homogeneous solution), placing this solution in an appropriate Teflon-covered state, and subsequently waiting for an aging time under a high-vacuum oven at 45°C, an orange-transparent and macroscopic material was obtained (Figure 4D). The SEM analysis highlighted formation of ordered aligned microscopic fibers extended over all of the material surface (Figure 4D). To our knowledge, this is the first example of a processable peptide based polymer, which results in large-scale fabrication of a bioinspired optical material. We

are planning to study its potentialities as material in a future work. **PAs 1-3** were characterized on the basis of their molecular weights and spectroscopic features. In Figure 5, we illustrate the results of the SEC analyses after polymerization. They highlighted the polymer molecular weight decrease as a function of the elongation of the corresponding monomeric peptide-ynes. A longer time of polymerization did not affect significantly the polymer lengths. In all cases, polymerization is almost complete after 5 h of reaction. The recovered material is quantitative for **PA 1** (1000 monomer units for polymer chain), while the yield decreases for **PAs 2** (400 monomer units for polymer chain) and **3** (80 monomer units for polymer chain). These results, together with the absence of reactivity for **4**, suggested that steric hindrance, combined with an efficient molecular packing, may decrease the polymerization efficiency. It is worth noting that Boc-Ala-NH-prop (similar to our **1** monomer) was used by Masuda and coworkers[50] to promote PA formation. In their work, the authors reported molecular weights similar to those found by us for monomer **1**. To our knowledge, studies on any β-sheet forming peptide, directly conjugated to an unsaturated polymer backbone, was not reported in the literature. **PAs 1-3** were characterized by solid-state FT-IR absorption (Figure 5A). The results of the N-H and C=O stretching regions indicated increasing β-sheet-like H-bonding interactions from **PA 1** to **PA 3** (both frequency maxima shift to lower wavelengths). The UV-Vis absorption spectra of **PAs 1-3** were recorded in DMSO to minimize the backbone···backbone interactions between the polymeric chains. The results reported in Figure 5B indicated that **PA 1** is characterized by an absorption maximum at 325 nm, while **PA 2** by a shoulder at the same wavelength and a maximum at 430 nm. Finally, **PA 3** displayed only the absorption maximum at 430 nm. The presence of a maximum at 325 nm suggested a less efficient conjugation in the unsaturated polymer backbone, while that at 430 nm indicated a more favorable conjugation between the double bonds of the polymer backbone. Thus, we may assume that the peptide segments contained in **PA 1** are randomly interacting with each other along their unsaturated backbone, probably due to the good solvation effect of DMSO that competes with all of the intra- and intermolecular H-bonding networks of **PA 1**. This solvation effect may be the reason for the poor conjugation in the corresponding polyacetylene that will tend to adopt many different conformations. On the other hand, in **PA 2** and **3** (**PA 3** more efficiently than **PA 2**) the corresponding peptide chains, even under a remarkable solvation, were able to efficiently (intramolecularly) interact along their parallel β-sheet axis thus to drive the unsaturated backbone in the preferred all-trans conformation. These results were confirmed by the CD

analysis, which showed that, despite their higher length with respect to that of **PA 1**, polymers **PAs 2** and **3** displayed a strong chiroptical positive signal with a maximum at 430 nm. These results highlight a steric-hindrance effect on the polymerization efficiency (shortest monomers produced longest polymers). In contrast, we observe that a positive stabilizing effect to the *transoid* PA conformation (with high electronic conjugation) is induced by the longest monomers. On the basis of these data, we conclude that **2** and especially **3**, once covalently connected to the unsaturated-conjugated system, are parallelly aligned along the PA backbone. This disposition efficiently templates them along all their amino acid sequence in two strands of an intramolecular, parallel β-sheet (one for each side of the unsaturated PA backbone). We believe that the overall alignment of the H-bonding interactions would represent the driving force for the stabilization of **PAs 2** and **3** in their *transoid* isomeric form.

run/entry	$[M]_0$ (mol/L)	$[M]_0/[Cat]$	temp (°C)	time	yield (%)	M_n	M_w/M_n
1 (**1** THF)	0.1	300	50	5h	95	232000	2.36
2 (**1** THF)	0.1	300	50	24h	97	244100	2.23
1 (**2** THF)	0.1	300	50	5h	72	123400	2.44
2 (**2** THF)	0.1	300	50	24h	76	135300	2.36
1 (**3** THF)	0.1	300	50	5h	58	39100	2.63
2 (**3** THF)	0.1	300	50	24h	61	41300	2.49
1 (**4** THF)	0.1	300	50	5h	0	-	-
2 (**4** THF)	0.1	300	50	24h	0	-	-

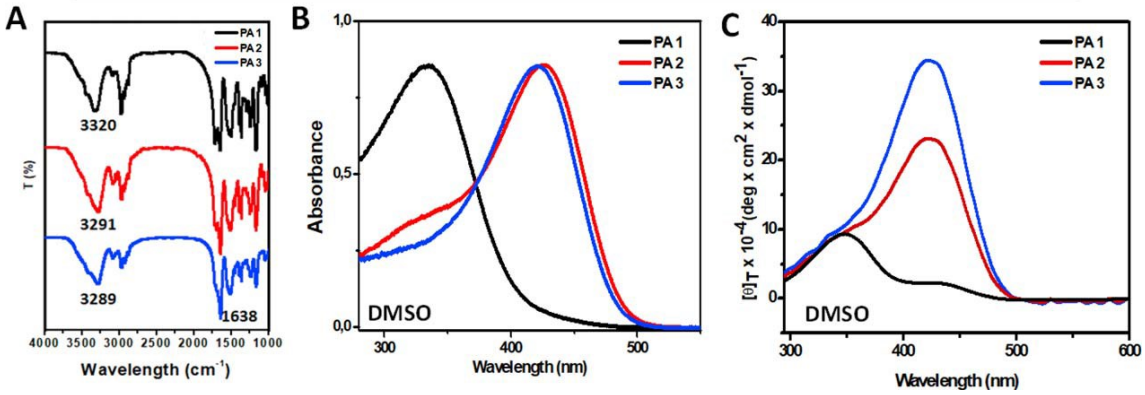

Fig. 5 Top, Results of the SEC analyses after polymerization under the reported experimental conditions. (A) Solid-state FT-IR absorption spectra for **PAs 1**–**3**. (B) UV–Vis absorption spectra in DMSO for **PAs 1**–**3**. (C) CD spectra in DMSO for **PAs 1**–**3**.

Peptide polydiacetylenes

Our next step was to apply to our peptide-acetylene hybrids the alkyne-alkyne cross-coupling reaction[52] that is expected to lead to formation of **1'-4'** diacetylene homo-dimers (Figure 6A). Traditionally, a molecular alignment with only minimal packing rearrangements of the diacetylenic (DA) monomer, satisfies the requisite to undergo a (thermal- or photochemical-

induced) topochemical polymerization. Recently, we demonstrated that not only single crystals of monomers can be transformed into highly conjugated polydiacetylenes,[22–25] but also DAs efficiently packed as organogels.[53] Thus, according with the alkyne-alkyne cross-coupling reaction, all of the **1**–**4** compounds were dissolved in THF at concentration 0.5 M and allowed to react (as indicated in the Experimental section) with the aim at obtaining homodiacetylene peptides **1'-4'**. Quite surprisingly, the reactions involving the **1-3** compounds turned rapidly (from 5 to 8 h) into the corresponding **PdAs 1-3** polymers providing well colored solutions with a gel-like consistence (Figure 6B). In the case of the reaction involving **4**, it did afford neither **4'** nor the corresponding **PdA 4** (4 was recovered quantitatively from the reaction mixture). Addition of MeOH to the crude **PdA 1-3** mixtures afforded the **PdA 1-3** series as solid compounds (from the crude mixtures we did not recover any **1'-3'** homodiacetylene peptides). In Figure 6C we show the UV–vis diffuse reflectance spectra of the **PdA 1-3** polymers, which confirmed that the topochemical polymerizations did indeed take place. A careful spectral comparison provided information on the degrees of their polymerization. On the basis of the wavelength absorption maxima (that is related to the double-triple bond repetition along the polymer backbone), we were able to establish formation of longer polymeric chains for **PdAs 2** and **3**. We characterized morphologically **PdAs 1-3** by dissolving small amounts of each polymer in DMSO. The TEM analyses of these samples gave information on the polymer molecular organizations and lengths. In more detail, after drying a drop of DMSO solution of each PdA over the TEM grid, we observed: (i) for **PdA 1**, formation of short strip-like structures with a length of 20–200 nm (Figure 6D); (ii) for **PdA 2**, a large distribution in size (100 nm to 2 μm) of similar strip-like structures as seen for **PdA 1** (Figure 6E); (iii) for **PdA 3**, compact, large rod-like structures (Figure 6F). Considering the size of the structures obtained for **PdA 1**, we assume that the topochemical condensation of four homo-diacetylenic monomers would result in an end-to-end linear distance of 2 nm. Thus, each of the average 100 nm-long **PdA 1** molecules contains as many as 100 diacetylenic monomers.[54] We extended a similar consideration to **PdA 2**, where apparently the large distribution of size affords from 1- to 2-μm-long strips each containing up to 2000 homo-diacetylenic monomers.

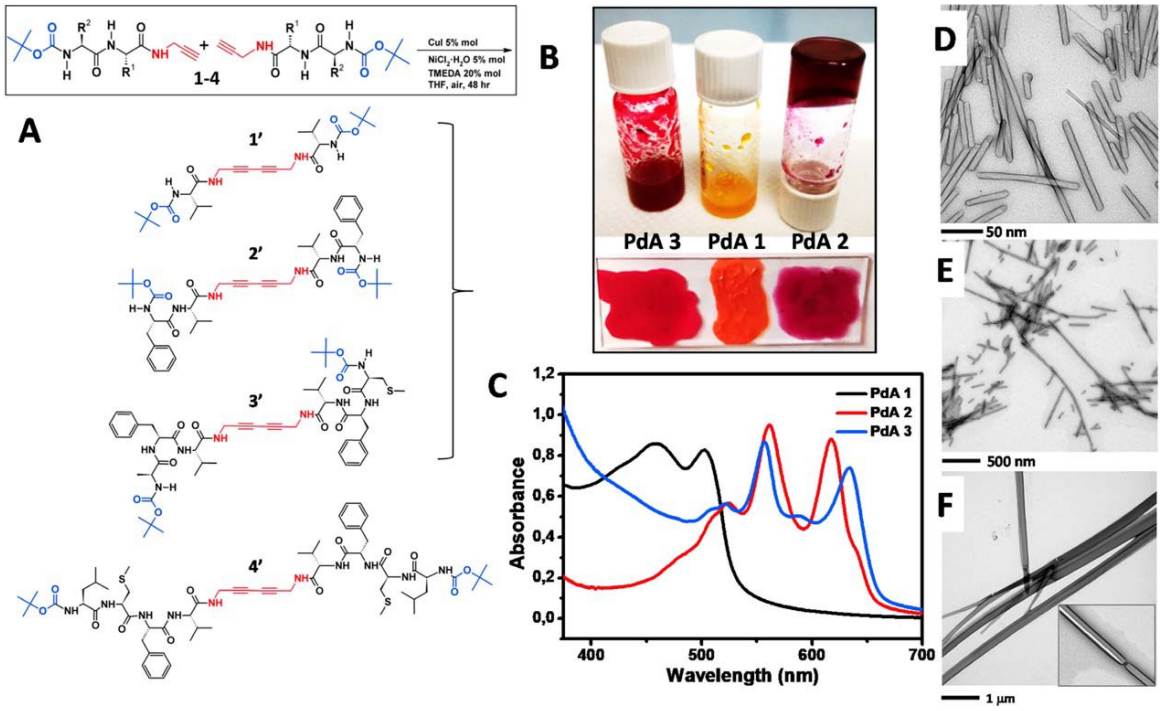

Fig. 6 (A) Schematic representations of the alkyne-alkyne cross-coupling reaction and the expected homo-diacetylene products. (B) PdAs obtained from the alkyne-alkyne cross-coupling reaction. (C) UV–Vis diffuse reflectance spectra of **PdAs 1–3**. (D-F) TEM images of PdAs obtained from diluted solutions.

As for **PdA 3,** the TEM analysis showed very large aggregates with crystalline features (Figure 6 F, inset). Taken together, the results obtained in the case of formation of the PdAs showed an intriguing templation effect for compounds **1-3**. While compound **4** was not able to afford the corresponding homodiacetylene dimer **40** (probably due to its strong tendency to self-associate), monomers **1-3** were rapidly converted into their homoacetylene dimers (**1'-3'**) and polymerized (**PdAs 1-3**). In particular, we observed that the polymerization degree increases, while the polymerization yield decreases, from **1** to **3**.

In conclusion, we assume that in the course of the PdA polymerizations, once the homo-acetylene dimers (**1'-3'**) formed, they self-assembled in such a way to adopt the appropriate disposition to undergo a moderately thermally (50°C) induced topochemical polymerization.

Conclusions

To summarize, we found that Boc-L-Val-NH-prop (**1**), Boc-L-Phe-L-Val-NH-prop (**2**), Boc-L-Cys(Me)-L-Val-NH-prop (**3**), and Boc-L-Leu-L-[Cys(Me)]-L-Val-NH-prop (**4**) are able to hierarchically selfassemble in well-defined organogels. These structures are build-up through networks of intermolecular β-sheet interactions and show critical concentration values (for **1**-**4** in THF) that decrease with mainchain elongation. The presence of a propargyl unit at the C-terminus of **2**-**4** allowed us to investigate for the first time formation of peptidebased polyacetylene (PAs) and polydiacetylene (PdAs) organogels. According with the schematic representation reported in Figure 1, both PA and PdA backbones are able to template formation of parallelly oriented β-sheet structures within their respective polymeric systems, thanks to the onset of geometrically perfect repetitions of highly conjugated double and double-triple bonds, respectively.[55–57] We are currently exploring the limits (dictated by the negative steric hindrance) and potentialities (governed by the positive template effect of well-ordered networks) of the organogel-forming peptide-acetylene hybrid compounds for a further development of this fascinating optoelectronic-active, stimuli-responsive, peptide-based, polymer field.[17–19]

Experimental section

Instruments and Methods

Nuclear magnetic resonance. ^{1}H and ^{13}C NMR spectra were recorded at room temperature on a Bruker AC-500 instrument using TMS (tetramethylsilane) as the internal reference. The multiplicity of a signal is indicated as s, singlet; d, doublet; t, triplet; m, multiplet; and br, broad. Chemical shifts (δ) are expressed in ppm.

Fourier-transform infrared absorption. FT-IR absorption spectra in KBr disk were recorded using a Perkin-Elmer 1720X spectrophotometer. The frequency maxima values for the main absorption bands are given.

Mass spectrometry. Mass spectra were obtained by electrospray ionization (ESI) on a Perceptive Biosystem Mariner ESI-ToF 5220 spectrometer. Data were collected in the positive mode.

Ultraviolet–Visible absorption. UV–Vis absorption spectra were recorded using a Shimadzu model UV-2501 PC spectrophotometer. A 1-cm path length quartz cell was used.

Electronic circular dichroism. ECD measurements were carried out at room temperature using a Jasco J-715 spectropolarimeter. A fused quartz cell of 1-mm path length (Hellma) was used.

Transmission Electron Microscopy. Samples were analyzed on a Jeol 300 PX TEM instrument. A glow discharged carbon coated grid was floated on a small drop of the nanosphere suspension and excess was removed by #50 hardened Whatman filterpaper. All TEM samples were negatively stained with a 2% (w/v) uranyl acetate aqueous solution.

Scanning Electron Microscopy. A Carl Zeiss Merlin field emission SEM instrument operating at 5 kV accelerating voltage was used. A small drop of the nanosphere suspension was placed on a microscope glass coverslip and allowed to dry overnight.

Size-exclusion chromatography. SEC analyses were performed on an Agilent 1260 Infinity system equipped with 1260 isopump, 1260 TCC, 1260 VWD VL, 1260 RID, Phenogel 5-μm linear/mixed guard column (30 x 4.6 mm^2), followed by a Phenomenex Phenogel 5-μm 104 Å (300 x 4.6 mm^2) column working at 60°C. DMF (N,N-dimethylformamide) was used as eluant at a flow rate of 1 mL min^{-1}. Before SEC analysis, the samples were filtered through a 0.2-μm PTFE filter (15 mm, Phenomenex). Molecular weights were calculated according to a calibration using polystyrene standards.

Synthesis and Characterization

Materials

The 1-hydroxy-7-aza-1,2,3-benzotriazole (HOAt) was purchased from GL Biochem (Shanghai). Tert-butyloxycarbonyl (Boc)-protected a-amino acids and N-(3-dimethylaminopropyl)-N'-ethylcarbodiimide (EDC) hydrochloride were obtained from Iris Biotech. Propargylamine, triethylamine (TEA), N,N,N',N'-tetramethylethylenediamine (TMEDA), copper(I) iodide and nickel(II) chloride hydrate were obtained from Sigma-Aldrich. The deuterated solvent dimethylsulfoxide (DMSO-d_6), acetonitrile (CH_3CN-d_3) and chloroform ($CDCl_3$) were purchased from Euriso-Top, while the anhydrous solvents for peptide coupling reactions were purchased from Sigma-Aldrich. All other chemicals and solvents are Sigma-Aldrich, Fluka or Acros products and used as provided without further purifications.

Boc-L-Val-NH-CH_2-C≡CH (1)

Boc-L-Val-OH (3.53 g, 16.2 mmol) was dissolved in 20 mL of anhydrous DCM (dichloromethane) and C-activated with HOAt (2.19 g, 16.1 mmol) and EDC·HCl (3.09 g, 16.1 mmol). Propargylamine (1.5 mL, 23.4 mmol) and TEA (2.3 mL, 16.1 mmol) were added to the solution of the active ester to pH 8-9. The mixture was stirred at room temperature for 4 days. The solvent was removed under reduced pressure and the residue was dissolved in ethyl acetate (EtOAc). The organic phase was washed with 5% $KHSO_4$(aq) (4v), water (1v), 5% $NaHCO_3$(aq) (3v), and brine. Then, the organic layer was dried over Na_2SO_4, filtered, and evaporated under reduced pressure. The residue was dissolved in EtOAc and precipitated by addition of petroleum ether. After filtration and drying, the product was obtained as a colorless solid (3.35 g, 82% yield).

MS (ESI+): m/z $[M+H]^+$ calcd. for $C_{13}H_{22}N_2O_3$ 255.3334, found 255.1760.

FT-IR absorption: ῡ 3296 (m), 1657 (s), 1538 (m) cm^{-1}.

^{1}H NMR (400 MHz, $CDCl_3$) δ 6.52 (br, 1H, NH propargyl), 5.10 (br, 1H, NH urethane), 4.06-4.02 (m, 2H, CH_2 propargyl), 3.94-3.86 (m, 1H, αCH Val), 2.20 (t, 1H), 2.14-2.07 (m, 1H, -CH Val), 1.43 (s, 9H), 0.93 (t, 6H). ^{1}HNMR (500 MHz, CH_3CN-d_3) δ 6.83 (br, 1H, NH amide), 5.38 (br, 1H, NH urethane), 4.01–3.92 (m, 2H, CH_2 propargyl), 3–86-3.83 (m, 1H, αCH Val), 2.43 (t, 1H), 2.07-2.01 (m, 1H), 1.45 (s, 9H), 0.93 (dd, 6H). ^{13}C NMR (50 MHz, $CDCl_3$) d 172.83, 157.32, 81.52, 75.16, 70.94, 56.27, 30.28, 29.91, 27.13, 17.03.

Boc-L-Phe-L-Val-NH-CH_2-C≡CH (2)

TFA^- $^+H_2$-L-Val-NH-CH_2-C≡CH [obtained after TFA/DCM treatment of **1**] was dissolved in 10 mL of anhydrous DCM with addition of TEA (1.2 mL, 8.61 mmol). This solution was added to a solution of Boc-L-Phe-OH (1.15 g, 4.34 mmol) dissolved in 10 mL of anhydrous DCM and C-activated with HOAt (593 mg, 4.36 mmol) and EDC·HCl (826 mg, 4.31 mmol). A few mL of TEA was added to pH 8–9. The mixture was stirred at room temperature for 24 h. The solvent was removed under reduced pressure and the yellowish residue was acidified with 5% $KHSO_4$(aq) and diluted with EtOAc. The organic phase was washed with 5% $KHSO_4$ (aq) (3v), water (1v), 5% $NaHCO_3$ (aq) (3v), and brine. The organic layer was dried over Na_2SO_4, filtered, and evaporated under reduced pressure. The product was obtained as a colorless solid (1.39 g, 88% yield).

MS (ESI+): m/z $[M+H]^+$ calcd. for $C_{22}H_{31}N_3O_4$ 402.2395, found 402.2359.

FT-IR absorption: ῡ 3275 (br), 2128 (w), 1684 (m), 1643 (s) cm^{-1}.

^{1}H NMR (500 MHz, CH_3CN-d_3) δ 7.35-7.25 (m, 5H, Ar Phe), 6.78 (br, 2H, 2 x NH amide), 5.54 (br, 1H, NH urethane), 4.34-4.30 (m, 1H, αCH Phe), 4.19-4.16 (m, 1H, αCH Val), 3.95-3.94 (m, 2H, CH_2 propargyl), 3.16-2.87 (m, 2H, βCH_2 Phe), 2.44 (t, 1H), 2.15-2.10 (m, 1H, βCH Val), 1.40 (s, 9H), 0.92 (dd, 6H). ^{13}C NMR (50 MHz, $CDCl_3$) δ 172.59, 171.01, 157.15, 135.68, 127.15, 126.95, 125.11, 79.62, 74.20, 71.23, 56.03, 55.09, 37.03, 30.59, 27.14, 18.40.

Boc-L-Cys(Me)-L-Phe-L-Val-NH-CH_2-C≡CH (3)

Boc-L-Cys(Me)-OH (492 mg, 2.09 mmol) was dissolved in 10 mL of anhydrous DCM and C-activated with addition of HOAt (284 mg, 2.09 mmol) and EDC·HCl (400 mg, 2.09 mmol). TFA^- $^+H_2$-L-Phe-L-Val-NH-CH_2-C≡CH (obtained after TFA/DCM treatment of **2**) was added to the solution of the active ester with TEA (584 mL, 4.18 mmol), monitoring the basicity of the resulting mixture (pH 8–9). Because a gel was formed, a few mL of CH3CN were added to promote the dissolution of the compound. The mixture was stirred at room temperature for 2 days. The solvent was removed under reduced pressure. The residue was acidified with 5% $KHSO_4$(aq) and dissolved in EtOAc. The organic phase, where the product formed a gel, was washed with 5% $KHSO_4$ (aq) (4v), 5% $NaHCO_3$(aq) (1v), and brine (2v). The organic layer, after dissolution of the gel under thermal treatment, was evaporated under reduced pressure. The product was obtained as a colorless solid (640 mg, 65% yield).

MS (ESI+): m/z $[M+H]^+$ calcd. for $C_{26}H_{38}N_4O_5S$ 519.6767, found 519.2637.

FT-IR absorption: ῡ 3281 (s), 2126 (w), 1693 (s), 1638 (s) cm^{-1}.

^{1}H NMR (500 MHz, CH_3CN-d_3) δ 7.33-7.25 (m, 5H, Ar Phe), 7.10 (d, 1H, NH amide), 6.86-6.81 (m, 2H, 2 x NH amide), 5.57 (br, 1H, NH urethane), 4.65-4.61 (m, 1H, αCH Cys), 4.20-4.15 (m, 2H, 2 x αCH Phe and αCH Val), 3.96-3.94 (m, 2H, CH_2 propargyl), 3.21-2.96 (m, 2H, βCH_2), 2.86-2.61 (m, 2H, βCH_2), 2.44 (t, 1H), 2.15-2.09 (m, 4H, SCH_3 Cys and βCH Val), 1.44 (s, 9H), 0.92-0.88 (m, 6H, 2 x CH3 Val). ^{13}C NMR (50 MHz, $CDCl_3$) δ 171.39, 170.11, 169.72, 157.13, 135.96, 127.93, 127.50, 125.51, 78.56, 74.03, 69.58, 56.30, 53.56, 52.11, 36.01, 31.73, 29.21, 27.14, 17.40, 13.77.

Boc-L-Leu-L-Cys(Me)-L-Phe-L-Val-NH-CH_2-C≡CH (4)

Boc-L-Leu-OH (123 mg, 0.53 mmol) was dissolved in 6 mL of anhydrous CH_3CN and C-activated with addition of HOAt (72 mg, 0.53 mmol) and EDC·HCl (102 mg, 0.53 mmol). TFA^- $^+H_2$-L-Cys(Me)-L-Phe-L-Val-NH-CH_2-C≡CH (obtained after TFA/DCM treatment of **3**) was added to the active ester with DIPEA (diisopropylethylamine) (93 μl, 0.53 mmol), monitoring the basicity of the resulting mixture (pH 8-9). An organogel was formed within a few seconds in the reaction mixture, which was stirred at room temperature for 20 h. The resulting suspension was filtered and the colorless solid was washed with diethyl ether (245 mg, 69% yield).

MS (ESI+): m/z $[M+H]^+$ calcd. for $C_{32}H_{49}N_5O_6S$ 632.3484, found 632.3520.

FT-IR absorption: ῡ 3270 (s), 2958 (m), 1698 (s), 1660 (s), 1634 (s), 1540 (s) cm^{-1}.

^{1}H NMR (500 MHz, CH_3CN-d_3) δ 7.33-7.25 (m, 6H, 5H Ar Phe and 1H NH amide), 7.15 (br, 1H, NH amide), 6.94 (br, 2H, 2 x NH amide), 5.64 (br, 1H, NH amide), 4.61-4.57 (m, 1H, αCH), 4.37-4.36 (m, 1H, αCH), 4.16-4.13 (m, 1H, αCH), 4.05-4.01 (m, 1H, αCH), 3.95-3.94 (m, 2H, CH_2 propargyl), 3.24-2.98 (m, 2H, βCH_2), 2.87-2.74 (m, 2H, βCH_2), 2.43 (br, 1H), 2.13-2.10 (m, 4H, SCH_3 Cys and βCH Val), 1.74-1.68 (m, 1H, γCH Leu), 1.54-1.53 (m, 2H, βCH_2 Leu), 1.46 (s, 9H), 0.98-0.91 (m, 12H, 2 x δCH_3 Leu and 2 x γCH_3 Val). ^{13}C NMR (50 MHz, $CDCl_3$) δ 172.97, 171.48, 171.03, 169.97, 157.25, 135.96, 127.53, 127.01, 125.37, 79.54, 74.25, 70.91, 57.03, 54.23, 53.82, 51.39, 39.66, 37.53, 32.59, 30.74, 29.31, 26.89, 24.10, 22.93, 17.31, 14.09.

Determination of critical self-assembly concentration

Peptides were dissolved in THF solutions thermostatted at 50°C in a range of concentrations from 1 to 20 mM. The solutions were allowed to equilibrate at room temperature. As critical self-assembly concentration, we assumed those peptide concentrations able to form stable organogel *via* the tube inversion test. All of the organogel processes were found to be thermoreversible.

Rh-catalyzed polymerization (reported example for 1)

Polymerization was carried out in a dry three-neck flask under dry nitrogen atmosphere. Compound **1** (500 mg, 1.97 mmol) was placed in the dry flask, which was then evacuated on a vacuum line and flushed with dry N_2. The evacuation-flush procedure was repeated three times. Then, THF (20 mL) and TEA (345 μl, 2.46 mmol), prepared in N_2 atmosphere, were added with a syringe. Finally, a solution of catalyst $[Rh(nbd)Cl]_2$ (nbd, 2,5-norbornadiene) (5 mg, 0.011 mmol), prepared under a dry N_2 atmosphere in 0.5 mL of THF, was added at room temperature. The polymerization proceeded rapidly: the solution changed color from yellow to brown and the polymer appeared as a viscous mixture after few seconds. The polymer was stirred at 50°C for 5 or 24 h. The resulting polymer was precipitated into a large amount of methanol and the yellow solid was collected by centrifugation, washed twice, and dried.

Direct topochemical polymerization (reported example for 1)

CuI (5 mol%) and $NiCl_2 \cdot H_2O$ (5 mol%) were dissolved in 500 μl of THF (tetrahydrofuran). Then, TMEDA (20 mol%) was added. The resulting solution was stirred at room temperature under air for 2 min. Compound **1** (500 mg, 1.97 mmol) was dissolved in 4 mL of THF. The mixture was stirred at 50°C under air for 8 h giving a yellow, gel like, solution. The resulting polymer was precipitated into a large amount of methanol (MeOH) and the orange solid was collected by centrifugation, washed twice, and dried.

References

1. S. I. Stupp, R. H. Zha, L. C. Palmer, H. Cui, and R. Bitton, *Faraday Discuss.*, **2013**, 166, 9.
2. S. Kim, J. H. Kim, J. S. Lee, and C. B. Park, *Small*, **2015**, 11, 3623.
3. X. Du, J. Zhou, J. Shi, and B. Xu, *Chem. Rev.*, **2015**, 115, 13165.
4. T. Aida, E. W. Meijer, and S. I. Stupp, *Science*, **2012**, 335, 813.
5. M. J. Webber, E. A. Appel, E. W. Meijer, and R. Langer, *Nat. Mater.*, **2016**, 15, 13.
6. D. W. P. M. L€owik, and J. C. M. van Hest, *Chem. Soc. Rev.*, **2004**, 33, 234.
7. R. Fairman, and K. S. Åkerfeldt, *Curr. Opin. Struct. Biol.*, **2005**, 15, 453.
8. B. J. Pepe-Mooney, and R. Fairman, *Curr. Opin. Struct. Biol.*, **2009**, 19, 483.
9. D. W. P. M. Lowik, E. H. P. Leunissen, M. van den Heuvel, M. B. Hansen, and J. C. M. van Hest, *Chem. Soc. Rev.*, **2010**, 39, 3394.
10. A. L. Boyle, and D. N. Woolfson, *Chem. Soc. Rev.*, **2011**, 40, 4295.
11. J. B. Matson, R. H. Zha, and S. I. Stupp, *Curr. Opin. Solid State Mater. Sci.*, **2011**, 15, 225.
12. J. B. Matson, and S. I. Stupp, *Chem. Commun.*, **2012**, 48, 26.
13. Q. Zou, M. Abbas, L. Zhao, S. Li, G. Shen, and X. Yan, *J. Am. Chem. Soc.*, **2017**, 139, 1921.
14. J. Wang, K. Liu, R. Xing, and X. Yan, *Chem. Soc. Rev.*, **2016**, 45, 5589.
15. K. Tao, B. Xue, S. Frere, I. Slutsky, Y. Cao, W. Wang, and E. Gazit, *Chem. Mater.*, **2017**, 29, 4454.
16. K. Tao, A. Levin, L. Adler-Abramovich, and E. Gazit, *Chem. Soc. Rev.*, **2016**, 45, 3935.
17. T. Masuda, *Polym. Rev.*, **2017**, 57, 1.
18. A. Xu, T. Masuda, and A. Zhang, *Polym. Rev.*, **2017**, 57, 138.
19. J. Liu, J. W. Y. Lam, and B. Z. Tang, *Chem. Rev.*, **2009**, 109, 5799.
20. K. Shimomura, T. Ikai, S. Kanoh, E. Yashima, and K. Maeda, *Nat. Chem.*, **2014**, 6, 429.
21. Y. Yoshida, Y. Mawatari, A. Motoshige, R. Motoshige, T. Hiraoki, M. Wagner, K. Müllen, and M. Tabata, *J. Am. Chem. Soc.*, **2013**, 135, 4110.
22. S. R. Diegelmann, N. Hartman, N. Markovic, and J. D. Tovar, *J. Am. Chem. Soc.*, **2012**, 134, 2028.

23. L. Hsu, G. L. Cvetanovich, and S. I. Stupp, *J. Am. Chem. Soc.*, **2008**, 130, 3892.
24. R. Jelinek, and M. Ritenberg, *RSC Adv.*, **2013**, 3, 21192.
25. P. van der Asdonk, M. Keshavarz, P. C. M. Christianen, and P. H. J. Kouwer, *Soft Matter*, **2016**, 12, 6518.
26. C. Tomasini, and N. Castellucci, *Chem. Soc. Rev.*, **2013**, 42, 156.
27. E. De Santis, and M. G. Ryadnov, *Chem. Soc. Rev.*, **2015**, 44, 8288.
28. S. Fleming, and R. V. Ulijn, *Chem. Soc. Rev.*, **2014**, 43, 8150.
29. C. K. Smith, J. M. Withka, and L. Regan, *Biochemistry*, **1994**, 33, 5510.
30. E. R. Blout, in *Polyamino Acids, Peptides, and Proteins* (Ed: M. A. Stahmann), The University of Wisconsin Press, Madison WI **1962**, pp. 275.
31. C. Toniolo, and G. M. Bonora, in *Peptides: Chemistry, Structure and Biology* (Eds: R. Walter, J. Meienhofer), Ann Arbor Science, Ann Arbor MI **1975**, pp. 145.
32. M. Palumbo, S. Da Rin, G. M. Bonora, and C. Toniolo, *Makromol. Chem.*, **1976**, 177, 1477.
33. M. Goodman, and C. Toniolo, *Biopolymers*, **1968**, 6, 1673.
34. C. Toniolo, and G. M. Bonora, M. Mutter, *J. Am. Chem. Soc.*, **1979**, 101, 450.
35. K. Wüthrich, *NMR of Proteins and Nucleic Acids*, Wiley, New York, NY **1986**.
36. T. Miyazawa, in *Poly-a-Amino Acids: Protein Models for Conformational Studies* (Ed.: G. D. Fasman), Dekker New York **1967**, pp. 69.
37. M. H. Baron, C. De Loze, C. Toniolo, and G. D. Fasman, *Biopolymers*, **1979**, 18, 411.
38. G. Zandomeneghi, M. R. H. Krebs, M. G. McCammon, and M. Fändrich, *Protein Sci.*, **2004**, 13, 3314.
39. C. Toniolo, and G. M. Bonora, *Can. J. Chem.*, **1976**, 54, 70.
40. A. G. Walton, *Polypeptides and Protein Structure*, Elsevier North Holland, New York, NY **1981**.
41. C. Toniolo, F. Formaggio, and R. W. Woody, in *Comprehensive Chiroptical Spectroscopy* (Eds: N. Berova, P. L. Polavarapu, K. Nakanishi, R. W. Woody), Vol. 2, Wiley, Hoboken NJ **2012**, pp. 499.
42. K. Maeda, K. Morino, Y. Okamoto, T. Sato, and E. Yashima, *J. Am. Chem. Soc.*, **2004**, 126, 4329.
43. Y. Kishimoto, P. Eckerle, T. Miyatake, T. Ikariya, and R. Noyori, *J. Am. Chem. Soc.*, **1994**, 116, 12131.

44. Y. Kishimoto, M. Itou, T. Miyatake, T. Ikariya, and R. Noyori, *Macromolecules*, **1995**, 28, 6662.
45. Y. Kishimoto, P. Eckerle, T. Miyatake, M. Kainosho, A. Ono, T. Ikariya, and R. Noyori, *J. Am. Chem. Soc.*, **1999**, 121, 12035.
46. S. Kumazawa, J. R. Castanon, M. Shiotsuki, T. Sato, and F. Sanda, *Polym. Chem.*, **2015**, 6, 5931.
47. F. Sanda, G. Gao, and T. Masuda, *Macromol. Biosci.*, **2004**, 4, 570.
48. F. Sanda, K. Terada, and T. Masuda, *Macromolecules*, **2005**, 38, 8149.
49. K. Maeda, and E. Yashima, *Top. Curr. Chem.*, **2017**, 375, 72.
50. G. Gao, F. Sanda, and T. Masuda, *Macromolecules*, **2003**, 36, 3932.
51. M. Tabata, T. Sone, and Y. Sadahiro, *Macromol. Chem. Phys.*, **1999**, 200, 265.
52. W. Yin, C. He, M. Chen, and H. Zhang, A. Lei, *Org. Lett.*, **2009**, 11, 709.
53. D. Mazzier, D. Mosconi, G. Marafon, A. Reheman, C. Toniolo, and A. Moretto, *J. Pept. Sci.*, **2017**, 23, 155.
54. Y. Ishihara, and S. Kimura, *Biopolymers (Pept. Sci.)*, **2012**, 98, 155.
55. H. Cui, T. Muraoka, A. G. Cheetham, and S. I. Stupp, *Nano Lett.*, **2009**, 9, 945.
56. N. Faruqui, A. Bella, J. Ravi, S. Ray, B. Lamarre, and M. G. Ryadnov, *J. Am. Chem. Soc.*, **2014**, 136, 7889.
57. S. Mondal, M. Varenik, D. N. Bloch, Y. Atsmon-Raz, G. Jacoby, L. Adler-Abramovich, L. J. W. Shimon, R. Beck, Y. Miller, O. Regev, and E. Gazit, *Nat. Commun.*, **2017**, 8, 14018.

2.2 Light-driven topochemical polymerization under organogel conditions of a symmetrical dipeptide-diacetylene system[d]

Nowadays, the bottom-up self-assembly approach is considered one of the most powerful to precisely design small molecule organizations at the nanoscale level[1–4]. By means of a hierarchical process, under suitable conditions, the combination of a multiplicity of non-covalent interactions allows appropriately designed molecules to form ordered aggregates that can progress into nano-, micro-, and macroscale materials. These systems may be characterized by precise 3D-architectures with definite shapes, dimensions, and functions, with applications in a number of fields going from chemistry to materials science and medicine[5–7]. In this perspective, peptides are excellent building blocks, because of their molecular diversity and secondary structure variety[8–17]. In particular, self-assemblies formed by short, terminally unprotected peptides resulted in nanotubes and nanofiber molecular architectures[18–22]. On the contrary, only a limited number of examples of short terminally protected peptides, characterized by nanotube shapes in their crystal structures, was reported, but their self-assembly attitude was not deeply investigated[23–26]. In this connection, we recently showed that the terminally protected peptide Boc-L-Cys(Me)-L-Leu-Me (Boc, *tert*-butyloxycarbonyl; OMe, methoxy) is able to hierarchically self-assemble in a variety of superstructures, including hollow rods, ranging from the nano to the macroscale, and organogels (fibers)[27]. Diacetylenes (DAs) can be polymerized via a photochemical or thermal process[28,29] to a highly conjugated, rigid polydiacetylene (PDAs) system with unique chromatic properties[30]. Importantly, the topochemical polymerization of DAs can only take place if thesemoieties are closely packed[31]. Molecules linked to DA may become versatile building blocks for the construction of supramolecular polymeric structures[32,33]. These novel structures have attracted considerable attention for various types of applications [30]. Despite these excellent properties, the design of appropriately substituted DAs remains a challenge. We report synthesis and topochemical polymerization of a symmetrically disubstituted DA based on the Boc-L-Cys(Me)-L-Leu dipeptide alkylamide sequence, which allowed formation of a peptide-based PDA through the intermediacy of a self-assembled, organized, molecular architecture (organogel).

[d] Reprinted (adapted) with permission from (J. Pept. Sci. 2017; 23,: 155). Copyright (2019) John Wiley and Sons."

Results and Discussion

Synthesis and topochemical polymerization

The chemical structures of the functionalized peptide molecules reported in this work are presented in Scheme 1. Briefly, the ester **1** was first converted to **2** via a nucleophilic substitution with propargylamine in the presence of catalytic DBU[34]. Then, the corresponding peptide-DA conjugate **3** was prepared via the Ni catalyzed oxidative homo-coupling reaction of terminal alkynes (Scheme 1)[35]. The propensity to form organogels of this novel polymeric construct was subsequently examined.

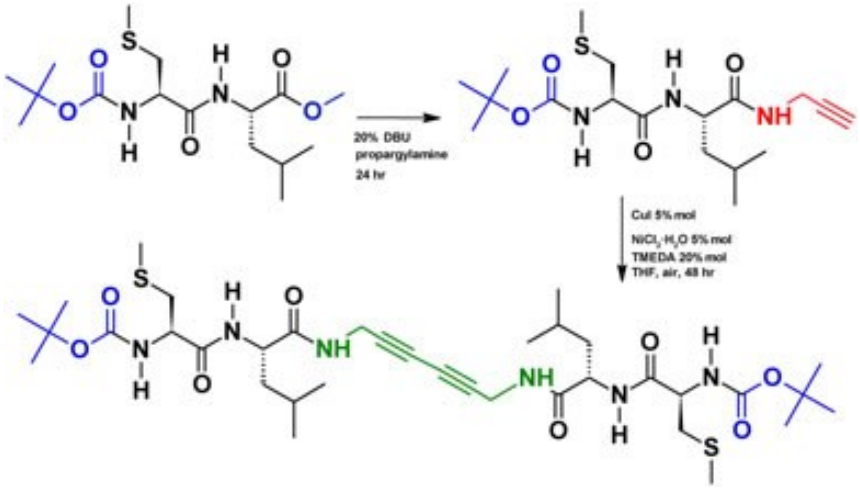

Scheme 1. Synthesis of compounds **2** and **3**. Reagents and conditions: i) propargylamine, DBU (20% mol), r.t., 48 h; ii) CuI (5% mol), $NiCl_2$·H2O (5% mol), TMEDA(20% mol), THF, r.t., air, 48 h.

In particular, it was found that at a concentration ranging from 5 to 20 mg/ml in CH_2Cl_2 stable organogels were obtained (Figure 1). We recorded the solid-state FT-IR absorption spectra for peptide-DA conjugate (**3**) after its deposition on a KBr disk from the organogel state. We found (see the *Experimental Section*, synthesis of compound **3**) a frequency of 1646 cm^{-1} for amide I and 1521 cm^{-1} for amide II, both indicative of the onset of a self-aggregated structure. Then, after a prolonged irradiation at 254 nm (2 h), the gel was converted to a solid orange-colored material. To confirm formation of PDAs after UV irradiation, Raman spectroscopy was exploited to probe the spectroscopic changes. As shown in Figure 1B, the original DA stretching band appears at 2267 cm^{-1}. After UV irradiation of the gel, two new peaks are seen, which were assigned to the typical conjugated alkyne-alkene structures of PDAs[31].

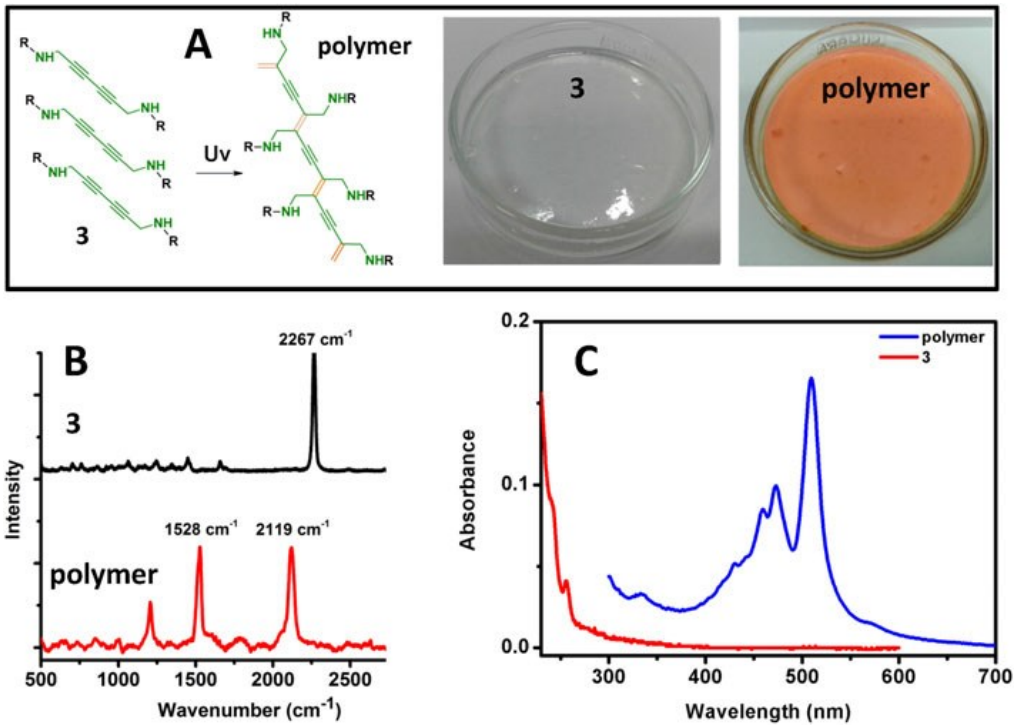

Fig. 1 (A) (left) Schematic representation of the UV-light induced topochemical polymerization reaction and (right) the **3**-organogel prior (left) and after (right) exposition to the UV-light; (B) Raman spectra recorded for **3** prior (top) and after (bottom) exposition to the UV-light; (C) UV-Vis absorption spectra recorded for **3** prior (red line) and after (blue line) exposition to the UV-light.

This result confirmed that the **3** organogel was directly converted into its PDA by UV irradiation. Furthermore, UV-Vis spectroscopy further probed the occurrence of the polymerization, as the resulting photo-polymerized PDA material displays an intense absorption profile in the Vis region, which is missing in the DA precursor (Figure 1C).

Morphological Studies

The topochemical polymerization was morphologically studied with the following set of microscopies: transmission electron microscopy (TEM), atomic force microscopy (AFM), and scanning electron microscopy (SEM). In particular, **3**-organogel, examined by TEM, revealed formation of a dense fiber network (Figure 2A). The TEM analyses were repeated on the same sample after 30 min (Figure 2B) and 2 h (Figure 2C) of UV-irradiation. The results showed formation of large stripe-like structures and the concomitant disappearance of the original fiber network. The photo-irradiated sample was additionally examined by SEM (Figure 2D) and AFM (Figures 2E and 2F): both techniques confirmed the results obtained by TEM.

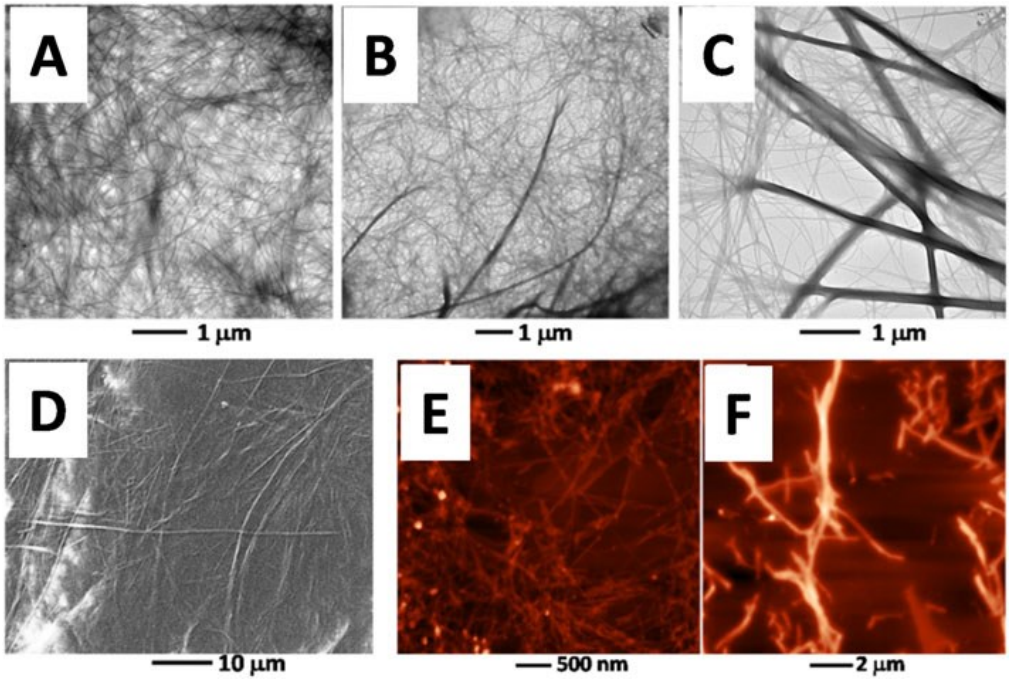

Fig. 2 (A) TEM image of **3**-organogel. (B–C) TEM images of **3**-organogel recorded, respectively, after 30min and 2 h of UV irradiation. (D) SEM image of **3**-organogel recorded after 2 h of UV irradiation. (E–F) AFM images of **3**-organogel recorded, respectively, prior and after UV-light exposure.

Subsequently, it was found that slow evaporation of a 2 mg/ml solution in 1,1,1,3,3,3-hexafluoroisopropanol of **3** afforded regularly round sponge-like microstructures, ranging in size from 5 to 10 μm, as detected by SEM (Figures 3A and 3B). Interestingly, starting from a more concentrated (50 mg/ml) solution of **3**, the same types of structures were obtained with a macroscopic size extended to 2 mm (Figure 3C), as detected by optical microscope. These last microstructures were subsequently irradiated using UV-light at different times. The results indicated that a topochemical polymerization took place within these microstructures, as shown by the different color detected by optical microscopy (Figures 3D and 3E). Furthermore, by SEM, we observed the morphological transition occurring for these microstructures after their exposition to UV light (Figures 3F and 3G).

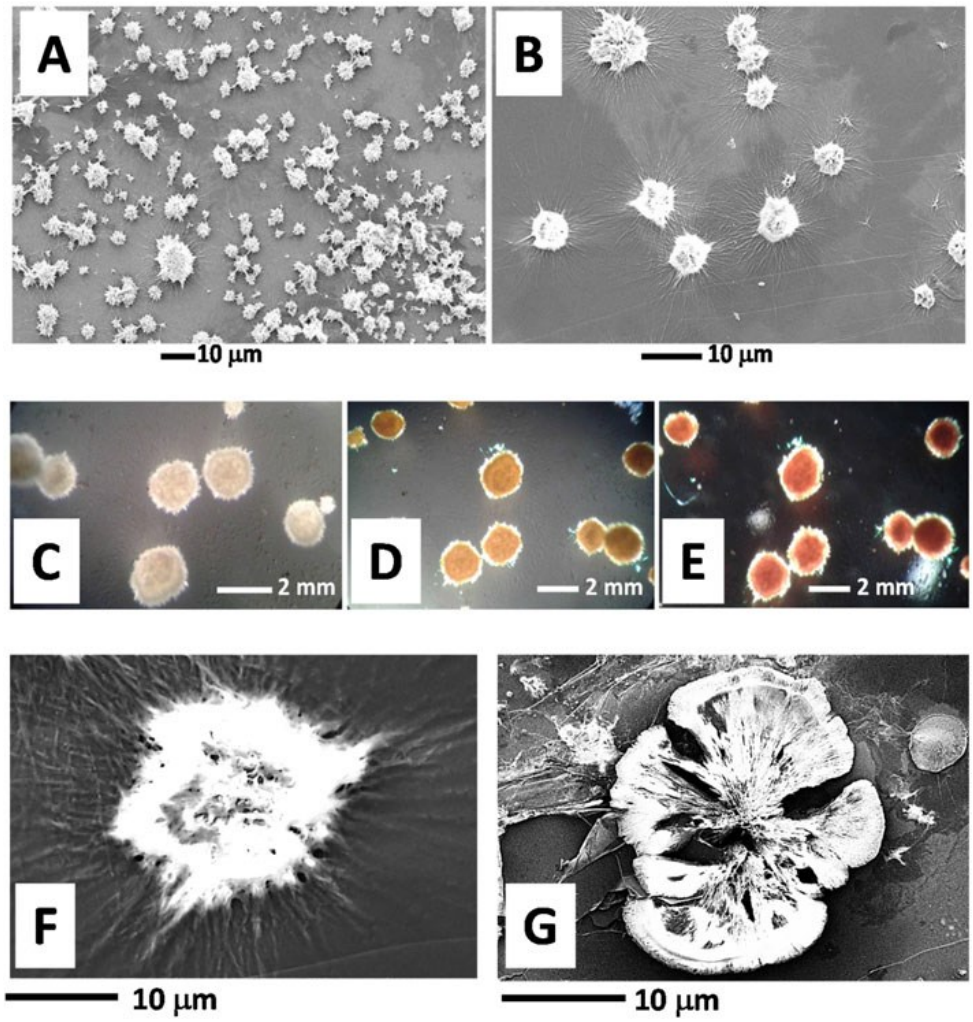

Fig. 3 (A–B) SEM images showing formation of round sponge-like microstructures for a 2 mg/ml solution in 1,1,1,3,3,3-hexafluoroisopropanol of **3**; (C–E) Optical microscope images recorded for a 50 mg/ml solution in 1,1,1,3,3,3-hexafluoroisopropanol of **3** at different times of UV-light exposure (T = 0, 30, and 60min, respectively); (F–G) SEM details of the sponge-like microstructure prior and after UV-light exposure, respectively.

Conformational Studies

Because of the presence of a chiral peptide linked to the polymer backbone, the resulting **3**-PDA was investigated by ECD spectroscopy. Specifically, DA **3** was converted into its organogel directly in a UV quartz-cuvette at the concentration of 10mg/ml in CH_2Cl_2 and the corresponding ECD spectrum was recorded as shown in Figure 4A (black curve). As expected, the contribution of the peptide chromophore was detected in the far-UV region (below 250 nm). The ECD spectra were also recorded after two different times of irradiation with UV light (Figure 4A; red line: 30 min; blue line: 60 min). In both cases, a set of intense

ECD bands were detected in the Vis range (400–50 nm) which may be attributed to the PDA chromophores that may be forced to chirally bend by the nearly chiral peptide substituents. Subsequently, the Boc protecting groups were removed from PDA by treatment with trifluoroacetic acid to allow formation of a water-soluble, terminally unprotected polymer. The corresponding ECD spectrum recorded in water (in the entire 200–600 nm range) is reported in Figure 4B. Above 300 nm it resembles in shape obtained for the terminally protected PDA discussed above. Interestingly, the unprotected PDA in water solution display a multi-wavelength fluorescence emission, as shown in Figure 4C. Finally, after adjusting the pH to 8, the water solution containing unprotected PDA rapidly turns into a hydrogels with formation of a dense fiber network, as detected by TEM (Figure 4D). The good solubility in DMF of this unprotected PDA has allowed its molecular weight characterization using SEC. We found a moderate polymerization degree (about 65 DA units) with a large polydispersity index (M: 183, monomer molecular weight; Mn: 11553, number average molecular weight; Mw: 14247, weight-average molecular weight; D: 1.21 molecular weight distribution index). This number of conjugated DA units is associated to the red-orange color of the resulting polymeric material. As reported in the literature, high DA polymerization degrees, as those occurring in reorganized DA-peptide based nanotubes, afford a blue colored polymer[36]. Moreover, the large degree of polydispersity occurring in our system may be responsible for the multi-wavelength fluorescence emission seen for this PDA (Figure 4C).

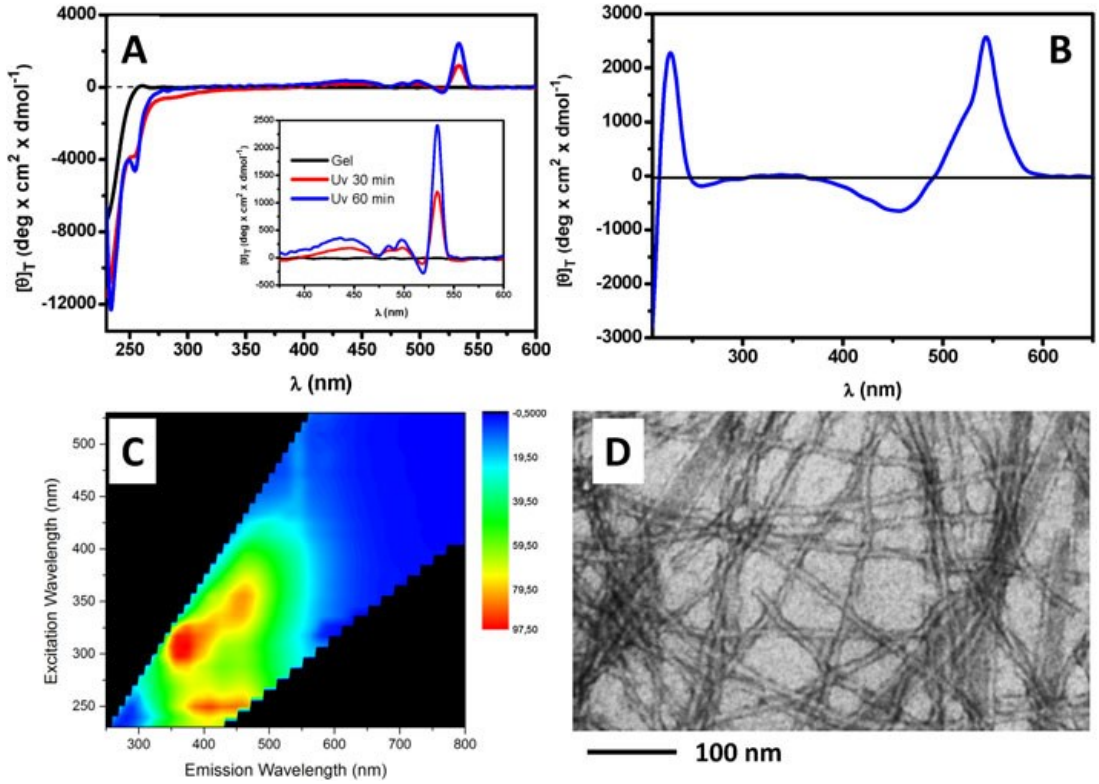

Fig. 4 (A) ECD spectra recorded in CH_2Cl_2 for: **3**-organogel (black curve) and **3**-organogel irradiated with UV light for 30 and 60min (red and blue curves, respectively). (B) ECD spectrum recorded for the terminally unprotected PDA in water solution. (C) Contour map of the fluorescence emission seen for the terminally unprotected PDA in water solution. (D) TEM image recorded for the hydrogel obtained starting from a water solution of the terminally unprotected PDA.

Electrospinning

We also decided to process **3** using the electrospinning technique by mixing it with PMMA. The strategy employed in this particular experiment initially involves DA monomers that are randomly distributed in an organic solvent before electrospinning. As the solvent evaporates during fiber formation, self-assembly of DA monomers does take place because the attractive forces among them are larger than those between the DA monomers and the matrix polymer molecules. Thus, polymerization of the self-assembled DA monomers should result in the formation of PDAs embedded within the polymer fibers[37]. In detail, a solution at the concentrations of 2% wt of **3** and 12% wt of PMMA was prepared by dissolving the two compounds in CH_2Cl_2 at room temperature. Electrospinning was performed for about 2 h to obtain a non-colored fiber matrix, which was subsequently irradiated under UV light, as illustrated in Figure 5A. Characterization of the resulting colored material was extended to

optical microscopy (Figure 5B) and SEM (Figure 5C). This latter technique clearly showed formation of a straight fiber network.

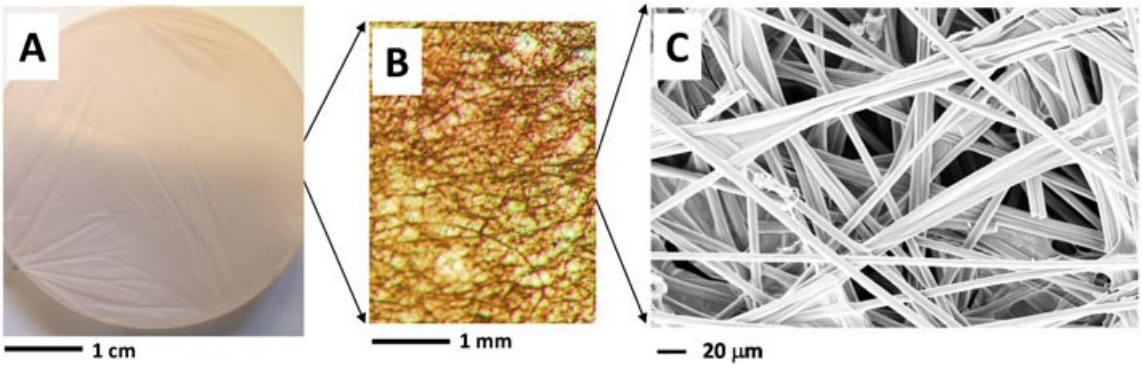

Fig. 5 (A) Solid material obtained using the electrospinning technique, starting from solution of **3** at 15% wt in dicloroacetic acid. (B) Optical microscope details of the resulting material. (C) SEM images showing the microarchitecture of the material obtained from electrospinning.

Conclusion

In this work, we report the synthesis and the self-assembly studies of a novel dipeptide-based diacetylene system able to forma stable organogel via the generation of an organized supramolecular fiber network. In these conditions, we took advantage of such molecular organization to promote the light-induced topochemical polymerization typically occurring for diacetylene monomers. This polymerization was studied with a set of spectroscopic and morphological techniques that confirmed the occurrence of the photochemical process in the organogel phase, which results in the formation of dipeptide-based polydiacetylene.

Experimental section

Instruments and Methods

Nuclear Magnetic Resonance. ^{1}H and ^{13}C NMR spectra were recorded at room temperature on a Bruker AC-200 (200MHz) instrument using tetramethylsilane (TMS) as the internal reference. The multiplicity of a signal is indicated as s, singlet; d, doublet; t, triplet; m, multiplet; and br, broad. Chemical shifts (δ) are expressed in ppm.

Fourier-Transform Infrared Absorption. FT-IR absorption spectra in KBr disk were obtained using a Perkin-Elmer 1720X spectrophotometer. The ν maxima values for the main absorption bands are given.

High-Resolution Mass Spectrometry. Mass spectra were obtained by electrospray ionization (ESI) on a Perseptive Biosystem Mariner ESI-ToF 5220 spectrometer. Data were collected in the positive mode.

Ultraviolet-Visible Absorption. UV-Vis absorption spectra were recorded using a Shimadzu model UV-2501 PC spectrophotometer. A 1-cm path length quartz cell was used.

Electronic Circular Dicroism. ECD measurements were carried out at room temperature using a Jasco J-715 spectropolarimeter. A fused quartz cell of 1-mm path length (Hellma) was used.

Raman Spectroscopy. Raman spectra of samples drop-casted on pre-cleaned glass micro slides (Corning) and annealed at 110 °C were recorded with an Invia Renishaw Raman microspectrometer (50x objective) using the 633-nm line of a He–Ne laser at room temperature with a low laser power.

Transmission Electron Microscopy. Samples were analyzed on a Jeol 300 PX TEM instrument. A glow discharged carbon coated grid was floated on a small drop of the nanosphere suspension, and excess was removed by #50 hardened Whatman filterpaper.

Fluorescence Emission Spectroscopy. The fluorescence spectra were measured upon excitation at different wavelengths using a Varian Cary Eclipse fluorimeter. A 1-cm path length quartz cell was used. The samples prepared for UV-Vis absorption were used to collect the fluorescence data.

Scanning Electron Microscopy. A Carl Zeiss Merlin field emission SEM operating at 5-kV accelerating voltage was used. A small drop of the nanosphere suspension was placed on a microscope glass coverslip and allowed to dry overnight.

Atomic Force Microscopy. AFM experiments were performed on Ntegra Aura (NT-MDT)

instrument operating in tapping mode at 200 to 400-kHz drive frequency and using a single crystal silicon tip coated with TiN (NSG01/TiN, 0.01-0.025 Ω-cm, antimony dope).

Size-Exclusion Chromatography. SEC analyses were performed on an Agilent 1260 Infinity system equipped with 1260 isopump, 1260 TCC, 1260 VWD VL, 1260 RID, Phenogel 5-µm linear/mixed guard column (30 x 4.6mm), followed by Phenomenex Phenogel 5-µm 104 Å (300 x 4.6mm) column working at 60°C. Dimethylformamide (DMF) was used as eluant at a flow rate of 1 ml/min. Before SEC analysis, the samples were filtered through a 0.2-µm PTFE filter (15 mm, Phenomenex). Molecular weights were calculated according to a calibration using polystyrene standards.

Electrospinning. A 2-ml SGE syringe with stainless steel needle was used as an electrode. Syringes with 2 ml of **3**/polymethyl methacrylate (PMMA) mixture were loaded in a syringe to control the flow rate of the solutions. Electrospinning was performed at ambient conditions with a constant applied voltage of +8 kV at needle and -5 kV at collector with the flow rate set at 0.01 ml/min to maintain a constant size of droplet at the tip of the syringe needle. A circular aluminum plate was used as the collector. The tip-to-collector distance was kept at 15 cm.

Synthesis and Characterization

Materials

1-Hydroxy-7-aza-1,2,3-benzotriazole (HOAt) was purchased from GL Biochem (Shanghai) Ltd. H-L-Cys(Me)-OH, HCl·H-L-Leu-OMe, Boc-L-Leu-OH, and N-(3-dimethylaminopropyl)-N′-ethylcarbodiimide hydrochloride (EDC·HCl) were obtained from Iris Biotech (Germany). Trifluoroacetic anhydride, N,N′-diisopropylcarbodiimide (DIC), 2,4,6-trichloro-1,3,5-triazine, 4-(dimethylamino)pyridine (DMAP), di-*tert*-butyl dicarbonate (Boc_2O), thionyl chloride, propargylamine, 1,8-diazabicyclo[5.4.0]undec-7-ene (DBU), triethylamine (TEA), N,N,N′,N′-tetramethylethylenediamine (TMEDA), copper(I) iodide, and nickel(II) chloride hydrate were obtained from Sigma-Aldrich. The deuterated solvent dimethylsulfoxide (DMSO-d_6) and $CDCl_3$ were purchased from Euriso-Top (France). All other chemicals and solvents are Sigma-Aldrich, Fluka, or Acros products and used as provided without further purifications.

Boc-L-Cys(Me)-OH

H-L-Cys(Me)-OH (5 g, 36.7mmol) was dissolved in 80 ml of the CH_3CN/H_2O (1:1 v/v)

solvent mixture in the presence of TEA (6ml, 43mmol). Boc_2O (8.4 g, 38.4mmol) was dissolved in 25ml of CH_3CN and added to the solution of the N-protected amino acid. The mixture was stirred at r.t. for 18 h. The organic solvent was removed under reduced pressure, and the aqueous solution was acidified with 1M HCl. The precipitate was extracted with ethyl acetate (EtOAc) (3v), then the organic phase was washed with water (2v) and brine. The organic layer was dried over Na_2SO_4, filtered, and evaporated to dryness under reduced pressure. The product was recovered as an oil (8.2 g, 94% yield).

HRMS (ESI+): m/z calcd. for $C_9H_{17}NO_4S$ 235.0878, found 236.1029 $[M+H]^+$.

FT-IR absorption: 3318, 3103, 1716, 1510 cm^{-1}.

^{1}HNMR (200 MHz,$CDCl_3$) δ 7.60 (br, 1H), 5.42 (d, J = 6.9 Hz, 1H, NH), 4.54 (d, J = 5.5 Hz, 1H, αCH), 2.97 (d, J = 4.6 Hz, 2H, βCH2), 2.14 (s, 3H), 1.44 (s, 9H). ^{13}CNMR (50 MHz, $CDCl_3$) δ 175.52, 155.70, 80.74, 53.02, 36.46, 28.42, 16.39.

Boc-L-Cys(Me)-L-Leu-OMe (1)

Boc-L-Cys(Me)-OH (6.76 g, 28.6 mmol) was dissolved in CH_2Cl_2 and C-activated with HOAt (3.9 g, 28.6 mmol) and EDC·HCl (5.48 g, 28.6mmol). Separately HCl·H-L-Leu-OMe (10.4 g, 38.8 mmol) was dissolved in CH_2Cl_2 with addition of TEA (10 ml, 71.8 mmol), and the resulting solution was added to that of the active ester. The mixture was stirred at r.t. for 18 h. The solvent was removed under reduced pressure and the residue dissolved in EtOAc. The organic phase was washed with 5% $KHSO_4$(aq) (4v), 5% $NaHCO_3$(aq) (3v), and brine. The organic layer was dried over Na_2SO_4, filtered, and evaporated under reduced pressure. The residue was dissolved in EtOAc and precipitated by addition of petroleum ether. After filtration and drying, the product was obtained as a white solid (8.35 g, 84% yield).

HRMS (ESI+): m/z calcd. for $C_{16}H_{30}N_2O_5S$ 362.1875, found 363.1966 $[M+H]^+$.

FT-IR absorption: 3342, 3281, 1756, 1682, 1656, 1557, 1522 cm^{-1}.

^{1}H NMR (200 MHz, $CDCl_3$) δ 6.84 (d, J = 8.1Hz, 1H, NH amide), 5.37 (d, J = 6.0 Hz, 1H, NH urethane), 4.66–4.55 (m, 1H, αCH), 4.30–4.20 (m, 1H, αCH), 3.73 (s, 3H, OMe), 2.98–2.67 (m, 2H, βCH_2 Cys), 2.17 (s, 3H), 1.68–1.60 (m, 3H, βCH_2 and γCH Leu), 1.46 (s, 9H), 0.93 (d, 6H, δCH_3 Leu). ^{13}C NMR (50 MHz, $CDCl_3$) δ 173.08, 170.68, 155.53, 80.65, 53.59, 52.46, 51.09, 41.63, 36.41, 28.40, 24.93, 22.92, 22.02, 16.04.

Boc-L-Cys(Me)-L-Leu-NH-CH_2-C≡CH (2)

A mixture of Boc-L-Cys(Me)-L-Leu-OMe (500 mg, 1.38 mmol), propargylamine (1 ml, 15.6 mmol), and DBU (40 µl, 0.27 mmol) was stirred at r.t. for 48 h. The mixture was diluted with EtOAc, and the organic phase was washed with 5% $KHSO_4$(aq) (3v) and brine. The solution was dried over Na_2SO_4, filtered, and the solvent was evaporated under reduced pressure. The product was obtained as a white solid (490 mg, 92% yield).

HRMS (ESI+): m/z calcd. for $C_{18}H_{31}N_3O_4S$ 385.2035, found 386.2110 $[M+H]^+$.

FT-IR absorption: 3283, 1693, 1646, 1548, 1525 cm^{-1}.

^1H NMR (200 MHz, $CDCl_3$) δ 7.00 (s, 1H, NH amide), 6.70 (d, J = 8.2 Hz, 1H, NH amide), 5.41 (d, J = 6.2 Hz, 1H, NH urethane), 4.50 (m, 1H, αCH), 4.24 (m, 1H, αCH), 4.01 (m, 2H, CH_2 propargyl), 2.87 (d, J = 5.2Hz, 2H, βCH_2 Cys), 2.19 (t, J = 2.5 Hz, 1H, -C≡CH), 2.14 (s, 3H), 1.91–1.52 (m, 3H, βCH_2 and γCH Leu), 1.45 (s, 9H), 0.92 (t, J = 6.2 Hz, 6H). ^{13}C NMR (50MHz, CDCl3) δ 171.42, 171.10, 155.92, 81.14, 79.46, 71.67, 54.07, 51.91, 40.61, 36.17, 29.34, 28.41, 24.92, 23.17, 21.81, 15.92.

[Boc-L-Cys(Me)-L-Leu-NH-CH2-C≡C-]$_2$ (3)

CuI (5 mol%) and $NiCl_2 \cdot H_2O$ (5 mol%) were dissolved in 500 µl of tetrahydrofuran (THF), then TMEDA (20 mol%) was added. The solution was stirred at r.t. under air for 2min. Boc-L-Cys(Me)-LLeu-NH-CH_2-C≡CH (500 mg, 1.30 mmol) was dissolved in 3 ml of THF. The mixture was stirred at r.t. under air for 48 h. The solvent was removed under reduced pressure, and the residue was purified by flash chromatography (eluant: 97:3 v/v CH_2Cl_2/MeOH). The product was recovered as a solid (260 mg, 50% yield).

HRMS (ESI+): m/z calcd. for $C_{36}H_{60}N_6O_8S_2$ 768.3914, found 769.3878 $[M+H]^+$.

FT-IR absorption: 3287, 1693, 1647, 1521 cm^{-1}.

^1H NMR (200 MHz, $CDCl_3$) δ 7.57 (t, 2H, NH amide), 7.07 (d, J = 8.2Hz, 2H, NH amide), 5.51 (d, J = 6.9Hz, 2H, NH urethane), 4.58 (m, 2H, αCH), 4.46–4.10 (m, 4H, αCH and CH_2 propargyl), 3.90 (m, 2H, CH_2 propargyl), 2.88 (d, J = 4.8 Hz, 4H, βCH_2 Cys), 2.14 (s, 6H), 1.87–1.52 (m, 6H, βCH_2 and γCH Leu), 1.46 (s, 18H, Boc), 0.92 (dd, J = 8.1, 6.0Hz, 12H). ^{13}C NMR (50 MHz, $CDCl_3$) δ 171.65, 171.35, 155.88, 80.91, 74.39, 68.01, 54.03, 51.91, 40.71, 36.49, 30.08, 28.43, 24.93, 23.07, 21.94, 16.01.

References

1. J. M. Lehn, *Angew. Chem. Int. Ed*., **1988**, 27, 89.
2. J. M. Lehn, *Angew. Chem. Int. Ed.*, **1990**, 29, 1304.
3. J. M. Lehn, *Science*, **1993**, 260, 1762.
4. J. M. Lehn, *Science*, **2002**, 295, 2400.
5. J. M. Lehn, *Proc. Natl. Acad. Sci. USA*, **2002**, 99, 4763.
6. G.M. Whitesides, and B. Grzybowski, *Science*, **2002**, 295, 2418.
7. G. Marafon, D. Mosconi, D. Mazzier, B. Biondi, M. De Zotti, and A. Moretto, *RSC Adv.*, **2016**, 6, 73650.
8. A. Rui, A. Mendes, and L. Gales, *J. Mater. Chem.*, **2012**, 22, 1709.
9. R. Chapman, M. Danial, M. L. Koh, K. A. Jolliffe, and S. Perrier, *Chem. Soc. Rev*., **2012**, 41, 6023.
10. E. Gazit, *Chem. Soc. Rev.*, **2007**, 36, 1263.
11. D. Mazzier, M. Maran, O. Polo Perucchin, M. Crisma, M. Zerbetto, V. Causin, C. Toniolo, and A. Moretto, *Macromolecules*, **2014**, 47, 7272.
12. Z. Luo, and S. Zhang, *Chem. Soc. Rev.*, **2012**, 41, 4736.
13. D. Mazzier, M. Favaro, S. Agnoli, S. Silvestrini, G. Granozzi, M. Maggini, and A. Moretto, *Chem. Commun.*, **2014**, 50, 6592.
14. X. Yan, P. Zhu, and J. Li, *Chem. Soc. Rev.*, **2010**, 39, 1877.
15. D. Mazzier, M. Mba, M. Zerbetto, and A. Moretto, *Chem. Commun.*, **2014**, 50, 4571.
16. M. Mba, A. Moretto, L. Armelao, M. Crisma, C. Toniolo, and M. Maggini, *Chem. Eur. J.*, **2011**, 17, 2044.
17. M. Mba, A. I. Jiménez, and A. Moretto, *Chem. Eur. J.*, **2014**, 20, 3888.
18. C. H. Görbitz, *Chem. Commun.*, **2006**, 22, 2332.
19. C. H. Görbitz, *Chem. Eur. J.*, **2007**, 13, 1022.
20. A. K. Das, D. Haldar, R. P. Hedge, N. Shamala, and A. Banerjee, *Chem. Commun.*, **2005**, 14, 1836.
21. P. P. Bose, A. K. Das, R. P. Hedge, N. Shamala, and A. Banerjee, *Chem. Mater.*, **2007**, 19, 6150.
22. M. Reches, and E. Gazit, *Science*, **2003**, 300, 625.
23. S. Ray, D. Haldar, M.G.B. Drew, and A. Banerjee, *Org. Lett.*, **2004**, 6, 4463.

24. M. Crisma, C. Toniolo, S. Royo, A.I. Jiménez, and C. Cativiela, *Org. Lett.*, **2006**, 8, 6091.
25. U.S. Raghavender, A.S. Kantharaju, N. Shamala, and P. Balaram, *J. Am. Chem. Soc.*, **2010**, 132, 1075.
26. U.S. Raghavender, B. Chatterjee, I. Saha, A. Rajagopal, N. Shamala, and P. Balaram, *J. Phys. Chem. B*, **2011**, 115, 9236.
27. D. Mazzier, F. Carraro, M. Crisma, M. Rancan, C. Toniolo, and A. Moretto, *Soft Matter*, **2016**, 12, 238.
28. G. Wegner, *Z. Naturforsch*, **1969**, 24b, 824.
29. D. Bloor, and R.R. Chance, Polydiacetylenes. NATO ASI Series, Applied Science, vol. 102 E, Nijhoff, Dordrecht, The Netherlands, **1985**.
30. R. Jelinek, and M. Ritenberga, *RSC Adv.*, **2013**, 3, 21192.
31. S. Wang, Y. Li, H. Liu, J. Li, T. Li, Y. Wu, S. Okada, and H. Nakanishi, *Org. Biomol. Chem*., **2015**, 13, 5467.
32. I. Levesque, S. Rondeau-Gagné, J.R. Néabo, and J.F. Morin, *Org. Biomol. Chem.*, **2014**, 12, 9236.
33. J. Liu, J.W.Y. Lam, and B.Z. Tang, *Chem. Rev.*, **2009**, 109, 5799.
34. E.C. de Lima, C.C. de Souza, R.O. Soares, B.G. Vaz, M.N. Eberlin, A.G. Dias, and P.R.R. Costa, *J. Braz. Chem. Soc*., **2011**, 22, 2186.
35. W. Yin, C. He, M. Chen, H. Zhang, and A. Lei, *Org. Lett.*, **2009**, 11, 709.
36. Y. Ishihara, and S. Kimura, *Biopolymers, Pept. Sci.*, **2012**, 98, 155.
37. S.K. Chae, H.K. Park, J. Yoon, C.H. Lee, D.J. Ahn, and J.M. Kim, *Adv. Mater*., **2007**, 19, 521.

3.1 Effect on the conformation of a terminally blocked, (E) β,γ-unsaturated δ-amino acid residue induced by carbon methylation

Introduction

Only in the late 1970's / early 1980's, in the medicinal chemistry and pharmacological fields the desirability of investigating proteolytically stable and successfully transportable synthetic analogs of bioactive peptides endowed with greatly reduced flexibility properties was first emphasized.[1-3] To this end, conformational restrictions, and sometimes even complete rigidity,[4,5] were envisaged as essential peptide prerequisites for the unambiguous elucidation of their structure – activity relationships. Peptide main-chain changes, involving either α-carbon modifications or amide bond replacements furnished novel families of compounds (termed peptidomimetics or pesudopeptides)[3,6,7] with significantly enhanced, more favorable physical and biological properties. More recently, it was observed that the enormous rise in the number of publications in this area is not only associated to compounds with therapeutic applications, but related to new properties of peptides in materials science as well.[8-10] In this connection, more than 20 years ago[4,11] it was clearly established that easy insertion of commercially available, achiral ω- (in particular β, γ, and δ-) amino acid residues into α-peptides generates peptidomimetics with replacement of the amide bonds by single or multiple methylene units in their backbones. Interestingly, the number of atoms (six) in a δ-amino acid is precisely matching that of a dipeptide segment. The saturated main chain of δ-amino valeric acid (δ-Ava) or 5-amino-pentanoic acid reflects with an acceptable approximation that of the Gly-Gly sequence.[10-13] By spectroscopic experiments, X-ray diffraction studies, and energy calculations it was also demonstrated that the simplest, rather flexible δ-Ava residue either prefers a *g-g-t-g-g* torsion angle sequence, thus allowing its accommodation into a folded (helical) peptide conformation, or a more elongated, β-sheet like, 3D-structure, the latter contributing to produce a hydrogel material with nanofibrous morphology at the supramolecular level.[10]

In this perspective, some conformational restrictions to the sp^3 CH_2 carbon chain of ω-amino acids were considered essential to construct appropriate model peptidomimetics with specific 3D-structural stabilizations. The most promising and extensively investigated constraint is the incorporation of a C=C moiety in the backbone. For example: (i) the introduction of one (or

multiple, even consecutive) units of the (*E, trans*)/(*Z, cis*) 3-aminoprop-2-enoic acid, -NH-CH=CH-CO-, in a β-peptidomimetic compound allowed its tunable (reversible) photoisomerization between two states, the former (*E*) being more extended and self-associating through N-H…O=C intermolecular H-bonds, while the latter (*Z*) being folded and characterized by a six-membered *pseudo*cycle energetically facilitated by an intramolecular N-H…O=C H-bond.[14,15] (ii) The base-induced double-bond migration of the (*E*) C^{α}=C^{β} moiety to the (*E*) C^{β}=C^{γ} positions of a γ-peptidomimetic, -NH-C^{γ}HR-C^{β}H=C^{α}H-CO- to -NH-C^{γ}R=C^{β}H-$C^{\alpha}H_2$-CO-, results in a conformational change from an open-chain to an intramolecularly H-bonded 3D-structure.[16] (iii) Semi-empirical conformational energy calculations on an (*E*) C^{β}=C^{γ} δ-peptidomimetic showed an increased flexibility with respect to the parent peptide, but mono-methylation on the C=C bond was predicted to induce a higher rigidity and a strong preference for backbone folding.[17] Unfortunately, however, subsequent NMR experimental data could not confirm this latter theoretical result.[18]

Figure 1 illustrates the chemical structures of a set of four N^{δ}-acetylated, C′-methylamidated δ-Ava peptidomimetic analogs (compounds **A** – **D**), exhibiting an (*E*) alkene unit in their main chain. Among *carbon* derivatives, exclusively *methylated* compounds were examined. These derivatives range from the *un*methylated compound **A**, to the *bis*-methylated compounds **B** and **C** (with *bis*-methylation either on the C^{β}=C^{γ} double bond, compound **B**, or on the C^{α} / C^{δ} atoms, external to the double bond, compound **C**), to the *ter*-methylated compound **D** (with C^{α}, C^{β}, and C^{δ} methylated atoms). Conformational analyses on terminally-blocked (or protected) analogs of them were already performed to a limited extent by other research groups,[19-22] but their preferred 3D-structures have been reanalyzed in this work, in particular using modern density functional theory (DFT) calculations.

In addition, the present study was aimed at expanding our general knowledge on this peptidomimetic system by and studying in detail the conformational preferences of the novel compound **E** (Figure 1) or its N^{δ}-Boc (*tert*-butyloxycarbonyl) protected, isopropyl amidated analog, (Boc)**E 10**, by use of computational analysis, and crystal-state (X-ray diffraction) and solution (FT-IR absorption and NMR spectroscopies) investigations. Our main focus was to further highlight and explain in depth the reasons for the beneficial effect, already suggested in limited cases,[17,19-23] produced by the introduction of methyl substituents on the sp^3 and/or sp^2 carbons of δ-Ava on folding (in particular on formation of the popular β-turns)[24-27] in

these peptidomimetics. The most representative β-turns, energetically favored by the occurrence of a C=O···H-N intramolecular H-bond, forming a ten-membered *pseudo*cycle, are the non-helical types I (I′) and II (II′), accompanied by type III (III′), the consecutive repetition of the latter generating the right- (or left-) handed 3_{10}-helical polypeptide structure.[6,28-32]

Finally, for a better comparison, an experimental conformational investigation analogous to that mentioned above for the carbon *tetra*methylated compound (Boc)**E 10** was also carried out on the *un*methylated compound (Boc)**A 6**. Interestingly, the two *gem*-dimethyl groups present in compound **E** make it to closely resemble the homo-dipeptide sequence based on the α-amino acid Aib (α-aminoisobutyric acid).[30,33,34] Indeed, this sequence, the most prone among those known to adopt a stable type III (III′) β-turn and to afford a regular 3_{10}-helix thanks to a double Thorpe-Ingold effect,[35] is expected to be a very promising choice.

Specifically, here we will discuss in detail the conformational propensities of the *achiral* compounds **A** and **B** unmethylated at both -CH_2- ("Gly-Gly" dipeptide mimics) and the *achiral* compound **E** *bis*-methylated at each -CH_2- ("Aib-Aib" dipeptide mimic). In addition, our attention will also focus on the chiral compounds **C** and **D**, both *mono*-methylated at each -CH_2- ("L-Ala-D-Ala" dipeptide mimics).[19-21] The chosen combination of configurations in these two latter compounds corresponds to that which is the most apt to accommodate a type-II β-turn conformation in an α-peptide chain. Note that related literature studies on other examples of *chiral* dipeptide mimetics ("Val-Gly",[36] "Leu-Gly",[37] "Ala-Gly",[18] "Phe-Gly",[17] "Phe-Ala",[38] and "Phe-Phe"[39-41]) of this type were not further treated in this paper because these compounds exhibit at least one carbon replacement different from simple methylation.

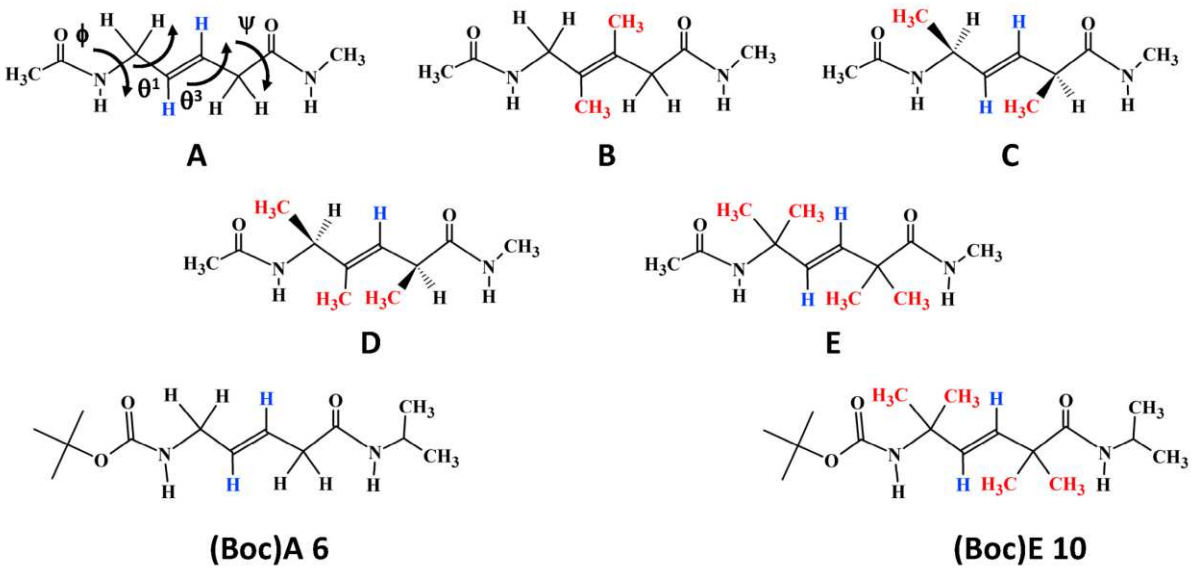

Fig. 1 Chemical structures of the compounds investigated in this work either by DFT calculations (compounds **A** – **E**) or experimentally (compounds **6** and **10**). In **A**, the backbone torsion angles conformationally relevant for this set of compounds are indicated.

Results and discussion

Theoretical conformational analysis

A systematic conformational search procedure was conducted to study the free energy (ΔG) landscape of peptides **A**-**E** (Figure 1) *in vacuo*.

DFT calculations at the M06L/6-31+G(d,p) level on achiral **A** (R_i= H with *i*= 1 to 6) and **B** (R_3= R_4= CH_3, R_i= H with $i \neq$ 3, 4) led to 9 minimum energy conformations (Tables 1 and 2, respectively), which are degenerated (*i.e.* minima with $\{\varphi,\theta^1,\theta^3,\psi\}$ and $\{-\varphi,-\theta^1,-\theta^3,-\psi\}$ are energetically equivalent) in a ΔG interval of 4.3 and 4.8 kcal/mol, respectively. However, according to a Boltzmann distribution, only two minima of **A** and one of **B** showed a population higher than 5%. These minima, named **a1** and **a2** in Figure 2a and **b1** in Figure 2b, are stabilized by a specific intramolecular interaction, forming a ten-membered H-bonded ring (C_{10}) that is characteristic of the β-turn.[24-27] Indeed, all these minima mainly differ in the arrangement of the central region, which is defined by the dihedral angles θ^1 and θ^3 (Figure 1). In the case of the unmethylated **A**, the backbone is slightly more strained for **a2** than for **a1**, causing an improving in the H-bonding geometry but a destabilization of 0.1 kcal/mol. Detailed inspection of Table 1 indicates than such minima present intramolecular H-bonds, whereas the rest do not display any specific interaction. Comparison of these results with the very limited amount of β-turn found by Gellman and co-workers[19,20] in solution for the

strictly related N^{δ} *i*Pr-CO-, C′ -NH*i*Pr blocked analog and corroborated by our experimental results on the N^{δ} Boc analog (see below) suggests that the stability of the latter conformations (those without intramolecular H-bonds) increases in condensed phases. In the case of the *bis*-methylated **B**, the backbone torsion angles of **b1** are relatively similar to those of **a2** and, therefore, the H-bonding parameters are close to the ideal geometry. An additional minimum with torsion angles resembling those of **a1** and stabilized by a C_{10} H-bonded ring (Figure 9) is also detected for **B**. This 3D-structure results disfavored by 1.8 kcal/mol due to the steric hindrance caused by the side methyl groups (R_3 and R_4).

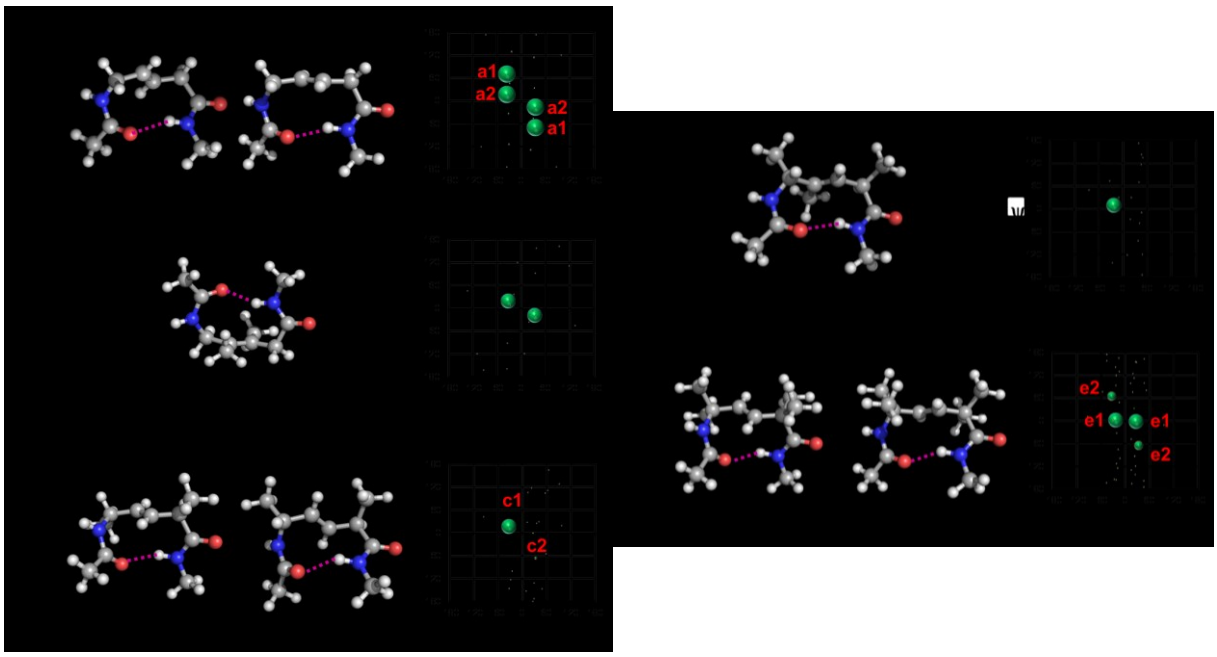

Fig. 2 Representative minimum energy conformations and "ϕ", "ψ" maps of compounds **A**, **B**, **C**, **D**, and **E** (**a** - **e**, respectively). Calculated torsion angles and ΔG values are presented in Tables 1-5.

In order to facilitate the representation of the conformational preferences of **A** and **B**, a Ramachandran-like map was plotted using two virtual torsion angles, φ′ and ψ′ (see Experimental Section), which were selected to account for the relative position of each amide group with respect to the central double bond (Fig. 8). The position of all minima was plotted in the maps using dots sized according to ΔG (Figures 2a-b). The map obtained for **A** indicates that both φ' and ψ' display low, but non-negligible, conformational flexibilities. This observation explains the very weak band associated to intramolecularly H-bonded N-H that was identified by IR absorption spectroscopy by Gellman and coworkers in solution.[19,20] In contrast, the map depicted for **B** shows that methylation at both C^{β} and C^{γ} atoms causes

strong restrictions in the conformational preferences, which is also consistent with previous experimental results[19,20] indicating a significant amount of β-turn in solution.

Energy minimization of the starting conformations constructed for the *bis*-methylated **C** (R_1= R_5= CH_3) led to 23 minimum energy conformations, which are listed in Table 3. These minima are distributed in the following way: two minima with $\Delta G \leq 1.5$ kcal/mol, which concentrate a population of 90.7%, while the remaining 21 show $\Delta G_{gp} \geq 1.9$ kcal/mol. The two preferred conformations of **C**, hereafter denoted **c1** and **c2**, are stabilized by a C_{10} H-bond (Figure 2c) and show some resemblance with **a2** and **a1**, respectively. Thus, the substitution of the H atom by a CH_3 group at both R_1 and R_5 inverts the order of stability of the two β-turn folds obtained for **A**. There is an additional conformation stabilized by an intramolecular C_{10} H-bonded ring, named **c6**, which is destabilized by 2.4 kcal/mol (*i.e.*, population at 298 K: 1.3%, Table 3). Inspection of the φ'-ψ' map obtained for **C** (Figure 2c) indicates that substitutions in R_1 and R_5 not only alter the energy landscape but also restrict the conformational flexibility with the respect to **A**, favoring considerably the β-turn folding.

Because of its trimethylation (at the R_1, R_3, and R_5 positions), **D** combines the conformational restrictions found for **B** and **C**. The relevant structural parameters of the 18 minimum energy conformations identified for **D** are listed in Table 4. The population of the global minimum amounts to almost 99%, the ΔG of the other minima ranging from 2.8 to 9.4 kcal/mol. The torsion angles of the global minimum (**d1** in Figure 2d), which is stabilized by a C_{10} H-bonded ring, are very similar to those found for **b1**, indicating that the methylation at C^{γ} has a higher influence than that at either C^{α} or C^{δ}. As it is illustrated in the φ'-ψ' map, the contribution of the rest of the minima is practically negligible, even though two of them are stabilized by intramolecular H-bonds. Again, the energy landscape predicted for **D** is fully consistent with the observed preferences for the β-turn conformation.[24-27]

Finally, compound **E**, which is tetramethylated at the C^{α} and C^{δ} atoms, shows 23 degenerated minima (Table 5). However, only two of them, named **e1** and **e2** (Figure 2e), with populations of 74.2% and 25.4%, respectively, are representative. These 3D-structures, which exhibit torsion angles that resemble those of **a2** and **a1**, respectively, are stabilized by a C_{10} H-bonded ring. It is worth noting that the 21 remaining conformers are disfavored by at least 3.9 kcal/mol, strongly suggesting that their contribution in terms of population is practically null.

Overall, our results extracted from DFT calculations indicate that the conformational preferences for the unmethylated **A** are intrinsically constrained by the double bond

connecting the C^{β} and C^{γ} atoms. These restrictions increase upon methylation at C_{sp2} (C^{β} and C^{γ}) and/or C_{sp3} (C^{α} and C^{δ}) atoms because of the induced repulsive interactions. The conformational flexibility of **C** decreases with respect to **A** because of $CH_3\cdots H$ interactions, which are much more repulsive than the H···H interactions. The principles of these interactions are analogous to the steric strain balance characteristic of substituted annular compounds (Thorpe-Ingold effect).[35] According to this phenomenon, which was originally extended to peptides by Balaram and coworkers[6] and by Toniolo and coworkers,[28] the peptide folding can be governed through the restrictions imposed by the incorporation of methyl groups at the C_{sp3} atoms, as it is observed for **C**. On the other hand, compounds methylated at the C_{sp2} atoms exhibit the steric 1,3-allylic strain.[19,42] This phenomenon is clearly displayed by **D**, which incorporates a methyl R_3-substituent at the *Z* position of the double bond relative to the C^{δ} chiral center. As shown in Tables 3-4, **D** displays conformational changes with respect to **C** that are caused by the addition of the 1,3-allylic strain to the Thorpe-Ingold effect. The resemblance between the torsion angles of **b1** (1,3-allylic strain), **c1** (Thorpe-Ingold effect), and **d1** (Thorpe-Ingold effect combined with 1,3-allylic strain), which are close to those of **a2** rather than to those of **a1**, suggests that the structural consequences of both repulsive effects are similar.

Amazingly, the conformational behavior of **E** resembles that of **A** more than those of **B**-**D**. Thus, the *bis*-methylation at each of the two sp^3 carbon atoms eliminates the effect associated to the steric 1,3-allylic strain, which was observed for **B** and **D**. Moreover, the Thorpe-Ingold effect in **E** results in a slight destabilization of the local minima with respect to **A**, even though the number of minima increases significantly. Thus, the 9 degenerated minima found for **A** are comprised within a ΔG interval of 4.3 kcal/mol, whereas the first 9 minima of **E** are within a range of 4.9 kcal/mol. However, 14 additional local minima, which were not detected for **A**, were identified for **E**. We attribute these features to the fact that the potential surface is more abrupt for **E** than for **A** because the $CH_3\cdots CH_3$ interactions are more repulsive than the H···H interactions. Consequently, the minima are less stable and more numerous in compound **E**. On the other hand, considering that, as mentioned above, Thorpe-Ingold and 1,3-allylic strain effects have a similar impact on the structure and that they are additive, the stability of the β-turn motif should be higher for **E** than for **B**, **C** and, probably, **D**.

Synthesis

The overall synthetic strategy for the preparation of the unmethylated compound **6** and its tetramethylated counterpart **10** is illustrated in Scheme 1. Fischer esterification of *trans*-β-hydromuconic acid **1** afforded both the mono- and the diethyl ester derivatives (**2** and **3**, respectively) which were easily separated. Compound **6** was synthesized following essentially the protocol previously reported by Gellman and coworkers.[20] Briefly, the mono-ester **2** was converted into the N^{δ} Boc-protected compound **4** under Curtius rearrangement conditions in the presence of diphenylphosphoryl azide (DPPA), N,N-di*iso*propylethylamine (DIPEA), and *tert*-butanol (*t*BuOH). The subsequent saponification of **4** with LiOH in a water/THF mixture afforded the free acid **5**. Then, amination of **5** under 1-hydroxy-1,2,3-benzotriazole (HOBt) / N-(3-dimethylaminopropyl)-N′-ethylcarbodiimide (EDC) mediated coupling with *iso*propylamine provided **6**.

Compound **10** was obtained starting from the diethyl ester of *trans*-β-hydromuconic acid **3** that was tetra-methylated at its acidic methylene positions by treatment with LDA and methyl iodide, yielding **7**. Attempts to carry out a partial saponification of **7** to isolate the corresponding mono-acid in an amount large enough to proceed with the synthesis failed. Therefore, we were forced to postpone the de-symmetrization of the molecule to a subsequent synthetic step. *Full* saponification of diester **7** by treatment with LiOH in a water/THF mixture at 0°C afforded the dicarboxylic acid **8.** Mono-amidation of **8** to provide **9** was performed through HOBt/EDC mediated coupling with *iso*propylamine. Then, **9** was converted into the N^{δ} Boc-protected compound **10** under Curtius rearrangement conditions in the presence of DPPA, DIPEA, and *t*BuOH. Workup of the reaction mixture leading to **10** also allowed the isolation of a side product which was identified (*inter alia* by single crystal X-ray diffraction analysis; see below) as the carbamoylazido derivative **11**. The possible formation of such a side product in this type of reaction is documented in the literature.[43]

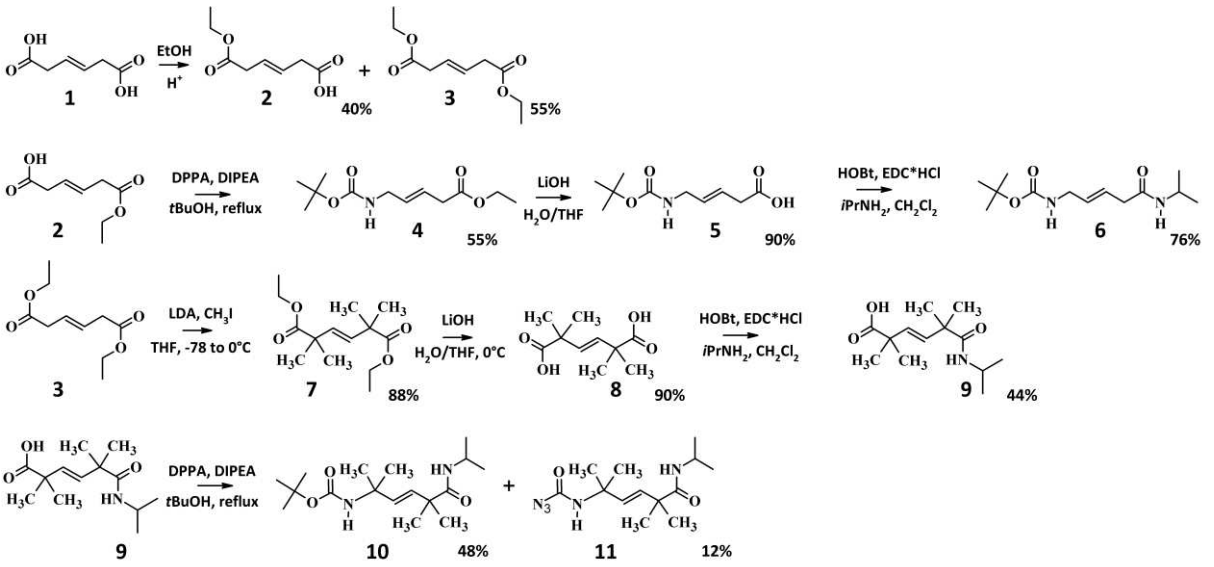

Scheme 1 Representation of the synthetic strategy for the preparation of the unmethylated compound **6** and its tetramethylated counterpart **10**.

Crystal-state conformational analysis

The crystal-state conformations of the unmethylated compound Boc-5-aminopent-3-(*E*)-enoyl-NH*i*Pr and its *tetra*-methylated analog Boc-5-amino-2,2,5,5-tetramethyl-pent-3-(*E*)-enoyl-NH*i*Pr (compounds **6** and **10**, respectively, in Scheme 2) were determined by X-ray diffraction analysis. In addition, the N^{δ}-azidocarbonyl analog of compound **10** (denoted as **11** in Scheme 2 and obtained as a minor side product in the synthesis of **10**) was also characterized by single crystal X-ray diffraction analysis. In general, bond distances and bond angles are in agreement with values typical for the Boc-urethane group,[44] the alkene and azido moieties,[45] and the amide unit.[46] In all three structures the -C-CH=CH-C- moiety is found in the expected *E* disposition, with deviations from the *trans* planarity not exceeding 4.7°. The urethane and amide bonds are also found in the *trans* disposition, the largest deviation [12.59(16)°] from 180° being found for ω^{N} of molecule 3 in the structure of Boc-5-aminopent-3-(*E*)-enoyl-NH*i*Pr [(Boc)**A**, **6**].

Three crystallographically independent molecules compose the asymmetric unit in the structure of Boc-5-aminopent-3-(*E*)-enoyl-NH*i*Pr (**6**) (Figure 3) in the monoclinic centrosymmetric space group C2/c. The values of the backbone torsion angles (Experimental Section, Table 9) adopted by the three molecules indicate that molecules 1 and 2 have in common a succession of similar ϕ, θ^{1}, and θ^{3} values [141.8(2)°, 119.8(3)°, and -121.2(3)°,

respectively, in molecule 1, whereas 140.2(2)°, 125.6(2)°, and -117.9(3)° in molecule 2], but differ by almost 20° in the value of ψ [-123.2(2)° *vs* -142.2(2) °]. Overall, molecules 1 and 2 are essentially extended.

The conformation adopted by molecule 3 is more kinked at the ϕ level [87.9(2)°], while the remaining θ^1, θ^3, and ψ torsion angles [127.4(2)°, -107.4(2)°, and -138.7(2)°, respectively] are not far from those of the other two molecules. As a consequence of the (more or less) extended backbone conformation, all molecules are devoid of any intramolecular H-bond. Conversely, an extended network of intermolecular N-H···O=C H-bonds is observed in the packing mode (Experimental Section, Table 10 and Figure 10). Each molecule is involved in four intermolecular H-bonds with two flanking molecules (either within the same asymmetric unit or symmetry related), on one side as the donor [through the N-terminal (N) and the C-terminal (NT) N-H groups] and on the other side as the acceptor (through the urethane O0 and the C-terminal O carbonyl oxygen atoms).

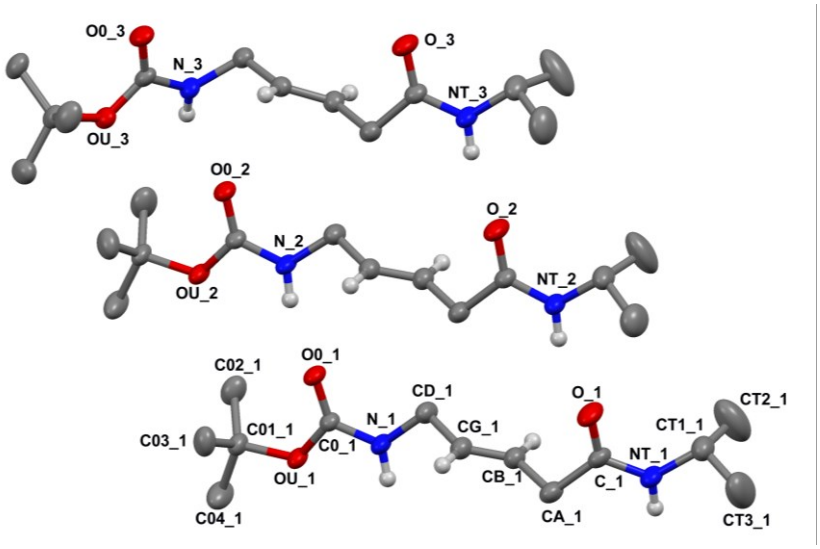

Fig. 3 X-Ray diffraction structure of Boc-5-aminopent-3-(E)-enoyl-NHiPr (**6**). Anisotropic displacement ellipsoids are drawn at the 30% probability level. Most of the H-atoms are omitted for clarity. Only nitrogen and oxygen atoms of the three crystallographically independent molecules are labeled, except for molecule 1 (bottom) for which full atom numbering is reported.

At variance with its unmethylated counterpart described above, Boc-5-amino-2,2,5,5-tetramethyl-pent-3-(*E*)-enoyl-NH*i*Pr (**10**) adopts a folded conformation in the crystal state (Figure 4), stabilized by an intramolecular N-H···O=C H-bond between the C-terminal *iso*propylamide NT-H group and the urethane carbonyl O0 oxygen atom [N···O and H···O distances 3.120(3) Å and 2.30 Å, respectively; N-H···O angle 160.6°].[47-50] In the molecule arbitrarily selected as the asymmetric unit in this centrosymmetric structure, the values of the

ϕ, θ^1, θ^3, and ψ torsion angles are 60.4(3)°, 8.9(4)°, 98.7(3)°, and -3.3(3)°, respectively. These values are not far from the backbone torsion angles typical for the *i*+1 and *i*+2 corner positions of a regular type-I′ β-turn conformation (60°, 30° and 90°, 0°, respectively).[24-27] Interestingly, the near-zero value of θ^1 allows the staggering of the C1G-H bond relative to the two methyl substituents on C1D. As a result, the (ethylenic) H-atom linked to C1G is at 2.62 Å from C1D1 and 2.80 Å from C1D2. Similarly, as a consequence of the value of ψ, the C1=O1 group is staggered with respect to the C1A1 and C1A2 methyl groups.

In the packing mode, an intermolecular H-bond is observed between the (urethane) N1-H1 group and a (*x*, *y*-1, *z*) translational equivalent of the (amide) O1 carbonyl oxygen atom, generating rows of molecules (of the same handedness within each row) along the *b* direction (Experimental Section, Table 12 and Figure 12). Packing is then completed through van der Waals interactions.

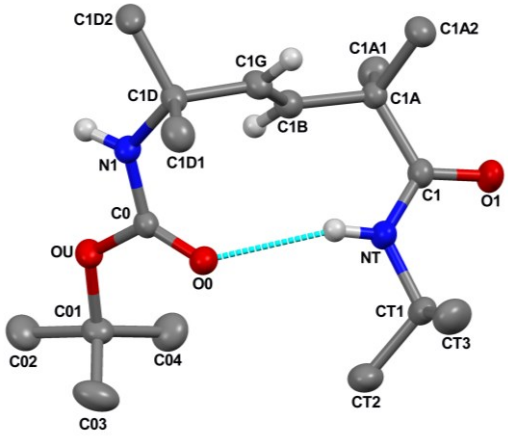

Fig. 4 X-Ray diffraction structure of Boc-5-amino-2,2,5,5-tetramethyl-pent-3-(*E*)-enoyl-NH*i*Pr (**10**). Anisotropic displacement ellipsoids are drawn at the 30% probability level. Most of the H-atoms are omitted for clarity. The (urethane) C=O···H-N (amide) intramolecular H-bond is represented by a dashed line.

The crystal-state conformation of azidocarbonyl-5-amino-2,2,5,5-tetramethyl-pent-3-(*E*)-enoyl-NH*i*Pr (**11**) (Figure 5) is also folded and stabilized by an intramolecular H-bond between the C-terminal *iso*propylamide NT-H group and the carbonyl O0 oxygen atom [N···O and H···O distances 3.0641(15) Å and 2.25 Å, respectively; N-H···O angle 158.7°].[47-50] The values of the backbone torsion angles of the molecule arbitrarily selected as the asymmetric unit in the centrosymmetric structure are: ϕ = 50.7(2)°, θ^1 = -130.52(15)°, θ^3 = -110.48(15)°, and ψ = 32.42(17)°. Therefore, at variance with the Boc-analog **10** described above, the folding of **11** resembles that of a type-II′ β-turn,[24-27] in which the typical ϕ,ψ

values for the *i*+1 and *i*+2 corner positions are 60°,-120° and -80°,0°. Basically, the main difference in the backbone folding between **10** and **11** is represented by a 180° flipping of the central ethylenic unit. As a result, in the structure of **11**, the (ethylenic) C1G-H bond is *anti*periplanar to the C1D-C1D1 bond, thus bringing the H-atom linked to C1G closer to C1D2 (2.76 Å) than to C1D1 (3.37) Å.

The packing mode of **11** is similar to that of **10**, being characterized by an intermolecular H-bond between the N1-H1 group and a (*x*, *y*-1, *z*) translational equivalent of the O1 carbonyl oxygen atom, generating rows of molecules along the *b* direction (Supporting Information, Table S14 and Figure S7).

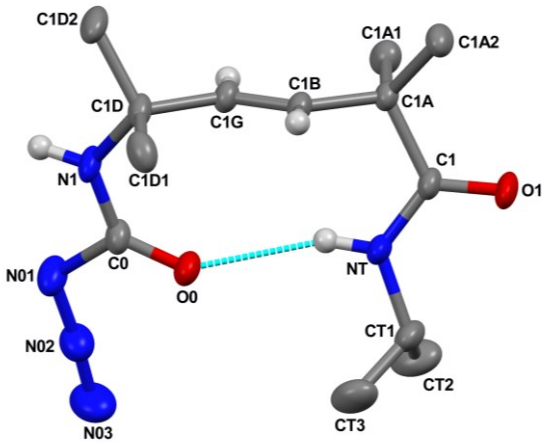

Fig. 5 X-Ray diffraction structure of azidocarbonyl-5-amino-2,2,5,5-tetramethyl-pent-3-(*E*)-enoyl-NH*i*Pr (**11**). Anisotropic displacement ellipsoids are drawn at the 30% probability level. Most of the H-atoms and the second position for the methyl groups of the disordered C-terminal isopropyl group are omitted for clarity. The (carbamoylazido) C=O···H-N (amide) intramolecular H-bond is represented by a dashed line.

The different β-turn-like conformations adopted by **10** and **11**, namely type-I′ (I) in **10**, whereas type-II′ (II) in **11**, might at least in part related to the different packing requirements associated to the N-terminal groups (Boc in **10** *vs* azidocarbonyl in **11**). In any case, however, it is clear that both conformations are accessible to the -CO-NH-C(CH_3)$_2$-CH=CH-C(CH_3)$_2$-CO-NH- sequence. Interestingly, the results of the gas-phase DFT calculations on the related compound **E** (Figure 1) indicate as the most stable and more populated (74.2% at 298 K) a conformation characterized by φ, θ^1, θ^3, and ψ values of the backbone torsion angles of 58.1°, -125.8°, -107.4°, and 23.8°, respectively (conformer **e1** in Figure 2; see also Supporting Information, Table S5). These values are close to those found in the structure of **11**. In addition, the conformer **e2** (Figure 2 and Supporting Information, Table S5), which is only 0.6

kcal/mol above the global minimum, with a population of 25.4% *in vacuo* at 298 K according to the theoretical results, exhibits backbone torsion angles (φ, θ^1, θ^3, ψ = 60.4º, 8.8º, 98.6º, -3.2º) not far from those observed in the structure of **10**.

Conformational analysis in solution

To obtain information on the tendency toward intramolecularly H-bonded, folded 3D-structure formation of the unmethylated "Gly-Gly" dipeptide mimic compound **A** and its tetramethylated "Aib-Aib" dipeptide mimic compound **E**, both achiral, we carried out FT-IR absorption and ^{1}H NMR investigations in $CDCl_3$ solution on their more soluble, N^δ-Boc protected, C′-*iso*propylamide analogs (Boc)**A 6** and (Boc)**E 10** (Figure 1).

In the FT-IR absorption spectra [amide A (N-H stretching) region] (Figure 6), the bands (shoulders) above 3415 cm^{-1} for the two compounds are assigned to the free (solvated) urethane and amide NH groups, while the band near 3358 cm^{-1} to C=O···H-N H-bonded NH groups.[51-54] The ratio of the integrated intensity of the free / H-bonded bands is hugely in favor of the free spectral component in the case of (Boc)**A 6**, whereas the H-bonded spectral component is even prevailing in the case of (Boc)**E 10**. Moreover, this ratio changes, but slightly, for (Boc)**A 6**, whereas it remains remarkably unmodified for (Boc)**E 10** upon a tenfold dilution (from 1.0 to 0.1 mM concentration; Supporting Information, Figures S8 and S9). This finding strongly suggests that the observed H-bonding is essentially *intra*molecular in the case of (Boc)**E 10**, while intermolecular H-bonds contribute, but only to some extent, to the weak H-bonded band of (Boc)**A 6**. These results, in excellent agreement with those already published by Gellman and coworkers[19,20] on an N^δ-acylated analog of **A** and one of its *bis*-methylated derivatives in DCM solution, clearly support the view that there is very little intramolecular H-bonding in this backbone structure in the absence of significant methylation and of the related preorganization induced by either allylic strain[42] (as in the Gellman's β,γ *bis*-methylated derivative) or the double Thorpe-Ingold effect operative in our compound (Boc)**E 10**, *gem*-dimethylated at both C^α and C^δ. From these IR absorption data we also tend to conclude, again in parallel to refs. 19 and 20, that the almost exclusive type of intramolecular H-bond in compound (Boc)**E 10** refers to that with the C-terminal amide NH group as donor and the N-terminal urethane C=O group as acceptor (formation of the common C_{10}- or β-turn) as observed in the crystal state (see above), without any relevant

contribution from the rather unusual C_8- or δ-turn[55] formation (with the N-terminal urethane NH group as donor and the C-terminal amide C=O group as acceptor). Finally, it is worth emphasizing that the H-bonded spectral component is significantly larger in our tetramethylated compound (Boc)**E 10** than in the Gellman's β,γ *bis*-methylated compound (labeled **1** in ref. 19 and **2** in ref. 20).

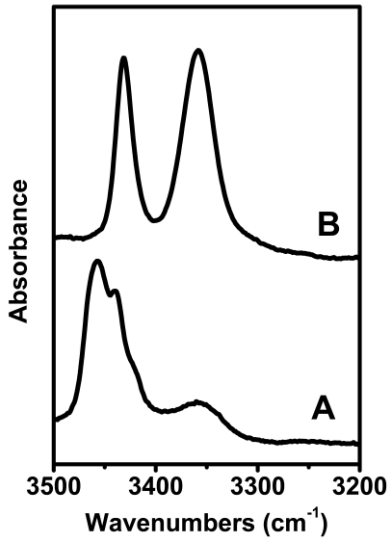

Fig. 6 FT-IR absorption spectra in $CDCl_3$ solution (1.0 mM concentration) of compounds (Boc)**A 6** (top) and (Boc)**E 10** (bottom) in the 3500-3200 cm^{-1} wavenumber (N-H stretching) region.

Our FT-IR absorption conclusions on the conformational preferences of (Boc)**E 10** in $CDCl_3$ solution at 1.0 mM concentration were confirmed by a 400 MHz ^1H NMR investigation. The delineation of intramolecularly H-bonded NH group(s) was carried out by use of solvent dependence of NH proton chemical shifts by adding increasing amounts of the strong H-bonding acceptor solvent DMSO[56] to the $CDCl_3$ solution (Figure 7). The upfield resonance in $CDCl_3$ (5.2 ppm) is unambiguously assigned to the N-terminal urethane NH proton.[52] This NH resonance is remarkably sensitive to the addition of DMSO, whereas the other (amide) resonance displays a behavior suggesting insensitivity of the chemical shift to solvent composition. In summary, our ^1H NMR results allow us to reasonably conclude that in a solvent of low polarity ($CDCl_3$) and in the absence of self-association the C-terminal *iso*propylamide NH proton is almost inaccessible to the perturbing agent and is therefore most probably intramolecularly H-bonded.

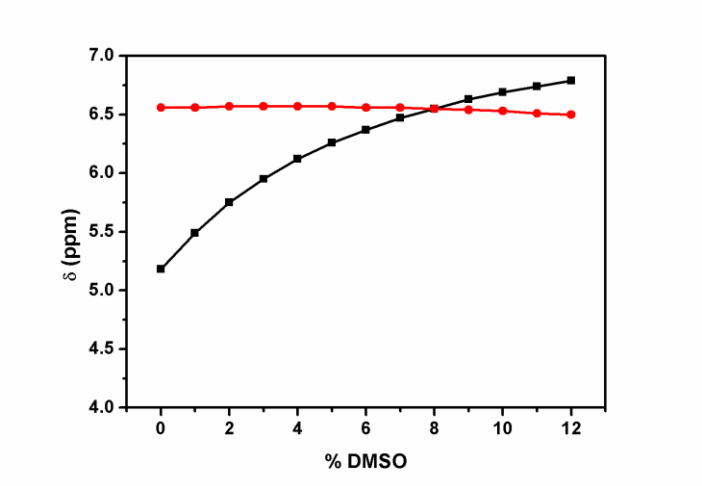

Fig. 7 Plot of the chemical shifts of the NH proton signals in the NMR spectrum of Boc-5-amino-2,2,5,5-tetramethyl-pent-3-(*E*)-enoyl-NH*i*Pr (**10**) as a function of the addition of increasing percentages (*v*/*v*) of deuterated DMSO to the $CDCl_3$ solution. Peptide concentration: 1.0 mM. The Boc-urethane and the C-terminal *iso*propylamido NH proton signals are displayed in black and red colors, respectively.

Conclusions

(*Trans*) amide-to-(*E*) olefin is an ideal replacement in a peptide because both the overall geometrical and conformational preferences of the former backbone are essentially maintained in the latter. In particular, the number of intervening atoms in the saturated -$C^{\delta}H_2$-$C^{\gamma}H_2$-$C^{\beta}H_2$-$C^{\alpha}H_2$- δ-amino acid δ-Ava corresponds exactly to that in the "original" -Gly-Gly- dipeptide sequence. As a result, not surprisingly in recent years the conformational propensities of terminally blocked (or protected) δ-Ava analogs with a central (*E*) olefin moiety have been the subject of a few investigations.[17-21,37-41] However, their potentially large variety has been covered only partially and the conclusions extracted appear sometime contradictory.

In this work, we focused our DFT computational and experimental (X-ray diffraction, FT-IR absorption, and NMR) studies on the conformation of the -NH-CH_2-CH=CH-CH_2-CO- system of β,γ-olefin δ-Ava derivatives with only simple methyl substitution on its carbon atoms, including the hitherto unexplored *bis*-methylation at each -CH_2- (in addition to the unsubstituted sequence). The obtained in-depth information on the 3D-structural preferences (specifically, on the folding tendencies) confirm the initial findings by Gellman,[19,20] Wipf[21] and their coworkers of the role of the allylic 1,3-strain[42] as a favorable controlling 3D-structural factor in inducing β-turn formation. However, the most relevant piece of additional

information comes from our investigation on the (2,2,5,5) *tetra*-methylated derivative which exhibits the remarkably highest tendency to fold known so far in this series, generated by a combination of positive 1,3-strain and Thorpe-Ingold effect[7,35] (double *gem*-methylation). Finally, our results suggest that the stability of the β-turn pattern of the -CH_2-CH=CH-CH_2- sequence of a δ-Ava derivative might be even further enhanced in the case of the completely (hexa-) methylated system.

Experimental Section

Instruments and Methods

High-Performance Liquid Chromatography. The HPLC measurements were performed using an Agilent 1200 apparatus (Palo Alto, CA), equipped with a UV detector at 216 nm and a column Agilent extend-C18 (stationary phase). Eluants: A= 9:1 H_2O/CH_3CN, 0.05 % TFA; B= 1:9 H_2O/CH_3CN, 0.05 % TFA.

Nuclear Magnetic Resonance. ^1H NMR and 2D-NMR spectra were recorded at 25°C on a Bruker Avance 400 or 500 MHz instruments. ^1H and ^{13}C spectra were referenced relative to the solvent residual peaks and chemical shifts (δ) reported in ppm downfield of tetramethylsilane ($CDCl_3$ δ H: 7.26 ppm, δ C: 77.16 ppm; CD_3CN δ H: 1.94 ppm, δ C: 118.26 ppm). The multiplicity of a signal is indicated as br, broad; s, singlet; d, doublet; t, triplet; m, multiplet.

Mass Spectrometry. Mass spectra by electrospray ionization (ESI), collected in the positive mode, were performed on Perseptive Biosystem Mariner ESI-ToF 5220 spectrometer (Foster City, CA).

Fourier Transform-Infrared Spectroscopy. FT-IR absorption spectra were recorded with a Nicolet Nexus FT-IR spectrometer, nitrogen flushed, equipped with a sample-shuttle device. The KBr disk technique was used for the characterization of solid compounds, while oily products were placed between two KBr windows. The frequency maxima for the main absorption bands are given. FT-IR absorption spectra in $CDCl_3$ (99.8%, *d*) solution were recorded at 293 K, averaging 100 scans. Solvent (baseline) spectra were obtained under the same conditions. For spectral elaboration, the software SpectraCalc, provided by Galactic (Salem, MA) was employed. Cells with path lengths of 1.0 mm and 10.0 mm (with CaF_2 windows) were used.

Synthesis and Characterization

Materials

DIPEA, *trans*-β-hydromuconic acid, lithium hydroxide hydrate, lithium diisopropylamide solution (LDA, 2.0 M in THF/heptane/ethylbenzene), methyl iodide, DPPA, glacial acetic acid, EDC hydrochloride, isopropylamine (*i*Pr-NH_2), ethanol (EtOH), *tert*-butanol (*t*BuOH), diethyl ether (Et_2O), CH_3CN, TFA, DCM, EtOAc, THF, deuterated $CDCl_3$, and deuterated

DMSO were obtained from Sigma-Aldrich and used without further purification. HOBt was purchased from GL Biochem (Shanghai, China).

Compounds 2 [5-ethoxycarbonyl-3-(*E*)-pentenoic acid] and 3 [hex-3-(*E*)-enedioic acid diethyl ester].

Commercially available trans-β-hydromuconic acid (5 g, 34.7 mmol) was dissolved in 30 mL of anhydrous EtOH. To this solution two drops of concentrated H_2SO_4 were added, and the mixture was heated under reflux for 3 h. After cooling the reaction mixture to room temperature, the solvent was removed under reduced pressure. The reaction crude was dissolved in diethyl ether (Et_2O) and washed with $NaHCO_3$ (5%) and brine. The organic layer was dried with Na_2SO_4 and filtered. Pure compound **3** was obtained as a colorless oil after evaporation of Et_2O (3.8 g, 19 mmol, 55%). The aqueous basic solution was acidified with solid $KHSO_4$ and extracted with Et_2O. The solution was dried over Na_2SO_4, filtered, and concentrated to dryness. Compound **2** was obtained as a colorless waxy solid (2.39 g, 13.9 mmol, 40%).

Compound 2: ^{1}H NMR (400 MHz, $CDCl_3$) δ 7.54 (br, 1H), 5.74 – 5.48 (m, 2H), 4.06 (q, J = 7.1 Hz, 2H), 3.00 (d, J = 5.0 Hz, 4H), 1.18 (t, J = 7.1 Hz, 3H) ppm.

IR (KBr) ν (cm^{-1}) 2984, 2901, 1737, 1710, 1691, 1401, 1293, 1218, 1157.

MS (ESI) calcd for $C_8H_{13}O_4^+$ $[M+H]^+$ *m/z* 173.0808, found 173.0966.

Compound 3: ^{1}H NMR (400 MHz, $CDCl_3$) δ 5.78 – 5.63 (m, 2H), 4.15 (q, J = 7.1 Hz, 4H), 3.09 (dd, J = 3.7, 1.3 Hz, 4H), 1.27 (t, J = 7.1 Hz, 6H) ppm.

IR (KBr) ν (cm^{-1}) 2983, 2939, 1737, 1371, 1275, 1249, 1177, 1158.

MS (ESI) calcd for $C_{10}H_{17}O_4^+$ $[M+H]^+$ *m/z* 201.1121, found 201.1308.

Compound 4 [ethyl-5-t-butoxycarbonylaminopent-3-(*E*)-enoate].[20]

Compound **2** (1.0 g, 5.8 mmol) was dissolved in dry tetrahydrofuran (THF) and cooled with an ice bath. DIPEA (1.0 mL, 5.8 mmol) and DPPA (1.25 mL, 5.8 mmol) were added, and the solution was stirred for 30 min. Then, the ice bath was removed and the solution was allowed to reach room temperature. *t*-BuOH (15 mL) was added and the reaction was stirred under reflux overnight. The solvent was removed under reduced pressure and the residue dissolved in EA. The organic phase was washed with $KHSO_4$ (5%), $NaHCO_3$ (5%) and brine, dried over Na_2SO_4, filtered, and concentrated to dryness. The crude product was purified by flash

chromatography (eluant: 1:3, EtOAc/hexane) to give 0.78 g (3.19 mmol, 55%) of **4** as a colorless oil.

^{1}H NMR (400 MHz, $CDCl_3$) δ 5.81 – 5.51 (m, 2H), 4.63 (br, 1H), 4.14 (q, J = 7.1 Hz, 2H), 3.74 (t, 2H), 3.06 (d, J = 6.8 Hz, 2H), 1.45 (s, 9H), 1.27 (d, J = 7.1 Hz, 2H) ppm. ^{13}C NMR (101 MHz, $CDCl_3$) δ 171.52, 155.70, 130.69, 123.74, 60.61, 42.07, 37.56, 28.32, 14.11 ppm.

IR (KBr) ν (cm^{-1}) 3364, 2979, 2931, 1737, 1715, 1518, 1366, 1249.

MS (ESI) calcd for $C_{12}H_{22}NO_4^+$ $[M+H]^+$ *m/z* 244.1543, found 244.1701.

Compound 5 [5-[N-(tert-butyloxycarbonyl)amino]-pent- 3-(*E*)-enoic acid].[20]

Compound **4** (0.6 g, 2.5 mmol) was dissolved in THF (10 mL) and $LiOH{\cdot}H_2O$ (0.17 g, 3.9 mmol), dissolved in water (10 mL), was added dropwise. The reaction was followed by TLC. After formation of the mono-ester (observed by TLC), the mixture was acidified with solid $KHSO_4$, and extracted with EtOAc. The organic phase was dried over Na_2SO_4, filtered and concentrated to dryness. The crude product was purified by flash chromatography (eluant: 2:1, EtOAc/hexane) to give 0.477 g (2.22 mmol, 90%) of **5** as a colorless oil.

MS (ESI) calcd for $C_{10}H_{18}NO_4^+$ $[M+H]^+$ *m/z* 216.1230, found 216.1392.

Compound 6 [tert-butyl{(2E)-5-oxo-5-[(propan-2-yl)amino]pent-2-en-1-yl}carbamate].[20]

Compound **5** (1.0 g, 4.6 mmol) was dissolved in dry ACN and HOBt (0.63 g, 4.6 mmol) and EDC·HCl (0.89 g, 4.6 mmol) were added. After 15 min *i*Pr-NH_2 (474 μL, 5.52 mmol) was added to the reaction mixture, and DIPEA was used to reach basic pH. The reaction was allowed to stir overnight. The solvent was removed under reduced pressure and the residue dissolved in EtOAc. The organic phase was washed with $KHSO_4$ (5%), $NaHCO_3$ (5%) and brine, dried over Na_2SO_4, filtered, and concentrated to dryness. The crude product was purified by flash chromatography (eluant: 1:3, EtOAc/hexane) to give 0.89 g (3.5 mmol, 76%) of **6** as a colorless solid.

Mp 118-120°C (lit. 116-119°C)[20].

^{1}H NMR (400 MHz, $CDCl_3$) δ 5.76 – 5.54 (m, 3H), 4.76 (br, 1H), 4.12 – 4.01 (m, 1H), 3.73 (t, J = 5.3 Hz, 2H), 2.94 (d, J = 6.9 Hz, 2H), 1.45 (s, 9H), 1.15 (d, J = 6.6 Hz, 6H) ppm. ^{13}C NMR (101 MHz, $CDCl_3$) δ 169.87, 155.88, 131.85, 124.67, 42.35, 41.45, 40.06, 28.40, 22.65 ppm.

IR (KBr) ν (cm^{-1}) 3349, 3308, 2973, 1683, 1641, 1529.

MS (ESI) calcd for $C_{13}H_{25}N_2O_3^+$ $[M+H]^+$ *m/z* 257.1860, found 257.2018.

Compound 7 [diethyl 2,2,5,5-tetramethylhex-3-(*E*)-enedioate].

Compound **3** (5.0 g, 24.9 mmol) was dissolved in dry THF, and cooled at -78°C. Then, Ar was fluxed in a three-neck round-bottom reaction flask. LDA (2M in THF, 25 mL, 50 mmol) was added to the solution. After 30 min CH_3I (3.11 mL, 50 mmol) was added at -78°C and the reaction mixture was stirred for 3 h at room temperature. The mixture was diluted carefully with an aqueous solution of $KHSO_4$ (6.8 g, 50 mmol) and extracted with EtOAc. The organic layer was additionally washed with $KHSO_4$ (5%), $NaHCO_3$ (5%), and brine, dried over Na_2SO_4, filtered and concentrated to dryness. After the work up, the alkylation procedure was repeated using the same quantities of LDA and CH_3I. After the completion of the reaction, the mixture was diluted carefully with an aqueous solution of $KHSO_4$ (6.8 g, 50 mmol) and extracted with EtOAc. The organic layer was additionally washed with $KHSO_4$ (5%), $NaHCO_3$ (5%), and brine, dried over Na_2SO_4, filtered and concentrated to dryness. The crude product was purified by flash chromatography (eluant: 1:3, EtOAc/hexane) to give 5.63 g (22 mmol, 88%) of **7** as a colorless oil.

^{1}H NMR (400 MHz, $CDCl_3$) δ 5.68 (d, J = 0.7 Hz, 2H), 4.11 (qd, J = 7.1, 0.7 Hz, 4H), 1.27 (s, 12H), 1.22 (td, J = 7.1, 0.7 Hz, 6H). ^{13}C NMR (101 MHz, $CDCl_3$) δ 176.40, 132.94, 60.53, 43.85, 25.04, 14.09.

MS (ESI) calcd for $C_{14}H_{25}O_4^+$ $[M+H]^+$ *m/z* 257.1747, found 257.1906.

Compound 8 [2,2,5,5-tetramethylhex-3-(*E*)-enedioic acid].

Compound **7** (2.0 g, 7.8 mmol) was dissolved in THF (20 mL) and $LiOH{\cdot}H_2O$ (0.65 g, 15.6 mmol), dissolved in water (20 mL), was added dropwise. The reaction was stirred at 40°C overnight. The mixture was acidified with solid $KHSO_4$, and extracted with EtOAc. The organic phase was dried over Na_2SO_4, filtered and concentrated to dryness to give compound **8** as a waxy solid (1.4 g, 7.02 mmol, 90%).

^{1}H NMR (400 MHz, DMSO) δ 12.22 (br, 2H), 5.65 (s, 2H), 1.19 (s, 12H). ^{13}C NMR (101 MHz, DMSO) δ 177.70, 133.05, 43.60, 25.47.

MS (ESI) calcd for $C_{10}H_{17}O_4^+$ $[M+H]^+$ *m/z* 201.1121, found 201.1279.

Compound 9 [(3E)-2,2,5,5-tetramethyl-6-oxo-6-[(propan-2-yl)amino]hex-3-enoic acid].

Compound **8** (1.0 g, 5 mmol) was dissolved in dry DCM and HOBt (0.34 g, 2.5 mmol) and EDC·HCl (0.48 g, 2.5 mmol) were added. After 15 min *i*Pr-NH_2 (237 μL, 2.76 mmol) was added to the reaction mixture, and DIPEA was used to reach basic pH. The reaction was

allowed to stir overnight. The solvent was removed under reduced pressure and the residue dissolved in EtOAc. The organic phase was washed with $KHSO_4$ (5%) and brine, dried over Na_2SO_4, filtered, and concentrated to dryness. The crude product was purified by flash chromatography (eluant: 2:3, EtOAc/hexane) to give 0.53 g (2.2 mmol, 44%) of **9** as a colorless solid.

^{1}H NMR (400 MHz, $CDCl_3$) δ 5.87 (d, J = 4.5 Hz, 1H), 5.73 (q, 2H), 4.06 – 3.91 (m, 1H), 1.36 (s, 6H), 1.27 (s, 6H), 1.09 (d, J = 6.5 Hz, 6H).

MS (ESI) calcd for $C_{13}H_{24}NO_3^+$ $[M+H]^+$ *m/z* 242.1750, found 242.1937.

Compound 10 [Boc-5-amino-2,2,5,5-tetramethyl-pent-3-(*E*)-enoyl-NH*i*Pr].

Compound **9** (1.0 g, 4.14 mmol) was dissolved in dry tetrahydrofuran (THF) and cooled with an ice bath. DIPEA (722 μL, 4.14 mmol) and DPPA (893 μL, 4.14 mmol) were added, and the solution was stirred for 30 min. Then, the ice bath was removed and the solution was allowed to reach room temperature. *t*-BuOH (15 mL) was added and the reaction was stirred under reflux overnight. The solvent was removed under reduced pressure and the residue dissolved in EtOAc. The organic phase was washed with $KHSO_4$ (5%), $NaHCO_3$ (5%) and brine, dried over Na_2SO_4, filtered, and concentrated to dryness. The crude product was purified by flash chromatography (eluant: 1:3, EtOAc/hexane) to give 0.62 g (1.99 mmol, 48%) of **10** as a colorless solid.

Mp 131-133°C.

^{1}H NMR (400 MHz, $CDCl_3$) δ 6.60 (d, J = 6.3 Hz, 1H), 5.60 (q, 2H), 5.41 (s, 1H), 4.10 – 3.98 (m, 1H), 1.41 (s, 9H), 1.25 (s, 12H), 1.13 (d, J = 6.6 Hz, 6H). ^{13}C NMR (101 MHz, $CDCl_3$) δ 175.52, 155.21, 134.12, 133.90, 54.06, 44.08, 41.28, 27.38, 25.11, 22.33, 21.53.

IR (KBr) ν (cm^{-1}) 3328, 3251, 3034, 2968, 2930, 2872, 2117, 2139, 1698, 1645, 1530, 1458.

MS (ESI) calcd for $C_{17}H_{33}N_2O_3^+$ $[M+H]^+$ *m/z* 313.2486, found 313.2673.

Compound 11 ({(3E)-2,5,5-trimethyl-6-oxo-6-[(propan-2-yl)amino]hex-3-en-2-yl}carbamyl azide).

This compound was recovered as a main secondary product from flash chromatography of the crude product of the synthesis of **10** (0.14 g, 0.49 mmol, 12%).

Mp 149-151°C.

^{1}H NMR (400 MHz, $CDCl_3$) δ 6.64 (d, J = 6.3 Hz, 1H), 5.65 (q, 2H), 5.41 (s, 1H), 4.07 (m, 1H), 1.44 (s, 6H), 1.29 (s, 6H), 1.17 (d, J = 6.6 Hz, 6H).

IR (KBr) ν (cm^{-1}) 3353, 3303, 3253, 2132, 1694, 1644, 1525.
MS (ESI) calcd for $C_{13}H_{24}N_5O_2^+$ $[M+H]^+$ *m/z* 282.1924, found 282.2111.

Conformational Energy Calculations.

DFT calculations at the M06L/6-31+G(d,p) level[57] were performed in the gas phase. It should be noted that the M06L functional describes very satisfactorily the geometries and relative energies of conformations stabilized by electrostatic interactions and by π-electron-rich functional groups.[58] All quantum mechanics computations were carried out with the Gaussian09 software.[59] Frequency analyses were operated to verify the nature of the minimum state of all of the stationary points obtained and to calculate the zero-point vibrational energies (ZPVEs), and both thermal and entropic corrections. These statistical terms were then used to compute the conformational Gibbs free energies in the gas phase (ΔG) at 298 K.
The conformational potential energy surface of each compound studied was systematically explored using a procedure inspired by the build-up method of Gibson and Scheraga.[60] This approach assumes that the short-range interactions are dominant in determining the conformation of a given peptide. Accordingly, the accessible conformations of any peptide studied result from combining *N* independent rotamers (*i.e*,. the rotational isomeric approximation[61]), in which each independent rotational state corresponds to the most favored conformation of each residue. In practice, accessible starting geometries for each compound were constructed by varying the free rotation backbone torsion angles (Scheme 1) in steps of 60°. Consequently, 6 (minima of φ) × 6 (minima of θ^1) × 6 (minima of θ^3) × 6 (minima of ψ) = 1296 minima were anticipated for the potential energy hypersurface $E = E(\varphi, \theta^1, \theta^3, \psi)$ of each *chiral* compound (*i.e.*, **C** and **D**). In the case of **A**, **B** and **E**, the number of theoretical minima can be reduced to 648 due to the absence of chirality, since structures with (φ, θ^1, θ^3, ψ) and ($-\varphi$, $-\theta^1$, $-\theta^3$, $-\psi$) are energetically degenerated and equivalent. Hence, 1296 × 2 (**C**, **D**) + 648 × 3 (**A**, **B**, **E**) structures were built and subsequently their geometries were optimized.
In order to construct a list of unique minima for each compound, all optimized geometries were compared and all unique minima found were ordered by a rank of increasing energy. We identify unique minimum energy conformations based on the values of the backbone torsion angles and the presence of interaction patterns (*i.e* , H-bonds between backbone amide

groups). To facilitate the representation of the conformational space of the compounds in a simplified Ramachandran-like plot, two virtual torsion angles were selected to mimic the backbone torsion angles typically used for peptides based on α-amino acids. Each virtual rotation was chosen to account for the relative position of each amide group with respect to the central C=C double bond, which is a characteristic feature of all compounds investigated. These two virtual torsion angles were defined according to Figure 8.

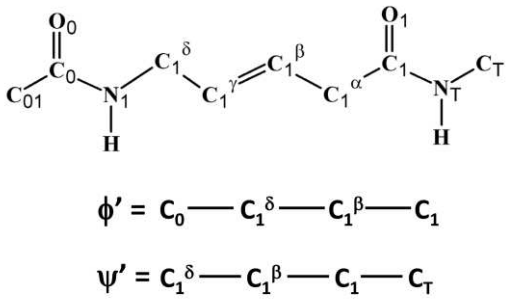

Fig.8 *Virtual* torsion angles used to represent the Ramachandran-like plots of the compounds investigated.

The validity of the two *virtual* torsion angles in reflecting the conformational properties of each compound was checked by comparing the clustering results with those achieved using the four main-chain torsion angles. The number of unique minima was identical for each case examined using both criteria. As for the analysis of the interactions, specific N–H···O H-bonds were defined to occur when the N-H···O distance is ≤ 3.0 Å and the ∠N–H···O angle is ≥ 120°.[62] Finally, two conformations were considered different when they diverge in at least one of their (*virtual*) torsion angles by more than 15° or in at least one of the interactions counted.

Table 1. Values obtained for the torsion angles (in degrees) of compound **A** in the minimum energy conformations calculated at the M06L/6-31+G(d,p) level and their corresponding free energies (ΔG) at 298K. H-Bonding parameters for the conformations with this type of specific interaction are included. Populations have been calculated according to a Boltzmann distribution of minima.

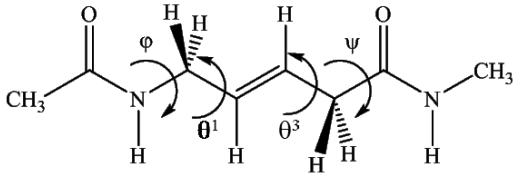

ΔG (kcal/mol)	d(N-H···O) (Å)	<N-H···O (º)	φ (º)	θ^1 (º)	θ^3 (º)	ψ (º)	Population (T=298 K)
0.0	2.17	155.5	-69.0	-6.0	-104.0	13.7	50.0
0.1	2.08	160.6	-66.1	116.0	105.0	-11.0	41.2
1.5	-	-	121.6	122.9	-111.0	25.4	3.8
1.6	-	-	97.8	119.8	-132.4	132.1	3.4
2.4	-	-	99.3	124.9	112.8	-26.5	0.8
2.7	-	-	99.1	120.2	130.5	-139.7	0.6
3.3	-	-	85.6	-110.9	111. 9	-20.3	0.2
3.8	-	-	81.5	-103.9	117.2	66.7	0.0
4.3	-	-	130.3	123.3	-106.2	-95.7	0.0

Table 2. Values obtained for the torsion angles (in degrees) of compound **B** in the minimum energy conformations calculated at the M06L/6-31+G(d,p) level and their corresponding free energies (ΔG) at 298K. H-Bonding parameters for the conformations with this type of specific interaction are included. Populations have been calculated according to a Boltzmann distribution of minima.

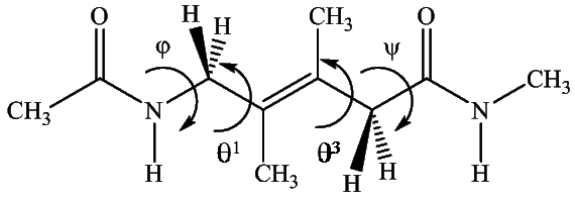

ΔG (kcal/mol)	d(N-H···O) (Å)	<N-H···O (º)	φ (º)	θ^1 (º)	θ^3 (º)	ψ (º)	Population (T=298 K)
0.0	2.07	157.7	61.6	-124.3	-95.2	14.1	93.4
1.8	2.11	152.3	51.3	56.2	91.0	-27.7	2.4
2.9	2.10	140.1	-106.8	-109.9	98.1	-96.6	0.8
3.3			-105.2	-101.6	-93.1	24.8	0.4
3.3			-85.9	108.9	-87.1	12.4	0.4
3.6			-104.9	-123.0	95.5	-21.7	0.2
3.7			-164.8	-81.9	-89.9	-159.6	0.2
4.6			-87.1	109.9	-84.7	-95.7	0.0
4.8			117.3	110.9	-92.5	-118.5	0.0

Table 3. Values obtained for the torsion angles (in degrees) of compound **C** in the minimum energy conformations calculated at the M06L/6-31+G(d,p) level and their corresponding free energies (ΔG) at 298K. H-Bonding parameters for the conformations with this type of specific interaction are included. Populations have been calculated according to a Boltzmann distribution of minima.

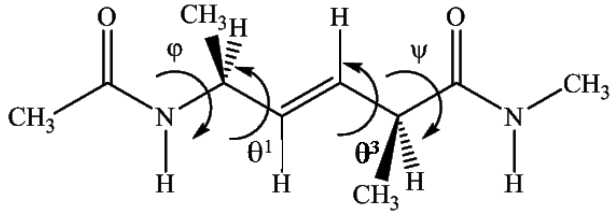

ΔG (kcal/mol)	d(N-H···O) (Å)	<N-H···O (º)	φ (º)	θ^1 (º)	θ^3 (º)	ψ (º)	Population (T=298 K)
0.0	2.07	159.6	-65.7	115.3	105.6	-12.1	76.9
1.0	2.16	154.2	-68.5	-5.6	-110.4	17.1	13.8
1.9	2.10	155.2	63.0	13.3	103.2	-15.3	3.1
2.2	-	-	-93.3	-125.7	111.4	-33.4	1.8
2.3	-	-	-145.1	-126.5	109.9	-29.3	1.5
2.4	2.06	156.7	59.4	-127.5	-107.7	25.4	1.3
2.8	-	-	-148.4	12.3	121.6	-116.1	0.7
3.8	-	-	-87.4	1.3	-9. 8	-82.1	0.1
3.8	-	-	-149.4	-124.5	-115.2	-92.7	0.1
3.8	-	-	-81. 8	103. 5	-119.4	25.1	0.1
3.9	-	-	-148.8	-130.5	-122.0	23.1	0.1
3.9	-	-	-160.7	118.0	-3.7	-97.0	0.1
4.1	-	-	-150.8	-127.2	-9.9	-93.5	0.1
4.2	-	-	-160.9	121.0	-116.1	26.7	0.1
4.3	-	-	-160.5	113.2	119.8	-108.5	0.1
4.4	-	-	-75.2	100.4	-12.9	-96.2	0.0
5.0	-	-	62.5	123.4	-116.0	32.7	0.0
5.3	-	-	-160.8	107.7	95.1	107.7	0.0
5.5	-	-	62.6	-130.3	116.5	-28.9	0.0
5.9	-	-	61.4	127.0	5.5	-80.2	0.0
6.0	-	-	71.2	1.2	-118.9	28.5	0.0
6.2	-	-	61.6	-134.7	125.0	-111.0	0.0
6.7	-	-	70.7	-1.6	-21.4	-92.9	0.0

Table 4. Values obtained for the torsion angles (in degrees) of compound **D** in the minimum energy conformations calculated at the M06L/6-31+G(d,p) level and their corresponding free energies (ΔG) at 298K. H-Bonding parameters for the conformations with this type of specific interaction are included. Populations have been calculated according to a Boltzmann distribution of minima.

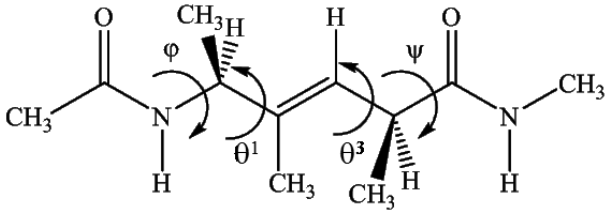

ΔG (kcal/mol)	d(N-H···O) (Å)	<N-H···O (º)	φ (º)	θ^1 (º)	θ^3 (º)	ψ (º)	Population (T=298 K)
0.0	2.07	154.0	-57.9	131.3	89.4	-13.5	98.6
2.8	2.12	151.6	52.8	55.4	93.2	-28.7	0.8
3.4	2.14	162.5	-60.1	-31.9	-51.1	-31.5	0.3
3.8	2.09	158.1	65.3	10.3	94.4	-4.3	0.1
4.3			54.7	-132.1	-49.7	-32.8	0.1
4.9			-103.1	-119.1	106.0	-85.5	0.0
4.9			-63.7	-30.3	149.5	-133.3	0.0
5.5			-79.5	105.6	-49.1	-41.1	0.0
5.7			-101.9	-123.1	-49.8	-37.2	0.0
6.2			61.6	-135.2	101.9	-21.0	0.0
6.5			-158.6	107.53	86.31	100.2	0.0
7.0			-162.37	106.5	109.7	-98.6	0.0
7.3			-159.5	110.2	-49.1	-41.2	0.0
7.4			57.5	-135.1	149.0	-133.2	0.0
7.7			84.3	129.2	-52.0	-34.0	0.0
7.9			83.1	116. 8	99.7	-90.7	0.0
8.0			-160.9	-34.2	-49.2	-37.6	0.0
9.4			74.2	0.6	-55.8	-36.3	0.0

Table 5. Values obtained for the torsion angles (in degrees) of compound **E** in the minimum energy conformations calculated at the M06L/6-31+G(d,p) level and their corresponding free energies (ΔG) at 298K. H-Bonding parameters for the conformations with this type of specific interaction are included. Populations have been calculated according to a Boltzmann distribution of minima.

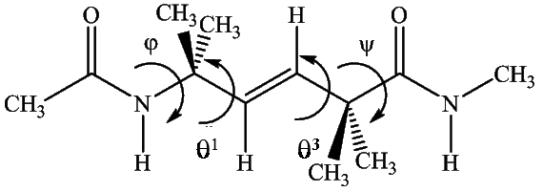

ΔG (kcal/mol)	d(N-H···O) (Å)	<N-H···O (º)	φ (º)	θ^1 (º)	θ^3 (º)	ψ (º)	Population (T=298 K)
0.0	2.04	155.7	58.1	-125.8	-107.4	23.8	74.2
0.6	2.05	157.3	-61.5	-14.0	-109.9	15.8	25.4
3.9	-	-	-176.7	-126.1	112.5	-28.7	0.3
4.2	-	-	-59.4	-125.2	113.1	-32.4	0.1
4.4	-	-	-63.3	-13.3	115. 8	-28.5	0.0
4.4	-	-	-59.8	-119.7	-113.8	32.4	0.0
4.5	-	-	61.1	-126.0	116.3	-27.7	0.0
4.7	-	-	58.9	122. 9	-126.6	117.4	0.0
4.8	-	-	177.4	-25.5	113.3	-29.7	0.0
4.9	-	-	-176.5	-126.5	-117.8	23.7	0.0
5.2	-	-	-178.5	19.2	115.1	-33.7	0.0
5.6	-	-	-176.4	-122.2	-1.0	99.0	0.0
5.7	-	-	-176.5	-117.8	-104.3	-103.2	0.0
5.8	-	-	58.3	120.4	127.7	-117.9	0.0
5.9	-	-	-179.3	21.0	126.8	-124.9	0.0
6.0	-	-	-61.3	-13.3	130.7	-122.3	0.0
6.1	-	-	-178.7	16.8	-131.2	120.2	0.0
6.4	-	-	60.5	-130.7	128.7	-120.3	0.0
6.5	-	-	65.6	7.4	-32.4	-45.9	0.0
6.7	-	-	-177.4	19.4	-29.3	-51.5	0.0
6.7	-	-	-176.8	-124.0	-8.6	-96.8	0.0
6.9	-	-	61.7	-111.5	22.5	56.6	0.0
7.0	-	-	179.2	-19.1	-19.9	-58.8	0.0

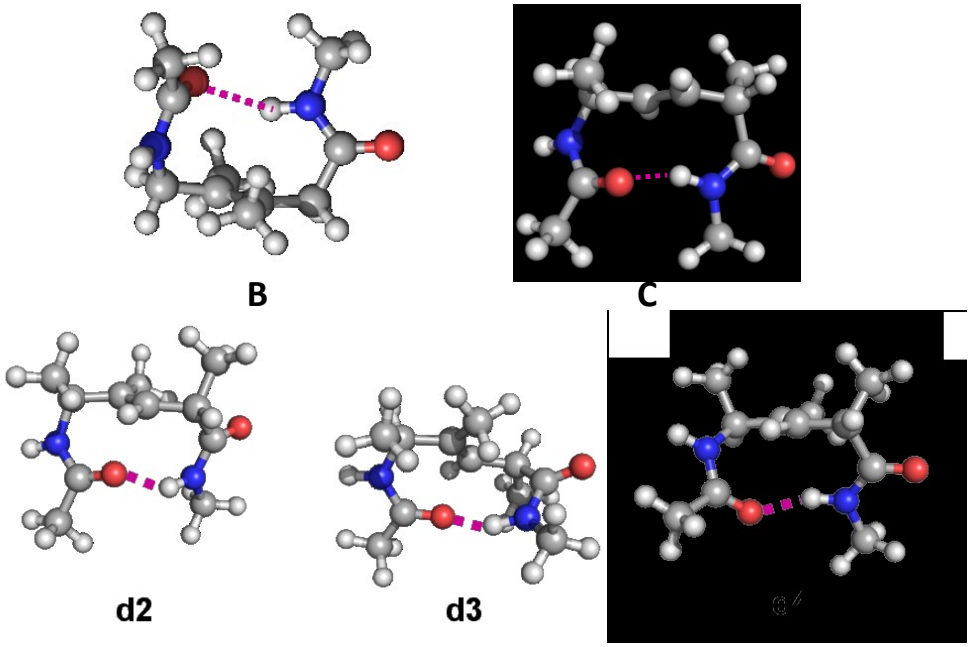

Fig. 9. Upper part: Minimum energy structure of compound **B** destabilized by 1.8 kcal/mol with respect to the global minimum (Table 2). Despite the high ΔG value, this structure presents a C_{10} H-bonded ring. Minimum energy structure of compound **C** destabilized by 2.4 kcal/mol with respect to the global minimum (Table 3). Despite the high ΔG value, this structure presents a C_{10} H-bonded ring. Lower part: minimum energy structures of compound **D** destabilized by 2.8 (**d2**), 3.4 (**d3**) and 3.8 (**d4**) kcal/mol with respect to the global minimum (Table 4). Despite the high ΔG values, each structure presents a C_{10} H-bonded ring.

X-Ray Diffraction

Boc-5-aminopent-3-(E)-enoyl-NHiPr [(Boc)**A 6**]. Crystals of this compound were grown from EA – *n*-hexane by vapor diffusion at 4°C. X-Ray diffraction data were collected with a Gemini E four-circle kappa diffractometer (Agilent Technologies) equipped with a 92 mm EOS CCD detector, using graphite monochromated Cu Kα radiation (λ = 1.54184 Å). Data collection and reduction were performed with the CrysAlisPro software system (Rigaku Oxford Diffraction). A semi-empirical absorption correction based on the multi-scan technique using spherical harmonics, implemented in the SCALE3 ABSPACK scaling algorithm, was applied. The structure was solved by *ab initio* procedures of the SIR 2014 program.[63] The trial solution with the best combined figure of merit allowed location of three independent molecules in the monoclinic space group C2/c. Refinement was carried out by full-matrix least-squares on F^2, using all data, by application of the SHELXL-2014 program,[64] with anisotropic displacement parameters for all of the non-H atoms. Restraints were applied to the bond distances and angles of the terminal Boc and NH*i*Pr groups, as well as to the anisotropic displacement parameters of all atoms (RIGU command in SHELXL-2014). H-Atoms were calculated at idealized positions and refined using a riding model.

Boc-5-amino-2,2,5,5-tetramethyl-pent-3-(E)-enoyl-NHiPr [(Boc)**E 10**]. Crystals of this compound were grown from EA – petroleum ether by vapor diffusion. Data collection was performed on a Philips PW1100 four-circle serial diffractometer in the θ-2θ scan mode using graphite monochromated Cu Kα radiation (λ = 1.54178 Å). The structure was solved by direct methods of the SIR 2002 program,[65] and refined by full-matrix least-squares on F^2, using all data, by application of the SHELXL-2014 program,[64] with anisotropic displacement parameters for all of the non-H atoms. H-Atoms were calculated at idealized positions and refined using a riding model.

Azidocarbonyl-5-amino-2,2,5,5-tetramethyl-pent-3-(E)-enoyl-NHiPr **11**. Crystals were grown from ethyl acetate – petroleum ether by vapor diffusion. Data collection and reduction, structure solution and refinement were performed similarly to what reported above for the structure of (Boc)**A 6**. The C-terminal *i*Pr group is disordered. Its methyl groups were refined on two sets of positions (atoms CT2,CT3 and CT2',CT3', respectively), each with 0.50

population parameter. Restraints were applied to the bond distances, bond angles, and anisotropic displacement parameters of the disordered atoms.

Relevant crystal data and structure refinement parameters for the structures of **6**, **10**, and **11** are listed in Tables S6-S8 (Supporting Information). CCDC 1948908, 1948909, and 1952416 contain the supplementary crystallographic data for this paper. The data can be obtained free of charge from The Cambridge Crystallographic Data Centre *via* www.ccdc.cam.ac.uk/structures.

Table 6. Crystal data and structure refinement parameters for Boc-5-amino-pent-3-(*E*)-enoyl-NH*i*Pr (**6**)

Identification code	mc309B2	
Empirical formula	$C_{13}H_{24}N_2O_3$	
Formula weight	256.34	
Temperature	293(2) K	
Wavelength	1.54184 Å	
Crystal system	Monoclinic	
Space group	C 2/c	
Unit cell dimensions	a = 54.6587(11) Å	α= 90°.
	b = 5.86885(11) Å	β= 99.241(2)°.
	c = 29.3845(4) Å	γ = 90°.
Volume	9303.7(3) $Å^3$	
Z	24	
Density (calculated)	1.098 Mg/m^3	
Absorption coefficient	0.630 mm^{-1}	
F(000)	3360	
Crystal size	0.10 × 0.10 × 0.02 mm^3	
Theta range for data collection	3.047 to 72.173°.	
Index ranges	$-66 \le h \le 62$, $-5 \le k \le 7$, $-36 \le l \le 34$	
Reflections collected	32059	
Independent reflections	9073 [R(int) = 0.0244]	
Completeness to theta = 67.684°	100.0 %	
Absorption correction	Semi-empirical from equivalents	
Max. and min. transmission	1.00000 and 0.78404	
Refinement method	Full-matrix least-squares on F^2	
Data / restraints / parameters	9073 / 405 / 502	
Goodness-of-fit on F^2	1.044	
Final R indices [I>2sigma(I)]	R_1 = 0.0548, wR_2 = 0.1502	
R indices (all data)	R_1 = 0.0821, wR_2 = 0.1660	
Extinction coefficient	n/a	
Largest diff. peak and hole	0.299 and -0.173 e.$Å^{-3}$	
CCDC deposition no.	1948908	

Table 7. Crystal data and structure refinement parameters for Boc-5-amino-2,2,5,5-tetramethyl-pent-3-(*E*)-enoyl-NH*i*Pr (**10**)

Identification code	mc92p2	
Empirical formula	$C_{17}H_{32}N_2O_3$	
Formula weight	312.44	
Temperature	293(2) K	
Wavelength	1.54178 Å	
Crystal system	triclinic	
Space group	P -1	
Unit cell dimensions	*a* = 5.990(2) Å	α= 88.95(5)°.
	b = 8.937(2) Å	β= 87.04(8)°.
	c = 17.928(3) Å	γ = 80.67(7)°.
Volume	945.7(5) $Å^3$	
Z	2	
Density (calculated)	1.097 Mg/m^3	
Absorption coefficient	0.594 mm^{-1}	
F(000)	344	
Crystal size	0.55 × 0.35 × 0.10 mm^3	
Theta range for data collection	4.940 to 60.001°.	
Index ranges	$-6 \le h \le 6$, $-10 \le k \le 10$, $0 \le l \le 20$	
Reflections collected	2793	
Independent reflections	2793 [R(int) = 0.000]	
Completeness to theta = 60.001°	99.9 %	
Absorption correction	none	
Refinement method	full-matrix least-squares on F^2	
Data / restraints / parameters	2793 / 0 / 200	
Goodness-of-fit on F^2	1.059	
Final R indices [I>2sigma(I)]	R_1 = 0.0692, wR_2 = 0.1924	
R indices (all data)	R_1 = 0.0736, wR_2 = 0.2017	
Extinction coefficient	0.026(4)	
Largest diff. peak and hole	0.612 and -0.336 $e.Å^{-3}$	
CCDC deposition no.	1948909	

Table 8. Crystal data and structure refinement parameters for Azidocarbonyl-5-amino-2,2,5,5-tetramethyl-pent-3-(*E*)-enoyl-NH*i*Pr (**11**)

Identification code	mc310	
Empirical formula	$C_{13}H_{23}N_5O_2$	
Formula weight	281.36	
Temperature	293(2) K	
Wavelength	1.54184 Å	
Crystal system	Triclinic	
Space group	P -1	
Unit cell dimensions	a = 9.1653(3) Å	α= 107.580(3)°.
	b = 9.4255(3) Å	β= 91.726(3)°.
	c = 10.5148(3) Å	γ = 106.465(3)°.
Volume	823.73(5) $Å^3$	
Z	2	
Density (calculated)	1.134 Mg/m^3	
Absorption coefficient	0.645 mm^{-1}	
F(000)	304	
Crystal size	0.50 × 0.40 × 0.20 mm^3	
Theta range for data collection	4.447 to 72.814°.	
Index ranges	$-11 \le h \le 11$, $-11 \le k \le 11$, $-13 \le l \le 10$	
Reflections collected	13055	
Independent reflections	3269 [R(int) = 0.0168]	
Completeness to theta = 67.684°	99.9 %	
Absorption correction	Semi-empirical from equivalents	
Max. and min. transmission	1.00000 and 0.80313	
Refinement method	Full-matrix least-squares on F^2	
Data / restraints / parameters	3269 / 44 / 203	
Goodness-of-fit on F^2	1.079	
Final R indices [I>2sigma(I)]	R_1 = 0.0523, wR_2 = 0.1533	
R indices (all data)	R_1 = 0.0550, wR_2 = 0.1567	
Extinction coefficient	n/a	
Largest diff. peak and hole	0.303 and -0.217 e.$Å^{-3}$	
CCDC deposition no.	1952416	

Table 9. Backbone torsion angles (°) for the three independent molecules in the X-ray diffraction structure of Boc-5-amino-pent-3-(*E*)-enoyl-NH*i*Pr (**6**)

Molecule	ω^N	ϕ	θ^1	θ^2	θ^3	ψ	ω^C
1	174.7(2)	141.8(2)	119.8(3)	178.5(2)	-121.2(3)	-123.2(2)	179.3(2)
2	174.96(19)	140.2(2)	125.6(2)	178.7(2)	-117.9(3)	-142.2(2)	-178.4(2)
3	-167.41(16)	87.9(2)	127.4(2)	-178.39(18)	-107.4(2)	-138.7(2)	-178.8(2)

Table 10. Intermolecular H-bond parameters [Å and °] in the X-ray diffraction structure of Boc-5-amino-pent-3-(*E*)-enoyl-NH*i*Pr (**6**)

D-H...A	d(D-H)	d(H...A)	d(D...A)	<(DHA)
N_1-H0_1...O0_3#1	0.86	2.13	2.982(2)	170.5
NT_1-HT_1...O_3#2	0.86	2.13	2.967(2)	163.1
N_2-H0_2...O0_1	0.86	2.12	2.9545(19)	163.7
NT_2-HT_2...O_1	0.86	2.07	2.905(2)	164.7
N_3-H0_3...O0_2	0.86	2.20	2.9459(19)	145.1
NT_3-HT_3...O_2	0.86	2.05	2.898(2)	169.9

Symmetry transformations used to generate equivalent atoms:

#1 x, -y+1, z-1/2 #2 x, -y, z-1/2

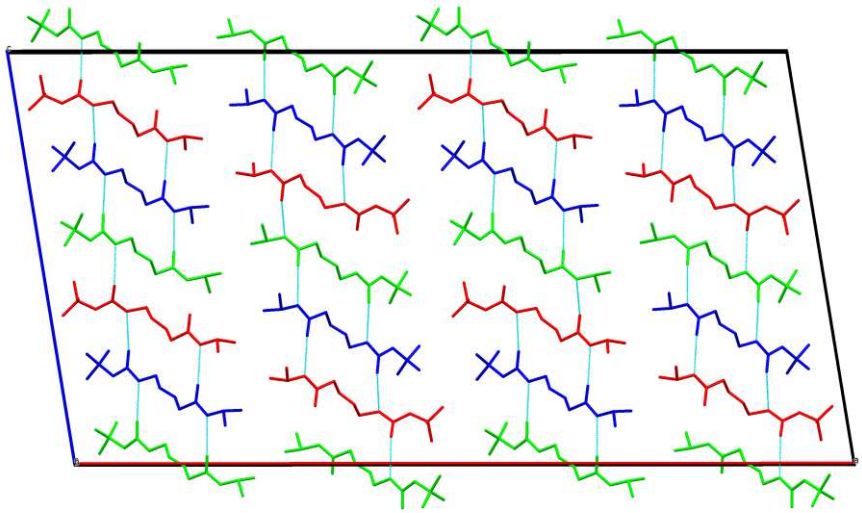

Fig. 10 Packing mode of Boc-5-amino-pent-3-(*E*)-enoyl-NH*i*Pr (**6**) as viewed nearly down the *b* direction. Each of the three independent molecules is shown in a different color. Intermolecular H-bonds are indicated by dashed lines.

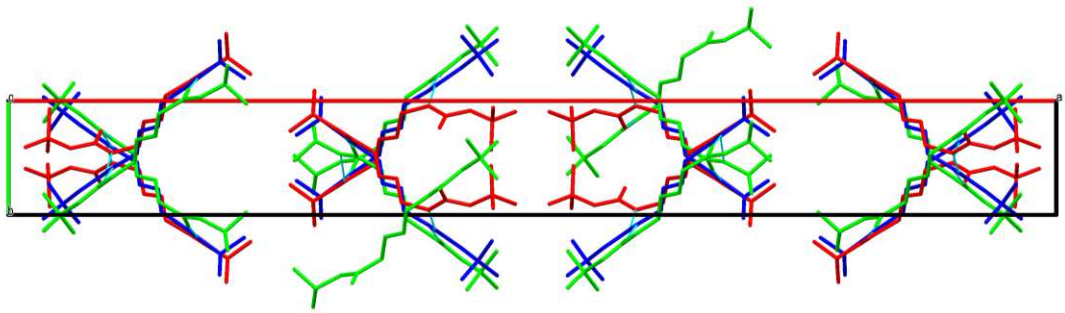

Fig. 11 Packing mode of Boc-5-amino-pent-3-(*E*)-enoyl-NH*i*Pr (**6**) as viewed down the *c* direction. Each of the three independent molecules is shown in a different color.

Table 11. Backbone torsion angles (°) in the X-ray diffraction structure of Boc-5-amino-2,2,5,5-tetramethyl-pent-3-(*E*)-enoyl-NH*i*Pr (**10**)

ω^N	ϕ	θ^1	θ^2	θ^3	ψ	ω^C
178.29(18)	60.4(3)	8.9(4)	-175.3(2)	98.7(3)	-3.3(3)	-177.9(2)

Table 12. Intra- and interermolecular H-bond parameters [Å and °] in the X-ray diffraction structure of Boc-5-amino-2,2,5,5-tetramethyl-pent-3-(*E*)-enoyl-NH*i*Pr (**10**)

D-H...A	d(D-H)	d(H...A)	d(D...A)	<(DHA)
NT-HT...O0	0.86	2.30	3.120(3)	160.6
N1-H1...O1#1	0.86	2.14	2.988(3)	166.9

Symmetry transformations used to generate equivalent atoms:

#1 *x*, *y*-1, *z*

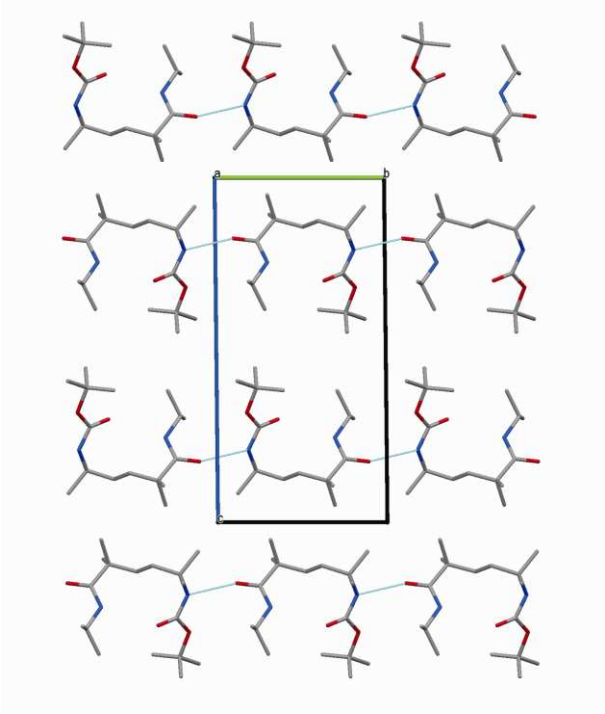

Fig. 12 Packing mode of Boc-5-amino-2,2,5,5-tetramethyl-pent-3-(*E*)-enoyl-NH*i*Pr (**10**) as viewed down the *a* direction. Intermolecular H-bonds are represented by dashed lines.

Table 13. Backbone torsion angles (°) in the X-ray diffraction structure of Azidocarbonyl-5-amino-2,2,5,5-tetramethyl-pent-3-(*E*)-enoyl-NH*i*Pr (**11**)

ω^N	ϕ	θ^1	θ^2	θ^3	ψ	ω^C
176.09(14)	50.7(2)	-130.52(15)	177.94(12)	-110.48(15)	32.42(17)	177.21(14)

Table 14. Intra- and interermolecular H-bond parameters [Å and °] in the X-ray diffraction structure of Azidocarbonyl-5-amino-2,2,5,5-tetramethyl-pent-3-(*E*)-enoyl-NH*i*Pr (**11**)

D-H...A	d(D-H)	d(H...A)	d(D...A)	<(DHA)
NT-HT...O0	0.86	2.25	3.0641(15)	158.7
N1-H1...O1#1	0.86	2.05	2.8694(15)	159.3

Symmetry transformations used to generate equivalent atoms:

#1 *x*, *y*-1, *z*

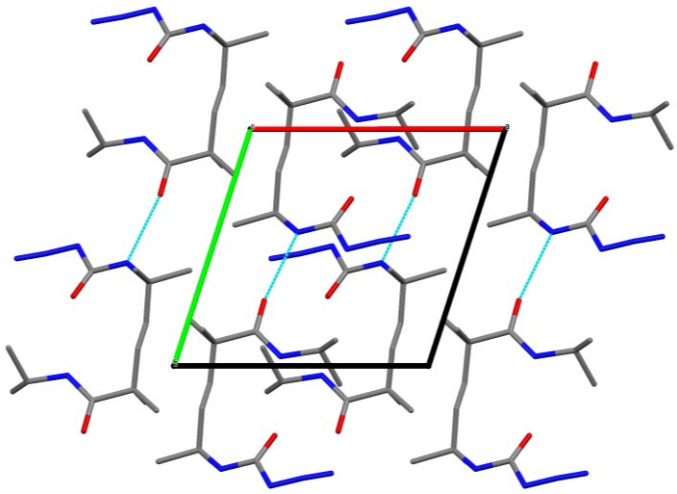

Fig. 13 Packing mode of Azidocarbonyl-5-amino-2,2,5,5-tetramethyl-pent-3-(*E*)-enoyl-NH*i*Pr (**11**) as viewed down the *c* direction. Intermolecular H-bonds are represented by dashed lines.

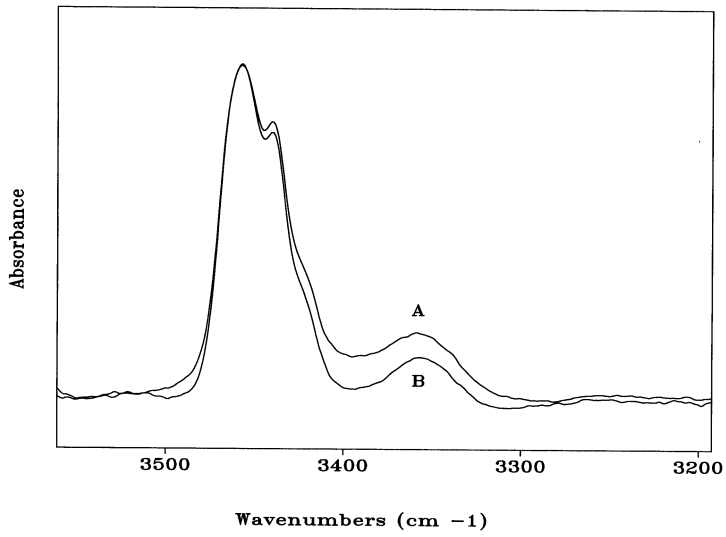

Fig. 14 FT-IR absorption spectra in $CDCl_3$ solution of compound (Boc)**A 6** in the 3500-3200 cm^{-1} wavenumber (N-H stretching) region in $CDCl_3$ solution at the concentrations of 1.0 mM (**A**) and 0.1 mM (**B**).

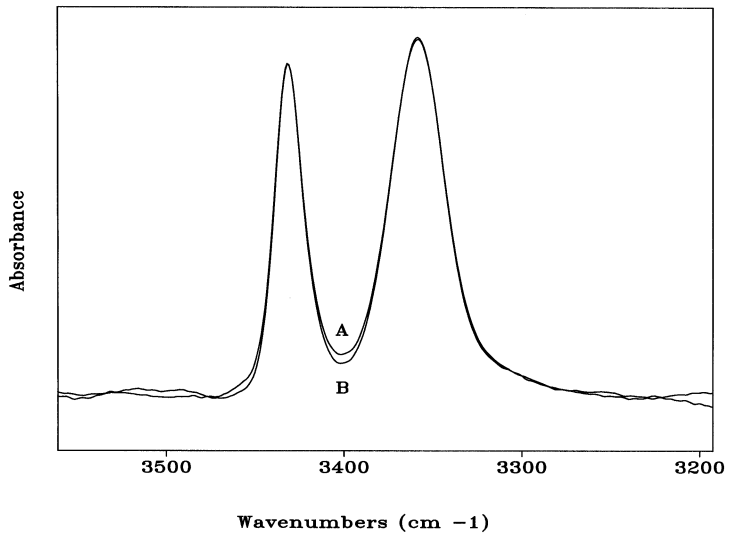

Fig. 15 FT-IR absorption spectra in $CDCl_3$ solution (1.0 mM concentration) of compound (Boc)**E 10** in the 3500-3200 cm^{-1} wavenumber (N-H stretching) region in $CDCl_3$ solution at the concentrations of 1.0 mM (**A**) and 0.1 mM (**B**).

References

1. E.J. Ariëns, *Trends Pharmacol.*, **1979**, 1, 11.
2. P. S. Farmer, and E. J. Ariëns, *Trends Pharmacol. Sci.,* **1982**, 3, 362.
3. A. F. Spatola, In *Chemistry and Biochemistry of Amino Acids, Peptides, and Proteins*; Weinstein, B., Ed.; Dekker: New York, NY, **1983**; Vol. 7, pp 267.
4. M. Mammen, E. I. Shakhnovich, G. M. Whitesides, *J. Org. Chem.,* **1998**, 63, 3168.
5. A. D. G. Lawson, M. MacCoss, and J. P. Heer, *J. Med. Chem.,* **2018**, 61, 4283.
6. N. Shamala, R. Nagaraj, and P. Balaram, *J. Chem. Soc., Chem. Commun.,* **1978**, 996.
7. C. Toniolo, M. Crisma, F. Formaggio, and C. Peggion, *Biopolymers (Pept. Sci.,)* **2001**, 60, 396.
8. R. T. Raines, and H. Wennemers, *Acc. Chem. Res.,* **2017**, 50, 2419, and articles in this Special Issue on "Chemical Biology of Peptides".
9. E. Gatto, A. Quatela, M. Caruso, R. Tagliaferro, M. De Zotti, F. Formaggio, C. Toniolo, A. Di Carlo, and M. Venanzi, *ChemPhysChem,* **2014**, 15, 64.
10. P. Tiwari, A. Basu, A. Vij, S. Bera, A.K. Tiwari, and A. Dutt Konar, *Chem. Select* **2019**, 4, 6896.
11. A. Banerjee, A. Pramanik, S. Bhattacharjya, and P. Balaram, *Biopolymers,* **1996**, 39, 69.
12. C. Baldauf, R. Günther, and H.-J. Hofmann, *J. Org. Chem.,* **2004**, 69, 6214.
13. C. Baldauf, and H.-J. Hofmann, *Helv. Chim. Acta,* **2012**, 95, 2348.
14. G. Marafon, M. Crisma, and A. Moretto, *Angew. Chem. Int. Ed.,* **2018**, 57, 10217.
15. G. Marafon, M. Crisma, and A. Moretto, *Org. Lett.,* **2019**, 21, 4182.
16. K. Veeresh, and H.N. Gopi, *Org. Lett.,* **2019**, 21, 4500.
17. S. Devadder, P. Verheyden, H. C. M. Jaspers, G. Van Binst, and D. Tourwé, *Tetrahedron Lett.,* **1996**, 37, 703.
18. P. Deschrijver, and D. Tourwé, *FEBS Lett.,* **1982**, 146, 353.
19. R.R. Gardner, G.-B. Liang, and S.H. Gellman, *J. Am. Chem. Soc.,* **1995**, 117, 3280.
20. R.R. Gardner, G.-B. Liang, and S.H. Gellman, *J. Am. Chem. Soc.,* **1999**, 121, 1806.
21. P. Wipf, T.C. Henninger, and S.J. Geib, *J. Org. Chem.,* **1998**, 63, 6088.
22. G.-B. Liang, G.P. Dado, and S.H. Gellman, *J. Am. Chem. Soc.,* **1991,** 113, 3994.
23. G.-B. Liang, J.M. Desper, and S.H. Gellman, *J. Am. Chem. Soc.,* **1993,** 115, 925.
24. C.M. Venkatachalam, *Biopolymers,* **1968**, 6, 1425.
25. J.A. Geddes, K.B. Parker, and E.D.T. Atkins, *J. Mol. Biol.,* **1968**, 32, 343.

26. C. Toniolo, *CRC Crit. Rev. Biochem.,* **1980**, 9, 1.
27. G.D. Rose, L.M. Gierasch, and J.A. Smith, *Adv. Protein Chem.,* **1985**, 37, 1.
28. E. Benedetti, A. Bavoso, B. Di Blasio, V. Pavone, C. Pedone, M. Crisma, G.M. Bonora, and C. Toniolo, *J. Am. Chem. Soc.,* **1982**, 104, 2437.
29. C. Toniolo, and E. Benedetti, *Trends Biochem. Sci*., **1991**, 16, 350.
30. I.L. Karle, and P. Balaram, *Biochemistry*, **1990**, 29, 6747.
31. R. Gessmann, H. Brückner, and K. Petratos, *J. Pept. Sci.*, **2003**, 9, 753.
32. J. Solà, M. Helliwell, and J. Clayden, *Biopolymers*, **2011**, 95, 62.
33. M.G. Lizio, V. Andrushchenko, S.J. Pike, A.D. Peters, G.F.S. Whitehead, I.J. Vitórica-Yrezábal, S.T. Mutter, J. Clayden, P. Bouř, E.W. Blanch, and S.J. Webb, *Chem. Eur. J.*, **2018**, 24, 9399.
34. G. Valle, M. Crisma, F. Formaggio, C. Toniolo, and G. Jung, *Liebigs Ann. Chem.*, **1987**, 1055.
35. R.M. Beesley, C.K. Ingold, and J.F. Thorpe, *J. Chem. Soc.*, **1915**, 107, 1080.
36. M. Drouin, J.L. Arenas, and J.-F. Paquin, *ChemBioChem*, **2019**, 20, 1817.
37. M.-C. Frantz, E.M. Skoda, J.R. Sacher, M.W. Epperly, J.P. Goff, J.S. Greenberger, and P. Wipf, *Org. Biomol. Chem.*, **2013**, 11, 4147.
38. P. Wipf, and J. Xiao, *Org. Lett.*, **2005**, 7, 103.
39. Y. Fu, J. Bieschke, and J.W. Kelly, *J. Am. Chem. Soc.*, **2005**, 127, 15366.
40. Y. Fu, J. Gao, J. Bieschke, M.A. Dendle, and J.W. Kelly, *J. Am. Chem. Soc.*, **2006**, 128, 15948.
41. J. Bieschke, S.J. Siegel, Y. Fu, and J.W. Kelly, *Biochemistry*, **2008**, 47, 50.
42. R.W. Hoffmann, *Chem. Rev.*, **1989**, 89, 1841.
43. Y. Yang, In *Side Reactions in Peptide Synthesis*; Academic Press: London, **2015**; pp. 110-113, and references therein.
44. E. Benedetti, C. Pedone, C. Toniolo, G. Némethy, M.S. Pottle, and H.A. Scheraga, *Int. J. Pept. Protein Res.*, **1980**, 16, 156.
45. F.H. Allen, O. Kennard, D.G. Watson, L. Brammer, A.G. Orpen, and R. Taylor, *J. Chem. Soc., Perkin Trans. II*, **1987**, S1.
46. P. Chakrabarti, and J.D. Dunitz, *Helv. Chim. Acta*, **1982**, 65, 1555.
47. C. Ramakrishnan, and N. Prasad, *Int. J. Protein Res.*, **1971**, 3, 209.
48. R. Taylor, O. Kennard, and W. Versichel, J. *Am. Chem. Soc.,* **1983**, 105, 5761.
49. R. Taylor, O. Kennard, and W. Versichel, *Acta Crystallogr. B*, **1984**, 40, 280.

50. C.H. Görbitz, *Acta Crystallogr. B*, **1989**, 45, 390.
51. M. Avignon, P.V. Huong, J. Lascombe, M. Marraud, and J. Néel, *Biopolymers*, **1969**, 8, 69.
52. E.S. Pysh, and C. Toniolo, *J. Am. Chem. Soc.*, **1977**, 99, 6211.
53. M.H. Baron, C. de Lozé, C. Toniolo, and G.D. Fasman, *Biopolymers*, **1978**, 17, 2225.
54. D.F. Kennedy, M. Crisma, C. Toniolo, and D. Chapman, *Biochemistry*, **1991**, 30, 6541.
55. C. Toniolo, M. Crisma, A. Moretto, C. Peggion, F. Formaggio, C. Alemán, C. Cativiela, C. Ramakrishnan, and P. Balaram, *Chem. Eur. J.*, **2015**, 21, 13866.
56. K. Wüthrich, *NMR of Proteins and Nucleic Acids*; Wiley: New York, NY, **1986**.
57. Y. Zhao, and D.G.A. Truhlar, *J. Chem. Phys.*, **2006**, 125, 194101.
58. Y. Wanga, X. Jina, H.S. Yub, D.G. Truhlar, and X. He, *Proc. Natl. Acad. Sci. USA*, **2017**, 114, 8487.
59. M.J. Frisch, G.W. Trucks, H.B. Schlegel, G.E. Scuseria, M.A. Robb, J.R. Cheeseman, G. Scalmani, V. Barone, B. Mennucci, G.A. Petersson, H. Nakatsuji, M. Caricato, X. Li, H.P. Hratchian, A.F. Izmaylov, J. Bloino, G. Zheng, J.L. Sonnenberg, M. Hada, M. Ehara, K. Toyota, R. Fukuda, J. Hasegawa, M. Ishida, T. Nakajima, Y. Honda, O. Kitao, H. Nakai, T. Vreven, J.A.Jr. Montgomery, J.E. Peralta, F. Ogliaro, M. Bearpark, J.J. Heyd, E. Brothers, K.N. Kudin, V.N. Staroverov, R. Kobayashi, J. Normand, K. Raghavachari, A. Rendell, J.C. Burant, S.S. Iyengar, J. Tomasi, M. Cossi, N. Rega, J.M. Millam, M. Klene, J.E. Knox, J.B. Cross, V. Bakken, C. Adamo, J. Jaramillo, R. Gomperts, R.E. Stratmann, O. Yazyev, A.J. Austin, R. Cammi, C. Pomelli, J.W. Ochterski, R.L. Martin, K. Morokuma, V.G. Zakrzewski, G.A. Voth, P. Salvador, J.J. Dannenberg, S. Dapprich, A.D. Daniels, O. Farkas, J.B. Foresman, J.V. Ortiz, J. Cioslowski, and D.J. Fox, *Gaussian 09*, Revision A.01. Gaussian, Inc.: Wallingford, CT, **2009**.
60. K.D. Gibson, and H.A. Scheraga, *J. Comput. Chem.,* **1987**, 8, 826.
61. P.J. Flory *Statistical Mechanics of Chain Molecules*; Interscience Publishers: New York, NY, **1969**.
62. B. Teixeira-Dias, D. Zanuy, J. Poater, M. Solà, F. Estrany, L.J. del Valle, and C. Alemán, *Soft Matter*, **2011**, 7, 9922.
63. M.C. Burla, R. Caliandro. B. Carrozzini, G.L. Cascarano, C. Cuocci, C. Giacovazzo, M. Mallamo, A. Mazzone, and G. Polidori, *J. Appl. Crystallogr.*, **2015**, 48, 306.
64. G.M. Sheldrick, *Acta Crystallogr. C*, **2015**, 71, 3.

65. M.C. Burla, M. Camalli, B. Carrozzini, G.L. Cascarano, C. Giacovazzo, G. Polidori, and R. Spagna, *J. Appl. Crystallogr.*, **2003**, 36, 1103.

3.2 Intrinsically photoswitchable α/β peptides toward two-state foldamers[e]

The field of foldamers[1] encompasses a growing set of conformationally controlled, oligomeric molecules able to develop well-defined 3D architectures. Examples include peptides based on non-coded α-amino acids, β- and γ-peptides, azapeptides, oligoureas, aromatic oligoamides.[2–9] Typically, α foldamer is designed to highly populate a single conformation. Development of foldamers able to switch their 3D structure between two states in a controlled way, although amenable in principle to interesting applications, is particularly challenging.[10–14] To this end, an appealing potential is offered by *E-Z* photoisomerization of double-bond containing molecules. We have recently shown that incorporation of a fumaramide or maleamide unit at the N-terminus of a peptidomimetic foldamer allows this latter to exhibit a functional response as a result of photoisomerization.[15] Furthermore, we expanded the photoinduced control of conformational switches to appropriately designed foldamers incorporating at an internal position an unsaturated β-amino acid residue, namely (*E/Z*)-3-aminoprop-2-enoic acid [or (*E/Z*)-3-aminoacrylic acid], which can be viewed as the $C^{\alpha,\beta}$ unsaturated analog of β-alanine (β-Ala). By combining this latter abbreviation with the Δ^E/Δ^Z terminology commonly used for $C^{\alpha,\beta}$-didehydro analogs of protein amino acids, the *E* and *Z* *i*somers of 3-aminoprop-2-enoic acid are herewith abbreviated as Δ^EβAla and Δ^ZβAla, respectively.

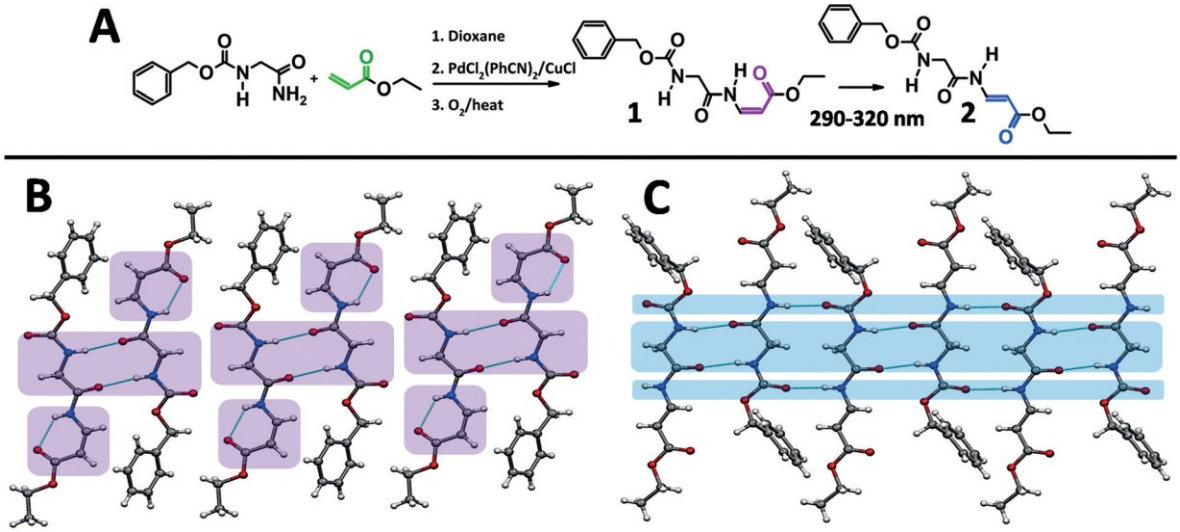

Fig. 1 (A) Synthesis of Z-Gly-Δ^ZβAla-OEt (**1**) and its photoconversion to Z-Gly-Δ^EβAla-OEt (**2**). (B,C) Packing modes in the crystal structures of **1** and **2**, respectively. Intra- and intermolecular H-

[e]Reprinted (adapted) with permission from (Angew. Chem. Int. Ed. 2018, 57, 10217). Copyright (2019) John Wiley and Sons."

bonds are indicated by dashed lines.

The instability of Δ^{E}βAla/ Δ^{Z}βAla derivatives carrying the free amino group hampers their use as amino component in standard peptide coupling reactions. Not surprisingly, peptides containing this residue have not been reported yet. Away around the synthetic problem may be offered by an approach based on the oxidative amidation of conjugated olefins, reported by Kim, Chang and co-workers, who efficiently prepared simple *Z*-configured enamides by reacting primary amides with conjugated olefins in the presence of a Pd/Cu co-catalyst system.[16]

By adapting this strategy, starting from Z-Gly-NH_2 (Z, benzyloxycarbonyl) and ethyl acrylate we successfully synthesized the (*Z*) dipeptide Z-Gly-Δ^{Z}βAla-OEt **1**, which was subsequently quantitatively photoconverted to its *E*-isomer **2** by irradiation at 290–320 nm (Figure 1A). Compounds **1** and **2** were crystallographically characterized. In the structure of **1** (Figure 1B) Gly(1) is nearly fully-extended (ϕ_1,ψ_1=156.1°, -176.0°).[6] The conformation of Δ^{Z}βAla(2) is described by three torsion angles, related to rotations about the N-C^{β} (ϕ_2= -176.2°), C^{β}-C^{α} (θ_2=1.5°), and C^{α}-C (ψ_2=176.9°) bonds. This arrangement allows formation of an N-H···O=C intraresidue H-bond which closes a 6-atom pseudocycle. In the structure of 2 (Figure 1C), not only Gly(1) is fully extended (ϕ_1,ψ_1=178.5°, -178.8°), but also all of the ϕ, θ, and ψ backbone torsion angles of Δ^{E}βAla(2) are within -179.2° and 173.2°. The packing modes of **1** and **2** are in part similar, being characterized by layers of antiparallel molecules (Figures 1B and C). However, they differ by the number of intermolecular H-bonds. Specifically, each molecule of **1** makes two N-H···O=C intermolecular H-bonds on one side only, whereas on the opposite side only C-H···O and van der Waals contacts are observed (Figure 1B; see also Table S5) because the intramolecularly H-bonded conformation adopted by Δ^{Z}βAla prevents its N-H group from being approached within H-bonding distance by any other potential H-bond acceptor of the flanking molecule. Conversely, for **2**, each molecule is connected to its neighbors by four intermolecular H-bonds, two on each side (Figure 1C), giving rise to a flattened β-sheet. Notably, attempts to carry out the olefin oxidative amidation by replacing either the benzyloxycarbonyl N^{α}-protecting group (with Fmoc or Boc), or Gly with other amino acids (e.g., Ala, Leu, Val) did not afford any product, in all probability owing to the different stability of the protecting groups close to the reaction site and to the steric hindrance exerted by the side chains, respectively.

Next, we explored the introduction of the unsaturated β-amino acid internally to the peptide

backbone. To this aim, a set of N^{α}-acrylamide-functionalized α-amino acid ester derivatives of the type Acr-Aaa-OR [Acr = acryloyl; Aaa =Gly, Ala, Leu, Aib (α-amino-isobutyric acid); R =methyl or ethyl] were prepared and placed to react with Z-Gly-NH_2 through olefin oxidative amidation to afford the corresponding tripeptides of general formula Z-Gly-Δ^{Z}βAla-Aaa-OR. Yields decreased from excellent to poor with increasing bulk of Aaa (Gly: 88%; Ala: 53%; Leu: 28%; Aib: 8%). However, the *Z/E* stereoselectivity of product formation was comparable in all cases (≈15:1). A representative example of the photoconversion of these *Z*-configured tripeptides to the corresponding E-isomers and back to their *Z*-form is illustrated in Figure 2 in the case of the Z-Gly-Δ^{Z}βAla-Leu-OMe (**3**)/ Z-Gly-Δ^{E}βAla-Leu-OMe (**4**) pair. We found by HPLC monitoring (Figure 2A, right panel) that the **3**-to-**4** conversion occurs quantitatively within 20 minutes by irradiation at 290–320 nm, whereas the reverse process, carried out by irradiation at 254 nm (to exploit a slight difference in the UV/Vis absorption profiles of **3** and **4**; see Fig. 3), reaches a photostationary equilibrium in which (*E*) **4** and (*Z*) **3** are present in a 30% : 70% molar ratio. Photoconversions (*Z* to *E* and *E* to *Z*) were also monitored by ^{1}HNMR spectrometry (Figure 2B).

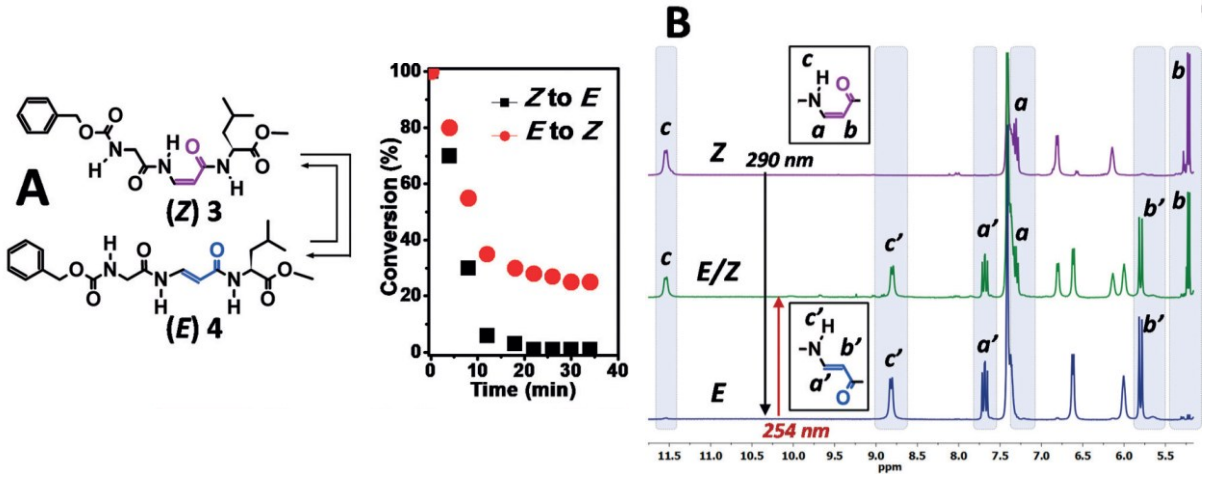

Fig. 2 (A) Left: formulas of Z-Gly-Δ^{Z}βAla-Leu-OMe (**3**) and Z-Gly-Δ^{E}βAla-Leu-OMe (**4**). Right: time evolution of their photoconversions monitored by HPLC. (B) ^{1}HNMR spectra (CD_3CN) of (*Z*) **3** (top), its (*E*) isomer **4** obtained by irradiation at 290–320 nm (bottom), and the mixture of *E/Z* isomers resulting as photostationary equilibrium upon irradiation of the *E* isomer at 254 nm (center). Diagnostic signals are marked. ^{3}J coupling constants between olefinic protons are 9 Hz for (*Z*) **3** and 14 Hz for (*E*) **4**.

As a further step, we placed a Δ^{Z}βAla residue as the junction between two conformationally distinct peptide domains. Specifically, Z-(Ala-Aib)$_2$-Ala-Gly-NH_2 **5** (highly folded, 3_{10}-helical)[18-21] was combined through olefin oxidative amidation with the β-amyloid[22] 16–20 segment derivative Acr-Lys(Boc)-Leu-Val-Phe-Phe-OH **6**, giving Z-(Ala-Aib)$_2$-Ala-Gly-

Δ^{Z}βAla-Lys(Boc)-Leu-Val-Phe-Phe-OH **7** in 64% yield (Figure 4A). Again, photoconversion from (*Z*) **7** to (*E*) **8** was achieved quantitatively.

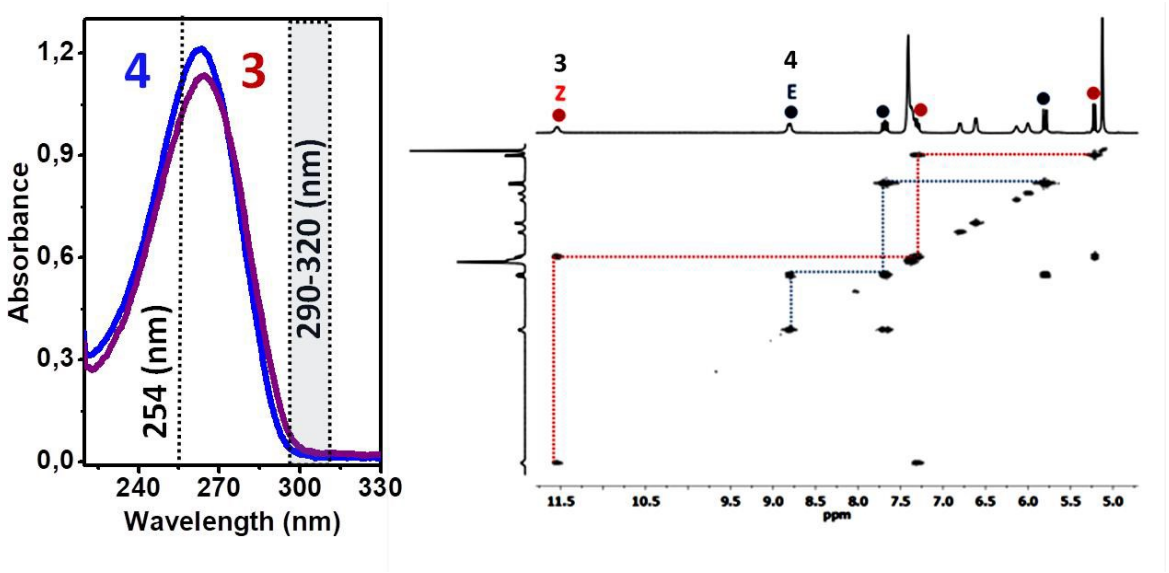

Fig. 3 (Left) UV-Vis spectra of **3** and **4** in MeOH solution. The two absorption ranges used for the isomerization processes are highlighted. (Right) 2D COSY NMR (400 MHz) spectrum of Z-Gly-ΔβAla-Leu-OMe (Z/E 40:60 %) mixture in CD_3CN.

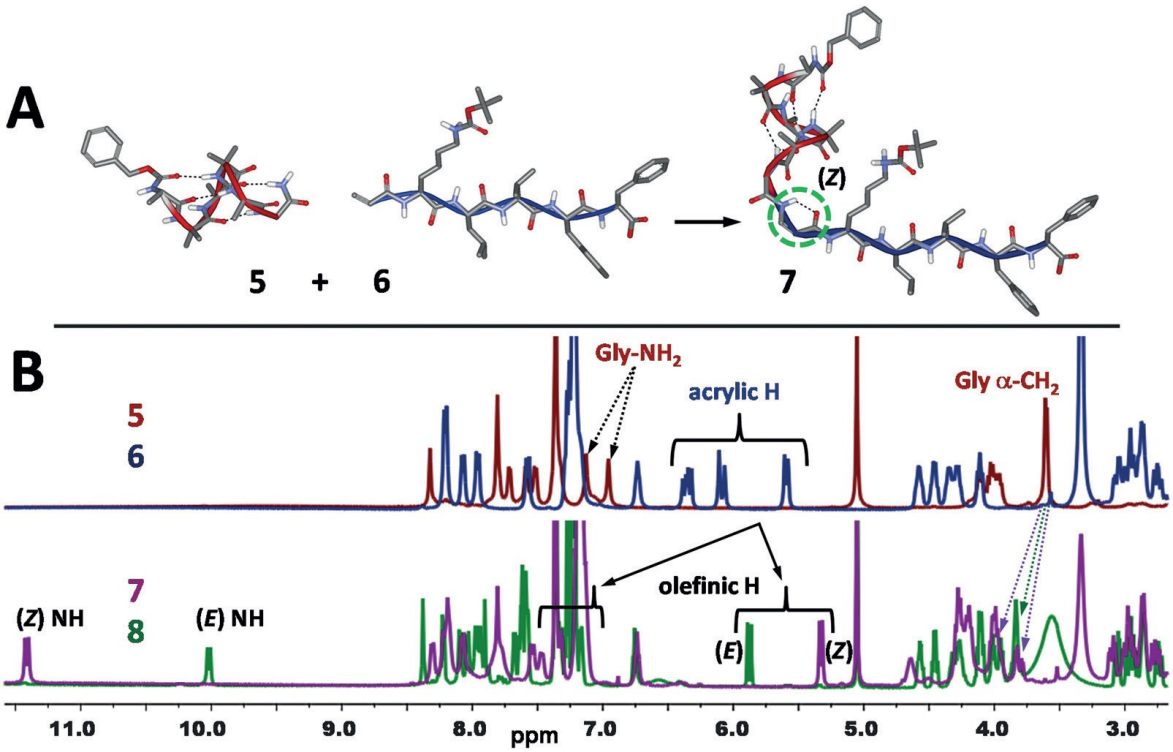

Fig. 4 (A) Computer-generated model of Z-(Ala-Aib)$_2$-Ala-Gly-Δ^{Z}βAla-Lys(Boc)-Leu-Val-Phe-Phe-OH (**7**), which combines a helical domain (from **5**) with a β-sheet promoting segment (from **6**) The -Δ^{Z}βAla- junction is circled. (B) Overlap of the ^{1}HNMR spectra (DMSO) of the two reactants (upper

part, **5**, red trace, and **6**, blue trace) and (lower part) of the resulting product (*Z*) **7** (violet) and its *E* isomer **8** (green). Diagnostic signals are marked.

Figure 4B compares the ^{1}HNMR spectra of the two reactants **5** and **6** with that of the resulting product (Z) **7**, highlighting the disappearance of the acrylate proton signals belonging to **6** and of the Gly-NH_2 signals belonging to **5**, accompanied in **7** by a downfield shift of the Gly α-CH_2 signals and the onset of the olefinic signals and of the lowfield Δ^{Z}βAla NH.

The latter signal moves upfield upon photoisomerization to (E) **8**. Notably, the Lys side-chain Boc-protection survived in **7**. Its subsequent removal afforded Z-(Ala-Aib)$_2$-Ala-Gly-Δ^{Z}βAla-Lys-Leu-Val-Phe-Phe-OH **9** which, in turn, was photoconverted to its Δ^{E}βAla-containing isomer **10**. Upon standing, the 5 mm water solution of (E) **10** turned into a stable hydrogel, suggesting that the *E*-isomeric state of the olefinic junction allows efficient β-sheet formation involving the β-amyloid-derived segment of the foldamer without interference from the helical domain (Figure 5B). Hydrogelation is not observed in the case of **9**, in all probability because the *Z* configuration of the olefinic junction, in addition to sequestering the Δ^{Z}βAla NH group from intermolecular H-bonding, makes a kink in the overall shape of the foldamer (Figure 5A). According to our model (Figure 5B), **9** may thus self-associate at best into dimers (as indirectly supported by the crystal structure of **2**), but extensive β-sheet formation does not occur. Interestingly, the hydrogel formed by **10**, upon 15 minutes irradiation at 254 nm, returns to a fluid state, in which the (*E*) **10** and (*Z*) **9** isomers are present in nearly equimolar amounts.

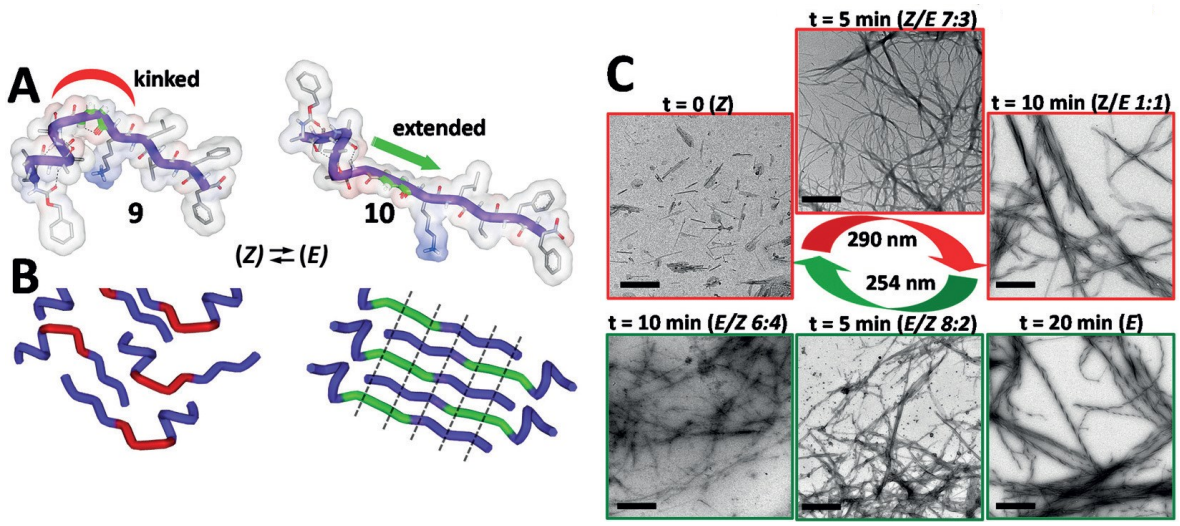

Fig. 5 (A) Models of the two-domain foldamers Z-(Ala-Aib)$_2$-Ala-Gly-Δ^{Z}βAla-Lys-Leu-Val-Phe-Phe-OH (*Z*) **9** and its *E*-isomer **10**. (B) Schematic representation of the self-assembly modes of (*Z*) **9** and (*E*) **10**. (C) TEM images taken at time intervals monitoring the photoconversion of (*Z*) **9** to (*E*) **10** and back from (*E*) **10** to a 6:4 mixture of (*E*) **10** to (*Z*) **9** (scale bars: 500 nm).

Morphological insight on these phenomena was provided by TEM analysis (Figure 5C). Specifically, we recorded a set of TEM images, beginning with a sample cast from a 5 mm water solution of **9** and then analyzing samples taken after 5, 10 and 20 minutes of irradiation at 290–320 nm. The increasing (*E*) **10**/ (*Z*) **9** molar ratio (from 0 to 95%) resulting from the photoconversion gives rise to formation of fibers of increasing size. Such fibers significantly dissociate upon partial back photoconversion (from 95% 10 to a 6:4 mixture of **10** and **9**) promoted by 254 nm irradiation.

Conclusions

To summarize, we succeeded in introducing the simplest unsaturated (E–Z photoisomerizable) β-amino acid, namely (*Z*)-3-aminoprop-2-enoic acid (Δ^{Z}βAla), into peptide foldamers, via a one-pot chemical coupling based on Pd/Cu catalyzed olefin oxidative amidation. A limitation to such synthetic approach, at least in our hands, is that among protein amino acids only Gly seems to be allowed at the position preceding the in situ generated Δ^{Z}βAla unit. Higher versatility is tolerated about the nature of the following residue, although yields decrease with increasing bulk of its side chain. This novel type of ligation gives access to peptidomimetics and foldamers, some properties of which, including 3D structure and self-association tendency, can be tuned photochemically. This view is supported by our crystallographic analyses on two model compounds. As a specific case, the switch between the Z and E isomers of a 3-aminoprop-2-enoic acid residue, inserted as the junction between two different peptide domains (one helical while the other β-sheet promoter), allows supramolecular self-association to be reversibly turned on/off. We are confident that the photoswitchable Δ^{Z}βAla/Δ^{E}βAla system may provide a valuable structural element in the design of two-state functional foldamers for biomimetic and nanotechnological applications.[10–14, 23, 24]

Experimental section

Instruments and Methods

High-Performance Liquid Chromatography. The HPLC measurements were performed using an Agilent 1200 apparatus (Palo Alto, CA), equipped with a UV detector at 216 nm and a column Agilent extend-C18 (stationary phase). Eluants: A= 9:1 H_2O/CH_3CN, 0.05 % TFA; B= 1:9 H_2O/CH_3CN, 0.05 % TFA.

Nuclear Magnetic Resonance. ^1H NMR and 2D-NMR spectra were recorded at 25°C on a Bruker Avance 400 or 500 MHz instruments. ^1H and ^{13}C spectra were referenced relative to the solvent residual peaks and chemical shifts (δ) reported in ppm downfield of tetramethylsilane ($CDCl_3$ δ H: 7.26 ppm, δ C: 77.16 ppm; CD_3CN δ H: 1.94 ppm, δ C: 118.26 ppm). The multiplicity of a signal is indicated as br, broad; s, singlet; d, doublet; t, triplet; m, multiplet.

Mass Spectrometry. Mass spectra by electrospray ionization (ESI), collected in the positive mode, were performed on Perseptive Biosystem Mariner ESI-ToF 5220 spectrometer (Foster City, CA).

Transmission Electron Microscopy. Samples were analyzed on a Jeol 300PX instrument. Samples were prepared immediately before used, by dilution of the dialyzed solutions with MilliQ water. A small drop of solutions was floated on a glow discharged carbon coated grid and excess was removed by #50 hardened Whatman filter paper. For the samples with negative staining, the grid was then floated on 2% uranyl acetate solution for 10 seconds, and the excess was removed by #50 hardened Whatman filter paper.

Fourier Transform-Infrared Spectroscopy. Solid state FT-IR (KBr disk technique) absorption spectra were recorded with a Nicolet Nexus FT-IR spectrometer. The ν maxima for the main absorption bands are given.

UV lamp. Two handheld UV Lamps (Vilber) with bulbs emitting wavelength of 254 nm (6W) or 290-320 nm (8W) were used in the photoisomerization experiments.

UV-Vis Absorption. The UV-Vis absorption spectra were recorded using a Shimadzu model UV-2501 PC spectrophotometer. A 1-cm path length quartz cell was used.

Photoisomerization experiments [conversion from **3** to **4** to **3**] The sample was dissolved in deuterated solvent (CD3CN) and placed in a quartz NMR tube (Norrell S-500-QTZ). The sealed NMR tube was directly irradiated under the UV lamp without protective filter at a distance of about 1 cm from the light bulb. The NMR spectra were recorded before and after

different irradiation times.

Synthesis and Characterization

Materials

N,N-diisopropylethylamine (DIPEA), trifluoroacetic acid (TFA), triethylamine (TEA), glycine ethyl ester hydrochloride, L-amino acids methyl ester hydrochloride, HATU, Fmoc-L-amino acids, acryloyl chloride, bis(benzonitrile)palladium(II) chloride, Z-glycinamide, ethyl acrylate, tetraethyl methylenediphosphonate, and copper monochloride were obtained from Sigma-Aldrich. 1-Hydroxy-7-aza-1,2,3-benzotriazole (HOAt) was purchased from GL Biochem (Shanghai).

The deuterated solvents DMSO-d_6, $CDCl_3$, and $CDCN_3$ were purchased from Euriso-Top (France).

Synthesis of Z-Gly-Δ^ZβAla-OEt (1)

A dry round bottom flask was charged with Z-Gly-NH_2 (4.8 mmol), $PdCl_2(PhCN)_2$ (0.24 mmol), CuCl (0.48 mmol). The reaction vessel was charged with oxygen followed by the addition of dioxane (20 mL). The reaction mixture was stirred at 70°C for 1 min and then ethyl acrylate (14 mmol) was added. The reaction mixture was stirred overnight at 70°C under oxygen atmosphere. After the reaction was over (typically 2 days), the solvent was removed by distillation and the crude residue was purified via flash chromatography (as eluant: DCM/MeOH 93:7), giving 1 as a white solid in a 83% yield. Compound **2** was also recovered in a 5% yield.

M.p. = 101-103°C.

MS (ESI+, MeOH) *m/z* calcd. for $C_{15}H_{19}N_2O_5$ ($[M+H]^+$) 307.1288, found 307.1284; *m/z* calcd. For $C_{15}H_{19}N_2O_5Na$ ($[M+Na]^+$) 329.1107, found 329.1123.

FT-IR ν_{max} 3316, 2982, 1709, 1686, 1630, 1485, 1397, 1245, 1199 cm^{-1}.

^1H NMR (400 MHz, $CDCl_3$) δ 10.87 (br, J = 9.1 Hz, 1H), 7.53-7.44 (m, 1H), 7.44-7.32 (m, 5H), 5.40 (br, J = 25.0 Hz, 1H), 5.21 (d, J = 9.0 Hz, 1H), 5.19 (s, 2H), 4.21 (q, J = 7.1 Hz, 2H), 4.05 (d, J = 4.8 Hz, 2H), 1.32 (t, J = 7.1 Hz, 3H). ^{13}C NMR (101 MHz, $CDCl_3$) δ 168.91, 167.59, 136.91, 128.56, 128.28, 128.18, 97.93, 67.44, 60.34, 44.76, 14.33.

Synthesis of Z-Gly-Δ^EβAla-OEt (2)

Compound **2** was obtained in 95 % yield starting from a 20 mM solution of 1 in CH_3CN. This

solution was placed in an open air crystallizer and directly irradiated at 290-320 nm. Under these conditions **2** precipitated almost quantitatively and it was collected by filtration.
M.p. = 131-133°C.
MS (ESI+, MeOH) *m/z* calcd. for $C_{15}H_{19}N_2O_5$ ($[M+H]^+$) 307.1288, found 307.1285; *m/z* calcd. For $C_{15}H_{19}N_2O_5Na$ ($[M+Na]^+$) 329.1107, found 329.1112.
FT-IR ν_{max} 3300, 2981, 1710, 1694, 1694, 1639, 1524, 1248, 1140 cm^{-1}.
^1H NMR (400 MHz, $CDCl_3$) δ 8.40 (br, 1H), 8.09-7.89 (m, 1H), 7.46-7.32 (m, 5H), 5.51 (d, J = 14.3 Hz, 1H), 5.47 (br, 1H), 5.17 (s, 2H), 4.22 (q, J = 7.1 Hz, 2H), 3.98 (d, J = 4.6 Hz, 2H), 1.31 (t, J = 7.1 Hz, 3H). ^{13}C NMR (101 MHz, $CDCl_3$) δ 167.41, 167.09, 136.58, 135.69, 128.69, 128.52, 128.15, 103.18, 67.72, 60.33, 45.04, 14.33.

Synthesis of Acr-Aaa-OR (Aaa = Gly; L-Ala;L-Leu, Aib; R = Me, Et)
Typically, HCl·Aaa-OR (21 mmol) was dissolved in dry DCM in the presence of DIPEA (33 mmol) and cooled with an ice bath, then acryolyl chloride (18.9 mmol) was added dropwise. The reaction was stirred overnight at room temperature. After evaporation of the solvent, the residue was dissolved in ethyl acetate and washed with saturated $KHSO_4$ 5% and $NaHCO_3$ 5%, dried, filtered and concentrated. The crude product was purified by silica-gel column chromatography using diethyl ether/petroleum ether as eluant to give the desired N-acryloyl amino acid methyl (or ethyl) esters as colorless products (87-95%).

Acr-Gly-OEt MS (ESI+, MeOH) *m/z* calcd. for $C_7H_{11}NO_3$ ($[M+H]^+$) 158.0811, found 158.0815; *m/z* calcd. for $C_7H_{11}NO_3Na$ ($[M+Na]^+$) 180.0631, found 180.0630. ^1H NMR (500 MHz, $CDCl_3$) δ 6.55 (br, 1H), 6.25 (ddd, J = 27.2, 17.0, 5.8 Hz, 2H), 5.67 (dd, 1H), 4.21 (q, J = 7.1, 5.2 Hz, 2H), 4.10 (d, J = 5.3 Hz, 2H), 1.28 (t, J = 7.2 Hz, 3H). M.p. = 88-90°C.

Acr-Ala-OMe MS (ESI+, MeOH) *m/z* calcd. for $C_7H_{11}NO_3Na$ ($[M+Na]^+$) 180.0631, found 180.0630. ^1H NMR (400 MHz, $CDCl_3$) δ 6.67 (br, 1H), 6.40-6.04 (m, 2H), 5.63 (d, J = 10.1 Hz, 1H), 4.75-4.47 (m, 1H), 3.72 (s, 3H), 1.44 (d, 3H). Oil.

Acr-Leu-OMe MS (ESI+, MeOH) *m/z* calcd. for $C_{10}H_{17}NO_3Na$ ($[M+Na]^+$) 222.1100, found 222.1121. ^1H NMR (500 MHz, $CDCl_3$) δ 6.47 (br, 1H), 6.22 (ddd, J = 27.2, 17.0, 5.8 Hz, 2H), 5.65 (dd, J = 10.2, 1.3 Hz, 1H), 4.81-4.60 (m, J = 8.8, 4.8 Hz, 1H), 3.73 (s, 3H), 1.78-1.42 (m, 3H), 0.93 (t, J = 6.1 Hz, 6H). Oil.

Acr-Aib-OMe MS (ESI+, MeOH) *m/z* calcd. for $C_8H_{13}NO_3$ ($[M+H]^+$) 172.0968, found 172.0975; *m/z* calcd. for $C_8H_{13}NO_3Na$ ($[M+Na]^+$) 194.0787, found 194.0809. ^{1}H NMR (500 MHz, $CDCl_3$) δ 6.37-5.98 (m, 2H), 6.24 (br, 1H), 5.67 (dd, J = 10.3, 1.4 Hz, 1H), 3.79 (s, 3H), 1.63 (s, 6H). Waxy solid.

Synthesis of 3 and related compounds of general formula Z-Gly-Δ^ZβAla-Aaa-OR

Typically, a dry round bottom flask was charged with Z-Gly-NH_2 (1.7 mmol), $PdCl_2(PhCN)_2$ (0.085 mmol), and CuCl (0.17 mmol). The reaction vessel was charged with oxygen followed by the addition of dioxane (8 mL) and tetraethyl methylenediphosphonate (0.17 mmol). The reaction mixture was stirred at 70°C for 1 min and then Acr-Aaa-OR (5 mmol) dissolved in dioxane (5 ml) was added. The reaction mixture was stirred 2/3 days at 70°C under oxygen atmosphere. After the reaction was over, the solvent was removed by evaporation and the crude residue was purified by flash chromatography using diethyl ether/petroleum ether as the eluant.

Z-Gly-Δ^ZβAla-Gly-OEt. 88% yield. MS (ESI+, MeOH) *m/z* calcd. for $C_{17}H_{21}N_3O_6$ ($[M+H]^+$) 364.1503, found 364.1503; *m/z* calcd. for $C_{17}H_{21}N_3O_6Na$ ($[M+Na]^+$) 386.1322, found 386.1321. FT-IR ν_{max} 3329, 2981, 2933, 1726, 1705, 1658, 1619, 1532, 1470, 1393, 1237, 1202 cm^{-1}.

^{1}H NMR (500 MHz, CD_3CN) δ 11.56 (d, J = 8.9 Hz, 1H), 7.52-7.18 (m, 6H), 6.85 (t, 1H), 6.22 (t, 1H), 5.19 (d, J = 25.3, 9.1 Hz, 1H), 5.10 (s, 2H), 4.13 (q, 2H), 3.93 (d, J = 5.9 Hz, 2H), 3.82 (d, J = 6.1 Hz, 2H), 1.23 (t, 3H). ^{13}C NMR (101 MHz, CD_3CN) δ 169.82, 168.61, 168.28, 134.44, 128.46, 127.95, 127.80, 99.27, 66.53, 44.44, 40.61, 13.50. M.p: 165-167 °C. Note: Its Δ^EβAla isomer was also recovered from chromatography in a 6% yield.

Z-Gly-Δ^ZβAla-Ala-OMe. 56% yield. MS (ESI+, MeOH) *m/z* calcd. for $C_{17}H_{21}N_3O_6$ ($[M+H]^+$) 364.1503, found 364.1503; *m/z* calcd. for $C_{17}H_{21}N_3O_6Na$ ($[M+Na]^+$) 386.1322, found 386.1321. FT-IR ν_{max} 3325, 2954, 1729, 1706, 1656, 1618, 1534, 1472, 1455, 1393, 1235 cm-1. ^{1}H NMR (500 MHz, $CDCl_3$) δ 11.49 (d, J = 10.2 Hz, 1H), 7.43-7.31 (m, 6H), 6.11 (d, J = 6.7 Hz, 1H), 5.46 (br, 1H), 5.17 (s, 2H), 5.10 (d, J = 8.8 Hz, 1H), 4.67-4.57 (m, J = 7.2 Hz, 1H), 4.03 (d, J = 5.5 Hz, 2H), 3.79 (s, 3H), 1.65 (s, 2H), 1.46 (d, J = 8.0 Hz, 3H). ^{13}C NMR (101 MHz, $CDCl_3$) δ 167.64, 135.10, 128.53, 128.20, 128.14, 99.55, 67.30, 52.65,

47.81, 30.33, 18.49. M.p: 141-143 °C. Note: Its Δ^{E}βAla isomer was also recovered from chromatography in a 4% yield.

Z-Gly-Δ^{Z}βAla-Leu-OMe (3). 28% yield. MS (ESI+, MeOH) m/z calcd. for $C_{20}H_{27}N_3O_6$ ($[M+H]^+$) 406.1972, found 406.1957; m/z calcd. for $C_{20}H_{27}N_3O_6Na$ ($[M+Na]^+$) 428.1792, found 428.1790. FT-IR ν_{max} 3324, 2957, 1730, 1707, 1657, 1619, 1469, 1393, 1242, 1217 cm-1. ^{1}H NMR (400 MHz, CD_3CN) δ 11.54 (d, J = 9.5 Hz, 1H), 7.50-7.20 (m, 5H), 6.81 (d, J = 7.5 Hz, 1H), 6.14 (t, 1H), 5.22 (d, J = 8.9 Hz, 1H), 5.12 (s, 2H), 4.53-4.40 (m, J = 15.0, 7.7 Hz, 1H), 3.85 (d, J = 6.1 Hz, 2H), 3.68 (s, 3H), 1.76-1.53 (m, 3H), 0.95 (dd, 6H). ^{13}C NMR (101 MHz, CD_3CN) δ 173.10, 168.34, 134.44, 128.47, 127.96, 127.79, 99.26, 66.56, 51.74, 50.52, 44.43, 40.14, 24.63, 22.07, 20.86. M.p: 151-155 °C. Note: Its Δ^{E}βAla isomer was also recovered from chromatography in a <2% yield.

Z-Gly-Δ^{Z}βAla-Aib-OMe. 8% yield. MS (ESI+, MeOH) *m/z* calcd. for $C_{18}H_{23}N_3O_6Na$ ([M+Na]+) 400.1479, found 400.1477. FT-IR ν_{max} 3332, 2951, 1724, 1707, 1656, 1618, 1534, 1468, 1456, 1393, 1235 cm^{-1}. ^{1}H NMR (500 MHz, CD_3CN) δ 11.41 (d, J = 9.2 Hz, 1H), 7.43-7.29 (m, 5H), 7.25 (t, 1H), 6.86 (s, 1H), 6.09 (t, 1H), 5.14 (d, J = 8.9 Hz, 1H), 5.08 (s, 2H), 3.81 (d, J = 6.1 Hz, 2H), 3.61 (s, 3H), 1.43 (s, 6H). ^{13}C NMR (101 MHz, CD_3CN) δ 174.71, 167.89, 134.17, 128.50, 127.99, 99.60, 66.60, 55.67, 51.78, 44.32, 29.65, 24.40. Oil.

Synthesis of 4 and related compounds of general formula Z-Gly-Δ^{E}βAla-Aaa-OR

These compounds were obtained by direct irradiation at 290-320 nm of a 15 mM solution (CH_3CN) of the corresponding Δ^{Z}βAla-containing isomers placed in an open air crystallizer. The products were collected by filtration.

Z-Gly-Δ^{E}βAla-Gly-OEt. 95% yield. MS (ESI+, MeOH) *m/z* calcd. for $C_{17}H_{21}N_3O_6$ ([M+H]+) 364.1503, found 364.1505; *m/z* calcd. for $C_{17}H_{21}N_3O_6Na$ ([M+Na] +) 386.1322, found 386.1320. FT-IR ν_{max} 3325, 3295, 2920, 1738, 1687, 1665, 1531 cm^{-1}. ^{1}H NMR (400 MHz, DMSO-d_6) δ 10.49 (d, J = 10.8 Hz, 1H), 8.28 (t, J = 5.9 Hz, 1H), 7.65-7.52 (m, 2H), 7.39-7.26 (m, 5H), 5.74 (d, J = 14.0 Hz, 1H), 5.02 (s, 2H), 4.07 (q, J = 7.1 Hz, 2H), 3.86 (d, J = 5.9 Hz, 2H), 3.73 (d, J = 5.9 Hz, 2H), 1.17 (t, J = 7.1 Hz, 3H). ^{13}C NMR (101 MHz, DMSO-d_6) δ 170.61, 169.12, 166.69, 157.02, 137.43, 134.21, 128.83, 128.30, 128.22, 104.42,

66.05, 60.83, 44.14, 41.13, 14.57. M.p: 178-180 °C.

Z-Gly-Δ^{E}βAla-Leu-OMe (4). 76% yield. MS (ESI+, MeOH) *m/z* calcd. for $C_{20}H_{27}N_3O_6$ ($[M+H]^+$) 406.1972, found 406.1961; *m/z* calcd. for $C_{20}H_{27}N_3O_6Na$ ($[M+Na]^+$) 428.1792, found 428.1790. FT-IR ν_{max} 3278, 2956, 1731, 1698, 1659, 1609, 1522, 1241, 1200 cm-1. ^{1}H NMR (400 MHz, CD_3CN) δ 8.82 (d, J = 10.4 Hz, 1H), 7.68 (dd, J = 13.8, 11.1 Hz, 1H), 7.47-7.30 (m, 5H), 6.62 (d, J = 7.6 Hz, 1H), 6.01 (t, 1H), 5.80 (d, J = 14.0 Hz, 1H), 5.13 (s, 2H), 4.48 (q, J = 7.6 Hz, 1H), 3.84 (d, J = 6.0 Hz, 2H), 3.68 (s, 3H), 1.74-1.64 (m, J = 12.0, 6.0 Hz, 1H), 1.60 (t, J = 7.2 Hz, 2H), 0.94 (dd, J = 13.3, 6.5 Hz, 6H). ^{13}C NMR (101 MHz, CD_3CN) δ 173.39, 166.06, 133.74, 128.50, 128.00, 104.15, 66.44, 51.61, 50.80, 40.34, 24.62, 22.10, 20.84. M.p: 171-173 °C.

Z-Gly-Δ^{E}βAla-Aib-OMe. 80% yield. MS (ESI+, MeOH) *m/z* calcd. for $C_{18}H_{23}N_3O_6Na$ ([M+Na]+) 400.1479, found 400.1476. FT-IR ν_{max} 3274, 3200, 3037, 1731, 1697, 1659, 1607, 1528 cm^{-1}. ^{1}H NMR (500 MHz, CD_3CN) δ 8.81 (d, J = 10.5 Hz, 1H), 7.63 (dd, J = 13.9, 11.0 Hz, 1H), 7.46-7.29 (m, 5H), 6.71 (s, 1H), 6.01 (t, 1H), 5.75 (d, J = 14.0 Hz, 1H), 5.12 (s, 2H), 3.83 (d, J = 6.0 Hz, 2H), 3.63 (s, 3H), 1.44 (s, 6H). ^{13}C NMR (101 MHz, CD_3CN) δ 133.44, 128.50, 128.01, 104.44, 66.44, 51.62, 24.49. Waxy solid.

Synthesis of Z-(Ala-Aib)2-Ala-Gly-NH_2 (5)

The compound **5** was prepared using standard solid-phase peptide synthesis (SPPS) and Fmoc chemistry on a Fmoc-Rink amide resin. The dry resin was swelled with DMF for 30-45 minutes before use and the Fmoc-protecting group on the resin was removed with a solution of 20% piperidine in DMF. Peptide was synthesised on 2 g of resin (loading 0.76 mmol/g). After linking the first amino acid (Fmoc-Gly-OH) to the resin, the latter was capped with a solution of DMF/Ac_2O/DIPEA (20:2:1). In each step, the Fmoc-protecting group was removed with a solution of 20% piperidine in DMF. Successive amino acids were added step-by-step, using the following protocol: 4.0 eq (relative to the resin's loading) of Fmoc-protected amino acid were activated with 4.0 eq of HOAt, 4.0 eq of HATU and 8 eq of DIPEA in DMF (about 0.5 M). This mixture was added in a reactor containing the resinbound peptide and mixed for 2 hours under N_2 flux. The resin was dried and rinsed with DMF (3x), DCM (2x), MeOH (1x) and it was swelled again with DMF. After drying the resin, the resin-

bound peptide was unblocked with a mixture 95:2,5:2,5 (v/v/v) of TFA:H_2O:TIS mixture. The peptide was obtained, in high purity, in 80% yield.

MS (ESI+, MeOH) *m/z* calcd. for $C_{27}H_{41}N_7O_8$ ($[M+H]^+$) 592.3089, found 592.3078; *m/z* calcd. For $C_{27}H_{41}N_7O_8Na$ ($[M+Na]^+$) 614.2908, found 614.2919. FT-IR ν_{max} 3311, 2985, 2938, 1705, 1659, 1535, 1455 cm^{-1}. ^1H NMR (400 MHz, DMSO-d_6) δ 8.32 (s, 1H), 7.80 (s, 2H), 7.71 (d, J = 4.7 Hz, 1H), 7.58 (d, J = 5.3 Hz, 1H), 7.51 (d, J = 6.7 Hz, 1H), 7.36 (s, 5H), 7.12 (s, 1H), 6.95 (s, 1H), 5.05 (s, 2H), 4.16-3.90 (m, 3H), 3.60 (d, J = 5.7 Hz, 2H), 1.42-1.19 (m, 21H). ^{13}C NMR (101 MHz, DMSO-d_6) δ 175.57, 174.98, 173.99, 173.59, 172.85, 171.51, 156.62, 137.40, 128.81, 128.29, 128.06, 65.98, 56.37, 56.14, 51.20, 50.88, 49.64, 42.63, 25.86, 25.39, 25.02, 24.84, 17.63, 17.41, 16.92, 14.54.

Synthesis of Acr-Lys(Boc)-Leu-Val-Phe-Phe-OH (6)

Compound **6** was prepared using standard solid-phase peptide synthesis (SPPS) and Fmoc chemistry on a 2-Chlorotrityl chloride resin. The dry resin was swelled with DMF for 30-45 minutes before use. The peptide was synthesised on 1 g of resin (loading 1.6 mmol/g). After linking the first amino acid (Fmoc-Phe-OH) to the resin, the latter was capped with a solution of DMF/MeOH/DIPEA (20:2:1). In each step, the Fmoc-protecting group was removed with a solution of 20% piperidine in DMF. Successive amino acids were added step-by-step, using the following protocol: 4.0 eq (relative to the resin loading) of Fmoc-protected amino acid were activated with 4.0 eq of HOAt, 4.0 eq of HATU and 8 eq of DIPEA in DMF (about 0.5 M). This mixture was added in a reactor containing the resin-bound peptide and mixed for 2 hours under N2 flux. After the last coupling with Fmoc-Lys(Boc)-OH, the Fmocprotecting group was removed with a solution of 20% piperidine in DMF. A solution of DIPEA (8.0 eq) in DMF was added in the reactor and then acryloyl chloride (4.0 eq) in DMF was added dropwise. The operation was repeated twice. The resin was dried and rinsed with DMF (3x), DCM (2x), MeOH (1x) and it was swelled again with DMF. After drying the resin, the resin-bound peptide was unblocked with a mixture 18:2 (v/v) of DCM/TFA. The peptide was obtained, in high purity, in 75% yield.

MS (ESI+, MeOH) *m/z* calcd. for $C_{43}H_{62}N_6O_9$ ($[M+H]^+$) 807.4651, found 807.4634; *m/z* calcd. For $C_{43}H_{62}N_6O_9Na$ ($[M+Na]^+$) 829.4470, found 829.4501. FT-IR ν_{max} 3287, 2960, 2934, 1717, 1686, 1638, 1539 cm^{-1}. ^1H NMR (400 MHz, DMSO-d_6) δ 12.68 (br, 1H), 8.20 (d, J = 7.4 Hz, 1H), 8.07 (d, J = 7.7 Hz, 1H), 7.95 (d, J = 8.0 Hz, 1H), 7.57 (d, J = 8.8 Hz, 1H), 7.30-7.14 (m, 16H), 6.73 (t, 1H), 6.35 (dd, J = 17.0, 10.2 Hz, 1H), 6.08 (d, J = 17.0 Hz, 1H),

5.59 (d, J = 10.2 Hz, 1H), 4.62-4.53 (m, 1H), 4.50-4.41 (m, 1H), 4.39-4.24 (m, 2H), 4.11 (t, J = 7.6 Hz, 1H), 3.10-2.82 (m, 4H), 2.79-2.70 (m, 1H), 1.86 (dd, J = 13.2, 6.6 Hz, 1H), 1.68-1.49 (m, 3H), 1.37 (s, 9H), 1.29-1.16 (m, 2H), 0.86 (d, J = 6.3 Hz, 3H), 0.80 (d, J = 6.2 Hz, 3H), 0.71 (d, J = 6.2 Hz, 6H). ^{13}C NMR (101 MHz, DMSO-d_6) δ 173.07, 172.03, 171.96, 171.35, 170.88, 164.84, 138.07, 137.77, 132.08, 129.54, 128.65, 128.42, 126.90, 126.62, 125.80, 77.80, 57.83, 53.82, 52.85, 51.51, 38.02, 37.22, 32.44, 31.21, 29.78, 28.75, 24.58, 23.53, 23.20, 22.11, 19.60, 18.35.

Synthesis of Z-(Ala-Aib)$_2$-Ala-Gly-Δ^ZβAla-Lys(Boc)-Leu-Val-Phe-Phe-OH (7)

A dry round bottom flask was charged with **5** (0.34 mmol), $PdCl_2(PhCN)_2$ (0.017 mmol), and CuCl (0.034 mmol). The reaction vessel was charged with oxygen followed by the addition of dioxane (4 mL) and tetraethyl methylenediphosphonate (0.034 mmol). The reaction mixture was stirred at 70°C for 1 min and then **6** (1 mmol) dissolved in a DMF/dioxane (1 + 5 ml) mixture was added. The reaction mixture was stirred 4 days at 60°C under oxygen atmosphere. After the reaction was over, the solvent was removed by evaporation and the crude residue was purified by flash chromatography using $CHCl_3$/MeOH as the eluant.

MS (ES+, MeOH) *m/z* calcd. for $C_{70}H_{101}N_{13}O_{17}Na$ ($[M+Na]^+$) 1418.7330, found 1418.7351. FT-IR ν_{max} 3274, 2931, 1643, 1536, 1229, 1173 cm^{-1}. ^{1}H NMR (400 MHz, DMSO) δ 11.41 (d, J = 10.5 Hz, 1H), 8.30 (d, J = 6.9 Hz, 1H), 8.20 (d, J = 13.2 Hz, 3H), 8.07 (d, J = 7.8 Hz, 1H), 7.80 (s, 3H), 7.53 (d, J = 8.9 Hz, 1H), 7.46 (d, J = 5.9 Hz, 1H), 7.41-7.27 (m, 5H), 7.27-7.05 (m, 12H), 6.73 (t, 1H), 5.32 (d, J = 8.9 Hz, 1H), 5.05 (s, 2H), 4.69-4.55 (m, 1H), 4.33-4.11 (m, 5H), 4.05-3.91 (m, 3H), 3.80 (dd, J = 17.0, 5.0 Hz, 1H), 3.09 (dd, J = 13.3, 4.8 Hz, 1H), 3.04-2.91 (m, 2H), 2.90-2.81 (m, 2H), 2.76 (dd, J = 13.9, 9.4 Hz, 1H), 1.88-1.76 (m, 1H), 1.66-1.42 (m, 6H), 1.39-1.28 (22H), 1.27-1.11 (12H), 0.86 (d, J = 6.1 Hz, 3H), 0.81 (d, J = 6.1 Hz, 3H), 0.70 (dd, 6H).

Synthesis of Z-(Ala-Aib)$_2$-Ala-Gly-Δ^EβAla-Lys(Boc)-Leu-Val-Phe-Phe-OH (8)

Compound **8** was obtained in 60 % yield starting from a 5 mM solution of 7 in MeOH. This solution was placed in a quartz cuvette and directly irradiated at 290-320 nm. Under these conditions the compound was recovered after flash chromatography using $CHCl_3$/MeOH as eluant.

MS (ESI+, MeOH) *m/z* calcd. for $C_{70}H_{101}N_{13}O_{17}Na$ ($[M+Na]^+$) 1418.7330, found 1418.7352. FT-IR ν_{max} 3282, 2931, 1668, 1629, 1536 cm^{-1}. ^{1}H NMR (400 MHz, DMSO) δ 9.99 (d, J =

10.7 Hz, 1H), 8.34 (s, 1H), 8.18 (d, J = 7.8 Hz, 1H), 8.06 (d, J = 7.8 Hz, 1H), 8.00 (d, J = 8.0 Hz, 1H), 7.97-7.85 (m, 3H), 7.69-7.52 (m, 4H), 7.38-7.30 (m, 5H), 7.27-7.12 (m, 12H), 6.72 (t, 1H), 5.87 (d, J = 14.0 Hz, 1H), 5.05 (s, 2H), 4.61-4.52 (m, 1H), 4.49-4.41 (m, 1H), 4.36-4.21 (m, 2H), 4.14-4.05 (m, 2H), 4.04-3.91 (m, 2H), 3.83 (d, 2H), 3.09-2.66 (m, 6H), 1.91-1.81 (m, 1H), 1.64-1.31 (m, 30H), 1.28 (d, J = 7.2 Hz, 3H), 1.22 (dd, J = 12.6, 7.1 Hz, 6H), 0.85 (d, J = 6.4 Hz, 3H), 0.79 (d, J = 6.4 Hz, 3H), 0.70 (d, J = 6.6 Hz, 6H).

Synthesis of Z-(Ala-Aib)2-Ala-Gly-Δ^{Z}βAla-Lys-Leu-Val-Phe-Phe-OH (9)

Compound **7** (0.14 mmol) was dissolved in dry DCM (5 ml) and then trifluoroacetic acid (5 ml) was added. After the reaction was over (typically 30 minutes), the solvent was removed by evaporation and the product was collected almost quantitatively after lyophilisation from water.

MS (ESI+, MeOH) *m/z* calcd. for $C_{65}H_{93}N_{13}O_{15}Na$ ($[M+Na]^+$) 1318.6806, found 1318.6827. ^{1}H NMR (400 MHz, DMSO-*d*$_6$) δ 12.76 (br, 1H), 11.37 (d, J = 10.5 Hz, 1H), 8.31-8.21 (m, 2H), 8.13 (t, 1H), 8.05 (d, J = 7.9 Hz, 1H), 7.94 (d, J = 8.4 Hz, 1H), 7.76 (s, 1H), 7.71-7.57 (m, 6H), 7.39-7.32 (m, 5H), 7.29-7.14 (m, 12H), 5.33 (d, J = 8.9 Hz, 1H), 5.04 (s, 2H), 4.63-4.53 (m, 1H), 4.50-4.42 (m, 1H), 4.40-4.20 (m, 2H), 4.15-4.06 (m, 2H), 4.04-3.95 (m, 2H), 3.81 (d, J = 5.4 Hz, 2H), 3.11-2.87 (m, 3H), 2.80-2.65 (m, 3H), 1.91-1.81 (m, 1H), 1.68-1.45 (6H), 1.42-1.14 (23H), 0.86 (d, J = 6.4 Hz, 3H), 0.81 (d, J = 6.5 Hz, 3H), 0.71 (d, J = 6.7 Hz, 6H).

Synthesis of Z-(Ala-Aib)$_2$-Ala-Gly-Δ^{E}βAla-Lys-Leu-Val-Phe-Phe-OH (10)

Compound **10** was obtained in quantitative yield starting from a 10 mM solution of **9** in MeOH. This solution was placed in a quartz cuvette and directly irradiated at 290-320 nm. Under these conditions the compound was recovered after the evaporation of the solvent.

MS (ESI+, MeOH) *m/z* calcd. for $C_{65}H_{93}N_{13}O_{15}Na$ ([M+Na]+) 1318.6806, found 1318.6826. ^{1}H NMR (400 MHz, DMSO) δ 12.76 (br, 1H), 10.00 (d, J = 10.8 Hz, 1H), 8.35 (s, 1H), 8.20 (d, J = 7.8 Hz, 1H), 8.10 (d, J = 8.1 Hz, 1H), 8.00 (d, J = 7.9 Hz, 1H), 7.92 (dd, J = 15.1, 9.2 Hz, 2H), 7.71-7.54 (m, 6H), 7.40-7.31 (m, 5H), 7.30-7.12 (m, 12H), 5.87 (d, J = 14.0 Hz, 1H), 5.05 (s, 2H), 4.61-4.50 (m, 1H), 4.46 (dd, J = 13.5, 8.0 Hz, 1H), 4.41-4.21 (m, 2H), 4.09 (dd, J = 14.3, 7.0 Hz, 2H), 4.05-3.89 (m, 2H), 3.88-3.76 (m, 2H), 3.13-2.86 (m, 3H), 2.83-2.63 (m, 3H), 1.94-1.78 (m, 1H), 1.70-1.44 (6H), 1.44-1.13 (23H), 0.89-0.77 (m, 6H), 0.74-0.65 (m, 6H).

X-Ray Diffraction

Single crystals of Z-Gly-Δ^{Z}βAla-OEt (**1**) and Z-Gly-Δ^{E}βAla-OEt (**2**) were grown by slow evaporation from ethyl ether and an ethyl ether-petroleum ether solvent mixture, respectively. X-Ray diffraction data were collected with a Gemini E four-circle kappa diffractometer (Rigaku Oxford Diffraction) equipped with a 92 mm EOS CCD detector, using graphite monochromated Cu Kαradiation (λ = 1.54184 Å) for **1**, while Mo Kα radiation (λ = 0.71073 Å) for **2**. Data collection and reduction were performed with the CrysAlisPro software (Rigaku Oxford Diffraction). A semiempirical absorption correction based on the multi-scan technique using spherical harmonics, implemented in the SCALE3 ABSPACK scaling algorithm, was applied. The structures were solved by ab initio procedures of the SIR 2014 program.[25] Refinements were carried out by full-matrix least-squares on F2, using all data, by application of the SHELXL-2014 program,[26] with anisotropic displacement parameters for all of the non-H atoms. H-Atoms were calculated at idealized positions and refined using a riding model. Relevant crystal data and structure refinement parameters are listed in Tables 1 and 2. The molecular structures of **1** and **2** with atom numbering are illustrated in Figures 6 and 7, respectively. Selected torsion angles and hydrogen bond parameters are reported in Tables 3-6. CCDC 1840922 and 1840923 contain the supplementary crystallographic data for this paper. The data can be obtained free of charge from The Cambridge Crystallographic Data Centre via www.ccdc.cam.ac.uk/structures.

Table S1. Crystal data and structure refinement for Z-Gly-$\Delta^{Z}\beta$Ala-OEt (**1**).

Identification code	mc290	
Empirical formula	$C_{15}H_{18}N_2O_5$	
Formula weight	306.31	
Temperature	293(2) K	
Wavelength	1.54184 Å	
Crystal system	Triclinic	
Space group	P -1	
Unit cell dimensions	a = 5.3222(3) Å	α= 79.248(5)°.
	b = 8.8920(5) Å	β= 83.650(4)°.
	c = 16.5607(9) Å	γ = 86.864(4)°.
Volume	764.79(8) $Å^3$	
Z	2	
Density (calculated)	1.330 Mg/m^3	
Absorption coefficient	0.844 mm^{-1}	
F(000)	324	
Crystal size	0.45 × 0.35 × 0.05 mm^3	
Theta range for data collection	2.730 to 72.787°.	
Index ranges	$-6 \le h \le 5$, $-10 \le k \le 11$, $-20 \le l \le 20$	
Reflections collected	12253	
Independent reflections	3040 [R(int) = 0.0286]	
Completeness to theta = 67.684°	100.0 %	
Absorption correction	Semi-empirical from equivalents	
Max. and min. transmission	1.00000 and 0.48238	
Refinement method	Full-matrix least-squares on F^2	
Data / restraints / parameters	3040 / 0 / 199	
Goodness-of-fit on F^2	1.034	
Final R indices [I>2sigma(I)]	R_1 = 0.0462, wR_2 = 0.1289	
R indices (all data)	R_1 = 0.0579, wR_2 = 0.1420	
Extinction coefficient	n/a	
Largest diff. peak and hole	0.184 and -0.182 $e.Å^{-3}$	
CCDC deposition number	1840923	

Table S2. Crystal data and structure refinement for Z-Gly-Δ^{E}βAla-OEt (**2**).

Identification code	mc293	
Empirical formula	$C_{15}\ H_{18}\ N_2\ O_5$	
Formula weight	306.31	
Temperature	293(2) K	
Wavelength	0.71073 Å	
Crystal system	Triclinic	
Space group	P -1	
Unit cell dimensions	a = 8.8090(5) Å	α= 84.064(3)°.
	b = 9.4789(3) Å	β= 66.122(5)°.
	c = 10.7200(5) Å	γ = 71.104(4)°.
Volume	774.00(7) $Å^3$	
Z	2	
Density (calculated)	1.314 Mg/m^3	
Absorption coefficient	0.100 mm^{-1}	
F(000)	324	
Crystal size	0.60 × 0.40 × 0.25 mm^3	
Theta range for data collection	2.652 to 29.286°.	
Index ranges	$-11 \le h \le 11$, $-12 \le k \le 12$, $-14 \le l \le 14$	
Reflections collected	16903	
Independent reflections	3833 [R(int) = 0.0194]	
Completeness to theta = 25.242°	99.9 %	
Absorption correction	Semi-empirical from equivalents	
Max. and min. transmission	1.00000 and 0.80408	
Refinement method	Full-matrix least-squares on F^2	
Data / restraints / parameters	3833 / 0 / 200	
Goodness-of-fit on F^2	1.033	
Final R indices [I>2sigma(I)]	R_1 = 0.0452, wR_2 = 0.1218	
R indices (all data)	R_1 = 0.0613, wR_2 = 0.1356	
Extinction coefficient	0.027(4)	
Largest diff. peak and hole	0.239 and -0.148 e.$Å^{-3}$	
CCDC deposition number	1840922	

Table S3. Selected torsion angles [°] for **1**.

C06-C01-C07-OU	-33.8(2)
C02-C01-C07-OU	150.02(16)
C01-C07-OU-C0	140.45(16)
C07-OU-C0-N1	176.54(16)
OU-C0-N1-C1A	-176.85(17)
C0-N1-C1A-C1	156.06(17)
N1-C1A-C1-N2	-176.03(16)
C1A-C1-N2-C2B	-177.68(18)
C1-N2-C2B-C2A	-176.2(2)
N2-C2B-C2A-C2	1.5(3)
C2B-C2A-C2-OT	176.88(19)
C2A-C2-OT-CT1	-179.91(19)
C2-OT-CT1-CT2	-176.3(2)

Table S4. Selected torsion angles [°] for **2**.

C06-C01-C07-OU	-21.32(19)
C02-C01-C07-OU	160.74(12)
C01-C07-OU-C0	-77.90(15)
C07-OU-C0-N1	175.63(11)
OU-C0-N1-C1A	-179.46(13)
C0-N1-C1A-C1	178.45(13)
N1-C1A-C1-N2	-178.82(13)
C1A-C1-N2-C2B	178.89(12)
C1-N2-C2B-C2A	178.07(14)
N2-C2B-C2A-C2	-179.15(13)
C2B-C2A-C2-OT	173.24(14)
C2A-C2-OT-CT1	-177.30(14)
C2-OT-CT1-CT2	173.61(16)

Table S5. Hydrogen bonds and intermolecular C-H···O contacts for **1** [Å and °].

D-H···A	d(D-H)	d(H···A)	d(D···A)	<(DHA)
N1-H1···O1	0.86	2.35	2.654(2)	101.3
N2-H2···O2	0.86	2.15	2.7432(19)	125.8
C07-H07A···O2#1	0.97	2.36	3.299(2)	162.8
C07-H07B···O0#2	0.97	2.51	3.457(2)	164.4
N1-H1···O1#3	0.86	2.19	3.0234(19)	162.6
C1A-H1A2···OU#4	0.97	2.62	3.547(3)	160.1

Symmetry transformations used to generate equivalent atoms:

#1 -x+1,-y+2,-z+2 #2 x+1,y,z #3 -x+2,-y+1,-z+2

#4 x-1,y,z

Table S6. Hydrogen bonds for **2** [Å and °].

D-H···A	d(D-H)	d(H···A)	d(D···A)	<(DHA)
N1-H1···O1	0.86	2.34	2.6864(15)	104.3
N1-H1···O1#1	0.86	2.09	2.9300(13)	165.8
N2-H2···O0#2	0.86	2.03	2.8916(13)	174.8

Symmetry transformations used to generate equivalent atoms:

#1 -x,-y,-z #2 -x,-y+1,-z

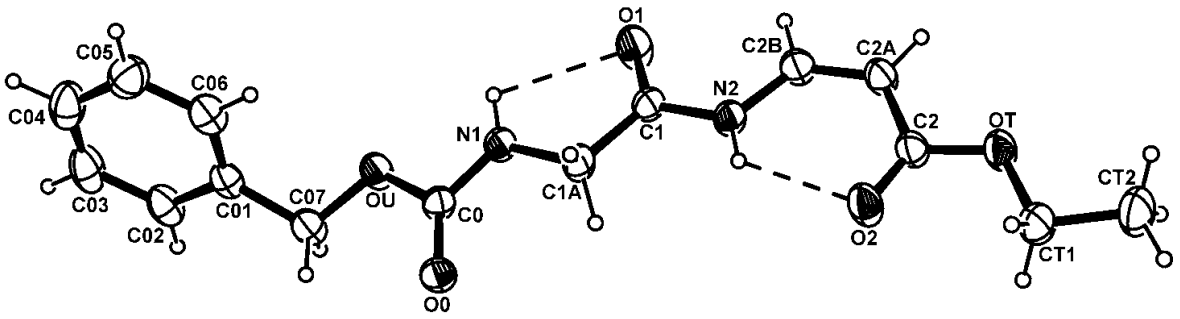

Fig. 6 X-ray diffraction structure of **1** with atom numbering. Displacement ellipsoids for the non-H atoms are drawn at the 30% probability level. The intramolecular H-bonds are represented by dashed lines.

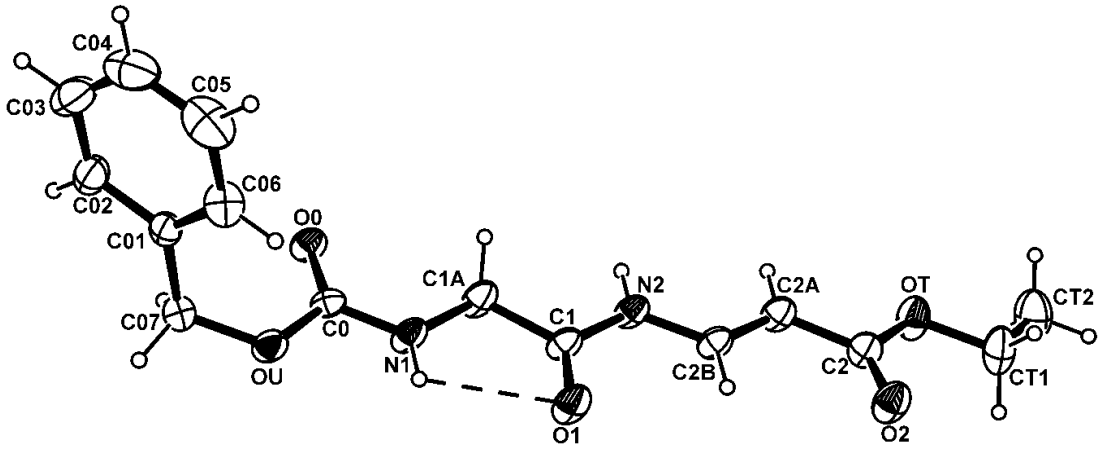

Fig. 7 X-ray diffraction structure of **2** with atom numbering. Displacement ellipsoids for the non-H atoms are drawn at the 30% probability level. The intramolecular H-bond is represented by a dashed line.

Morphological transition studies

A 5 mM water solution of **9** was prepared and placed in a quartz cuvette. This solution was irradiated at 290-320 nm for 5, 10 and 20 min. After each irradiation time an aliquot of solution was deposited on a TEM grid and stained with uranyl acetate. The same aliquots were also dissolved in MeOH solution and checked by reverse phase HPLC (conditions: 1 ml/min, 10 to 60 % B in 20 min; see general method part, HPLC). After 20 minutes of irradiation at 290-320 nm the UV source was changed at 254 nm. The irradiation process was performed in the same cuvette and TEM and HPLC samples were collected as described above after 5 and 10 minutes.

TEM images are reported below.

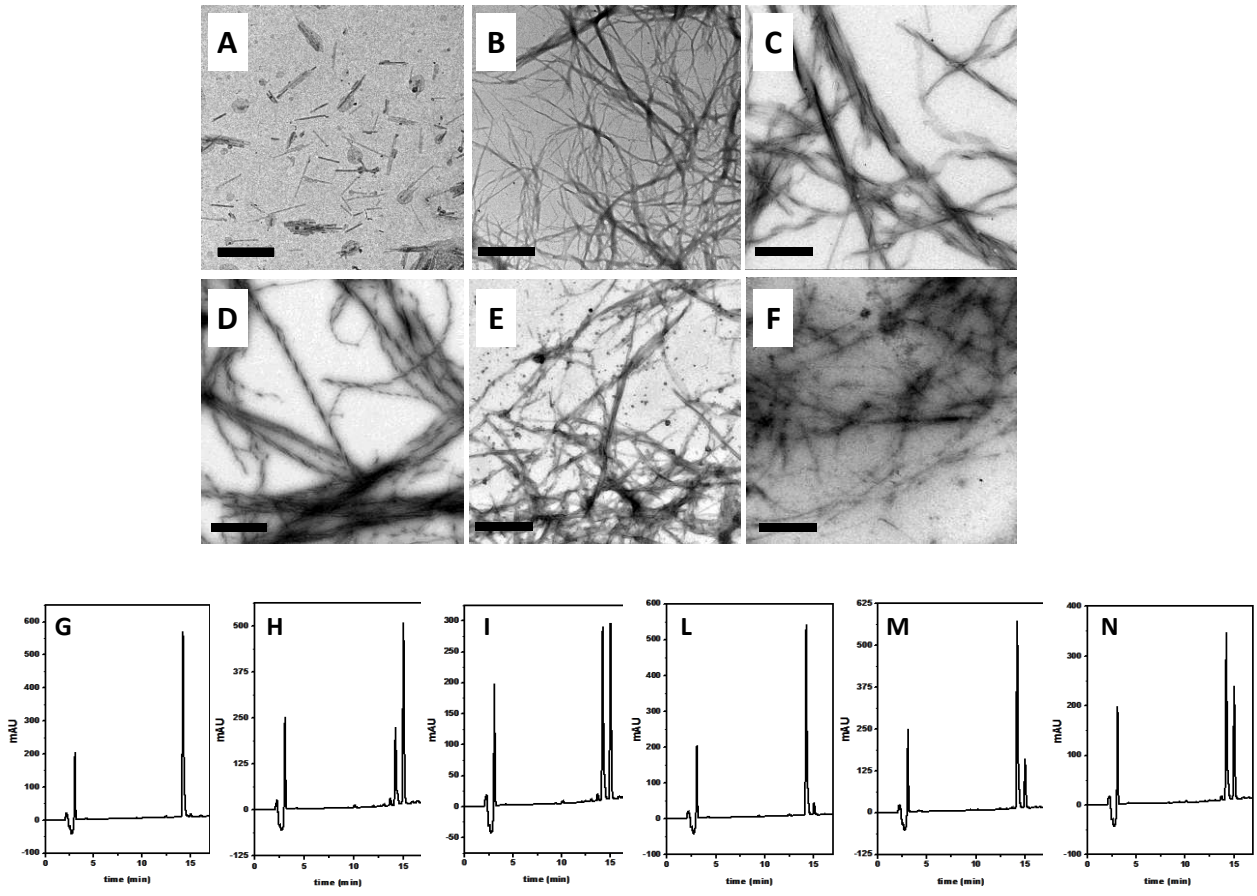

Fig. 8 (A-D) TEM images of a 5 mM solution of **9** after 0, 5, 10, 20 minutes of irradiation at 290-320 nm and (E, F) after 5 and 10 minutes of irradiation at 254 nm starting from the previous solution. (G-N) HPLC chromatograms of the corresponding isomerization experiments.

References

1. S. H. Gellman, *Acc. Chem. Res*., **1998**, 31, 173.
2. C. Toniolo, M. Crisma, F. Formaggio, and C. Peggion, *Biopolymers,* **2001**, 60, 396.
3. S. Hecht, and I. Huc, *Foldamers: Structure, Properties and Applications*, Wiley-VCH, Weinheim, **2007**.
4. C. M. Goodman, S. Choi, S. Shandler, and W. F. DeGrado, *Nat. Chem. Biol*., **2007**, 3, 252.
5. D. Seebach, and J. Gardiner, *Acc. Chem. Res*., **2008**, 41, 1366.
6. W. S. Horne, and S. H. Gellman, *Acc. Chem. Res*., **2008**, 41, 1399.
7. I. Saraogi, and A. D. Hamilton, *Chem. Soc. Rev*., **2009**, 38, 1726.
8. Z. T. Li, J. L. Hou, and C. Li, *Acc. Chem. Res.,* **2008**, 41, 1343.
9. T. A. Martinek, and F. Fülöp, *Chem. Soc. Rev*., **2012**, 41, 687.
10. M. Crisma, M. De Zotti, F. Formaggio, C. Peggion, and A. Moretto, C. Toniolo, *J. Pept. Sci.*, **2015**, 21, 148.
11. R. Wechsel, M. Zabka, J. W. Ward, and J. Clayden, *J. Am. Chem. Soc*., **2018**, 140, 3528.
12. M. De Poli, W. Zawodny, O. Quinonero, M. Lorch, S. J. Webb, and J. Clayden, *Science*, **2016**, 352, 575.
13. M. Barboiu, A.-M. Stadler, and J.-M. Lehn, *Angew. Chem. Int. Ed.*, **2016**, 55, 4130; *Angew. Chem*., **2016**, 128, 4200.
14. P. C. Knipe, S. Thompson, and A. D. Hamilton, *Chem. Commun*., **2016**, 52, 6521.
15. D. Mazzier, M. Crisma, M. De Poli, G. Marafon, C. Peggion, J. Clayden, and A. Moretto, *J. Am. Chem. Soc*., **2016**, 138, 8007.
16. J. M. Lee, D.-S. Ahn, D. Y. Jung, J. Lee, Y. Do, S. K. Kim, and S. Chang, *J. Am. Chem. Soc*., **2006**, 128, 12954.
17. C. Peggion, A. Moretto, F. Formaggio, M. Crisma, and C. Toniolo, *Biopolymers*, **2013**, 100, 621.
18. C. Toniolo, and E. Benedetti, *Trends Biochem. Sci*., **1991**, 16, 350.
19. C. Toniolo, A. Polese, F. Formaggio, M. Crisma, and J. Kamphuis, *J. Am. Chem. Soc*., **1996**, 118, 2744.
20. V. Pavone, E. Benedetti, B. Di Blasio, C. Pedone, A. Santini, A. Bavoso, C. Toniolo, M. Crisma, and L. Sartore, *J. Biomol. Struct. Dyn*., **1990**, 7, 1321.

21. A. Aubry, D. Bayeul, H. Brgckner, N. Schiemann, and E. Benedetti, *J. Pept. Sci*. **1999**, 4, 502.
22. M. J. Krysmann, V. Castelletto, A. Kelarakis, I. W. Hamley, R. A. Hule, and D. J. Pochan, *Biochemistry*, **2008**, 47, 4597.
23. G. Wei, Z. Su, N. P. Reynolds, P. Arosio, I. W. Hamley, E. Gazit, and R. Mezzenga, *Chem. Soc. Rev*., **2017**, 46, 4661.
24. A. S. Lubbe, T. van Leeuwen, S. J. Wezenberg, and B. L. Feringa, *Tetrahedron*, **2017**, 73, 4837.
25. M.C. Burla, R. Caliandro, B. Carrozzini, G.L. Cascarano, C. Cuocci, C. Giacovazzo, M. Mallamo, A. Mazzone, and G. Polidori, *J. Appl. Crystallogr,.* **2015**, 48, 306.
26. G.M. Sheldrick, *Acta Crystallogr. C,* **2015**, 71, 3.

3.3 Tunable E−Z photoisomerization in α,β-peptide foldamers featuring multiple (E/Z)-3-aminoprop-2-enoic acid units[f]

Foldamers are oligomeric molecules based on building blocks other than those characterizing naturally occurring biopolymers, able to highly populate a specifi c conformation, thus giving rise to a stable and well-defi ned three-dimensional (3D) architecture.[1] Peptides based on β-amino acids, γ-amino acids, and noncoded α-amino acids, aromatic oligoamides, azapeptides, and oligoureas are among the most extensively investigated classes of compounds in this area.[2] The possibility of triggering the switch of a foldamer between two distinct but structurally defined states (for such systems, the term " dynamic foldamers" has been coined)[3] may offer interesting opportunities. For example, a foldamer undergoing elongation and contraction of its end-to-end distance resulting from the transition between two conformations, each characterized by a different pitch, can be viewed as a molecular spring.[4] Moreover, a conformational transition can convey chemical information across the entire length of a foldamer from a signaling unit at one end to a reporter at the other end, even at multinanometer distances.[5] In this regard, we exploited the (*E*)-fumaramide/(*Z*)-maleamide photoswitchable system as a linker between a chiral and an achiral helical peptide foldamer segment to turn on-off transmission of stereochemical information (a preferred helical screw sense) to the latter.[6] However, such an approach results in the antiverse orientation of the two peptide chains connected to the linker. We therefore became interested in developing peptide-based foldameric systems in which the photoswitchable unit itself would be an amino acid.[7] For this aim, we selected (*E/Z*)-3-aminoprop-2-enoic acid [or (*E/Z*)-3-aminoacrylic acid]. Considering this β-amino acid as the $C^{\alpha,\beta}$-unsaturated analogue of β-alanine (β-Ala) and exploiting the Δ^E/Δ^Z terminology commonly used for $C^{\alpha,\beta}$-didehydro analogues of protein amino acids, we abbreviate the *E*- and *Z*- isomers of 3-aminoprop-2-enoic acid as Δ^EβAla and Δ^ZβAla, respectively.

We recently succeeded in introducing Δ^ZβAla into a peptide sequence through a synthetic methodology based on the oxidative amidation of conjugated olefins.[8] Specifically, the reaction involved two peptide segments, one requiring a glycinamide at the C-terminus and the other an acryloyl group at the N-terminus. Although successful, such a strategy suffers from limitations, the most important being that it allows the in situ generation of only a single

[f] Reprinted (adapted) with permission from (Org. Lett. 2019, 21, 4182). Copyright (2019) American Chemical Society."

Δ^ZβAla residue within a peptide sequence.

To overcome these limitations, we developed a novel and more versatile synthetic approach suitable for the stepwise incorporation of multiple Δ^ZβAla units, even consecutively, in peptides. The processes of *Z-E* and *E-Z* photoisomerization and the properties of the resulting foldamers are also described. To achieve multiple insertions of Δ^ZβAla residues into a peptide sequence, a derivative compatible with the multistep chemical strategy involved in the solution protocol for peptide synthesis was needed, owing to the intrinsic instability of the unprotected amine group conjugated to the unsaturated C=C bond that does not tolerate removal of any N-protecting group.

Compound **8** [*exo*-3-tert-butoxycarbonylamino-7-oxabicyclo-(2.2.1)hept-5-ene-exo-2-carboxylic acid] was selected as our Δ^ZβAla precursor (Figure 1 a).

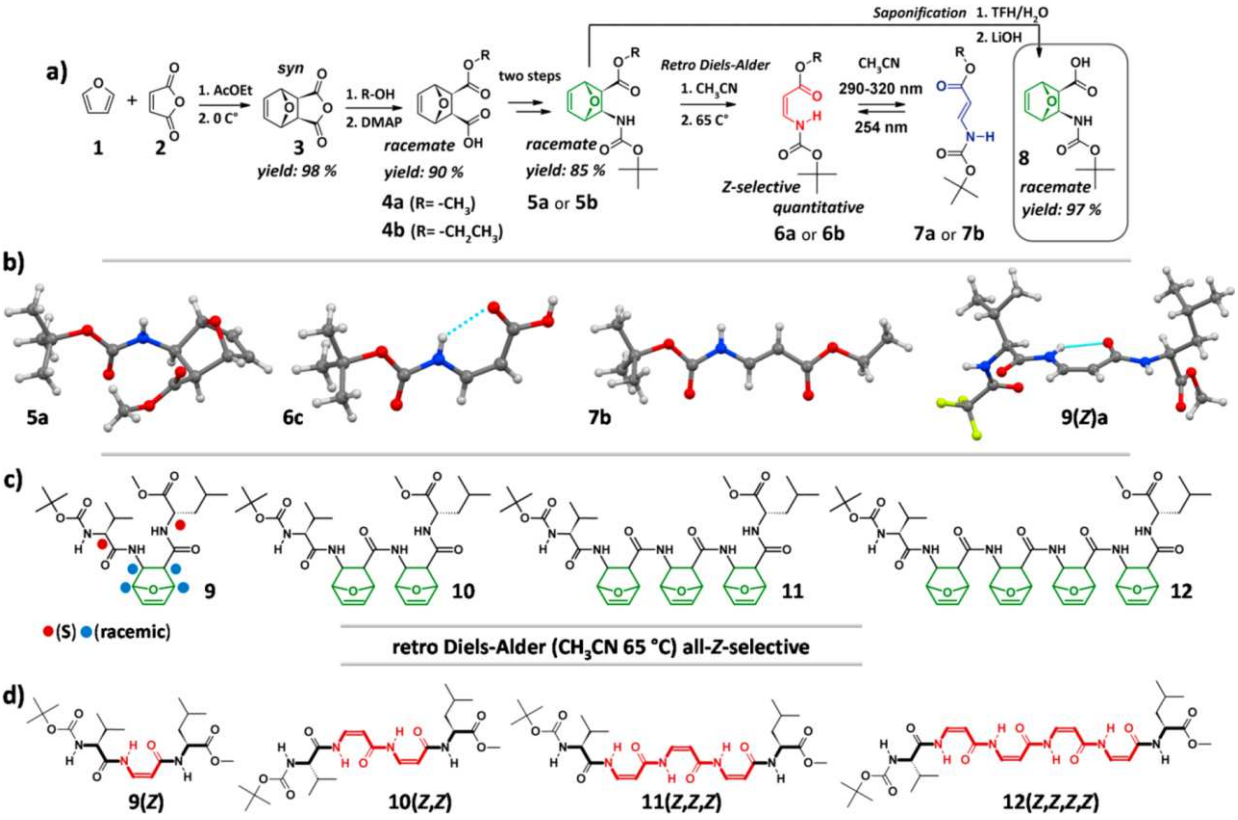

Fig. 1 (A) Synthesis of Boc-*fm*Δ^ZβAla-OH (**8**) and Δ^ZβAla/Δ^EβAla photoconversion. (B) X-ray diffraction structures of **5a**, **6c**, **7b**, and **9(*Z*)a**. Intramolecular hydrogen bonds are indicated by dashed lines. (C) Chemical structures of foldamers built by incorporation of consecutively coupled *fm*Δ^ZβAla residues. (D) Chemical structures of the synthesized foldamers characterized by a row of one to four consecutive Δ^ZβAla residues.

In this compound, the olefinic C=C bond is masked by the formal cycloaddition of furan to

Boc-Δ^ZβAla-OH, therefore allowing removal of the Boc group to produce a stable amino derivative. Following our protocol, the cycloaddition of furan (**1**) to maleic anhydride (**2**) afforded selectively the *syn* (*exo*) cycloadduct (**3**), which was subsequently converted to the racemic form of (*exo*,*exo*) cycloadduct **5a** (R = CH_3) or **5b** (R = CH_2CH_3) after a few synthetic steps, namely, monoesterification (yielding **4a** and **4b**) and acyl azide formation followed by a Curtius rearrangement carried out in the presence of *tert*-butyl alcohol and *p*-toluenesulfonic acid as the catalyst (70% overall yield). By heating **5a** and **5b** in acetonitrile, we obtained Boc-Δ^ZβAla-OR (**6a** and **6b**) quantitatively via the retro-Diels-Alder mechanism. Upon irradiation at 290-320 nm (UV-B), **6a** and **6b** were quantitatively converted to the Boc-Δ^EβAla-OR isomer (**7a** and **7b**). The back-conversion was achieved in 75% yield by irradiation at 254 nm. Finally, precursor **8** (Boc-*fm*Δ^ZβAla-OH, where *fm* stands for furan masking of the olefinic double bond) was obtained after saponification of **5a** and **5b**. The stereochemical output of this series of reactions (see the *Experimental Section* for NMR spectra) was verified by single-crystal X-ray diffraction analysis of compounds **5a**, **6c**, and **7b**. Analysis of **5a** (Figure 1 b) unambiguously confirms the *syn,syn* (*exo,exo*)-type structure of the resulting racemic cycloadduct.[9] The structure of Boc-Δ^ZβAla-OH (**6c**, obtained after saponification of **6a** and **6b**) shows the occurrence of an intramolecular N− H···O=C H-bond that closes a six-atom pseudocycle (C_6 structure) (Figure 1 b), made possible by the almost exact (within 1.0°) *trans*, *cis*, and *trans* arrangement of the ϕ, θ, and ψ backbone torsion angles (rotations about the N-C^β, C^β=C^α, and C^α-C bonds, respectively) of Δ^ZβAla. Finally, in **7b** the molecule is perfectly flat in that all non-H atoms, except two methyl carbons of the Boc group, lay on the same plane (Figure 1 b) and the value of all backbone torsion angles is 180°. The results described above prompted us to plan the synthesis of foldamers in which Δ^ZβAla would be combined with α-amino acid residues characterized by a good propensity to adopt the β-sheet conformation, namely, Val and Leu. Accordingly, starting from H-Leu-OMe, through a series of conventional peptide couplings (each involving either **8** or a Boc-protected α-amino acid) and Boc deprotection steps, a set of oligomers containing up to four consecutively coupled *fm*Δ^ZβAla residues were prepared. Because **8** was used in its racemic form while all α-amino acids were of the S configuration, each foldamer was obtained as a mixture of diastereomers [compounds **9**-**12** (Figure 1 c)]. However, upon thermal treatment of these mixtures to induce retro-Diels-Alders reaction (which proceeded with quantitative *Z* stereoselectivity and yield), restoration of the Δ^ZβAla C=C double bond removed the chiral heterogeneity. The synthesized peptide foldamers comprised a set of compounds of the

general sequence Boc-Val-(Δ^{Z}βAla)$_n$-Leu-OMe [n = 1, **9(*Z*)**; n = 2, **10(*Z*,*Z*)**; n = 3, **11(*Z*,*Z*,*Z*)**; n = 4, **12(*Z*,*Z*,*Z*,*Z*)**] characterized by a row of one to four consecutive Δ^{Z}βAla residues flanked by one α-amino acid at each end (Figure 1 d). An analogue of **9(*Z*)** in which Boc protection is replaced by a trifluoroacetyl group was also synthesized, and its structure determined by X-ray diffraction [Figure 1 b, structure **9(*Z*)a**]. The conformation of the central Δ^{Z}βAla residue closely matches that reported above for the Boc-protected derivative **6a**, giving rise to an intraresidue N-H···O=C H-bond (C_6 structure) internal to the tripeptide backbone.

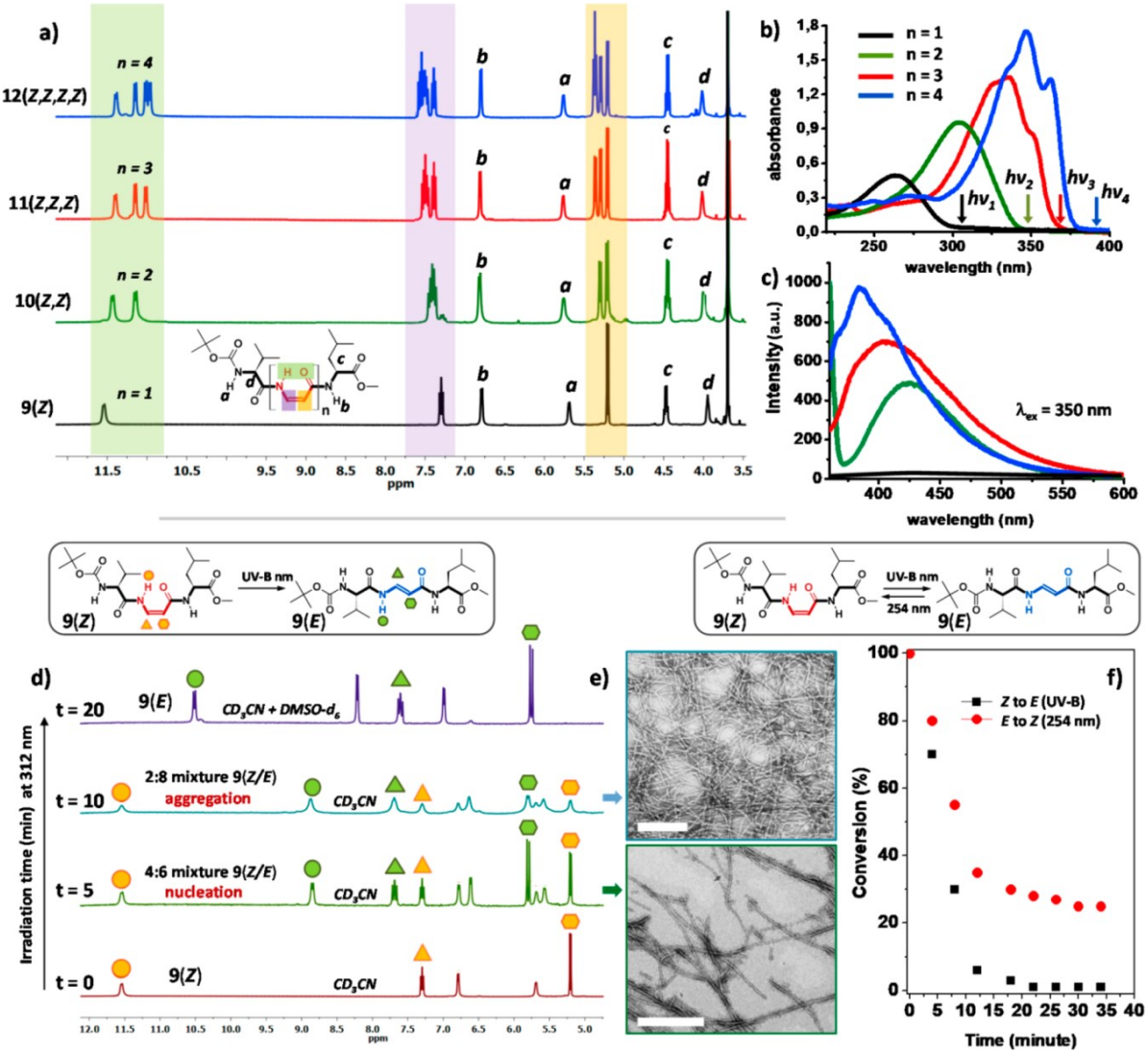

Fig. 2 (A) ^{1}H NMR spectra of Boc-Val-(Δ^{Z}βAla)$_n$-Leu-OMe [n = 1−4; **9(*Z*)**, **10(*Z*,*Z*)**, **11(*Z*,*Z*,*Z*)**, and **12(*Z*,*Z*,*Z*,*Z*)**, respectively] (peptide concentration of 3 mM in CD_3CN). NH protons involved in an intraresidue H-bond are highlighted in green, while α- and β-olefinic protons are highlighted in orange and purple, respectively. (B and C) UV−Vis absorption spectra and fluorescence emission (λ_{ex} at 350 nm), respectively, of Boc-Val-(Δ^{Z}βAla)$_n$-Leu-OMe (n = 1−4). (D) ^{1}H NMR spectra of **9(*Z*)**−**9(*E*)** isomerization recorded under different periods of exposition during UV-B illumination. Proton signals belonging to Δ^{Z}βAla and Δ^{E}βAla units are highlighted. (E) TEM images recorded for 4:6 (bottom) and

2:8 (top) **9(*Z*)/9(*E*)** isomeric mixtures (scale bar of 100 nm, stained samples). (F) Kinetics of **9(*Z*)→9(*E*)** (UV-B, black squares) and **9(*E*)→9(*Z*)** (254 nm, red circles) photoconversions (data from HPLC).

However, the N-H groups of Val(1) and Leu(3) are oriented nearly perpendicular to each other, and the same holds true for the corresponding carbonyl groups. Such a disposition of the potential intermolecular H-bonding donors and acceptors, combined with the inaccessibility of the N-H and C=O groups of Δ^{Z}βAla (already intramolecularly engaged), hampers the possibility that intermolecular H-bonding may give rise to a sheetlike arrangement in the crystal packing. The ^{1}H NMR spectra of the foldamers belonging to the Boc-Val-(Δ^{Z}βAla)$_n$-Leu-OMe series (n = 1-4; 2 mM in CH_3CN) are reported in Figure 2 a.
The NH proton of each Δ^{Z}β Ala residue is found in the low-field spectral region, indicative of its involvement in an intraresidue (C_6) H-bond. As a function of foldamer elongation in the Boc-Val-(Δ^{Z}βAla)$_n$-Leu-OMe series, a remarkable red-shift of the maximum is observed in the corresponding UV-Vis absorption spectra (Figure 2 b), from 260 nm (n = 1) to 310 nm (n = 2), 337 nm (with a shoulder at 362 nm) (n = 3), and 350 nm (with a shoulder at 370 nm) (n = 4). The increasing number of consecutive Δ^{Z}βAla residues in the foldamer backbone seems to give rise to a progressively expanded, conjugated π-system involving both olefin and amide groups. Such a conjugation is expected to be maximized if all Δ^{Z}βAla residues adopt a conformation similar to that found for **6a** and **9(*Z*)a** (see above), i.e., a fully planar system. The UV-Vis absorption profiles of the **9(*Z*)-12(*Z,Z,Z,Z*)** series suggested that we explore a set of different wavelengths (hν as reported in Figure 2b) to induce the photoisomerization of these foldamers to their corresponding *E* isomers and for the reverse process, as well. Clearly, on the way from the all-*Z* to all-*E* isomeric states of the -(ΔβAla)$_n$ oligomers, when n >1 additional combinations of isomeric forms are also implicated, for a total of 2^n isomers. The **9(*Z*)** → **9(*E*)** isomerization was monitored by NMR spectroscopy (Figure 2 d, red trace). Experimental condition: 3 mM **9(*Z*)** in CD_3CN, quartz NMR tube. After irradiation under UV-B light for 5 min, the new isomer **9(*E*)** started to form, yielding a **9(*Z*)** /**9(*E*)** mixture in 4:6 molar ratio (determined by HPLC), which gave rise to a weak organogel state (Figure 2 d, green trace, and corresponding TEM image). Irradiation for an additional 5 min generated a **9(*Z*)/9(*E*)** mixture in a 2:8 molar ratio (by HPLC), which turned the NMR trace in a set of broad NMR proton signals and in a robust organogel state (Figure 2 d, blue trace, and corresponding TEM image). After addition of DMSO-d_6 to the CD_3CN solution, the organogel collapsed to a liquid state, and upon irradiation for an additional 10 min, the

isomerization process produced **9(*E*)** in quantitative yield (Figure 2 d, violet trace). TEM analyses clearly show how the progressive formation of ordered supramolecular fibers is related to the incremental conversion of **9(*Z*)** to **9(*E*)** (Figure 2 e). The latter compound at the critical concentration of 2.4 mM (referenced to its own concentration in the mixture) was the origin of a dense fiber network that could entrap the solvent (acetonitrile). The reversible **9(*E*)** → **9(*Z*)** conversion was achieved by irradiation at 254 nm (Figure 2 e, experiments run in MeOH to avoid aggregation). While the **9(*Z*)** → **9(*E*)** transformation occurred quantitatively, the back process **9(*E*)** → **9(*Z*)** reached a photostationary equilibrium at 77% conversion. In our view, the strong tendency of **9(*E*)** to self-associate into fibers, at variance with its **9(*Z*)** counterpart, might arise from an extended conformation adopted by Δ^{E}βAla (similar to that described above for **7** in the crystal state), combined with the availability for intermolecular H-bonding of an additional NH group free from intramolecular interactions. As for the higher oligomers, we found that photoconversions from the all-*Z* isomer to a mixture in which the all-*E* isomer was by far the most abundant component required successive irradiation steps at different wavelengths. On the basis of the UV-Vis absorption profiles of Boc-Val-(Δ^{Z}βAla)$_n$-Leu-OMe (n = 1-4) reported in Figure 2 b, we selected four wavelengths (indicated by arrows in Figure 2 b) that fall each in the red tail of the absorption profile of one of the compounds: irradiation at 350 nm, followed by UV-B, for **10(*Z,Z*)**; 365 nm, followed by 350 nm, for **11(*Z,Z,Z*)**; and 395 nm, followed by 365 nm and successively by 350 nm, for **12(*Z,Z,Z,Z*)** (Figure 3 a-c, respectively). Indeed, on the way from the all-*Z* to the all-*E* isomers, a mixture of isomers in which *Z* and *E* units are variously combined is likely to be formed, somehow resembling the conjugation state of some of the lower all-*Z* homologues. These latter require progressively higher irradiation energies for their *Z*-*E* conversion as the number of consecutive *Z* units decreases. It is noteworthy that these processes can be achieved in high conversion yields (as shown in the reported HPLC profiles) when concentrations are <5 μM. These conditions are required because of the strong aggregation tendency of **10(*E,E*)**-**12(*E,E,E,E*)** and their mixed intermediate species. All HPLC peaks were found to be *iso* mass with the corresponding precursors.

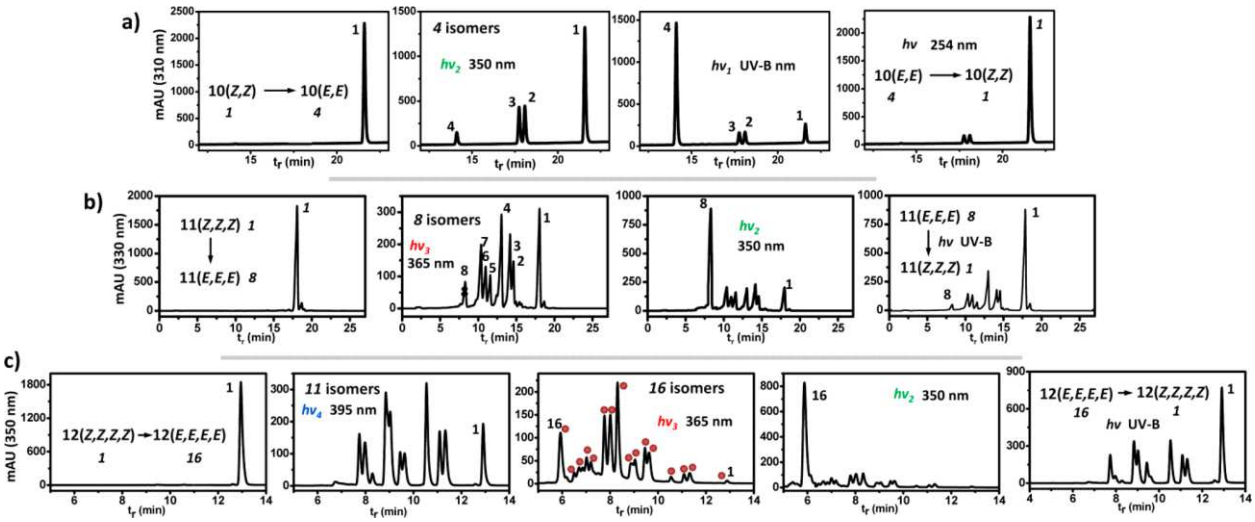

Fig. 3 (A−C) HPLC profiles of the photoconversion process from the all-*Z* isomer to mainly the all-*E* isomer starting from **10(*Z,Z*)**, **11(*Z,Z,Z*)**, and **12(*Z,Z,Z,Z*)**, respectively. Solvent MeOH, concentrations of 5 μM for all samples. The HPLC profiles reported at the right of each row show the corresponding all-*E* → all-*Z* back-isomerization process.

Interestingly, if compared to their all-*Z* counterparts, foldamers **10(*E,E*)**, **11(*E,E,E*)**, and **12(*E,E,E,E*)** are characterized by blue-shifted UV-Vis absorption profiles (see the *Experimental Section*, Fig. 9), accompanied by a loss of fluorescence. The back-isomerization process was also investigated [from all-*E* to all-*Z* isomers (Figure 3, right HPLC profiles)]. High levels of conversion were found in the case of **10(*Z,Z*)** (at 254 nm) and **11(*Z,Z,Z*)** (at UV-B), while moderate conversion was achieved in the case of **12(*Z,Z,Z,Z*)**. All compounds after reconversion to their corresponding all-*Z* isomers restored the native fluorescence.

To summarize, foldamers featuring consecutive Δ^{Z}βAla/Δ^{E}βAla units are endowed with interesting conformational, electronic, and supramolecular aggregation properties that can be modulated by selective *E*-*Z* photoisomerization. The synthetic route developed in this work offers possibilities for the exploitation of the Δ^{Z}βAla/Δ^{E}βAla dyad in photoresponsive systems.

Experimental section

Instruments and Methods

High-Performance Liquid Chromatography. The HPLC measurements were performed using an Agilent 1200 apparatus (Palo Alto, CA), equipped with a UV detector at various wavelengths and a column Agilent extend-C18 (stationary phase). Eluants: A= 9:1 H_2O/CH_3CN, 0.05 % TFA; B= 1:9 H_2O/CH_3CN, 0.05 % TFA.

Nuclear Magnetic Resonance. ^{1}H NMR, ^{13}C NMR, and 2D-NMR spectra were recorded at 25°C on Bruker Avance 200, 400 or 500 MHz instruments. ^{1}H and ^{13}C spectra were referenced relative to the solvent residual peaks and chemical shifts (δ) reported in ppm downfield of tetramethylsilane ($CDCl_3$ δ H: 7.26 ppm, δ C: 77.16 ppm; CD_3CN δ H: 1.94 ppm; DMSO δ H: 2.50 ppm). The multiplicity of a signal is indicated as br, broad; s, singlet; d, doublet; t, triplet; m, multiplet.

Mass Spectrometry. Mass spectra by electrospray ionization (ESI), collected in the positive mode, were performed on Perseptive Biosystem Mariner ESI-ToF5220 spectrometer (Foster City, CA).

Fourier Transform-Infrared Spectroscopy. FT-IR absorption spectra were recorded with a ATi Perkin Elmer Spectra RX1 FT-IR spectrometer. The ῡ maxima for the main absorption bands are given.

UV lamp. Two handheld UV Lamps (Vilber) with bulbs emitting wavelength of 254 nm (6W) or 290-320 nm (8W), 350 nm (8W), 365 nm (15W) and 395-410 nm (10W, MinChen 502B Ultraviolet LED Flashlight Torch) were used in the photoisomerization experiments.

UV-Vis Absorption. The UV-Vis absorption spectra were recorded using a Shimadzu model UV-2501 PC spectrophotometer. A 1-cm path length quartz cell was used.

Photoisomerization experiments. The sample was dissolved in deuterated solvent (CD_3CN) and placed in a quartz NMR tube (Norrell S-500-QTZ). The sealed NMR tube was directly irradiated under the UV lamp without protective filter at a distance of about 1 cm from the light bulb. The NMR spectra were recorded before and after different irradiation times.

Melting point. Melting point of the compounds were determined using a Leitz Laborlux 12 microscope equipped with a Mavotherm 32 thermometer (sensor: NiCr-Ni thermocouple; resolution: 0.1 K; inherent deviation: 199°C ± 0.5% meas. val.).

Synthesis and Characterization

Materials

N,N-diisopropylethylamine (DIPEA), trifluoroacetic acid (TFA), triethylamine (TEA), L-amino acids methyl ester hydrochloride, N-(3-Dimethylaminopropyl)-N′-ethylcarbodiimide hydrochloride, 4-(dimethylamino) pyridine, isobutyl chloroformate, Boc-L-amino acids, furan, and maleic anhydride were obtained from Sigma-Aldrich. 1-hydroxy-7-aza-1,2,3-benzotriazole (HOAt) was purchased from GL Biochem (Shanghai).

The deuterated solvents DMSO-d_6, $CDCl_3$, and $CDCN_3$ were purchased from Euriso-Top (France).

Synthesis of 3

Maleic anhydride (4 g, 40 mmol) was dissolved in EtOAc (20 ml) and furan (4 ml, 63 mmol) was added under strong stirring. The solution was refrigerated until the next day. The product was filtered, washed with ethyl acetate and dried.

Colourless solid, 98% yield, 6.513 g, m.p. 122°C.

^{1}H NMR (200 MHz, $CDCl_3$) δ 6.59 (t, 2H), 5.47 (t, 2H), 3.19 (s, 2H).

^{13}C NMR (101 MHz, $CDCl_3$) δ 169.88, 137.00, 136.50, 82.23, 48.72.

MS (ESI-TOF): $[M+H]^+$ calc. for $C_8H_6O_4$ = 167.0338 m/z; found = 167.0344 m/z.

FT-IR ν_{max} 3100, 3090, 3033, 2991, 1859, 1845, 1789 cm^{-1}.

Synthesis of 4a-b

Compound 3 (2 g, 12 mmol) was suspended in anhydrous methanol or ethanol (20 ml) and 4-(dimethylamino) pyridine (DMAP) was added as catalyst. The reaction was stirred at room temperature until complete dissolution of 3. The solvent was removed under vacuum and the residue was dissolved in EtOAc and washed with $KHSO_4$ 5% saturated with NaCl. The organic phase was dried over Na_2SO_4, filtered and concentrated providing the corresponding monoester.

Methyl ester (4a): colourless solid, 90% yield, 2.133 g, m.p. 94-95°C.

^{1}H NMR (400 MHz, $CDCl_3$) δ 10.78 (s, 1H), 6.49 (s, 2H), 5.31 (d, J = 16.6 Hz, 2H), 3.72 (s, 3H), 2.88 (q, J = 8.9 Hz, 2H).

MS (ESI-TOF): $[M+H]^+$ calc. for $C_9H_{10}O_5$ = 199.0601 m/z; found = 199.0604 m/z.

FT-IR ν_{max} 3059, 1706, 1637, 1590, 1567, 1459, 1433 cm^{-1}.

Ethyl ester (4b): colourless solid, 90% yield, 2.291 g, m.p. 96-98°C.

^{1}H NMR (400 MHz, $CDCl_3$) δ 10.16 (s, 1H), 6.48 (qd, J = 5.8, 1.3 Hz, 2H), 5.30 (d, J = 23.7 Hz, 2H), 4.18 (q, J = 7.1 Hz, 2H), 2.85 (q, 2H), 1.26 (t, J = 7.1 Hz, 3H).
^{13}C NMR (101 MHz, $CDCl_3$) δ 177.47, 171.31, 136.80, 136.39, 80.58, 80.32, 61.32, 47.21, 46.81,
13.89.
MS (ESI-TOF): $[M+H]^+$ calc. for $C_{10}H_{12}O_5$ = 213.0757 m/z; found = 213.0759 m/z.
FT-IR ν_{max} 3094, 2988, 1733, 1706 cm^{-1}.

Synthesis of Boc-fmΔ^{Z}βAla-OR (5a-b)

Isobutyl chloroformate (1.28 ml, 9.85 mmol) was added to a mixture of **4b** (1.3 g, 6.56 mmol) and TEA (1.83 ml, 13 mmol) in anhydrous THF (20 ml) at -20°C. the solution was stirred at this temperature for an hour. A solution of NaN_3 (1.066 g, 16 mmol) in H_2O (10 ml) was added at -10°C and the reaction was stirred for two hour at room temperature. The mixture was diluted with water and extracted with EtOAc. The organic phase was washed with $NaHCO_3$ 5% and brine and dried over anhydrous Na_2SO_4. Solvent was evaporated in vacuum to obtain the product, which was recrystallized from ethyl acetate/hexane and filtered.
Crude acyl azide was dissolved in anhydrous CH_2Cl_2 (30 ml) and was stirred at 50°C with reflux condenser for about 27 hours. Conversion from azide to isocyanate was followed by NMR spectroscopy. *Tert*-butanol (3 eq) and *p*-toluene sulfonic acid (catalytic quantity, 5% mol) were added. The reaction was stirred at 50°C reflux and followed with NMR until the formation of **5** (4 days). The solvent was removed under vacuum and the crude product was purified via flash chromatography (eluant: EtOAc/hexane 1:2).
5a-Colourless solid, 85% yield, 1.505 g, m.p. 111-112°C.
5b-Colourless solid, 83% yield, 1.542 g, m.p. 121-123°C.
Methyl ester (5a): ^{1}H NMR (400 MHz, CD_3CN) δ 6.46 (ddd, J = 15.1, 5.8, 1.6 Hz, 2H), 5.24 (s, 1H), 5.05 (s, 1H), 4.67 (s, 1H), 4.17 – 4.08 (m, 1H), 3.66 (s, 3H), 2.80 (d, J = 7.7 Hz, 1H), 1.42 (s, 9H).
MS (ESI-TOF): $[M+H]^+$ calc. for $C_{13}H_{19}NO_5$ = 270.1335 m/z; found = 270.1338 m/z.
Ethyl ester (5b): ^{1}H NMR (400 MHz, $CDCl_3$) δ 6.44 (qd, J = 5.8, 1.3 Hz, 2H), 5.22 (d, J = 9.9 Hz, 1H), 5.11 (s, 1H), 4.73 (s, 1H), 4.28 – 4.14 (m, J = 10.4, 6.7, 5.6 Hz, 3H), 2.80 (d, J = 7.8 Hz, 1H), 1.43 (s, 9H), 1.28 (t, J = 5.6 Hz, 3H).
^{13}C NMR (101 MHz, $CDCl_3$) δ 171.88, 155.38, 137.96, 135.23, 83.90, 79.98, 79.62, 61.00, 52.16, 47.15, 28.31, 28.06, 14.22.

MS (ESI-TOF): $[M+H]^+$ calc. for $C_{14}H_{21}NO_5$ = 284.1492 m/z; found = 284.1494 m/z.

FT-IR ν_{max} 3353, 2983, 1723, 1707, 1525 cm^{-1}.

Synthesis of Boc-Δ^ZβAla-OR (6a-b)

Compound **5a-b** was dissolved in acetonitrile and heated at 65°C for 12 hours in an open batch. The solvent was removed by evaporation in vacuum providing the crude product in its cis- isomer.

Waxy solid, quantitative yield.

Methyl ester (5a): ^1H NMR (400 MHz, CD_3CN) δ 9.55 (br, 1H), 7.28 (dd, J = 11.8, 8.9 Hz, 1H), 5.04 (d, J = 8.9 Hz, 1H), 3.71 (s, 3H), 1.51 (s, 9H).

^{13}C NMR (101 MHz, $CDCl_3$) δ 169.10, 140.26, 93.85, 81.66, 59.67, 28.01, 14.06.

MS (ESI-TOF): $[M+H]^+$ calc. for $C_{10}H_{17}NO_4$ = 216.1230 m/z; found = 216.1233 m/z.

FT-IR ν_{max} 3340, 2981, 1741, 1686, 1632 cm^{-1}.

Synthesis of Boc-Δ^EβAla-OR (7a-b)

Compound **6a-b** was isomerized in acetonitrile solution by irradiation under UV-B light, yielding **7**.

Methyl ester (7a): Colourless solid, quantitative yield, m.p. 101-104°C.

^1H NMR (400 MHz, CD_3CN) δ 7.97 (br, 1H), 7.68 (dd, J = 14.0, 11.8 Hz, 1H), 5.38 (d, J = 14.1 Hz, 1H), 3.67 (s, 3H), 1.49 (s, 9H).

^{13}C NMR (101 MHz, $CDCl_3$) δ 167.65, 151.86, 139.97, 98.76, 59.96 , 28.14, 14.31.

MS (ESI-TOF): $[M+H]^+$ calc. for $C_{10}H_{17}NO_4$ = 216.1230 m/z; found = 216.1233 m/z.

FT-IR ν_{max} 3297, 2981, 1749, 1697, 1684, 1639 cm^{-1}.

Synthesis of Boc-fmΔ^ZβAla-OH (8)

Compound **5** (0.7 g, 2.4 mmol) was dissolved in THF/H_2O (2:1 v/v), then LiOH·H2O (0.726 g, 17 mmol) dissolved in water was added dropwise to the solution. The reaction was followed by TLC. The organic solvent was evaporated, then the solution was diluted with water, acidified with solid $KHSO_4$, extracted with EtOAc, dried, filtered and concentrated.

Colourless solid, 97% yield, 0.590 g, m.p. 121°C.

^1H NMR (400 MHz, $CDCl_3$) δ 6.52 – 6.39 (m, 1H), 5.54 (d, J = 9.7 Hz, 1H), 5.15 (s, 1H), 4.76 (s, 1H), 4.26 – 4.17 (m, 1H), 2.81 (d, J = 7.8 Hz, 1H), 1.44 (s, 9H).

MS (ESI-TOF): $[M+H]^+$ calc. for $C_{12}H_{17}NO_5$ = 256.1179 m/z; found = 256.1182 m/z.

FT-IR ν_{max} 3291, 2972, 1736, 1650, 1551 cm^{-1}.

Synthesis of Boc-Val-*fm*Δ^ZβAla-OR

Compound **5b** (0.5 g, 1.7 mmol) was dissolved in DCM and TFA was added to achieve the removal of the Boc-protecting group. Once the reaction was over, solvent was evaporated to obtain the deprotected compound in quantitative yield. Boc-Val-OH (0.443 g, 2.04 mmol) was activated with HOAt (0.277 g, 2.04 mmol) and EDC·HCl (0.391 g, 2.04 mmol) in anhydrous DCM, then a solution of the deprotected compound 5 was added and pH adjusted to 8 with DIPEA. The reaction was stirred overnight. The solution was diluted with DCM, washed with $KHSO_4$ 5% and $NaHCO_3$ 5%, dried, filtered and concentrated. The product was purified by column chromatography (EtOAc/petroleum ether, 2:1).

Colourless solid, 73% yield, 0.472 g, m.p. 104-105°C.

^1H NMR: see Note1.

^{13}C NMR (101 MHz, $CDCl_3$) δ 172.10, 171.50, 137.77, 135.41, 84.37, 84.04, 80.71, 79.82, 61.32, 59.68, 50.36, 46.34, 46.13, 31.27, 30.72, 28.29, 19.27, 17.51, 17.00, 14.13.

MS (ESI-TOF): $[M+H]^+$ calc. for $C_{19}H_{30}N_2O_6$ = 383.2176 m/z; found = 383.2178 m/z.

FT-IR ν_{max} 3336, 3258, 2966, 1746, 1732, 1709, 1691, 1654 cm^{-1}.

Synthesis of Boc-Val-*fm*Δ^ZβAla-OH

Boc-Val-*fm*Δ^ZβAla-OR (0.3 g, 0.78 mmol) was dissolved in THF/H_2O (2:1 v/v), then LiOH·H_2O (0.225 g, 5.4 mmol) dissolved in water was added dropwise to the solution. The reaction was followed by TLC. The organic solvent was evaporated, then the solution was diluted with water, acidified with solid $KHSO_4$, extracted with EtOAc, dried, filtered and concentrated. The crude product was used for the following coupling reaction without any further purification.

Colourless solid.

MS (ESI-TOF): $[M+H]^+$ calc. for $C_{17}H_{26}N_2O_6$ = 355.1863 m/z; [M+H]+ found = 355.1866 m/z.

Synthesis of Boc-Val-*fm*Δ^ZβAla-Leu-OMe

Boc-Val-*fm*Δ^ZβAla-OH (0.277 g, 0.78 mmol) was activated with HOAt (0.106 g, 0.78 mmol) and EDC·HCl (0.150 g, 0.78 mmol) in anhydrous DCM, then HCl·H-Leu-OMe (0.156 g, 0.86

mmol) was added and pH adjusted to 8 with TEA (230 µl). The reaction was stirred overnight. The solution was diluted with DCM, washed with $KHSO_4$ 5% and $NaHCO_3$ 5%, dried, filtered and concentrated. The product was purified by column chromatography (EtOAc /petroleum ether, 2:1).

Colourless solid, 68% yield, 0.255 g, m.p. 136-138°C.

^{1}H NMR: see Note1.

MS (ESI-TOF): $[M+H]^+$ calc. for $C_{24}H_{39}N_3O_7$ = 482.2860 m/z; found = 482.2863 m/z.

Synthesis of 9(Z)

Boc-Val-*fm*Δ^ZβAla-Leu-OMe was dissolved in acetonitrile and heated at 65°C for 5 hours in an open batch. The solvent was removed by evaporation in vacuum providing the crude product in its *cis* isomer.

Colourless solid, quantitative yield, m.p. 108-110°C.

^{1}H NMR (500 MHz, CD_3CN) δ 11.54 (d, J = 8.8 Hz, 1H), 7.30 (t, 1H), 6.79 (d, J = 7.6 Hz, 1H), 5.69 (d, J = 5.4 Hz, 1H), 5.20 (d, J = 8.8 Hz, 1H), 4.47 (dd, J = 14.9, 7.7 Hz, 1H), 3.95 (t, 1H), 3.70 (s, 3H), 1.72 – 1.63 (m, 1H), 1.63 – 1.54 (m, 3H), 1.44 (s, 9H), 1.09 – 0.81 (m, 12H).

MS (ESI-TOF): $[M+H]^+$ calc. for $C_{20}H_{35}N_3O_6$ = 414.2598 m/z; found = 414.2602 m/z.

FT-IR ν_{max} 3341, 3240, 2963, 1740, 1718, 1685, 1660, 1630 cm^{-1}.

Synthesis of 9(E)

Compound **9(Z)** was isomerized in acetonitrile solution by irradiation under UV-B light, yielding **9(E)**.

Colourless solid, quantitative yield.

^{1}H NMR (400 MHz, DMSO) δ 10.51 (d, J = 11.0 Hz, 1H), 8.21 (d, J = 7.7 Hz, 1H), 7.60 (dd, 1H), 6.99 (d, J = 8.0 Hz, 1H), 5.76 (d, J = 14.1 Hz, 1H), 4.41 – 4.23 (m, 1H), 3.80 (t, J = 7.7 Hz, 1H), 3.62 (s, 3H), 2.02 – 1.83 (m, 1H), 1.71 – 1.45 (m, 3H), 1.38 (s, 9H), 0.87 (dd, J = 19.7, 6.4 Hz, 12H).

MS (ESI-TOF): $[M+H]^+$ calc. for $C_{20}H_{35}N_3O_6$ = 414.2598 m/z; found = 414.2602 m/z.

Synthesis of Boc-*fm*Δ^ZβAla-Leu-OMe

Compound **8** (0.15 g, 0.59 mmol) was dissolved in anhydrous DCM and HOAt (0.079 g, 0.59 mmol) and EDC·HCl (0.113 g, 0.59 mmol) were added. H-L-Leu-OMe hydrochloride (0.16

g, 0.88 mmol) was added to the solution of the active ester and pH was adjust to 8 with DIPEA. The reaction was stirred for 72 hours. The solution was diluted with DCM, washed with $KHSO_4$ 5% and $NaHCO_3$ 5%, dried, filtered and concentrated.

Colourless solid, 62% yield, 0.139 g.

^{1}H NMR: see Note1.

MS (ESI-TOF): $[M+H]^+$ calc. for $C_{19}H_{30}N_2O_6$ = 383.2176 m/z; found = 383.2179 m/z.

Synthesis of Boc-(*fm*Δ^ZβAla)$_2$-Leu-OMe

Boc-*fm*Δ^ZβAla-Leu-OMe (0.2 g, 0.52 mmol) was dissolved in DCM and TFA was added to achieve the removal of the Boc-protecting group. Once the reaction was over, solvent was evaporated to obtain the deprotected compound in quantitative yield. Compound 8 (0.16 g, 0.62 mmol) was activated with HOAt (0.085 g, 0.62 mmol) and EDC·HCl (0.12 g, 0.62 mmol) in anhydrous DCM and it was added to the product unprotected and pH was adjust to 8 with DIPEA. The reaction was stirred overnight. The solution was diluted with DCM, washed with $KHSO_4$ 5% and $NaHCO_3$ 5%, dried, filtered and concentrated.

Colourless solid, 49% yield, 0.132 g.

^{1}H NMR: see Note1.

MS (ESI-TOF): $[M+H]^+$ calc. for $C_{26}H_{37}N_3O_8$ = 520.2653 m/z; found = 520.2654 m/z.

Synthesis of 10(Z,Z)

Boc-(*fm*Δ^ZβAla)$_2$-Leu-OMe (0.132 g, 0.25 mmol) was dissolved in DCM and TFA was added to achieve the removal of the Boc-protecting group. Once the reaction was over, solvent was evaporated to obtain the deprotected compound in quantitative yield. Boc-Val-OH (0.083 g, 0.38 mmol) was activated with HOAt (0.052 g, 0.38 mmol) and EDC·HCl (0.073 g, 0.38 mmol) in anhydrous DCM and it was added to the product unprotected and pH was adjust to 8 with DIPEA. The reaction was stirred overnight. The solution was diluted with DCM, washed with $KHSO_4$ 5% and $NaHCO_3$ 5%, dried, filtered and concentrated. The crude product was dissolved in acetonitrile and heated at 80°C for 24 hours. The solvent was removed by evaporation in vacuum and the crude product was purified via flash chromatography (eluant: DCM/methanol 95:5).

Colourless solid, 54% yield, 0.065 g, m.p. decomposition above 210°C.

^{1}H NMR (400 MHz, CD_3CN) δ 11.43 (d, J = 10.4 Hz, 1H), 11.14 (d, J = 10.4 Hz, 1H), 7.41 (dt, J = 19.3, 9.8 Hz, 2H), 6.82 (d, J = 7.4 Hz, 1H), 5.75 (d, 1H), 5.30 (d, J = 8.7 Hz, 1H), 5.21

(d, J = 8.9 Hz, 1H), 4.45 (dd, J = 15.0, 7.6 Hz, 1H), 4.01 (t, 1H), 3.69 (s, 3H), 1.79 – 1.56 (m, 4H), 1.45 (s, 9H), 0.94 (dt, J = 9.3, 4.2 Hz, 12H).

^{13}C NMR (101 MHz, $CDCl_3$) δ 173.43, 170.55, 168.12, 165.88, 137.66, 135.59, 98.96, 98.60, 52.46, 50.45, 41.66, 30.96, 29.72, 28.30, 24.89, 22.74, 22.01, 19.27, 17.41.

MS (ESI-TOF): $[M+H]^+$ calc. for $C_{23}H_{38}N_4O_7$ = 483.2813 m/z; found = 483.2815 m/z.

FT-IR ν_{max} 3285, 1738, 1677, 1608 cm^{-1}.

Synthesis of Boc-(*fm*Δ^ZβAla)$_3$-Leu-OMe

Boc-(*fm*Δ^ZβAla)$_2$-Leu-OMe (0.2 g, 0.38 mmol) was dissolved in DCM and TFA was added to achieve the removal of the Boc-protecting group. Once the reaction was over, solvent was evaporated to obtain the deprotected compound in quantitative yield. Compound **8** (0.147 g, 0.57 mmol) was activated with HOAt (0.077 g, 0.57 mmol) and EDC·HCl (0.109 g, 0.57 mmol) in anhydrous DCM and it was added to the product unprotected and pH was adjust to 8 with DIPEA. The reaction was stirred overnight. The solution was diluted with DCM, washed with $KHSO_4$ 5% and $NaHCO_3$ 5%, dried, filtered and concentrated. The crude product was used for the following coupling reaction without any further purification.

Colourless solid, 46% yield, 0.114 g.

MS (ESI-TOF): $[M+H]^+$ calc. for $C_{33}H_{44}N_4O_{10}$ = 657.3130 m/z; found = 657.3133 m/z.

Synthesis of 11(Z,Z,Z)

Boc-(*fm*Δ^ZβAla)$_3$-Leu-OMe (0.114 g, 0.17 mmol) was dissolved in DCM and TFA was added to achieve the removal of the Boc-protecting group. Once the reaction was over, solvent was evaporated to obtain the deprotected compound in quantitative yield. Boc-Val-OH (0.073 g, 0.33 mmol) was activated with HOAt (0.046 g, 0.33 mmol) and EDC·HCl (0.065 g, 0.33 mmol) in anhydrous DCM and it was added to the product unprotected and pH was adjust to 8 with DIPEA. The reaction was stirred overnight. The solution was diluted with DCM, washed with $KHSO_4$ 5% and $NaHCO_3$ 5%, dried, filtered and concentrated. The crude product was dissolved in acetonitrile and heated at 80°C for 24 hours. The solvent was removed by evaporation in vacuum and the crude product was purified via flash chromatography (eluant: DCM/methanol 95:5), giving **11(Z,Z,Z)**.

Colourless solid, 57% yield, 0.054 g, m.p. decomposition above 220°C.

^{1}H NMR (500 MHz, CD_3CN) δ 11.40 (d, J = 10.6 Hz, 1H), 11.15 (d, J = 10.7 Hz, 1H), 11.01

(d, J = 10.9 Hz, 1H), 7.55 – 7.45 (m, 2H), 7.39 (dd, J = 10.4, 9.2 Hz, 1H), 6.81 (d, J = 7.7 Hz, 1H), 5.76 (d, J = 5.8 Hz, 1H), 5.36 (d, J = 8.7 Hz, 1H), 5.29 (d, J = 8.8 Hz, 1H), 5.21 (d, J = 8.9 Hz, 1H), 4.48 – 4.42 (m, 1H), 4.02 (t, 1H), 3.69 (s, 3H), 1.72 – 1.65 (m, 1H), 1.64 – 1.58 (m, 3H), 1.45 (s, 9H), 0.95 (dt, J = 10.5, 5.6 Hz, 12H).

^{13}C NMR (101 MHz, $CDCl_3$) δ 173.63, 170.69, 168.27, 166.02, 138.62, 138.24, 137.97, 135.34, 98.73, 98.30, 52.47, 50.44, 41.50, 30.83, 28.30, 24.88, 22.75, 21.94, 19.25, 17.43.

MS (ESI-TOF): $[M+H]^+$ calc. for $C_{26}H_{41}N_5O_8$ = 552.3027 m/z; found = 552.3029 m/z.

FT-IR ν_{max} 3316, 2978, 1729, 1678, 1645, 1621, 1600 cm^{-1}.

Synthesis of Boc-(*fm*Δ^ZβAla)$_4$-Leu-OMe

Boc-(*fm*Δ^ZβAla)$_3$-Leu-OMe (0.125 g, 0.19 mmol) was dissolved in DCM and TFA was added to achieve the removal of the Boc-protecting group. Once the reaction was over, solvent was evaporated to obtain the deprotected compound in quantitative yield. Compound 8 (0.073 g, 0.28 mmol) was activated with HOAt (0.038 g, 0.28 mmol) and EDC·HCl (0.055 g, 0.28 mmol) in anhydrous DCM and it was added to the product unprotected and pH was adjust to 8 with DIPEA. The reaction was stirred overnight. The solution was diluted with DCM, washed with KHSO4 5% and NaHCO3 5%, dried, filtered and concentrated. The crude product was used for the following coupling reaction without any further purification.

Colourless solid, 68% yield, 0.103 g.

MS (ESI-TOF): $[M+H]^+$ calc. for $C_{40}H_{51}N_5O_{12}$ = 794.3606 m/z; found = 794.3609 m/z.

Synthesis of 12(Z,Z,Z,Z)

Boc-(*fm*Δ^ZβAla)$_4$-Leu-OMe (0.1 g, 0.13 mmol) was dissolved in DCM and TFA was added to achieve the removal of the Boc-protecting group. Once the reaction was over, solvent was evaporated to obtain the deprotected compound in quantitative yield. Boc-Val-OH (0.041 g, 0.19 mmol) was activated with HOAt (0.025 g, 0.19 mmol) and EDC·HCl (0.036 g, 0.19 mmol) in anhydrous DCM and it was added to the product unprotected and pH was adjust to 8 with DIPEA. The reaction was stirred overnight. The solution was diluted with DCM, washed with $KHSO_4$ 5% and $NaHCO_3$ 5%, dried, filtered and concentrated. The crude product was dissolved in acetonitrile and heated at 80°C for 24 hours. The solvent was removed by evaporation in vacuum and the crude product was purified via flash chromatography (eluant: DCM/methanol 95:5), giving **12(Z,Z,Z,Z)**.

Colourless solid, 52% yield, 0.042 g, m.p. decomposition above 220°C.

^{1}H NMR (500 MHz, CD_3CN) δ 11.39 (d, J = 10.7 Hz, 1H), 11.15 (d, J = 10.7 Hz, 1H), 11.02 (d, J = 11.0 Hz, 1H), 10.96 (d, J = 11.1 Hz, 1H), 7.53 (ddd, J = 26.4, 14.2, 9.8 Hz, 3H), 7.44 – 7.36 (m, 1H), 6.80 (d, J = 7.7 Hz, 1H), 5.76 (s, 1H), 5.37 (t, J = 9.2 Hz, 2H), 5.29 (d, J = 8.8 Hz, 1H), 5.21 (d, J = 8.9 Hz, 1H), 4.45 (q, J = 7.6 Hz, 1H), 4.02 (t, 1H), 3.69 (s, 3H), 1.74 – 1.64 (m, 1H), 1.64 – 1.56 (m, 3H), 1.45 (s, 9H), 1.00 – 0.90 (m, 12H).

^{13}C NMR (101 MHz, $CDCl_3$) δ 173.46, 170.66, 168.17, 165.98, 138.45, 137.89, 135.53, 112.98, 98.60, 98.28, 97.93, 52.49, 50.47, 41.62, 30.85, 28.30, 24.90, 22.75, 21.99, 19.27, 17.41.

MS (ESI-TOF): $[M+H]^+$ calc. for $C_{29}H_{44}N_6O_9$ = 621.3242 m/z; found = 621.3244 m/z.

FT-IR ν_{max} 3307, 2978, 1732, 1675, 1640, 1626, 1593 cm^{-1}.

Note 1. The NMR spectra of the oligomers containing one or more -fmΔ^{Z} βAla- residues are reported below; different sets of signals are present, due to the fact that each foldamer was obtained as a mixture of diasteromers, and this makes the assignation of the spectrum difficult.

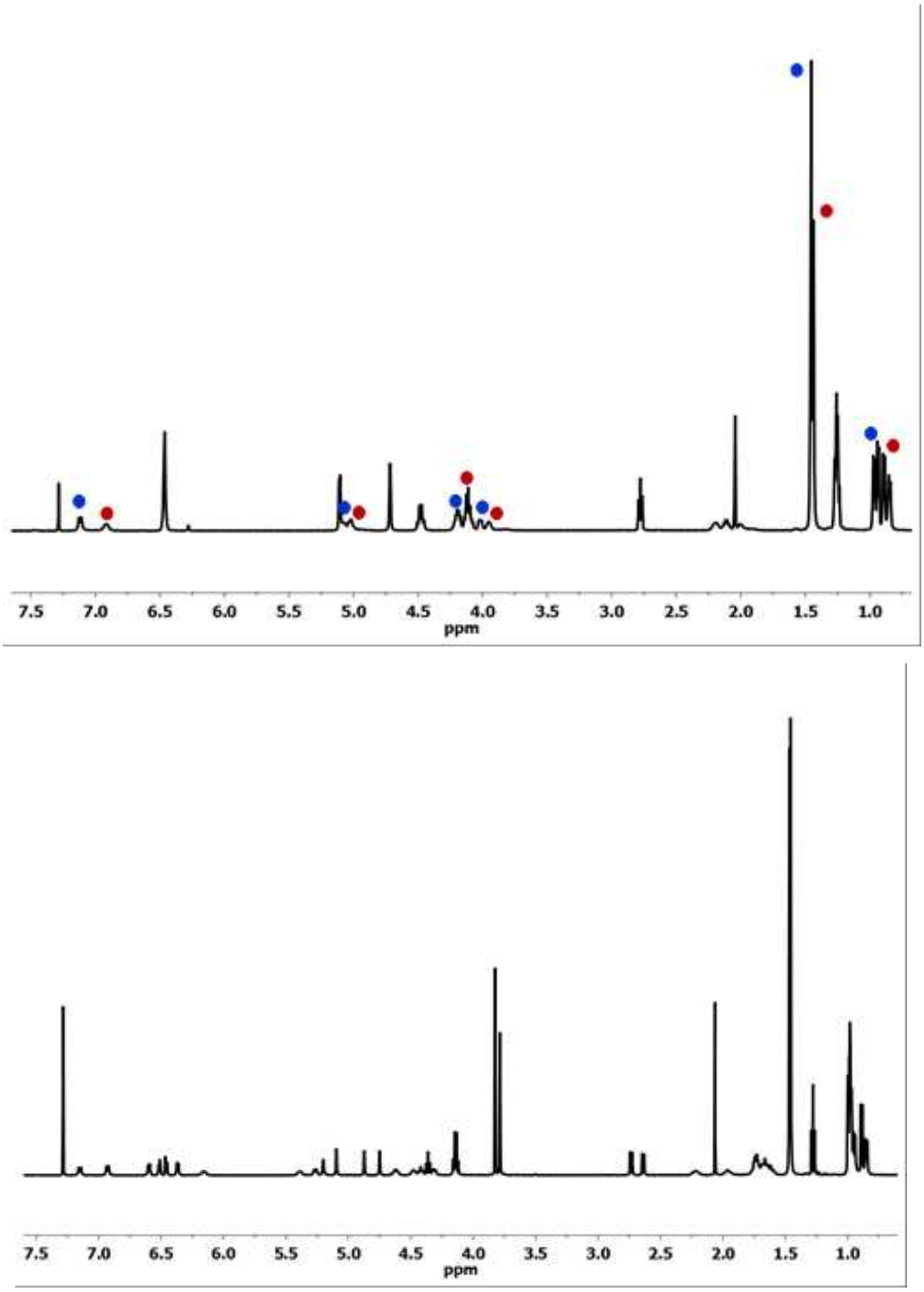

Fig. 4-5 ^{1}H NMR spectrum of Boc-Val-fmΔ^{Z}βAla-OR and Boc-Val-fmΔ^{Z}βAla-Leu-OMe.

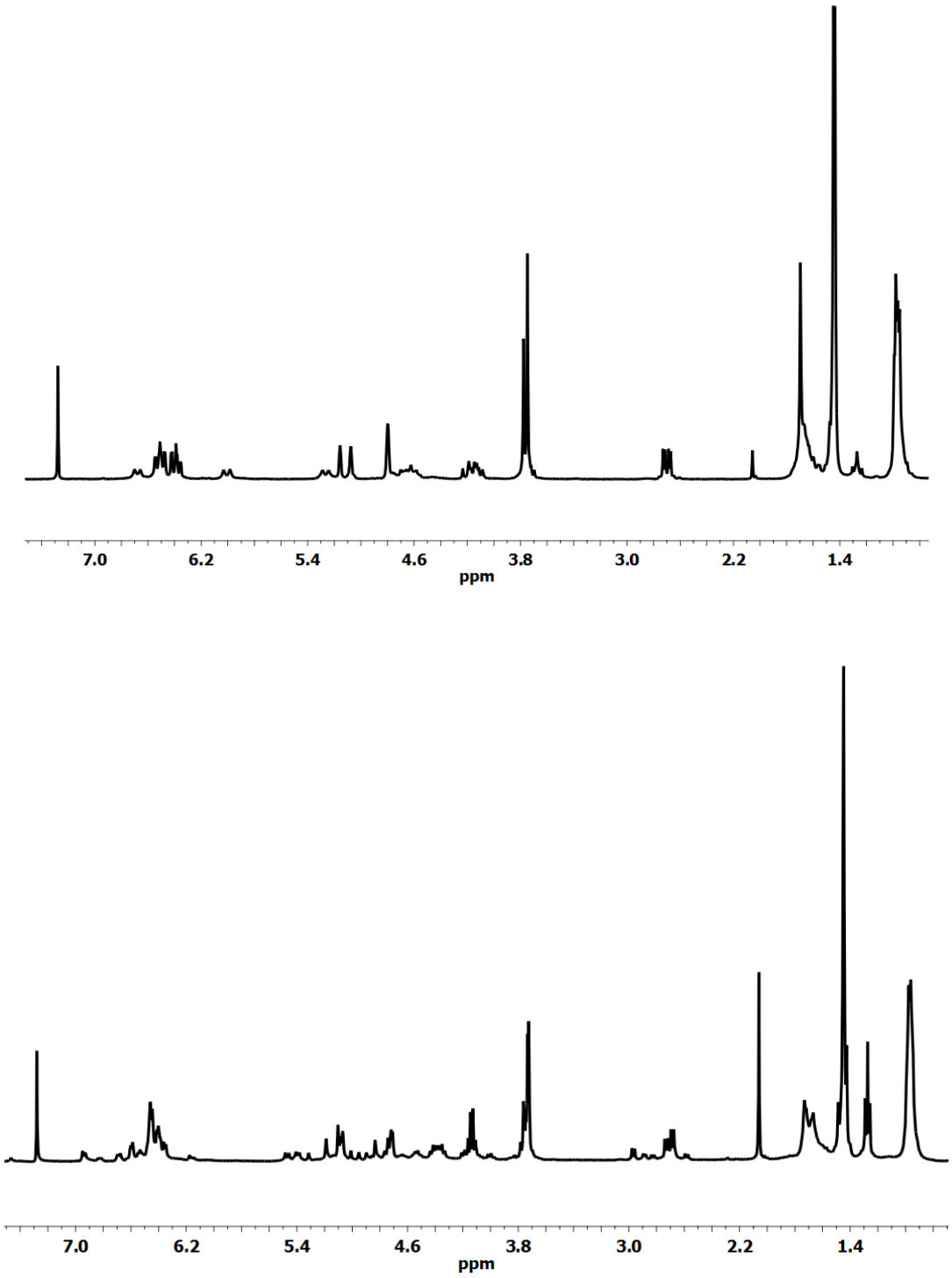

Fig. 6-7 ^{1}H NMR spectrum of Boc-fmΔ^{Z}βAla-Leu-OMe and Boc-(fmΔ^{Z}βAla)$_2$-Leu-OMe.

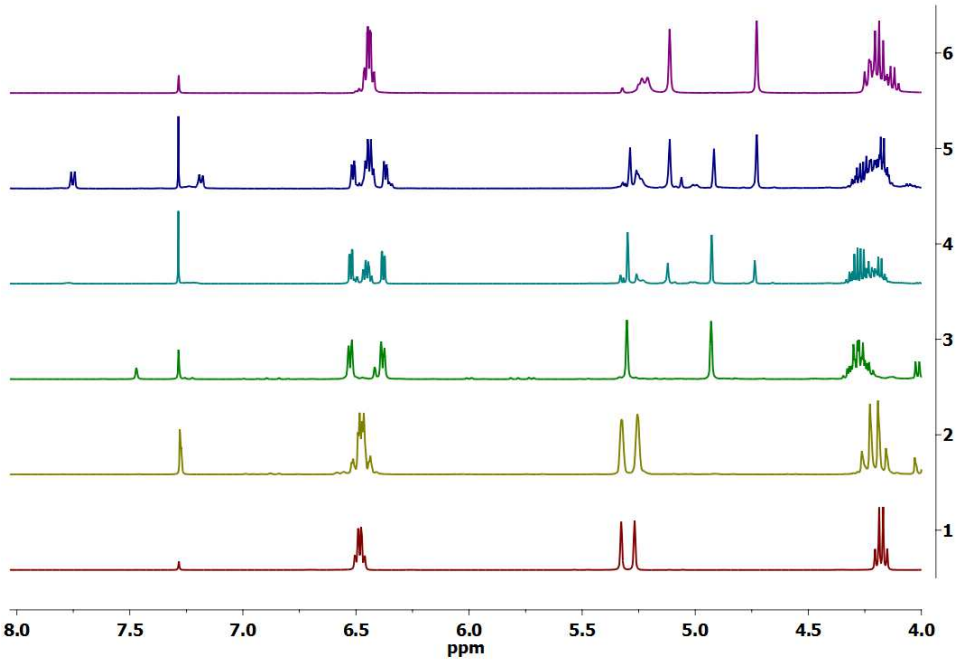

Fig. 8 ^{1}H NMR spectrum in $CDCl_3$ highlighting (from 1 to 6 traces) the chemical conversion from **4** (red line, first spectrum) to **5** (violet line, sixth spectrum). In-between spectra belong respectively to the azide intermediate (yellow line, second spectrum), to the isocianate intermediate (green line, third spectrum), to the reaction mixture of the Curtius rearrangement after 3 hr (light blue line, fourth spectrum), and to the reaction mixture of the Curtius rearrangement after 6 hr (blue line, fifth spectrum).

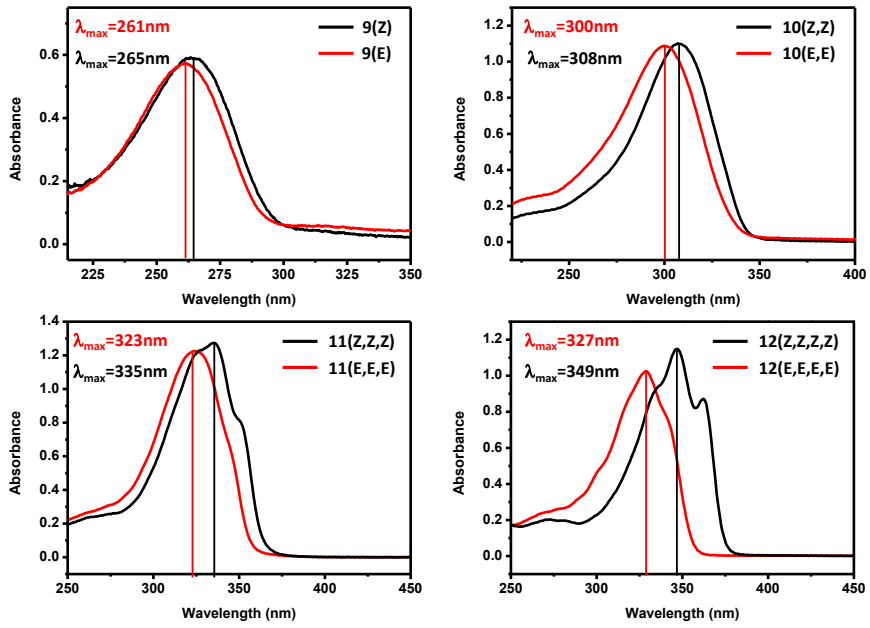

Fig. 9 UV-Vis spectra of **9(Z)**, **10(Z,Z)**, **11(Z,Z,Z)**, and **12(Z,Z,Z,Z)** in black and **9(E)**, **10(E,E)**, **11(E,E,E)**, and **12(E,E,E,E)** in red. Spectra were recorded by collecting all-Z and all-E corresponding componds from HPLC (see Figure 3).

X-Ray Diffraction

Single crystals of compounds **5**, **6a**, **7**, and **9(*Z*)a** were grown, respectively: by slow evaporation from ethyl acetate (**5**), by cooling of a warm petroleum ether solution (**6a**), from ethyl acetate - petroleum ether (**7**), and from acetone - water [**9(*Z*)a**]. X-Ray diffraction data were collected with a Gemini E four-circle kappa diffractometer (Rigaku Oxford Diffraction) equipped with a 92 mm EOS CCD detector, using graphite monochromated Cu Kα radiation (λ = 1.54184 Å) for **5**, **6a** and **9(*Z*)a**, while Mo Kα radiation (λ = 0.71073 Å) for **7**. For **9(*Z*)a** data collection was performed up to theta = 51°, as the crystal did not significantly diffract beyond 1.0 Å resolution. Data collection and reduction were performed with the CrysAlisPro software (Rigaku Oxford Diffraction). A semi-empirical absorption correction based on the multi-scan technique using spherical harmonics, implemented in the SCALE3 ABSPACK scaling algorithm, was applied.

The structures of **5**, **6a**, and **7** were solved by *ab initio* procedures of the SIR 2014 program.[9] In the structure of **7**, in space group *Pnma*, the non-H atoms of the molecule lie on a mirror plane (special position *x*, ¼, *z*), except for two carbon atoms of the Boc group. The structure of **9(*Z*)a** was eventually solved by application of the SHELXT program,[10] which allowed the location of 43 atoms (out of 56) in two independent molecules (A and B) in space group $P3_221$. The positions of the remaining atoms were recovered from subsequent difference Fourier maps. Refinements were carried out by full-matrix least-squares on F^2, using all data, by application of the SHELXL-2014 program,[11] with anisotropic displacement parameters for all of the non-H atoms.

Structural refinement of **9(*Z*)a** was somehow complicated by the occurrence of two independent molecules, both characterized by extensive disorder at the level of the N-terminal trifluoroacetyl group and the Val and Ile side chains. Specifically: (i) In each molecule the fluorine atoms were refined on two sets of positions, rotated approximately by 60°, with population parameters 0.53/0.47 in molecule A, while 0.55/0.45 in molecule B. (ii) In molecule A, the two methyl groups of the Val side chain were modeled on three sites (corresponding to the *trans*, *gauche*$^-$ and *gauche*$^+$ $\chi^{1,1}$ rotamers) to which a common population parameter of 0.6667 was imposed, whereas in molecule B two distinct sets of position could be identified for each of the methyl groups, with population parameters 0.60/0.40: (iii) Two sets of positions, with population parameters 0.55/0.45, were assigned to the methyl groups of the Leu side chain of molecule A. Some sort of disorder is likely to

occur at the level of the Leu side chain of molecule B, as suggested by the large displacement parameters of the terminal methyl groups. However, despite extensive effort, the data did not allowed us to model the disorder satisfactorily. Restraints on bond distances, bond angles, and anisotropic displacement parameters were applied to the disordered atoms.

In general, H-atoms were calculated at idealized positions and refined using a riding model. For **7**, the positions of methyl and methylene H-atoms linked to carbon atoms sitting on the mirror plane were recovered from a difference Fourier map and refined with restraints on their bond distances and bond angles.

Relevant crystal data and structure refinement parameters are listed in Tables S1-S4. CCDC 1901757-1901760 contain the supplementary crystallographic data for this paper. The data can be obtained free of charge from The Cambridge Crystallographic Data Centre via www.ccdc.cam.ac.uk/structures.

Table S1. Crystal data and structure refinement for methyl exo-3-tert-butoxycarbonylamino-7-oxabicyclo(2.2.1)hept-5-ene-exo-2-carboxylate [**5**].

Identification code	mc286	
Empirical formula	$C_{13}H_{19}NO_5$	
Formula weight	269.29	
Temperature	293(2) K	
Wavelength	1.54184 Å	
Crystal system	Triclinic	
Space group	P -1	
Unit cell dimensions	a = 7.0799(2) Å	α= 70.832(3)°.
	b = 8.5861(3) Å	β= 79.464(3)°.
	c = 12.7044(4) Å	γ = 74.335(3)°.
Volume	698.60(4) $Å^3$	
Z	2	
Density (calculated)	1.280 Mg/m^3	
Absorption coefficient	0.823 mm^{-1}	
F(000)	288	
Crystal size	0.70 × 0.40 × 0.04 mm^3	
Theta range for data collection	5.600 to 72.730°.	
Index ranges	$-8 \le h \le 8$, $-10 \le k \le 10$, $-15 \le l \le 15$	
Reflections collected	16264	
Independent reflections	2764 [R(int) = 0.0411]	
Completeness to theta = 67.684°	99.9 %	
Absorption correction	Semi-empirical from equivalents	
Max. and min. transmission	1.00000 and 0.41105	
Refinement method	Full-matrix least-squares on F^2	
Data / restraints / parameters	2764 / 0 / 176	
Goodness-of-fit on F^2	1.086	
Final R indices [I>2sigma(I)]	R_1 = 0.0482, wR_2 = 0.1401	
R indices (all data)	R_1 = 0.0509, wR_2 = 0.1438	
Extinction coefficient	n/a	
Largest diff. peak and hole	0.245 and -0.208 e.$Å^{-3}$	
CCDC deposition No.	1901757	

Table S2. Crystal data and structure refinement for Boc-Δ^{Z}βAla-OH [**6a**].

Identification code	mc285	
Empirical formula	$C_8H_{13}NO_4$	
Formula weight	187.19	
Temperature	293(2) K	
Wavelength	1.54184 Å	
Crystal system	Orthorhombic	
Space group	Pbca	
Unit cell dimensions	a = 9.8965(3) Å	α= 90°.
	b = 11.0326(3) Å	β= 90°.
	c = 18.6266(7) Å	γ = 90°.
Volume	2033.73(11) $Å^3$	
Z	8	
Density (calculated)	1.223 Mg/m^3	
Absorption coefficient	0.833 mm^{-1}	
F(000)	800	
Crystal size	0.40 × 0.15 × 0.05 mm^3	
Theta range for data collection	4.748 to 72.655°.	
Index ranges	$-12 \le h \le 12$, $-13 \le k \le 13$, $-22 \le l \le 22$	
Reflections collected	8435	
Independent reflections	2001 [R(int) = 0.0188]	
Completeness to theta = 67.684°	100.0 %	
Absorption correction	Semi-empirical from equivalents	
Max. and min. transmission	1.00000 and 0.35343	
Refinement method	Full-matrix least-squares on F^2	
Data / restraints / parameters	2001 / 0 / 122	
Goodness-of-fit on F^2	1.027	
Final R indices [I>2sigma(I)]	R_1 = 0.0404, wR_2 = 0.1162	
R indices (all data)	R_1 = 0.0539, wR_2 = 0.1277	
Extinction coefficient	n/a	
Largest diff. peak and hole	0.129 and -0.124 e.$Å^{-3}$	
CCDC deposition No.	1901758	

Table S3. Crystal data and structure refinement for Boc-Δ^{E}βAla-OEt [**7**].

Identification code	mc280	
Empirical formula	$C_{10}H_{17}NO_4$	
Formula weight	215.24	
Temperature	293(2) K	
Wavelength	0.71073 Å	
Crystal system	Orthorhombic	
Space group	Pnma	
Unit cell dimensions	a = 9.9702(4) Å	α= 90°.
	b = 8.1092(5) Å	β= 90°.
	c = 15.2259(7) Å	γ = 90°.
Volume	1231.02(11) Å^3	
Z	4	
Density (calculated)	1.161 Mg/m^3	
Absorption coefficient	0.089 mm^{-1}	
F(000)	464	
Crystal size	0.45 × 0.20 × 0.15 mm^3	
Theta range for data collection	2.442 to 26.371°.	
Index ranges	-12 ≤ h ≤ 11, -10 ≤ k ≤ 10, -19 ≤ l ≤ 19	
Reflections collected	9634	
Independent reflections	1346 [R(int) = 0.0353]	
Completeness to theta = 25.242°	99.9 %	
Absorption correction	Semi-empirical from equivalents	
Max. and min. transmission	1.00000 and 0.84151	
Refinement method	Full-matrix least-squares on F^2	
Data / restraints / parameters	1346 / 21 / 101	
Goodness-of-fit on F^2	1.068	
Final R indices [I>2sigma(I)]	R_1 = 0.0504, wR_2 = 0.1499	
R indices (all data)	R_1 = 0.0682, wR_2 = 0.1648	
Extinction coefficient	n/a	
Largest diff. peak and hole	0.285 and -0.187 e.Å^{-3}	
CCDC deposition No.	1901759	

Table S4. Crystal data and structure refinement for Tfa-L-Val-Δ^{Z}βAla-L-Leu-OMe [**9(*Z*)a**].

Identification code	mc294B	
Empirical formula	$C_{17}H_{26}F_3N_3O_5$	
Formula weight	409.41	
Temperature	293(2) K	
Wavelength	1.54184 Å	
Crystal system	Trigonal	
Space group	$P3_221$	
Unit cell dimensions	a = 15.7700(2) Å	α= 90°.
	b = 15.7700(2) Å	β= 90°.
	c = 32.1389(5) Å	γ = 120°.
Volume	6921.9(2) $Å^3$	
Z	12	
Density (calculated)	1.179 Mg/m^3	
Absorption coefficient	0.880 mm^{-1}	
F(000)	2592	
Crystal size	0.250 × 0.200 × 0.080 mm^3	
Theta range for data collection	3.236 to 51.247°.	
Index ranges	$-15 \le h \le 15$, $-15 \le k \le 15$, $-32 \le l \le 32$	
Reflections collected	39185	
Independent reflections	5006 [R(int) = 0.0377]	
Completeness to theta = 51.247°	100.0 %	
Absorption correction	Semi-empirical from equivalents	
Max. and min. transmission	1.00000 and 0.65184	
Refinement method	Full-matrix least-squares on F^2	
Data / restraints / parameters	5006 / 682 / 604	
Goodness-of-fit on F^2	1.008	
Final R indices [I>2sigma(I)]	R_1 = 0.0609, wR_2 = 0.1745	
R indices (all data)	R_1 = 0.0907, wR_2 = 0.2025	
Absolute structure parameter	-0.03(7)	
Extinction coefficient	n/a	
Largest diff. peak and hole	0.174 and -0.174 $e.Å^{-3}$	
CCDC deposition No.	1901760	

References

1. S.H. Gellman, *Acc. Chem. Res.*, **1998**, 31, 173.
2. (a) C. Toniolo, M. Crisma, F. Formaggio, and C. Peggion, *Biopolymers*, **2001**, 60, 396. (b) S. Hecht, and I. Huc, *Foldamers: Structure, Properties and Applications*; Wiley-VCH: Weinheim, Germany, **2007**. (c) C.M. Goodman, S. Choi, S. Shandler, and W.F. DeGrado, *Nat. Chem. Biol.*, **2007**, 3, 252. (d) D. Seebach, and J. Gardiner, *Acc. Chem. Res.*, **2008**, 41, 1366. (e) W.S. Horne, and S.H. Gellman, *Acc. Chem. Res.*, **2008**, 41, 1399. (f) I. Saraogi, and A.D. Hamilton, *Chem. Soc. Rev.*, **2009**, 38, 1726. (g) Z. T. Li, J. L. Hou, and C. Li, *Acc. Chem. Res.*, **2008**, 41, 1343. (h) T. A. Martinek, and F. Fülöp, *Chem. Soc. Rev.*, **2012**, 41, 687.
3. B. A. F. Le Bailly, and J. Clayden, *Chem. Commun.* **2016**, 52, 4852.
4. (a) C. Peggion, M. Crisma, C. Toniolo, and F. Formaggio, *Tetrahedron*, **2012**, 68, 4429. (b) M. Crisma, M. Saviano, A. Moretto, Q.B. Broxterman, B. Kaptein, and C. Toniolo, *J. Am. Chem. Soc.*, **2007**, 129, 15471.
5. (a) M. De Poli, W. Zawodny, O. Quinonero, M. Lorch, S.J. Webb, and J. Clayden, *Science*, **2016**, 352, 575. (b) B.A.F. Le Bailly, L. Byrne, and J. Clayden, *Angew. Chem., Int. Ed.*, **2016**, 55, 2132. (c) F.G.A. Lister, B.A.F. Le Bailly, S.J. Webb, and J. Clayden, *Nat. Chem*., **2017**, 9, 420.
6. D. Mazzier, M. Crisma, M. De Poli, G. Marafon, C. Peggion, J. Clayden, and A. Moretto, *J. Am. Chem. Soc.*, **2016**, 138, 8007.
7. For examples of photoisomerizable systems, see: (a) L. Wang, and Q. Li, *Chem. Soc. Rev*., **2018**, 47, 1044. (b) B.L. Feringa, *Angew. Chem., Int. Ed.*, **2017**, 56, 11059. (c) H.M.D. Bandara, and S.C. Burdette, *Chem. Soc. Rev.*, **2012**, 41, 1809. (d) Z. Yu, and S. Hecht, *Angew. Chem., Int. Ed.*, **2011**, 50, 1640. (e) S. Amirjalayer, A. Martinez-Cuezva, J. Berna, S. Woutersen, and W.J. Buma, *Angew. Chem., Int. Ed.*, **2018**, 57, 1792. (f) H. Wang, H.K. Bisoyi, L. Wang, A.M. Urbas, T.J. Bunning, and Q. Li, *Angew. Chem., Int. Ed.*, **2018**, *57*, 1627. (g) M. Irie, *Chem. Rev.*, **2000**, 100, 1685. (h) D. Han, B.L. Jiang, J. Feng, Y.D. Yin, and W.S. Wang, *Angew. Chem., Int. Ed.*, **2017**, 56, 7792. (i) J. Yoon, and A.P. de Silva, *Angew. Chem., Int. Ed.*, **2015**, 54, 9754.
8. G. Marafon, M. Crisma, and A. Moretto, *Angew. Chem., Int. Ed.*, **2018**, 57, 10217.
9. M.C. Burla, R. Caliandro, B. Carrozzini, G.L. Cascarano, C. Cuocci, C. Giacovazzo, M. Mallamo, A. Mazzone, and G. Polidori, *J. Appl. Crystallogr.*, **2015**, 48, 306.

10. G.M. Sheldrick, *Acta Crystallogr. A,* **2015**, 71, 3.
11. G.M. Sheldrick, *Acta Crystallogr. C,* **2015**, 71, 3.

APPENDIX

Copies of ^{1}H NMR, ^{13}C NMR and bidimensional NMR spectra of the principal compounds synthetized and studied in this work.

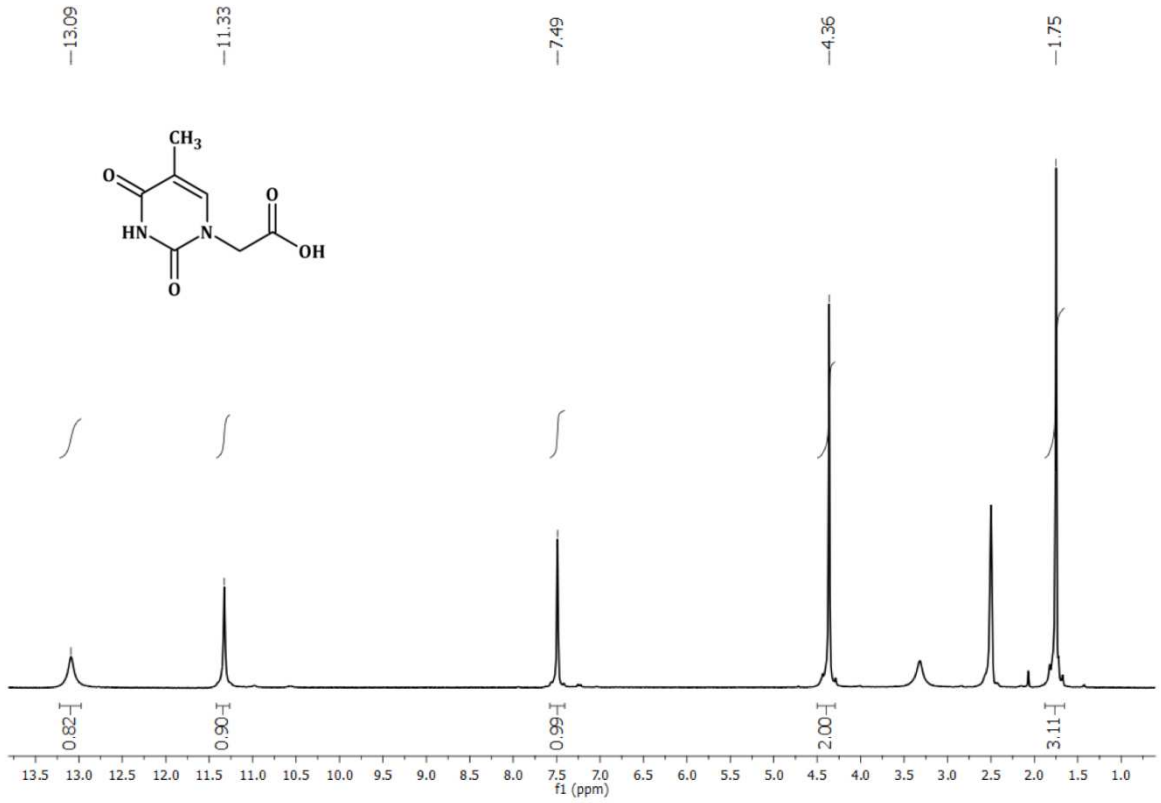

^{1}H NMR spectrum of thymine-1-acetic acid.

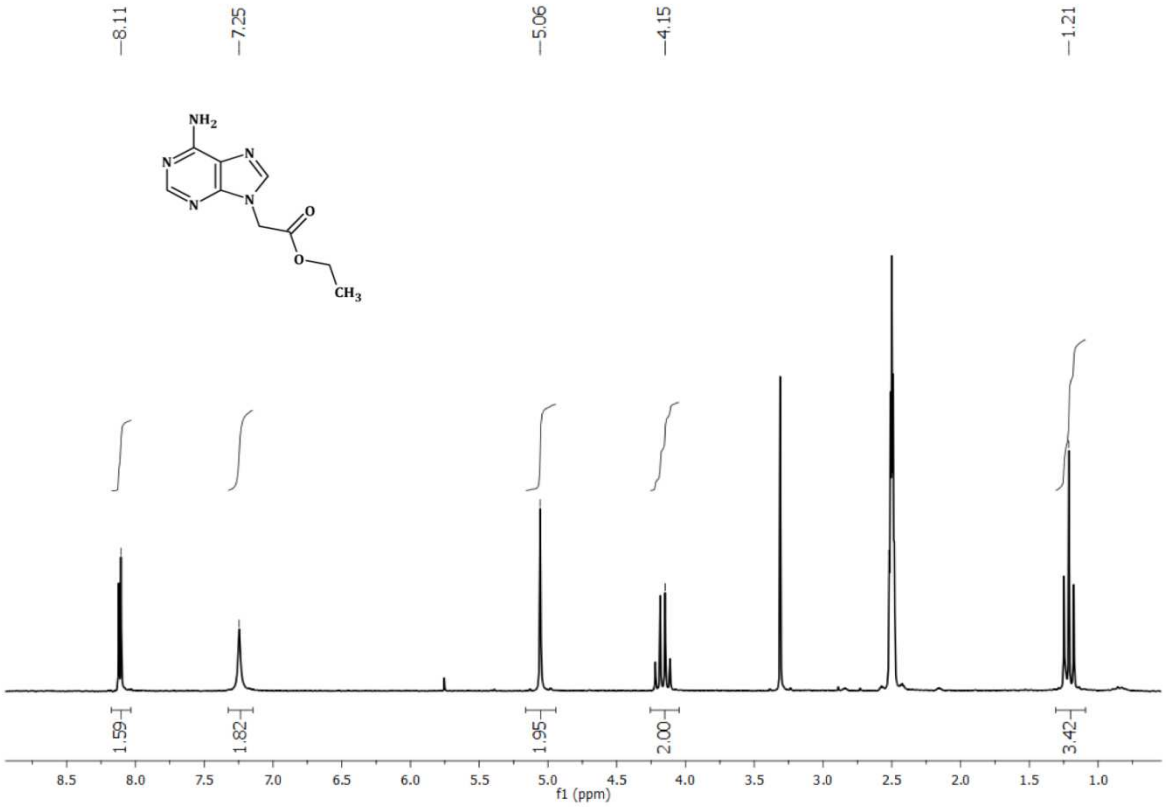

^{1}H NMR spectrum of ethyl adenine-9-acetate.

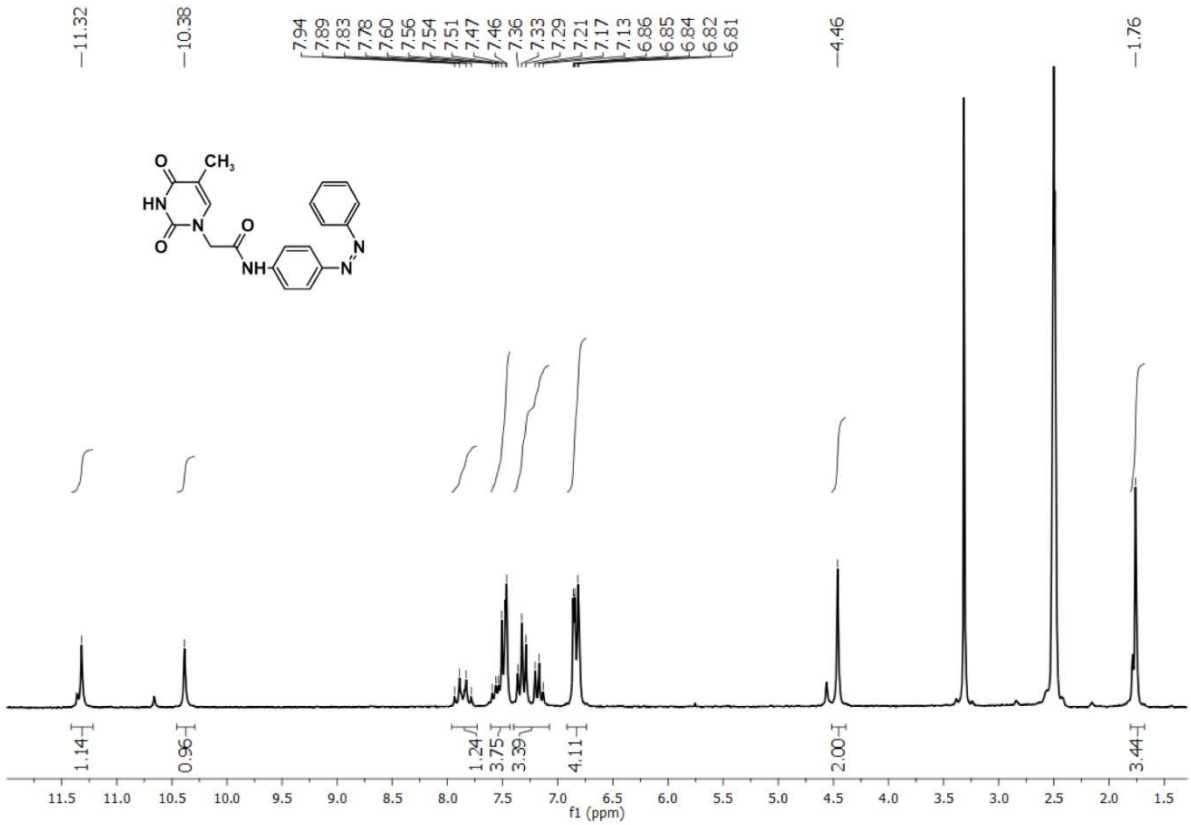

[1]H NMR spectrum of thymine-4-phenilazoanilide (*cis* form).

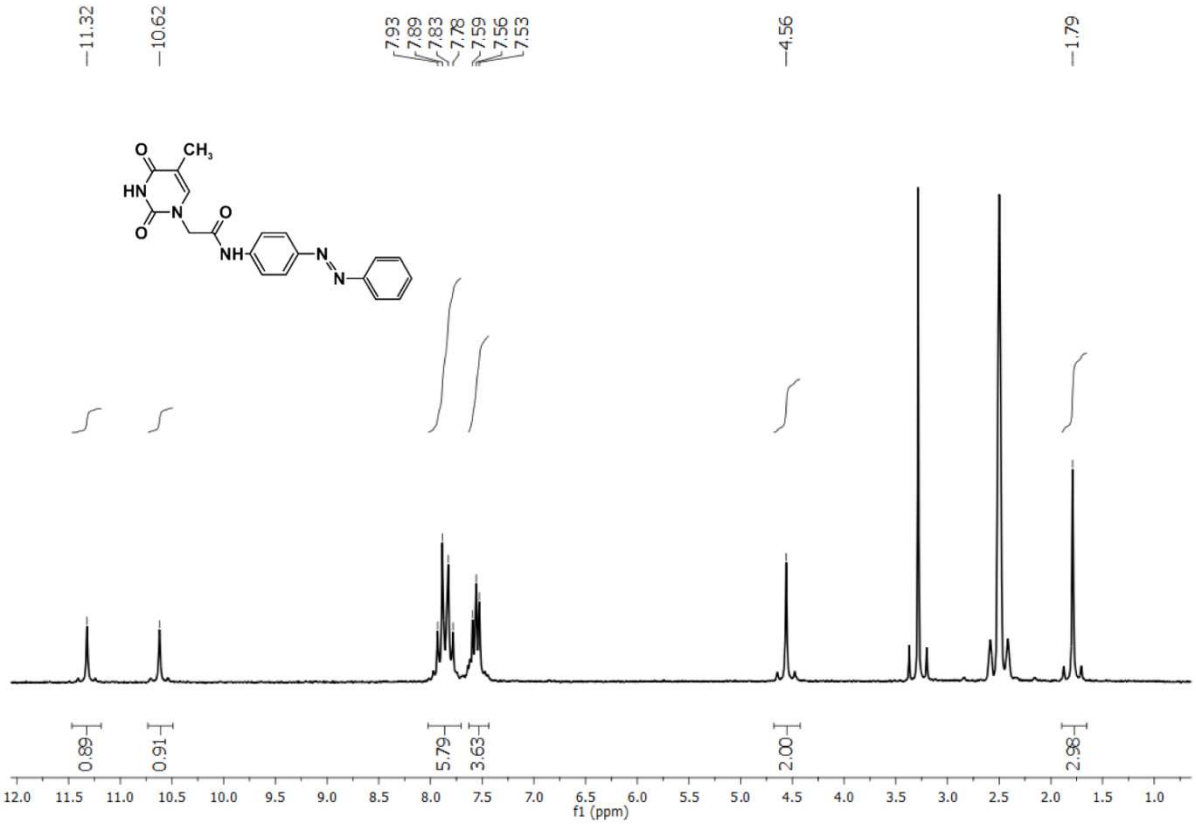

[1]H NMR spectrum of thymine-4-phenilazoanilide (*trans* form).

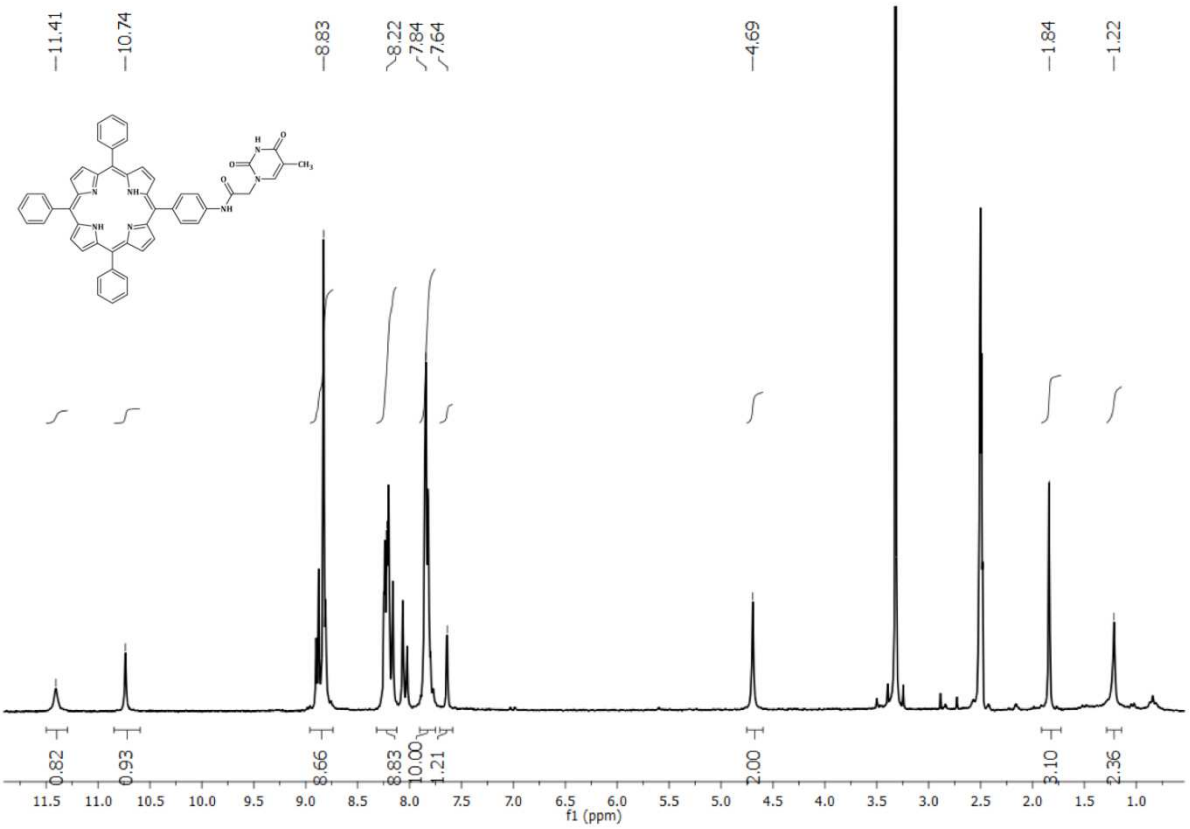

^{1}H NMR spectrum of thymine-(aminophenyl) porphyrin.

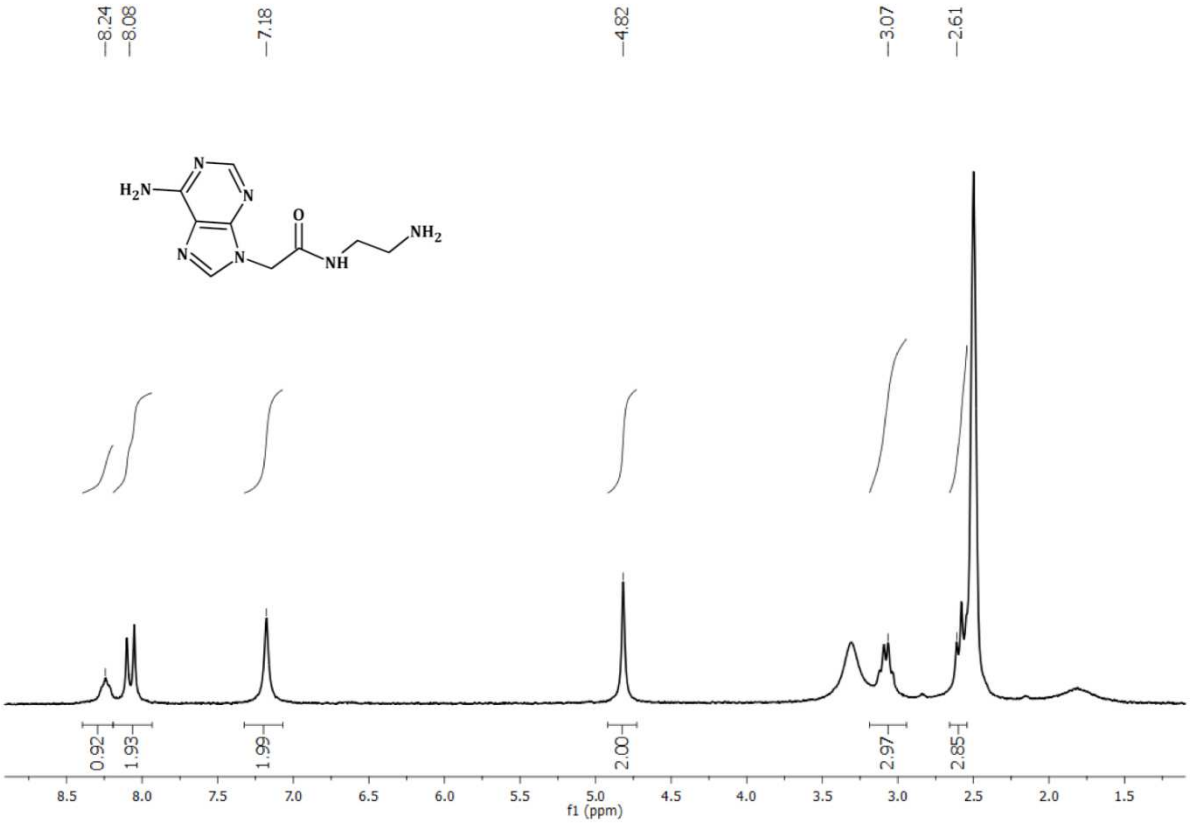

^{1}H NMR spectrum of adenine-9-ethylenamide amine.

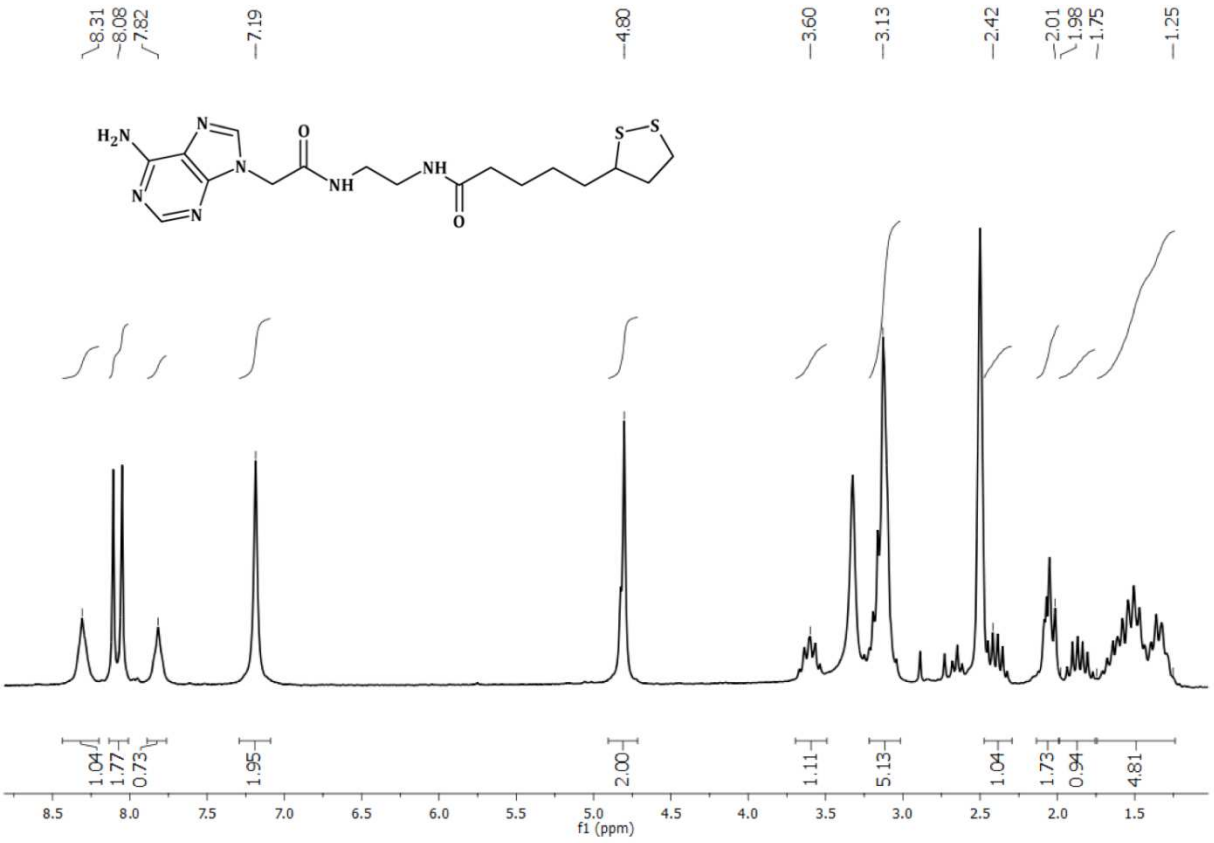

^{1}H NMR spectrum of **4**.

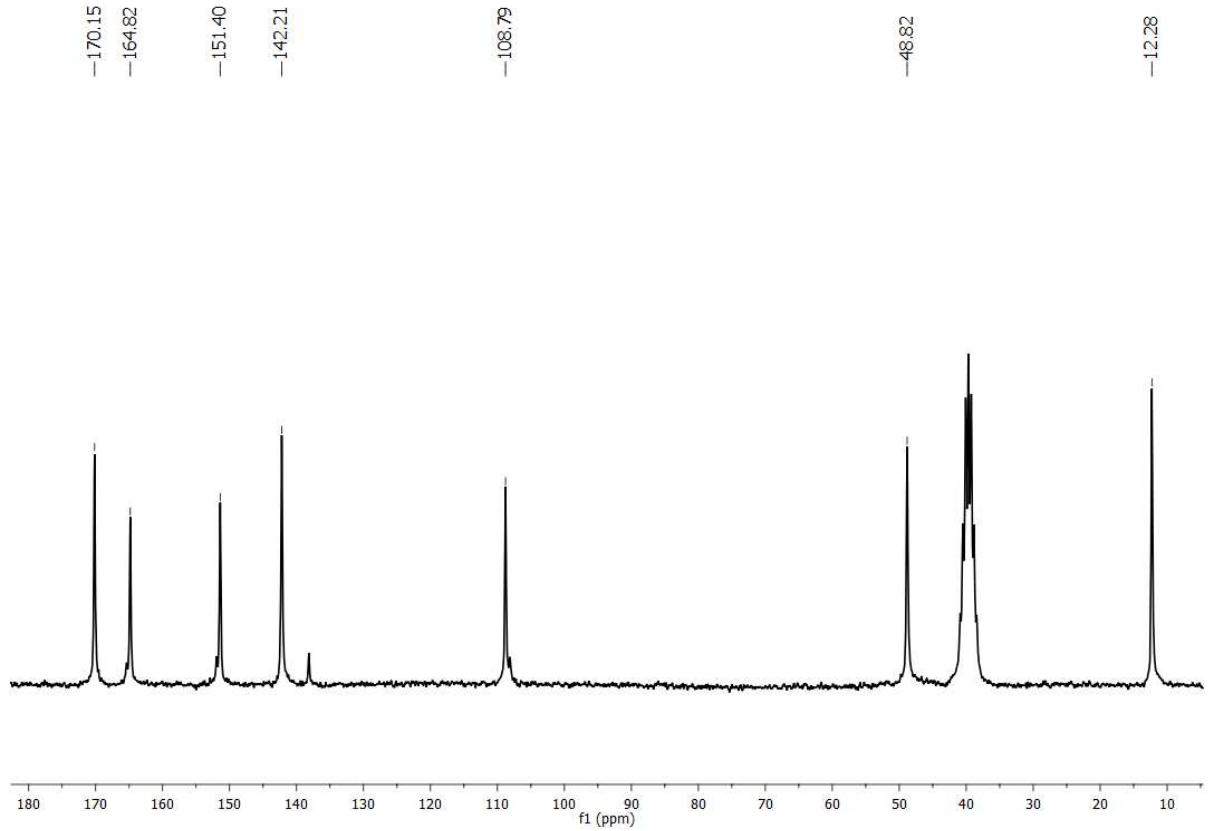

^{13}C NMR spectrum of thymine-1-acetic acid.

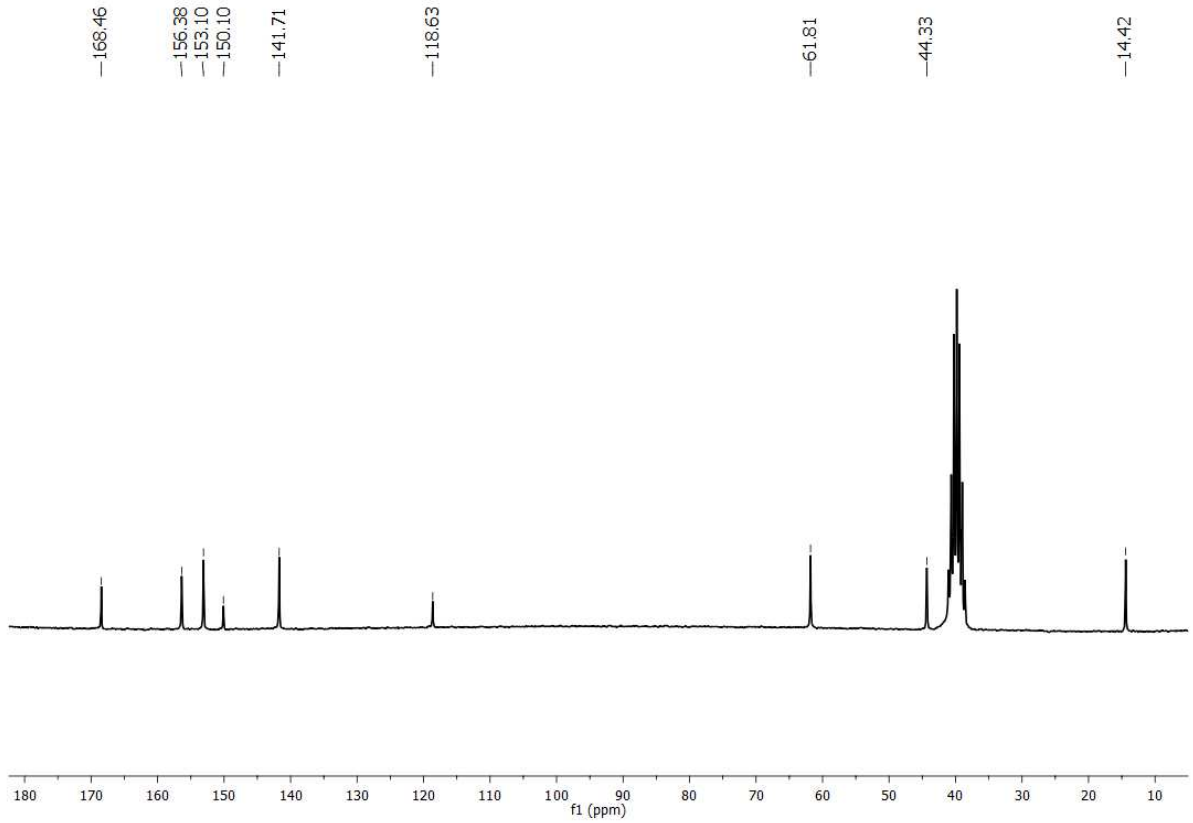

^{13}C NMR spectrum of ethyl adenine-9-acetate.

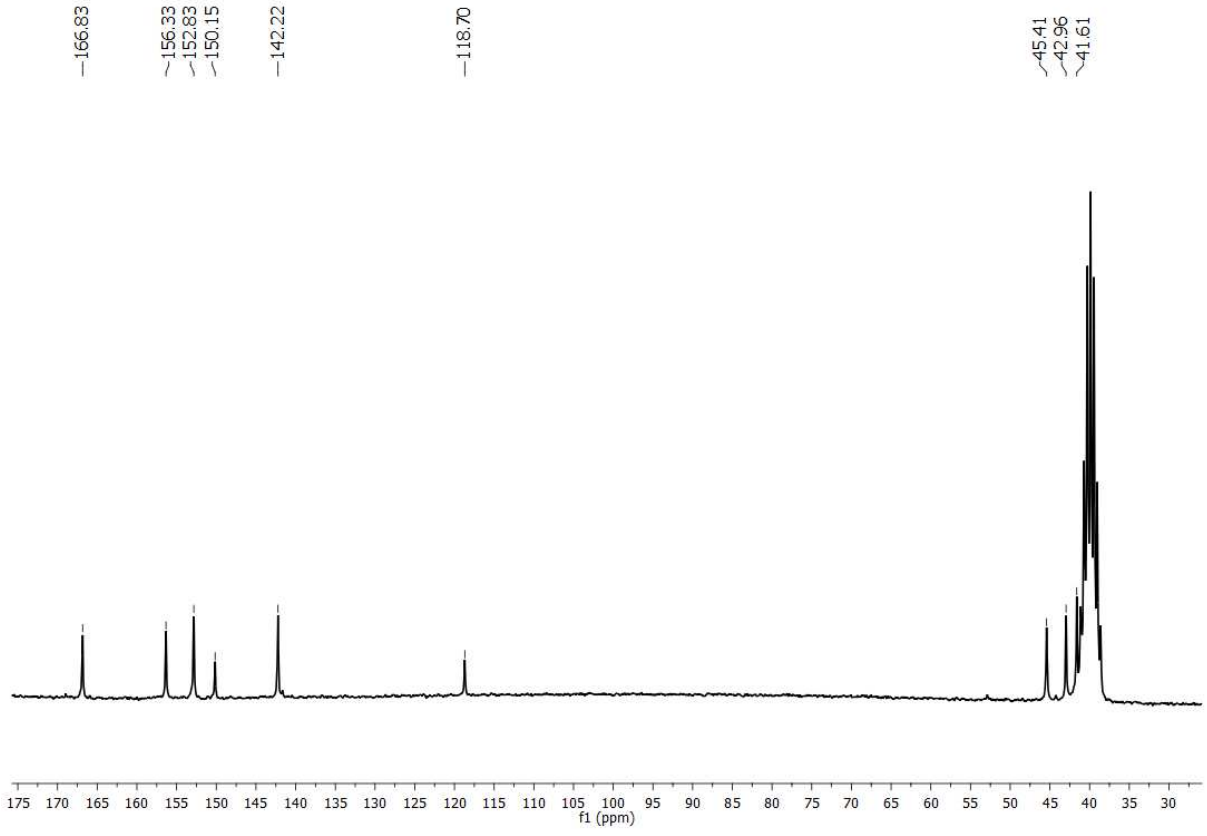

^{13}C NMR spectrum of ethyl adenine-9-ethylenamide amine.

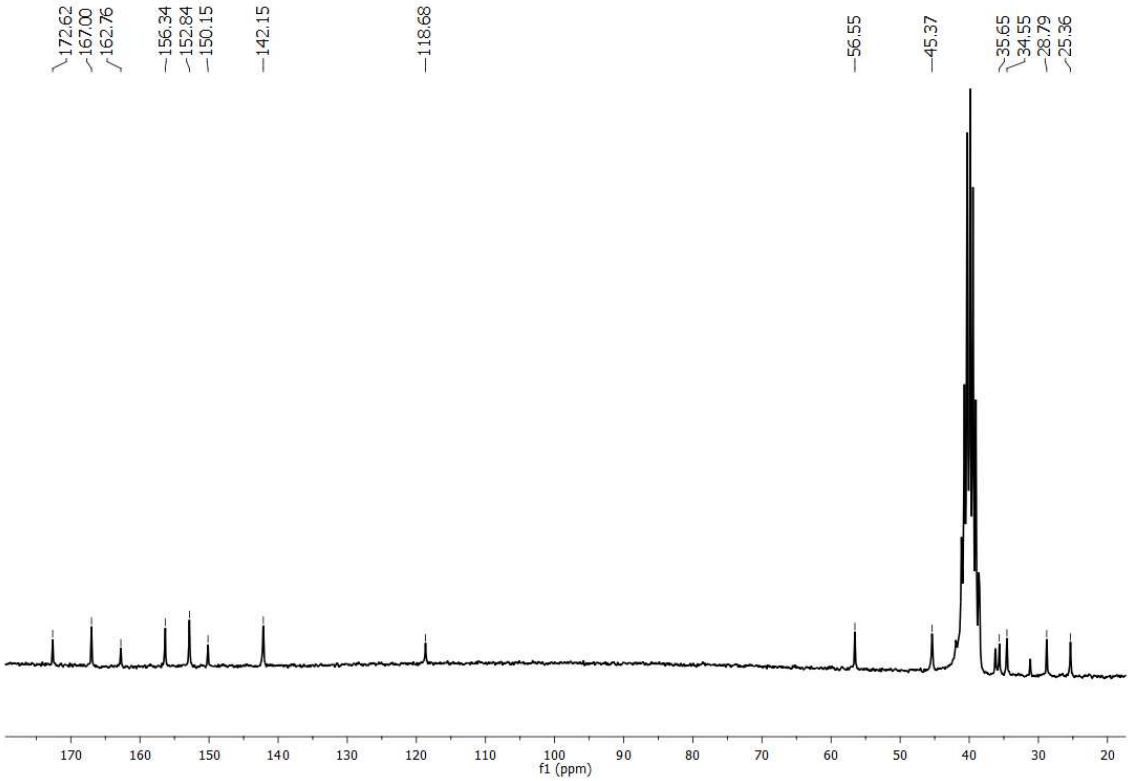

^{13}C NMR spectrum of ethyl **4**.

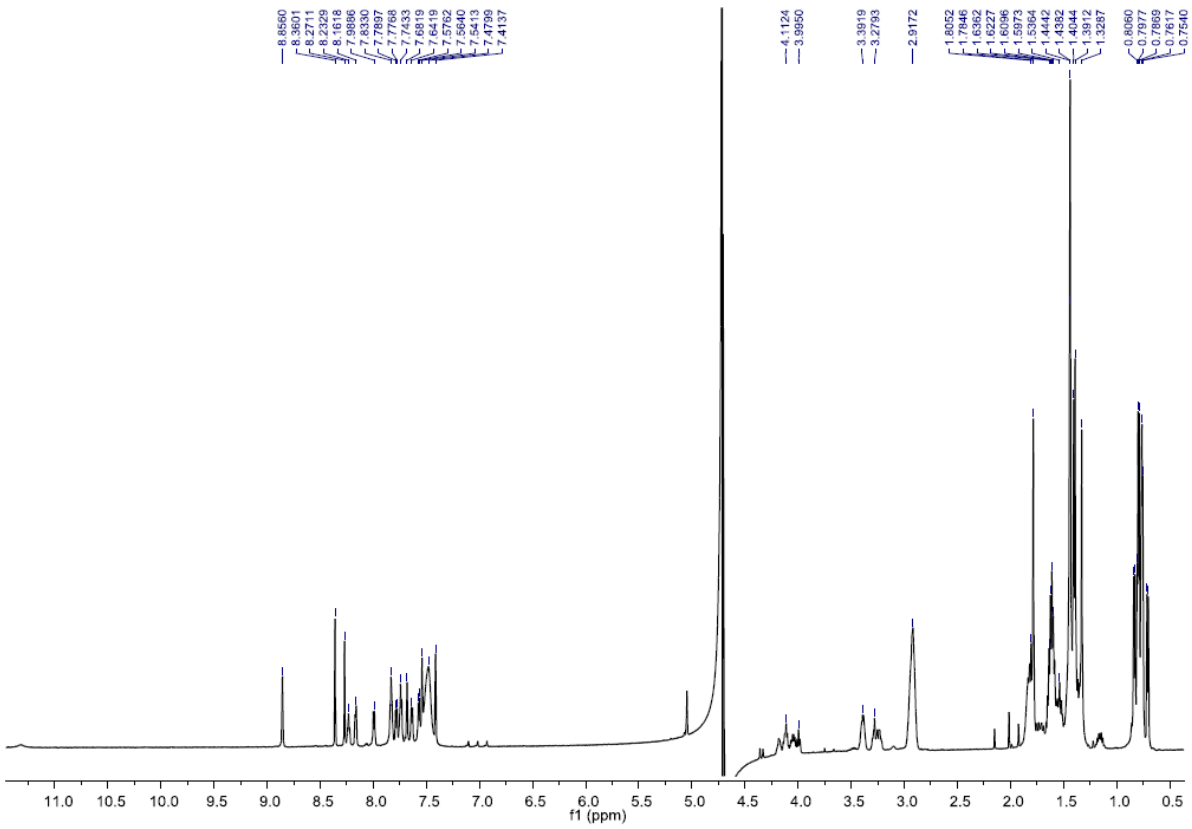

^{1}H NMR spectrum of **T-Tr(Lys)-A**.

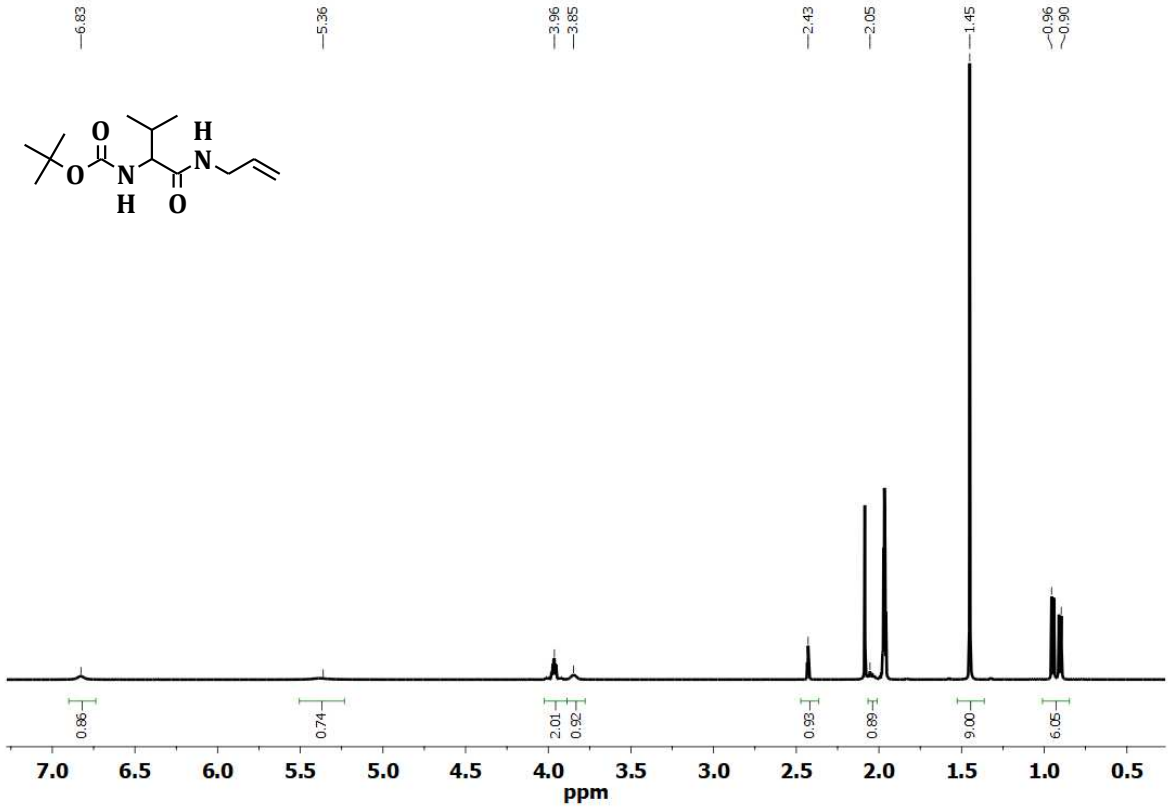

^{1}H NMR spectrum of **Boc-Val-NH-CH$_2$-C≡CH (1).**

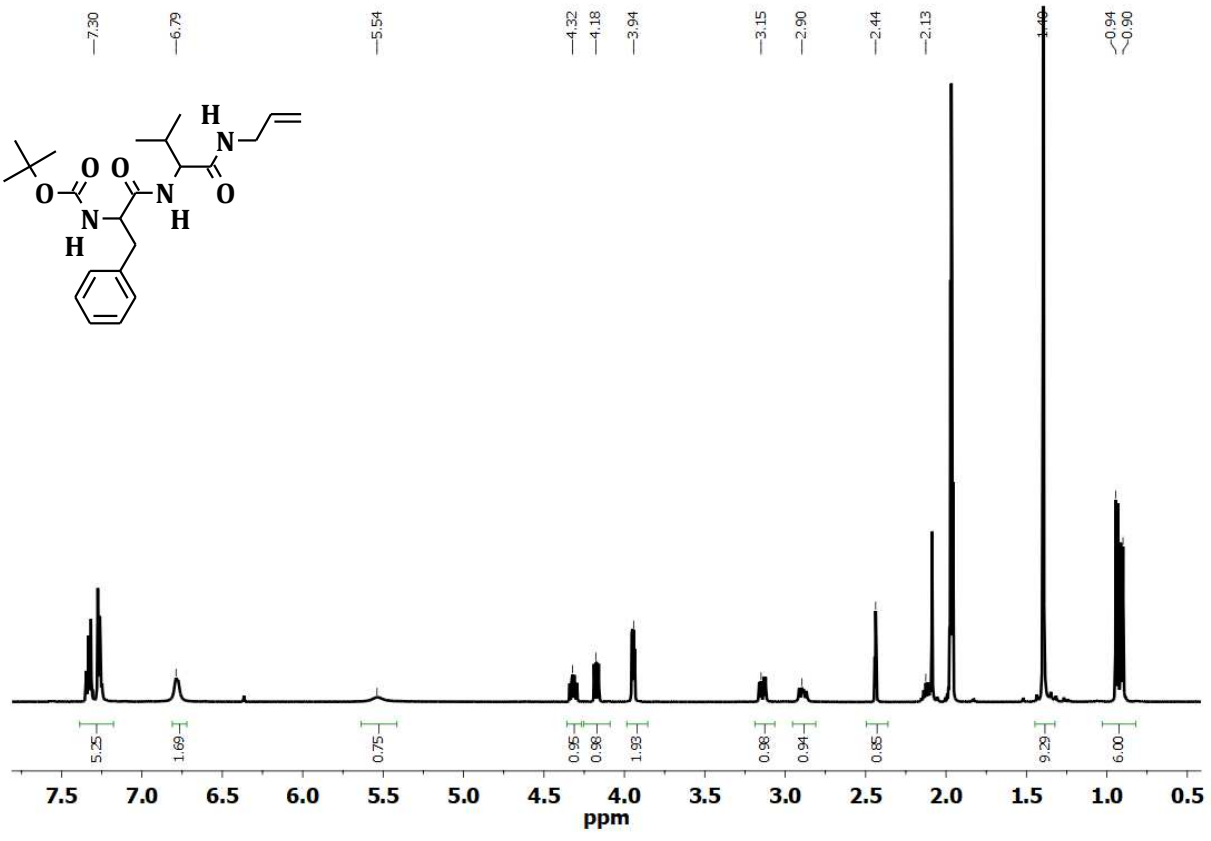

^{1}H NMR spectrum of **Boc-Phe-Val-NH-CH$_2$-C≡CH (2).**

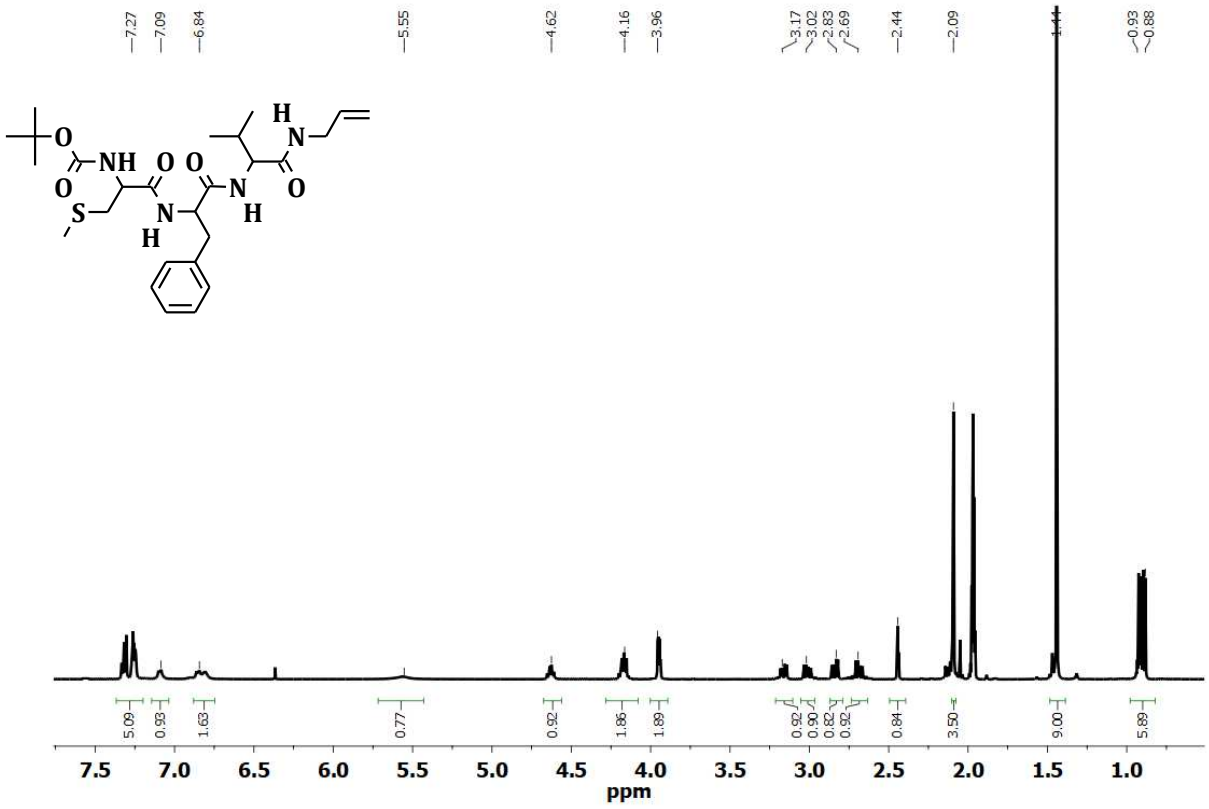

^{1}H NMR spectrum of **Boc-Cys(Me)-Phe-Val-NH-CH$_2$-C≡CH (3).**

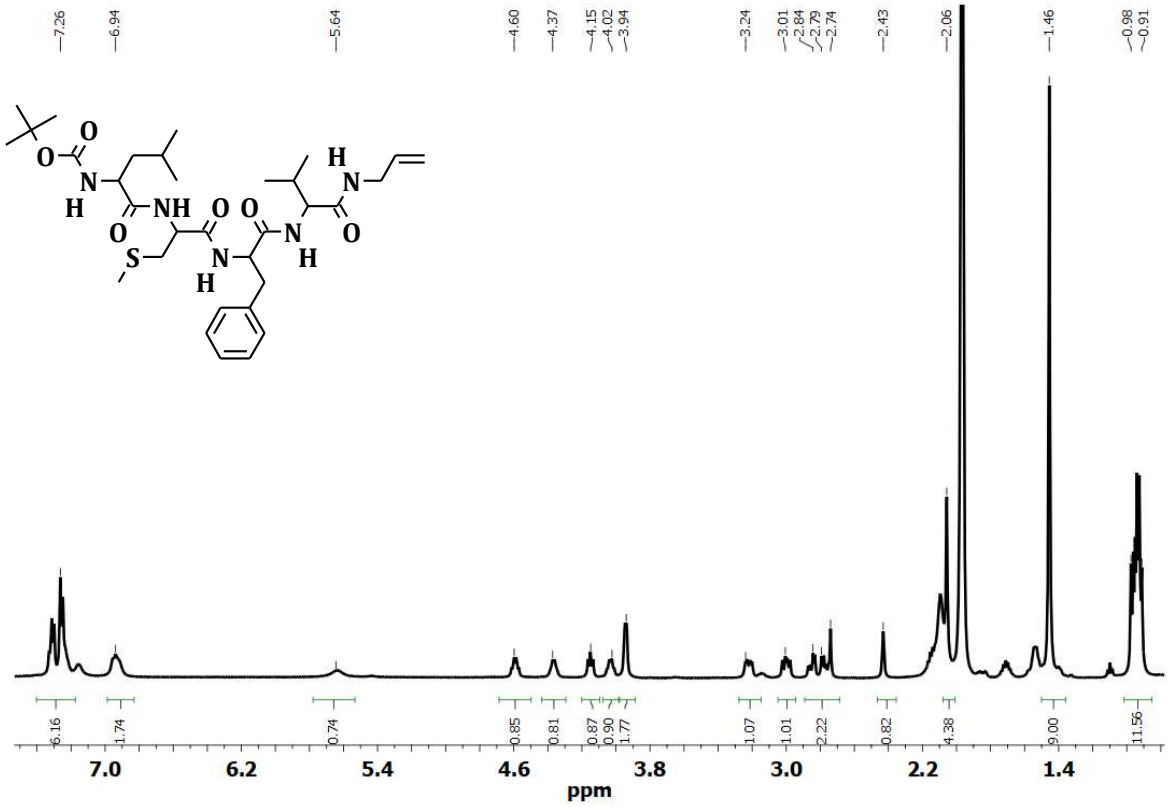

^{1}H NMR spectrum of **Boc-Leu-Cys(Me)-Phe-Val-NH-CH$_2$-C≡CH (4).**

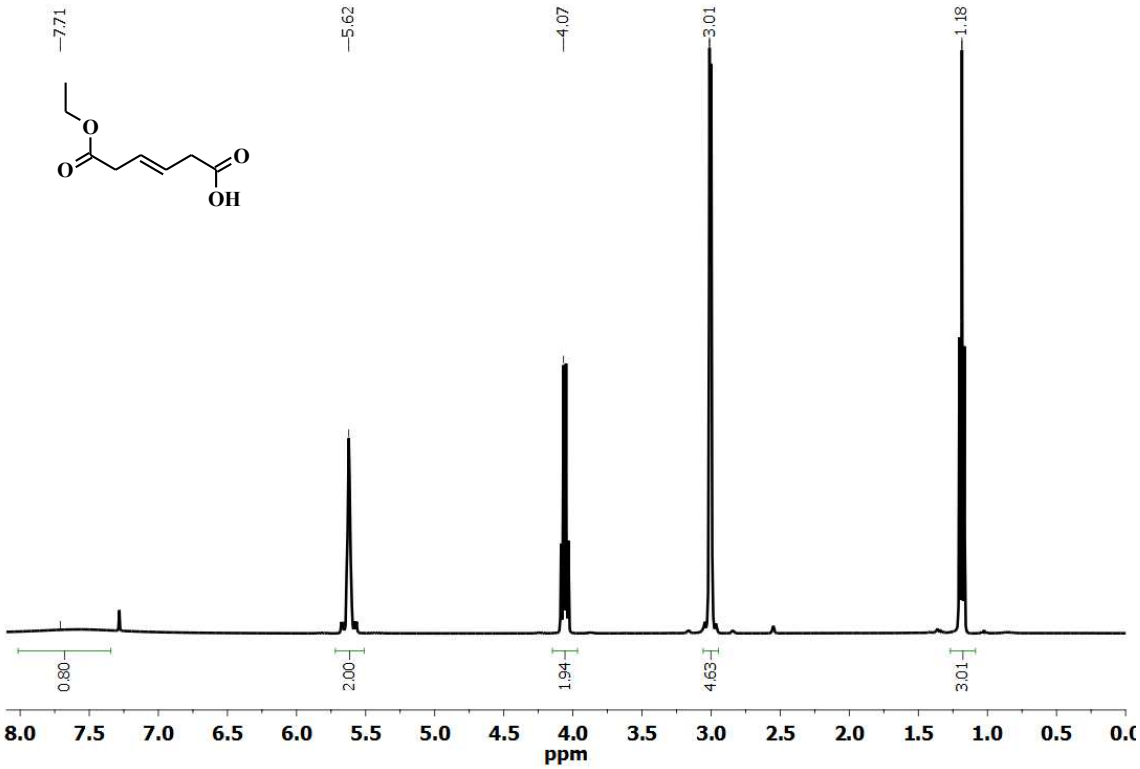

^{1}H NMR spectrum of **2**.

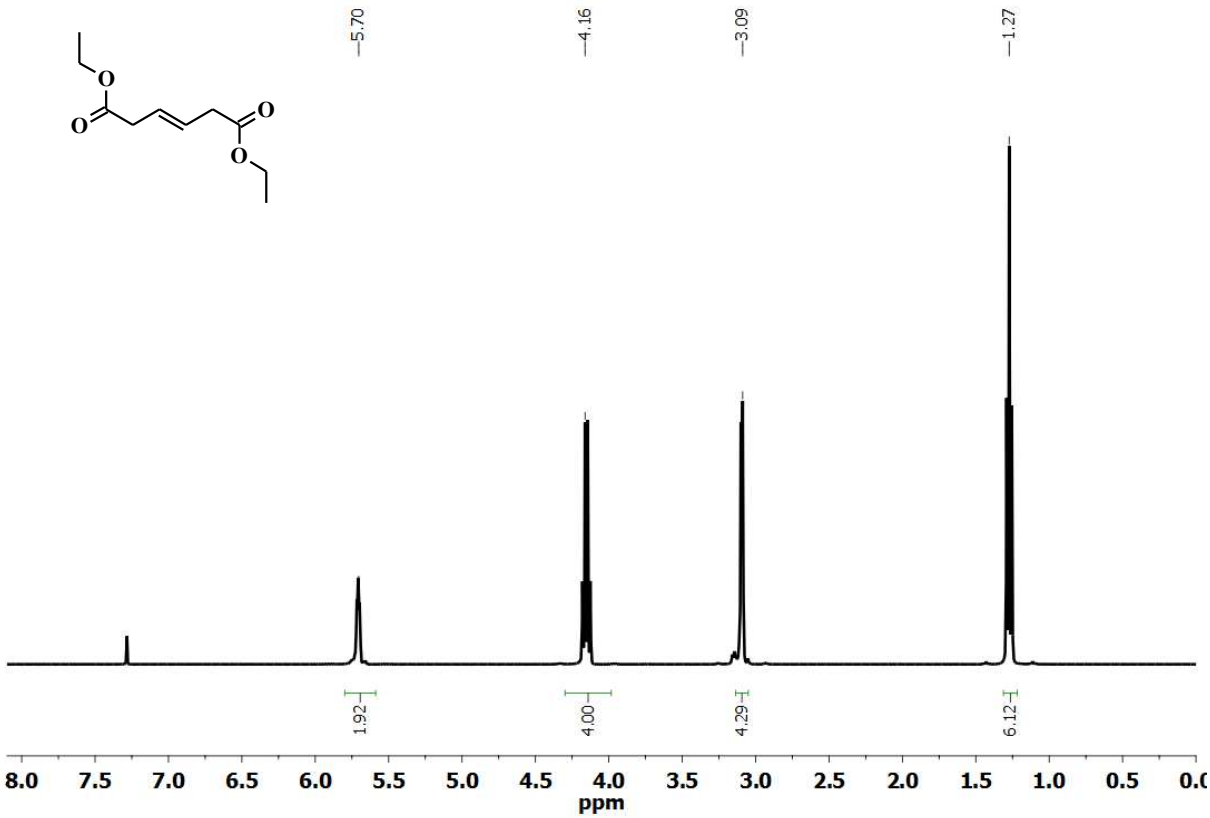

^{1}H NMR spectrum of **3**.

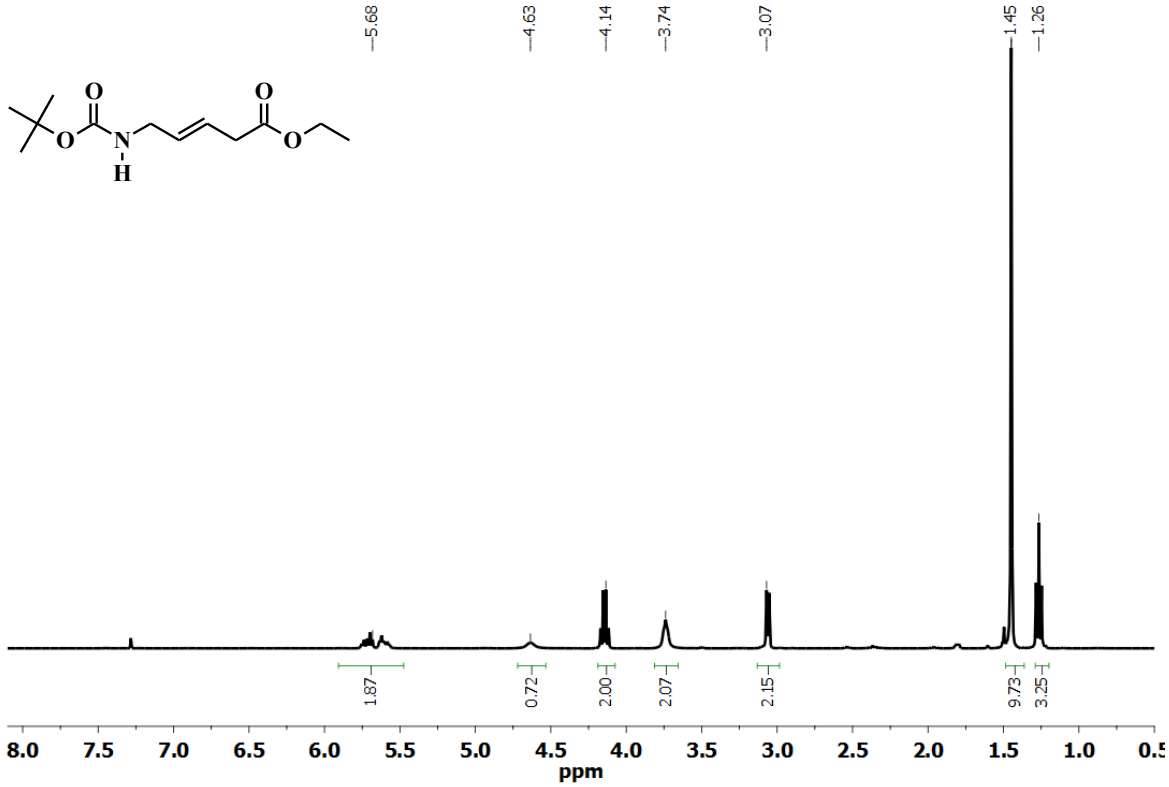

^{1}H NMR spectrum of **4**.

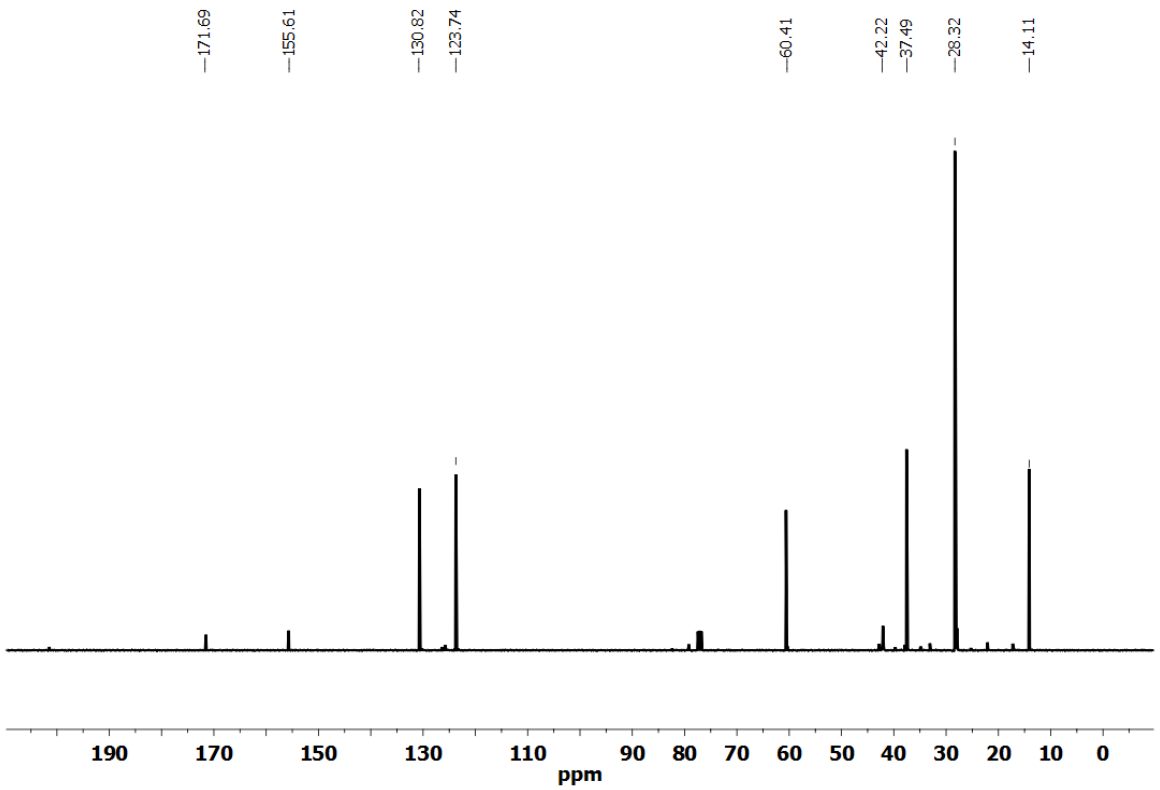

^{13}C NMR spectrum of **4**.

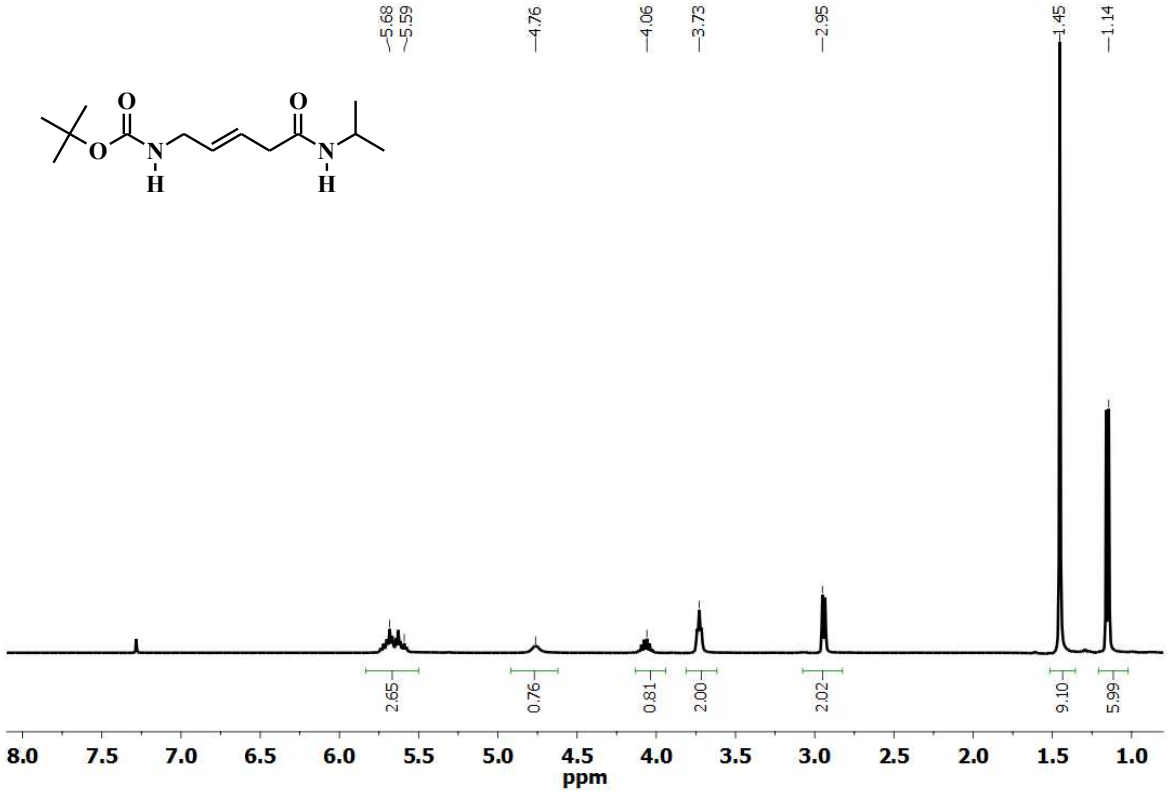

^{1}H NMR spectrum of **6**.

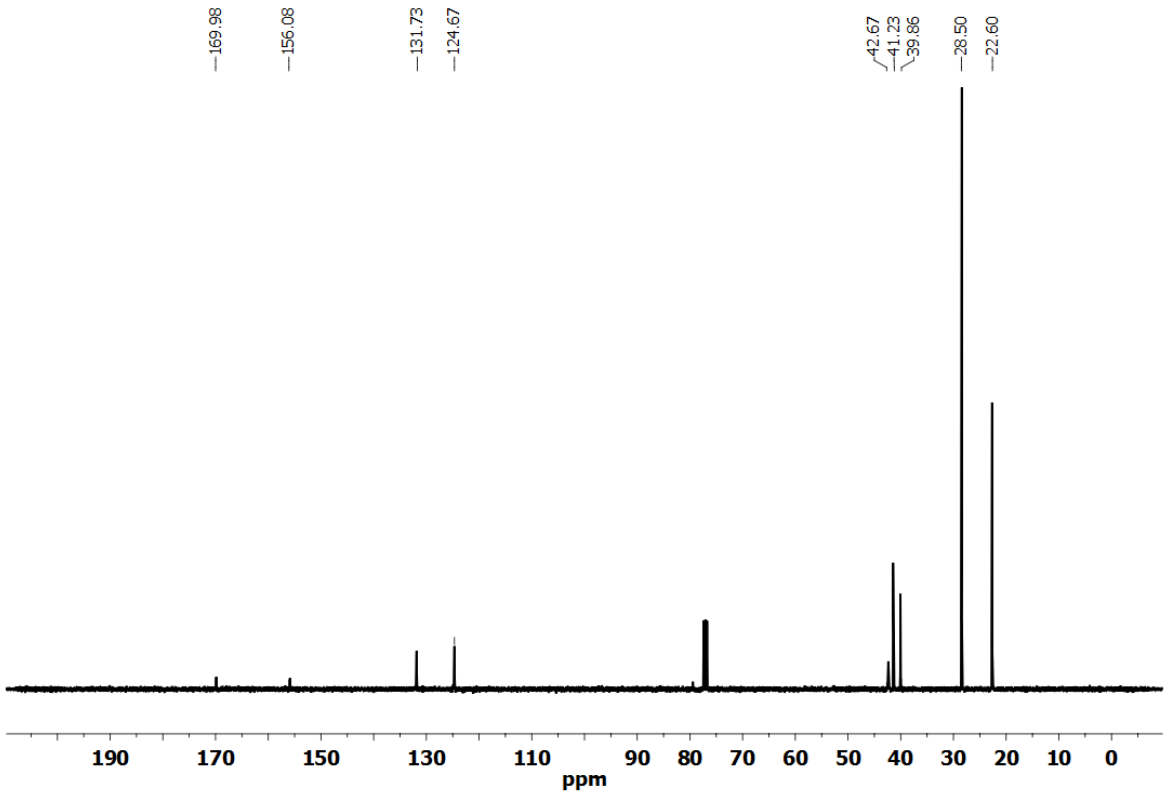

^{13}C NMR spectrum of **6**.

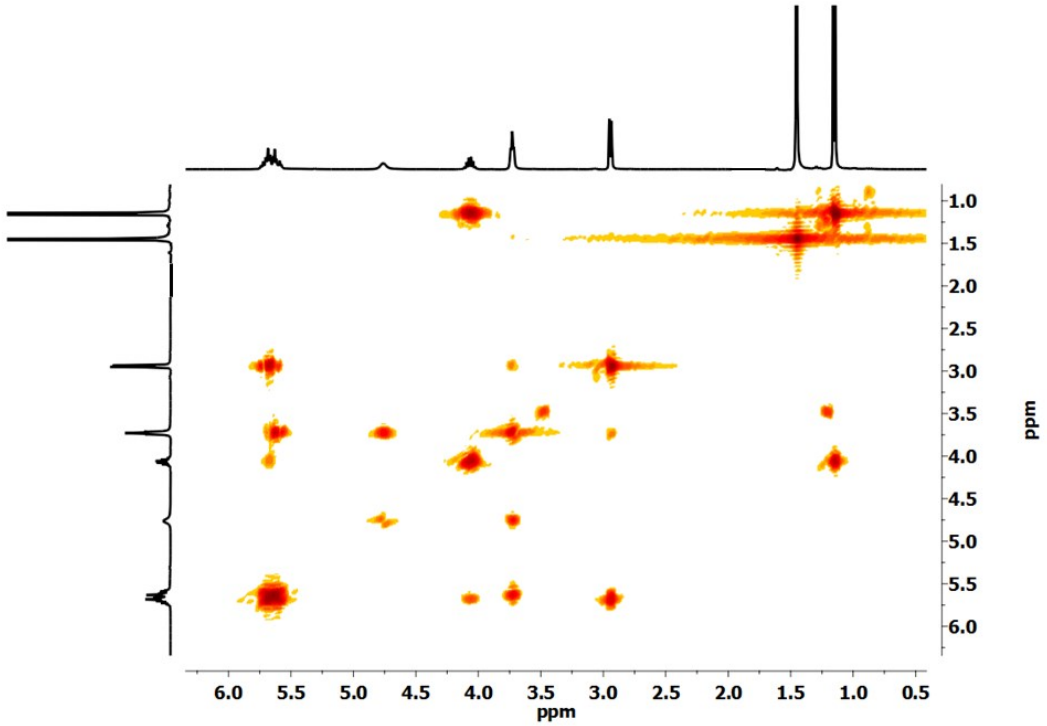

2D COSY NMR spectrum of **6.**

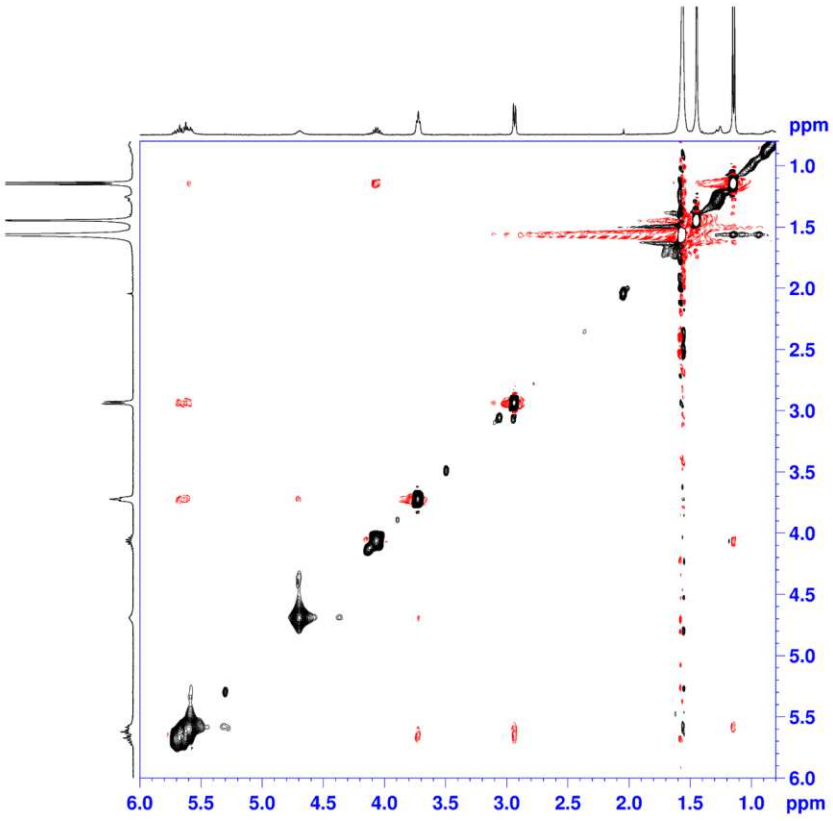

2D NOESY NMR spectrum of **6.**

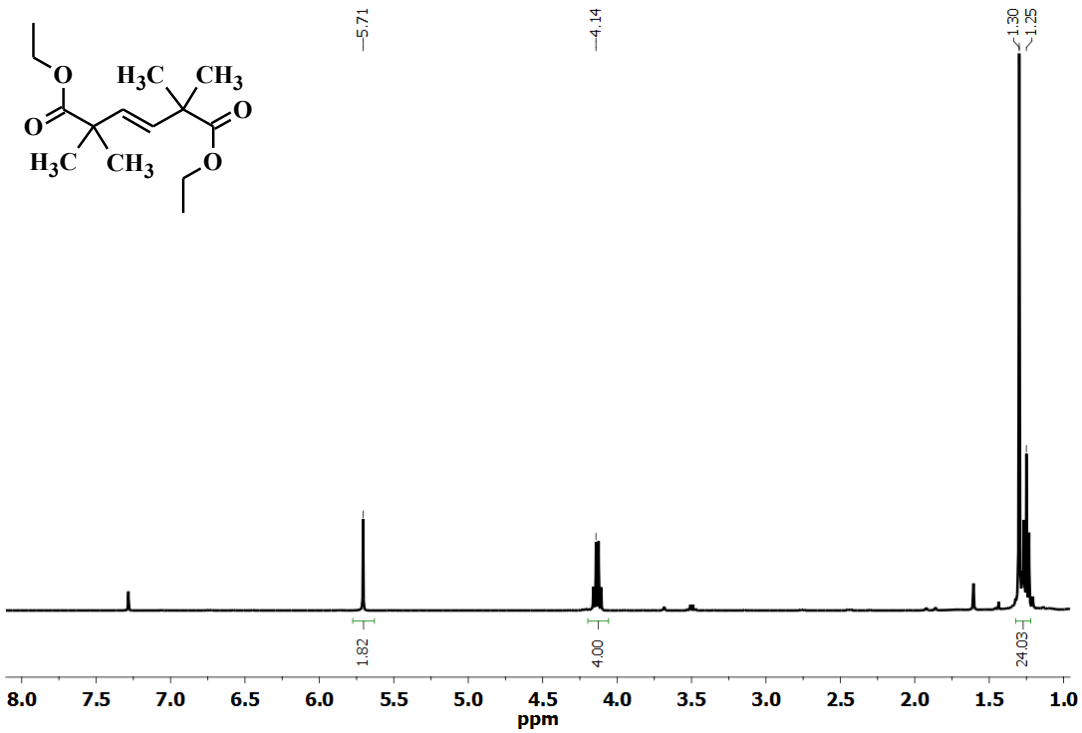

^{1}H NMR spectrum of **7.**

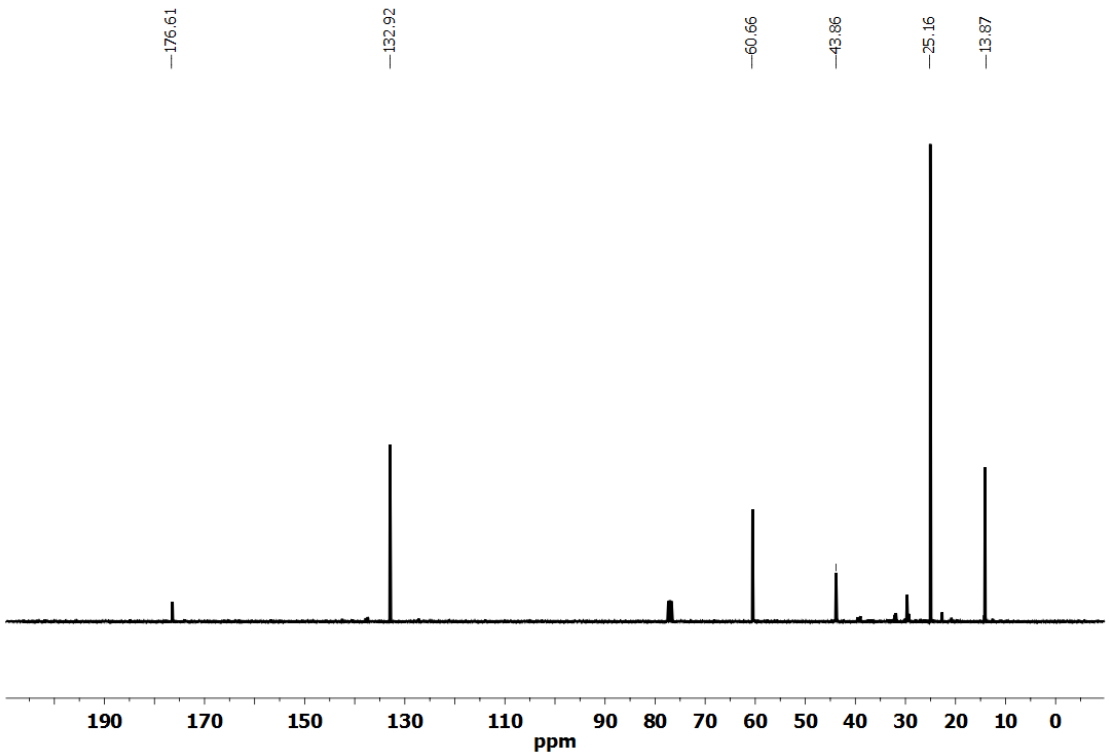

^{13}C NMR spectrum of **7.**

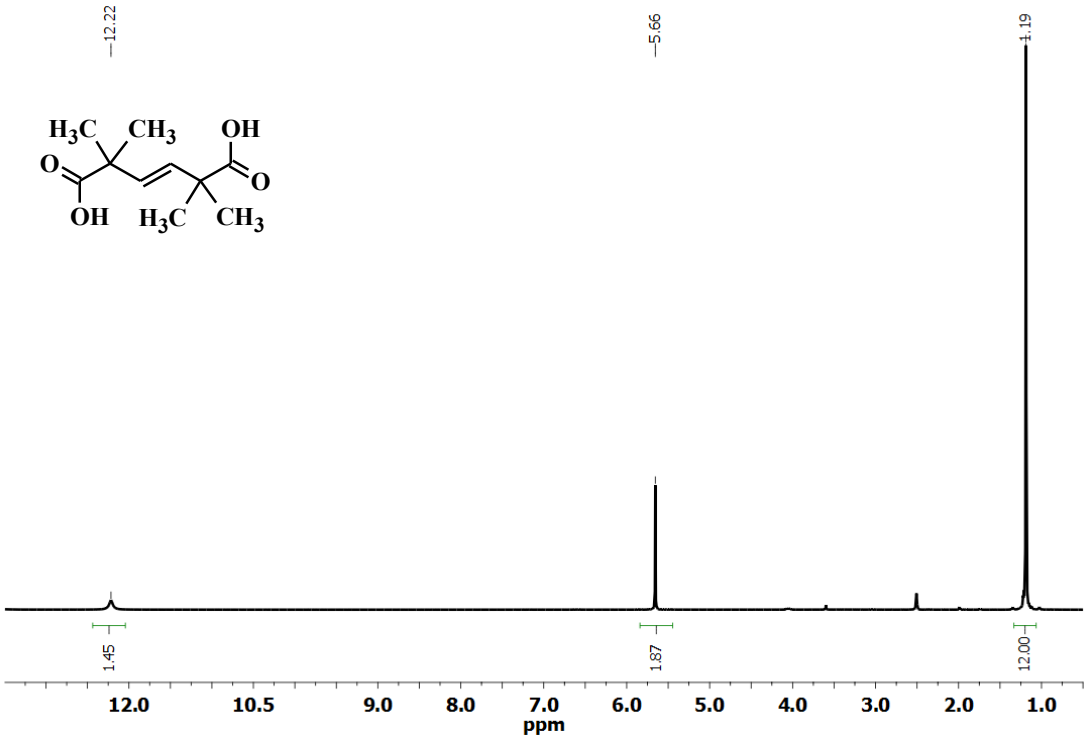

^{1}H NMR spectrum of **8.**

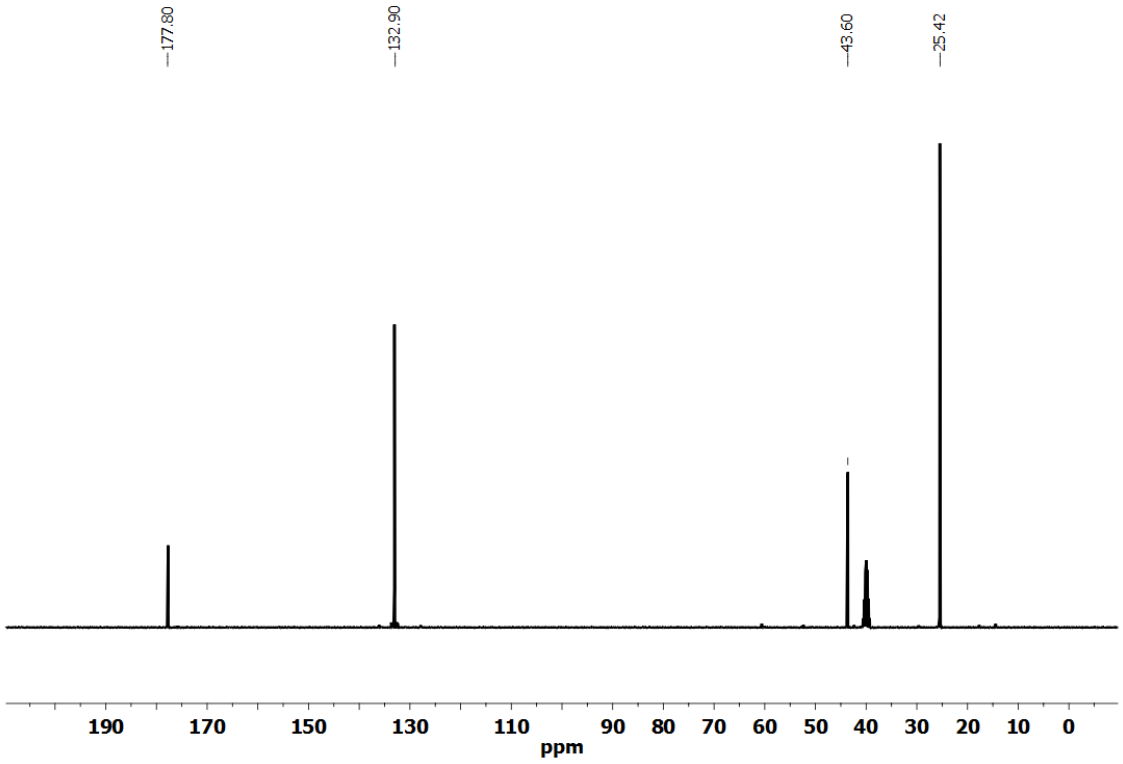

^{13}C NMR spectrum of **8.**

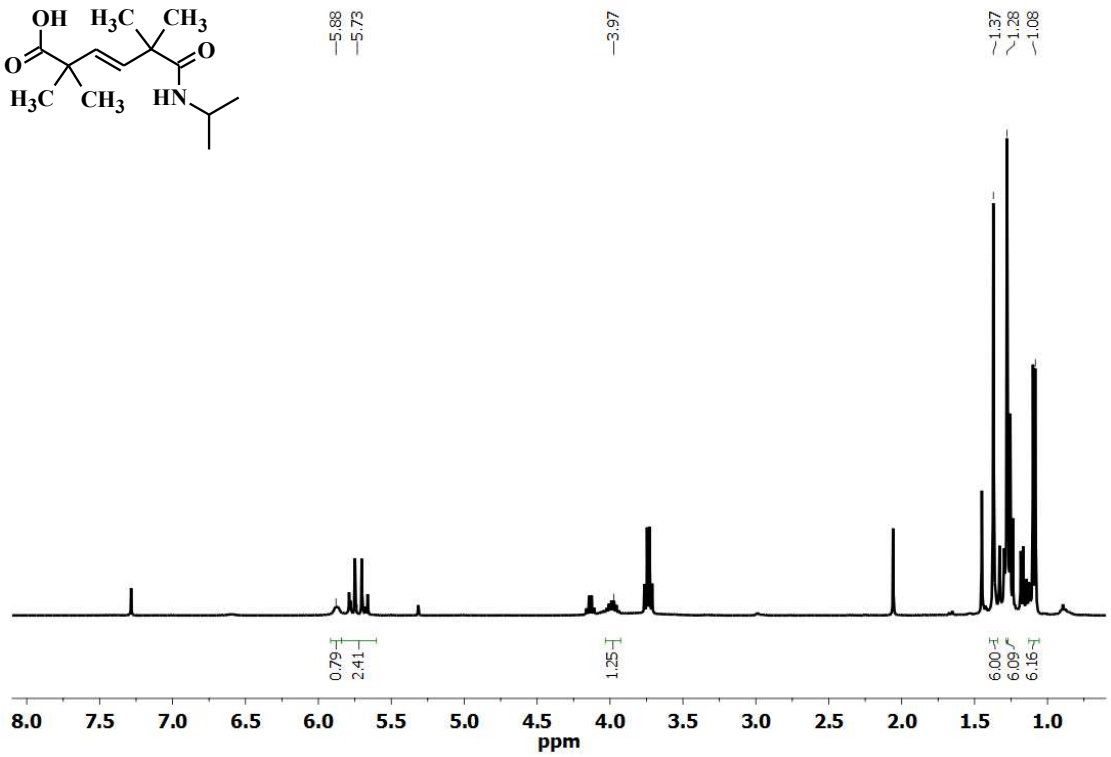

^{1}H NMR spectrum of **9.**

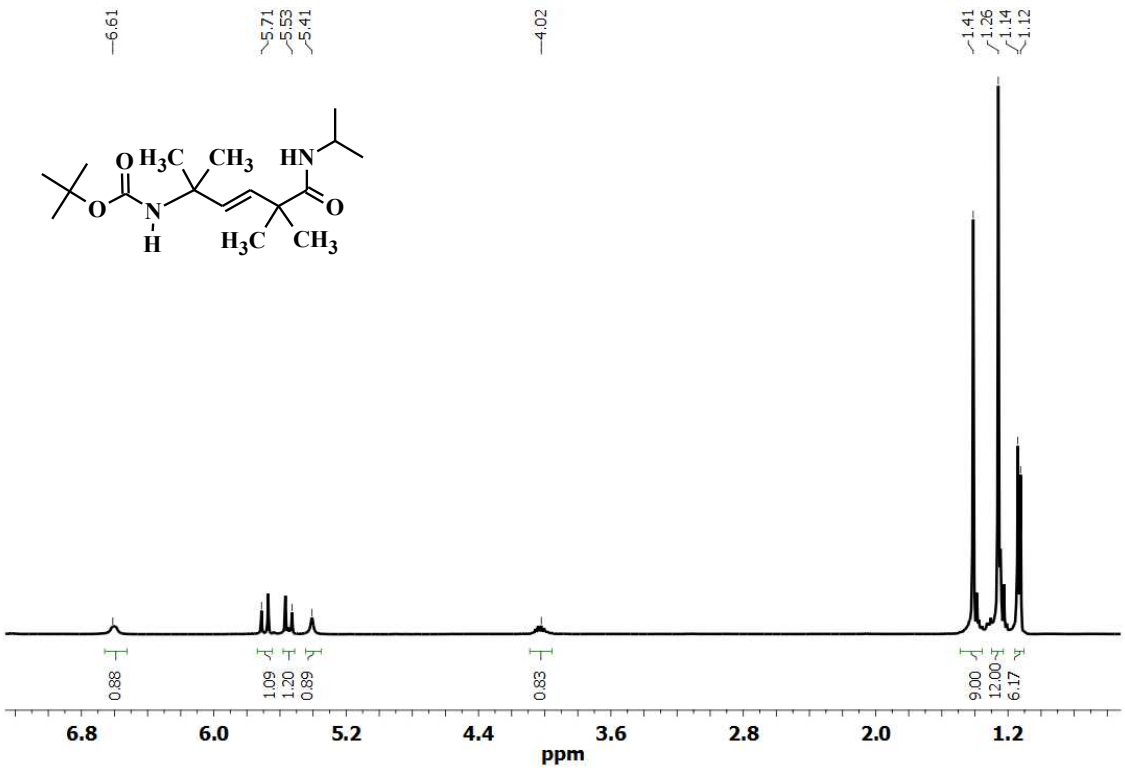

^{1}H NMR spectrum of **10.**

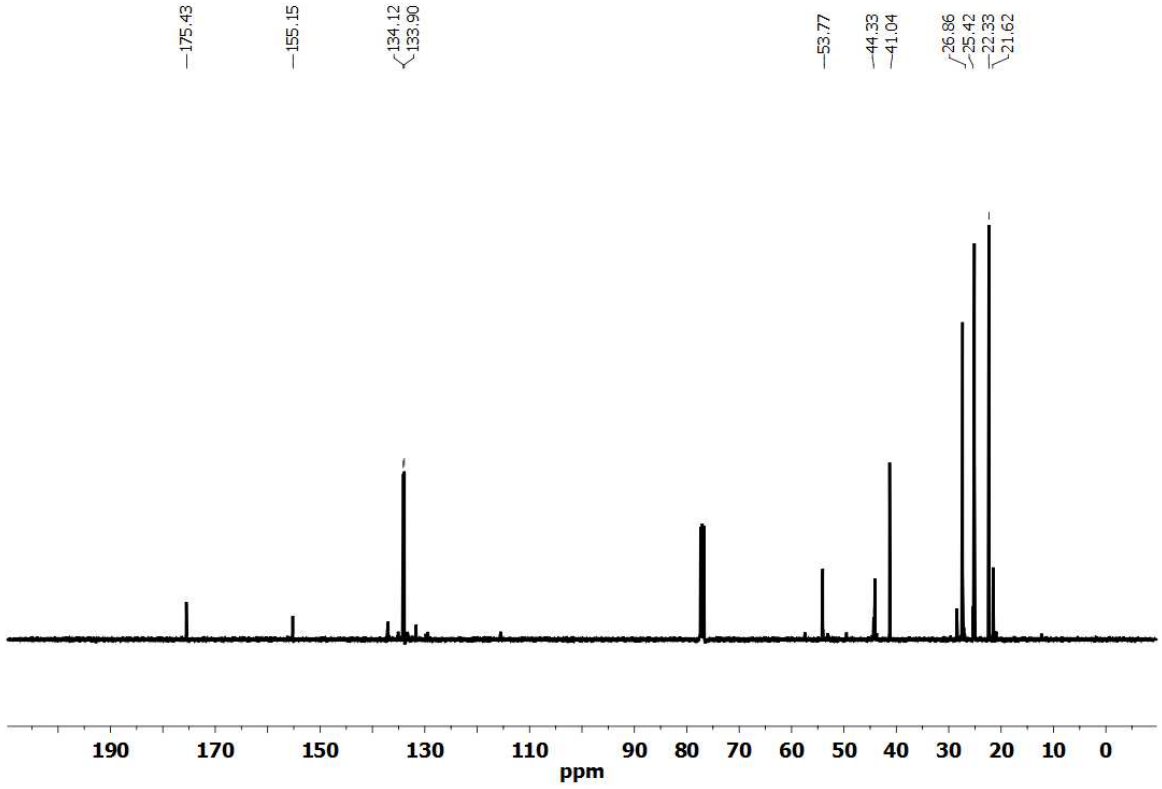

^{13}C NMR spectrum of **10.**

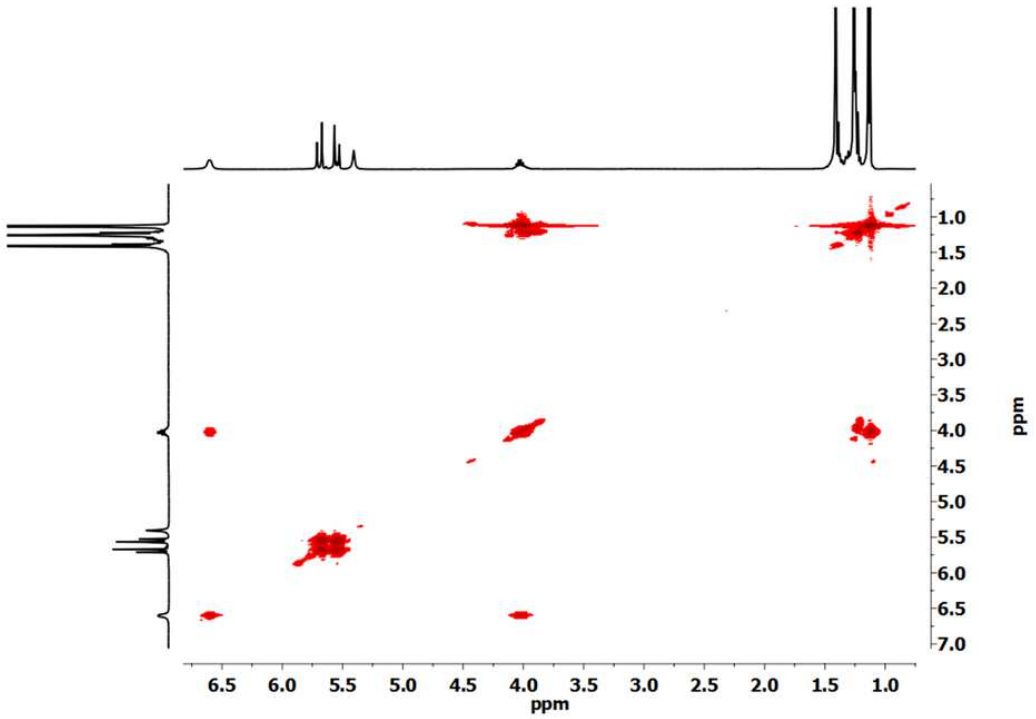

2D COSY NMR spectrum of **10**.

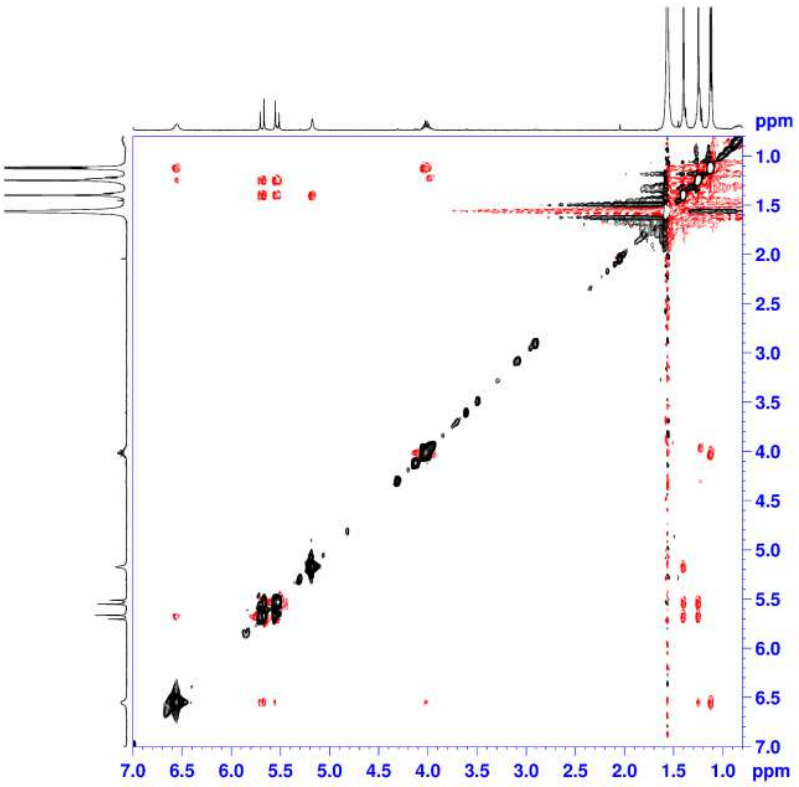

2D NOESY NMR spectrum of **10**.

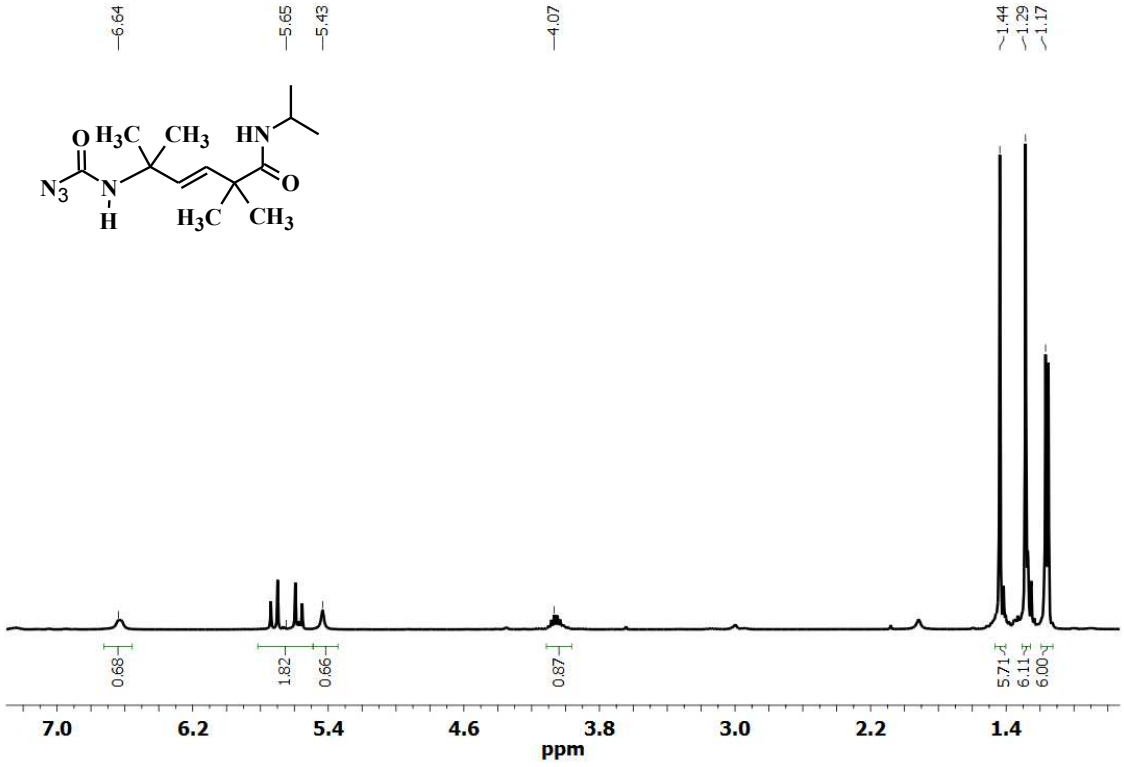

^{1}H NMR spectrum of **11.**

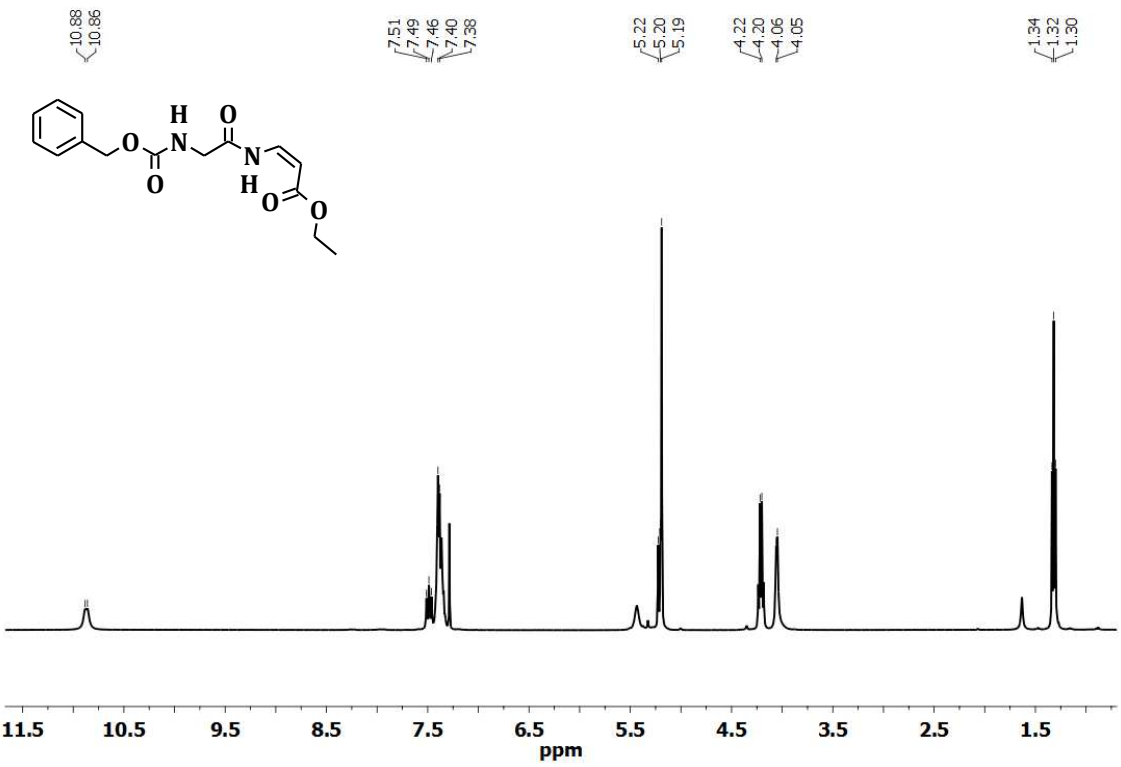

^{1}H NMR spectrum of **Z-Gly-Δ^{Z}βAla-OEt (1).**

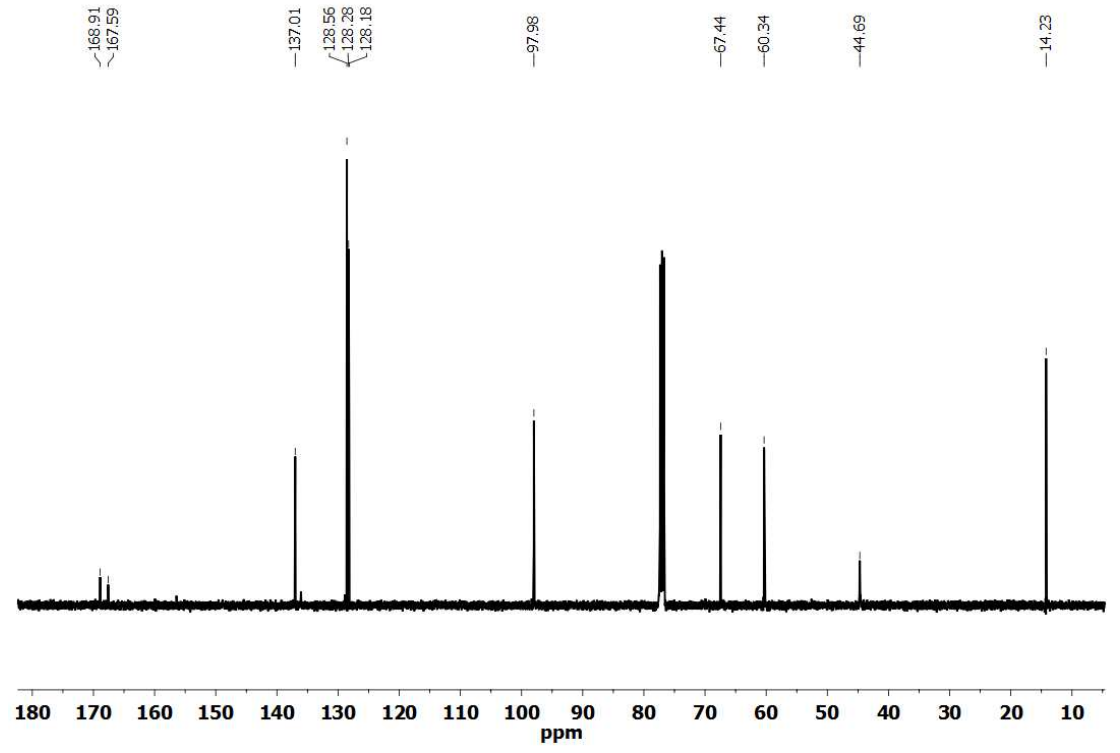

^{13}C NMR spectrum of **Z-Gly-Δ^{Z}βAla-OEt (1).**

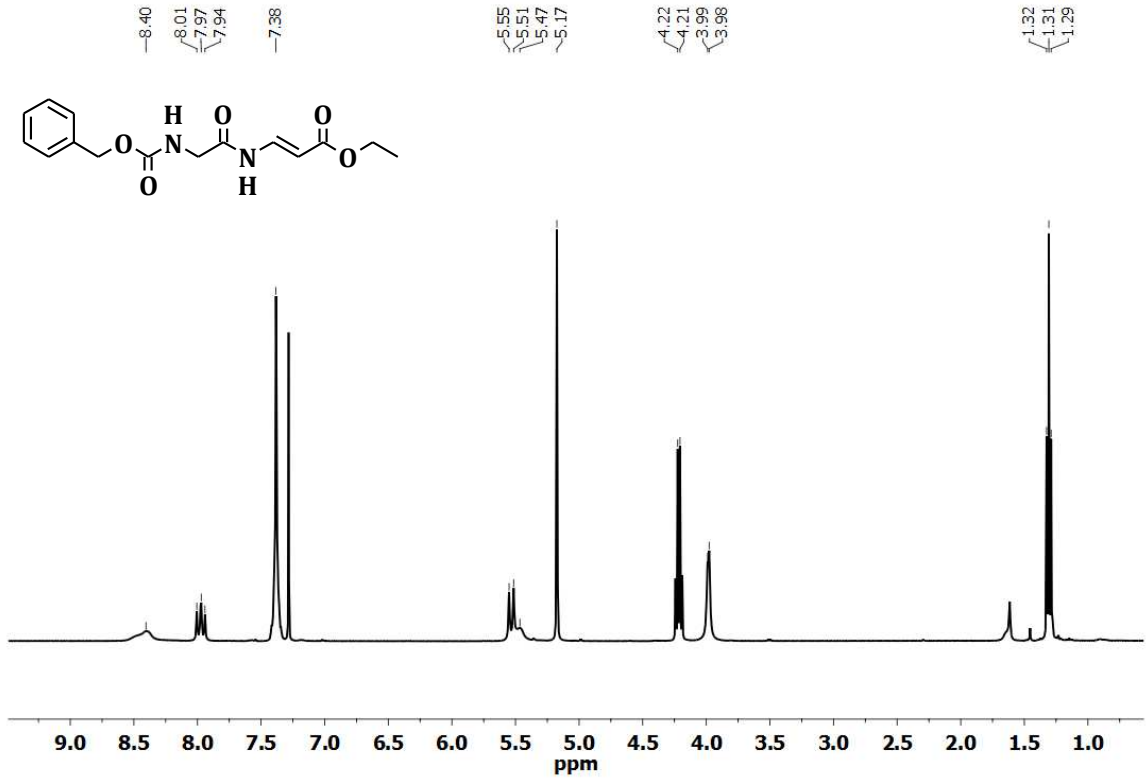

^{1}H NMR spectrum of **Z-Gly-Δ^{E}βAla-OEt (2).**

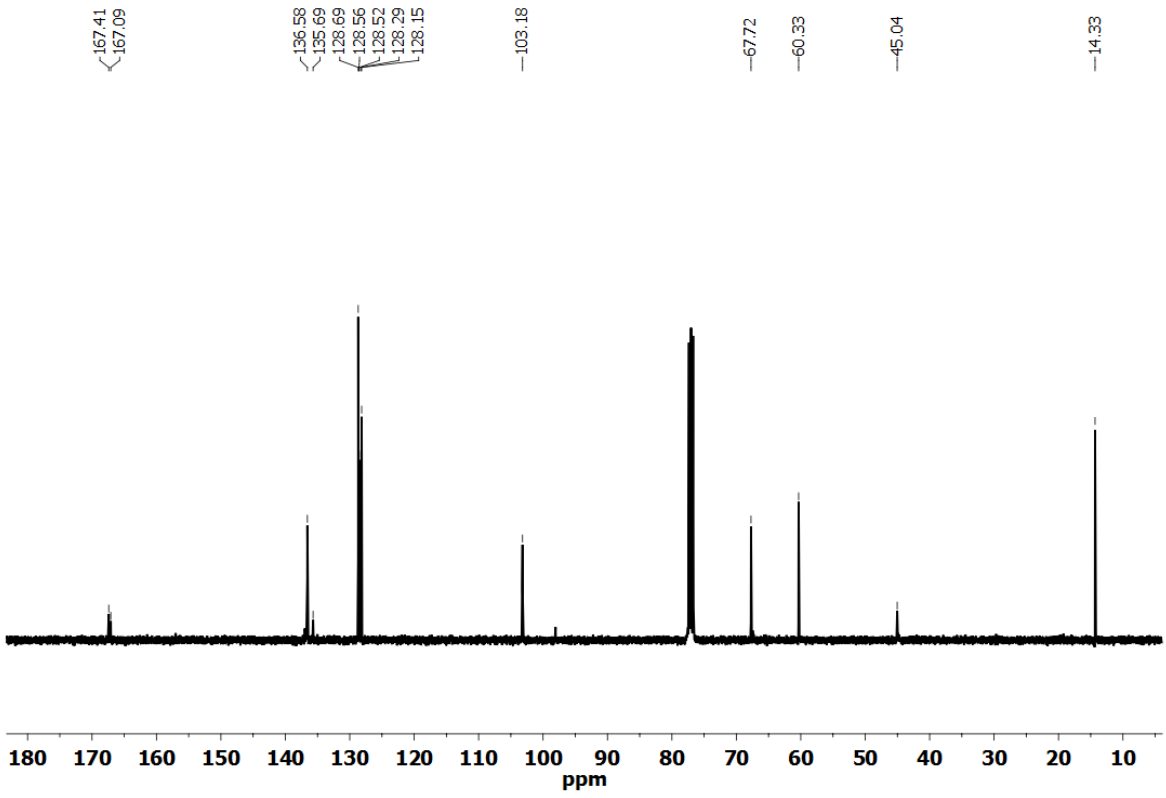

^{13}C NMR spectrum of **Z-Gly-Δ^{E}βAla-OEt (2).**

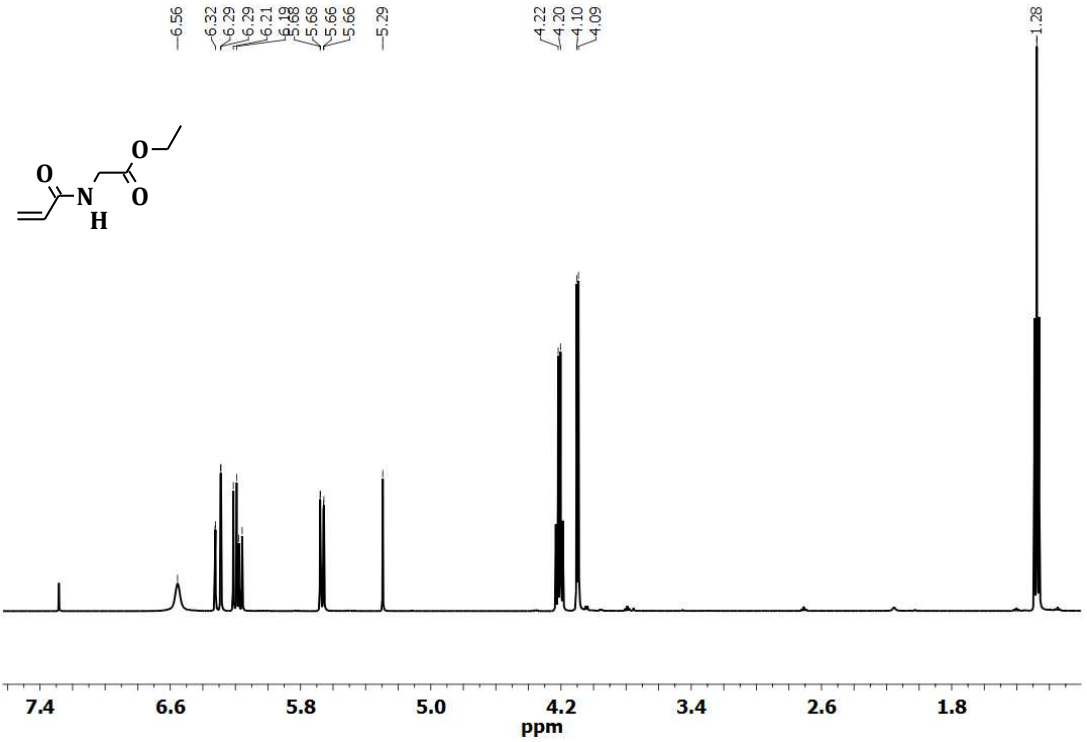

^{1}H NMR spectrum of **Acr-Gly-OEt.**

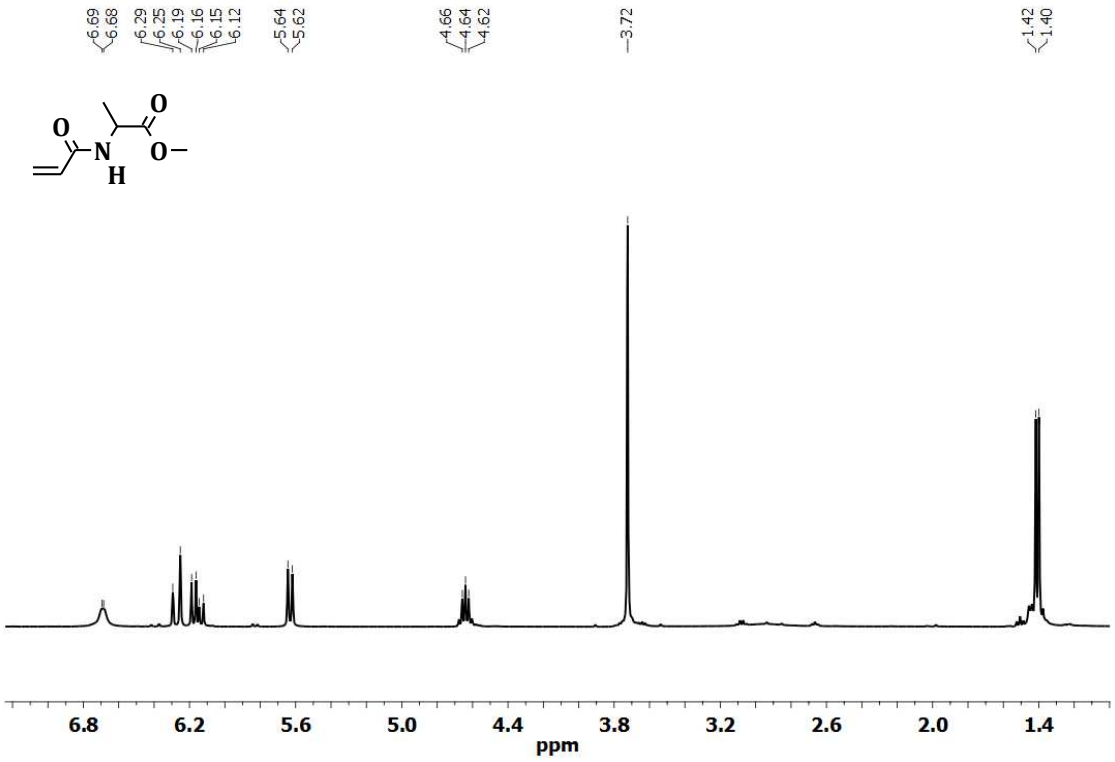

^{1}H NMR spectrum of **Acr-Ala-OMe.**

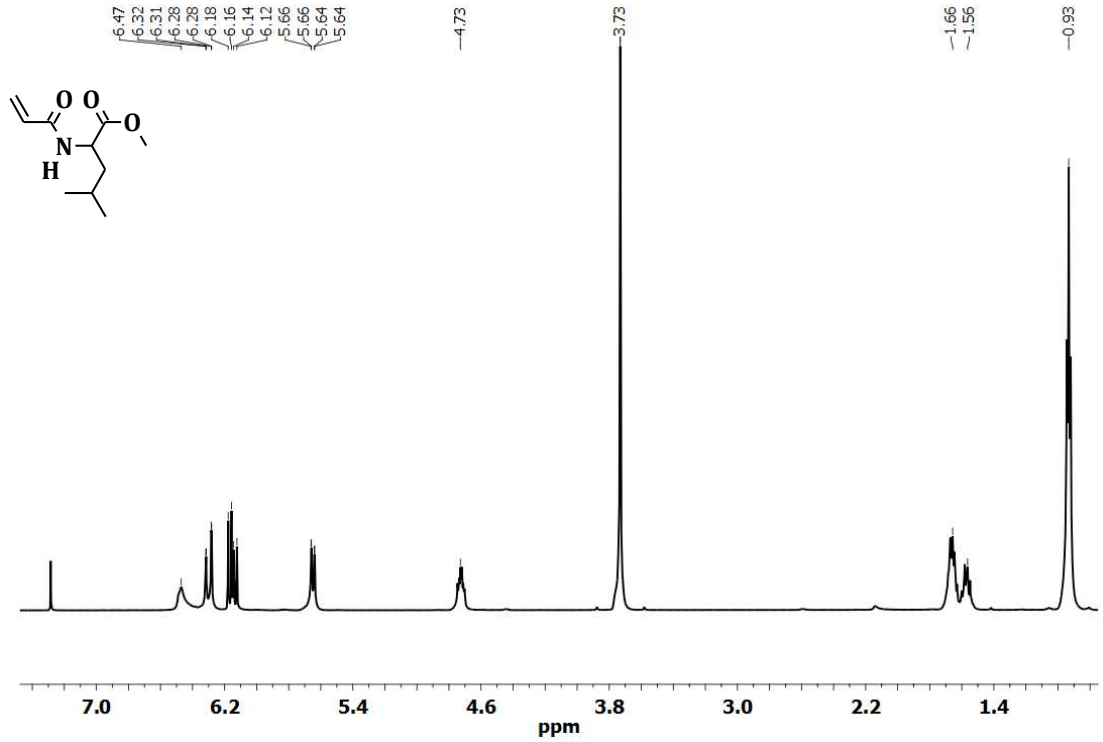

^{1}H NMR spectrum of **Acr-Leu-OMe.**

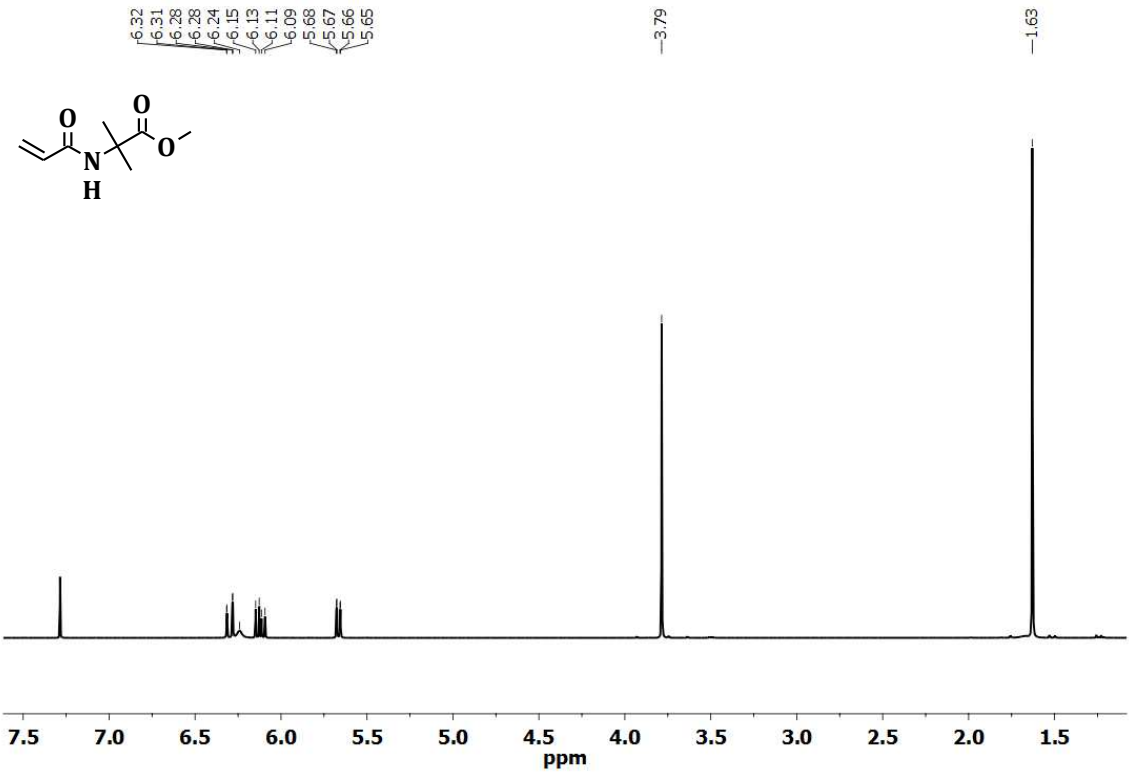

^{1}H NMR spectrum of **Acr-Aib-OMe.**

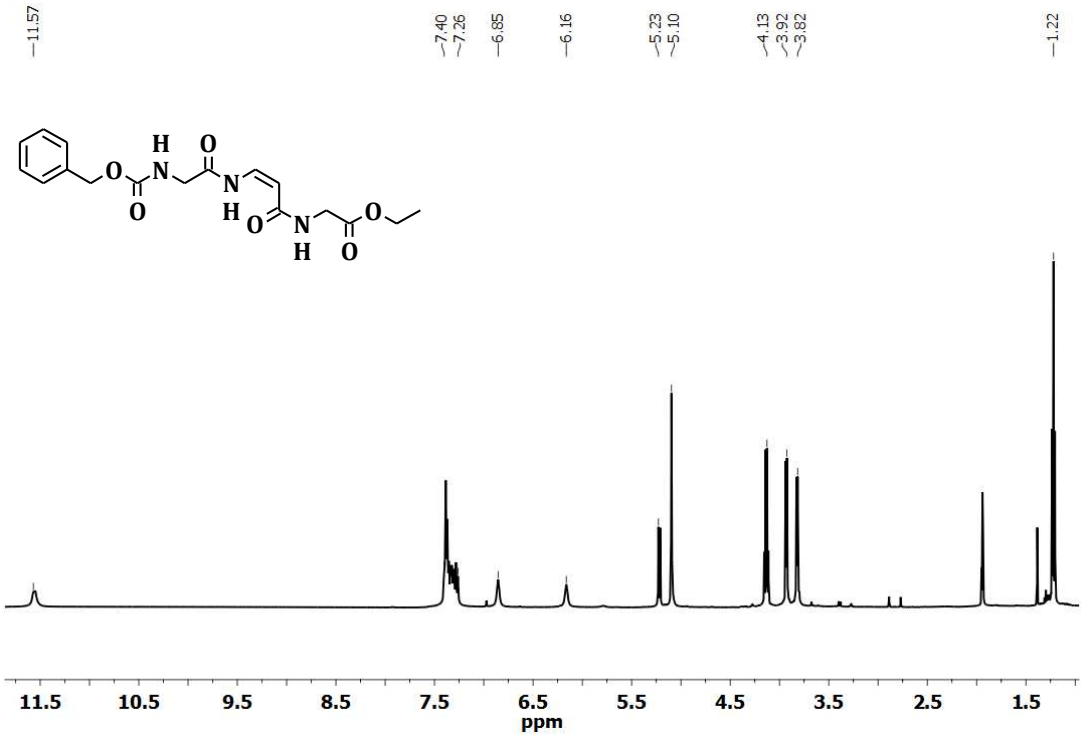

^{1}H NMR spectrum of **Z-Gly-Δ^{Z}βAla-Gly-OEt.**

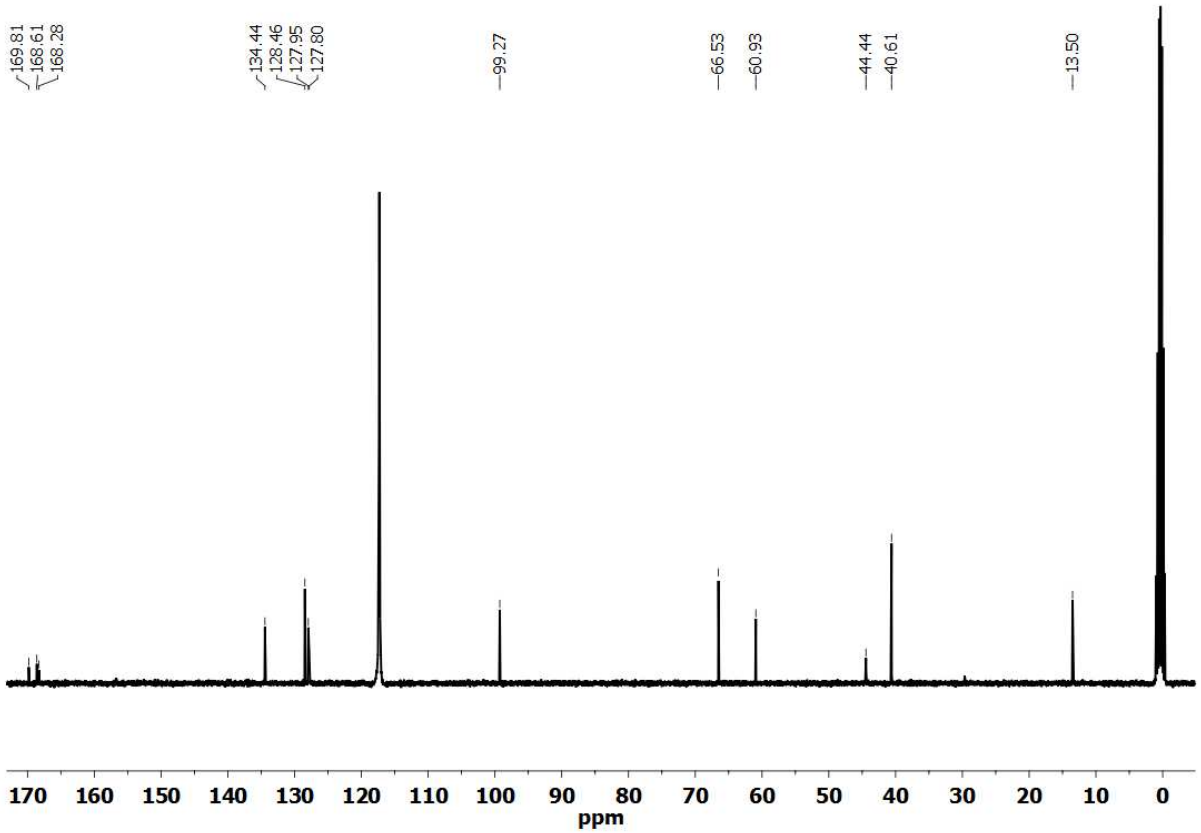

^{13}C NMR spectrum of **Z-Gly-Δ^{Z}βAla-Gly-OEt.**

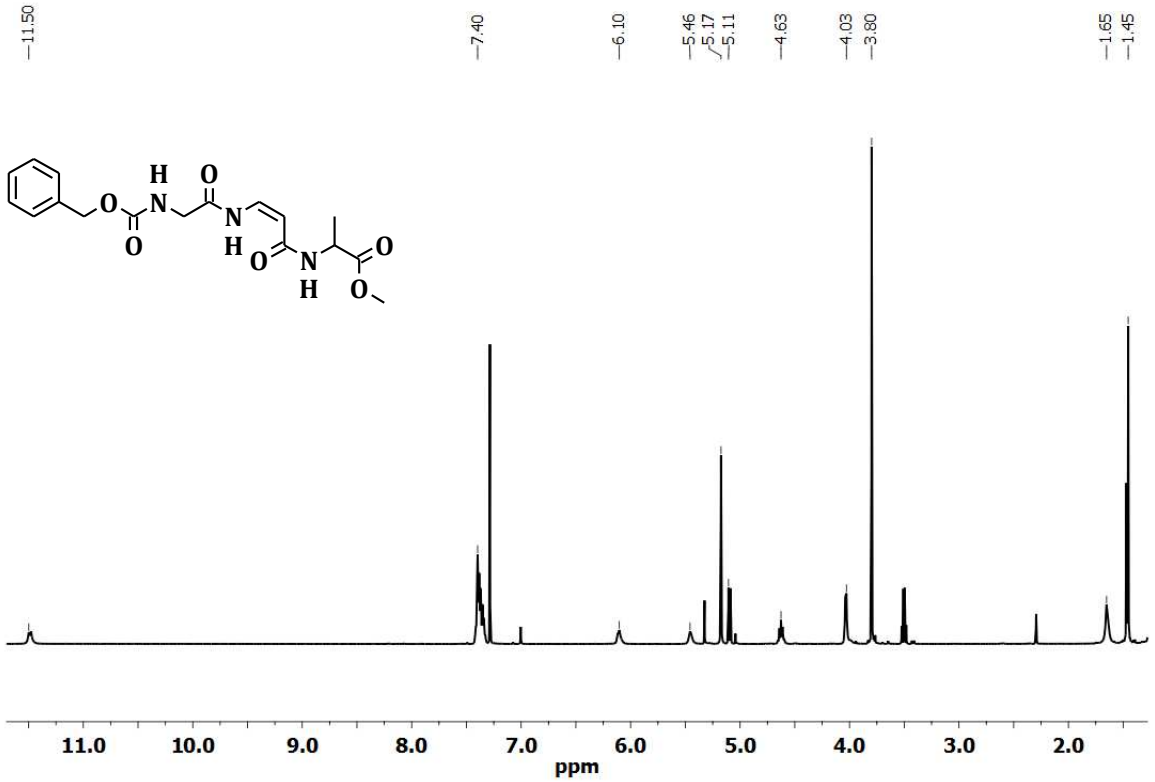

^{1}H NMR spectrum of **Z-Gly-Δ^{Z}βAla-Ala-OMe.**

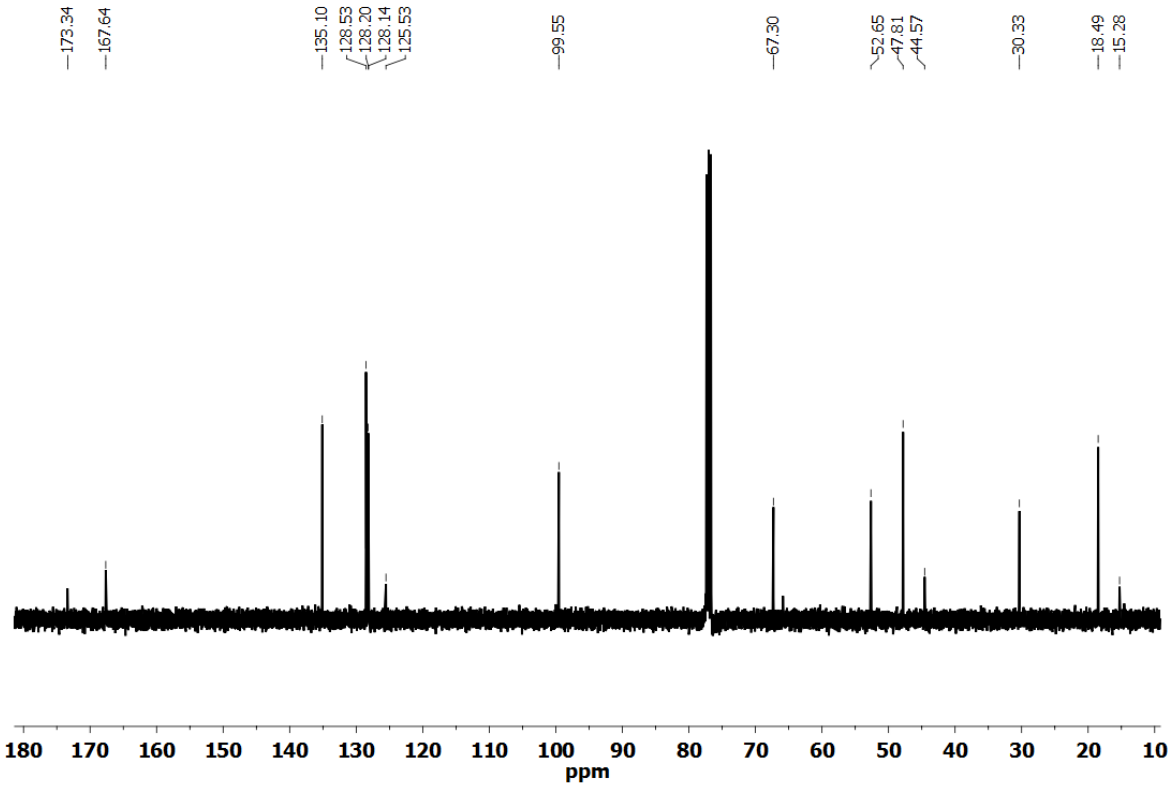

^{13}C NMR spectrum of **Z-Gly-Δ^{Z}βAla-Ala-OMe.**

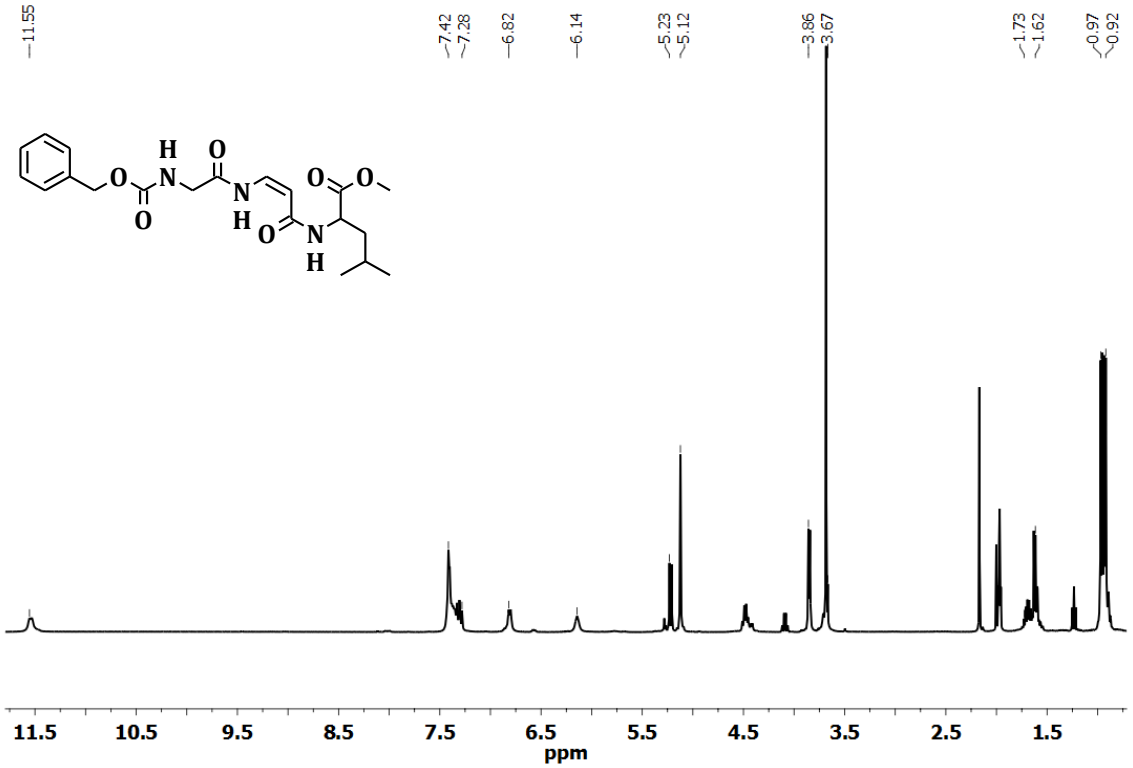

^{1}H NMR spectrum of **Z-Gly-Δ^{Z}βAla-Leu-OMe (3).**

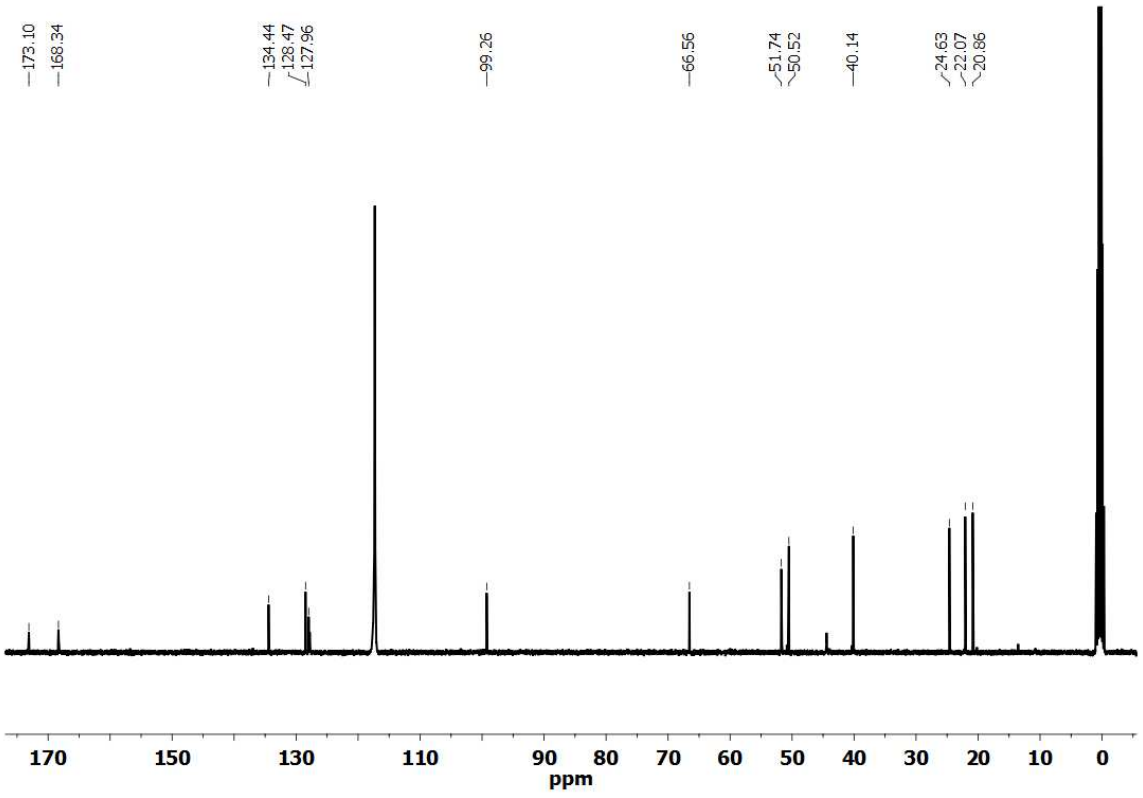

^{13}C NMR spectrum of **Z-Gly-Δ^{Z}βAla-Leu-OMe (3).**

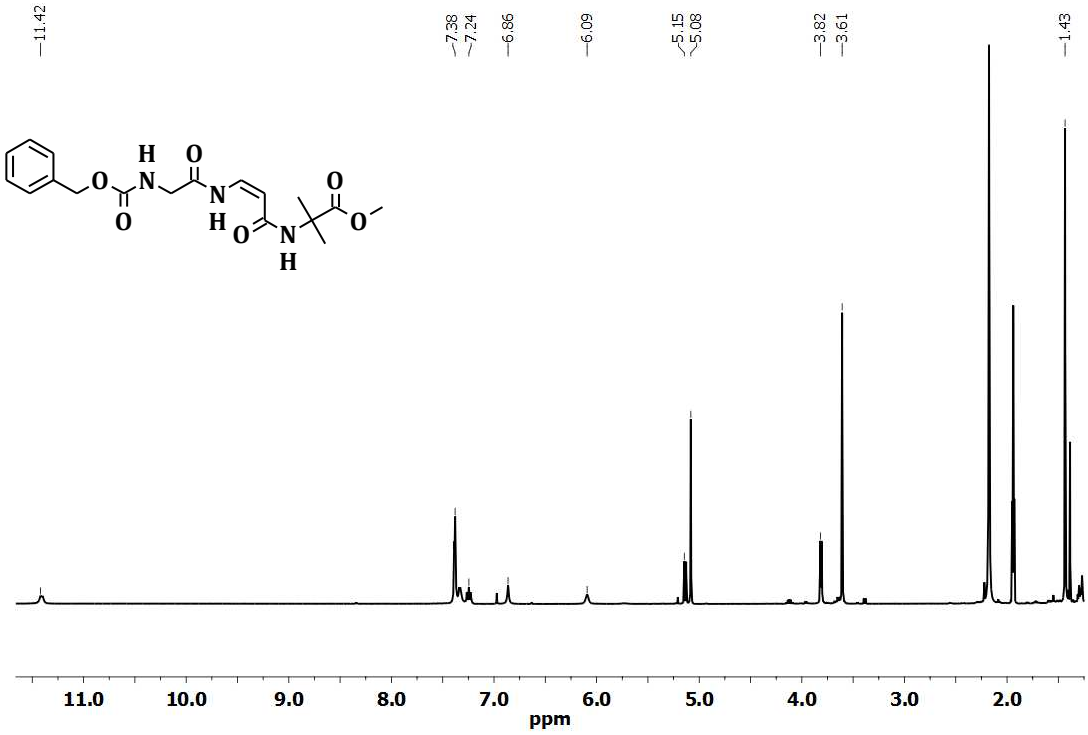

^{1}H NMR spectrum of **Z-Gly-Δ^{Z}βAla-Aib-OMe.**

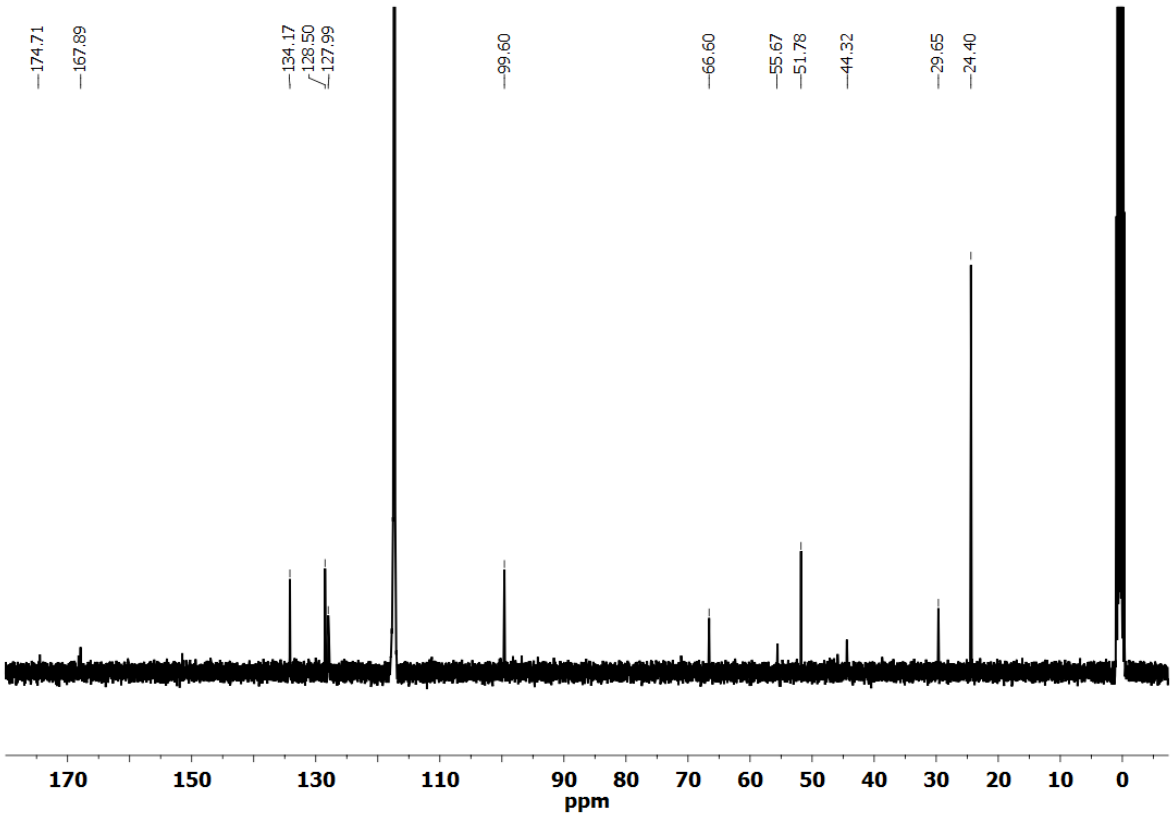

^{13}C NMR spectrum of **Z-Gly-Δ^{Z}βAla-Aib-OMe.**

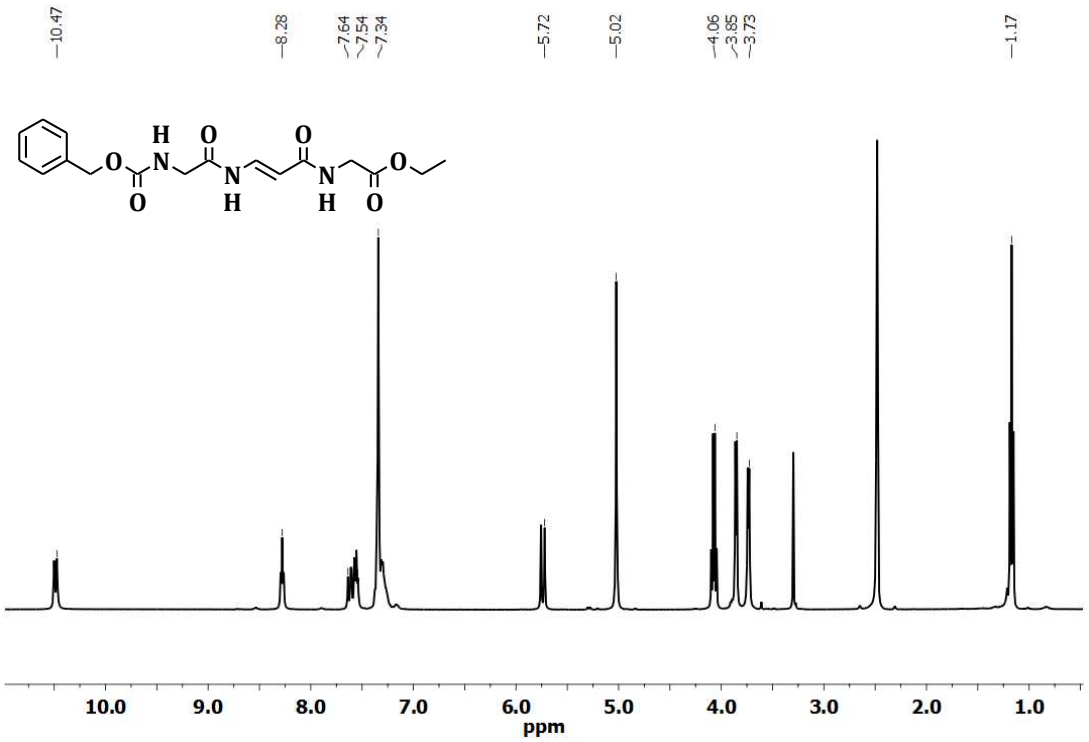

^{1}H NMR spectrum of **Z-Gly-Δ^{E}βAla-Gly-OEt.**

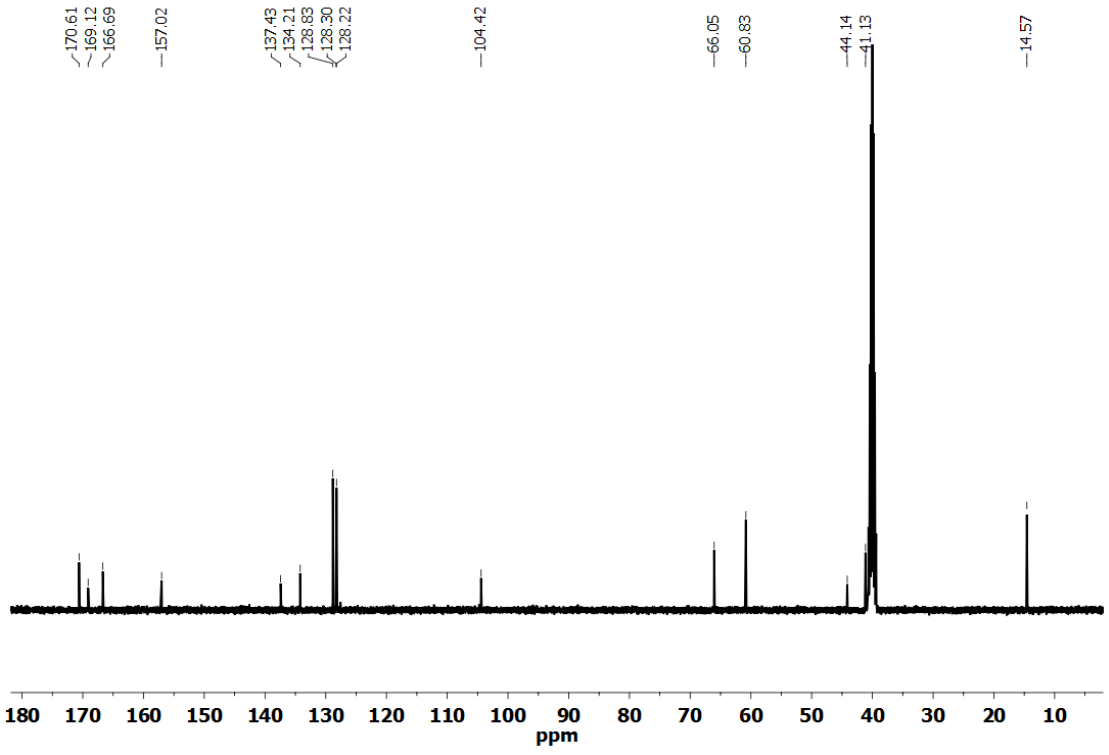

^{13}C NMR spectrum of **Z-Gly-Δ^{E}βAla-Gly-OEt.**

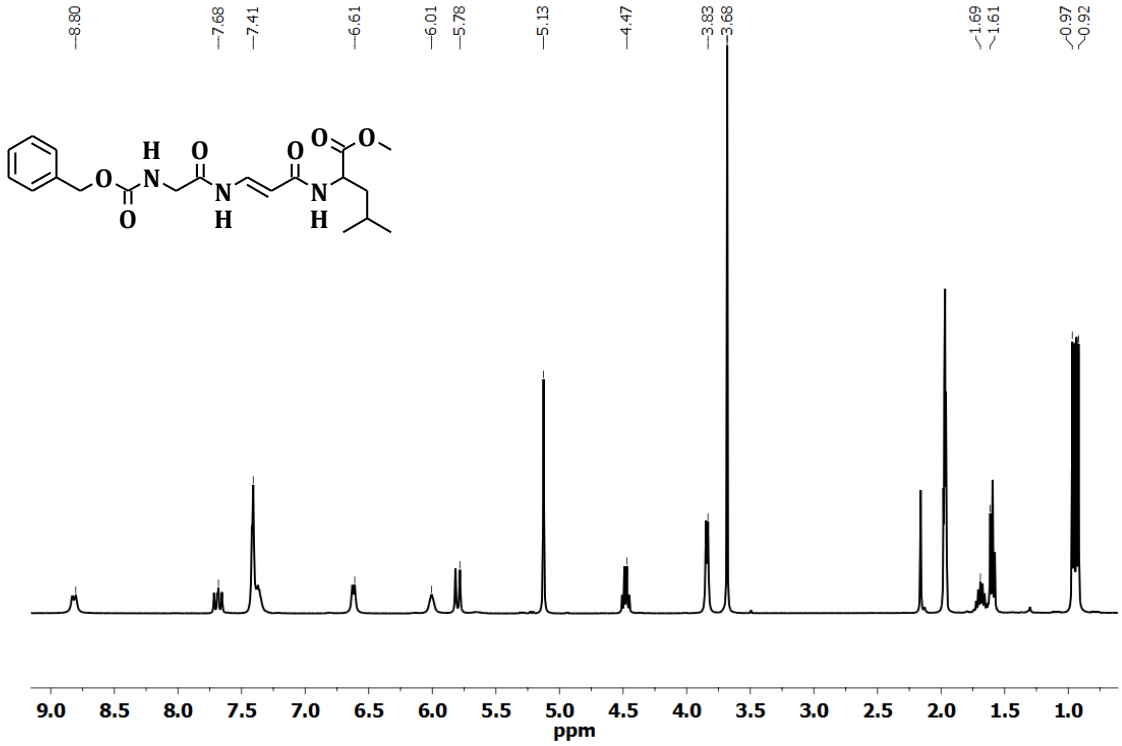

^{1}H NMR spectrum of **Z-Gly-Δ^{E}βAla-Leu-OMe (4).**

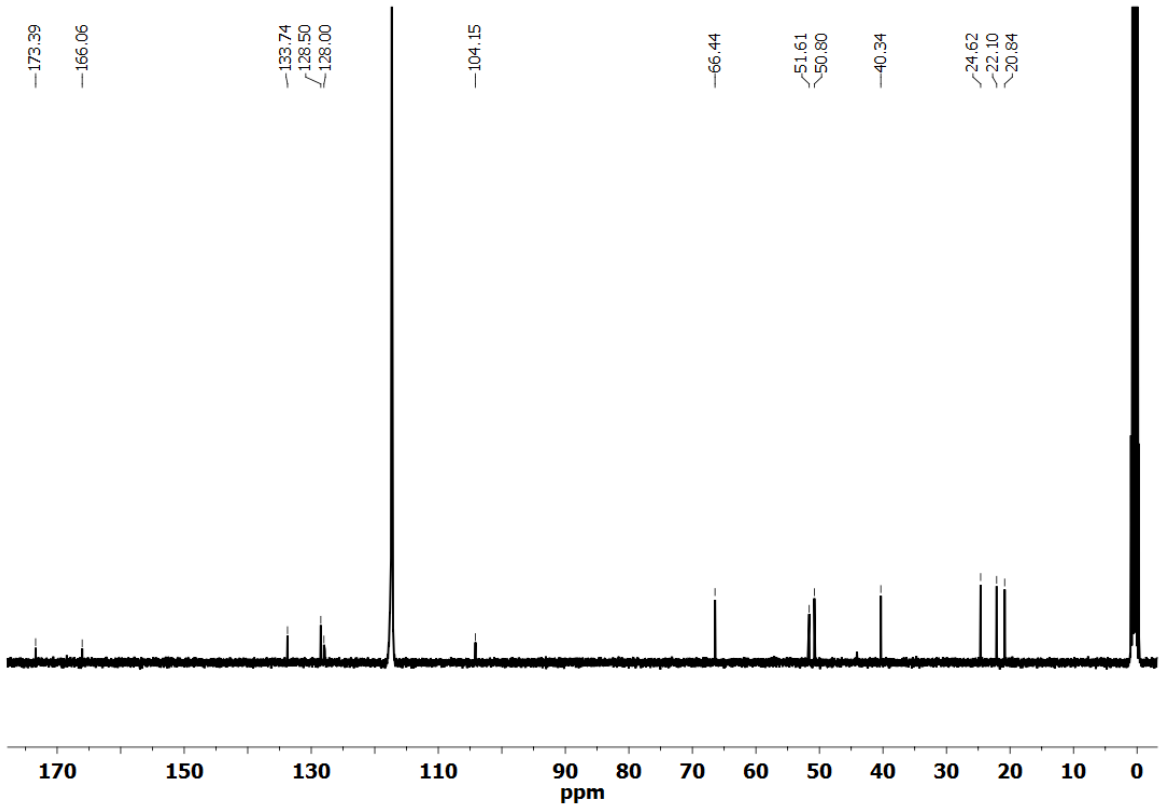

^{13}C NMR spectrum of **Z-Gly-Δ^{E}βAla-Leu-OMe (4).**

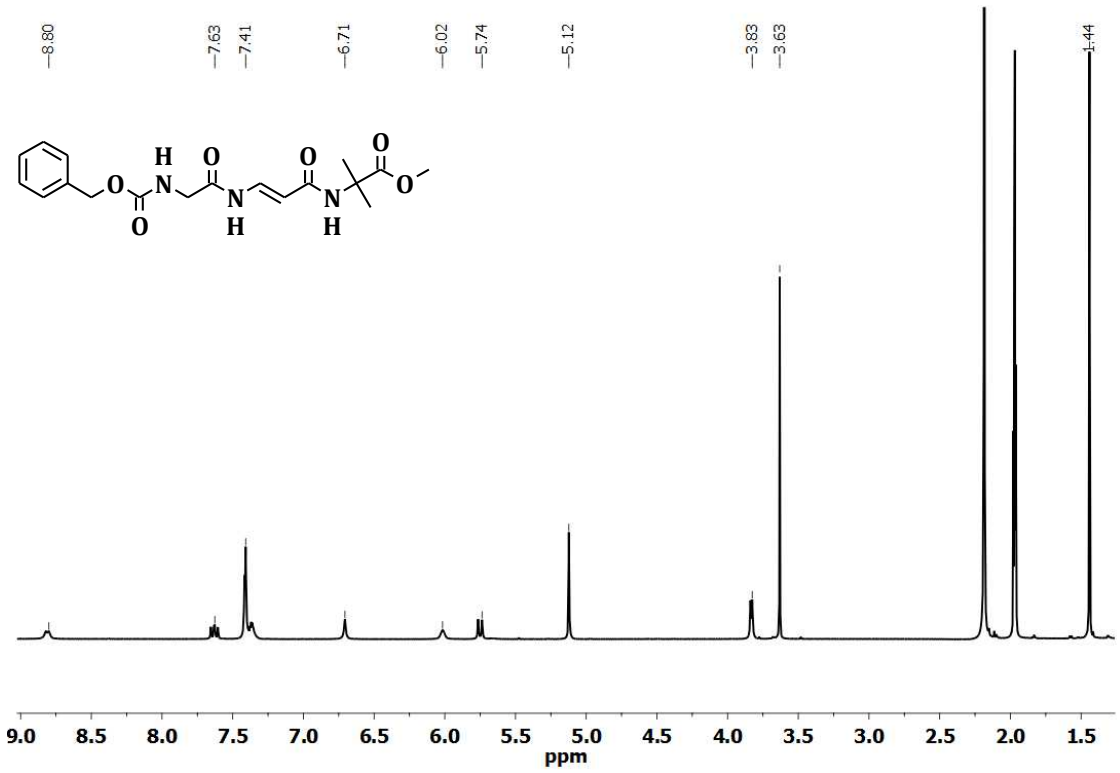

^{1}H NMR spectrum of **Z-Gly-Δ^{E}βAla-Aib-OMe.**

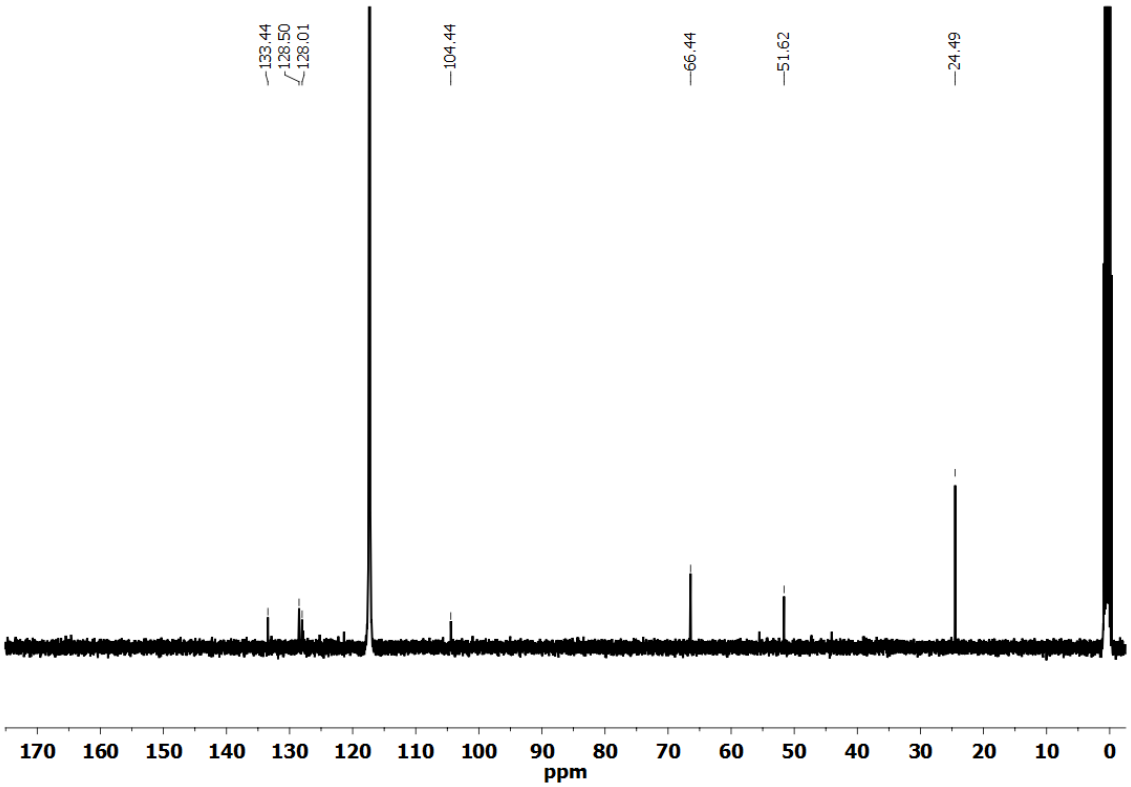

^{13}C NMR spectrum of **Z-Gly-Δ^{E}βAla-Aib-OMe.**

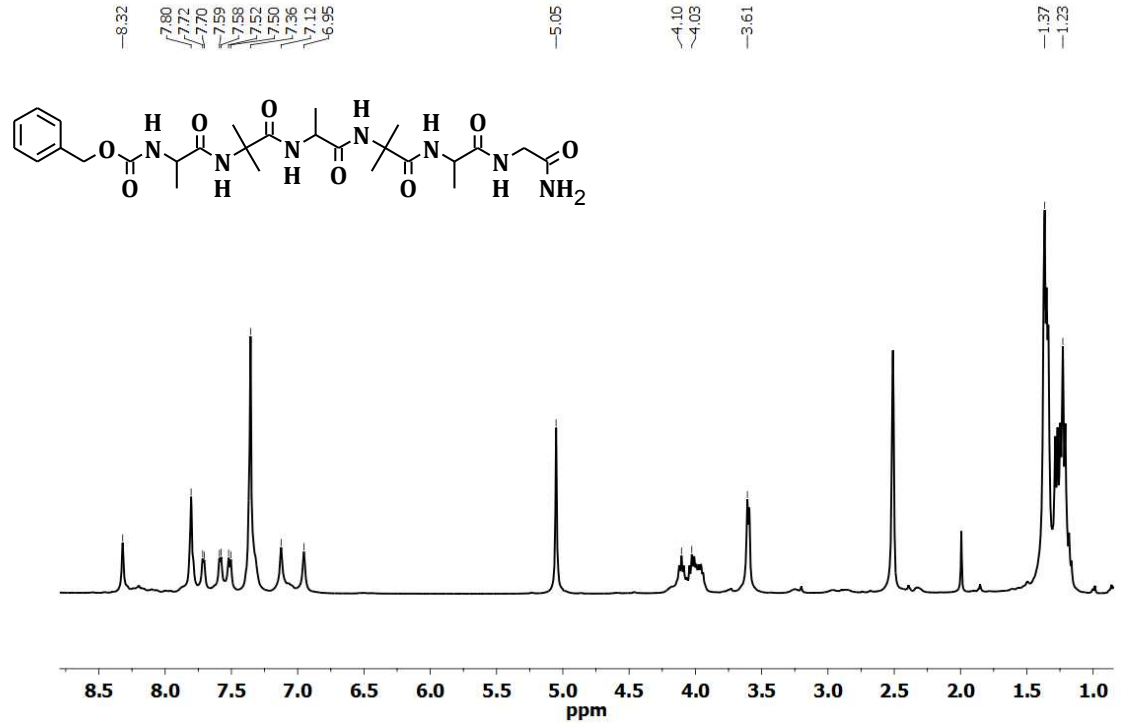

^{1}H NMR spectrum of **Z-(Ala-Aib)2-Ala-Gly-NH$_2$ (5).**

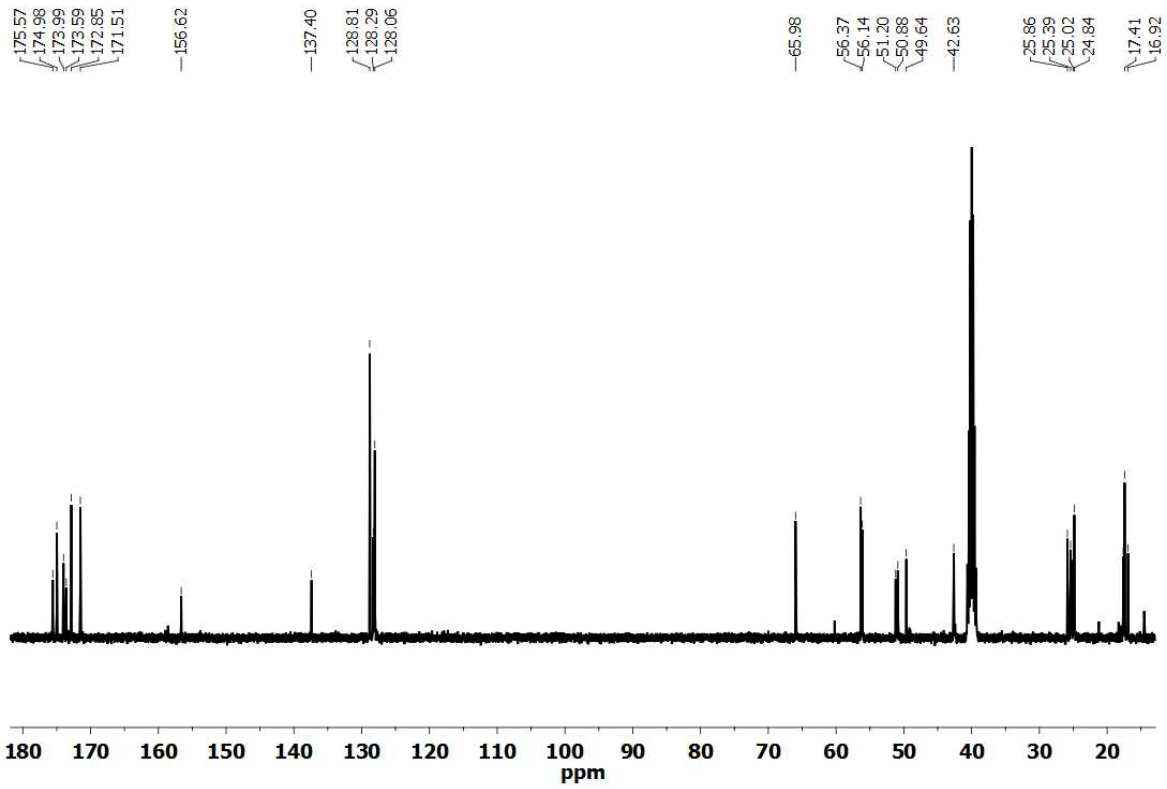

^{13}C NMR spectrum of **Z-(Ala-Aib)2-Ala-Gly-NH$_2$ (5).**

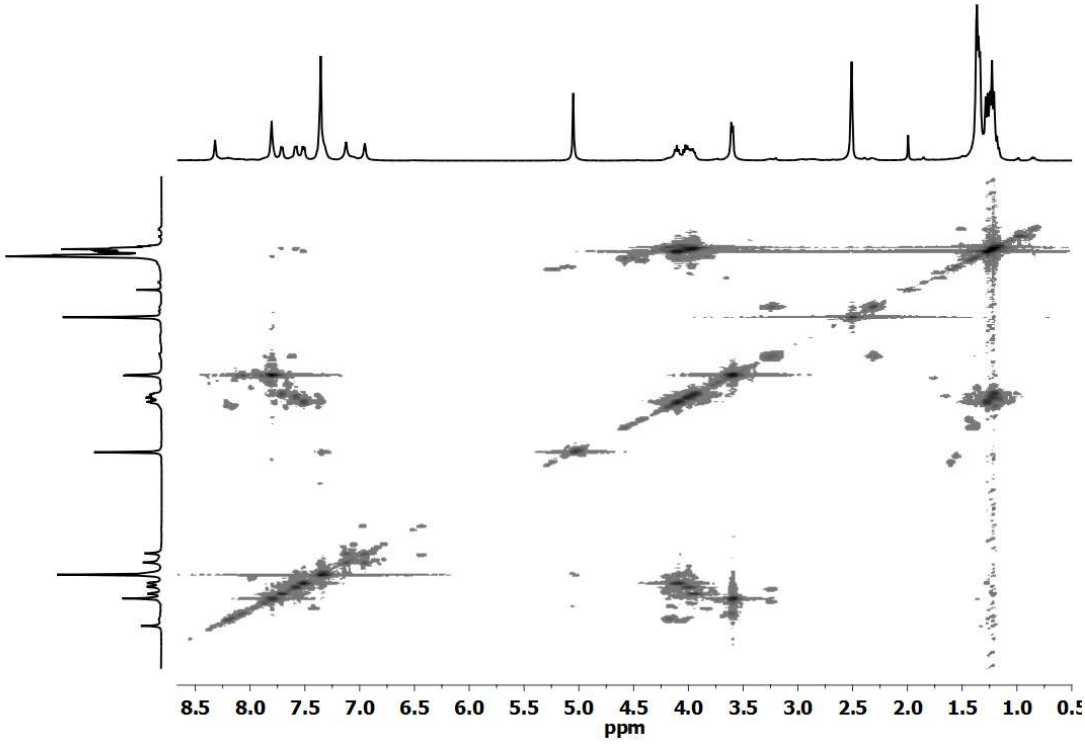

2D COSY NMR spectrum of **Z-(Ala-Aib)2-Ala-Gly-NH_2 (5).**

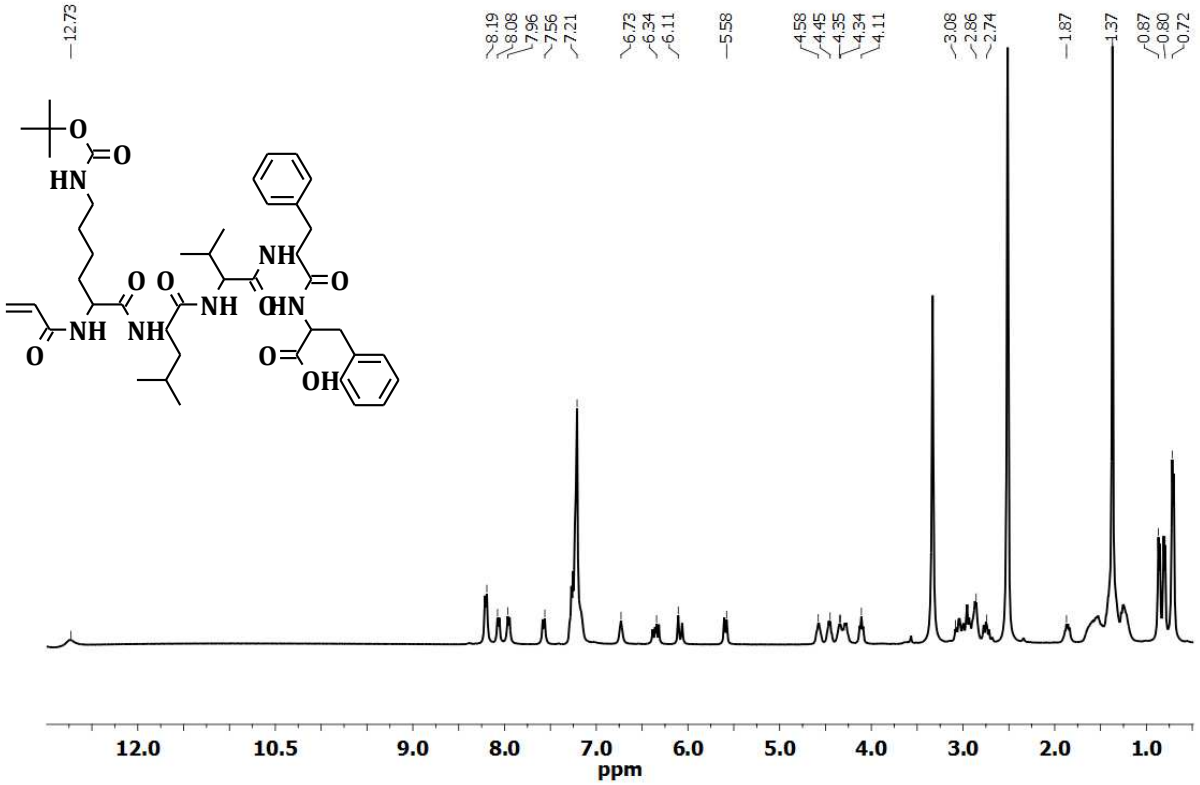

^{1}H NMR spectrum of **Acr-Lys(Boc)-Leu-Val-Phe-Phe-OH (6).**

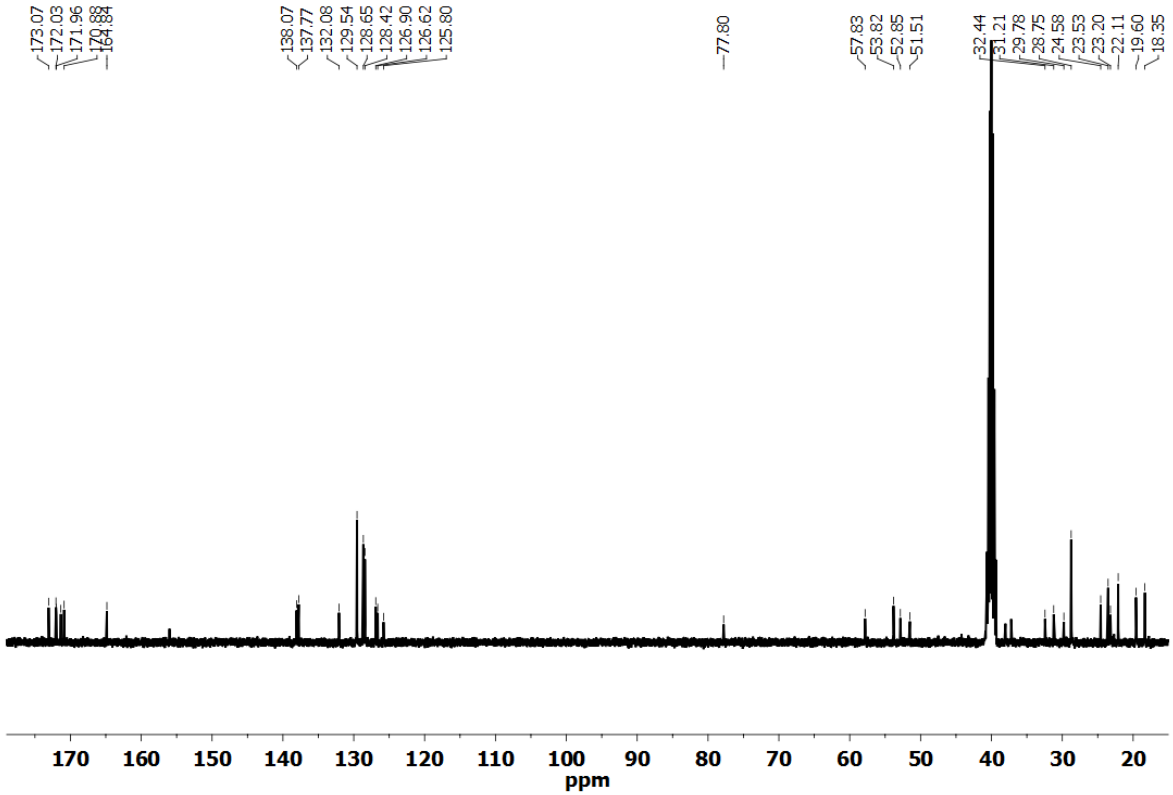

^{13}C NMR spectrum of **Acr-Lys(Boc)-Leu-Val-Phe-Phe-OH (6).**

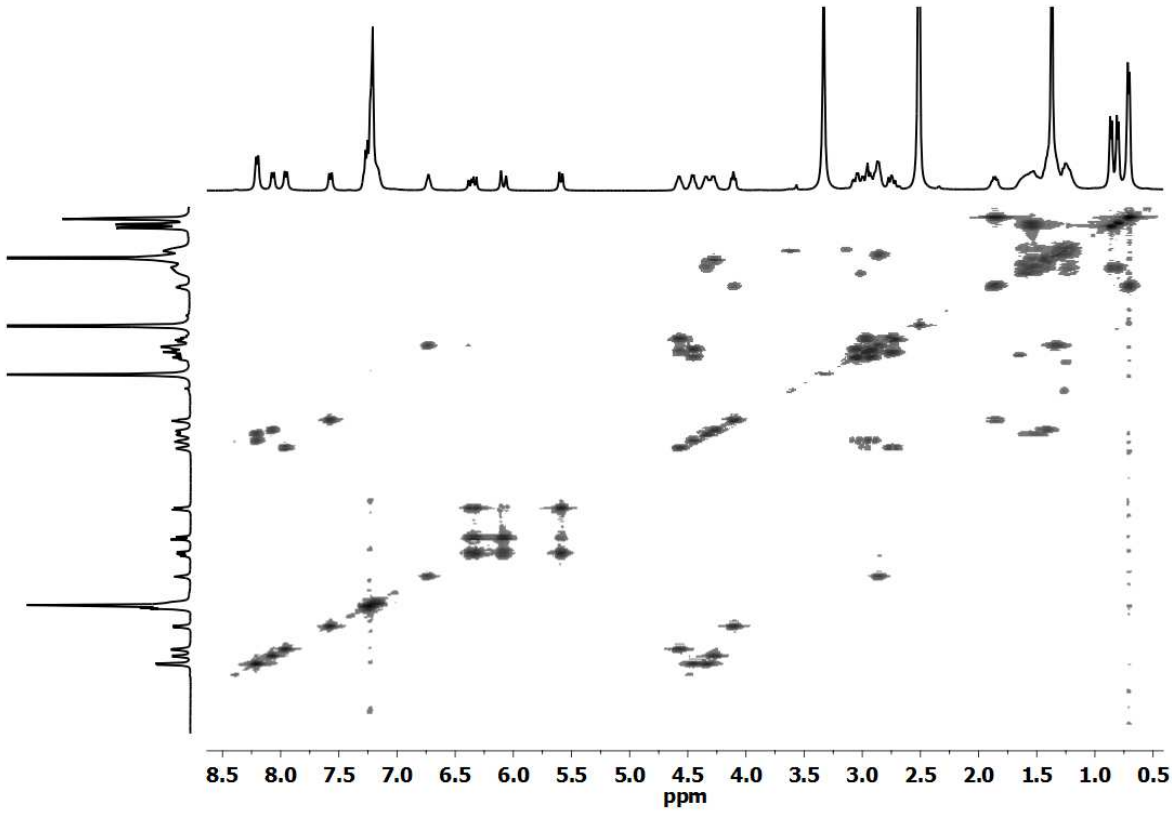

2D COSY NMR spectrum of **Acr-Lys(Boc)-Leu-Val-Phe-Phe-OH (6).**

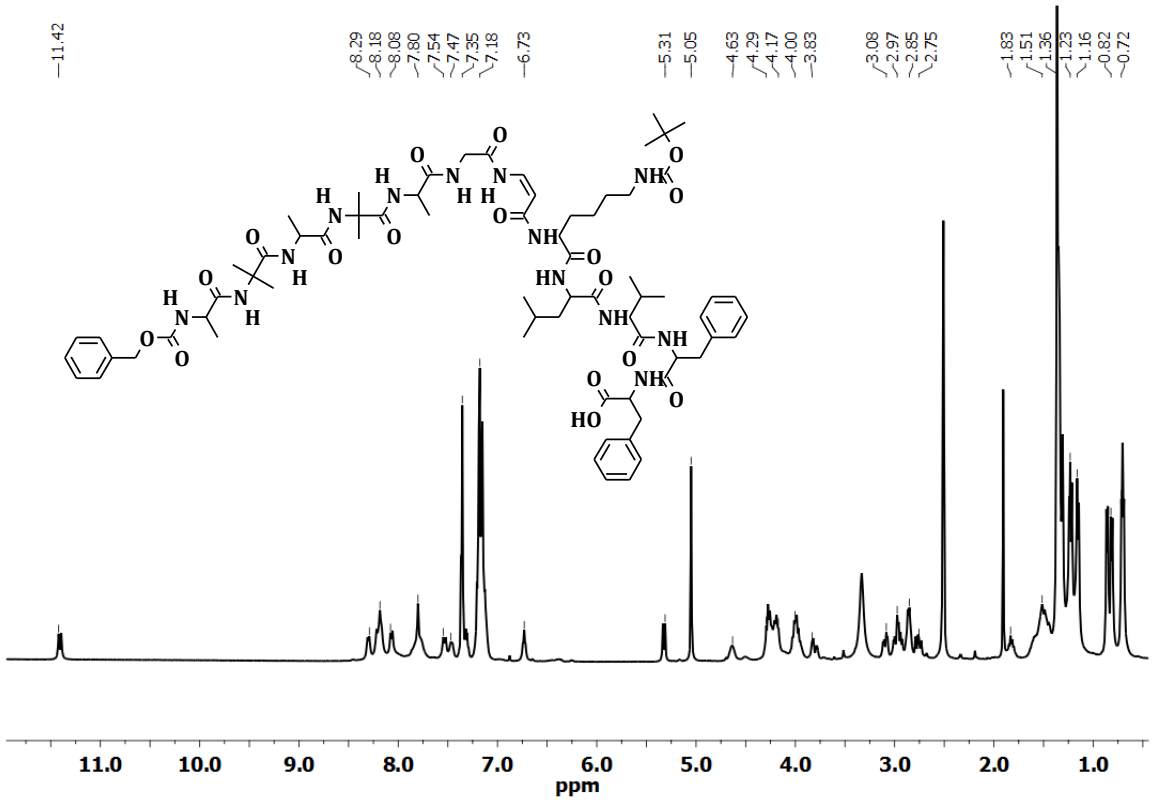

^{1}H NMR spectrum of **Z-(Ala-Aib)2-Ala-Gly-Δ^{Z}βAla-Lys(Boc)-Leu-Val-Phe-Phe-OH (7).**

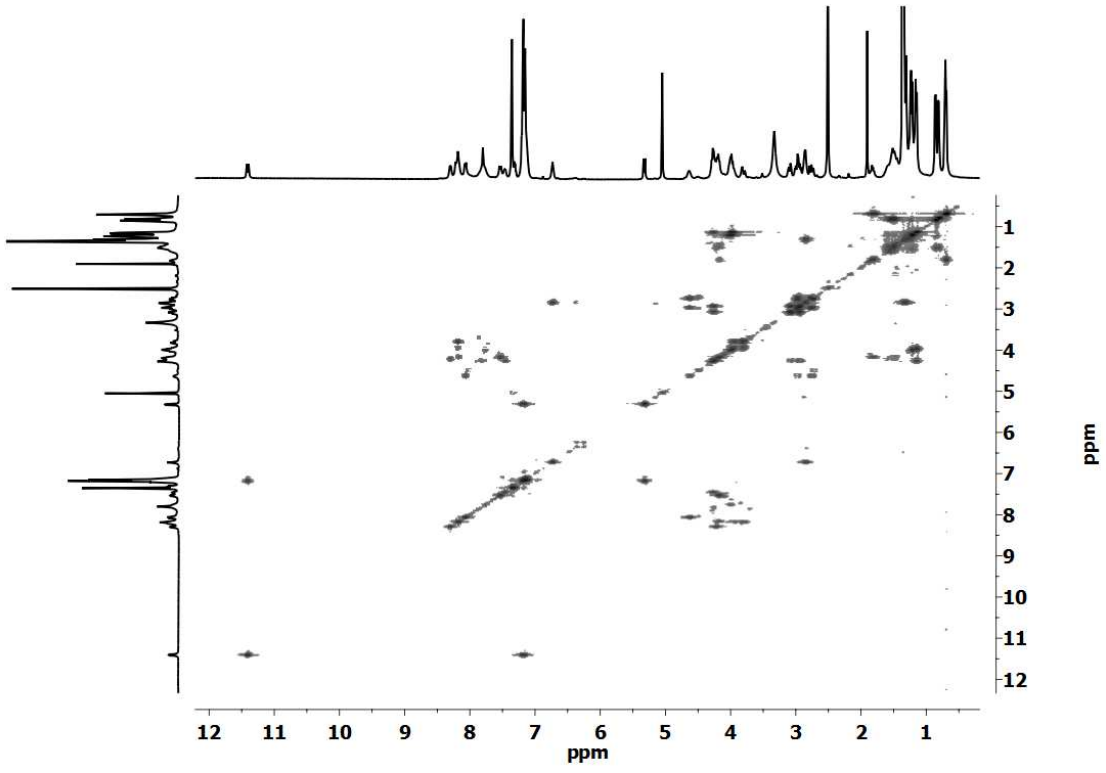

2D COSY NMR spectrum of **Z-(Ala-Aib)2-Ala-Gly-Δ^{Z}βAla-Lys(Boc)-Leu-Val-Phe-Phe-OH (7).**

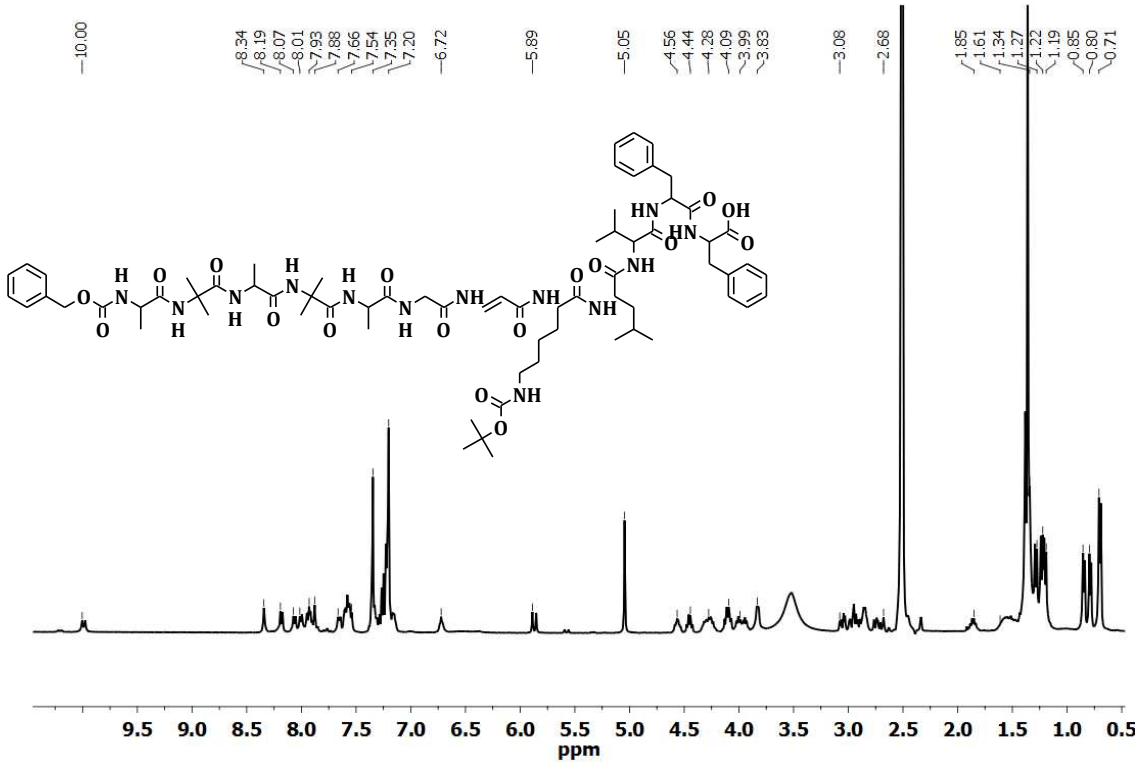

^{1}H NMR spectrum of **Z-(Ala-Aib)2-Ala-Gly-Δ^{E}βAla-Lys(Boc)-Leu-Val-Phe-Phe-OH (8).**

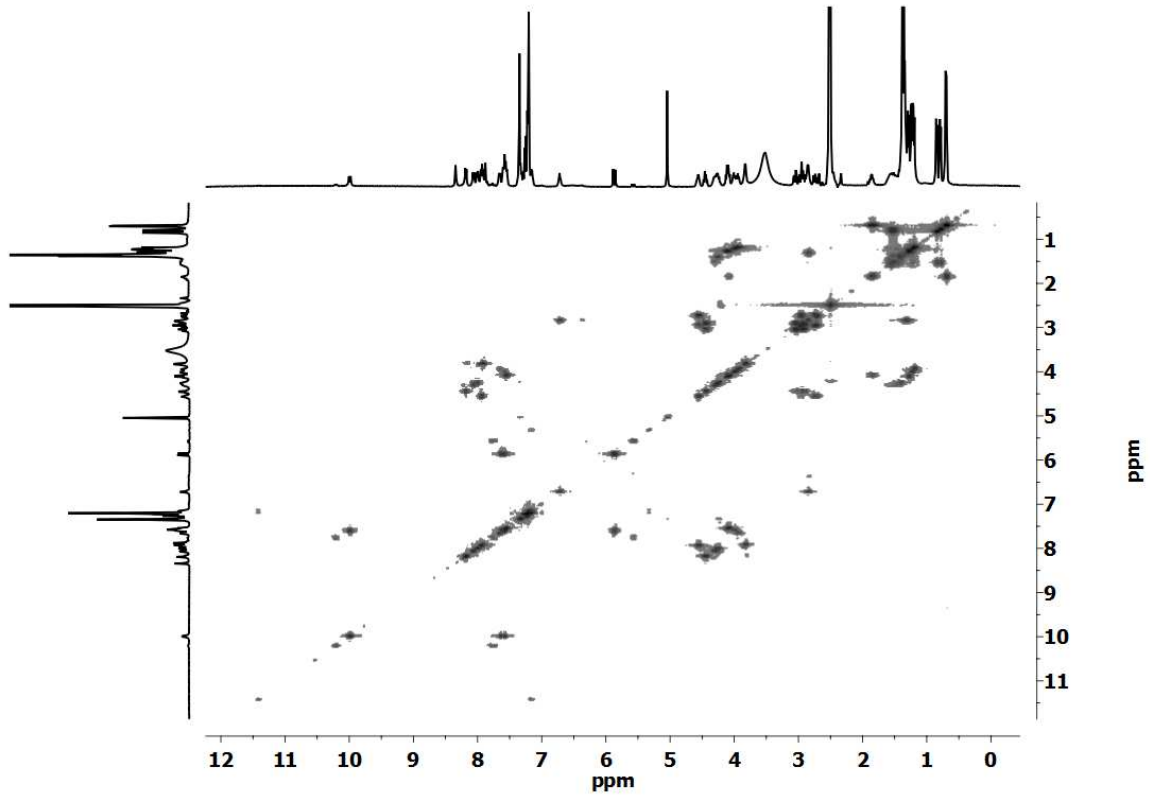

2D COSY NMR spectrum of **Z-(Ala-Aib)2-Ala-Gly-Δ^{E}βAla-Lys(Boc)-Leu-Val-Phe-Phe-OH (8).**

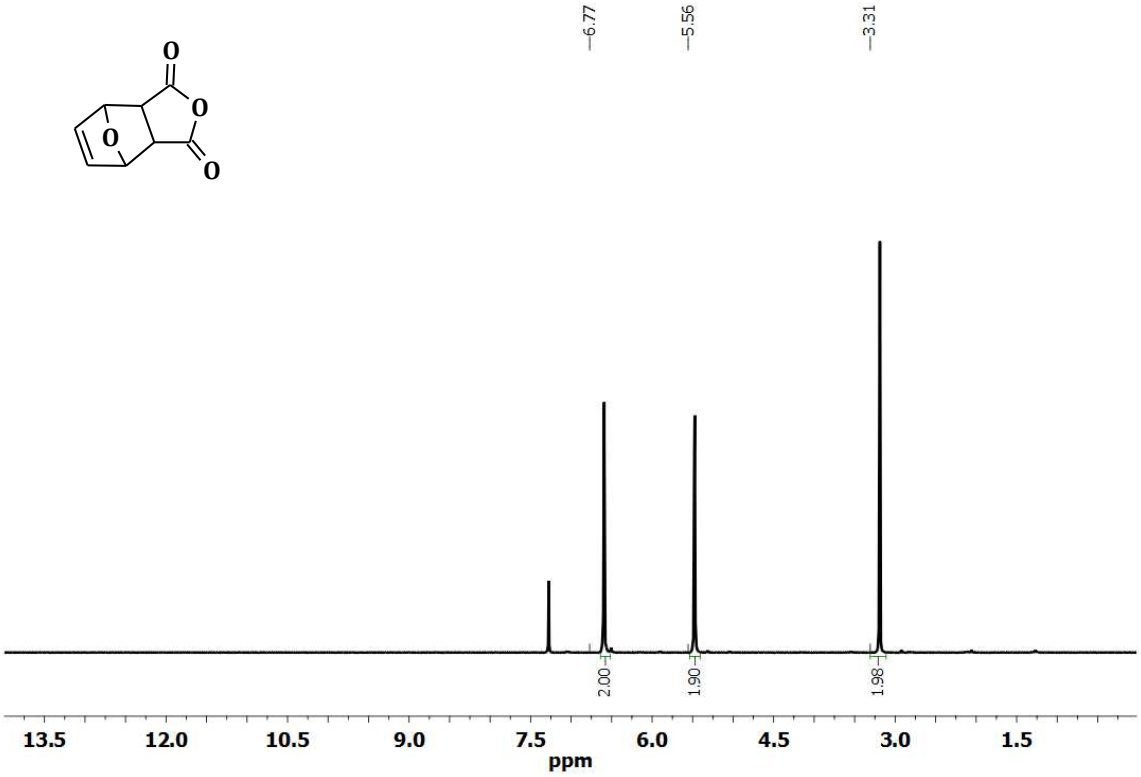

^{1}H NMR spectrum of **3**.

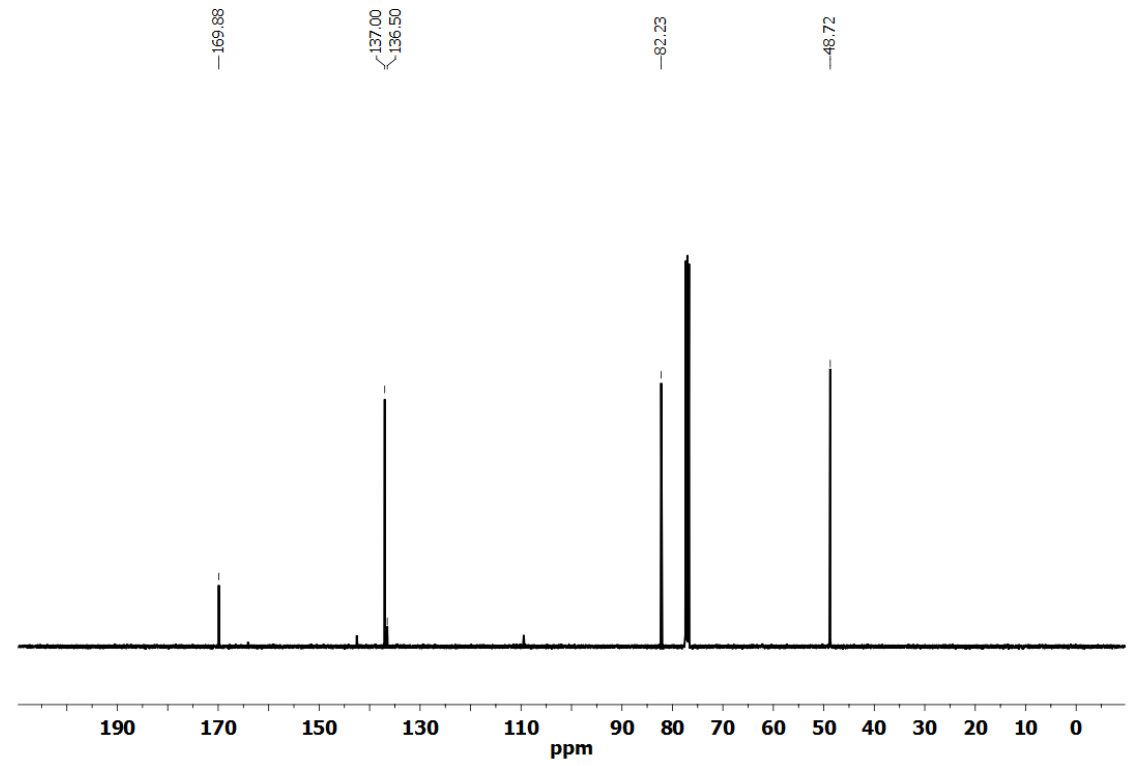

^{13}C NMR spectrum of **3**.

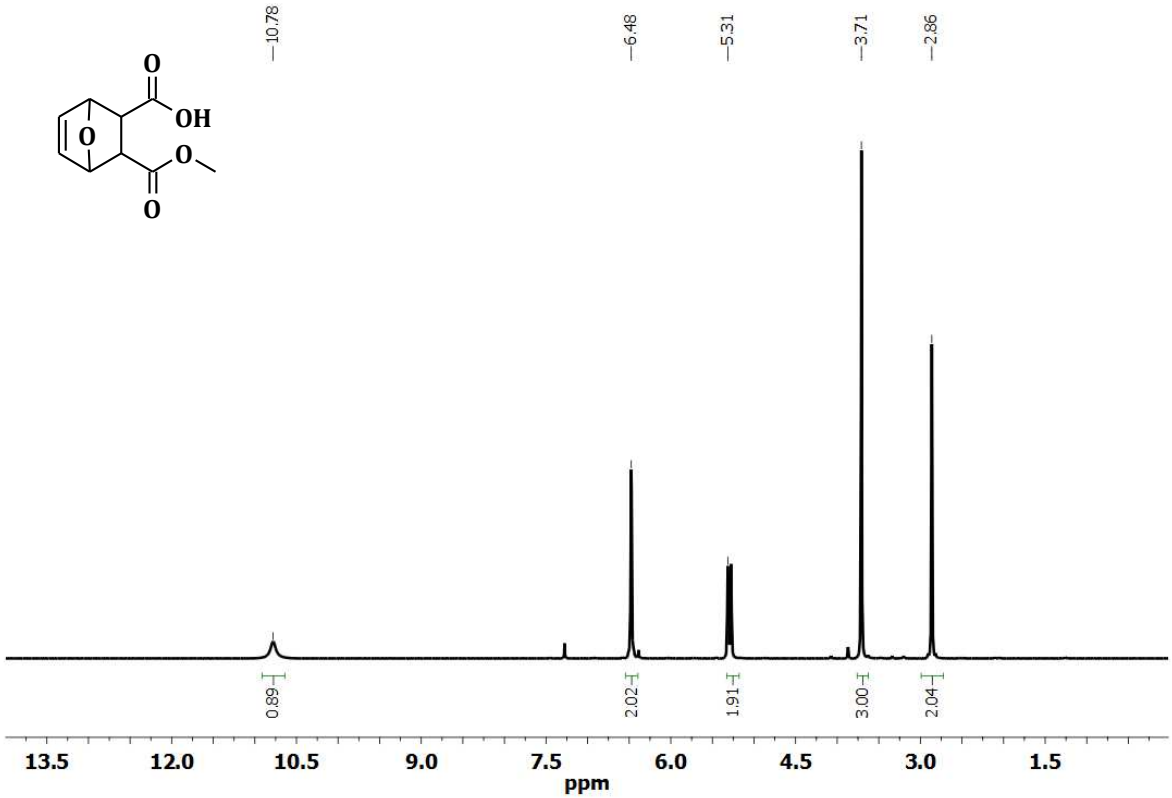

^{1}H NMR spectrum of **4 (methyl ester)**.

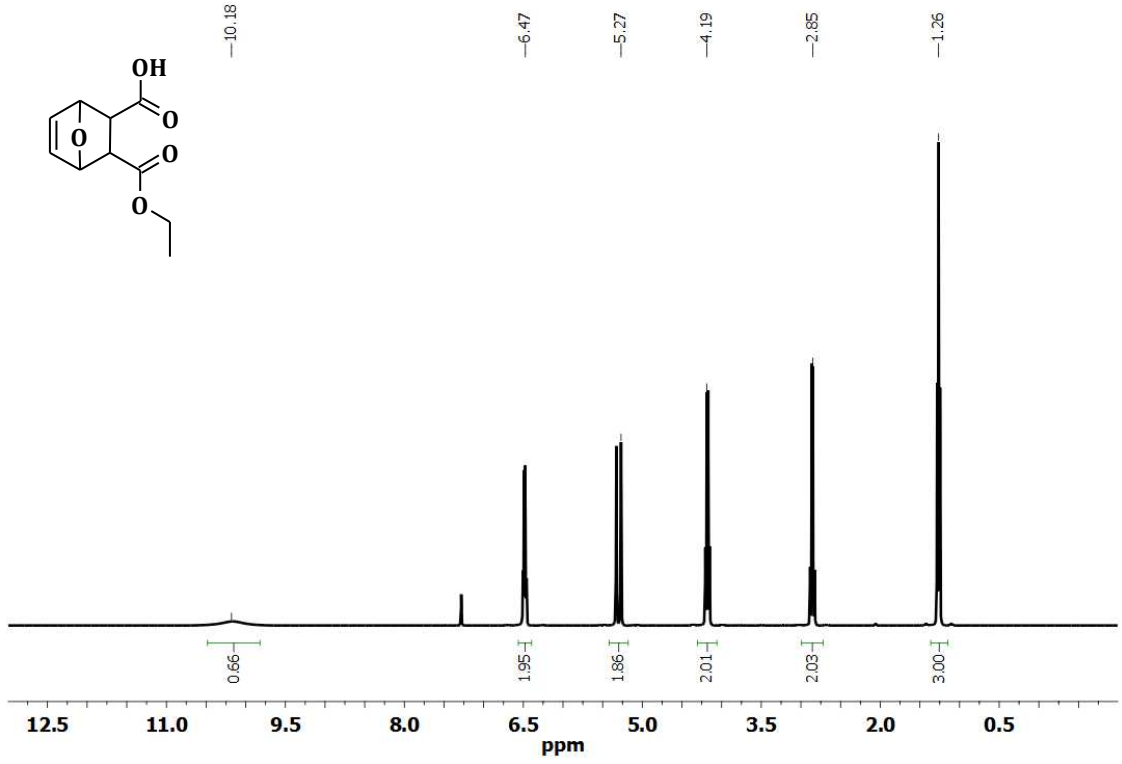

^{1}H NMR spectrum of **4 (ethyl ester)**.

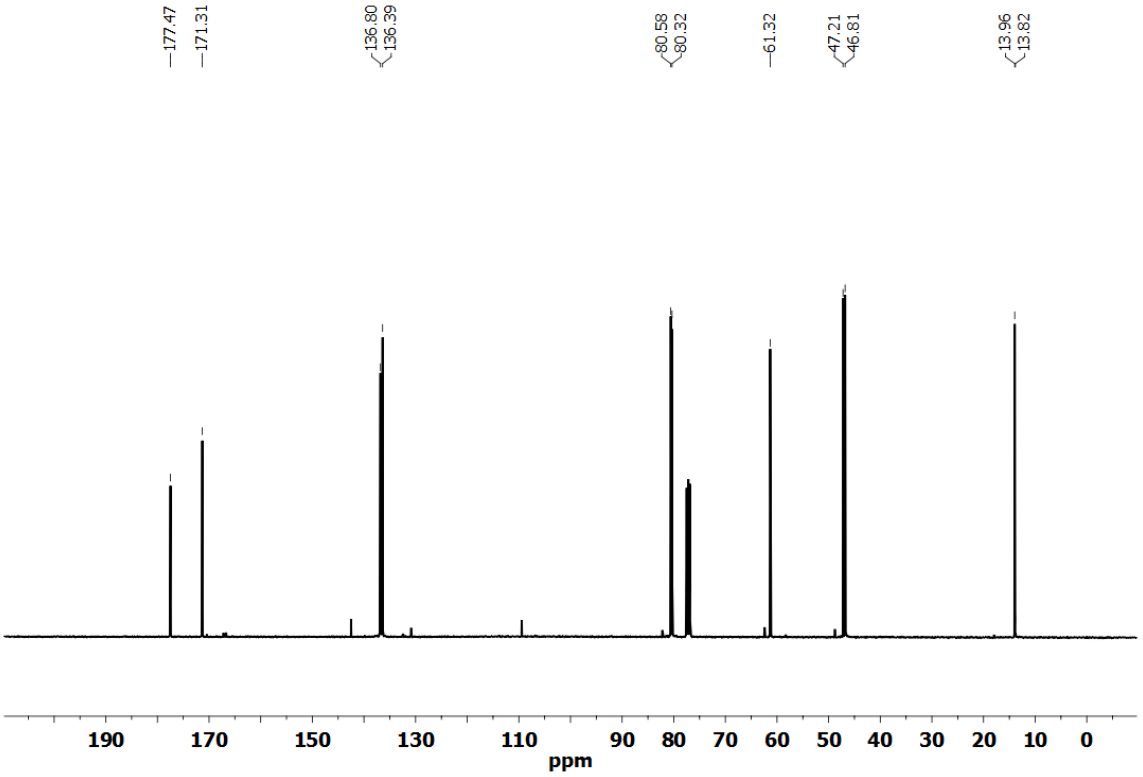

^{13}C NMR spectrum of **4 (ethyl ester)**.

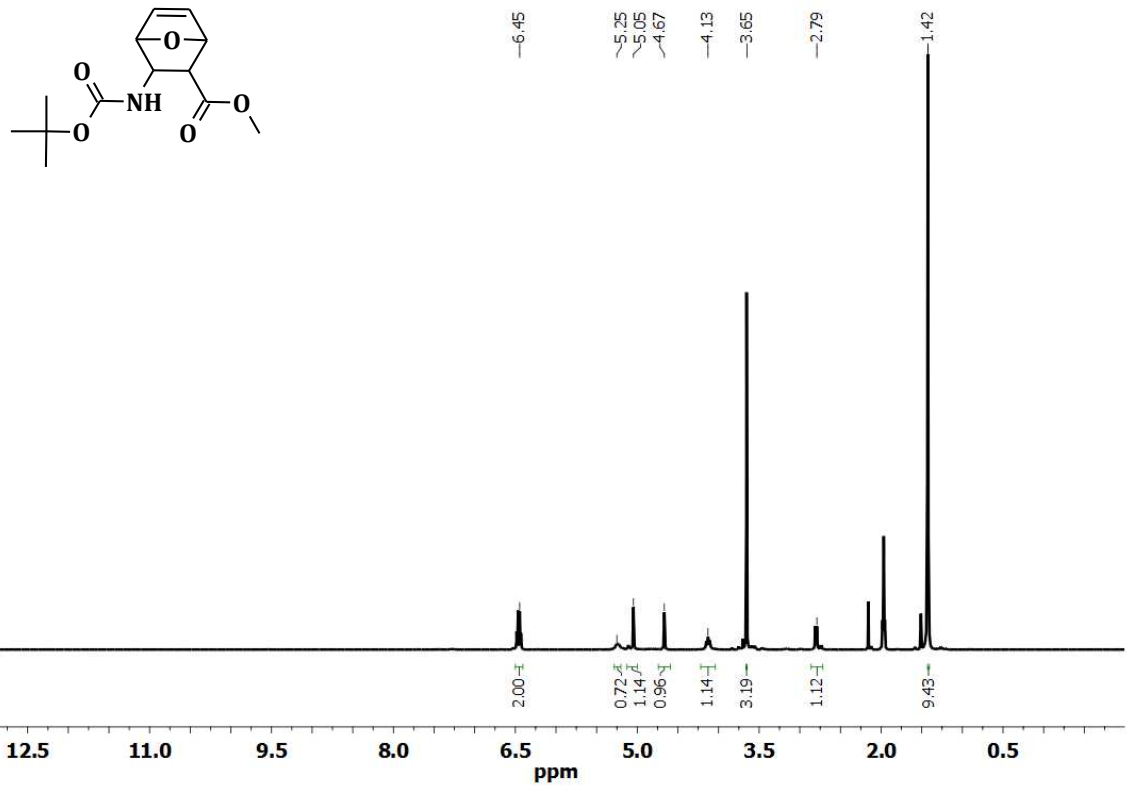

^{1}H NMR spectrum of **5 (methyl ester)**.

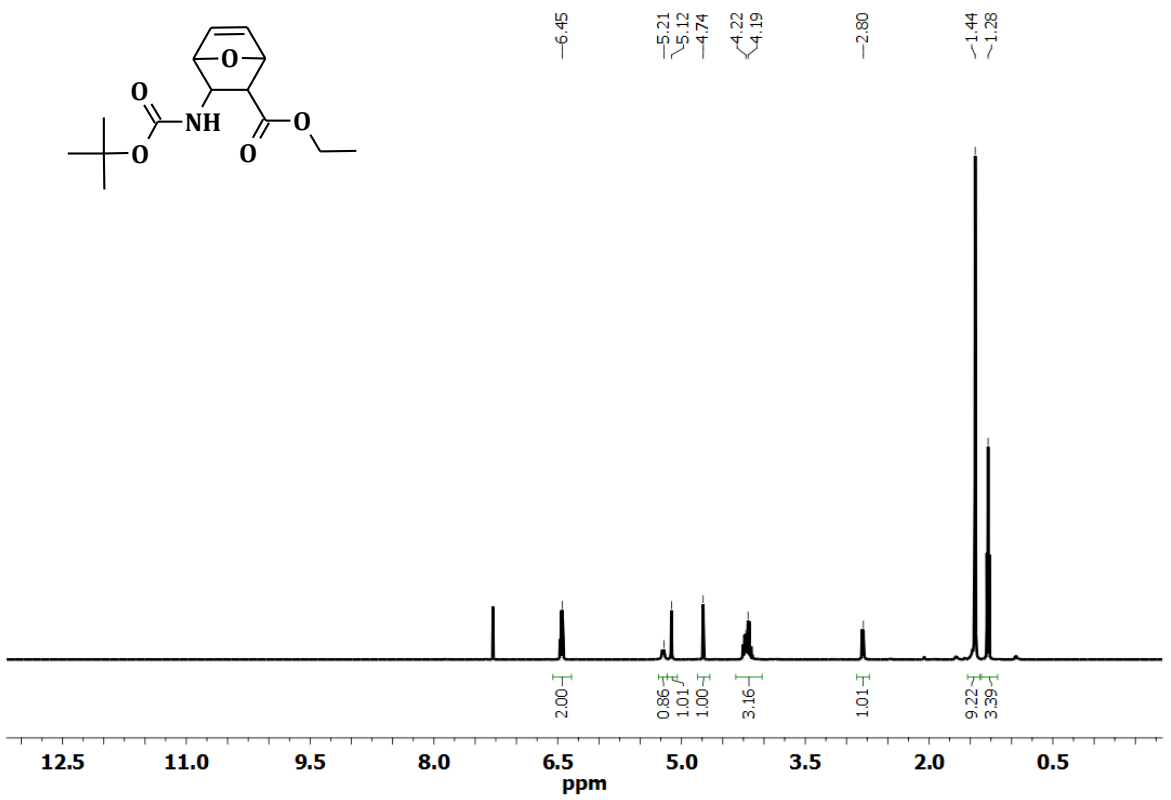

^{1}H NMR spectrum of **5 (ethyl ester)**.

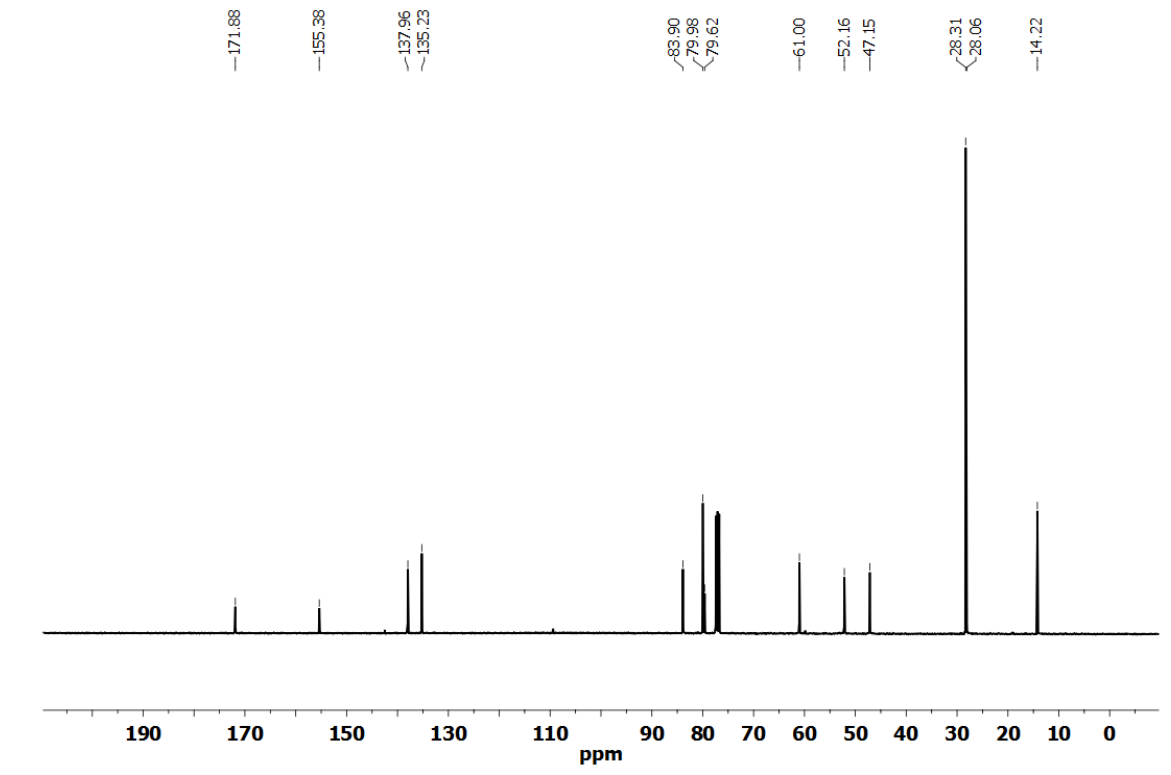

^{13}C NMR spectrum of **5 (ethyl ester)**.

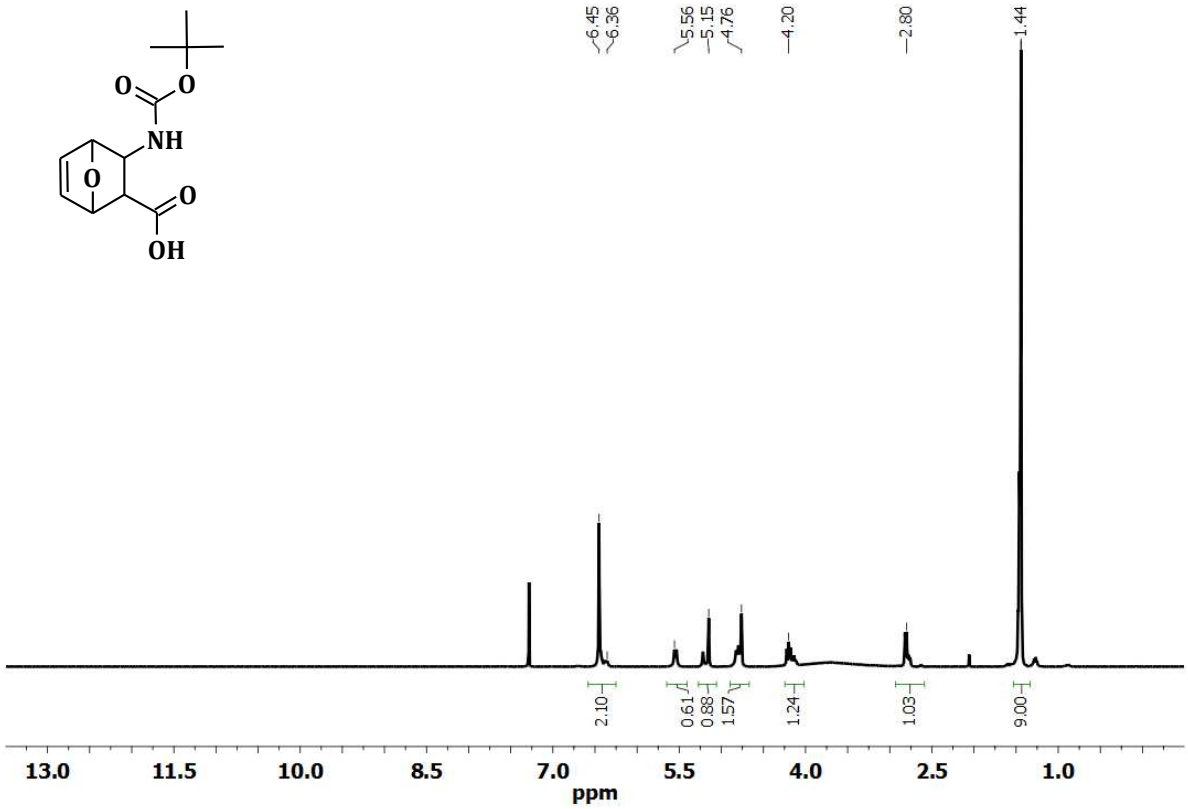

^{1}H NMR spectrum of **8**.

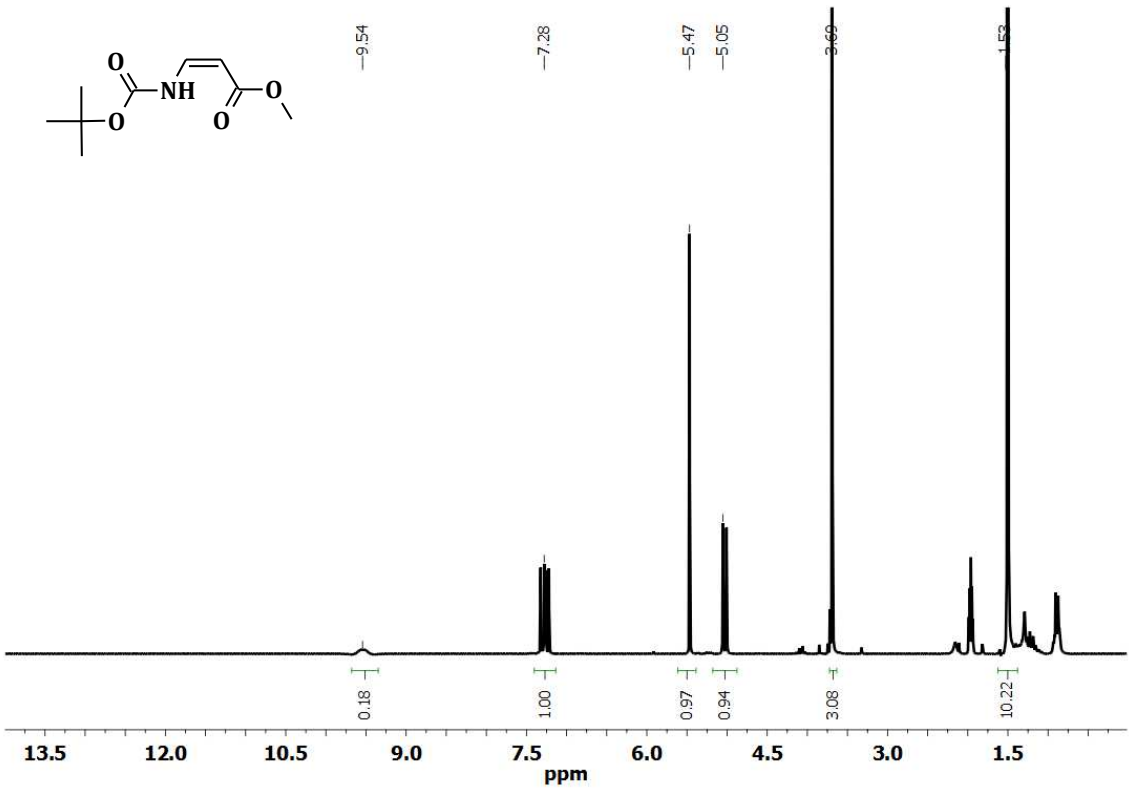

^{1}H NMR spectrum of **6**.

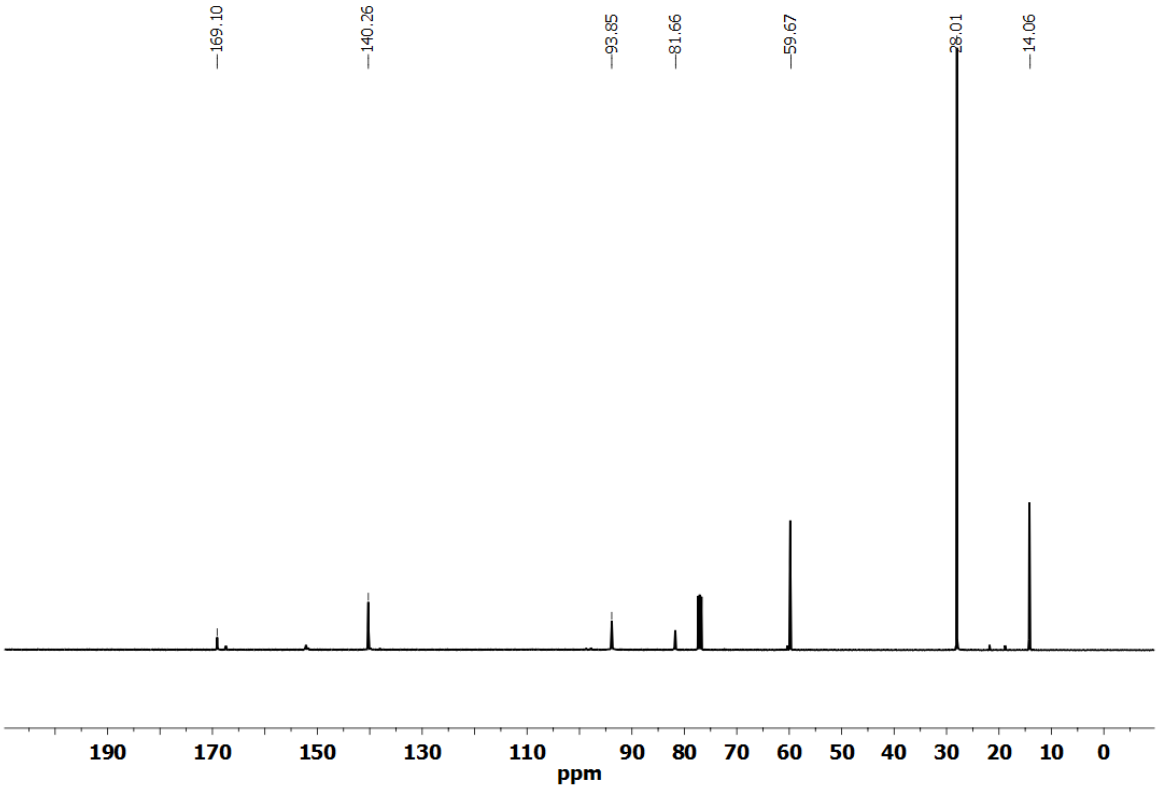

^{13}C NMR spectrum of **6**.

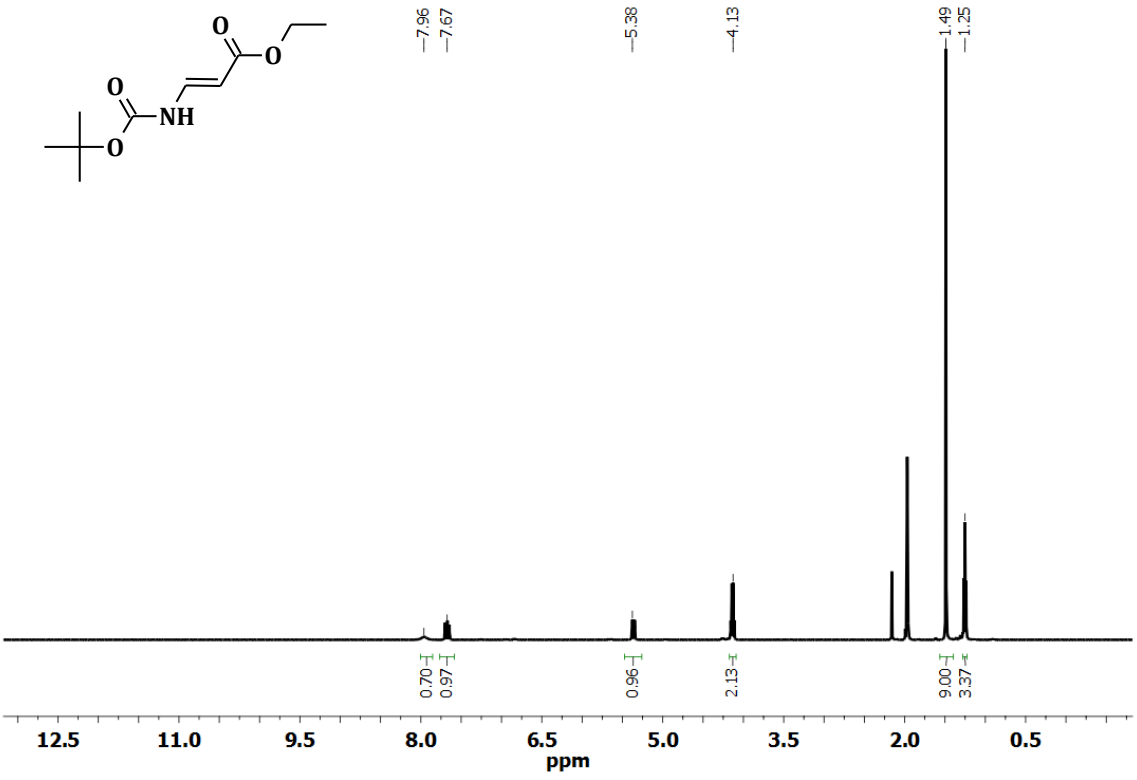

^{1}H NMR spectrum of **7**.

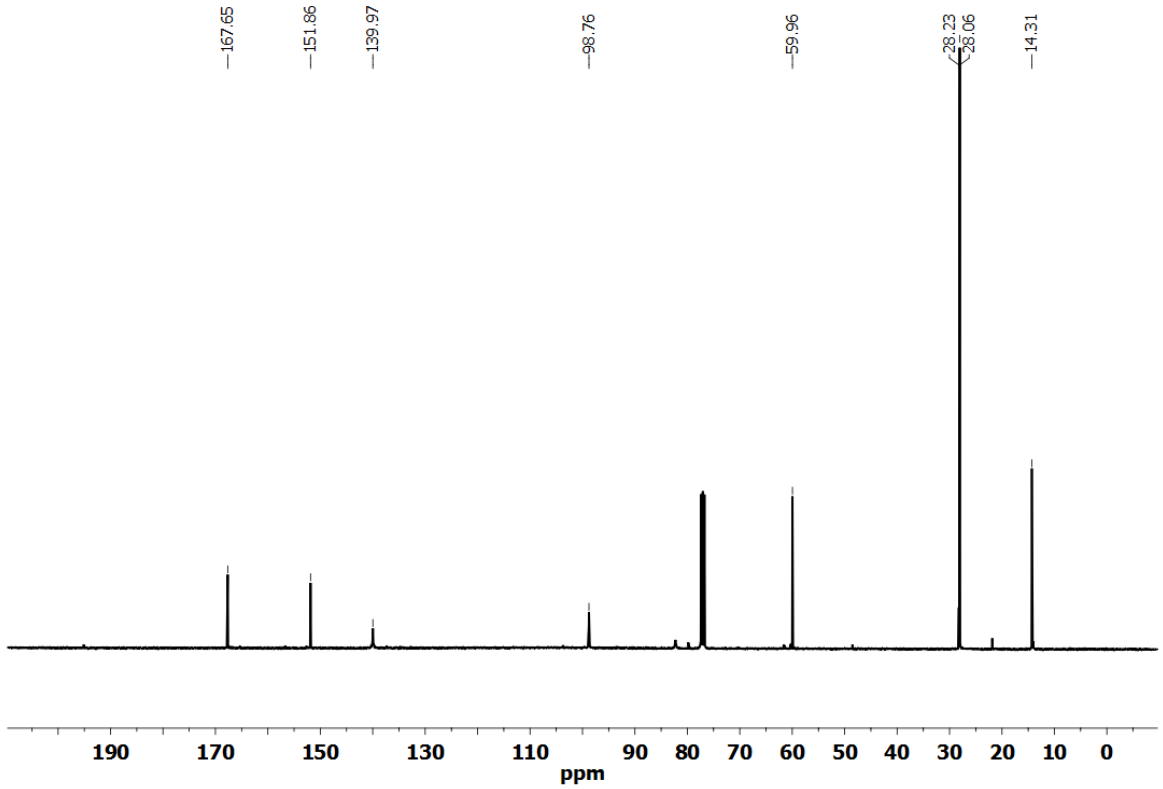

^{13}C NMR spectrum of **7**.

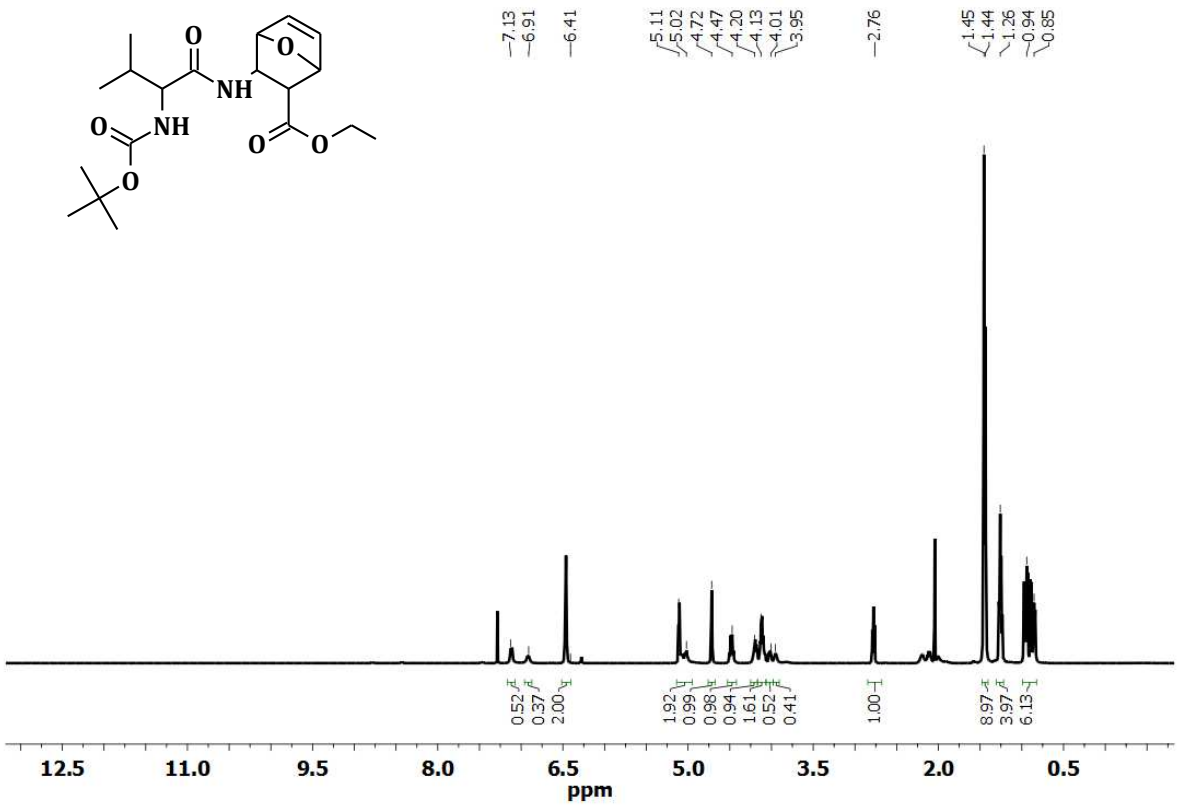

^{1}H NMR spectrum of **Boc-Val-fmΔ^{z}βAla-OR**.

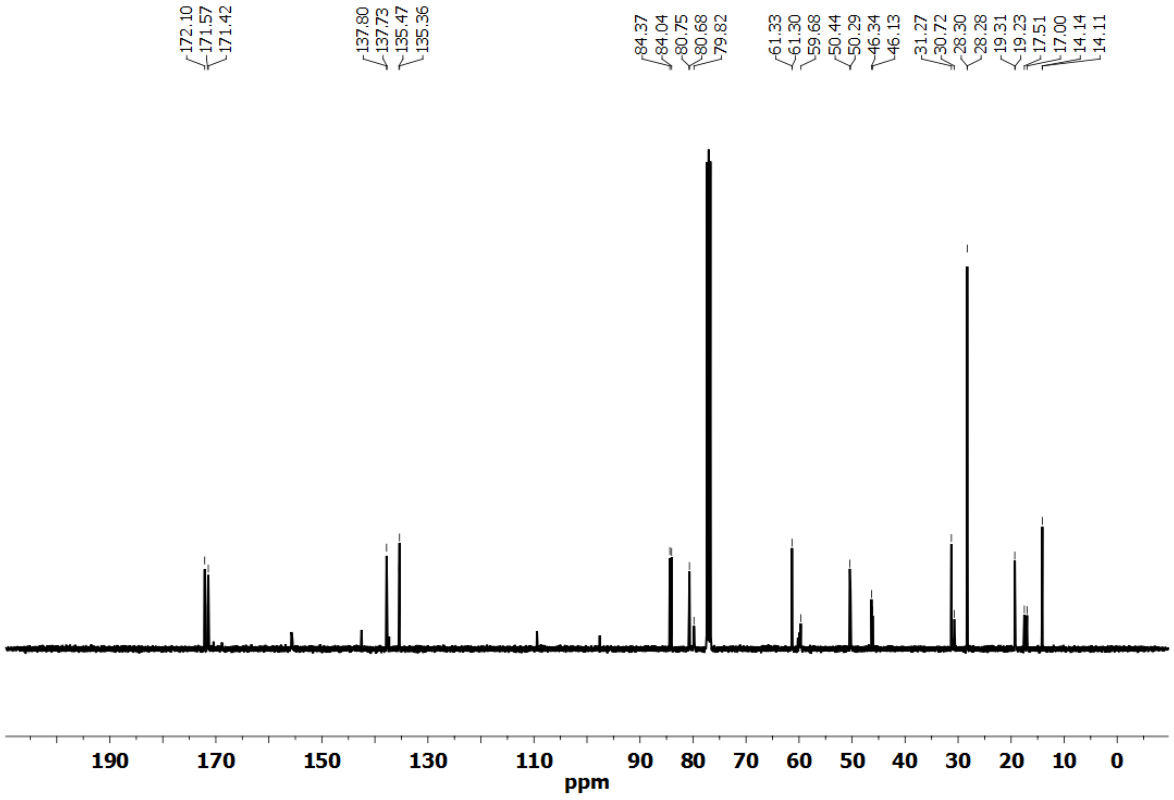

^{13}C NMR spectrum of **Boc-Val-fmΔ^{z}βAla-OR**.

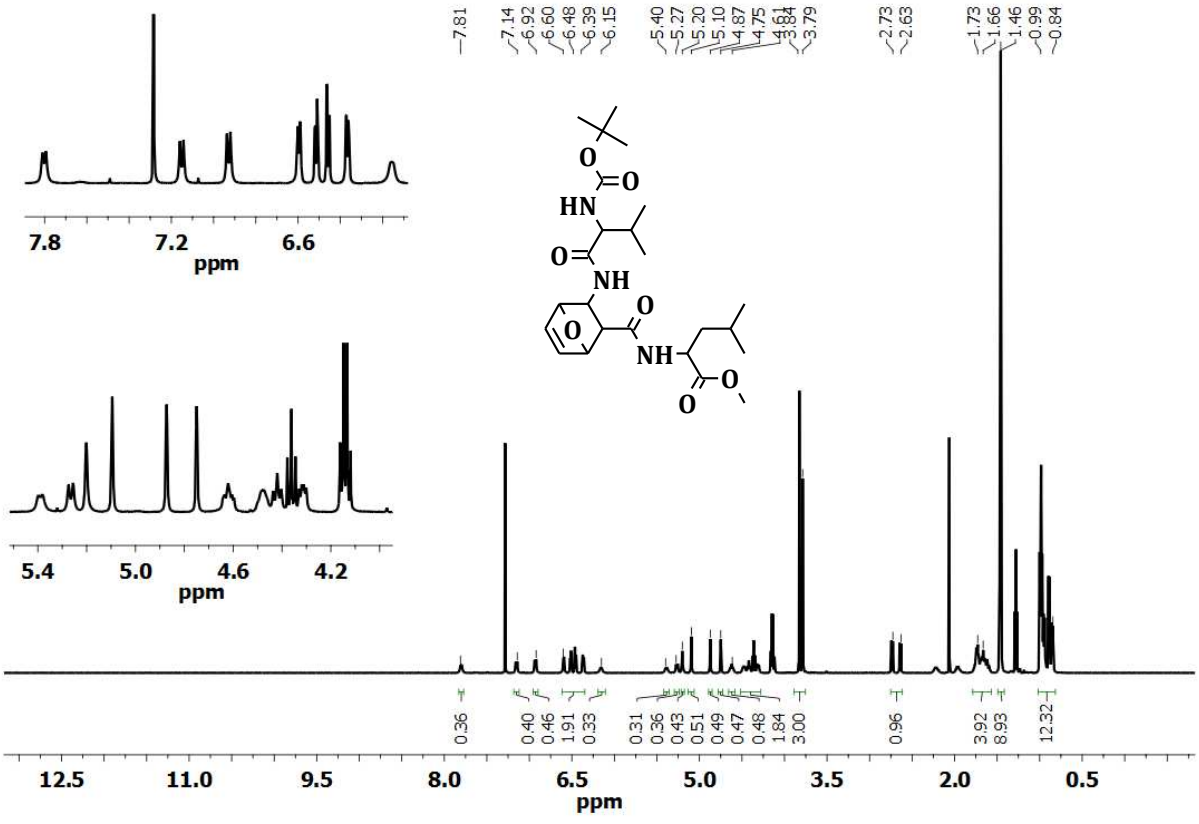

^{1}H NMR spectrum of **Boc-Val-fmΔ^{z}βAla-Leu-OMe**.

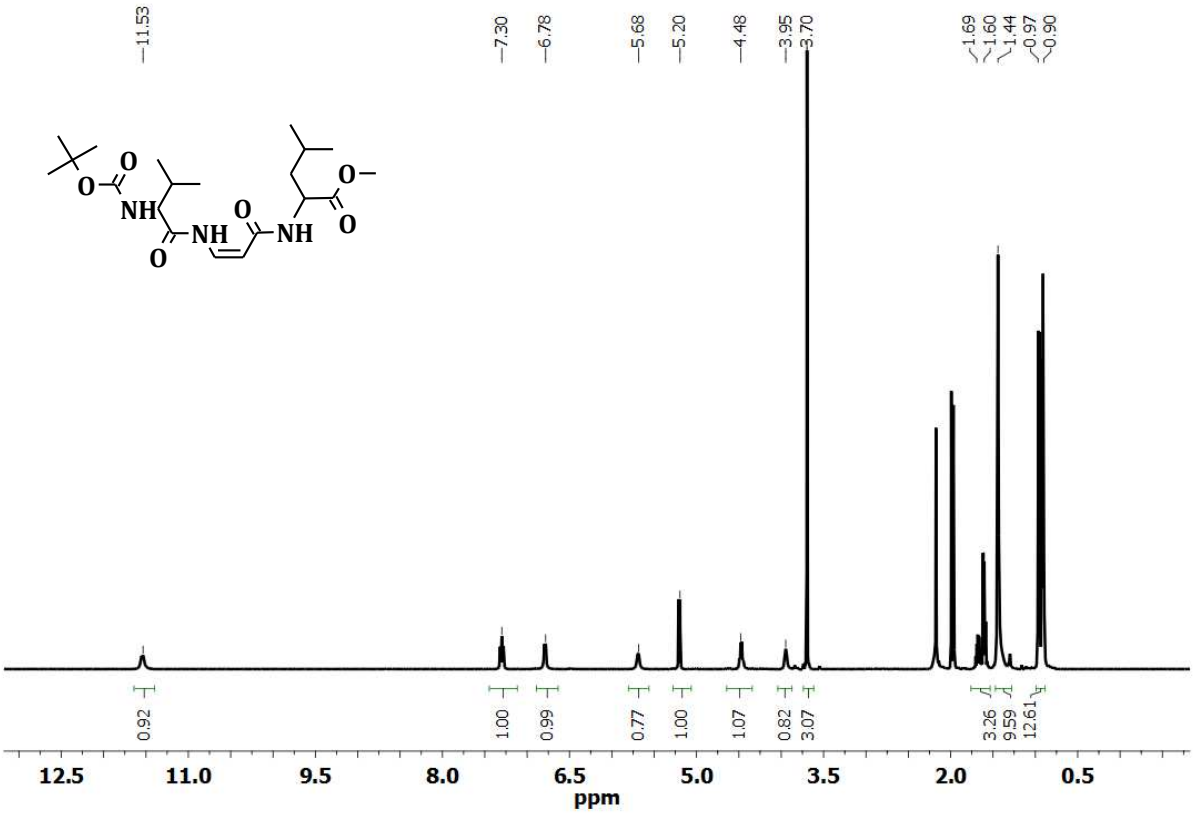

^{1}H NMR spectrum of **9(*Z*)**.

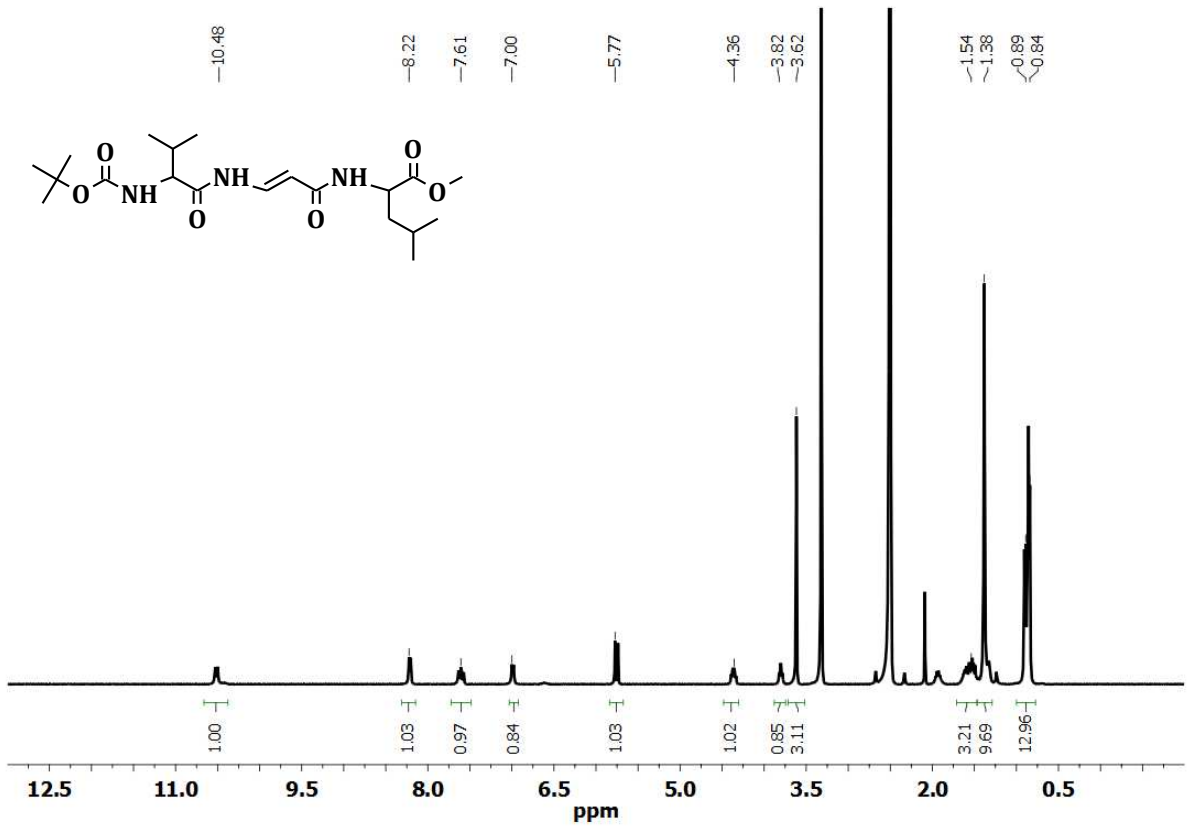

^{1}H NMR spectrum of **9(*E*)**.

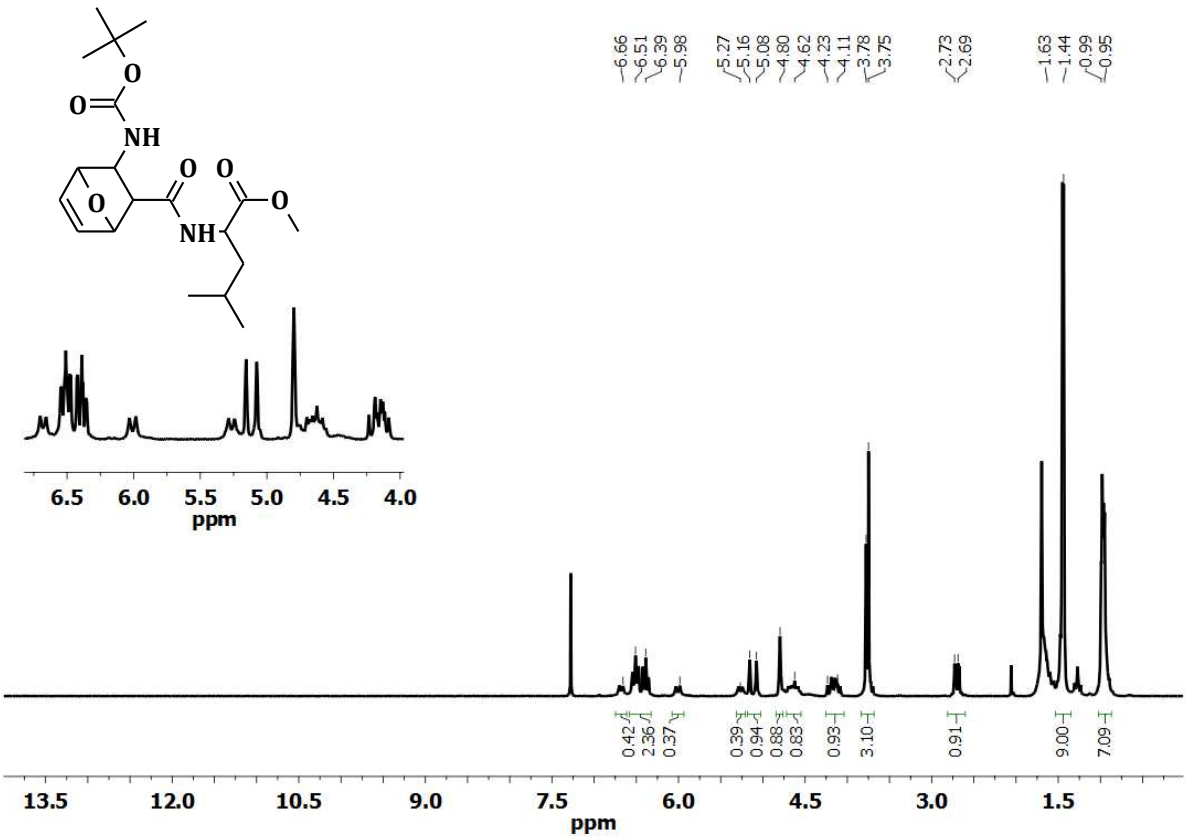

^{1}H NMR spectrum of **Boc-fmΔ^{z}βAla-Leu-OMe**.

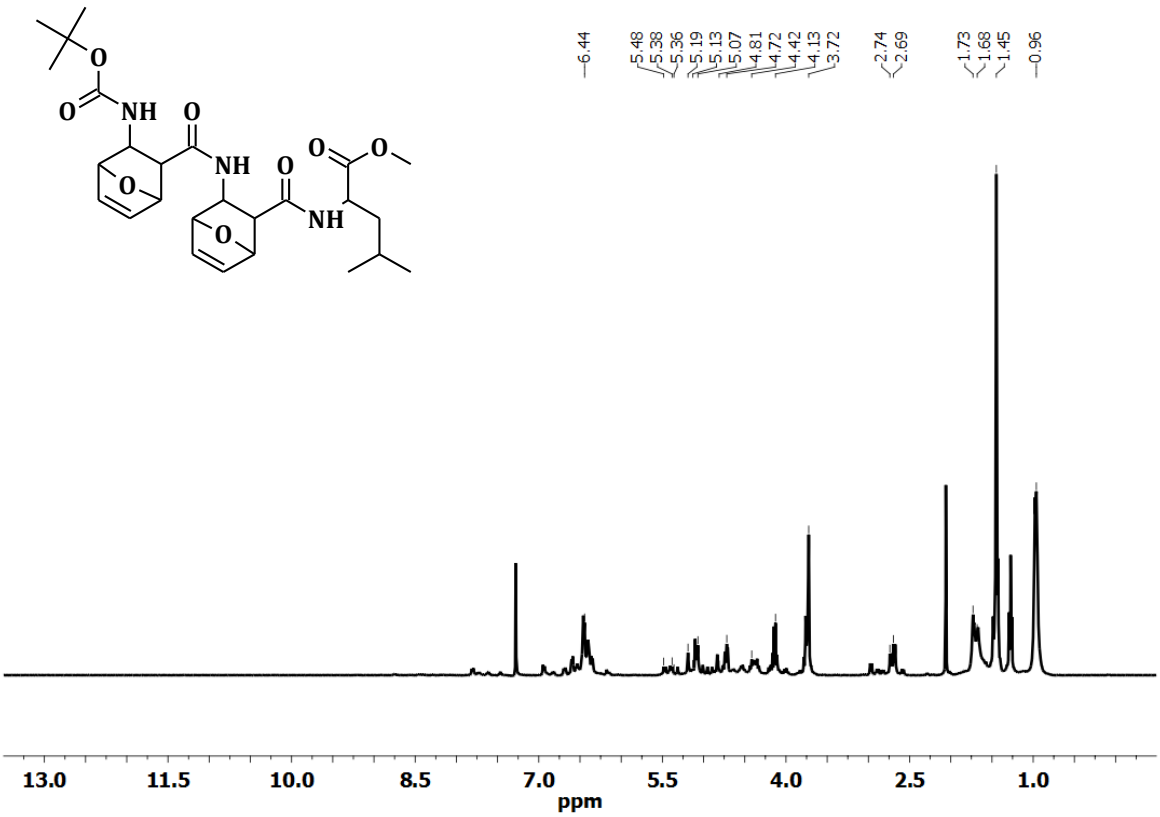

^{1}H NMR spectrum of **Boc-(fmΔ^{z}βAla)$_2$-Leu-OMe**.

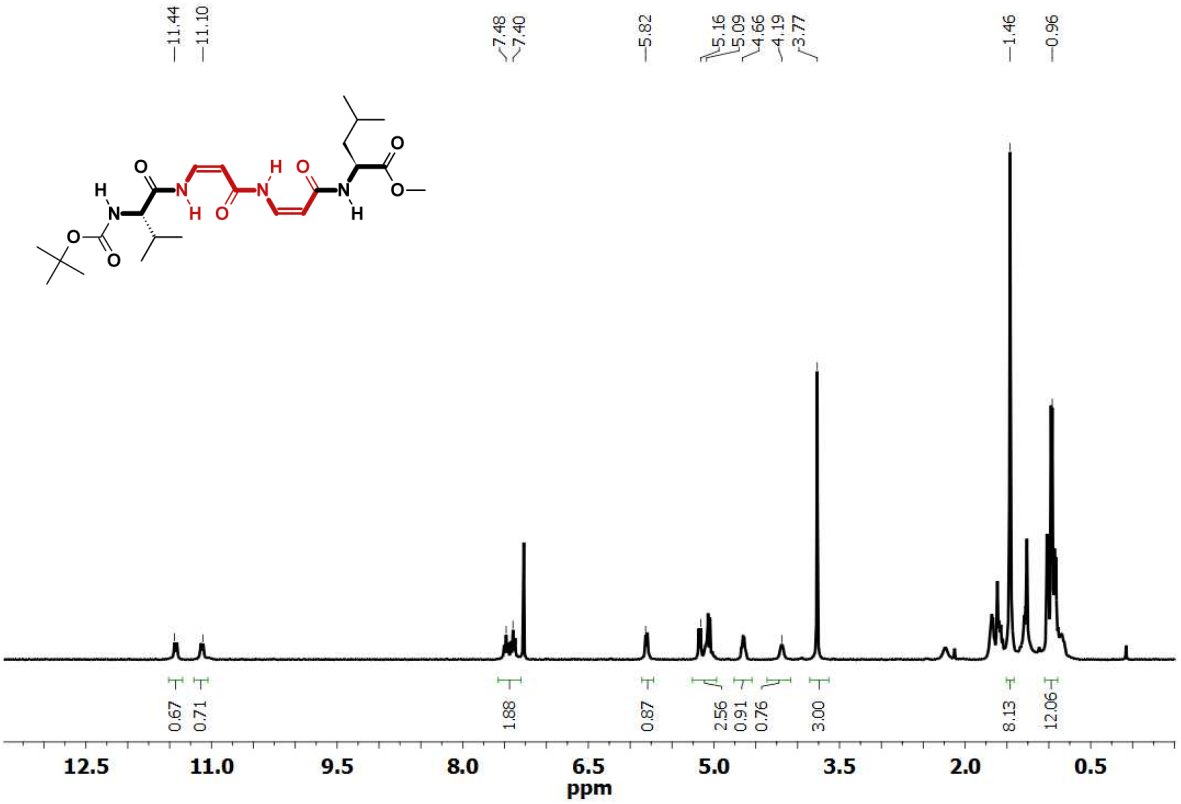

^{1}H NMR spectrum of **10(Z,Z)**.

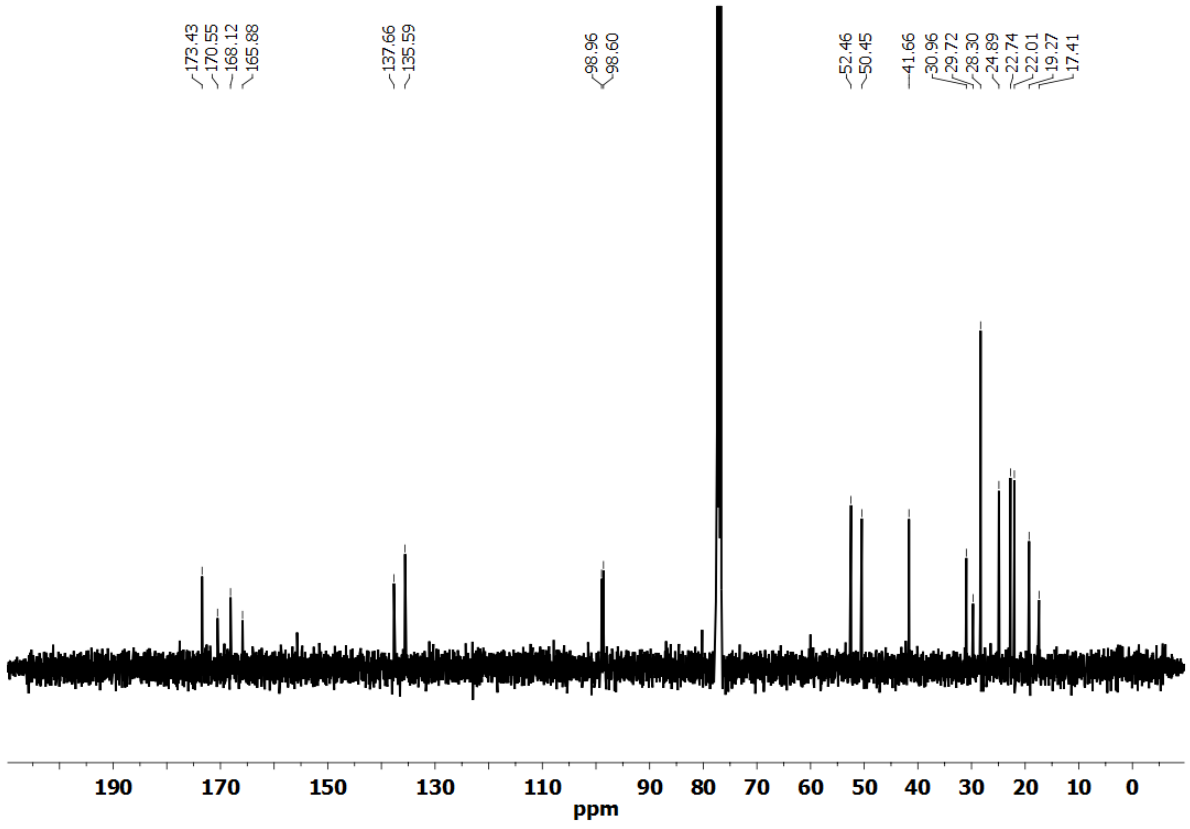

^{13}C NMR spectrum of **10(Z,Z)**.

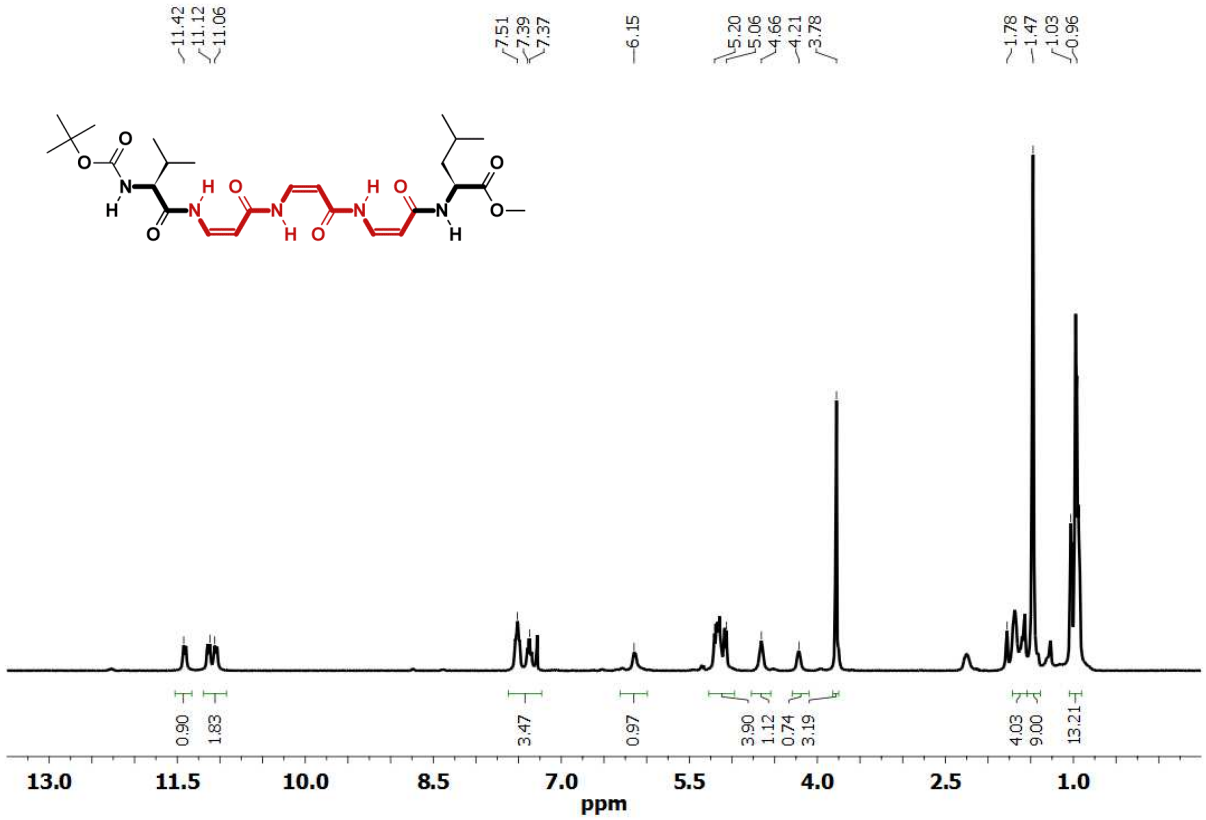

^{1}H NMR spectrum of **11(Z,Z,Z)**.

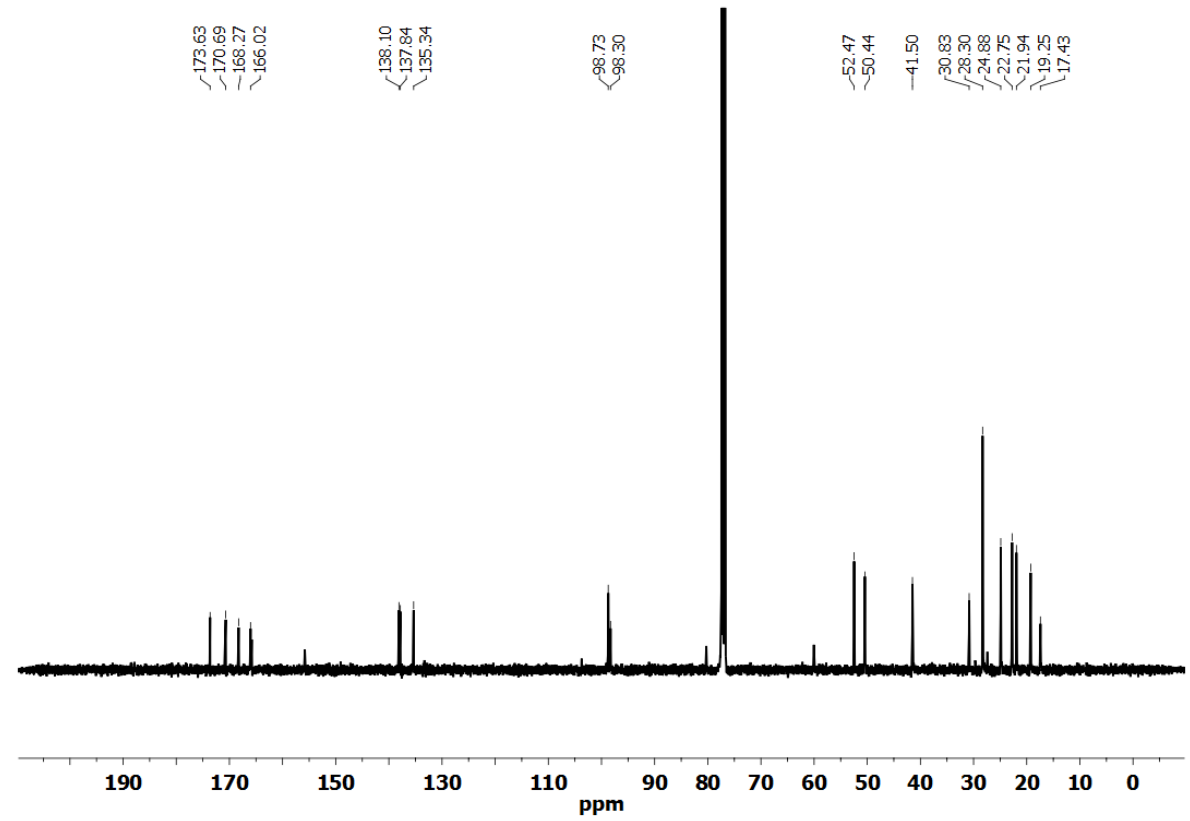

^{13}C NMR spectrum of **11(Z,Z,Z)**.

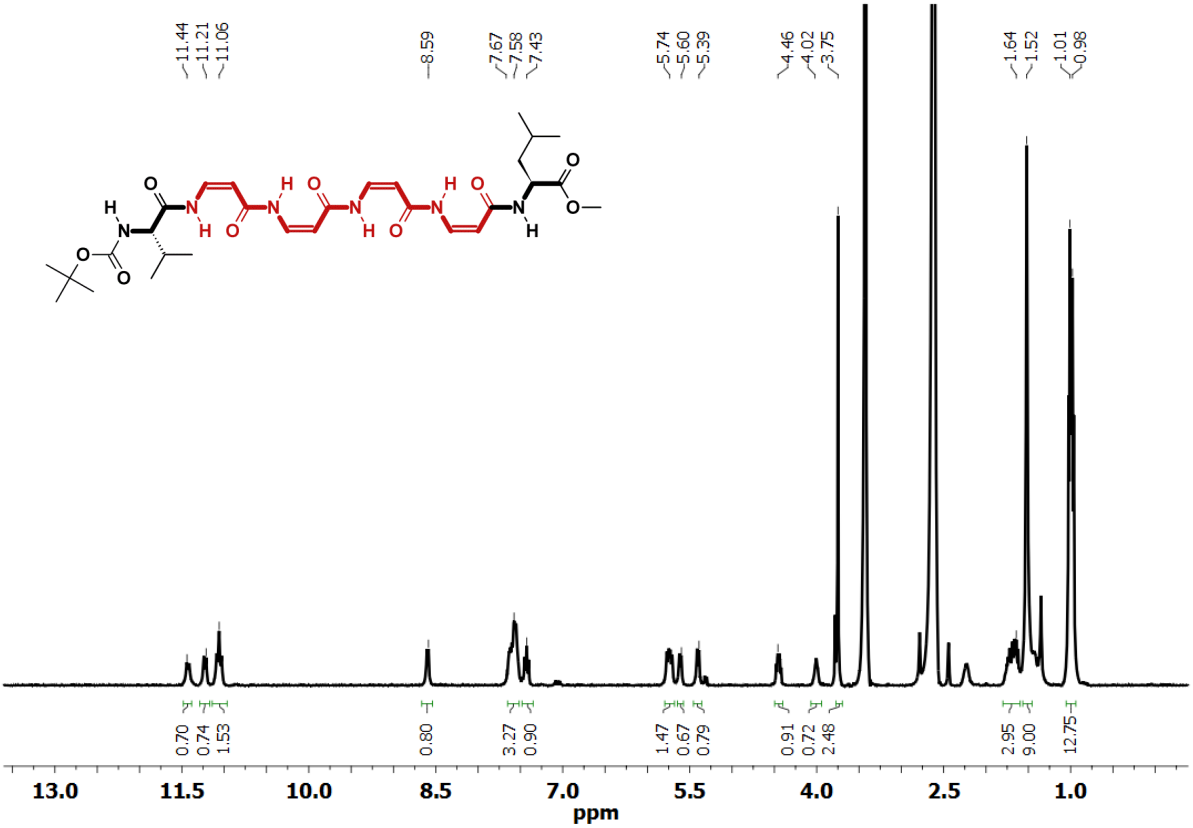

^{1}H NMR spectrum of **12(Z,Z,Z,Z)**.

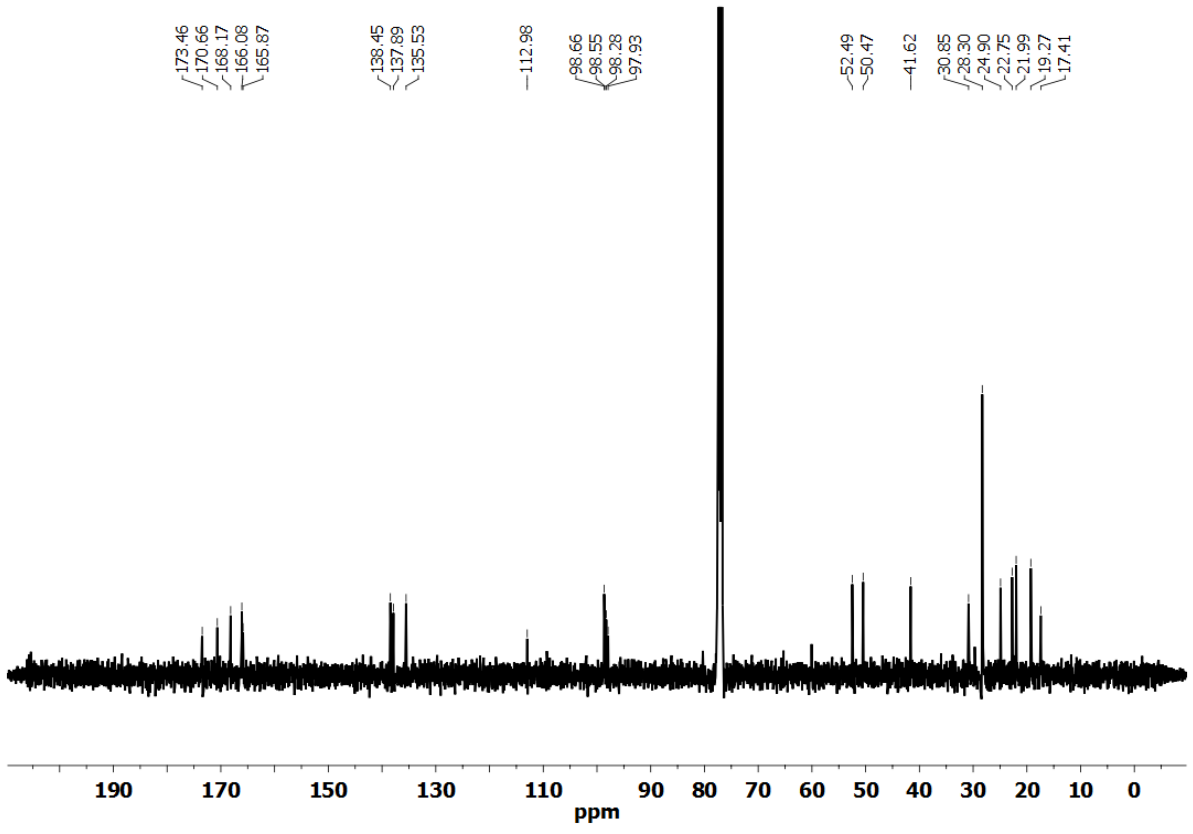

^{13}C NMR spectrum of **12(Z,Z,Z,Z)**.

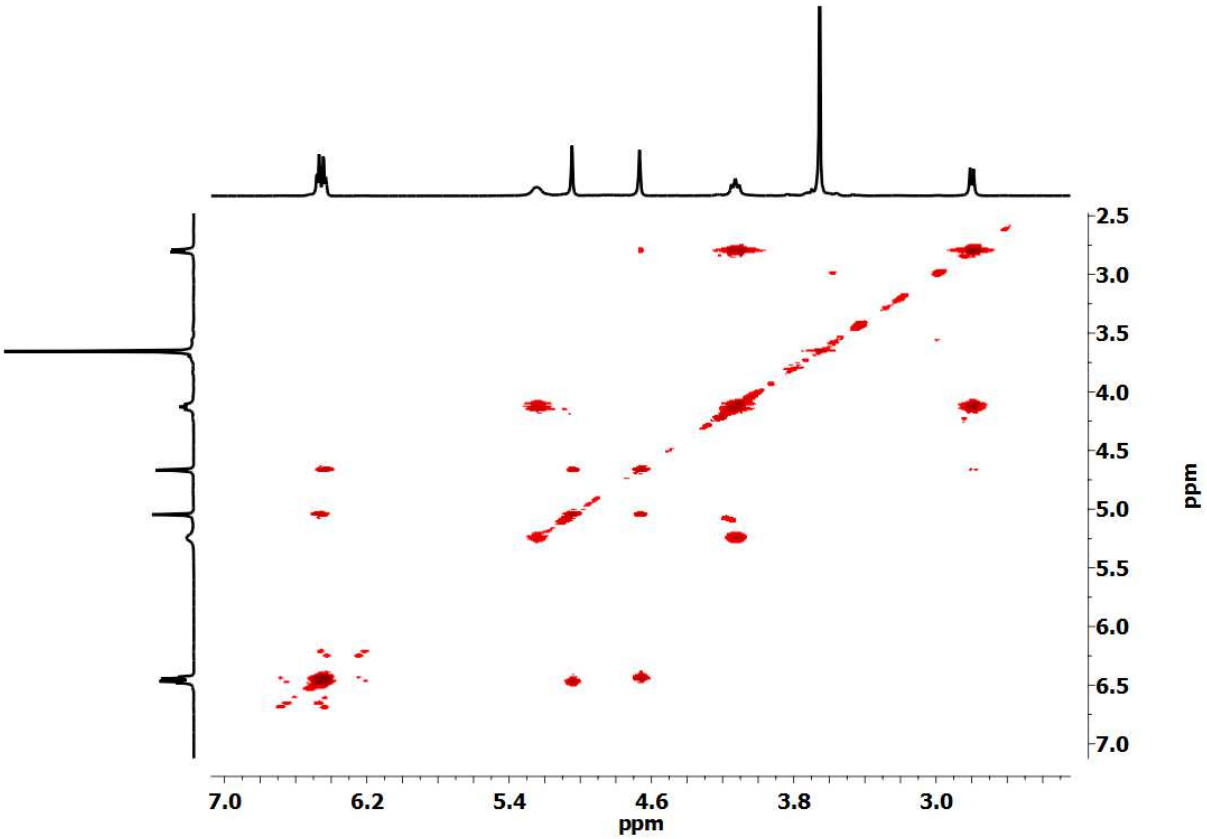

2D COSY NMR spectrum of **6**.

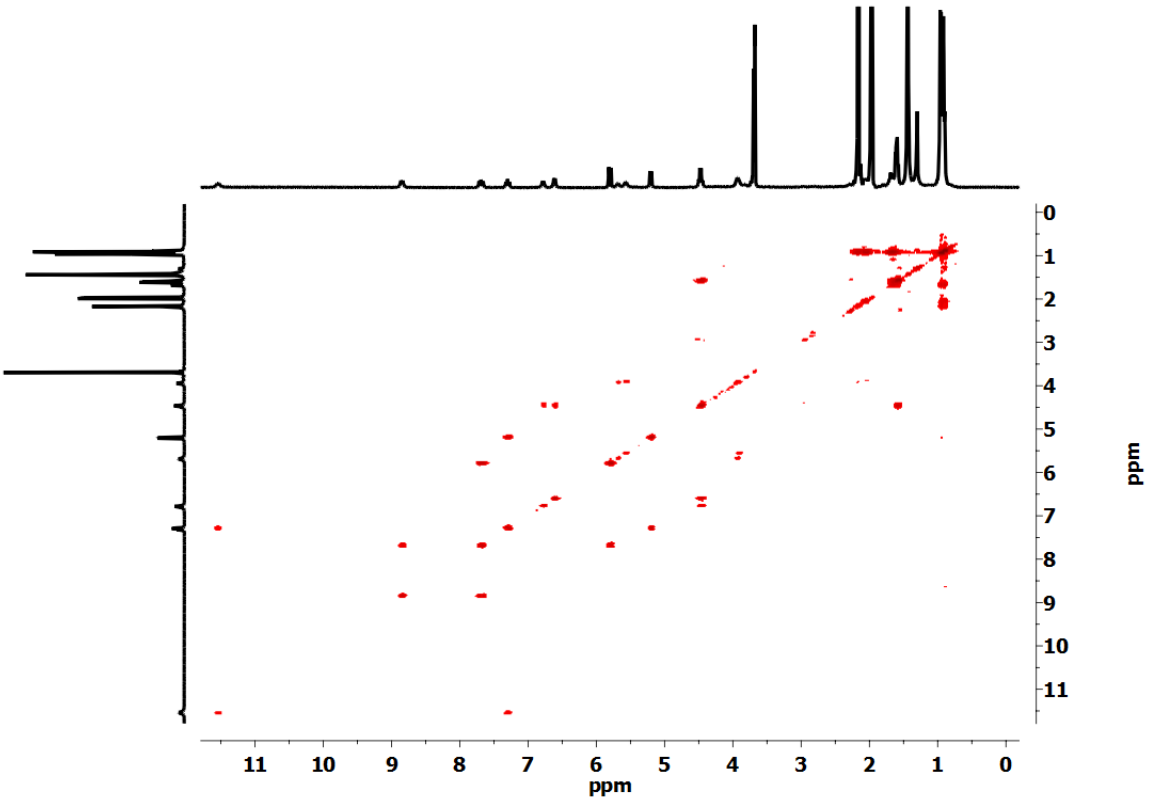

2D COSY NMR spectrum of **9(Z/E)**.

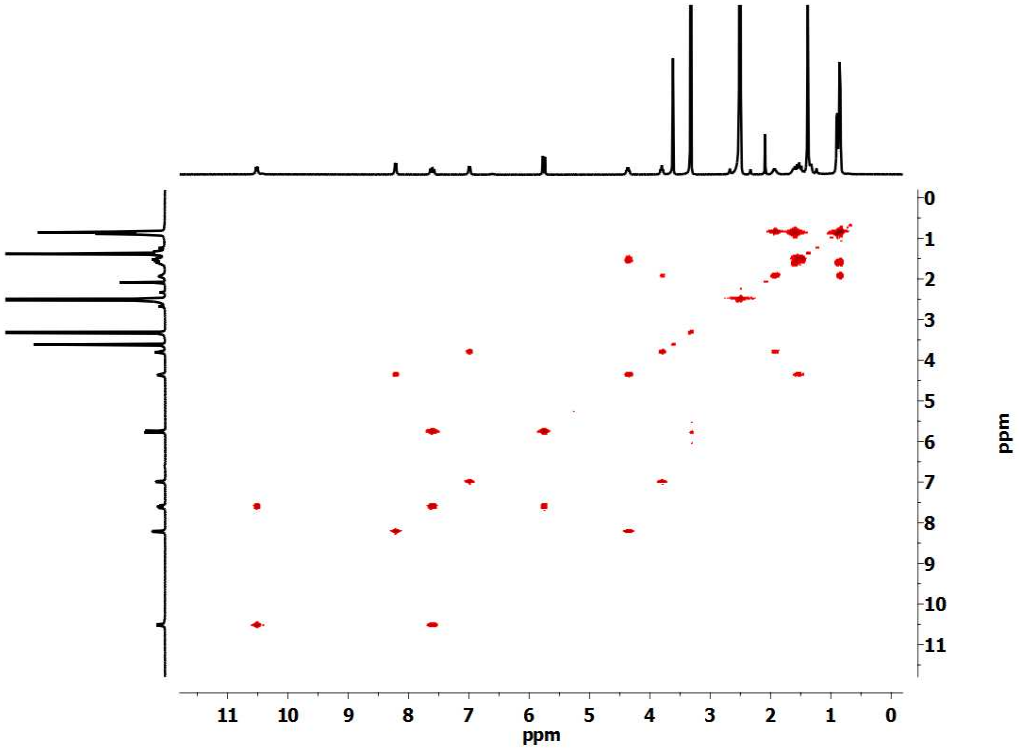

2D COSY NMR spectrum of **9(E)**.

List of Publications

[1] D. Mazzier, M. Crisma, M. De Poli, G. Marafon, C. Peggion, J. Clayden, and A. Moretto, *J. Am. Chem. Soc.,* **2016**, *138*, 8007-8018; https://onlinelibrary.wiley.com/doi/full/10.1002/psc.2941

[2] D. Mazzier, D. Mosconi, G. Marafon, A. Reheman, C Toniolo, and A. Moretto, *J. Pept. Sci.*, **2017**, *23*, 155-161; https://onlinelibrary.wiley.com/doi/full/10.1002/psc.2941

[3] G. Marafon, D. Mosconi, D. Mazzier, B. Biondi, M. De Zotti, and A. Moretto, *RSC Adv.*, **2016**, *6*, 73650-73659; https://pubs.rsc.org/en/content/articlelanding/2016/ra/c6ra17673a#!divAbstract

[4] G. Marafon, I. Menegazzo, M. De Zotti, M. Crisma, C. Toniolo, and A. Moretto, *Soft Matter*, **2017**, *13*, 4231-4240; https://pubs.rsc.org/en/content/articlelanding/2017/sm/c7sm00764g#!divAbstract

[5] G. Marafon, M. A. Motta, C. Toniolo, and A. Moretto, *Peptide Science*, **2018,** e24036, 10.1002/pep2.24036; https://onlinelibrary.wiley.com/doi/10.1002/pep2.24036

[6] G. Marafon, M. Crisma, and A. Moretto, *Angew. Chem. Int. Ed.*, **2018**, *57*, 10217-10220; https://onlinelibrary.wiley.com/doi/full/10.1002/anie.201806035

[7] E. Gatto, S. Kubitzky, M. Schriever, S. Cesaroni, C. Mazzuca, G. Marafon, M. Venanzi, and M. De Zotti, *Angew. Chem. Int. Ed.*, **2019**, *131*, 7386-7390; https://onlinelibrary.wiley.com/doi/full/10.1002/anie.201901683

[8] G. Marafon, M. Crisma, and A. Moretto, *Org. Lett.,* **2019**, *21*, 4182-4186; https://pubs.acs.org/doi/abs/10.1021/acs.orglett.9b01360

[9] Y. Lyu, G. Marafon, A. Martìnez, A. Moretto, and P. Scrimin, *Chem. Eur. J.*, **2019**, *25*, 11758-11764; https://onlinelibrary.wiley.com/doi/full/10.1002/chem.201902552

[10] G. Marafon, A. Moretto, D. Zanuy, C. Alemán, M. Crisma, and C. Toniolo, *J. Org. Chem.*, **2019**, accepted, DOI: 10.1021/acs.joc.9b02544. https://pubs.acs.org/doi/10.1021/acs.joc.9b02544

Ringraziamenti

In questi tre anni di lavoro, di ricerca, ma soprattutto di crescita, sono molte le persone che mi sono state vicino e mi hanno aiutata in molti modi diversi.

Primo fra tutti, devo ringraziare il Prof. Moretto, per avermi seguito e sopportato in questi anni in laboratorio, per tutto quello che mi ha insegnato, per la passione per la sintesi organica che mi ha trasmesso, e la fiducia che ripone in me. Grazie perché adesso so qual è il lavoro più bello del mondo.

Grazie al Prof. Claudio Toniolo e al Prof. Fernando Formaggio, per la disponibilità, le attenzioni e la gentilezza che mi hanno sempre dimostrato in questi anni.
Grazie al dott. Marco Crisma, per la risoluzione delle strutture molecolari tramite diffrazione di raggi X e per tutti i preziosi suggerimenti che mi ha saputo dare.
Grazie alla prof. Cristina Peggion, alla dottoressa Barbara Biondi, alla dottoressa Marta De Zotti, alla dottoressa Ileana Menegazzo e al dottor Renato Schiesari per non avermi mai fatto mancare il loro prezioso aiuto e per la grande disponibilità che hanno sempre dimostrato nei miei confronti.

Soprattutto, grazie a papà Silvio, mamma Dorella, Anna e Raffaele, perché non mi avete mai fatto mancare il vostro sostegno e l'incoraggiamento ad andare avanti, perchè mi spronate sempre a superare i miei limiti, perché siete i primi a fare il tifo per me e credete in me forse più di quanto io non creda in me stessa. A tutta la "banda" della mia famiglia: grazie.

Ora che sono giunta alla fine di questo percorso, ripenso a quando è iniziato e, sotto alcuni punti di vista, vorrei non trovarmi qui a scrivere questa pagina di ringraziamenti che ne sancisce la fine. Mi sento fortunata ad avere avuto la possibilità di intraprendere questo percorso, per le persone con cui ho potuto lavorare, per quello che ho imparato (chimicamente parlando e non solo) e per la persona che sento di essere ora, ben diversa dalla neolaureata che si è immatricolata a Ottobre di tre anni fa. Credo sinceramente che questo Dottorato sia stato una delle opportunità migliori che mi siano capitate, e anche se mi sento entusiasta nel cominciare un nuovo capitolo, non potrò evitare di ripensare con un po' di nostalgia a questo appena concluso.

Re-use permission requests

Material published by the Royal Society of Chemistry and other publishers is subject to all applicable copyright, database protection, and other rights. Therefore, for any publication, whether printed or electronic, permission must be obtained to use material for which the author(s) does not already own the copyright. This material may be, for example, a figure, diagram, table, photo or some other image.

Author reusing their own work published by the Royal Society of Chemistry

You do not need to request permission to reuse your own figures, diagrams, etc, that were originally published in a Royal Society of Chemistry publication. However, permission should be requested for use of the whole article or chapter except if reusing it in a thesis. If you are including an article or book chapter published by us in your thesis please ensure that your co-authors are aware of this.

Reuse of material that was published originally by the Royal Society of Chemistry must be accompanied by the appropriate acknowledgement of the publication. The form of the acknowledgement is dependent on the journal in which it was published originally, as detailed in 'Acknowledgements'.

JOHN WILEY AND SONS LICENSE TERMS AND CONDITIONS

Sep 19, 2019

This Agreement between via Marzolo 1 ("You") and John Wiley and Sons ("John Wiley and Sons") consists of your license details and the terms and conditions provided by John Wiley and Sons and Copyright Clearance Center.

License Number	4672370566740
License date	Sep 19, 2019
Licensed Content Publisher	John Wiley and Sons
Licensed Content Publication	Angewandte Chemie International Edition
Licensed Content Title	Intrinsically Photoswitchable α/β Peptides toward Two-State Foldamers
Licensed Content Author	Alessandro Moretto, Marco Crisma, Giulia Marafon
Licensed Content Date	Jul 15, 2018
Licensed Content Volume	57
Licensed Content Issue	32
Licensed Content Pages	4
Type of use	Dissertation/Thesis
Requestor type	Author of this Wiley article
Format	Print and electronic
Portion	Full article
Will you be translating?	No
Title of your thesis / dissertation	Peptide-based foldamers for applications in self-recognition, supramolecular propagation, and photo-induced folding.
Expected completion date	Apr 2020
Expected size (number of pages)	300
Requestor Location	via Marzolo 1 via Marzolo 1 3 Padova, PD 35131 Italy Attn: via Marzolo 1
Publisher Tax ID	EU826007151
Total	0.00 EUR
Terms and Conditions	

TERMS AND CONDITIONS

This copyrighted material is owned by or exclusively licensed to John Wiley & Sons, Inc. or one of its group companies (each a"Wiley Company") or handled on behalf of a society with which a Wiley Company has exclusive publishing rights in relation to a particular work (collectively "WILEY"). By clicking "accept" in connection with completing this licensing transaction, you agree that the following terms and conditions apply to this transaction (along with the billing and payment terms and conditions established by the Copyright Clearance Center Inc., ("CCC's Billing and Payment terms and conditions"), at the time that you opened your RightsLink account (these are available at any time at http://myaccount.copyright.com).

JOHN WILEY AND SONS LICENSE TERMS AND CONDITIONS

Sep 19, 2019

This Agreement between via Marzolo 1 ("You") and John Wiley and Sons ("John Wiley and Sons") consists of your license details and the terms and conditions provided by John Wiley and Sons and Copyright Clearance Center.

License Number	4672370850450
License date	Sep 19, 2019
Licensed Content Publisher	John Wiley and Sons
Licensed Content Publication	Journal of Peptide Science
Licensed Content Title	Light-driven topochemical polymerization under organogel conditions of a symmetrical dipeptide–diacetylene system
Licensed Content Author	Alessandro Moretto, Claudio Toniolo, Aikebaier Reheman, et al
Licensed Content Date	Nov 14, 2016
Licensed Content Volume	23
Licensed Content Issue	2
Licensed Content Pages	7
Type of use	Dissertation/Thesis
Requestor type	Author of this Wiley article
Format	Print and electronic
Portion	Full article
Will you be translating?	No
Title of your thesis / dissertation	Peptide-based foldamers for applications in self-recognition, supramolecular propagation, and photo-induced folding.
Expected completion date	Apr 2020
Expected size (number of pages)	300
Requestor Location	via Marzolo 1 via Marzolo 1 3 Padova, PD 35131 Italy Attn: via Marzolo 1
Publisher Tax ID	EU826007151
Total	0.00 EUR
Terms and Conditions	

TERMS AND CONDITIONS

This copyrighted material is owned by or exclusively licensed to John Wiley & Sons, Inc. or one of its group companies (each a"Wiley Company") or handled on behalf of a society with which a Wiley Company has exclusive publishing rights in relation to a particular work (collectively "WILEY"). By clicking "accept" in connection with completing this licensing transaction, you agree that the following terms and conditions apply to this transaction (along with the billing and payment terms and conditions established by the Copyright Clearance Center Inc., ("CCC's Billing and Payment terms and conditions"), at the time that you opened your RightsLink account (these are available at any time at http://myaccount.copyright.com).

JOHN WILEY AND SONS LICENSE TERMS AND CONDITIONS

Sep 19, 2019

This Agreement between via Marzolo 1 ("You") and John Wiley and Sons ("John Wiley and Sons") consists of your license details and the terms and conditions provided by John Wiley and Sons and Copyright Clearance Center.

License Number	4672371111031
License date	Sep 19, 2019
Licensed Content Publisher	John Wiley and Sons
Licensed Content Publication	Angewandte Chemie International Edition
Licensed Content Title	Building Supramolecular DNA-Inspired Nanowires on Gold Surfaces: From 2D to 3D
Licensed Content Author	Marta De Zotti, Mariano Venanzi, Giulia Marafon, et al
Licensed Content Date	Apr 24, 2019
Licensed Content Volume	58
Licensed Content Issue	22
Licensed Content Pages	5
Type of use	Dissertation/Thesis
Requestor type	Author of this Wiley article
Format	Print and electronic
Portion	Full article
Will you be translating?	No
Title of your thesis / dissertation	Peptide-based foldamers for applications in self-recognition, supramolecular propagation, and photo-induced folding.
Expected completion date	Apr 2020
Expected size (number of pages)	300
Requestor Location	via Marzolo 1 via Marzolo 1 3 Padova, PD 35131 Italy Attn: via Marzolo 1
Publisher Tax ID	EU826007151
Total	0.00 EUR
Terms and Conditions	

TERMS AND CONDITIONS

This copyrighted material is owned by or exclusively licensed to John Wiley & Sons, Inc. or one of its group companies (each a"Wiley Company") or handled on behalf of a society with which a Wiley Company has exclusive publishing rights in relation to a particular work (collectively "WILEY"). By clicking "accept" in connection with completing this licensing transaction, you agree that the following terms and conditions apply to this transaction (along with the billing and payment terms and conditions established by the Copyright Clearance Center Inc., ("CCC's Billing and Payment terms and conditions"), at the time that you opened your RightsLink account (these are available at any time at http://myaccount.copyright.com).

Title: Tunable E–Z Photoisomerization in α,β-Peptide Foldamers Featuring Multiple (E/Z)-3-Aminoprop-2-enoic Acid Units

Author: Giulia Marafon, Marco Crisma, Alessandro Moretto

Publication: Organic Letters

Publisher: American Chemical Society

Date: Jun 1, 2019

PERMISSION/LICENSE IS GRANTED FOR YOUR ORDER AT NO CHARGE

This type of permission/license, instead of the standard Terms & Conditions, is sent to you because no fee is being charged for your order. Please note the following:

- Permission is granted for your request in both print and electronic formats, and translations.
- If figures and/or tables were requested, they may be adapted or used in part.
- Please print this page for your records and send a copy of it to your publisher/graduate school.
- Appropriate credit for the requested material should be given as follows: "Reprinted (adapted) with permission from (COMPLETE REFERENCE CITATION). Copyright (YEAR) American Chemical Society." Insert appropriate information in place of the capitalized words.
- One-time permission is granted only for the use specified in your request. No additional uses are granted (such as derivative works or other editions). For any other uses, please submit a new request.

BACK | CLOSE WINDOW